UNIVERSITY OF CALIFORNIA SAN DIEGO

SAN DIEGO STATE UNIVERSITY

Selective Methodologies for Direct Functionalization of Arenes and Heterocycles

A dissertation submitted in partial satisfaction of the
requirements for the degree Doctor of Philosophy

in

Chemistry

by

Andrew Nguyen Dinh

Committee in charge:

Professor Jeffrey L. Gustafson, Chair
Professor William Fenical
Professor Byron Purse
Professor Valerie Schmidt
Professor Haim Weizman

2020

The dissertation of Andrew Nguyen Dinh is approved, and it is acceptable in quality and for publication on microfilm and electronically:

_____

_____

_____

_____

_____

Chair

University of California San Diego

San Diego State University

2020

DEDICATION

To everyone who’s made me who I am

TABLE OF CONTENTS

LIST OF FIGURES

LIST OF TABLES

LIST OF SCHEMES

ACKNOWLEDGEMENTS

It goes without saying that I wouldn't be in this fortuitous position if it weren't for the people around me who have provided their friendship, advice, support and love throughout my entire life. I'm blessed to have made these new connections during my time as a graduate student at San Diego State University. I could write an entirely different thesis about how much each person has impacted my life; for the sake of brevity, I'll try my best to condense it within this short acknowledgement section.

I learned very quickly that my apartment in San Diego was only a home by name, as I spent most of the time in my true abode of the laboratory. I still vividly remember my first day interviewing with different professors; this lab was the only one where I could speak to my boss about atropisomerism, baseball, The Simpsons and classic rock all within the span the less than an hour. The choice was simple. With every good setting, it is provided with a unique set of characters and the Gustafson Lab was no exception. To Sean Maddox and Chris Nalbandian as the senior graduate students; I looked up to both of you as mentors for guidance and wisdom. Every time I had a question or concern, one of you was there to provide an answer, and I can't understate enough how much I valued your patience, especially during that first year. Honestly, it was a frightening experience when you both graduated because I wasn't ready to the carry the responsibilities of the laboratory. To Mariel Cardenas, Ryan Noorbehesht and Sean Toenjes, the three graduate students who were in my cohort and entered the Gustafson Lab at the same time; you have all impacted my life heavily over the past five years not just as amazing researchers but as close friends. I couldn't have asked for a more intelligent, entertaining and understanding group of people to experience graduate school with. To Ashley Nguyen, Zach Brown, Bahar Heydari, Beeta Heydari and Mariam Basilaia, the graduate students who joined the lab after me; I cannot wait to see you continue to

flourish in the Gustafson lab and grow as individuals. You guys have done so much in your short time at SDSU, more than I accomplished during my time here. I'm happy to call you my friends and will be checking in to hear about your new adventures in the next few years. To Amy Jackson, Lalena Janke, Tiffany Duong, Ernesto Millan and Samuel Albright, the undergraduates who have assisted me directly; thank you for being reliable students who were with me throughout the entirelty of my research projects. I couldn't have accomplished my work without your help. Additionally, thank you for reminding me that I'm getting too old too quickly. I can't wait to read your future papers and see how much you all grow in graduate school. And to my primary investigator, Dr. Jeffrey Gustafson; I'm not exaggerating when I say that you are one of the most enthusiastic people I have ever met. Your excitement for discovery of new ideas drives me to improve every single day, and I am grateful to be able to call you my mentor and my friend.

I need to spend some time giving a shout out to my support network outside of SDSU. To Me, Bo, Jeannie and Vinnie; thank you for always being there throughout my success as well as my failures. I promise to continue being the best son and sibling I possibly can be. To my friends at Edmonds-Woodway and Stanford, I am thankful for all your support over the years, despite the distance. Your friendships are a welcome escape back to a simpler time. To Kelly; I love you. That's all that needs to be said.

The contents in Chapter 1 are in part a reformatted reprint of the following manuscript, with permission from the American Chemical Society: Maddox, S. M.; Dinh, A. N.; Armenta, F.; Um, J.; Gustafson, J. L. "The Catalyst-Controlled Regiodivergent Chlorination of Phenols." *Org. Lett.* **2016**, *18*, 5476. The dissertation author is one of the primary researchers for the data presented. Support of this work by San Diego State University is acknowledged.

The contents in Chapter 2 contains material that will be utilized in a future publication. The following are coauthors on the corresponding project: Dinh, A. N.; Maddox, S. M.; Vaidya, S.; Saputra, M.; Nalbandian, C.; Gustafson J. L. "Catalyst-controlled Regioselective Chlorination of Phenols and Anilines through a Lewis basic Selenoether catalyst." The dissertation author is the primary researcher for the data presented. Support of this work by the National Science Foundation is acknowledged (CHE-1664565).

The contents in Chapter 3 are in part a reformatted reprint of the following manuscript, with permission from Thieme E-Books & E-Journals: Dinh, A. N.; Nguyen, A. D.; Millan Aceves, E.; Albright, S. T.; Cedano, M. R.; Smith, D. K.; Gustafson J. L. "Photocatalytic Oxidative C-H Thiolation: Synthesis of Benzothiazoles and Sulfenylated Indoles." *Synlett*, **2019**, *30*, 1648-1655. The dissertation author is the primary research for the data presented. Support of this work by the National Science Foundation is acknowledged (CHE-1664565).

The contents in Chapter 4 are in part a reformatted reprint of the following manuscript, with permission from Thieme E-Books & E-Journals: Dinh, A. N.; Noorbehesht, R. R.; Toenjes, S. T.; Jackson, A. C.; Saputra, M. A.; Maddox, S. M.; Gustafson, J. L. "Toward a Catalytic Atroposelective Synthesis of Diaryl Ethers Through C(sp^2)-H Alkylation with Nitroalkanes." *Synlett*, **2018**, *29*, 2155-2160. The dissertation author is the primary research for the data presented. Support of this work by the National Science Foundation is acknowledged (CHE-1664565).

VITA

2009-2013 Bachelor of Science, Chemistry, Stanford University

2013-2015 Laboratory Technician, Medicinal Chemistry, University of Washington

2015-2017 Teaching Assistant, San Diego State University

2017-2020 Graduate Research, San Diego State University

2015-2020 Doctor of Philosophy, Chemistry, University of California San Diego and San Diego State University

PUBLICATIONS

1. Maddox, S. M.; Dinh, A. N.; Armenta, F.; Um, J.; Gustafson, J. L. "The Catalyst-Controlled Regiodivergent Chlorination of Phenols." *Org. Lett.* **2016**, *18*, 5476

2. Dinh, A. N.; Gustafson J. L. "A Catalytic Cycle of Discovery: Asymmetric Catalysis Gives Rise to New Chiral Catalyst Scaffolds." *Chem,* **2020**, *6*, 810-812

3. Dinh, A. N.; Nguyen, A. D.; Millan Aceves, E.; Albright, S. T.; Cedano, M. R.; Smith, D. K.; Gustafson J. L. "Photocatalytic Oxidative C-H Thiolation: Synthesis of Benzothiazoles and Sulfenylated Indoles." *Synlett*, **2019**, *30*, 1648-1655

4. Dinh, A. N.; Noorbehesht, R. R.; Toenjes, S. T.; Jackson, A. C.; Saputra, M. A.; Maddox, S. M.; Gustafson, J. L. "Toward a Catalytic Atroposelective Synthesis of Diaryl Ethers Through C(sp^2)-H Alkylation with Nitroalkanes." *Synlett*, **2018**, *29*, 2155-2160.

MANUSCRIPTS IN PREPARATION

1. Dinh, A. N.; Maddox, S. M.; Vaidya, S.; Saputra, M.; Gustafson J. L. "Catalyst-controlled Regioselective Chlorination of Phenols and Anilines through a Lewis basic Selenoether catalyst."

PRESENTATIONS

1. “Selective C-H Chlorination of Phenols and Anilines through Lewis base selenoether catalyst.” **Dinh, A. N.**; Maddox, S. M.; Vaidya, S.; Saputra, M.; Gustafson J., poster presentation at the Florida Heterocycles Conference, Gaineville, FL, March 2020.

2. “Regioselective Electrophilic Aromatic Substitution of Phenols and Anilines via Lewis base catalysis”, **Dinh, A. N.**, oral presentation at SDSU Student Research Symposium, San Diego State University, March 2020.

3. “Selective C-H Functionalization of Arenes and Heterocycles for Biological Applications”, **Dinh, A. N.**, Brown, Z., poster presentation at the 32nd Annual CSU Biotechnology Symposium, Santa Clara, CA, January 2020.

4. “Mechanistic Insights and Kinetic studies of Lewis base Chlorination of arenes and heterocycles.” **Dinh**, **A. N.**, Janke, L.; Maddox, S. M.; Addison, B.; Gustafson, J. L., poster presentation at the American Chemical Society Fall 2019 National Meeting, San Diego, CA, August 2019.

5. “Regioselective Chlorination of Phenol: Mechanistic Insights and Kinetic Studies of Lewis Base catalysts” **Dinh**, **A. N.**, Janke, L.; Maddox, S. M.; Addison, B.; Gustafson, J. L., poster presentation at the National Organic Symposium, Bloomington, IN, July 2019.

6. “Regioselective Halogenation of Phenol: Mechanistic Insights and Kinetic Studies of Lewis Base catalyst” **Dinh**, **A. N.**, Janke, L.; Maddox, S. M.; Addison, B.; Gustafson, J. L., poster presentation at SDSU Student Research Symposium, San Diego State University, March 2019.

7. “Investigative Mechanistic Studies of Lewis Base Catalyst-Controlled Regioselective Chlorination of Arenes and Heterocycle”, **Dinh**, **A. N.**, Janke, L.; Maddox, S. M.; Addison, B.;

Gustafson, J. L., poster presentation at the 31st Annual CSU Biotechnology Symposium, Orange County, CA, January 2019.

8. "Atroposelective dynamic kinetic resolution of diaryl ether naphthoquinones through alkylation" **Dinh, A. N.,** Jackson, A., poster presentation at the American Chemical Society Spring 2018 National Meeting, New Orleans, LA, March 2018.

9. "An Atroposelective Dynamic Kinetic Resolution of Diaryl Ether Naphthoquinones" **Dinh A. N.**, oral presentation at SDSU Student Research Symposium, San Diego State University, March 2018.

10. "The Catalyst-Controlled Regiodivergent Chlorination of Phenols Towards Drug Discovery Efforts" Maddox, S. M.; **Dinh, A. N.**, poster presentation at 30th Annual CSU Biotechnology Symposium, Santa Clara, CA, January 2018.

11. "The Atroposelective Dynamic Kinetic Resolution of Diaryl Ethers: A New Route to Chiral Pharmacophores" **Dinh, A. N.**, Noorbehesht, R., poster presentation at 30th Annual CSU Biotechnology Symposium, Santa Clara, CA, January 2018.

12. "An Atroposelective Dynamic Kinetic Resolution of Di-aryl Ether Naphthoquinones" **Dinh, A. N.**, Noorbehesht, R., poster presentation at the National Organic Symposium, Davis, CA, July 2017.

13. "An Atroposelective Dynamic Kinetic Resolution of Di-aryl Ether Naphthoquinones through Nitromethylation", **Dinh, A. N.**, Noorbehesht, R., poster presentation at SDSU Student Research Symposium, San Diego State University, March 2017.

14. "Atropisomeric Synthesis of Selective Kinase Inhibitors: A Scalable Solution to a Problem in Drug Discovery", Cardenas, M. M.; **Dinh, A. N.**, poster presentation at 29th Annual CSU Biotechnology Symposium, Santa Clara, CA, January 2017.

15. “The Catalyst-Directed *ortho*-Chlorination of Phenols”, **Dinh A.N.**, oral presentation at the Chemistry Graduate Research Award at SDSU, August 2016.

HONORS AND AWARDS

Tom Ragan Memorial Endowed Fellowship, San Diego State University (2019-2020)

University Graduate Fellow (2017-2019)

Harry Hamber Scholarship, San Diego State University (2017-2018)

MAJOR FIELD OF STUDY

Major Field: Chemistry (Organic)

Regioselective and Enantioselective C-H Functionalization Utilizing Organocatalytic Chemical Methodologies

Professor Jeffrey L. Gustafson

ABSTRACT OF THE DISSERTATION

Selective Methodologies for Direct Functionalization of Arenes and Heterocycles

by

Andrew Nguyen Dinh

Doctor of Philosophy in Chemistry

University of California San Diego 2020

San Diego State University, 2020

Professor Jeffrey L. Gustafson, Chair

The functionalization of arenes and heterocycles via direct C-H activation is a valuable tool in medicinal chemistry as it allows for the manipulation of a diversity of complex structures without the need for *de novo* methodologies. It can be utilized as a late-stage strategy to address pharmacological problems such as pharmacokinetic profile, metabolism and on-off target activity of a lead compound. One of the drawbacks to current methodologies is the lack of regioselectivity,

wherein a scaffold possesses multiple sites of reactivity, leading to multiple constitutional isomers. Our lab has developed a regioselective catalyst-controlled Lewis base halogenation of phenols and anilines, which is discussed in two manuscripts in Chapter 1 and 2. We also explore photoredox catalysis to explore the intramolecular synthesis of benzothiazoles and intermolecular sulfenylation of indoles, which is presented in Chapter 3. Last, Chapter 4 discusses an enantioselective functionalization of a diaryl ether naphthoquinone scaffold to access enantioenriched atropisomeric molecules. We believe these works can be utilized to obtain a diversity of highly regioselective and enantioselective heterocycle and arene motifs that are relevant towards drug discovery efforts.

CHAPTER 1: The Catalyst-Controlled Regiodivergent Chlorination of Phenols and Anilines via Lewis Base Catalysis

1.0 ACS Copyright

1.1 C-H Functionalization as a Useful Synthetic Strategy

The selective functionalization of C-H bonds has been a long-standing challenge and sought after goal in organic chemistry. Developing synthetic methodologies that selectively functionalize one bond over the many would allow for an endless number of useful transformations for a broader scope of molecules. Over the past fifteen years, there has been a renewed interest in the direct functionalization of inactivated C-H bonds.[1–4] Despite significant progress, activating a specific C-H bond in a practical manner is still a challenge. This is due to 1) the ubiquitous abundance of C-H bonds in all organic molecules and 2) unfavorable harsh conditions that are often needed to initiate activation.

In order to work around these shortcomings, Yu has categorized C-H functionalization broadly into two large subfields.[5] One strategy involves the transformation of completely unfunctionalized molecules, which he refers to as "first functionalization". Here, the molecules are classified as non-polar and may interact very weakly with transition metals or organic catalysts, meaning control of the chemoselectivity is extremely difficult. The second subfield of C-H functionalization that he describes has substrates with one or more functional groups, which he

called “further functionalization”. This approach utilizes the functional group as an intermediate handle to coordinate to a polar metal species or bond with a mediating catalyst via non-covalent interactions. This interaction can bias the substrate to overcome its innate selectivity of the C-H bond. Because the functional group plays an essential role in this system, it is desirable that the group is necessary for the final product so that extra steps can be avoided.

1.2 Late Stage C-H Functionalization in Medicinal Chemistry

Because the past fifteen years have seen a resurgence of new chemical methodologies in academia for C-H functionalization, medicinal chemists and chemists in industry are now looking to incorporate these strategies into more complex biologically relevant molecules. A recent analysis showed that there is a large bias towards “traditional” synthetic reactions in medicinal chemistry, such as the Suzuki cross coupling, Buchwald-Hartwig aminations and nucleophilic aromatic substitution (S_NAr); this is most likely due to commercial availability of starting materials, high chemoselectivity and overall reliability of the processes.[6] However, with the expansion of new C-H transformations being reported, these methods offer the opportunity to create a diverse library of complex analogues through late stage functionalization (LSF) without resorting to complex *de novo* syntheses.[7,8] Cernak describes the utility of LSF with their example of Aprepitant, a neurokinin receptor antagonist for the treatment of chemotherapy induced nausea and vomiting (Figure 1.2.1).[1] The precursor to Aprepitant is an advanced lead compound that failed in clinical trials due to lack of metabolic stability *in vivo*. Adding one or two simple functional groups such as a methyl and fluorine group changed the metabolic profile of the molecule, leading to the discovery of Aprepitant. The drug itself is not synthesized according to the hypothetical strategy shown in the figure since there are no reactions which can selectively convert the C-H bonds into their respective C-methyl and C-F bonds. Instead, a *de novo* 10 step synthesis was

optimized for this discovery. If such a process existed, one could imagine the utility of making drugs efficiently along with the diversification of multiple analogues for high-throughput evaluation.

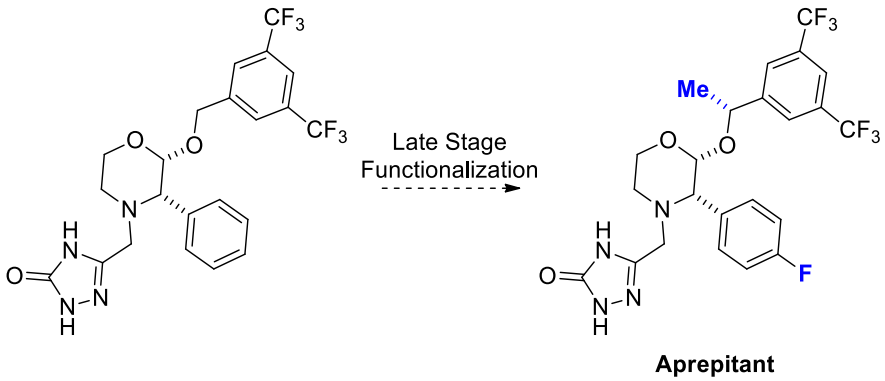

Figure 1.2.1 A Hypothetical Late Stage Functionalization Strategy for Aprepitant

1.3 The Chlorine Scaffold in Bioactive Arenes and Heterocycles

As mentioned in the previous section, synthesis in medicinal chemistry seeks to functionalize complex bioactive molecules with scaffolds that can enhance the general druglike properties of a molecule.[9] Specifically, halogen atoms such as chlorine are well-known as modulators for the electronic and physical properties of drugs as they can provide significant intermolecular interactions between the ligand and target protein.[10–13] Because of these favorable properties, aromatic scaffolds containing chlorine are common throughout the drug landscape and hundreds of aryl chlorides have been approved as clinical drugs, including numerous landmark small molecule pharmaceuticals such as the blockbuster drugs Zoloft, Claritin and Zelboraf (Figure 1.3.1).[14]

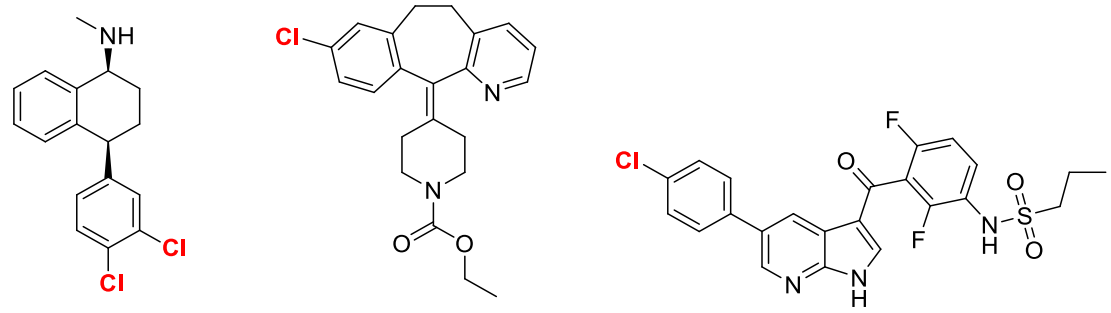

Sertraline (Zoloft)
antidepressant

Loratadine (Claritin)
antihistaminergic agent

Vemurafenib (Zelboraf)
against late-stage melanoma

Figure 1.3.1 The Chlorine Atom is Ubiquitous in Drug Discovery

Additionally, the chlorination of aromatics is one of the most common reactions in modern organic synthesis, largely because halogenated aromatics are among the most versatile and utilized precursors in modern cross-coupling chemistry, metal-halogen exchanges, nucleophilic aromatic substitution (S_NAr) and Buchwald-Hartwig aminations.[15–19] Aryl chlorides are also important starting materials for the synthesis of bulky phosphine ligands via C-C, C-N and C-O bond formation, which are frequently used in late stage functionalization for medicinal chemistry.[20–23] Hence, there is an ever-growing need to develop new methodologies for the chlorination of arenes and heterocycles.

1.4 Electrophilic Aromatic Substitution (S_EAr) as a Strategy for Direct Arene Functionalization

Halogenation of aromatics via electrophilic aromatic substitution (S_EAr) is a classic synthesis that had been studied for well over a century, often represented by the canonical Friedel-Crafts reaction. The presence of a strong Lewis acid catalyst is needed to activate the electrophilic species. However, this first iteration contained multiple shortcomings, which included a reliance on high temperatures and harsh acidic/basic conditions, reagents with low atom economy, reduced reactivity toward electron-poor arenes, and mixtures of constitutional isomers arising from multiple sites of reactivity. In order to avoid these problems, attempts at “greener” oxidative

chemistry was developed, taking inspiration from nature to obtain an electrophilic halogen species through milder oxidants such as oxygen and hydrogen peroxide.[24–26]

In order to replace classic electrophilic halogen reagents such as bromine (Br_2) and chlorine (Cl_2), more mild alternative reagents such as the N-halosuccinimides (NXS: X = Cl, Br, I) are commonly found both in academia and industry. However, these reagents are significantly less reactive and can be used to form the halide product only when the nucleophilic arene is electron rich or when harsh conditions are applied. These reagents can also be activated via catalysis, with Lewis or Brønsted catalysts traditionally utilized.[27–32] The mechanism of action is done via complexation or protonation of the succinimide carbonyl scaffold, creating a positively charged intermediate (Figure 1.4.1a). Another common strategy is the formation of reactive organometallic species through direct metalation of the C-H bond, which affords the halogenated product without needed prefunctionalization. If the aromatic possesses a directing group, regioselective halogenation is possible via adjacent coordination to a transition metal (Figure 1.4.1b).

Additionally, Lewis base catalysis has been used for halide functionalization, wherein a nucleophilic atom such as oxygen, sulfur, selenium, nitrogen or phosphorus will coordinate to the halogenating species to create a positively charged halenium complex (Figure 1.4.1c). This catalytic strategy will be the focus of the subsequent work in the next two chapters. When our lab initially began research on aromatic C-H functionalization in 2013, there was little precedence for a Lewis basic catalytic halogenation of arenes; most of the preceding literature explored the addition to alkene substrates via a halenium cation-π cyclization.[33,34] At of the time of this writing, there have been a number of reports for Lewis base-catalyzed aromatic functionalization.[35–40]

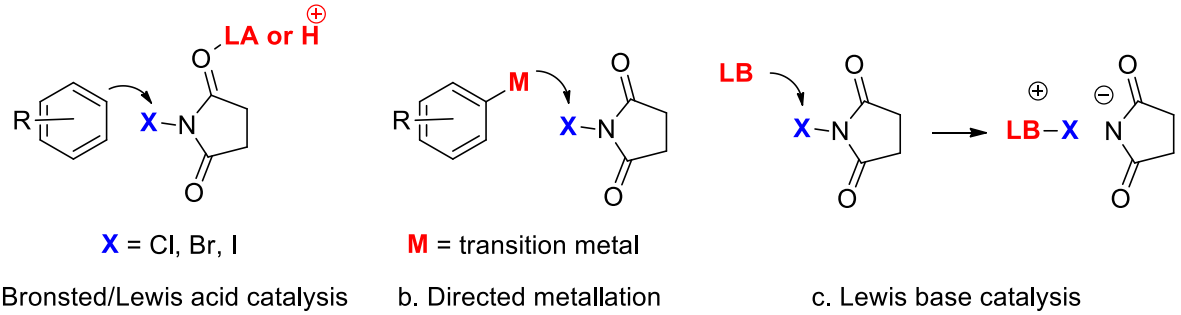

Figure 1.4.1 General Activation Strategies for Electrophilic Halogenation of Arenes

1.5 Theory of Lewis Base Activation of Electrophiles

To better understand the mechanism of Lewis base catalyzed activation of electrophilic halogenation, the following information is summarized from an elegant review from Scott Demark.[41] A Lewis base catalyzed reaction is one accelerated by the formation of an electron-pair donor (catalyst) on a electro pair acceptor (substrate or reagent). This binding will create a transfer of electron density in the newly formed adduct. Normally, one would expect the acceptor to have more nucleophilic character, but the opposite can also occur in which binding to a Lewis base provides the acceptor molecule to have more electrophilic character, a concept that initially appears counterintuitive. Regardless of the structure and electronic properties of the Lewis acid and base, the final acceptor adduct will always contain more electron density than the parent Lewis acid. However, it is overall distribution of electron density through the adjacent atoms which allows Lewis bases to be electrophilic catalysts. Such modes of electron density redistribution arise from analysis by Gutmann and is clearly described in Figure 1.5.1, which is adapted from a manuscript by Miura.[42,43] The binding of a Lewis base to the halogen center is a n-σ^* interaction, leading to polarization of the peripheral bonds to create an electron positive center within the complex. The lengths of the adjacent bonds will become longer while that of the donor-acceptor complex will shorten. If the polarization effect is strong enough, the complex will form a charge-

separated ion pair and the electrophilic character of the halogen will be highly activated and can readily undergo S_EAr.

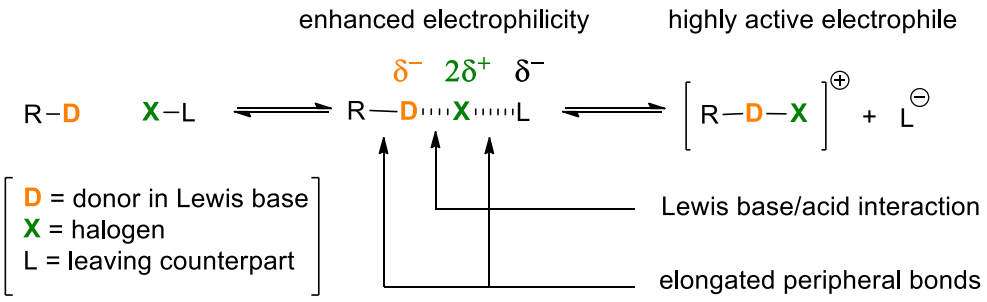

Figure 1.5.1 Charge Separation in Lewis Base Catalysis to Form Electrophilic Intermediate

1.6 Initial Work on Lewis base Catalyzed Electrophilic Chlorination of Arenes and Heterocycles

In 2015, our lab published its first paper in direct C-H chlorination; to our knowledge, there were no reports of Lewis base catalyzed chlorinations of arenes and heterocycles at the time. Stimulated by work from Denmark, our lab postulated that NCS activation with an appropriate Lewis base would represent a mild and efficient catalytic strategy.[44–46] Indeed, Lewis basic triphenylphosphine sulfide proved an excellent catalyst; it could be utilized in mild conditions combined with readily available NXS reagents and was applied to over 20 different arenes and heterocycles for chlorination, bromination and iodination (some examples are shown in Figure 1.6.1 and Scheme 1.6.1). Importantly, the dependence of the chemistry on the presence of a catalyst opens the possibility of next generation phosphine sulfide catalysts which can control enantioselective or regioselective chlorinations (i.e. lack of regioselectivity in Scheme 1.6.1 for

substrates with multiple sites of reactivity). The work towards the Lewis base regiodivergent chlorination of phenols are discussed in the following section.

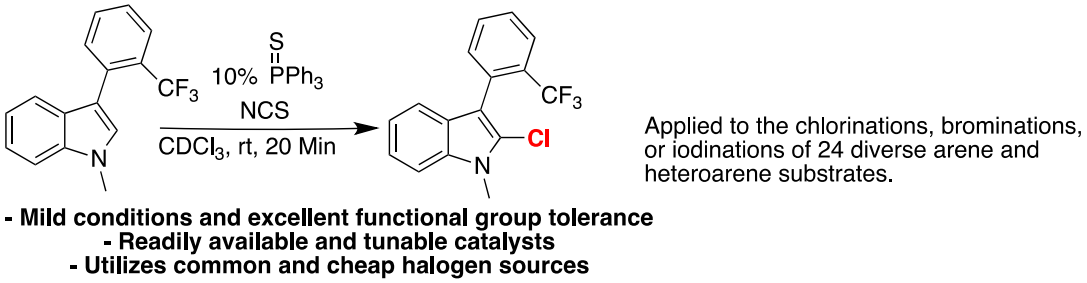

Figure 1.6.1 Lewis Basic Phosphine Sulfide Catalyzed Electrophilic Aromatic Halogenation of Arenes and Heterocycles

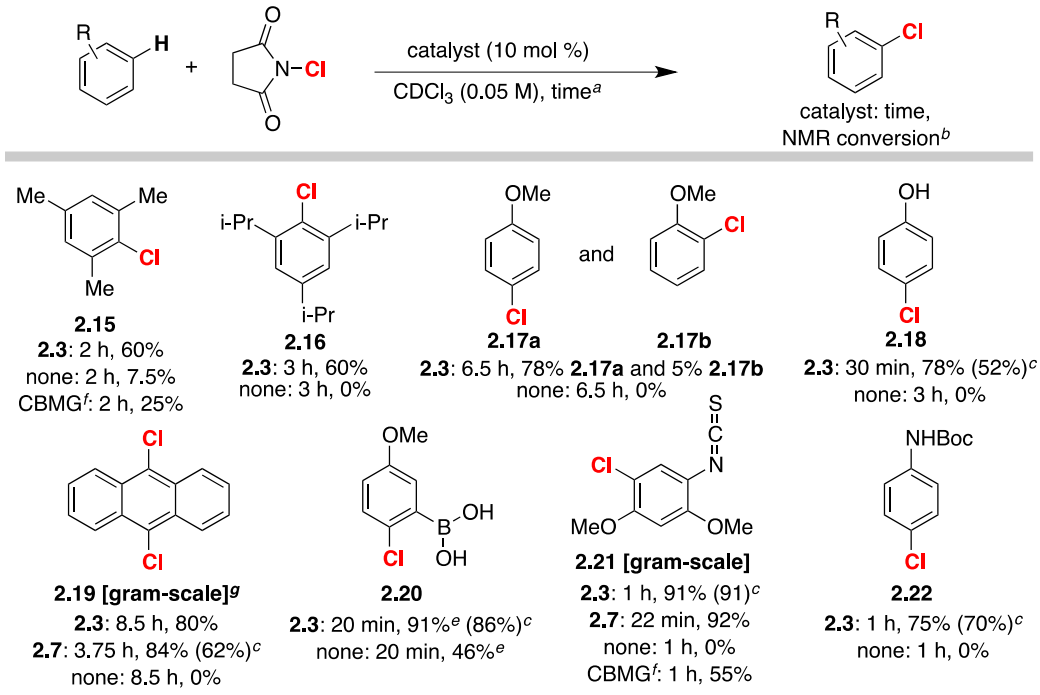

[a]Reactions were performed at room temperature by the addition of 0.03 mmol substrate, 0.003 mmol catalyst, and 600 μL $CDCl_3$ into an NMR tube, followed by the addition of 0.040 mmol NCS. [b]Percent conversions by NMR represent an average of three trials using tetramethylsilane as an internal standard. [c]Isolated yield represents an average of three trials (isolated yield on the gram-scale represents an average of two trials [See Supporting Information for gram-scale procedure]). [e]A 9:1 mixture of $CDCl_3$:CD_3OD was used as the solvent. [f]CBMG was used as the stoichiometric chlorine source instead of NCS, and no catalyst was added to the reaction. [g]2.4 equiv of NCS was used.

Scheme 1.6.1 Chlorination of Various Arenes

1.7 The Catalyst-Controlled Regiodivergent Chlorination of Phenols

As previously mentioned, electrophilic aromatic substitution represents a broadly utilized route to access aryl chlorides. Traditional electrophilic halogenations suffer from several

drawbacks such as a reliance on harsh reaction conditions, reduced reactivity towards electron poor arenes, and a lack of regioselectivity across many substrate classes.[47–49] While recent advances have largely addressed the first two issues, regioselectivity is still an unsolved problem as current electrophilic halogenations rely on substrate-controlled regioselectivity (Figure 1.7.1), often resulting in a mixture of constitutional isomers.[35,36,50–55] On the other hand, it becomes a synthetic challenge to obtain a non-favored isomer when the substrate possesses a strong innate reaction preference toward electrophilic aromatic chlorination.

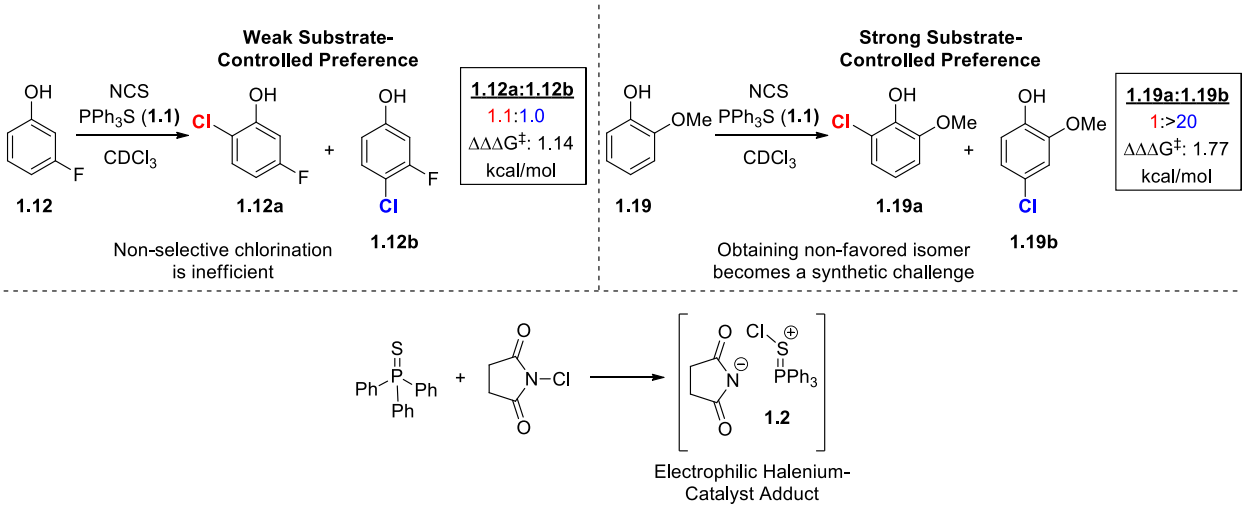

Figure 1.7.1 Reagent-Controlled Regioselectivities in S_EAr Chlorination with Triphenylphosphine Sulfide

Over the past decade, there have been relatively few examples of catalyst-controlled regioselectivities in the arena of S_EAr (Figure 1.7.2). Seminal work by Miller on complex natural products used peptide catalysts to provide a site-selective bromination of Vancomycin, exemplifying this catalyst-controlled strategy.[56] Alternatively, Lewis engineered mutants of the enzyme RebH that can overcome the innate regioselectivity of heterocycle chlorination.[57,58] After this chapter was published, Yeung developed novel methodologies that can regioselectively functionalize anilines and phenols using secondary ammonium catalysts, and enantioselectively

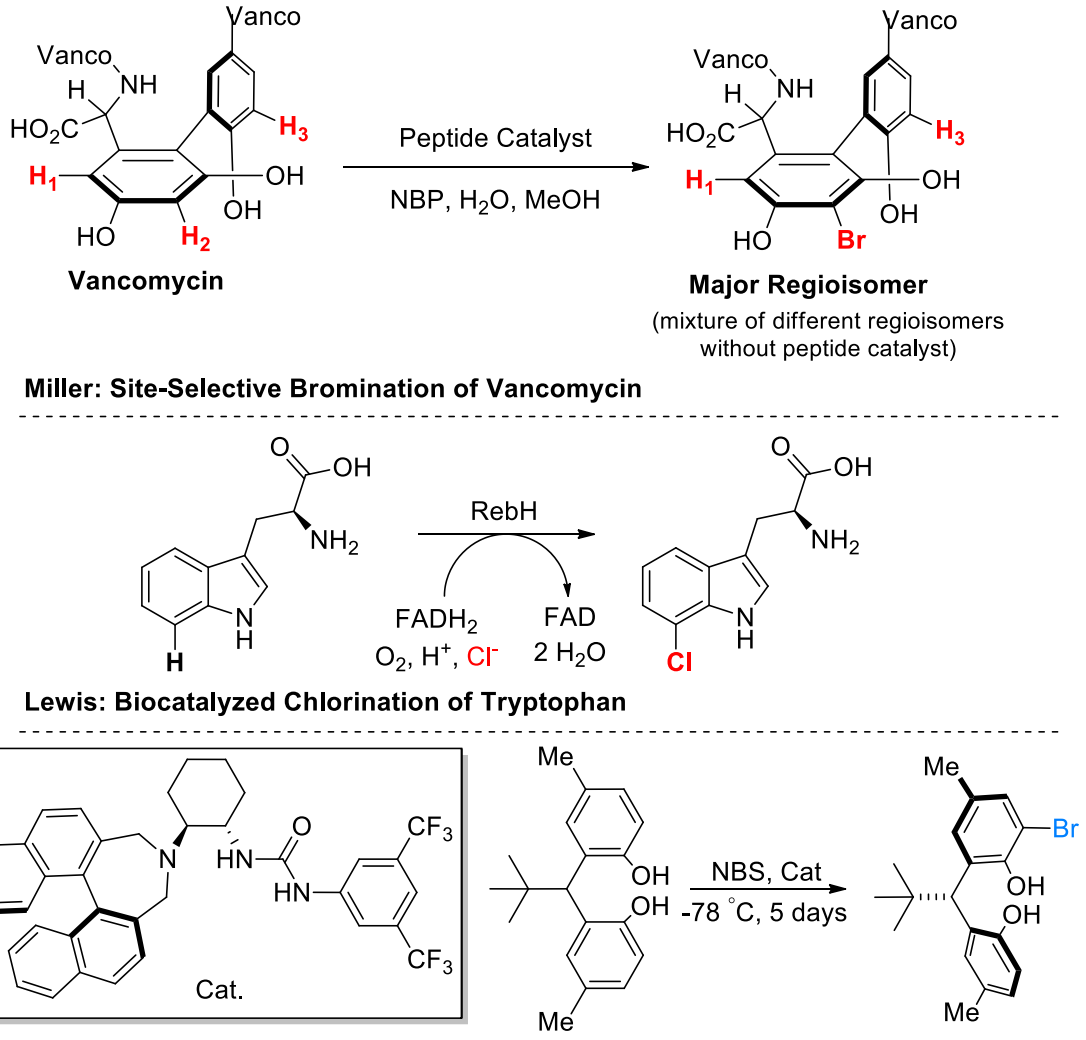

Figure 1.7.2 Previous Examples of Catalyst-Controlled Regioselective Electrophilic Halogenation of Arenes

functionalize aromatic diols to make chiral bisphenols through a desymmetrization strategy.[37,38,59] Herein, I disclose a novel approach to address these issues, in which we demonstrate the ability of different catalysts to control the regioselectivity of phenol in a divergent fashion.

As a proof of concept, I was interested in the development of a Lewis base catalyzed halogenation of arenes that possessed weakly coordinating directing groups such as phenol. As mentioned in earlier sections of this chapter, previous work from our lab showed that Lewis bases such as phosphine sulfides (**1.1**) could activate the halogen species and promote direct

halogenation of arenes and heterocycles by activation of N-halosuccinimides (NXS). These catalyst were able to affect the chlorination of diverse arenes according to the innate preference of a substrate with regioselectivities closely following those reported in literature.[36,53,55] Monitoring the course of the reaction by ^{31}P NMR (Figure 1.7.3) suggested the formation of an intermediate with a large degree of phosphonium character,[60] which would be expected if the chemistry proceeded through a catalyst-halenium adduct[44,61] (Figure 1.7.1, **1.2**). This observation was corroborated by DFT (Figure 1.7.4) studies that predict halogenation to proceed through such an intermediate.

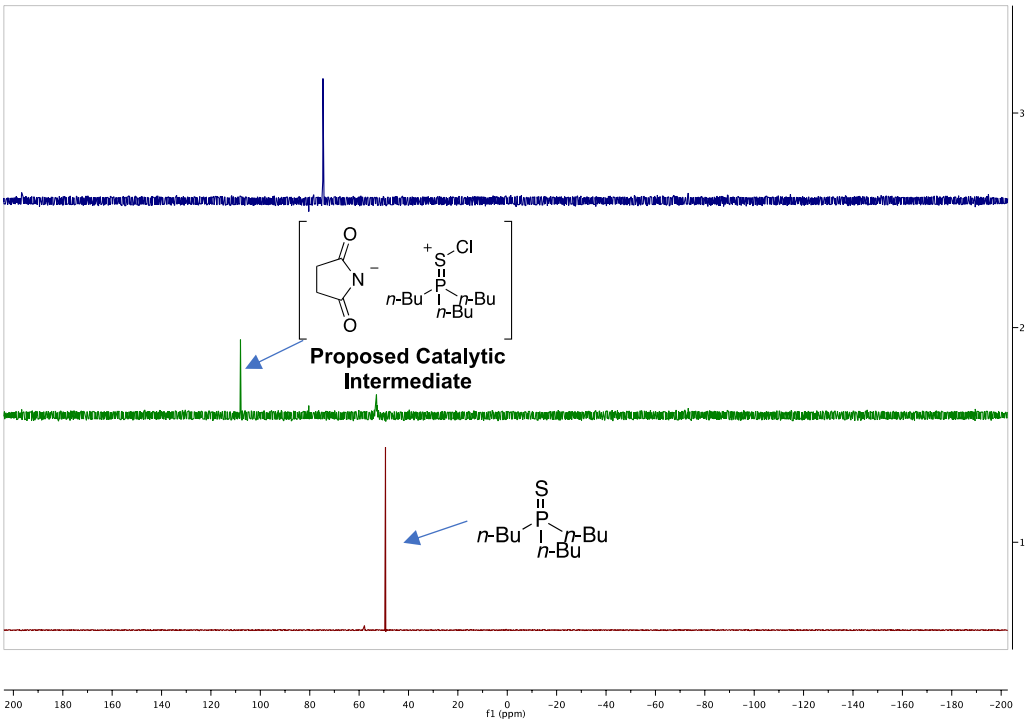

Figure 1.7.3 Lewis Base Catalyst Chlorination with Triphenylphosphine Catalyst (1.1), tracked by ^{31}P NMR.

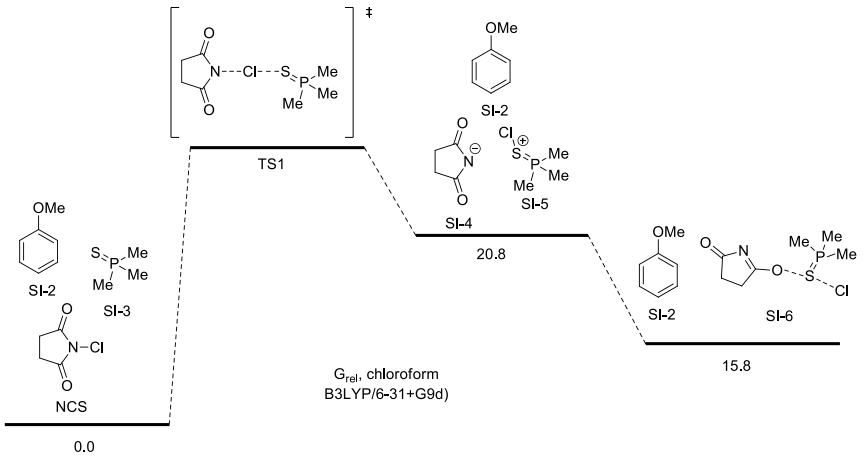

Figure 1.7.4 DFT Calculations of Predicted Catalytic Intermediates in Lewis Base Chlorination with Triphenylphosphine Sulfide (1.1)

As this *in silico* data suggests that the activated halenium is associated with the catalyst, I hypothesized that the Lewis base catalyst structure can alter the reaction outcome for the site-selectivity of electrophilic aromatic halogenation. As a proof of concept, I chose to test this in the context of the *ortho*-chlorination of phenols. Phenols represent an important class of arenes that typically display a moderate to high *para*-preference (Figure 1.7.1). While bulky amines are known to affect the *ortho*-chlorination of phenols,[49,62] these reactions operate under fairly harsh conditions (sulfuryl chloride at 70 ºC) and have been shown to have limited substrate scope.[63] Other commonly employed routes to *ortho*-chlorinated phenols involve multistep processes that include arene oxidation,[64,65] dehalogenation,[66,67] or *O*-methoxymethyl (MOM) directed lithiation.[68,69] A catalytic room temperature *ortho*-selective electrophilic chlorination would represent a more desirable approach that could be performed in one step with few precautions, lending it several practical advantages over current routes.

1.8 Discussion

I began these studies by evaluating several privileged catalyst structures that also possessed Lewis basic functional groups that are known to activate NXS.[45,70] Schreiner's thiourea (**1.4**)

efficiently catalyzed this reaction and yielded a 1.0:2.0 **1.3a:1.3b** ratio (Table 1.8.1, Entry 2).[71,72] While catalyst **1.4** still favored **1.3b**, we were intrigued by the moderate increase (compared to catalyst **1.1**) in *ortho*-isomer **1.3a** formed and decided to evaluate other thioureas. A slight increase in the *ortho*-selectivity for **1.3a** was observed with urea **1.5**, albeit at the expense of significantly reduced reactivity. I found that Nagasawa's bis-thiourea (**1.6**) overcame the substrate's innate preference, yielding a 5.4:1.0 mixture of isomers favoring **1.3a** (Table 1.8.1, Entry 4).[73] This ratio could be improved to 27:1.0 by diluting the reaction concentration (Table 1.8.1, Entry 7). This

Table 1.8.1 Catalyst Exploration towards the *ortho*-Chlorination of Phenol

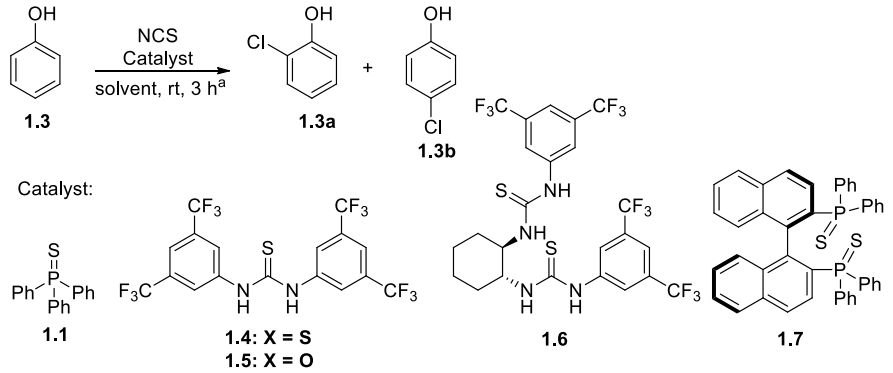

Entry	Cat (%)	Solvent (molarity)[b]	Conv. **1.3a** (%)[c]	**1.3a:1.3b**[d]	$\Delta\Delta G^{\ddagger}$ (kcal/mol)[f]
1	**1.1**(10)	$CDCl_3$ (0.05)	23	1.0:4.0	0
2	**1.4**(10)	$CDCl_3$ (0.025)	33	1.0:2.0	0.41
3	**1.5**(10)	$CDCl_3$ (0.025)	14	1.0:1.1	0.76
4	**1.6**(10)	$CDCl_3$ (0.05)	67	5.4:1.0	1.82
5	**1.6**(10)	C_6D_6 (0.05)	55	6.4:1.0	1.92
6	**1.6**(5)	C_6D_6 (0.025)	75	6.9:1.0	1.96
7	**1.6**(10)	$CDCl_3$ (0.025)	83	27:1.0	2.77
8	**1.6**(5)	$CDCl_3$ (0.025)	82	12:1.0	2.29
9	**1.1**(10)	$CDCl_3$ (0.025)	20	1.0:3.0	0.17
10	**1.7**(10)	$CDCl_3$ (0.025)	13	1.0:7.1	-0.33
11	**1.6**(10)	CD_2Cl_2 (0.025)	64	4.7:1.0	1.73
12	**1.7**(10)	CD_2Cl_2 (0.05)	16	1.0:5.0	-0.13

[a]All reactions were performed by addition of catalyst, solvent, and 0.03 mmol **1.3** at rt, followed by the addition of 0.036 mmol NCS. [b]Molarity of the reaction is in reference to **1.3**. [c]Percent conversion to **1.3a** was determined by ^{1}H NMR and represents an average of three trials using tetramethylsilane or tetrakis(trimethylsilyl)methane as an internal standard. [d]Isomeric ratios were determined by ^{1}H NMR and represent an average of three trials. [e]We observed only minor decreases in selectivites with CD_2Cl_2 as the solvent, allowing us to reliably use DCM as our solvent upon scale-up to mitigate loss of volatile products. [f]$\Delta\Delta\Delta G = \Delta\Delta G_{entry\#} - \Delta\Delta G^{\ddagger}_{entry1}$, with *ortho*-selectivity defined as positive $\Delta\Delta G^{\ddagger}$ and *para*-selectivity defined as negative $\Delta\Delta G^{\ddagger}$.

noticeable effect on the regioselectivity is likely due to a decrease in catalyst aggregation at lower concentration and is consistent with work by Seidel.[74] To put the efficiency of catalyst **1.6** into perspective, the $\Delta\Delta G^{\ddagger}$ between catalyst **1.6** and **1.1** towards *ortho*-chlorination is 2.77 kcal/mol, which corresponds to approximately 98% *ee* in the realm of enantioselective catalysis.

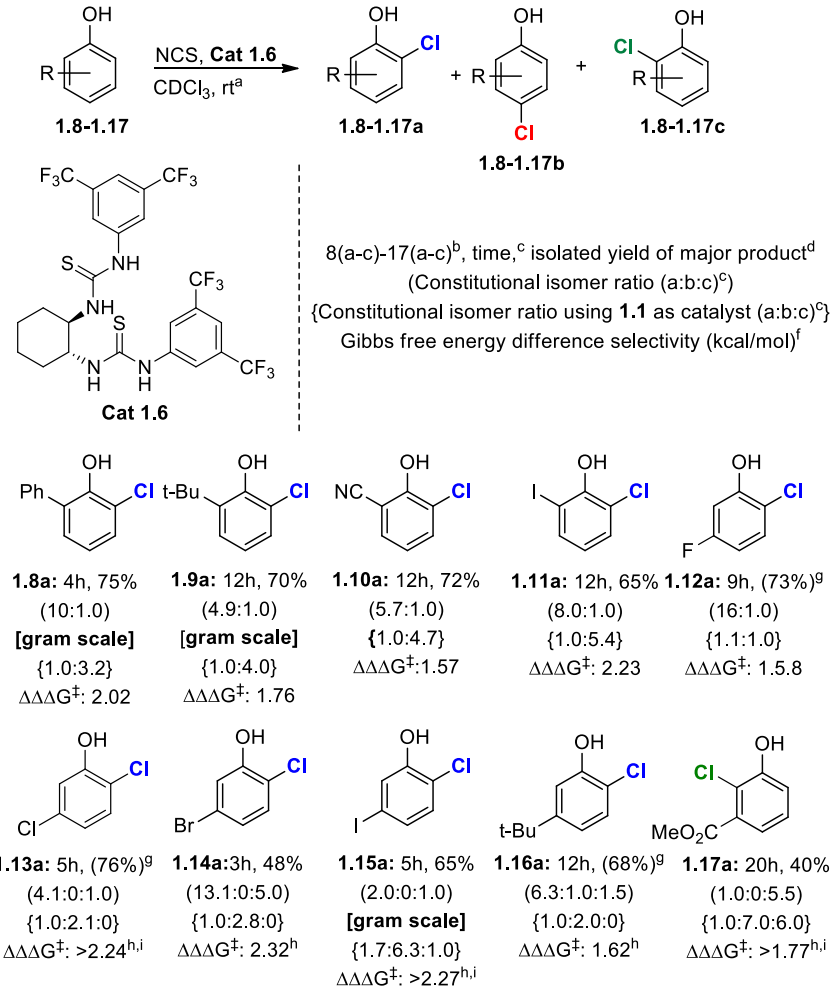

[a]Optimized reaction conditions were used with respect to the catalyst. [b]Only the major product is shown. [c]Reaction times and constitutional isomer ratios were determined by ^{1}H NMR and represent an average of two trials using tetramethylsilane or tetratis(trimethylsilyl)methane (TTMSM) as an internal standard. [d]Isolated yields were determined on the 50-1000mg scale, using DCM as the solvent (due to volatility), and represent an average of two trials. [e]The selectivities observed with catalyst **1.1** are included for comparison. [f]With *ortho*-selectivity defined as positive $\Delta\Delta G^{\ddagger}$ and *para*-selectivity defined as negative $\Delta\Delta G^{\ddagger}$. [g]Due to product volatility, as isolated yield could not be reported; therefore % conversion was reported as determined by ^{1}H NMR using TTMSM as an internal standard. [h]Both *ortho* products (**a** and **c**) combined to simplify calculation. [i]Assuming >20:1 *ortho*/*para* with **1.6**.

Scheme 1.8.1 *ortho*-Selective Chlorination of Substituted Phenols

To define the generality of this catalyst-controlled *ortho*-chlorination, I applied catalyst **1.6** across a series of differentially substituted phenols, observing predominantly *ortho*-chlorination across the substrate set (Scheme 1.8.1). This was in contrast to catalyst **1.1**, which predominantly yielded *para*-chlorination. For example, **1.6** effected the chlorination of phenol **1.8** to give an *ortho*:*para* ratio (**1.8a**:**1.8b**) of 10.0:1.0, with **1.8a** being isolated in 75% yield. I observed a decrease in *ortho*-selectivity for 2-*tert*-butyl substituted **1.9** (*ortho*:*para* ratio of 3:1), perhaps due to the bulky substituent interfering with a catalyst-substrate interaction. Nonetheless, I was able to isolate **1.9a** with a 70% yield. Nitrile-containing **1.10** and 2-iodophenol (**1.11**) also proved good substrates, affording *ortho*:*para* ratios of 5.7:1.0 and 8.0:1.0, respectively.

The chlorination of *meta*-substituted phenols also proceeded with *ortho*-selectivity in the presence of **1.6**. For example, the chlorination of 3-fluorophenol (**1.12**) yielded an excellent 16.0:1.0 **1.12a**:**1.12b** ratio. Substrates with less electronically withdrawing *meta*-substituents were also chlorinated *ortho* to the phenol by **1.6**, however now varying degrees of chlorination at the more hindered *ortho*-position was observed in line with expected electronic trends (see substrates **1.13**-**1.16** in Scheme 1.8.1). **1.17** possessed particularly interesting selectivity as **1.6** primarily effected chlorination at the more hindered *ortho*-position to give predominantly **1.17c** (1.0:0:5.5 ratio of **1.17a**:**1.17b**:**1.17c**). From an energetic perspective, catalyst **1.6** was less effective on these substrates than phenol, however the $\Delta\Delta\Delta G^{\ddagger}$ between catalyst **1.6** and catalyst **1.1** were still quite good, corresponding to a range of 85% to 96% *ee* when an analogy to enantioselective catalysis is made.

With an *ortho*-selective catalyst in hand, I then turned our attention to catalysts that augment the innate *para*-selectivity of phenols, finding that bis(diphenylphosphino)-1,1'-

binaphthyl (BINAP)-derived phosphine sulfide **1.7** could improve upon the innate *para*-selectivity of phenol, yielding a **1.3a**:**1.3b** ratio of 1.0:7.1 (Table 1.8.1, Entry 10).

I then evaluated catalyst **1.7** across the same set of substrates (Scheme 1.8.2). In general, **1.7** was found to yield markedly improved *para*-selectivities compared to those of **1.1**. For

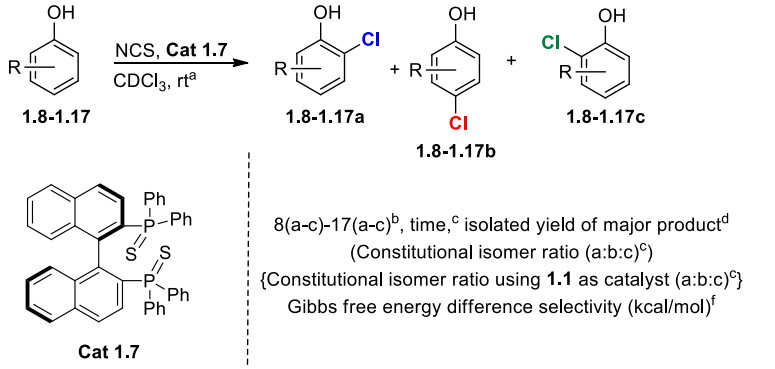

1.8b: 4h, 89% (1.0:12) **[gram scale]** {1.0:3.2} ΔΔΔG‡: -0.80

1.9b: 12h, 83% (1.0:17) {1.0:4.0} ΔΔΔG‡: -0.85

1.10b: 12h, 67% (1.0:7.4) **{**1.0:2.5} ΔΔΔG‡:-0.64

1.11b: 3h, 86% (1.0:20) {1.0:5.4} ΔΔΔG‡: -0.80

1.12b: 6h, (68%)[g] (1.0:2.1) {1.1:1.0} ΔΔΔG‡: -0.50

1.13b: 2h, 71% (1.0:3.5:0) {1.0:2.1:0} ΔΔΔG‡: -0.30[h]

1.14b: 2h, 72% (1.0:6:0:0) {1.0:2.8:0} ΔΔΔG‡: -0.45[h]

1.15b: 1h, 80% (1.7:8.3:1.0) {1.7:6.3:1.0} ΔΔΔG‡: >-0.16[h]

1.16b: 1h, 53% (1.0:6.0:0) {1.0:2.0:0} ΔΔΔG‡: -0.65[h]

1.17b: 2h, 57% (1.0:13:6.5) {1.0:7.0:6.0} ΔΔΔG‡: -0.32[h]

[a]Optimized reaction conditions were used with respect to the catalyst. [b]Only the major product is shown. [c]Reaction times and constitutional isomer ratios were determined by ^{1}H NMR and represent an average of two trials using tetramethylsilane or tetratis(trimethylsilyl)methane (TTMSM) as an internal standard. [d]Isolated yields were determined on the 50-1000mg scale, using DCM as the solvent (due to volatility), and represent an average of two trials. [e]The selectivities observed with catalyst **1.1** are included for comparison. [f]With *ortho*-selectivity defined as positive $\Delta\Delta G^{\ddagger}$ and *para*-selectivity defined as negative $\Delta\Delta G^{\ddagger}$. [g]Due to product volatility, as isolated yield could not be reported; therefore % conversion was reported as determined by ^{1}H NMR using TTMSM as an internal standard. [h]Both *ortho* products (**a** and **c**) combined to simplify calculation.

Scheme 1.8.2 Augmenting the Innate Chlorination of Phenol

example, **1.7** effected the chlorination of phenols **1.8** and **1.9** with *ortho*:*para* ratios of 1.0:12.0 (compared to 1.0:3.2 and 1.0:4.0, respectively, by **1.1**). I also observed a similar degree of *para*-

augmentation with **1.7** for nitrile-containing **1.10** (**1.10a**:**1.10b** of 1.0:7.4 vs. 1.0:2.5 with **1.1**), and 2-iodophenol (**1.11**) (*ortho*:*para* ratio of 1.0:20 vs. 1.0:5.4). Catalyst **1.7** also augmented the *para*-selectivity of *meta*-substituted phenols when compared to catalyst **1.1**. For example, while fluorophenol **1.12** gave a ratio of **1.12a**:**1.12b** as 1.1:1.0 with catalyst **1.1**, chlorination of **1.12** with catalytic **1.7** altered the reaction outcome to give *para*-chlorinated **1.12b** as the major product (ratio of **1.12a**:**1.12b** as 1.0:2.1). **1.7** also resulted in increases in *para*-selectivity of 2-3 fold for phenols **1.14**, **1.16**, and **1.17**. It should be noted that for some phenols, such as **1.13** and **1.15**, catalyst **1.7** increased selectivity minimally. Finally, the chlorination of ester-containing **1.17** was seemingly unselective with catalyst **1.1**, resulting in a mixture of **1.17a**:**1.17b**:**1.17c** as 1.0:7.0:6.0, yet in the presence of **1.7**, the chlorination proceeded to yield a *para*-favoring mixture of **1.17a**:**1.17b**:**1.17c** as 1.0:13.0:6.5. While the increase in *para*-selectivities are moderate, the ability to augment *para*-selectivities when using catalyst **1.7** over catalyst **1.1** complements the catalyst-directed *ortho*-chlorinations in Scheme 1.8.2, and serves as another proof of concept that catalyst structure can both augment (as with **1.7**) or override (as with **1.6**) innate regioselectivities.

I next probed whether these catalysts could also affect regioselective brominations. While there are robust conditions for *ortho*-bromination, catalyst-controlled bromination might find utility in late-stage functionalization. In these studies, I found little difference between catalysts **1.1** and **1.7**, with both yielding predominantly *para*-brominated products, however as with chlorination, **1.6** overcame this innate *para*-preference to give mostly *ortho*-brominated products. For example, phenol **1.3** yielded excellent regioselectivities (**1.3c**:**1.3d** ratio of 1.0:11.0, Scheme 1.8.3), albeit with a significant amount of polybromination, while **1.6** gave an observed **1.3c**:**1.3d** ratio of 3.3:1.0. *Ortho*-substituted phenols **1.8** and **1.18** proceeded more smoothly, with **1.1**

A. Regiodivergent Bromination

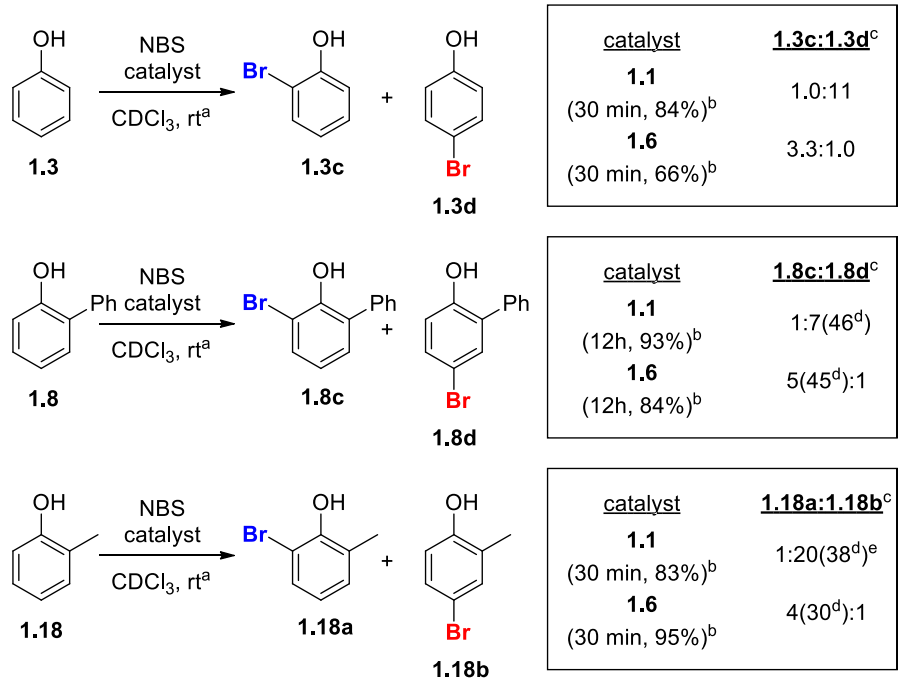

catalyst	1.3c:1.3d[c]
1.1 (30 min, 84%)[b]	1.0:11
1.6 (30 min, 66%)[b]	3.3:1.0

catalyst	1.8c:1.8d[c]
1.1 (12h, 93%)[b]	1:7(46[d])
1.6 (12h, 84%)[b]	5(45[d]):1

catalyst	1.18a:1.18b[c]
1.1 (30 min, 83%)[b]	1:20(38[d])[e]
1.6 (30 min, 95%)[b]	4(30[d]):1

B. Effect of Electron-Donating Substitution

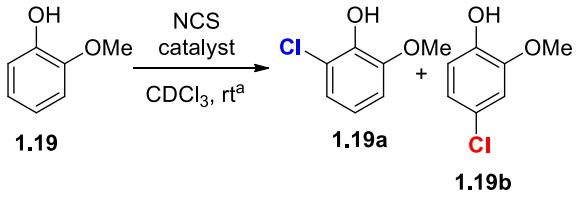

catalyst	1.19a:1.19b[c]
1.1 (1h, 88%)[b]	1:>20
1.6 (2h, 70%)[b]	1.8:1
$\Delta\Delta\Delta G^{\ddagger}$ = >2,12 kcal/mol[f]	

[a]Optimized reaction conditions were used with respect to the catalyst. [b]Reaction times and conversions to mono-brominated products were determined by ^{1}H NMR and represent an averageof two trials using tetramethylsilane or tetrakis(trimethylsilyl)methane as an internal standard.[c]Ratios were determined by ^{1}H NMR and represent an average of three trials. [d]Isolated yields in parentheses were determined on the 50-100 mg scale, using DCM as the solvent (due to volatility), and represent an average of two trials. [e]Ratio could not be determined by ^{1}H NMR, however **1.18b** was the predominant isomer. [f]$\Delta\Delta\Delta G^{\ddagger} = \Delta\Delta G^{\ddagger}_{\mathbf{1.6}} - \Delta\Delta G^{\ddagger}_{\mathbf{1.1}}$, with *ortho*-selectivity defined as positive $\Delta\Delta G^{\ddagger}$ and *para*-selectivity defined as negative $\Delta\Delta G^{\ddagger}$.

Scheme 1.8.3 Regiodivergent Bromination and the *ortho*-Chlorination of Guaiacol

yielding predominantly *para*-brominated **1.8d** and **1.18b**, and catalyst **1.6** favoring bromination *ortho*- to the hydroxy group each time (**1.8c**:**1.8d** ratio of 5.0:1.0; **1.18a**:**1.18b** ratio of 4.0:1.0). It should be noted that when using 1.2 equiv. NBS, I observed some di-bromination which complicated purification and resulted in isolated yields that were lower than observed NMR conversions.

I also evaluated the chlorination of substrates that possessed multiple directing groups such as guaiacol (**1.19**), finding catalyst **1.1** to effect chlorination exclusively *para*- to the hydroxy group, giving **1.19b** in high yields. Interestingly, catalyst **1.6** could overcome this large substrate preference to yield *ortho*-chlorinated **1.19a** as the major product, however with a more modest ratio than other substrates in Scheme 1.8.1. It is worth mentioning that this modest selectivity is due to the large innate *para*-preference of **1.19**, as from an energetic perspective, catalyst **1.6** overcomes roughly 2.1 kcal/mol, comparable, if not better than many of the substrates in Scheme 1.8.1.

In conclusion, I have demonstrated that the catalyst structure of Lewis bases can influence the regioselectivity of the electrophilic halogenation of phenols. A particularly exciting aspect of this work is the observed reversal of regioselectivity by Nagasawa's bis-thiourea **1.6**, presumably through a mechanism in which one thiourea interacts with the phenol hydroxy group, and the other activates NCS through Lewis basic (analogous to that depicted in Figure 1.7.1) or a Brönsted acidic manifold (H-bonding with NCS carbonyl). Mechanistic studies to understand how this chemistry works are ongoing. These results represent a novel and facile route to access arene substitution patterns that are not currently readily available. More broadly, these results represent a key proof of concept that a catalyst can indeed alter the reaction outcome of electrophilic halogenation.

1.9 Experimental Section

1.9.1 Initial Mechanistic Investigations (Figures 1.7.3 and 1.7.4)

Results in Figure 1.7.3 were obtained as follows: 2.4 mg (0.01 mmol, 1.0 equiv.) of tributylphosphinesulfide was added to an NMR tube followed by the addition of 600 μL $CDCl_3$. A ^{31}P NMR spectrum was obtained, represented as the bottom spectrum in red (Figure 1.7.3). 6.7 mg (0.05 mmol, 5.0 equiv.) NCS was then added to the NMR tube and shaken vigorously for 3 minutes. A second ^{31}P NMR spectrum was obtained, represented by the middle spectrum in green (Figure 1.7.3). Immediately after obtaining the second ^{31}P spectrum, 9.7 mg (0.5 mmol, 5.0 equiv.) of caffeine was added to the NMR tube and left for 30 minutes with 4 equally spaced out short periods of mixing. After the 30 minutes was up, a third ^{31}P NMR spectrum was obtained, represented by the blue spectrum (Figure 1.7.3). While the blue spectrum in Figure 1.7.3 is a different species than the starting catalyst by ^{31}P NMR, sequential additions of NCS followed by caffeine continued to effect catalytic chlorination. Mass spectral analysis of the reaction after chlorination revealed an observed mass of 437.5 m/z, suggesting the formation of a resting-state catalyst such as **1.20** (calculated mass of protonated **1.20** is 437.3 m/z).

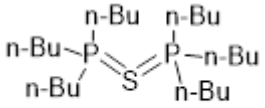

1.20

Figure 1.9.1 Proposed Resting-State Catalyst 1.20

As a control, 2.4 mg (0.01 mmol, 1.0 equiv.) of tributylphosphinesulfide was added to an NMR tube, followed by the addition of succinimide and 8-chlorocaffeine. The ^{31}P NMR spectrum of the control mixture was analogous to that of the **1.1** alone (red spectrum, Figure 1.7.3).

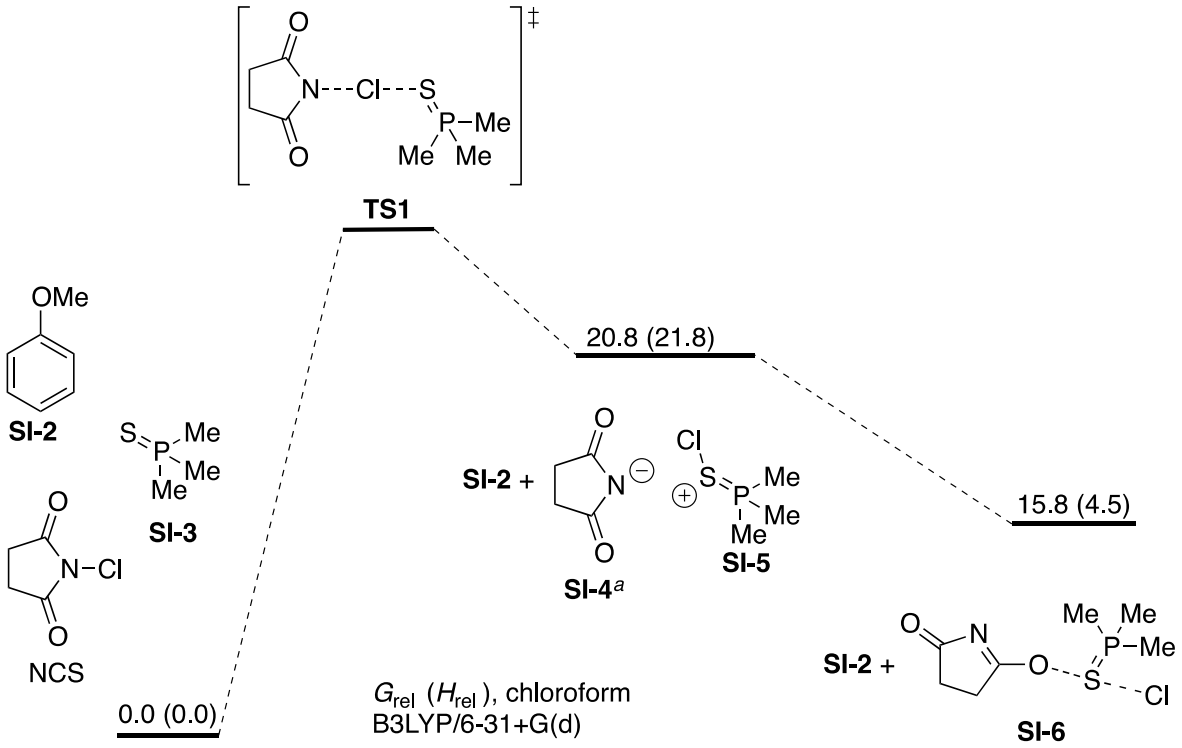

Scheme 1.9.1 Energies from Figure 1.7.4

Scheme 1.9.1 is a reformatted version of Figure 1.7.4. The energies given for **SI-4** and **SI-5** represent the separated ions with implicit solvent calculations. Explicit solvation may result in a lower energy ion pair. All attempts to locate ion-pair type interactions between **SI-4** and **SI-5** in the gas phase resulted in convergence to intermediate **SI-6** or higher energy species.

1.9.2 General Information

All ^{1}H and ^{13}C NMR spectra were recorded on either a Varian VNMRS 400 MHz, Varian Inova 500 MHz, Varian VNMRS 600 MHz or Bruker Avance III 600 MHz spectrometers at 25 ^{o}C. All chemical shifts were reported in parts per million (δ) and were internally referenced to residual protio solvents unless otherwise noted. ^{19}F NMR spectra were referenced to an external TFA standard. Spectral data were reported as follows: chemical shift (multiplicity [singlet (s), doublet (d), triplet (t), quartet (q), pentet (p), and multiplet (m)], coupling constants [Hz], integration). Carbon spectra were recorded with complete proton decoupling. Conventional mass spectra were obtained using Advion Expression^{s} CMS (APCI, ASAP). *N*-chlorosuccinimide was recrystallized from acetic acid, and *N*-bromosuccinimide was recrystallized from water. For the synthesis of **1.7**, toluene was degassed prior to use via the freeze-pump-thaw method. All other chemicals used were purchased from Sigma Aldrich, TCI, Frontier Scientific, Acros Organics, Strem, Oakwood, Matrix Scientific, Cambridge Isotope Laboratories, or Fisher and were used as received without further purification, unless specifically noted. All normal phase flash column chromatography (FCC) was performed using Grade 60 Silica Gel (230-400 mesh) purchased from Fisher Scientific. Reverse phase flash chromatography was performed on a Biotage Isolera One with a Biotage SNAP cartridge (KP-C18-HS 12g). Preparative Thin Layer Chromatography (TLC) plates contained grade 60 silica gel coated with fluorescent indicator F_{254}. Catalysts were either purchased (**1.1**), prepared from known literature procedures (**1.4**,[75] **1.5**,[75] **1.6**,[76]) or synthesized (**1.7**).

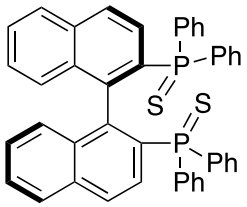

Figure 1.9.2 Catalyst 1.7

(*R*)-[1,1'-binaphthalene]-2,2'-diylbis(diphenylphosphine sulfide) (**1.7**): (*R*)-BINAP (1 g, 1.61 mmol, 1.0 equiv.) and ground elemental sulfur (210 mg, 6.42 mmol, 4.0 equiv.) was added to a round bottom (rb) flask equipped with a stir bar. The flask was evacuated and backfilled with nitrogen (1x), followed by the addition of degassed toluene (3.2 mL, 0.5 M). The flask was attached to a reflux condenser and a nitrogen line. The reaction was refluxed overnight at 120 ^{o}C under nitrogen. Upon reaction completion (determined by ^{31}P NMR), the solvent was removed by rotovap; and the remaining sulfur was removed via flash column chromatography. The fractions containing **1.7** were collected, dried over sodium sulfate, and evaporated by rotovap. The relatively pure material was then dissolved in a 2-dram vial with hot toluene (~3 mL), capped, and placed in the freezer for 24 hours. The resulting crystals were filtered, and washed with minimal cold toluene to afford **1.7** as off-white solid crystals (592 mg, 54%). **^{1}H NMR** (500 MHz, $CDCl_3$) δ 7.78 (dd, *J* = 8.7, 2.0 Hz, 2H), 7.75-7.61 (m, 10H), 7.46 (dd, *J* = 12.3, 8.7 Hz, 2H), 7.41-7.35 (m, 2H), 7.34-7.27 (m, 4H), 7.25-7.20 (m, 8H), 6.72 (d, *J* = 8.5 Hz, 2H), 6.63 (t, *J* = 7.4 Hz, 2H); **^{13}C NMR** (126 MHz, $CDCl_3$) δ 140.65 (dd, *J* = 8.2, 5.2 Hz), 135.83 (d, *J* = 86 Hz), 134.12 (d, *J* = 2.5 Hz), 133.57 (d, *J* = 11.5 Hz), 132.95 (d, *J* = 10 Hz), 132.30 (d, *J* = 11 Hz), 131.59, 130.97 (d, *J* = 3.0 Hz), 130.69 (d, *J* = 3.0 Hz), 129.49 (d, *J* = 12 Hz), 128.74 (d, *J* = 85 Hz), 128.11 (d, *J* = 13 Hz), 128.10 (d, *J* = 12 Hz), 127.95 (d, *J* = 13 Hz), 127.80, 127.56, 127.38 (d, *J* = 1.0 Hz), 125.81 (d, *J* = 1.0 Hz); **^{31}P NMR** (202 MHz, $CDCl_3$) δ 43.12 (referenced to external H_3PO_4 standard); **MS (APCI)**: **Calculated for** $C_{44}H_{33}P_2S_2$ $[M+H]^+$ 687.2. **Found:** 687.2 m/z.

1.9.3 General Regiodivergent Halogenation Procedure

Substrate (0.030 mmol, 1 equiv.), catalyst (0.0030 mmol, 0.1 equiv.), and $CDCl_3$ (600 μL or 1200 μL) were added to an NMR tube followed by the addition of either tetramethylsilane (TMS) or tetrakis(trimethylsilyl)methane (TTMSM) as an internal standard (when necessary). A ^1H spectrum of the reaction mixture was then obtained with a relaxation delay of 5.00 sec (number of scans = 4), representing the reaction mixture at time = 0. *N*-Halosuccinimide (0.036 mmol, 1.2 equiv.) was then added to the NMR tube, and the reaction was monitored by ^1H NMR. The reaction was considered complete once the substrate conversion had ceased. Isomeric ratios were determined via integration of the aromatic peaks of each product. Conversion to mono-Cl products represents the sum of the conversions of all identified mono-chlorinated products, and the value was determined via integration of mono-chlorinated products with respect to either the residual protio solvent or TMS. Isomeric ratios determined by analysis of non-obscure peaks. When necessary, clear coupling patterns were partially integrated, and full integration value was extrapolated from the partial integration. If multiple peaks were clear, the average of those peaks were used to determine the isomeric ratio. Each experiment was performed in triplicate, and the reported ratios are the average of the three trials. An example from each set is reported with the Spectral Data. Each example was zoomed in for clear visualization of each isomer.

Isolated yields were determined on a 50-1,000 mg scale using dichloromethane (DCM) as the reaction solvent instead of $CDCl_3$, due to the low boiling points of many of the products; all reagents and solvent were scaled equally, omitting TMS (or TTMSM). When catalyst **1.6** was used on these scales, the concentration with respect to the substrate was adjusted to 0.05 M to avoid using unnecessary volumes of solvent; the catalyst loading was subsequently adjusted to 0.025 mol% to avoid catalyst aggregation. Upon reaction completion, as determined by Thin-Layer

Chromatography (TLC), the reaction was filtered through a short normal phase silica plug with DCM to remove succinimide. The solvent was then removed by rotovap, and, for almost all substrates, the resulting crude mixture was purified by Flash Column Chromatography (FCC) on normal phase silica gel, eluting with hexanes and ethyl acetate (hexanes:ethyl acetate::100:0 → 99:1 → 98:2 → 97:3 → 95:5), unless otherwise noted. Many of the isolated products had low boiling points, thereby negatively affecting the isolated yield upon being exposed to strong vacuums for extended periods of time. For the chlorination and bromination of phenol (**1.3**), spectra were compared to literature precedents (**1.3a**,[77] **1.3b**,[35] **1.3c**,[78] **1.3d**[78]) to determine isomeric ratios. For the chlorination of guaiacol (**1.19**), spectra were compared to literature precedents (**1.19a**[79]) and the Spectral Database for Organic Compounds (**1.19b**).

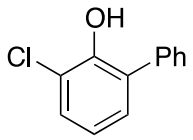

Figure 1.9.3 Product 1.8a

3-chloro-[1,1'-biphenyl]-2-ol (**1.8a**): Prepared according to the general procedure on a 1 g scale, using **1.6** as catalyst. 902 mg (75% yield) of **1.8a** was isolated as a white solid. **^{1}H NMR** (599 MHz, $CDCl_3$) δ 7.54 (dd, *J* = 7.8, 1.4 Hz, 2H), 7.46 (t, *J* = 7.5 Hz, 2H), 7.39 (tt, *J* = 7.4, 1.2 Hz, 1H), 7.33 (dd, *J* = 8.0, 1.6 Hz, 1H), 7.23 (dd, *J* = 7.8, 1.4 Hz, 1H), 6.95 (t, *J* = 7.9 Hz, 1H), 5.70 (s, 1H); **^{13}C NMR** (151 MHz, $CDCl_3$) δ 148.55, 137.19, 129.84, 129.56, 129.29, 128.66, 128.43, 127.89, 121.22, 120.81; **MS (APCI)**: **Calculated for** $C_{12}H_{10}ClO$ $[M+H]^+$ 205.0. **Found:** 205.0 m/z.

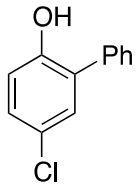

Figure 1.9.4 Product 1.8b

5-chloro-[1,1'-biphenyl]-2-ol (**1.8b**): Prepared according to the general procedure on a 1 g scale, using **1.7** as catalyst. 1.081 g (89% yield) of **1.8b** was isolated as a white solid. **^{1}H NMR** (400 MHz, $CDCl_3$) δ 7.54 – 7.47 (m, 2H), 7.47 – 7.40 (m, 3H), 7.24 – 7.19 (m, 2H), 6.95 – 6.90 (m, 1H), 5.17 (bs, 1H); **^{13}C NMR** (126 MHz, $CDCl_3$) δ 151.25, 135.97, 129.91, 129.66, 129.62, 129.07, 129.03, 128.57, 125.70, 117.32; **MS (APCI)**: **Calculated for** $C_{12}H_{10}ClO$ $[M+H]^+$ 205.0. **Found:** 205.0 m/z.

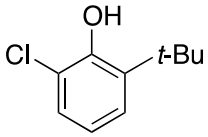

Figure 1.9.5 Product 1.9a

2-(*tert*-butyl)-6-chlorophenol (**1.9a**): Prepared according to the general procedure on a 1 g scale, using **1.6** as catalyst. 861 mg (70%) of **1.9a** was recovered as an orange oil. **^{1}H NMR** (500 MHz, $CDCl_3$) δ 7.21 – 7.17 (m, 2H), 6.80 (t, *J* = 7.9 Hz, 1H), 5.85 (bs, 1H), 1.41 (s, 9H); **^{13}C NMR** (126 MHz, $CDCl_3$) δ 149.83, 137.75, 126.61, 125.85, 121.05, 120.43, 35.34, 29.47; **MS (APCI)**: **Calculated for** $C_{10}H_{14}ClO$ $[M+H]^+$ 185.1. **Found:** 185.1 m/z.

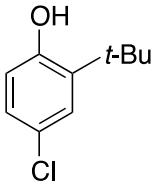

Figure 1.9.6 Product 1.9b

2-(*tert*-butyl)-4-chlorophenol (**1.9b**): Prepared according to the general procedure on a 500 mg scale, using **1.7** as catalyst. 514 mg (83% yield) of **1.9b** was isolated as an orange oil. **^{1}H NMR**

(500 MHz, $CDCl_3$) δ 7.22 (d, *J* = 2.6 Hz, 1H), 7.02 (dd, *J* = 8.4, 2.6 Hz, 1H), 6.59 (d, *J* = 8.4 Hz, 1H), 4.79 (s, 1H), 1.39 (s, 9H); **^{13}C NMR** (126 MHz, $CDCl_3$) δ 152.90, 138.18, 127.45, 126.67, 125.57, 117.73, 34.89, 29.48; **MS (APCI)**: **Calculated for** $C_{10}H_{14}ClO$ $[M+H]^+$ 185.1. **Found:** 185.1 m/z.

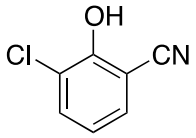

Figure 1.9.7 Product 1.10a

3-chloro-2-hydroxybenzonitrile (**1.10a**): Prepared according to the general procedure (except for purification) on a 100 mg scale, using **1.6** as catalyst. Upon reaction completion, the solvent was evaporated by rotovap, and the resulting crude material was immediately purified by FCC with an isocratic elution of 100% dichloromethane to obtain 93 mg (72% yield) of **1.10a** as a white solid. **^{1}H NMR** (500 MHz, $CDCl_3$) δ 7.56 (dd, *J* = 8.1, 1.5 Hz, 1H), 7.48 (dd, *J* = 7.8, 1.5 Hz, 1H), 6.97 (t, *J* = 7.9 Hz, 1H), 6.23 (s, 1H); **^{13}C NMR** (126 MHz, $CDCl_3$) δ 153.91, 133.87, 132.23, 121.69, 121.26, 115.16, 101.40; **MS (APCI)**: **Calculated for** C_7H_5ClNO $[M+H]^+$ 154.0. **Found:** 154.0 m/z.

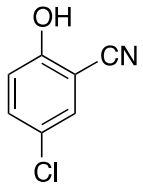

Figure 1.9.8 Product 1.10b

5-chloro-2-hydroxybenzonitrile (**1.10b**): Prepared according to the general procedure (except for purification) on a 100 mg scale, using **1.7** as catalyst. Upon reaction completion, the solvent was evaporated by rotovap, and the resulting crude material was immediately purified by FCC with an isocratic elution of 100% dichloromethane to obtain 86 mg (67% yield) of **1.10b** as a white solid, which consistently included about 12% starting material that could not be removed

by available chromatography methods. **^{1}H NMR** (500 MHz, acetone-D6) δ 10.09 (s, 1H), 7.65 (d, *J* = 2.7 Hz, 1H), 7.52 (dd, *J* = 8.9, 2.7 Hz, 1H), 7.12 (d, *J* = 8.9 Hz, 1H); **^{13}C NMR** (126 MHz, acetone-D6) δ 159.59, 135.30, 133.18, 124.92, 118.74, 115.86, 102.30; **MS (APCI)**: **Calculated for** C_7H_5ClNO $[M+H]^+$ 154.0. **Found:** 154.1 m/z.

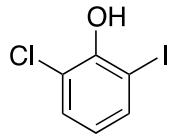

Figure 1.9.9 Product 1.11a

2-chloro-6-iodophenol (**1.11a**): Prepared according to the general procedure on a 100 mg scale, using **1.6** as catalyst. 75 mg (65% yield) of **1.11a** was isolated as a white solid. **^{1}H NMR** (599 MHz, $CDCl_3$) δ 7.62 (d, *J* = 8.0 Hz, 1H), 7.31 (d, *J* = 8.0 Hz, 1H), 6.63 (t, *J* = 8.0 Hz, 1H), 5.93 (s, 1H); **^{13}C NMR** (151 MHz, $CDCl_3$) δ 151.01, 137.92, 129.80, 122.98, 119.39, 83.63; **MS (APCI)**: **Calculated for** C_6H_4ClIO $[M]^+$ 253.9. **Found:** 254.0 m/z.

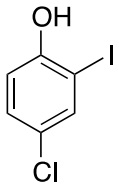

Figure 1.9.10 Product 1.11b

4-chloro-2-iodophenol (**1.11b**): Prepared according to the general procedure on a 100 mg scale, using **3.7** as catalyst. 99 mg (86% yield) of **1.11b** was isolated as a white solid. **^{1}H NMR** (500 MHz, $CDCl_3$) δ 7.63 (d, *J* = 2.4 Hz, 1H), 7.22 (dd, *J* = 8.7, 2.4 Hz, 1H), 6.92 (d, *J* = 8.7 Hz, 1H), 5.28 (s, 1H); **^{13}C NMR** (126 MHz, $CDCl_3$) δ 153.93, 137.28, 130.29, 126.24, 115.82, 85.58; **MS (APCI)**: **Calculated for** C_6H_4ClIO $[M]^+$ 253.9. **Found:** 253.9 m/z.

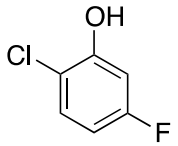

Figure 1.9.11 Product 1.12a

2-chloro-5-fluorophenol (**1.12a**): 5 g (44.6 mmol, 1.0 equiv.) of 3-fluorophenol was added to a 100 mL 2-necked round bottom flask, equipped with a stir bar, followed by the addition of 45 mL of dichloromethane. 131 mg (0.446 mmol, 0.01 equiv.) of **1.6** was subsequently added to the reaction mixture while stirring at room temperature. After five minutes, 6.6 g (49.1 mmol, 1.1 equiv.) of *N*-chlorosuccinimide was added to the stirring reaction at room temperature in 3 equal portions over the span of 10 minutes. After 24 hours stirring, 40 mL of hexanes was added to the reaction. Solid succinimide crashed out of solution and was filtered via vacuum filtration. The solid was disposed of, and the collected organic layer was purified via fractional distillation. **1.12a** and **1.12b** could not be isolated on this scale via distillation, however the fractions containing the highest purity of each isomer were collected for spectral analysis (spectra are provided). No isolated yield is reported. **1.12a** distilled at a lower temperature (90-150 ^{o}C), and significant amounts of hexane were present in the purest fraction. Constitutional isomer was assigned by contrast from spectra obtained from **1.12b**. **^{1}H NMR** (500 MHz, $CDCl_3$) δ 7.26 (dd, *J* = 8.9, 5.7 Hz, 1H), 6.77 (dd, *J* = 9.6, 2.9 Hz, 1H), 6.62 (ddd, *J* = 9.0, 8.0, 2.9 Hz, 1H), 5.65 (d, *J* = 1.5 Hz, 1H); **^{13}C NMR** (126 MHz, $CDCl_3$) δ 162.41 (d, *J* = 246 Hz), 152.45 (d, *J* = 12.8 Hz), 129.57 (d, *J* = 9.9 Hz), 115.22 (d, *J* = 3.5 Hz), 108.70 (d, *J* = 23.4 Hz), 104.17 (d, *J* = 26.5 Hz); **MS (APCI)**: **Calculated for** C_6H_4ClFO $[M]^+$ 146.0. **Found:** 145.9 m/z.

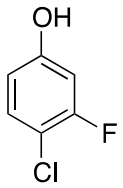

Figure 1.9.12 Product 1.12b

4-chloro-3-fluorophenol (**1.12b**): 5 g (44.6 mmol, 1.0 equiv.) of 3-fluorophenol was added to a 100 mL 2-necked round bottom flask, equipped with a stir bar, followed by the addition of 45 mL of dichloromethane. 131 mg (0.446 mmol, 0.01 equiv.) of **1.7** was subsequently added to the reaction mixture while stirring at room temperature. After five minutes, 6.6 g (49.1 mmol, 1.1 equiv.) of *N*-chlorosuccinimide was added to the stirring reaction at room temperature in 3 equal portions over the span of 10 minutes. After 24 hours stirring, 40 mL of hexanes was added to the reaction. Solid succinimide crashed out of solution and was filtered via vacuum filtration. The solid was disposed of, and the collected organic layer was purified via fractional distillation. **1.12a** and **1.12b** could not be isolated on this scale via distillation, however the fractions containing the highest purity of each isomer were collected for spectral analysis (spectra are provided). No isolated yield is reported. In later fractions, where **1.12b** distilled (120-200 ^{o}C), significant amounts of succinimide began to distill with the product. Spectral data matched the data provided by Sigma Aldrich. **^{1}H NMR** (500 MHz, $CDCl_3$) δ 7.21 (t, *J* = 8.6 Hz, 1H), 6.67 (dd, *J* = 10.3, 2.8 Hz, 1H), 6.58 (ddd, *J* = 8.8, 2.8, 1.3 Hz, 1H); **^{13}C NMR** (126 MHz, $CDCl_3$) δ 158.54 (d, *J* = 248 Hz), 155.68 (d, *J* = 10 Hz), 130.88 (d, *J* = 1.4 Hz), 112.40 (d, *J* = 17.7 Hz), 112.22 (d, *J* = 3.5 Hz), 104.68 (d, *J* = 23.9 Hz); **MS (APCI)**: **Calculated for** C_6H_4ClFO $[M]^+$ 146.0. **Found:** 145.9 m/z.

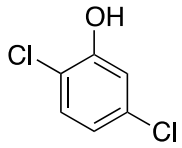

Figure 1.9.13 Product 1.13a

2,5-dichlorophenol (**1.13a**): Prepared according to the general procedure on a 100 mg scale, using **1.6** as catalyst. **1.13a** was isolated as an off-white solid, however the product quickly sublimes under vacuum. No isolated yield was reported, albeit 10 mg of pure material was obtained for spectral analysis. Spectral data matched the data provided by Sigma Aldrich. **^{1}H NMR** (500 MHz, $CDCl_3$) δ 7.24 (d, *J* = 8.6 Hz, 1H), 7.04 (d, *J* = 2.4 Hz, 1H), 6.87 (dd, *J* = 8.6, 2.4 Hz, 1H), 5.58 (s, 1H); **^{13}C NMR** (126 MHz, $CDCl_3$) δ152.05, 133.92, 129.69, 121.74, 118.49, 116.82; **MS (APCI)**: **Calculated for** $C_6H_4Cl_2O$ $[M]^+$ 162.0. **Found:** 161.9 m/z.

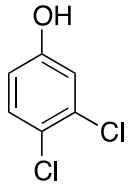

Figure 1.9.14 Product 1.13b

3,4-dichlorophenol (**1.13b**): Prepared according to the general procedure (not purified by FCC) on a 100 mg scale, using **1.7** as catalyst. After filtering reaction mixture through silica plug, solvent was removed under rotovap. The resulting crude material was dissolved in 300 μL of hexane. The resulting solution was purified by preparative TLC (hexane:ethyl acetate::90:10) to afford 90 mg (71% yield) of **1.13b** as a white solid. Spectral data matched the data provided by Sigma Aldrich. **^{1}H NMR** (500 MHz, $CDCl_3$) δ 7.28 (d, *J* = 8.7 Hz, 1H), 6.96 (d, *J* = 2.9 Hz, 1H), 6.69 (dd, *J* = 8.7, 2.9 Hz, 1H), 4.95 (s, 1H); **^{13}C NMR** (126 MHz, $CDCl_3$) δ 154.66, 133.08, 131.05, 124.39, 117.66, 115.38; **MS (APCI)**: **Calculated for** $C_6H_4Cl_2O$ $[M]^+$ 162.0. **Found:** 161.9 m/z.

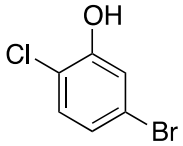

Figure 1.9.15 Product 1.14a

5-bromo-2-chlorophenol (**1.14a**): Prepared according to the general procedure on a 100 mg scale, using **1.6** as catalyst. 57 mg (48% yield) of **1.14a** was isolated as an off-white solid. The structure was assigned by comparison to computationally predicted ^{13}C NMR shifts [B3LYP63-1G+(d,p)]. **^{1}H NMR** (400 MHz, $CDCl_3$) δ 7.19 (d, *J* = 2.2 Hz, 1H), 7.18 (d, *J* = 8.6 Hz, 1H), 7.01 (dd, *J* = 8.5, 2.2 Hz, 1H), 5.56 (s, 1H); **^{13}C NMR** (101 MHz, $CDCl_3$) δ 152.15, 130.02, 124.64, 121.42, 119.68, 119.14; **MS (APCI)**: **Calculated for** $C_6H_4CBrClO$ $[M]^+$ 205.9. **Found:** 205.8 m/z.

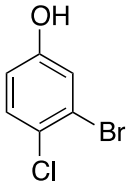

Figure 1.9.16 Product 1.14b

3-bromo-4-chlorophenol (**1.14b**): Prepared according to the general procedure on a 100 mg scale, using **3.7** as catalyst. 86 mg (72% yield) of **1.14b** was isolated as an off-white solid. The structure was assigned by comparison to computationally predicted ^{13}C NMR shifts [B3LYP63-1G+(d,p)]. **^{1}H NMR** (500 MHz, $CDCl_3$) δ 7.29 (d, *J* = 8.7 Hz, 1H), 7.13 (d, *J* = 2.9 Hz, 1H), 6.74 (dd, *J* = 8.7, 2.9 Hz, 1H), 4.90 (s, 1H); **^{13}C NMR** (126 MHz, $CDCl_3$) δ 154.62, 130.87, 126.37, 122.77, 120.80, 116.05; **MS (APCI)**: **Calculated for** $C_6H_4CBrClO$ $[M]^+$ 205.9. **Found:** 205.8 m/z

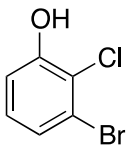

Figure 1.9.17 Product 1.14c

3-bromo-2-chlorophenol (**1.14c**): Prepared according to the general procedure on a 100 mg scale, using **1.6** as catalyst. 17 mg (14% yield) of **1.14c** was isolated as an off-white solid. **^{1}H NMR** (599 MHz, $CDCl_3$) δ 7.20 (dd, *J* = 8.0, 1.1 Hz, 1H), 7.06 (t, *J* = 8.1 Hz, 1H), 6.98 (dd, *J* = 8.2, 1.2 Hz, 1H), 5.66 (s, 1H); **^{13}C NMR** (151 MHz, $CDCl_3$) δ 152.69, 128.78, 125.50, 122.33, 121.00, 115.16; **MS (APCI)**: **Calculated for** $C_6H_4CBrClO$ $[M]^+$ 205.9. **Found:** 205.8 m/z.

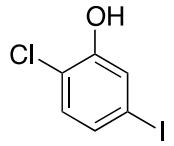

Figure 1.9.18 Product 1.15a

2-chloro-5-iodophenol (**1.15a**): Prepared according to the general procedure on a 1 g scale, using **1.6** as catalyst. 750 mg (65% yield) of **1.15a** was isolated as an off-white solid. Spectra obtained from **1.15a** match spectra reported in patent literature.[80] **^{1}H NMR** (400 MHz, $CDCl_3$) δ 7.54 (d, *J* = 2.0 Hz, 1H), 7.36 (dd, *J* = 8.4, 2.0 Hz, 1H), 7.19 (d, *J* = 8.4 Hz, 1H), 5.68 (s, 1H); **^{13}C NMR** (126 MHz, $CDCl_3$) δ 152.13, 130.65, 130.36, 125.56, 120.25, 92.16; **MS (APCI)**: **Calculated for** C_6H_4CClIO $[M]^+$ 253.9. **Found:** 254.0 m/z.

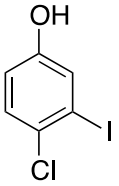

Figure 1.9.19 Product 1.15b

4-chloro-3-iodophenol (**1.15b**): Prepared according to the general procedure on a 50 mg scale, using **1.7** as catalyst. 46 mg (80% yield) of **1.15b** was isolated as a white solid. Constitutional isomer was assigned by contrast to spectra obtained from **1.15a**. **^{1}H NMR** (400 MHz, $CDCl_3$) δ 7.35 (d, *J* = 2.9 Hz, 1H), 7.28 (d, *J* = 8.7 Hz, 1H), 6.78 (dd, *J* = 8.7, 2.9 Hz, 1H), 4.87 (s, 1H); **^{13}C**

NMR (126 MHz, $CDCl_3$) δ 154.33, 130.50, 129.66, 126.99, 117.01, 98.04; **MS (APCI)**: **Calculated for** C_6H_4CClIO $[M]^+$ 253.9. **Found:** 254.0 m/z.

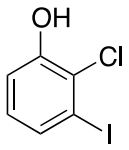

Figure 1.9.20 Product 1.15c

2-chloro-3-iodophenol (**1.15c**): Prepared according to the general procedure on a 1 g scale, using **1.6** as catalyst. 320 mg (28% yield) of **1.15c** was isolated as a white solid. **^{1}H NMR** (400 MHz, $CDCl_3$) δ 7.42 (dd, *J* = 7.8, 1.5 Hz, 1H), 7.00 (dd, *J* = 8.2, 1.5 Hz, 1H), 6.92 (t, *J* = 8.0 Hz, 1H), 5.59 (s, 1H); **^{13}C NMR** (126 MHz, $CDCl_3$) δ 151.80, 132.02, 129.60, 124.81, 116.15, 97.41; **MS (APCI)**: **Calculated for** C_6H_4CClIO $[M]^+$ 253.9. **Found:** 254.0 m/z.

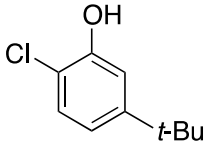

Figure 1.9.21 Product 1.16a

5-(*tert*-butyl)-2-chlorophenol (**1.16a**): Prepared according to the general procedure on a 100 mg scale, using **1.6** as catalyst. 44 mg of **1.16a** was isolated as an orange oil, however approximately 10% impurities were present that could not be removed using available purification techniques (*i.e.* FCC, preparative TLC, etc.). No isolated yield was reported, but the slightly impure material was used for spectral analysis in order to elucidate the structure of **1.16a** (2D NMR spectra are provided). **^{1}H NMR** (599 MHz, $CDCl_3$) δ 7.22 (d, *J* = 8.4 Hz, 1H), 7.06 (d, *J* = 2.3 Hz, 1H), 6.90 (dd, *J* = 8.4, 2.3 Hz, 1H), 5.52 (bs, 1H), 1.29 (s, 9H); **^{13}C NMR** (151 MHz, $CDCl_3$) δ 152.43, 150.94, 128.42, 118.73, 116.83, 113.63, 34.76, 31.34; **MS (APCI)**: **Calculated for** $C_{10}H_{14}ClO$ $[M+H]^+$ 185.1. **Found:** 185.1 m/z.

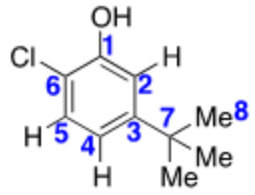

no.	δ_H (mult, *J* in Hz)	δ_C	HMBC (H->C)
1		150.9	H-5, H-2, H-4
2	7.06 (d, *J* = 2.3)	113.6	H-5, H-4
3		152.4	H-5, H-2, H-4, Me-8
4	6.90 (dd, *J* = 8.4, 2.3)	118.7	H-2
5	7.22 (d, *J* = 8.4)	128.4	H-4
6		116.8	H-5, H-2, H-4
7		34.8	H-2, H-4
8	1.29 (s)	31.3	

Figure 1.9.22 Multiple Bond Correlations of Product 1.16a

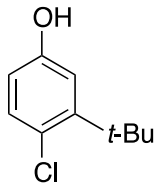

Figure 1.9.23 Product 1.16b

3-(*tert*-butyl)-4-chlorophenol (**1.16b**): Prepared according to the general procedure on a 100 mg scale, using **1.7** as catalyst. 65 mg (53% yield) of **1.16b** was isolated as an orange oil. The constitutional isomer was verified using 2-dimensional NMR analysis. **^{1}H NMR** (599 MHz, $CDCl_3$) δ 7.18 (d, *J* = 8.5 Hz, 1H), 6.91 (d, *J* = 3.0 Hz, 1H), 6.61 (dd, *J* = 8.5, 3.0 Hz, 1H), 1.45 (s, 9H); **^{13}C NMR** (151 MHz, $CDCl_3$) δ 154.12, 148.13, 132.77, 125.20, 115.25, 113.92, 36.13, 29.55; **MS (APCI)**: **Calculated for** $C_{10}H_{14}ClO$ $[M+H]^+$ 185.1. **Found:** 185.1 m/z.

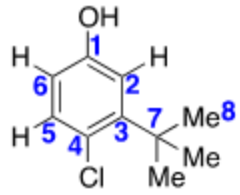

no.	δ_H (mult, *J* in Hz)	δ_C	HMBC (H->C)
1		154.1	H-2, H-5, H-6
2	6.91 (d, *J* = 3.0)	115.3	H-5, H-6
3		148.1	H-5, Me-8
4		125.2	H-2, H-5, H-6
5	7.18 (d, *J* = 8.5)	132.8	
6	6.61 (dd, *J* = 8.5, 3.0)	113.9	H-2
7		36.1	H-2, H-5
8	1.45 (s)	29.6	

Figure 1.9.24 Multiple Bond Correlations of Product 1.16b

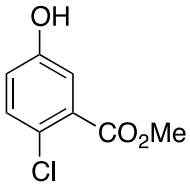

Figure 1.9.25 Product 1.17b

Methyl 2-chloro-5-hydroxybenzoate (**1.17b**): Prepared according to the general procedure on a 100 mg scale, using **1.7** as catalyst. 70 mg (57% yield) of **1.17b** was isolated as a clear oil, which settled to clear thin crystals shortly after. The constitutional isomer was verified using 2-dimensional NMR analysis. **^{1}H NMR** (500 MHz, $CDCl_3$) δ 7.34 (d, *J* = 3.1 Hz, 1H), 7.30 (d, *J* = 8.7 Hz, 1H), 6.93 (dd, *J* = 8.7, 3.1 Hz, 1H), 5.82 (s, 1H), 3.93 (s, 3H); **^{13}C NMR** (126 MHz, $CDCl_3$) δ 166.56, 154.37, 132.29, 130.50, 125.06, 120.32, 118.28, 52.85; **MS (APCI)**: **Calculated for** $C_8H_8ClO_3$ $[M+H]^+$ 187.0. **Found:** 187.0 m/z.

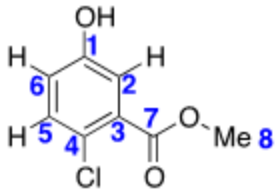

no.	δ_H (mult, *J* in Hz)	δ_C	HMBC (H->C)
1		154.1	H-2, H-5, H-6
2	7.34 (d, *J* = 3.1)	118.3	H-6
3		130.5	H-5, Me-8
4		125.1	H-2, H-5, H-6
5	7.30 (d, *J* = 8.7)	132.3	
6	6.93 (dd, *J* = 8.7, 3.1)	120.3	H-2
7		166.6	H-2, H-5, Me-8
8	1.45 (s)	52.9	

Figure 1.9.26 Multiple Bond Correlations of Product 1.17b

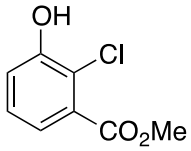

Figure 1.9.27 Product 1.17c

Methyl 2-chloro-3-hydroxybenzoate (**1.17c**): Prepared according to the general procedure (purified using reverse phase FCC) on a 100 mg scale, using **1.6** as catalyst. Upon completion, reaction was filtered thru a short silica plug with DCM. The filtrate was collected, and the solvent was removed by rotovap to afford a crude oil. The crude oil was then dissolved with minimal acetonitrile (50% v/v aqueous). This solution was purified on a Biotage Isolera using a C18 stationary phase SNAP cartridge (water:acetonitrile:: 90:10 → 85:15 → 80:20). Fractions containing the desired compound were combined and extracted with ethyl acetate (3x). The combined organic layers were washed with brine (1x). The organic layer was collected, dried over sodium sulfate, and filtered. The solvent was removed by rotovap to yield 49 mg (40% yield) **1.17c** as a clear oil. **^{1}H NMR** (599 MHz, $CDCl_3$) δ 7.45 (dd, *J* = 7.6, 1.7 Hz, 1H), 7.24 (t, *J* = 8.0 Hz, 1H), 7.19 (dd, *J* = 8.1, 1.7 Hz, 1H), 5.95 (s, 1H), 3.93 (s, 3H); **^{13}C NMR** (151 MHz, $CDCl_3$)

δ 165.88, 152.42, 146.80, 130.13, 127.74, 123.50, 119.56, 52.65; **MS (APCI)**: **Calculated for** $C_8H_8ClO_3$ $[M+H]^+$ 187.0. **Found:** 187.0 m/z.

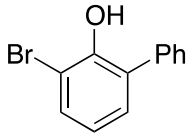

Figure 1.9.28 Product 1.8c

3-bromo-[1,1'-biphenyl]-2-ol (**1.8c**): Prepared according to the general procedure (Purified by preparative TLC) on a 50 mg scale, using **1.6** as catalyst. Upon completion, the reaction was filtered thru a silica plug with DCM. The filtrate was collected, and the solvent was removed by rotovap. The resulting crude material was dissolved in minimal hexane, and the solution was purified by preparative TLC (hexane:ethyl acetate = 90:10) to afford 33 mg (45% yield) of **1.8c** as a white solid. **^{1}H NMR** (500 MHz, $CDCl_3$) δ 7.55 – 7.51 (m, 2H), 7.49 – 7.44 (m, 3H), 7.39 (tt, *J* = 7.4, 1.5 Hz, 1H), 7.26 (dd, *J* = 7.6, 1.6 Hz, 1H), 6.89 (t, *J* = 7.8 Hz, 1H), 5.68 (s, 1H); **^{13}C NMR** (126 MHz, $CDCl_3$) δ 149.38, 137.33, 131.59, 130.30, 129.83, 129.30, 128.69, 127.93, 121.82, 111.15; **MS (APCI)**: **Calculated for** $C_{12}H_{10}BrO$ $[M+H]^+$ 249.0. **Found:** 248.8 m/z.

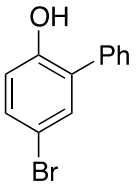

Figure 1.9.29 Product 1.8d

5-bromo-[1,1'-biphenyl]-2-ol (**1.8d**): Prepared according to the general procedure on a 100 mg scale, using **1.1** as catalyst. 68 mg (46% yield) of **1.8d** was isolated as a white solid. **^{1}H NMR** (500 MHz, $CDCl_3$) δ 7.52 – 7.47 (m, 2H), 7.45 – 7.40 (m, 3H), 7.38 – 7.33 (m, 2H), 6.88 (d, *J* = 8.7 Hz, 1H), 5.19 (s, 1H); **^{13}C NMR** (126 MHz, $CDCl_3$) δ 151.78, 135.84, 132.78, 131.97, 130.20, 129.62, 129.07, 128.59, 117.79, 112.91; **MS (APCI)**: **Calculated for** $C_{12}H_{10}BrO$ $[M+H]^+$ 249.0. **Found:** 248.9 m/z.

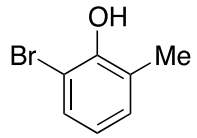

Figure 1.9.30 Product 1.18a

2-bromo-6-methylphenol (**1.18a**): Prepared according to the general procedure on a 50 mg scale, using **1.6** as catalyst. 26 mg (31% yield) of **1.18a** was isolated as a white solid. The yield was severely affected by the presence of dibromination product, which eluted in a similar manner to **1.18a** on normal phase silica gel. **^{1}H NMR** (500 MHz, $CDCl_3$) δ 7.29 (dd, *J* = 8.1, 1.1 Hz, 1H), 7.09 – 7.04 (m, 1H), 6.71 (t, *J* = 7.8 Hz, 1H), 5.54 (s, 1H), 2.30 (s, 3H); **^{13}C NMR** (126 MHz, $CDCl_3$) δ 150.52, 130.52, 129.49, 126.07, 121.35, 110.29, 16.75; **MS (APCI)**: **Calculated for** C_7H_7BrO $[M]^+$ 186.0. **Found:** 185.9 m/z.

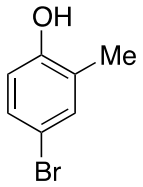

Figure 1.9.31 Product 1.18b

4-bromo-2-methylphenol (**1.18b**): Prepared according to the general procedure on a 50 mg scale, using **1.1** as catalyst. 33 mg (38% yield) of **1.18b** was isolated as a white solid. **^{1}H NMR** (500 MHz, $CDCl_3$) δ 7.24 (d, *J* = 2.0 Hz, 1H), 7.17 (dd, *J* = 8.6, 2.3 Hz, 1H), 6.65 (d, *J* = 8.5 Hz, 1H), 4.68 (s, 1H), 2.22 (s, 3H); **^{13}C NMR** (126 MHz, $CDCl_3$) δ 153.03, 133.67, 129.89, 126.30, 116.67, 112.73, 15.76; **MS (APCI)**: **Calculated for** C_7H_7BrO $[M]^+$ 186.0. **Found:** 185.9 m/z.

1.9.4 Molecular Geometries and Energies for Scheme 1.9.1

All structures were optimized in chloroform (CPCM model) using density functional theory, B3LYP/6-31+(d),[I,II] as implemented in the Gaussian 09[III] suite of programs.

SI-2 (anisole)
Number of imaginary frequencies: 0

C	2.2883130	0.3344250	-0.0000630
C	1.3366360	1.3550730	0.0000440
C	-0.0344860	1.0636280	0.0000760
C	-0.4534590	-0.2738530	-0.0000010
C	0.4992610	-1.3063260	-0.0001080
C	1.8583110	-1.0001340	-0.0001380
H	3.3487690	0.5704780	-0.0000870
H	1.6529520	2.3953050	0.0001040
H	-0.7526910	1.8758100	0.0001600
H	2.5861700	-1.8076840	-0.0002210
O	-1.7627840	-0.6732170	0.0000200
C	-2.7813690	0.3262940	0.0001240
H	-3.7277500	-0.2163140	0.0001220
H	-2.7196440	0.9550730	0.8967300
H	-2.7197090	0.9551950	-0.8964000

Energy (0K) = -346.7893763
Energy (0K) + ZPE = -346.656146
Enthalpy (298K) = -346.648318
Free Energy (298K) = -346.687233

***N*-chlorosuccinimide** (NCS)
Number of imaginary frequencies: 0

C-1.8910590 0.7703380 0.0000190
C-1.8910590-0.7703380 0.0000520
C-0.4306800-1.1878760 0.0000320
C-0.4306800 1.1878760-0.0000160
H-2.3748120 1.2001160-0.8823900
H-2.3747810 1.2001540 0.8824270
H-2.3748140-1.2001530-0.8823380
H-2.3747800-1.2001160 0.8824790
N 0.3203470 0.0000000-0.0000060
Cl 2.0278730 0.0000000-0.0000380
O 0.0402360 2.3042510-0.0000470
O 0.0402360-2.3042510 0.0000450

Energy (0K) = -820.24114
Energy (0K) + ZPE = -820.159520
Enthalpy (298K) = -820.151369
Free Energy (298K) = -820.192270

SI-3 (trimethylphosphine sulfide)
Number of imaginary frequencies: 0

P 0.0000000 0.0000000-0.1921990
C 0.0000000 1.6836960-0.9182330
H-0.8896040 2.2226230-0.5791860

H 0.8896040 2.2226230-0.5791860
H 0.0000000 1.6329080-2.0124860
C 1.4581240-0.8418480-0.9182330
H 2.3696500-0.3408920-0.5791860
H 1.4800460-1.8817310-0.5791860
H 1.4141400-0.8164540-2.0124860
C-1.4581240-0.8418480-0.9182330
H-1.4800460-1.8817310-0.5791860
H-2.3696500-0.3408920-0.5791860
H-1.4141400-0.8164540-2.0124860
S 0.0000000 0.0000000 1.8077340

Energy (0K) = -859.3396157
Energy (0K) + ZPE = -859.223656
Enthalpy (298K) = -859.214659
Free Energy (298K) = -859.254473

SI-4
Number of imaginary frequencies: 0

C-0.7643710-1.2299740 0.0000160
C 0.7643710-1.2299740 0.0000570
C 1.1116880 0.2726960 0.0000090
C-1.1116880 0.2726960-0.0000250
H-1.2078630-1.7065960-0.8820410
H-1.2079150-1.7065640 0.8820640
H 1.2079150-1.7066160-0.8819630
H 1.2078630-1.7065440 0.8821420
N 0.0000000 1.0590930-0.0000320
O-2.2873380 0.6812510-0.0000510
O 2.2873380 0.6812510 0.0000110

Energy (0K) = -360.2074013
Energy (0K) + ZPE = -360.128665
Enthalpy (298K) = -360.122096
Free Energy (298K) = -360.158564

SI-5
Number of imaginary frequencies: 0

P-0.8463320 0.3697160 0.0000000
C-1.4025170 2.0967260 0.0000000
H-1.0445590 2.6089520 0.8966020
H-1.0445590 2.6089520-0.8966020
H-2.4973460 2.0896980 0.0000000
C-1.4025170-0.4986530-1.4910600
H-1.0765900 0.0503850-2.3778210
H-0.9914620-1.5114930-1.5094600
H-2.4958800-0.5539570-1.4693150
C-1.4025170-0.4986530 1.4910600
H -0.9914620-1.5114930 1.5094600

H-1.0765900 0.0503850 2.3778210
H-2.4958800-0.5539570 1.4693150
S 1.2686850 0.5607500 0.0000000
Cl 1.8444510-1.4348070 0.0000000

Energy (0K) = -1319.33797132
Energy (0K) + ZPE = -1319.219840
Enthalpy (298K) = -1319.209133
Free Energy (298K) = -1319.254998

SI-6
Number of imaginary frequencies: 0

N-1.8047390 0.0271570 0.5565690
C-3.1408990 0.1944700 0.9344830
C-4.0951230-0.3053340-0.1605050
H-4.7158760-1.1137130 0.2395520
C-3.1463750-0.7655280-1.2737360
C-1.7873800-0.5016650-0.6454570
H-3.2457200-0.1959030-2.2040620
H-3.2364630-1.8265490-1.5292920
H-4.7665130 0.5054970-0.4604620
O-3.4940790 0.6836720 2.0000100
O-0.7181550-0.7826550-1.3241720
Cl 3.0280010-1.6390220 0.8589800
P 1.5188010 0.9356960-0.1968220
C 3.1748280 1.2196460-0.8987550
H 3.3930160 2.2909590-0.8358100
H 3.9244260 0.6538170-0.3448940
H 3.1772720 0.9080200-1.9469310
C 1.4617330 1.4833890 1.5340830
H 2.1583390 0.8885980 2.1287380
H 0.4420190 1.3432550 1.9028730
H 1.7392980 2.5412580 1.5845450
C 0.3746560 1.9626140-1.1684200
H 0.7710200 2.9836990-1.1560480
H 0.3250450 1.6046640-2.1989300
H-0.6186940 1.9534310-0.7188830
S 0.9798250-1.1145540 0.3339730

Energy (0K) = -1679.575544
Energy (0K) + ZPE = -1679.376536
Enthalpy (298K) = -1679.358874
Free Energy (298K) = -1679.421581

Calculation Citations:

(I) (a) Becke, A. D. *J. Chem. Phys.* **1993**, *98,* 5648. (b) Becke, A. D. *J. Chem. Phys.* **1993**, *98,* 1372. (c) Lee, C.; Yang, W.; Parr, R. G. *Phys. Rev. B* **1988**, *98,* 785.

(II) (a) Ditchfield, R.; Hehre, W. J.; Pople, J. A. *J. Chem. Phys.* **1971**, *54*, 724. (b) Hehre, W. J.; Ditchfield, R.; Pople, J. A. *J. Chem. Phys.* **1972**, *56*, 2257. (c) Hariharan, P. C.;

Pople, J. A. *Theor. Chim. Acta* **1973**, *28*, 213. (d) Clark, T., J.; Chandrasekhar, C.; Spitznagel, G. W.; Schleyer, P. v. R. *J. Comp. Chem.* **1983**, *4*, 294.

(III) Gaussian 09, Revision D.01. M. J. Frisch, G. W. Trucks, H. B. Schlegel, G. E. Scuseria, M. A. Robb, J. R. Cheeseman, G. Scalmani, V. Barone, B. Mennucci, G. A. Petersson, H. Nakatsuji, M. Caricato, X. Li, H. P. Hratchian, A. F. Izmaylov, J. Bloino, G. Zheng, J. L. Sonnenberg, M. Hada, M. Ehara, K. Toyota, R. Fukuda, J. Hasegawa, M. Ishida, T. Nakajima, Y. Honda, O. Kitao, H. Nakai, T. Vreven, J. A. Montgomery, Jr., J. E. Peralta, F. Ogliaro, M. Bearpark, J. J. Heyd, E. Brothers, K. N. Kudin, V. N. Staroverov, T. Keith, R. Kobayashi, J. Normand, K. Raghavachari, A. Rendell, J. C. Burant, S. S. Iyengar, J. Tomasi, M. Cossi, N. Rega, J. M. Millam, M. Klene, J. E. Knox, J. B. Cross, V. Bakken, C. Adamo, J. Jaramillo, R. Gomperts, R. E. Stratmann, O. Yazyev, A. J. Austin, R. Cammi, C. Pomelli, J. W. Ochterski, R. L. Martin, K. Morokuma, V. G. Zakrzewski, G. A. Voth, P. Salvador, J. J. Dannenberg, S. Dapprich, A. D. Daniels, O. Farkas, J. B. Foresman, J. V. Ortiz, J. Cioslowski, and D. J. Fox, Gaussian, Inc., Wallingford CT, 2013.

1.9.5 Spectral Data for Purified Products

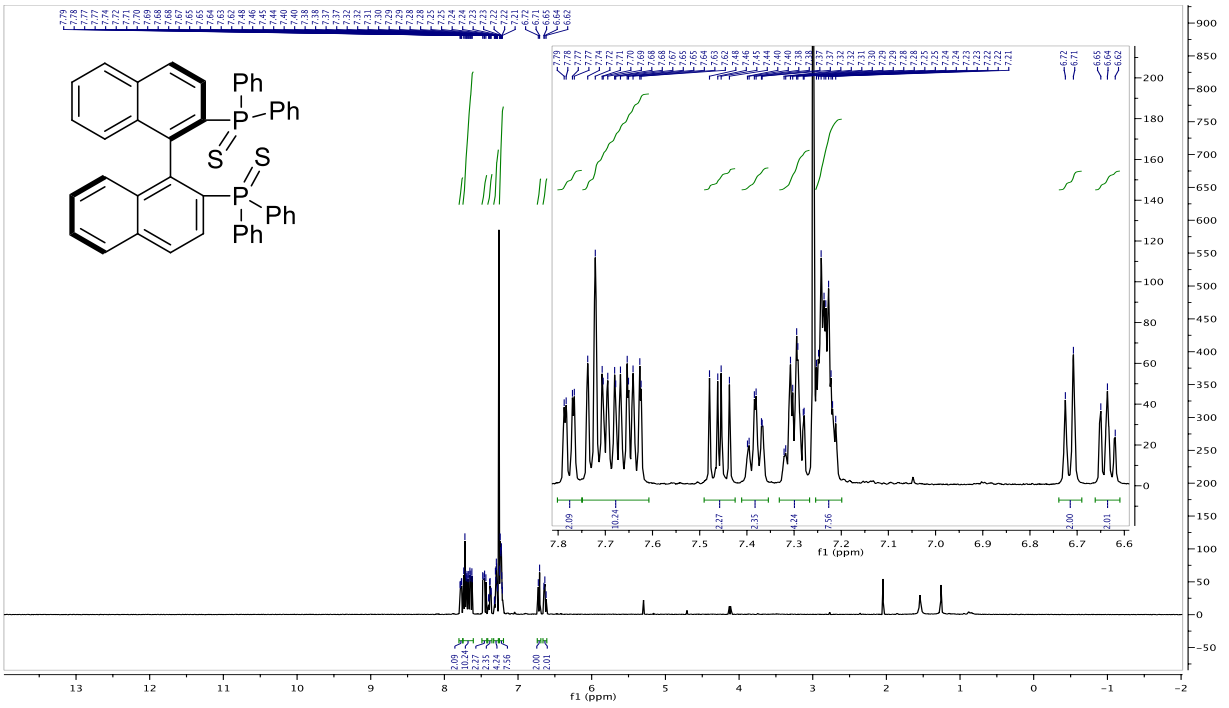

Figure 1.9.32 500 MHz ^{1}H NMR Spectrum of 1.7

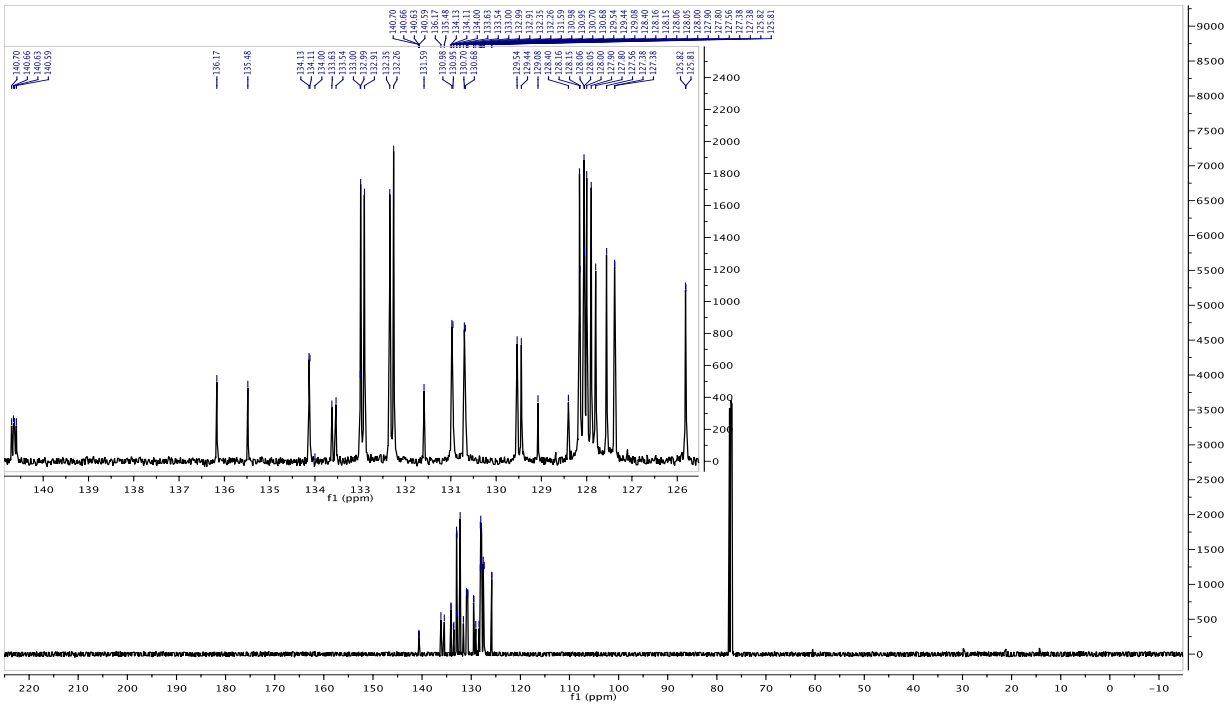

Figure 1.9.33 126 MHz ^{13}C NMR Spectrum of 1.7

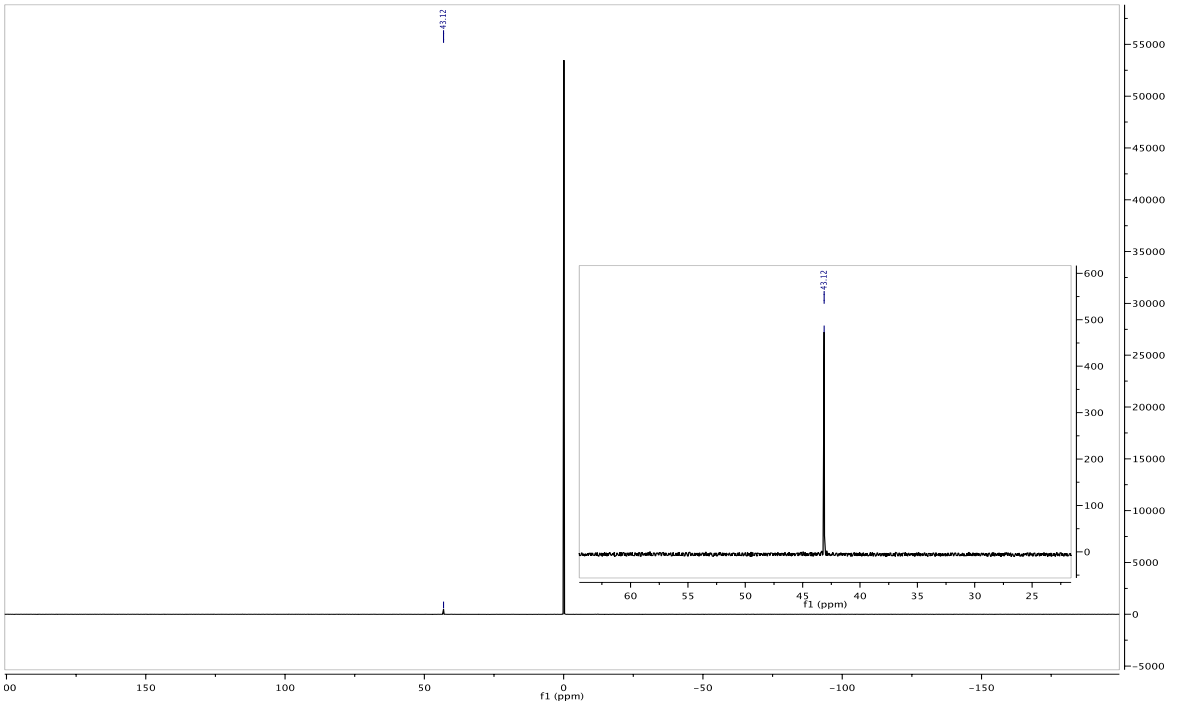

Figure 1.9.34 202 MHz ^{31}P NMR Spectrum of 1.7

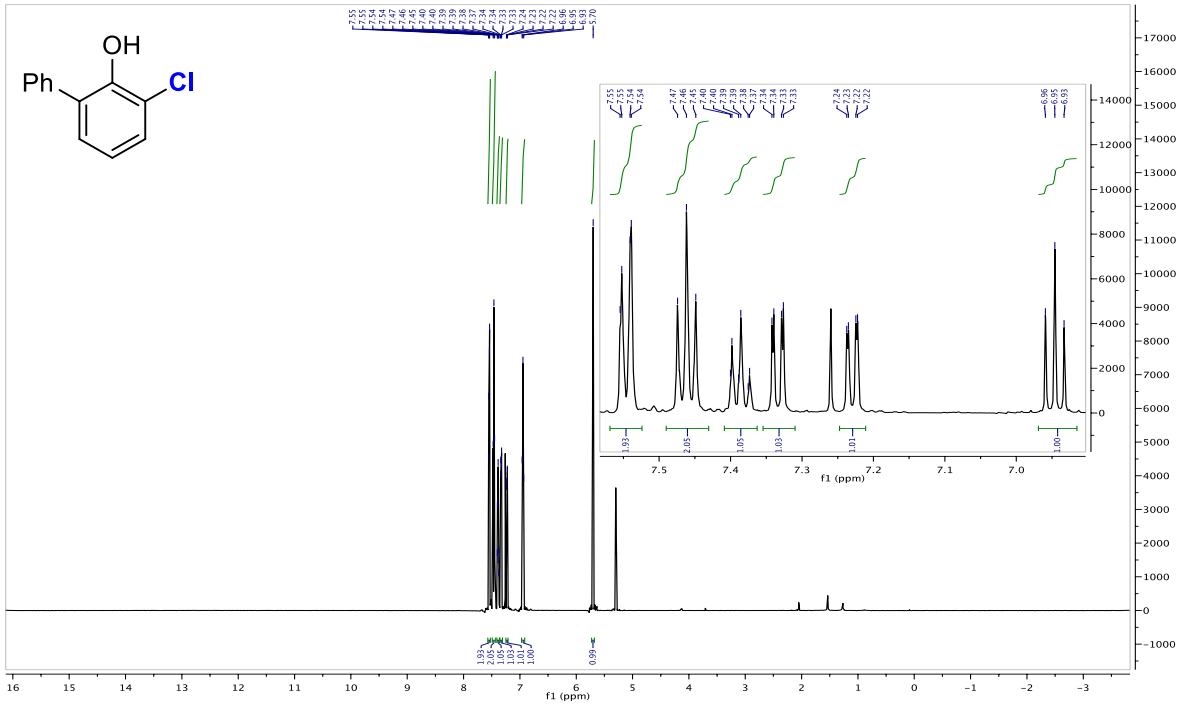

Figure 1.9.35 599 MHz ^{1}H NMR Spectrum of 1.8a

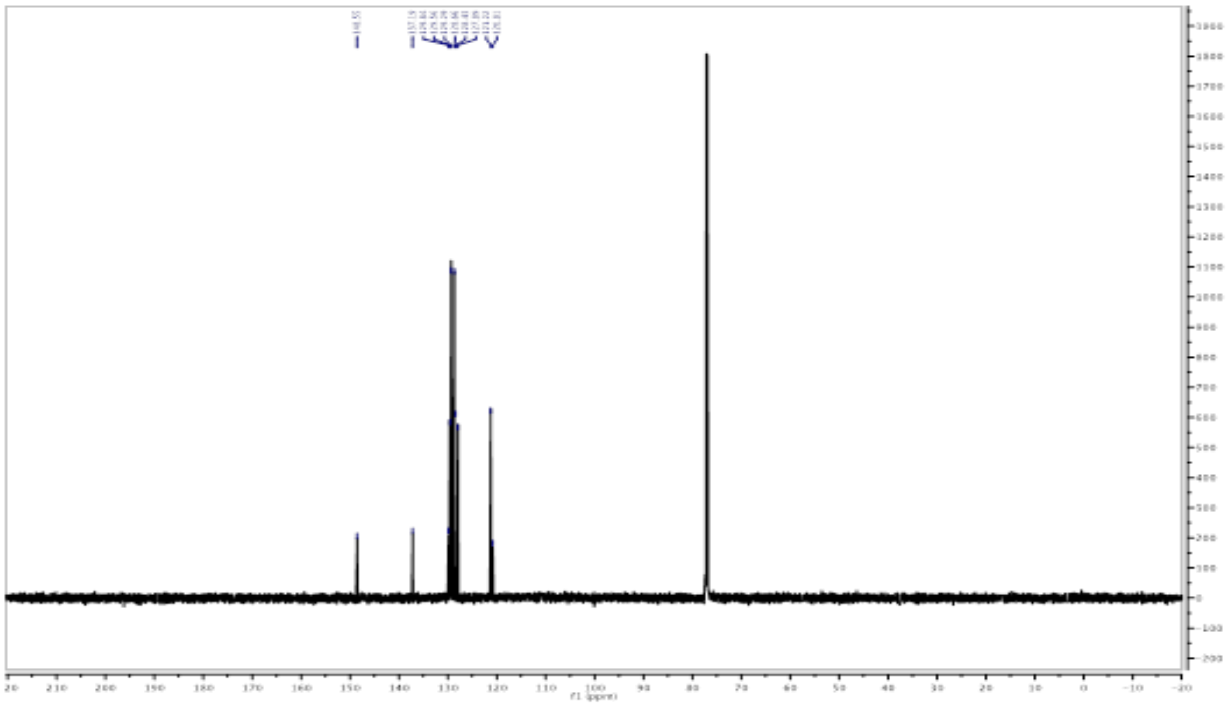

Figure 1.9.36 151 MHz ^{13}C NMR Spectrum of 1.8a

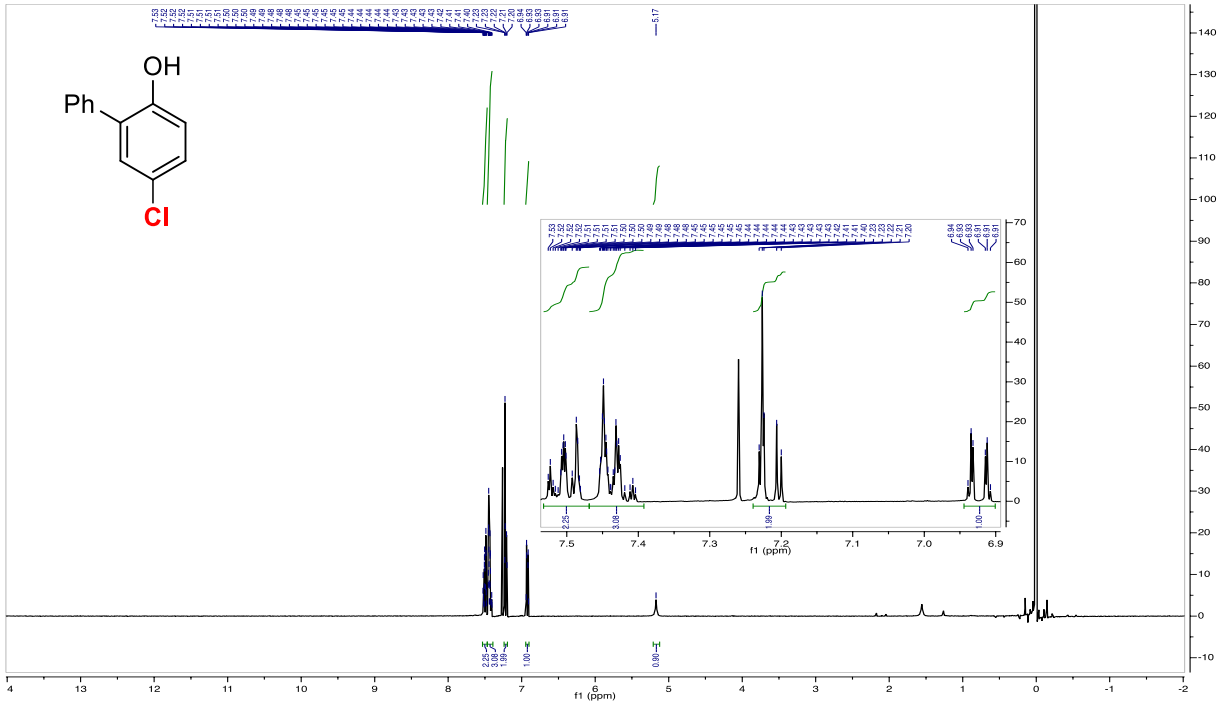

Figure 1.9.37 400 MHz ^{1}H NMR Spectrum of 1.8b

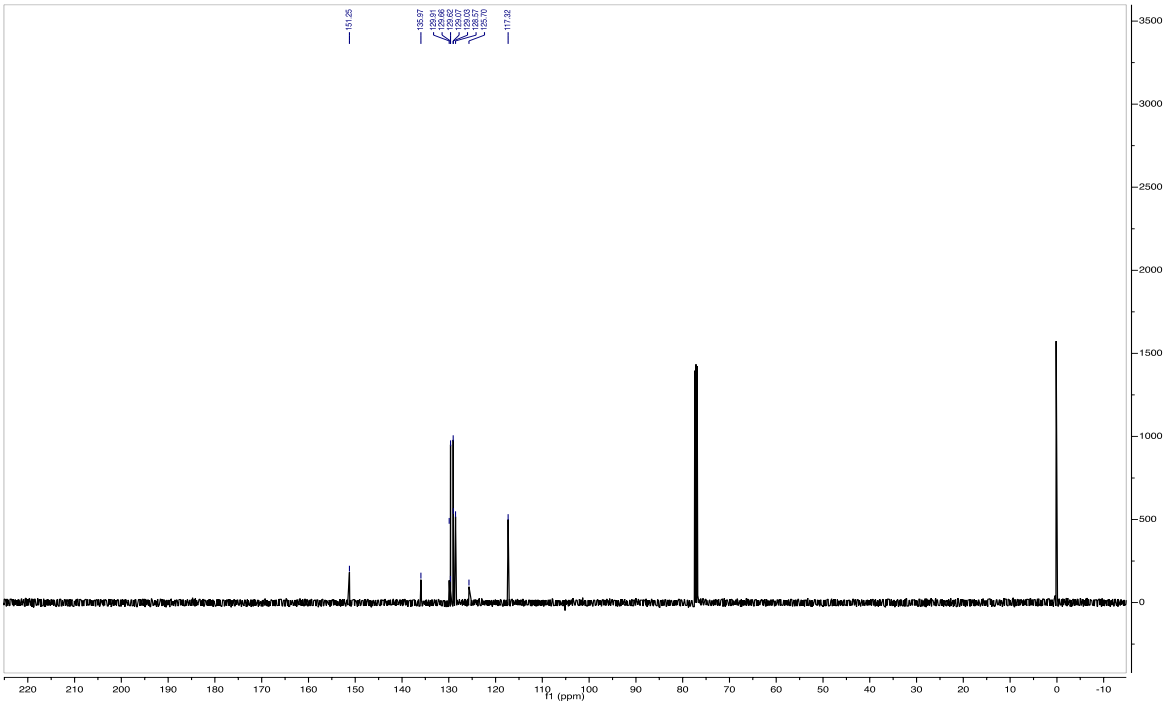

Figure 1.9.38 126 MHz ^{13}C NMR Spectrum of 1.8b

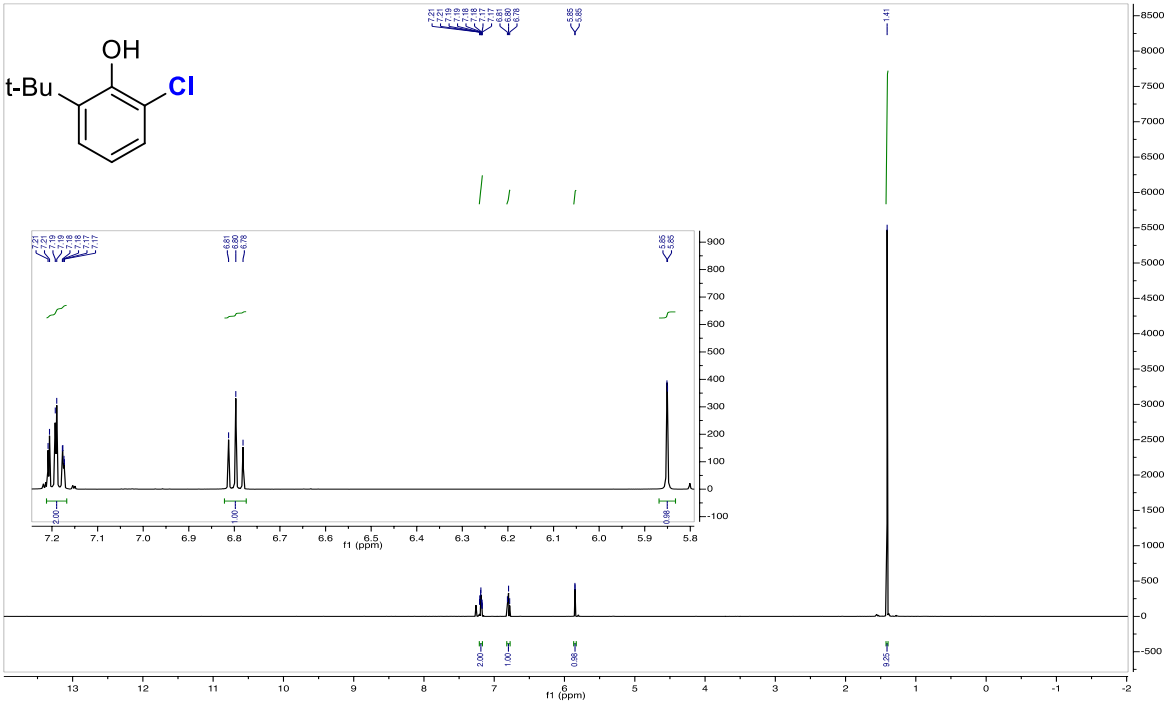

Figure 1.9.39 500 MHz ^{1}H NMR Spectrum of 1.9a

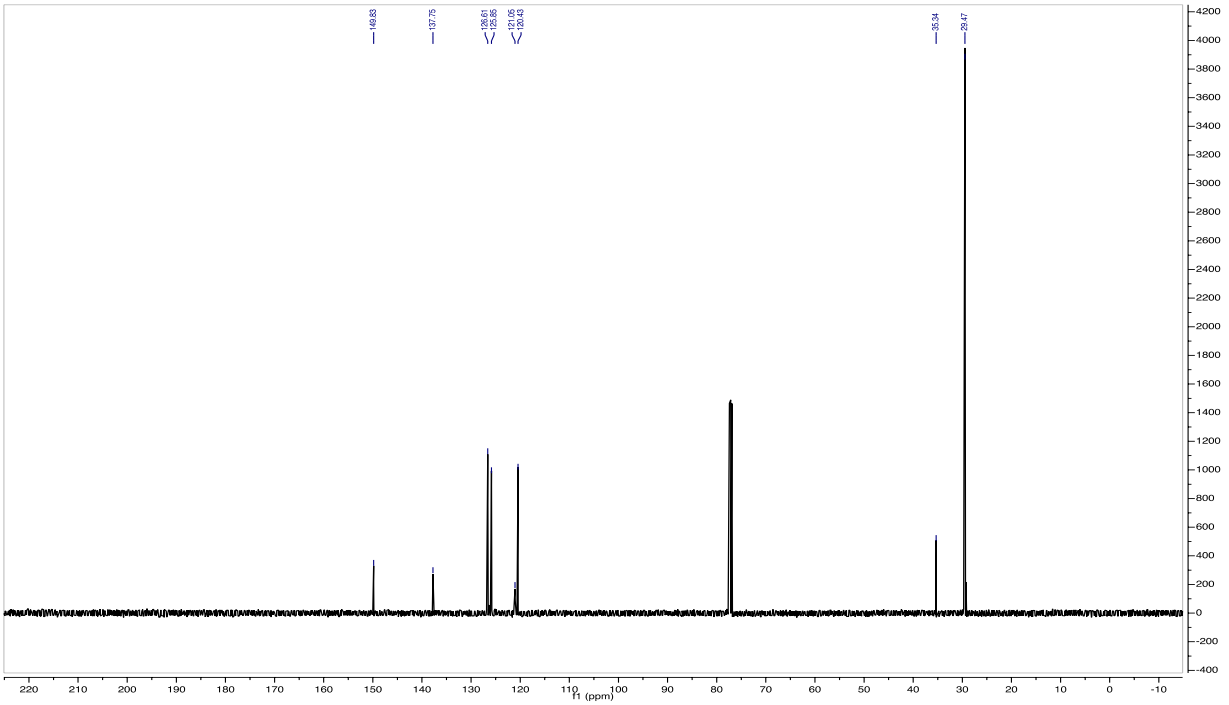

Figure 1.9.40 126 MHz ^{13}C NMR Spectrum of 1.9a

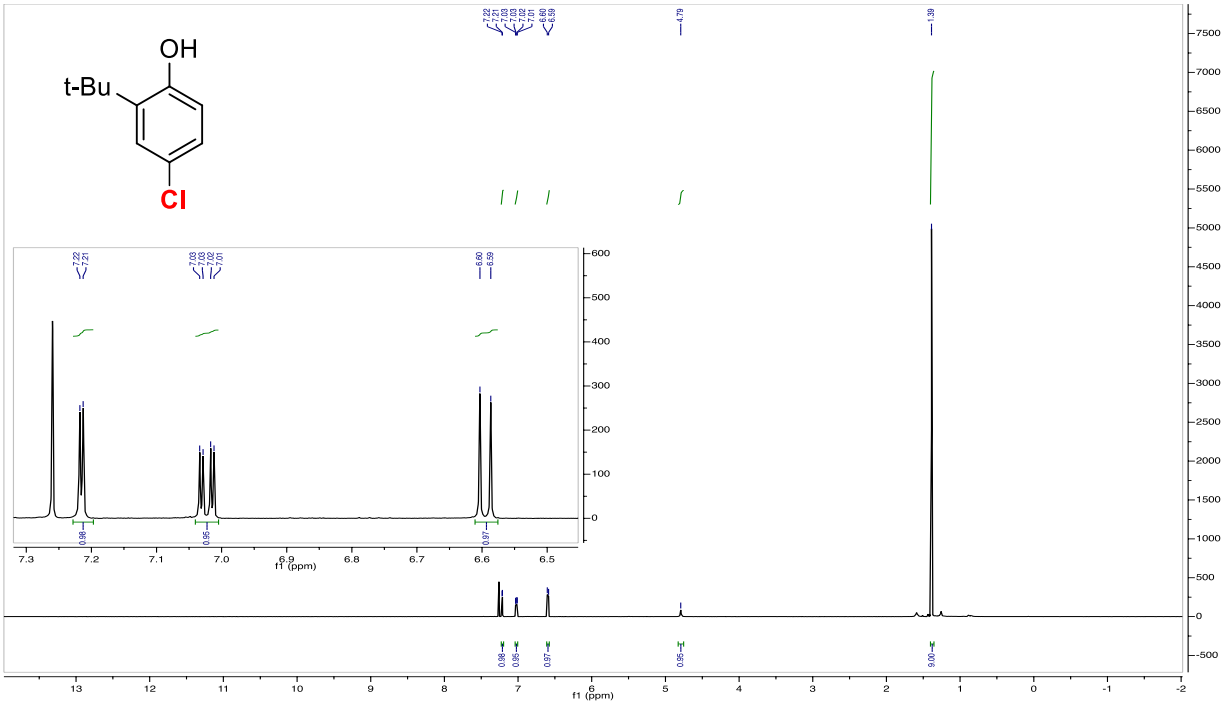

Figure 1.9.41 500 MHz ^{1}H NMR Spectrum of 1.9b

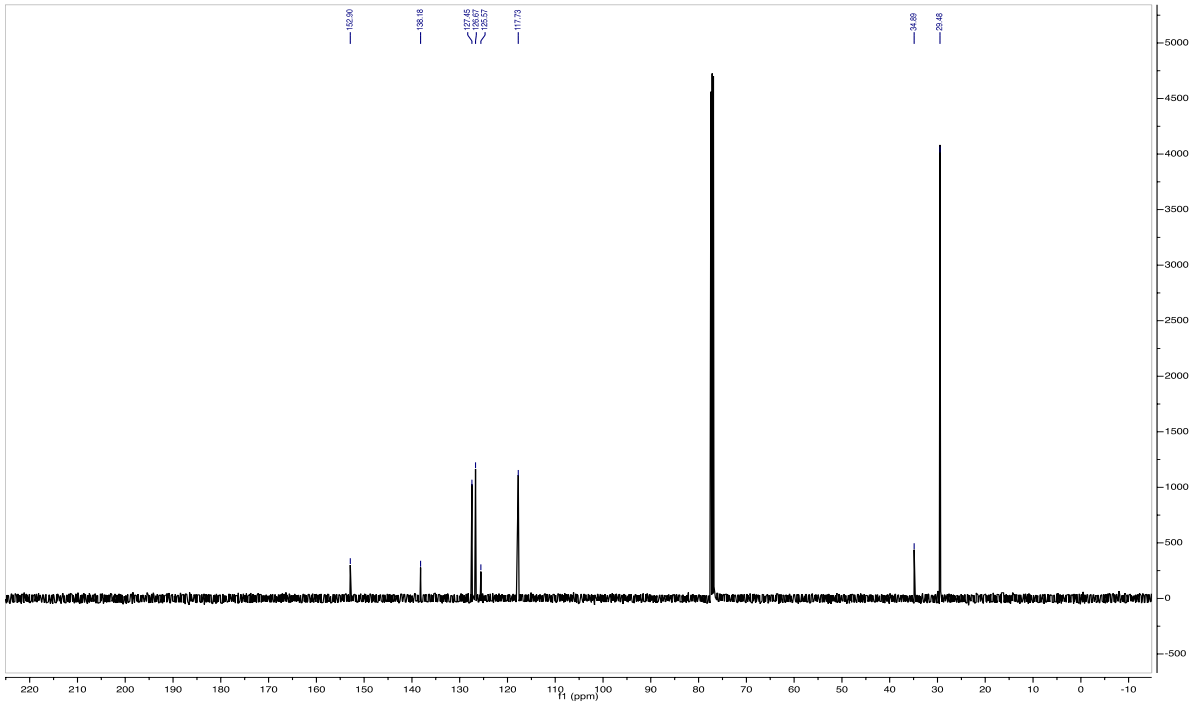

Figure 1.9.42 126 MHz ^{13}C NMR Spectrum of 1.9b

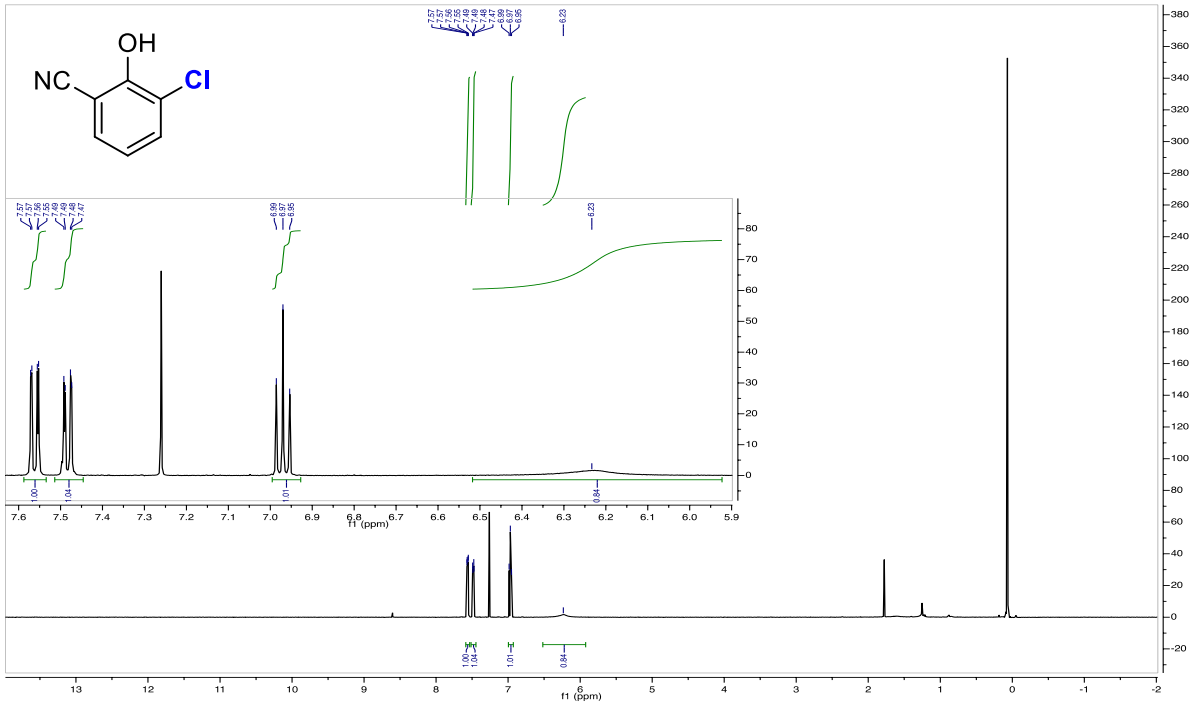

Figure 1.9.43 500 MHz ^{1}H NMR Spectrum of 1.10a

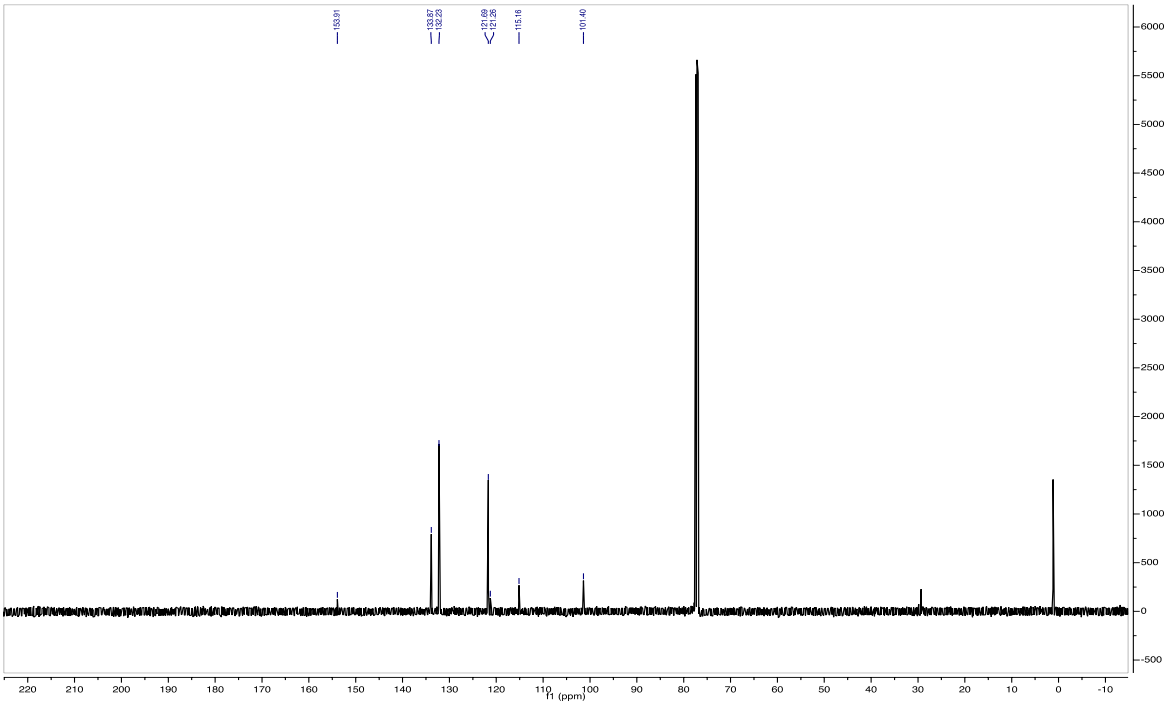

Figure 1.9.44 126 MHz ^{13}C NMR Spectrum of 1.10a

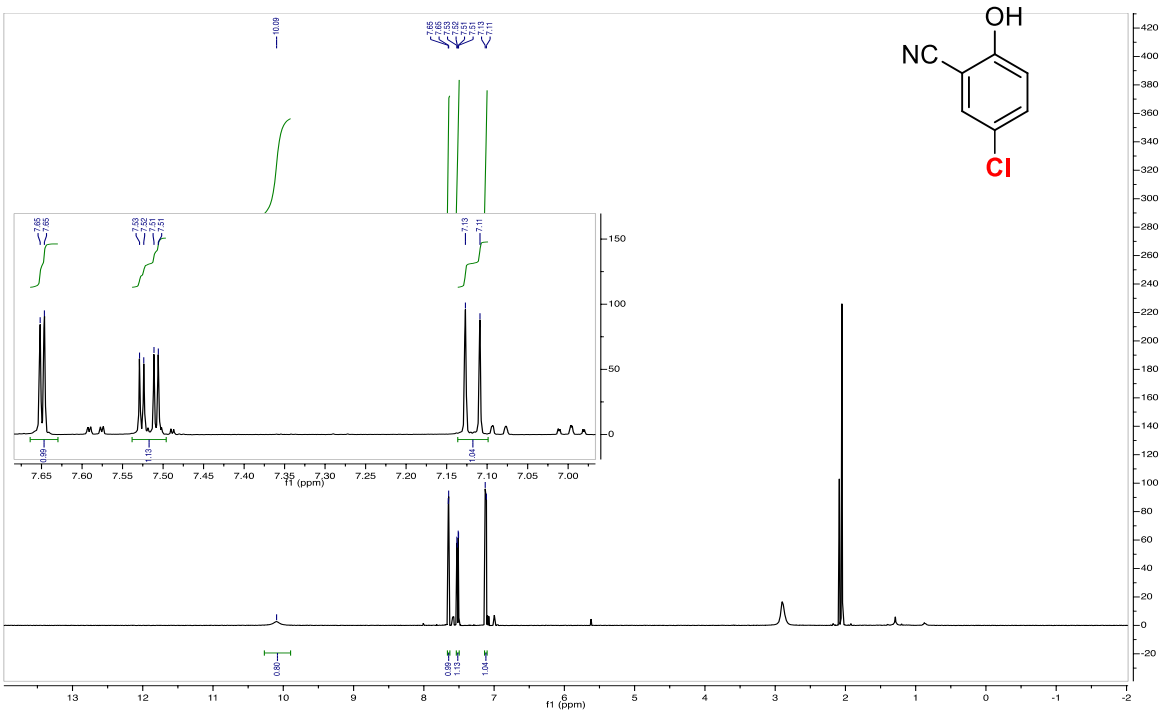

Figure 1.9.45 500 MHz ^{1}H NMR Spectrum of 1.10b

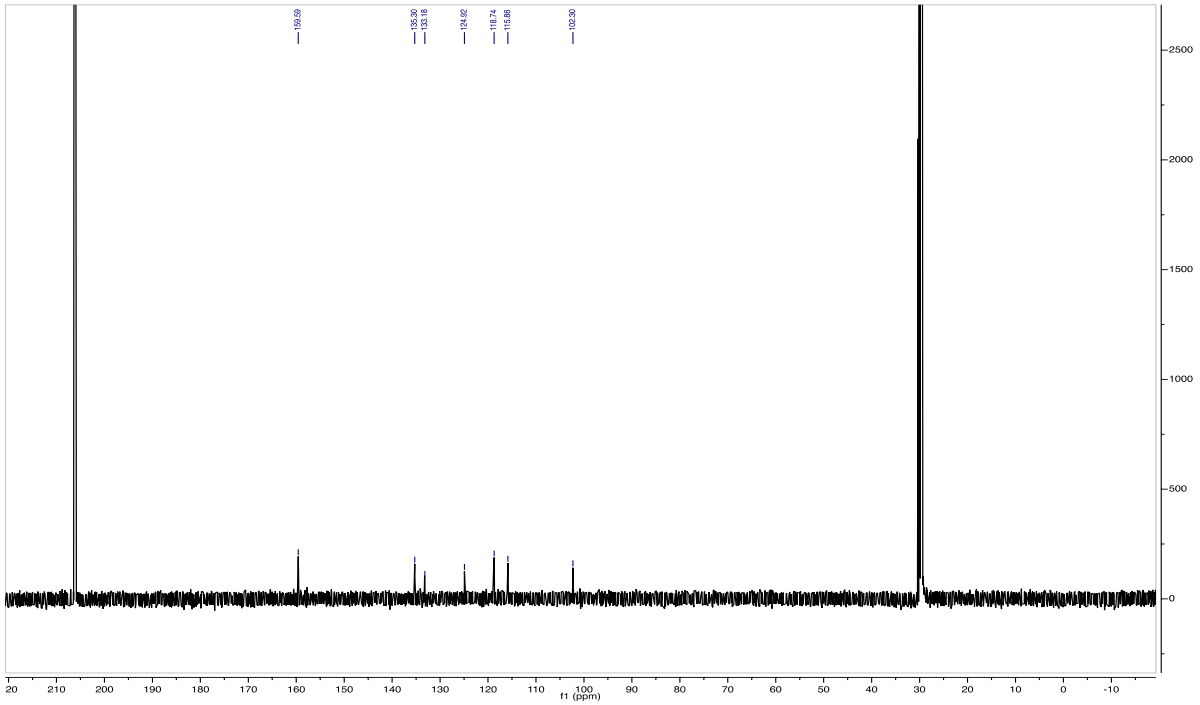

Figure 1.9.46 126 MHz ^{13}C NMR Spectrum of 1.10b

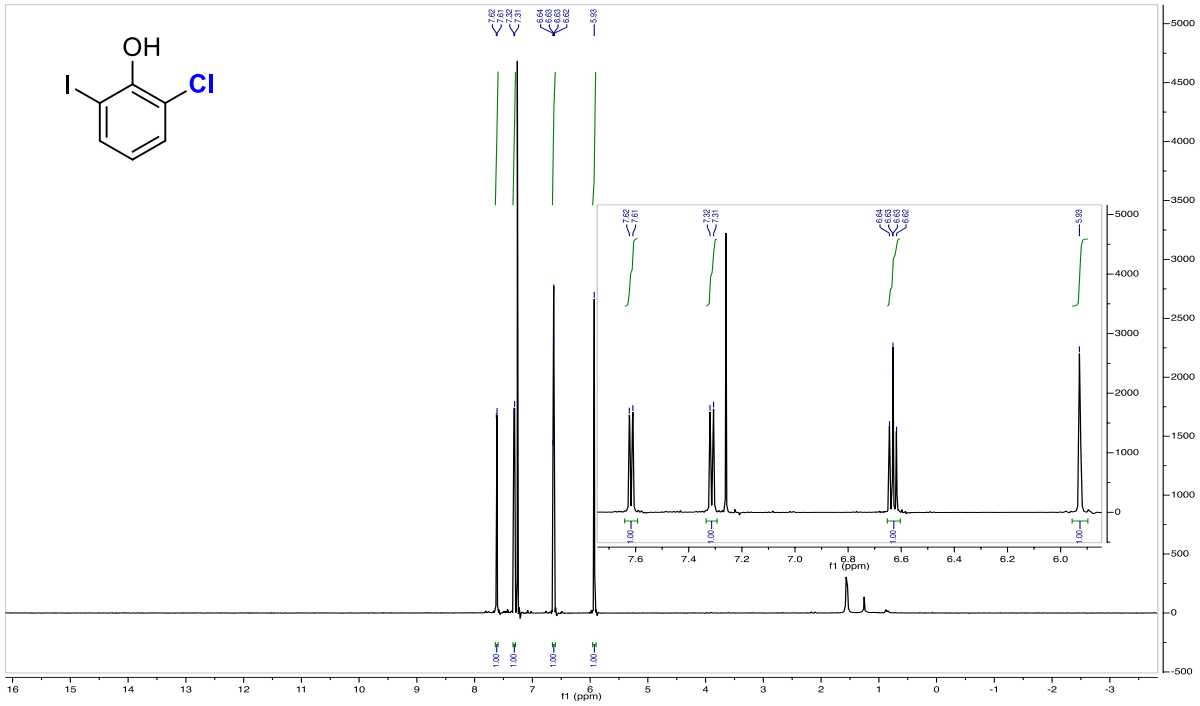

Figure 1.9.47 599 MHz ^{1}H NMR Spectrum of 1.11a

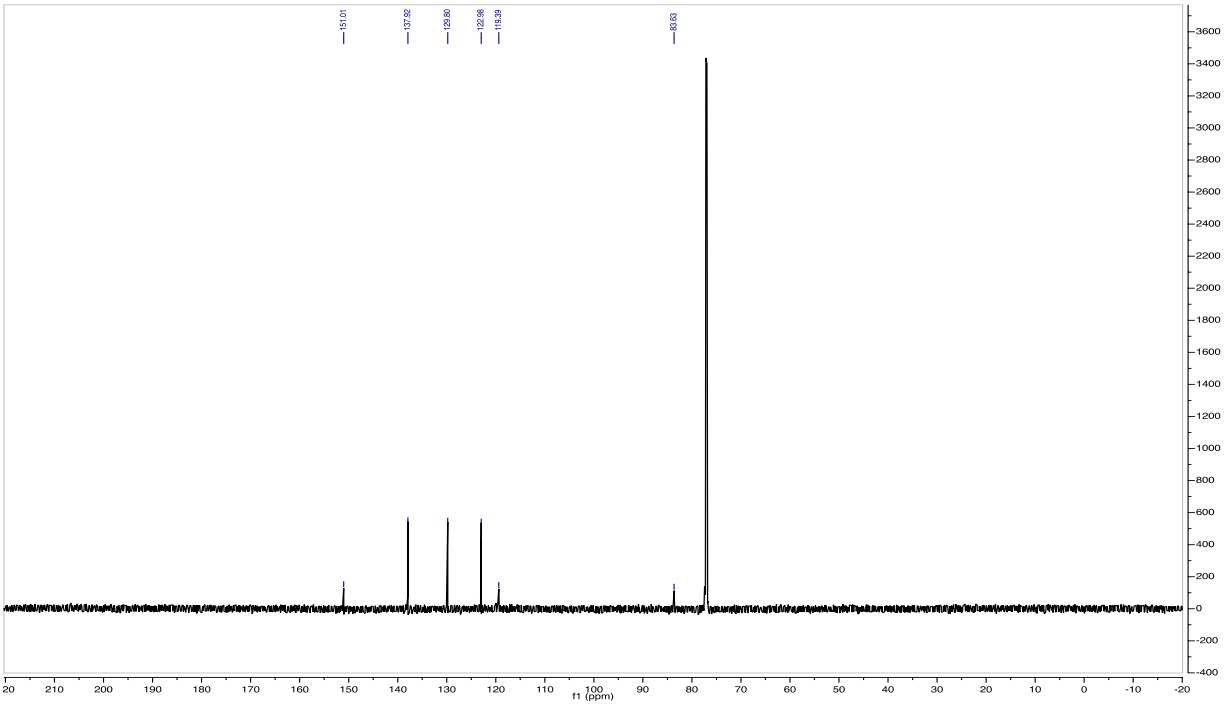

Figure 1.9.48 151 MHz ^{13}C NMR Spectrum of 1.11a

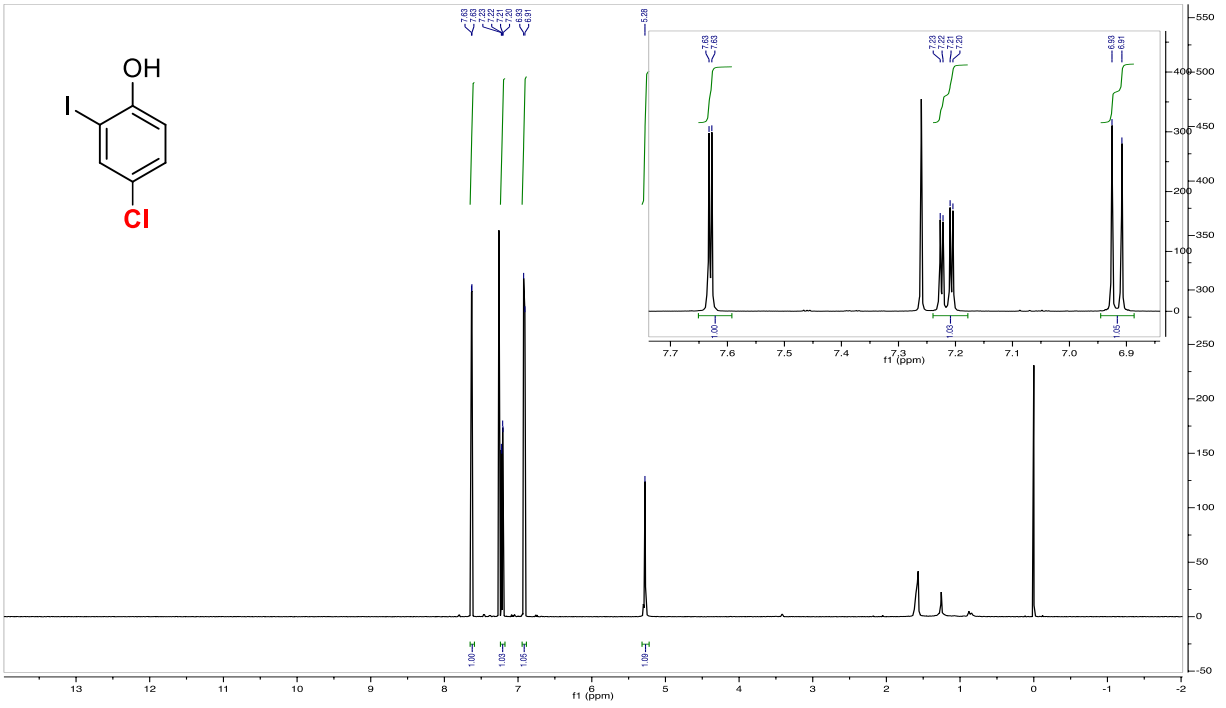

Figure 1.9.49 500 MHz ^{1}H NMR Spectrum of 1.11b

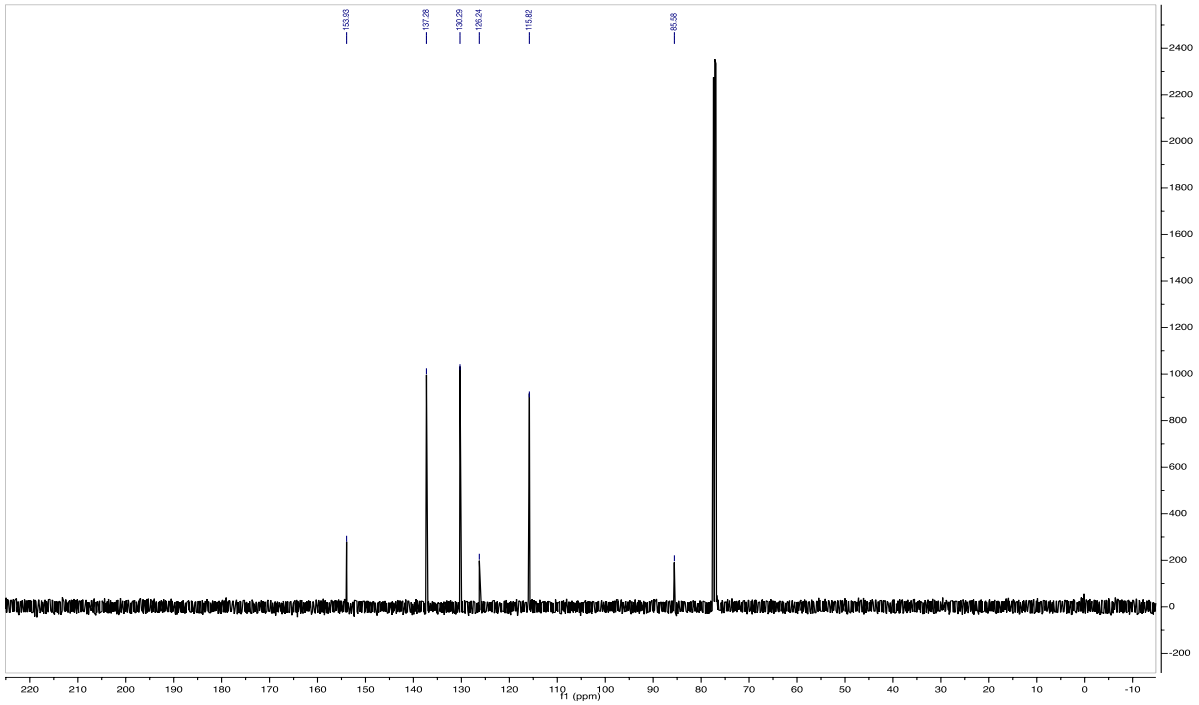

Figure 1.9.50 126 MHz ^{13}C NMR Spectrum of 1.11b

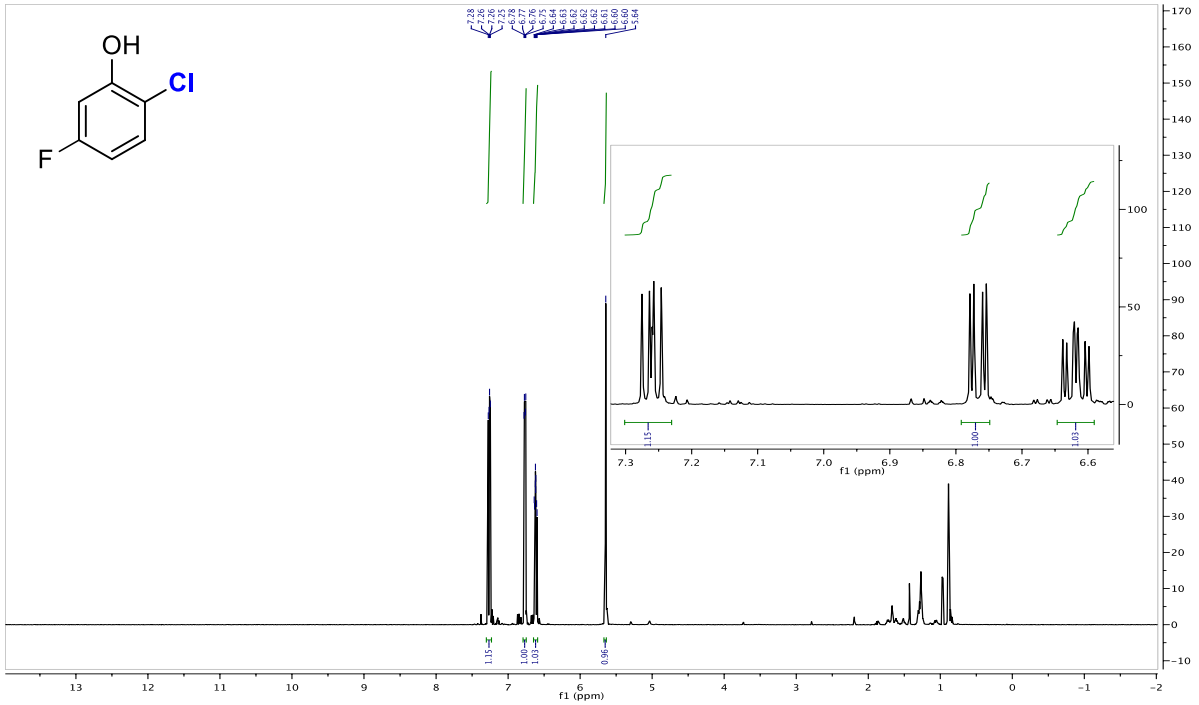

Figure 1.9.51 500 MHz ^{1}H NMR Spectrum of 1.12a

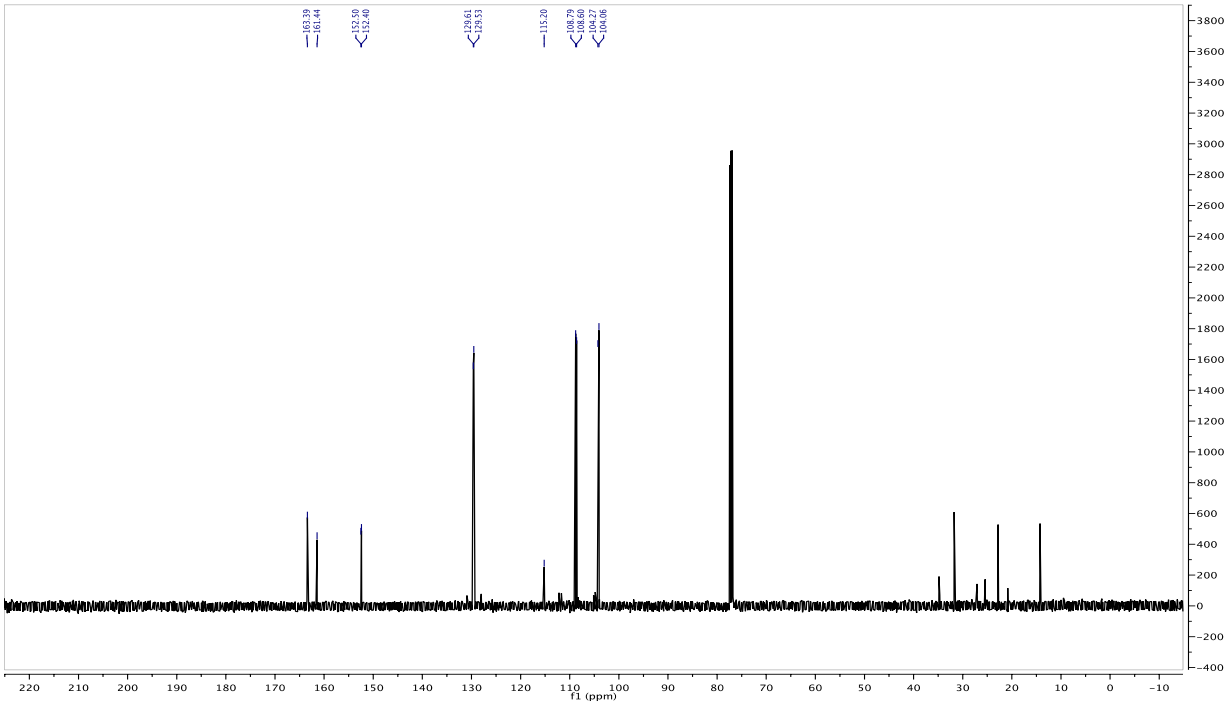

Figure 1.9.52 126 MHz ^{13}C NMR Spectrum of 1.12a

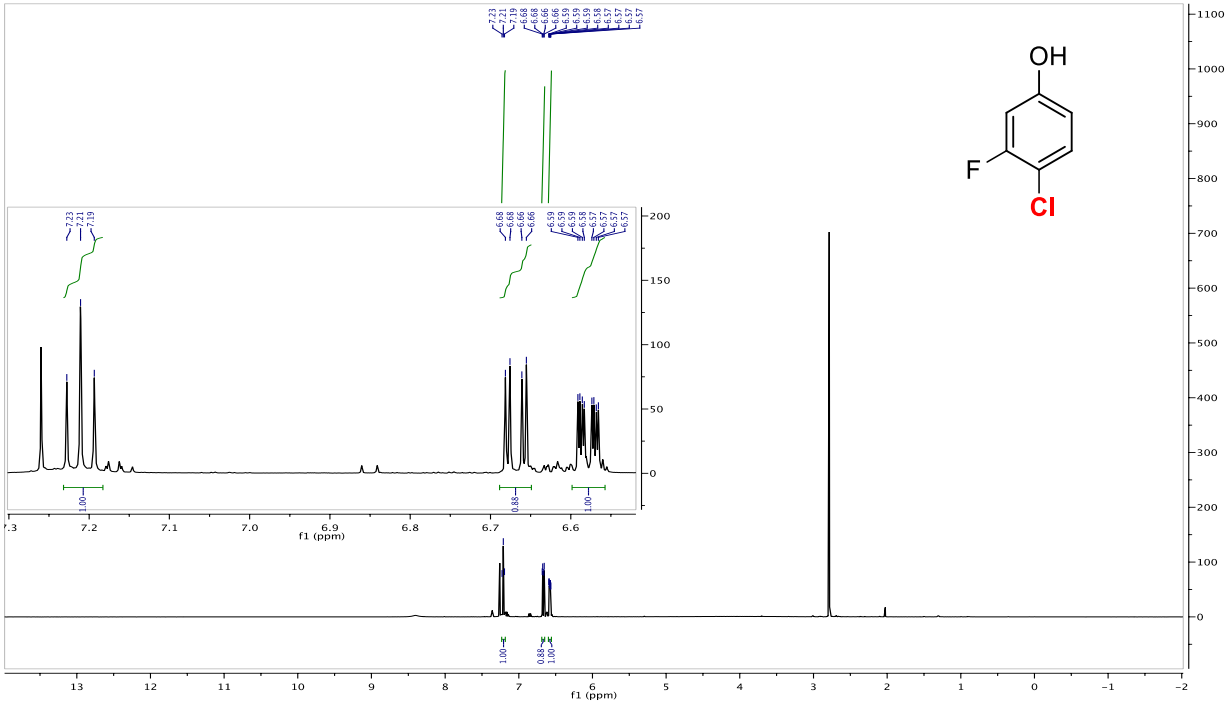

Figure 1.9.53 500 MHz ^{1}H NMR Spectrum of 1.12b

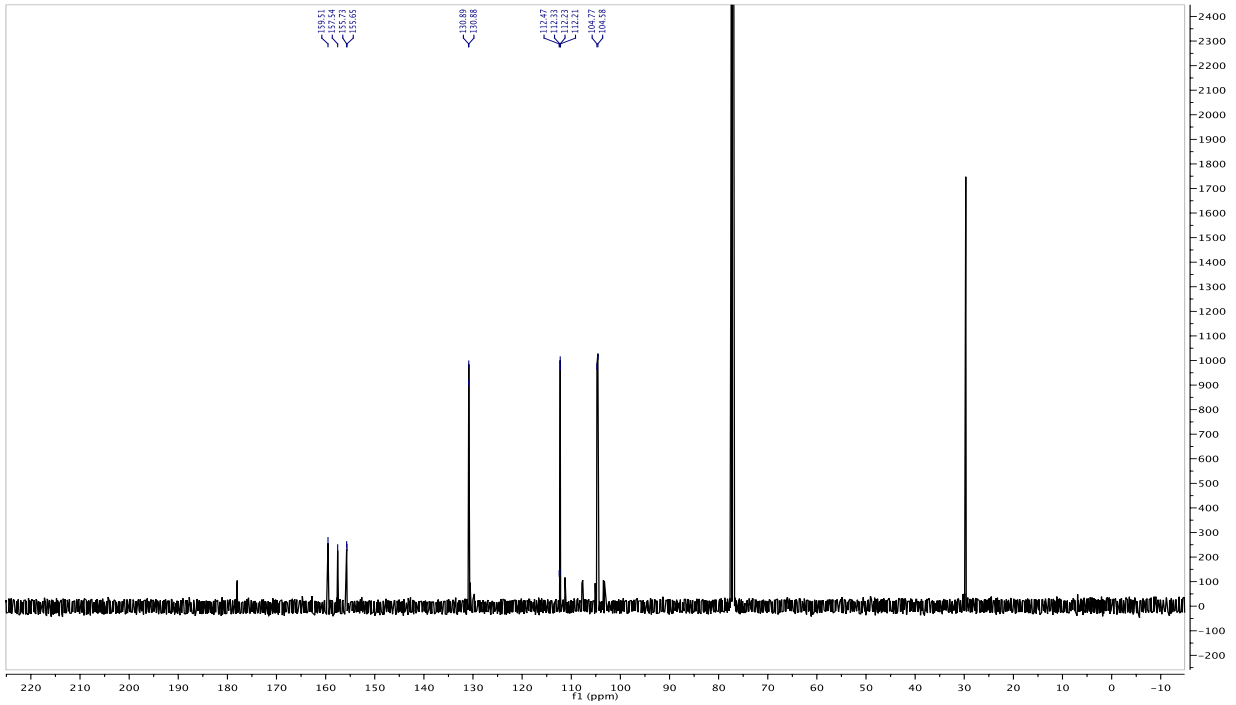

Figure 1.9.54 126 MHz ^{13}C NMR Spectrum of 1.12b

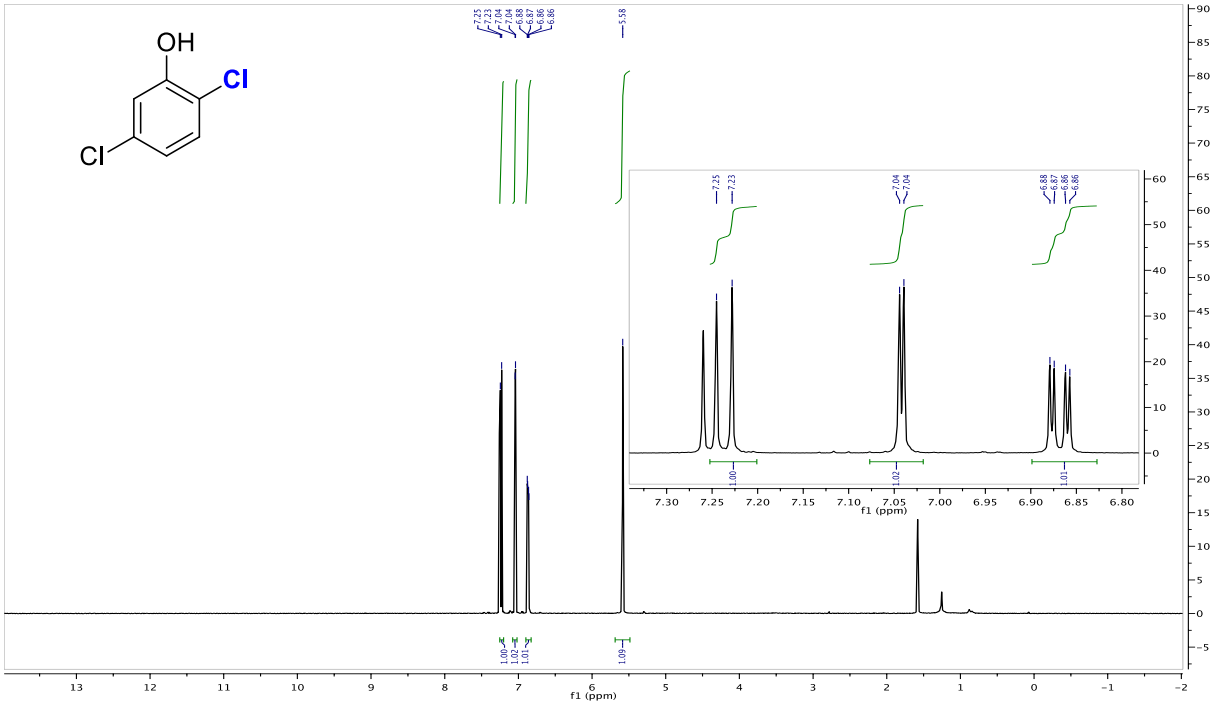

Figure 1.9.55 500 MHz ^{1}H NMR Spectrum of 1.13a

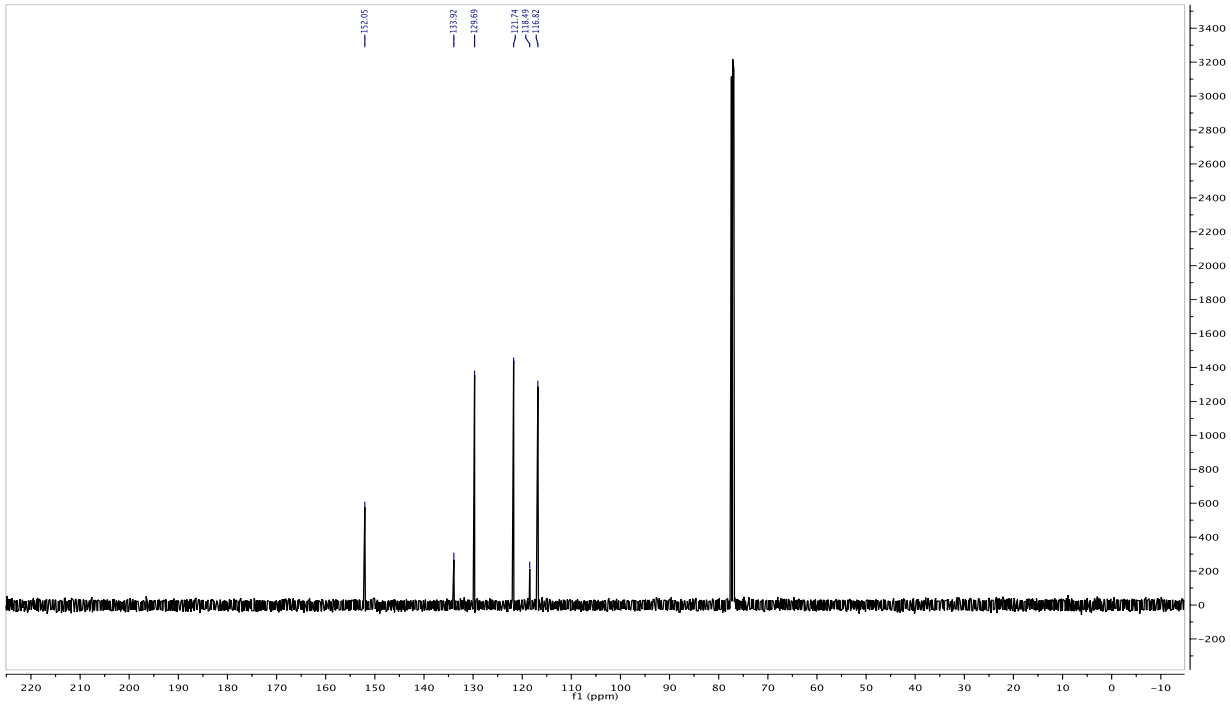

Figure 1.9.56 126 MHz ^{13}C NMR Spectrum of 1.13a

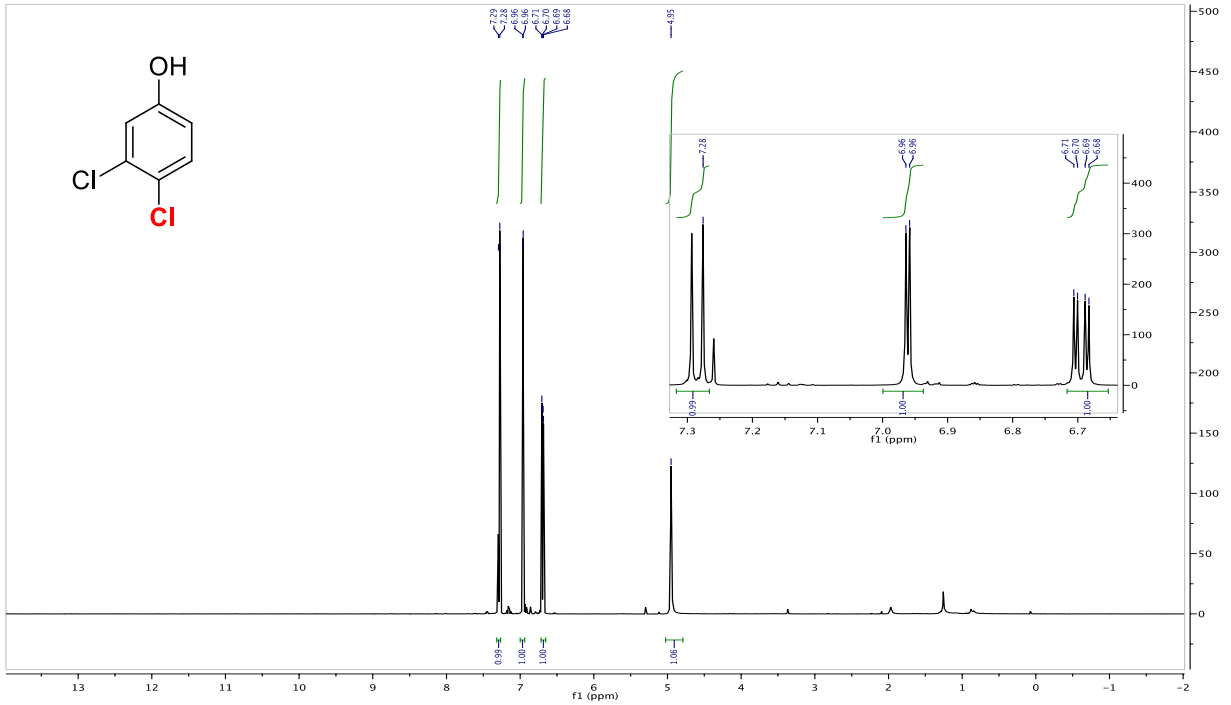

Figure 1.9.57 500 MHz ^{1}H NMR Spectrum of 1.13b

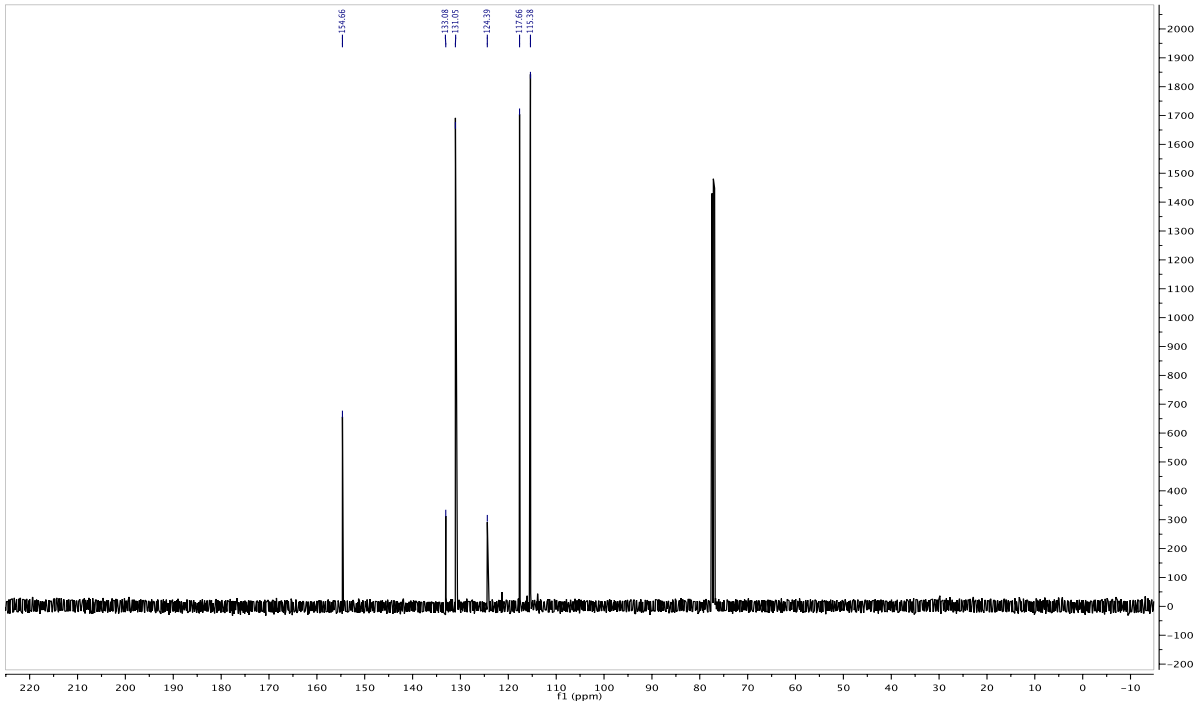

Figure 1.9.58 126 MHz ^{13}C NMR Spectrum of 1.13b

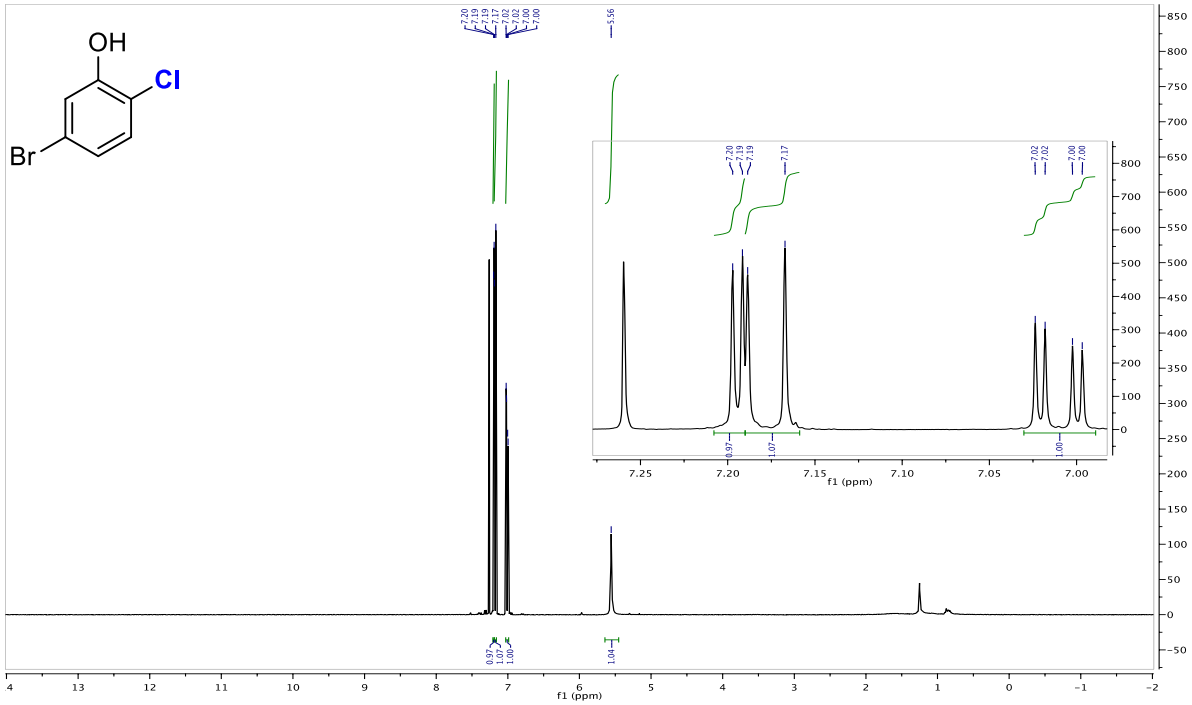

Figure 1.9.59 400 MHz ^{1}H NMR Spectrum of 1.14a

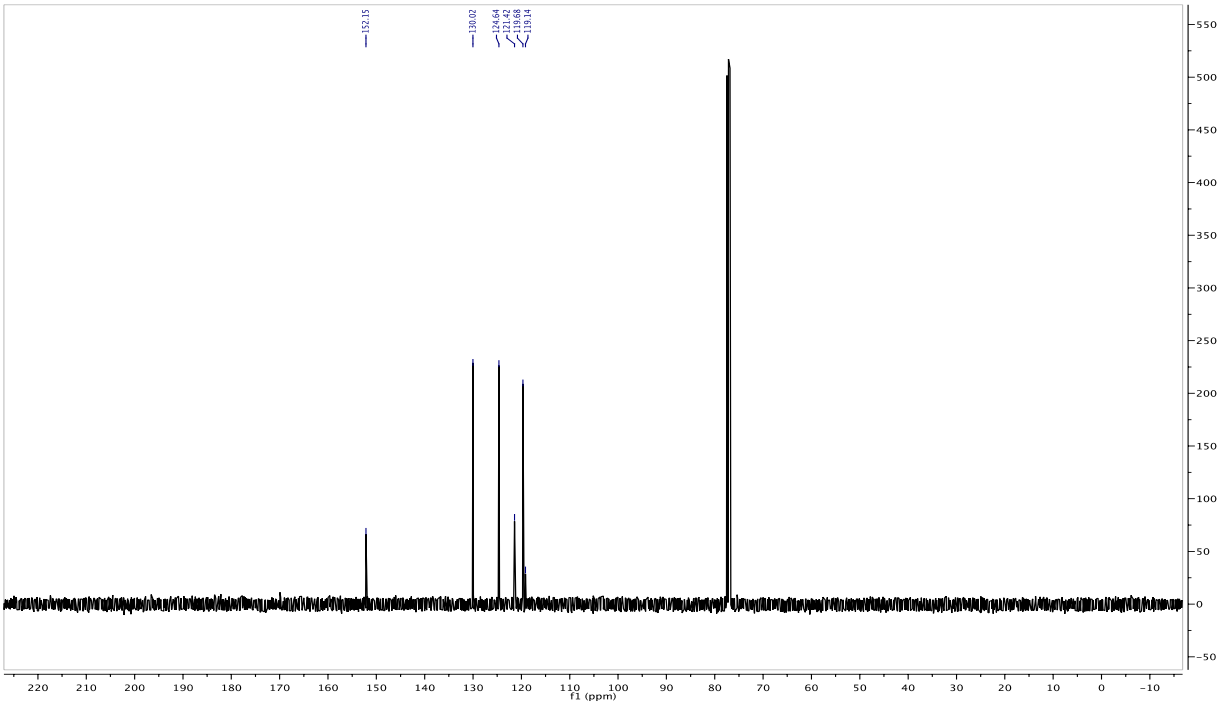

Figure 1.9.60 101 MHz ^{13}C NMR Spectrum of 1.14a

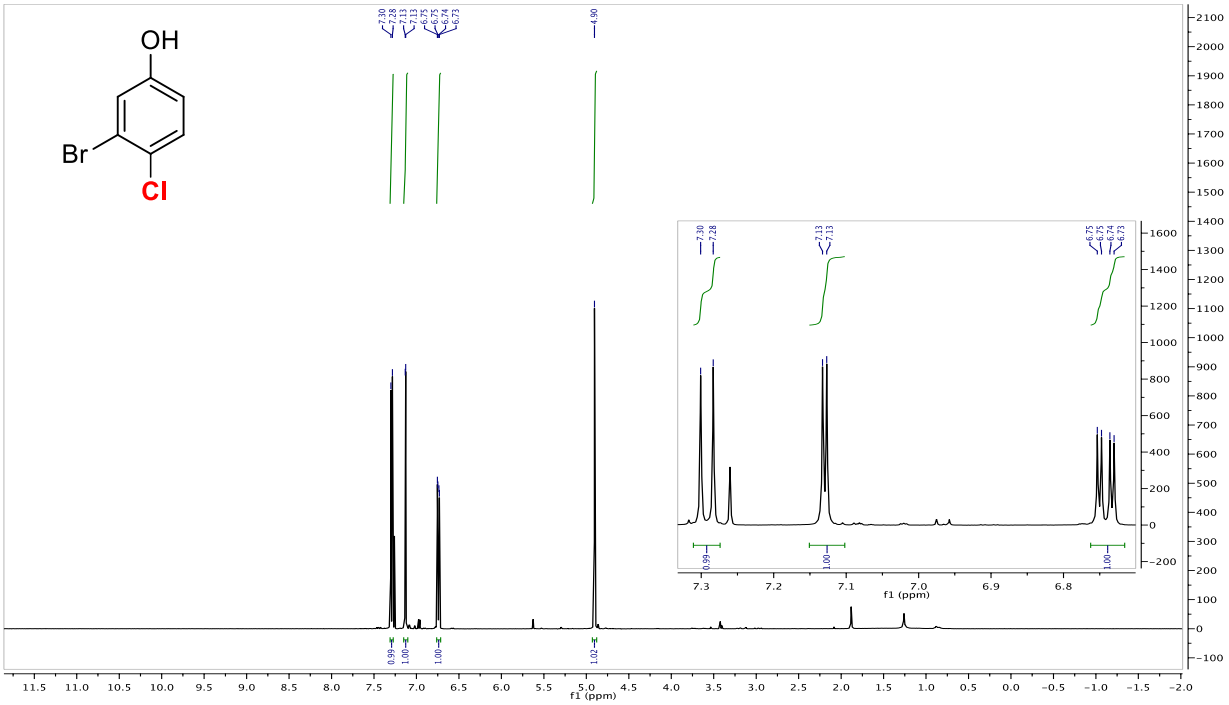

Figure 1.9.61 500 MHz ^{1}H NMR Spectrum of 1.14b

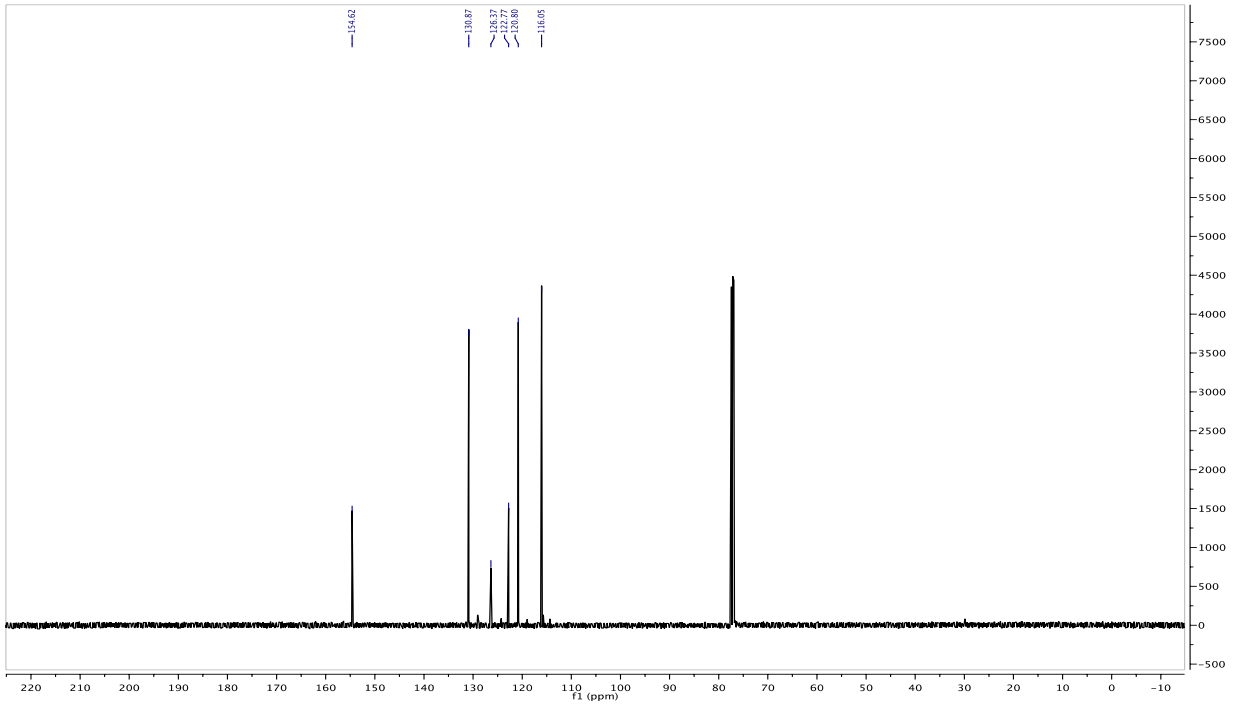

Figure 1.9.62 126 MHz ^{13}C NMR Spectrum of 1.14b

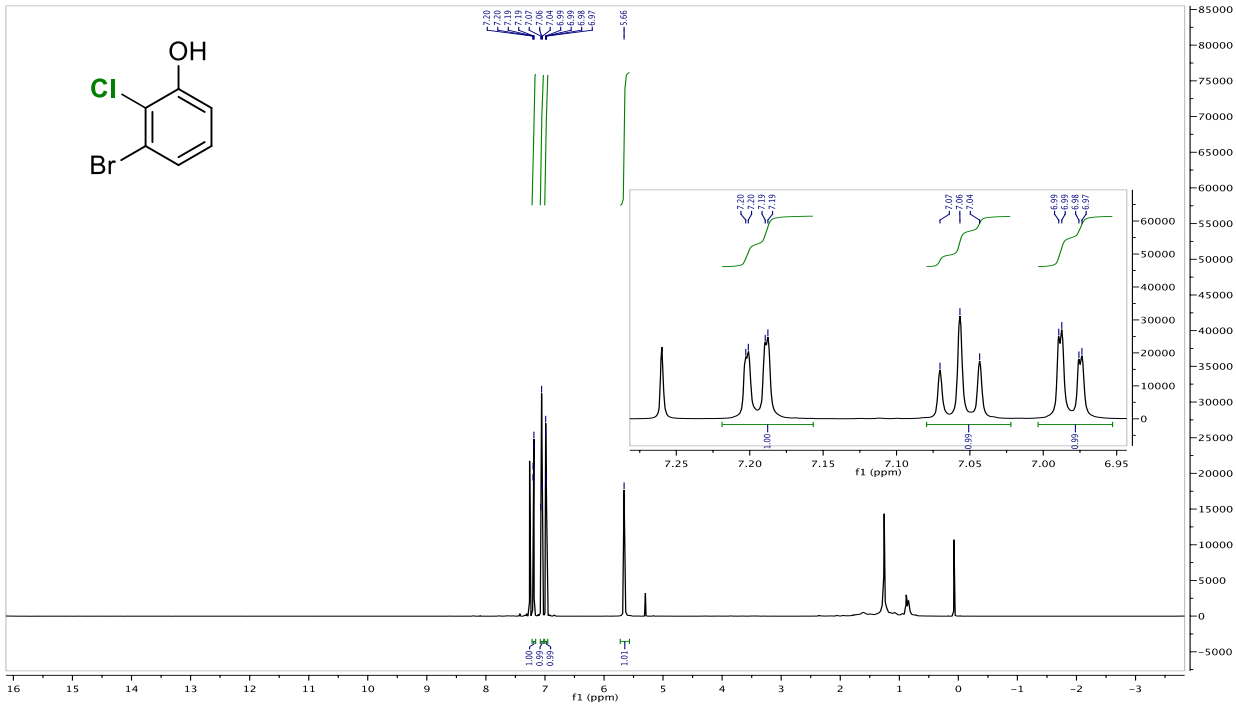

Figure 1.9.63 599 MHz ^{1}H NMR Spectrum of 1.14c

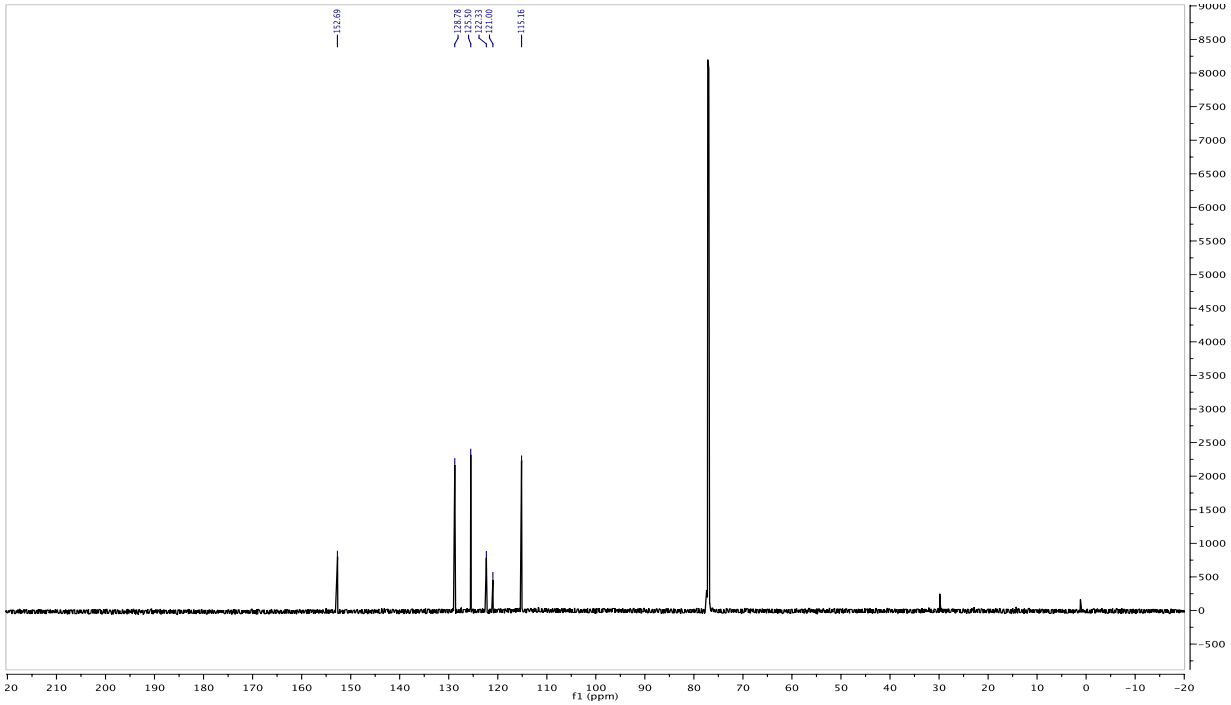

Figure 1.9.64 151 MHz ^{13}C NMR Spectrum of 1.14c

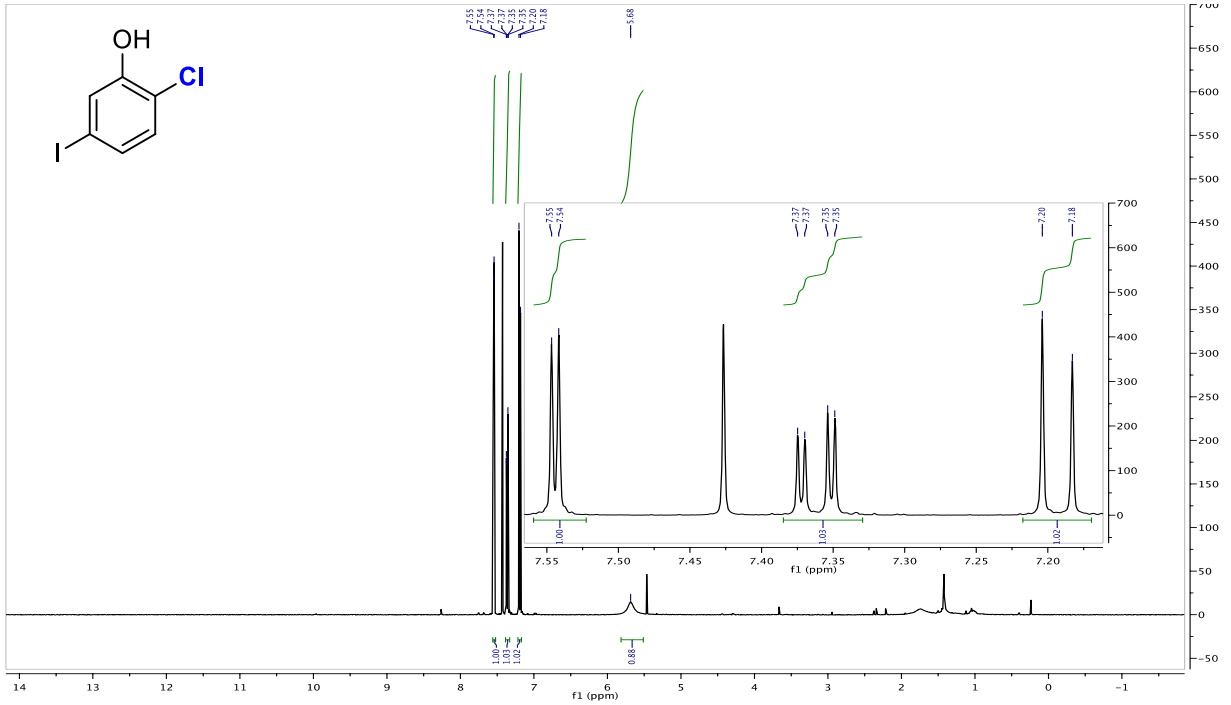

Figure 1.9.65 400 MHz ^{1}H NMR Spectrum of 1.15a

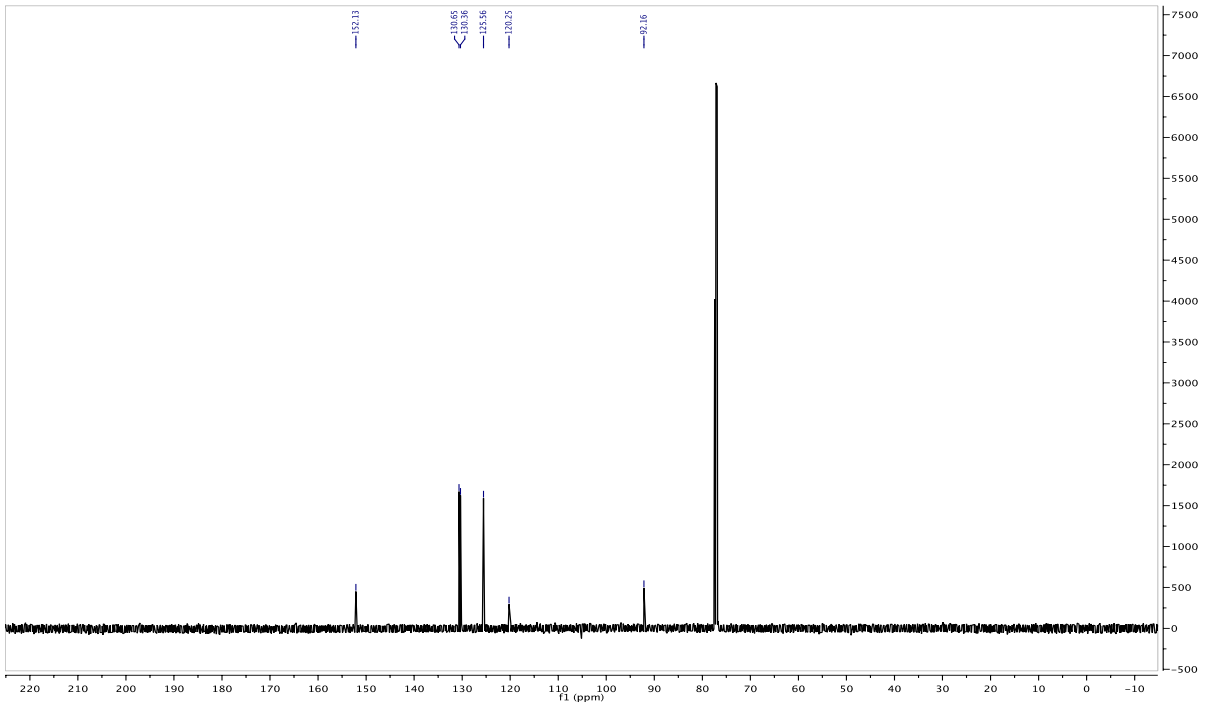

Figure 1.9.66 126 MHz ^{13}C NMR Spectrum of 1.15a

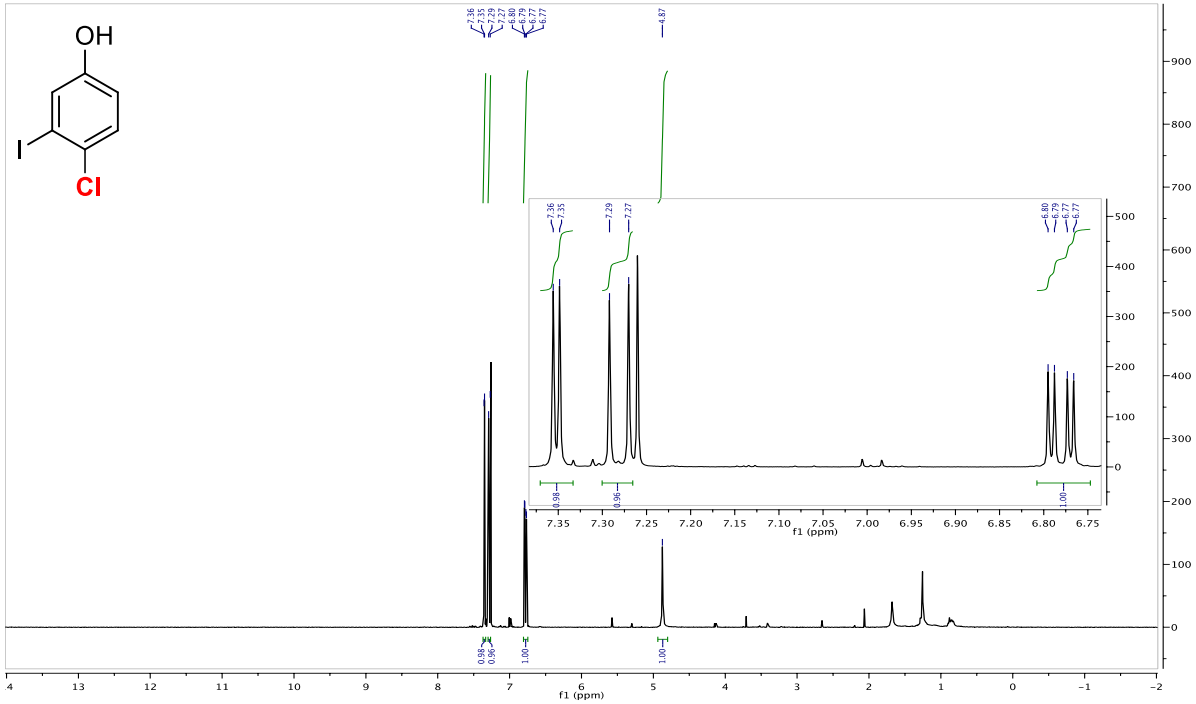

Figure 1.9.67 400 MHz ^{1}H NMR Spectrum of 1.15b

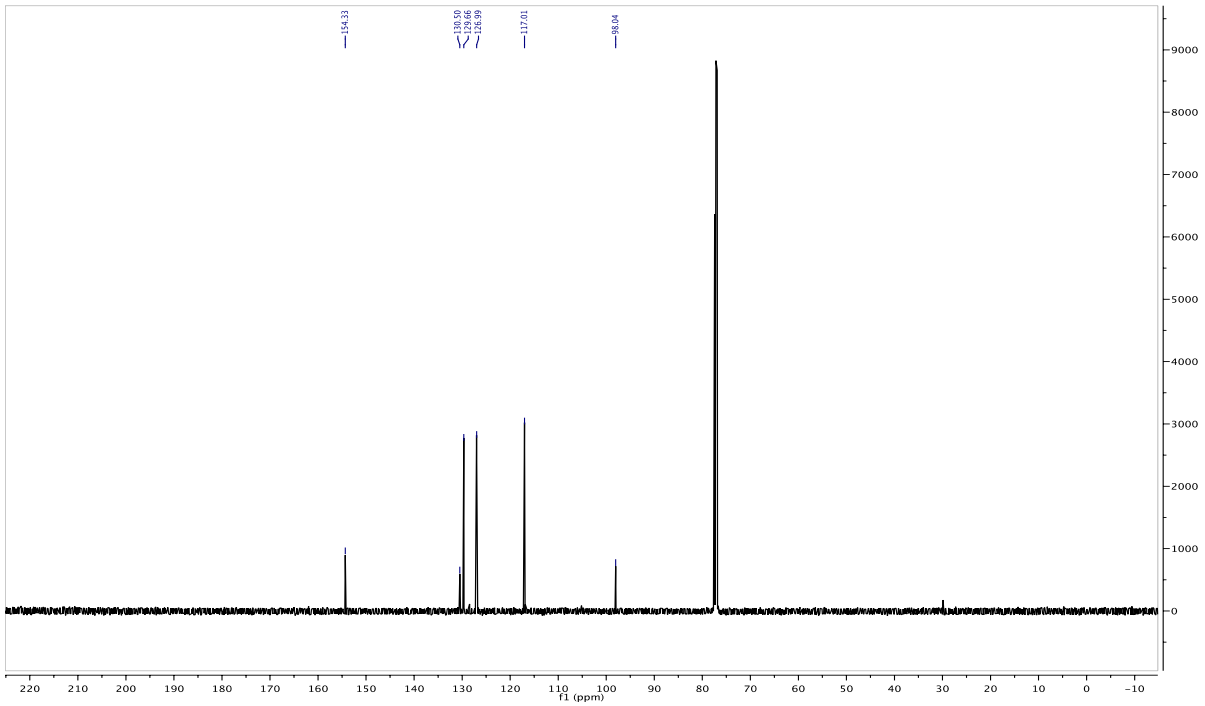

Figure 1.9.68 126 MHz ^{13}C NMR Spectrum of 1.15b

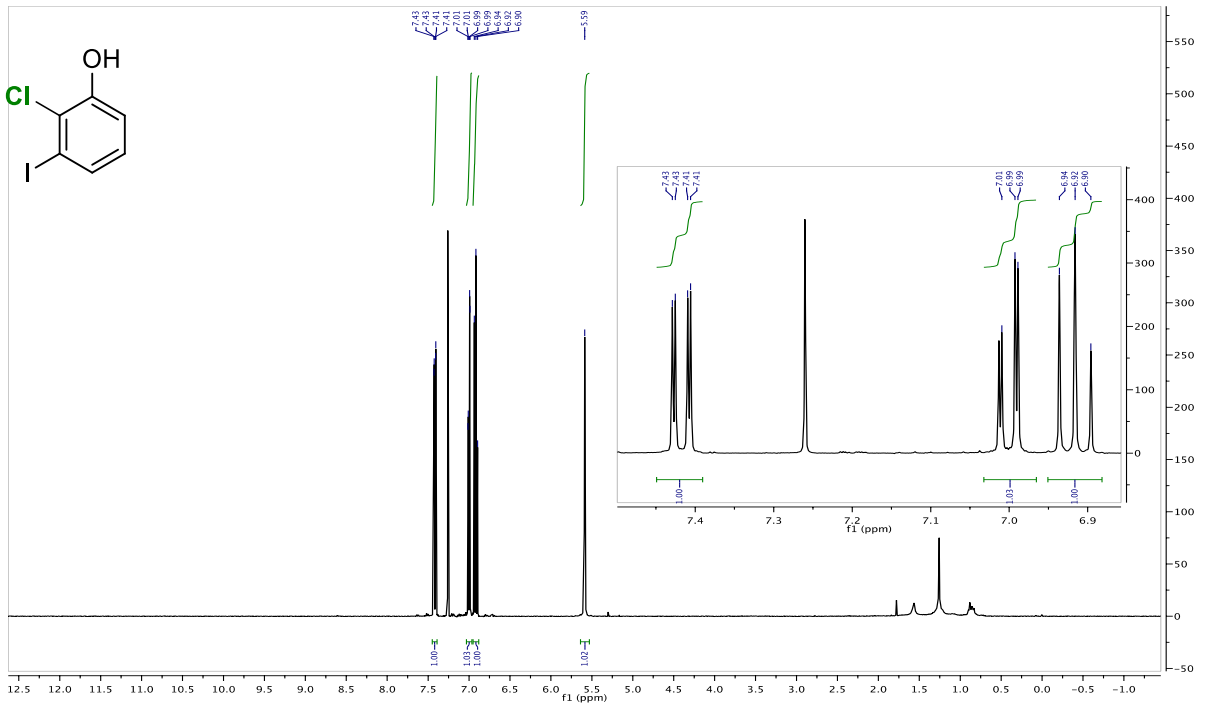

Figure 1.9.69 400 MHz ^{1}H NMR Spectrum of 1.15c

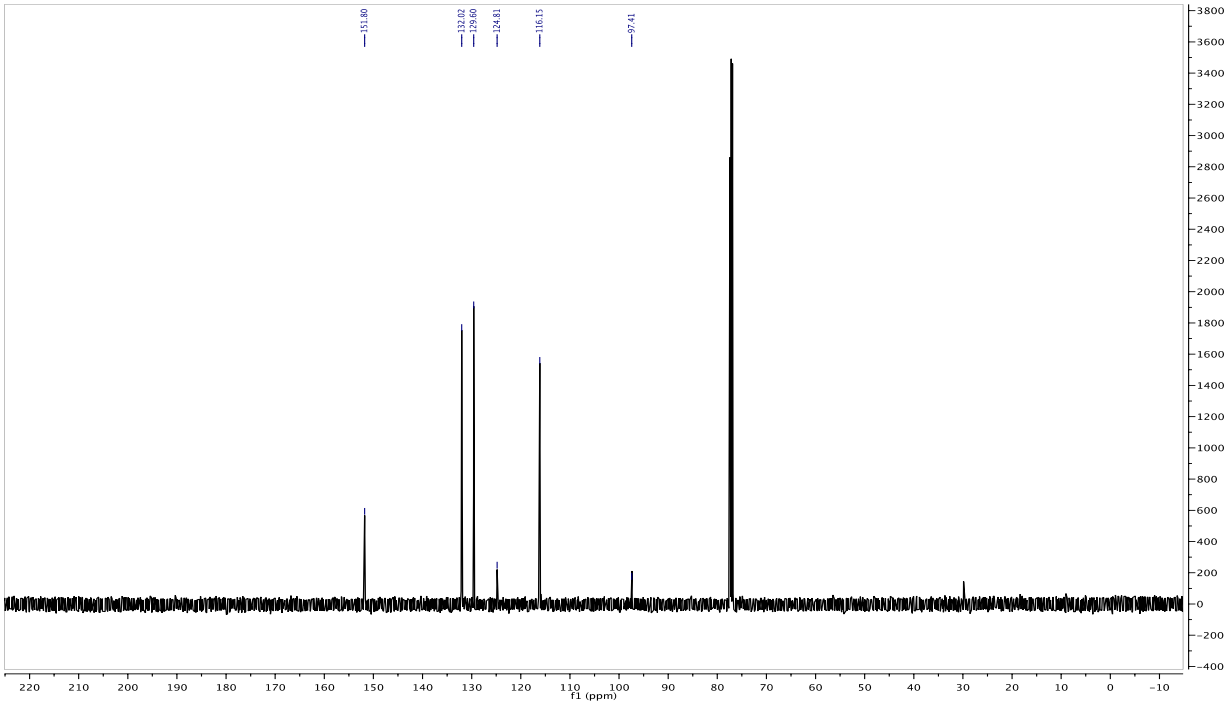

Figure 1.9.70 126 MHz ^{13}C NMR Spectrum of 1.15c

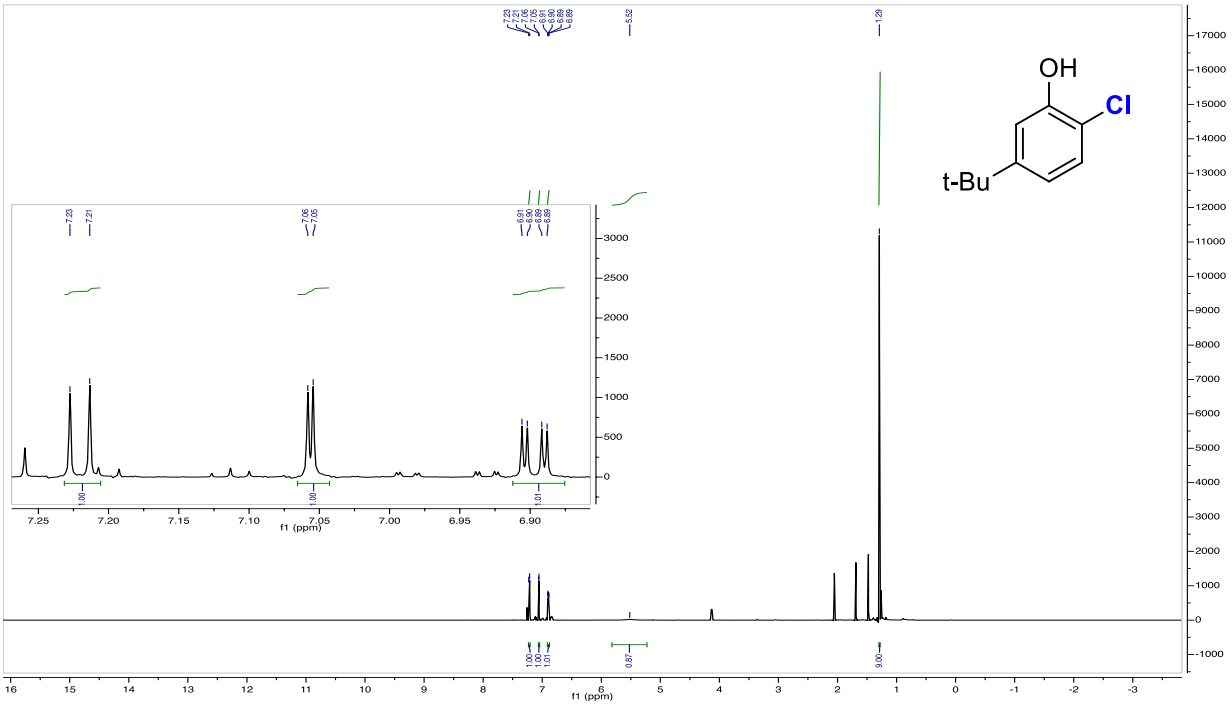

Figure 1.9.71 599 MHz ^{1}H NMR Spectrum of 1.16a

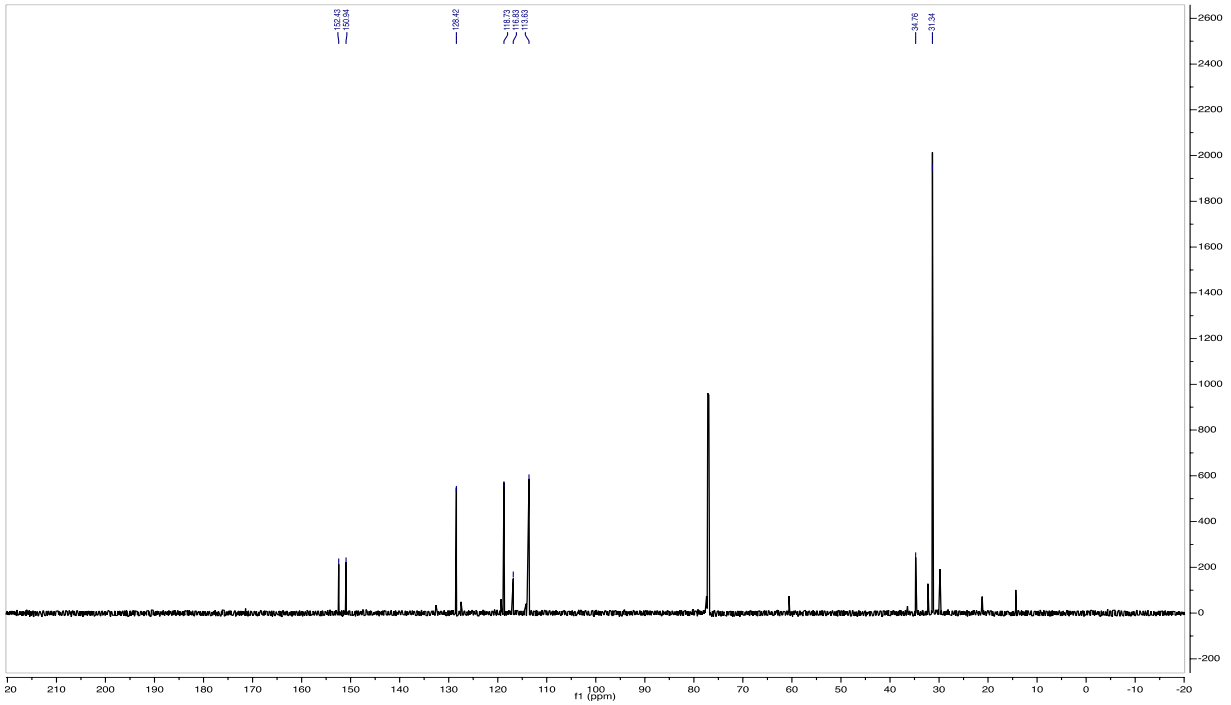

Figure 1.9.72 151 MHz ^{13}C NMR Spectrum of 1.16a

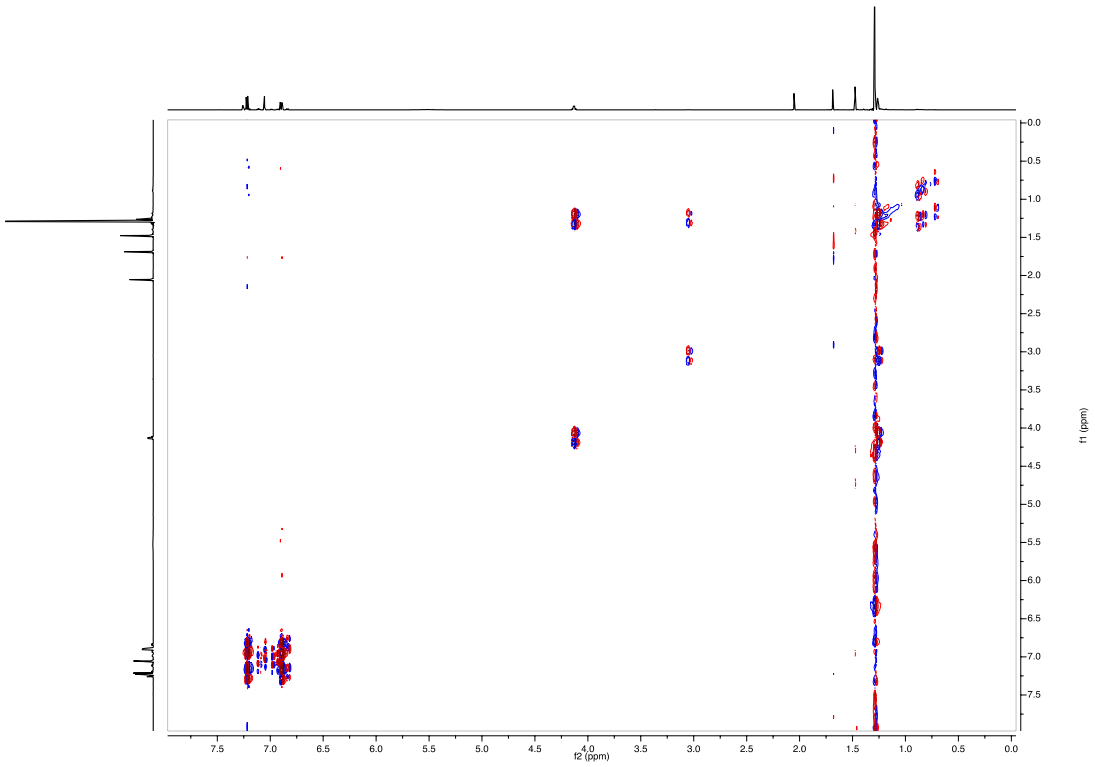

Figure 1.9.73 COSY (^{1}H/^{1}H) Spectrum of 1.16a

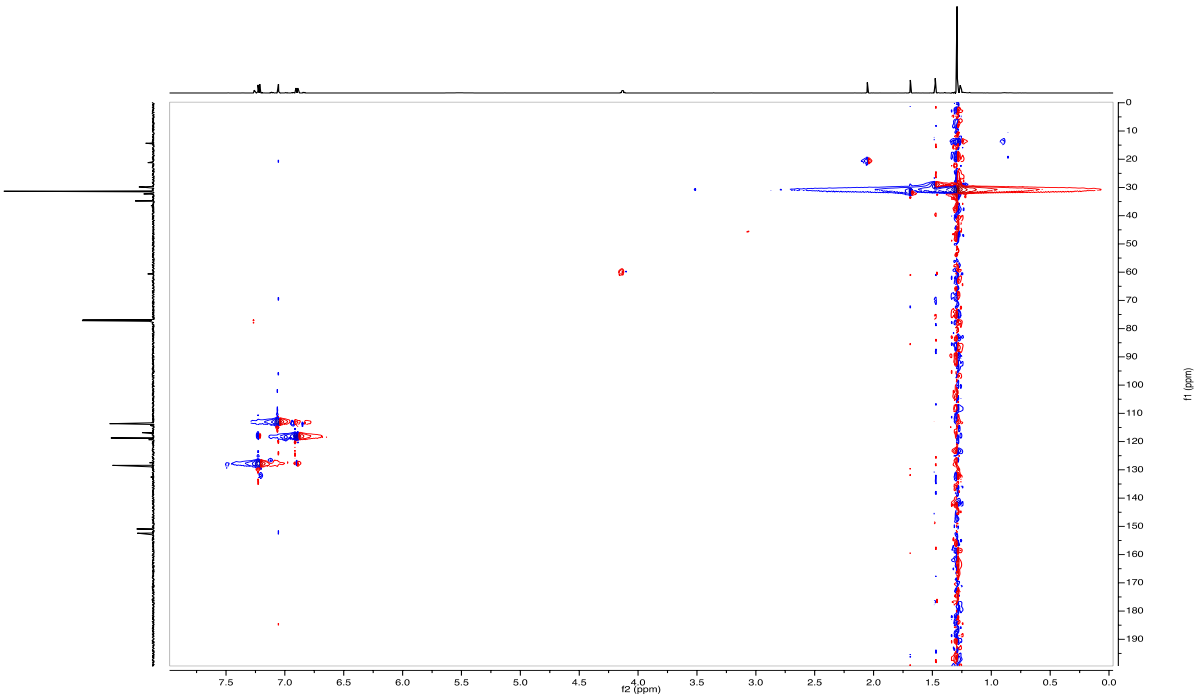

Figure 1.9.74 HSQC ($^{1}H/^{13}C$) Spectrum of 1.16a

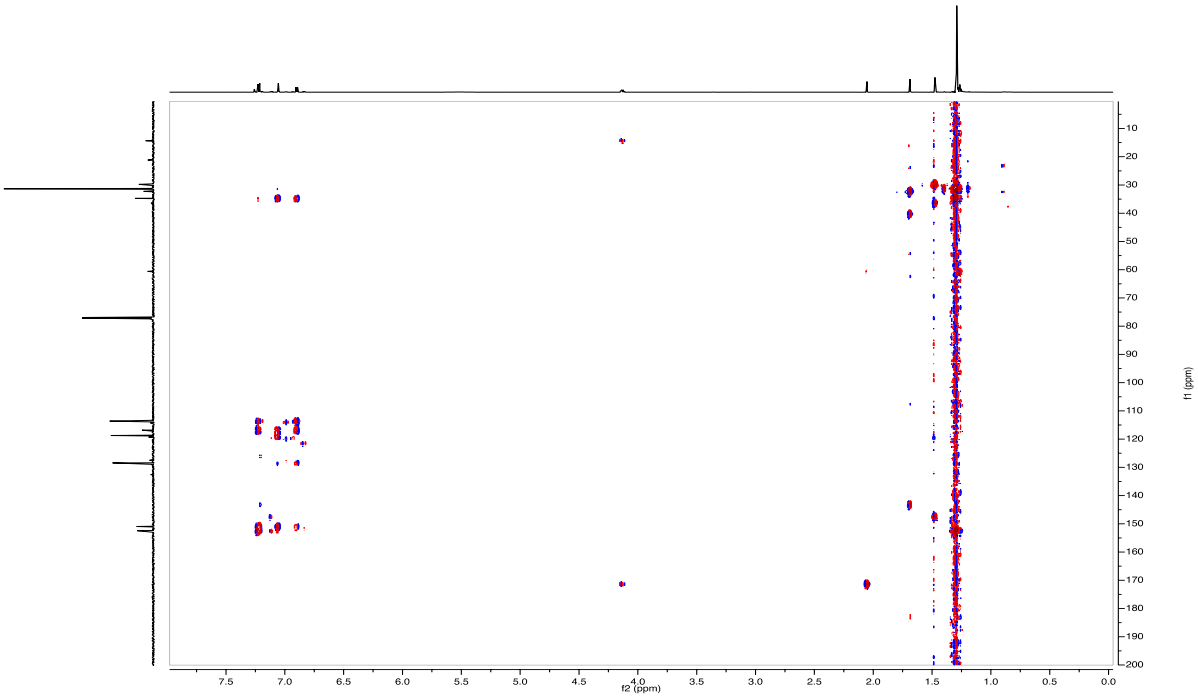

Figure 1.9.75 HMBC ($^{1}H/^{13}C$) Spectrum of 1.16a

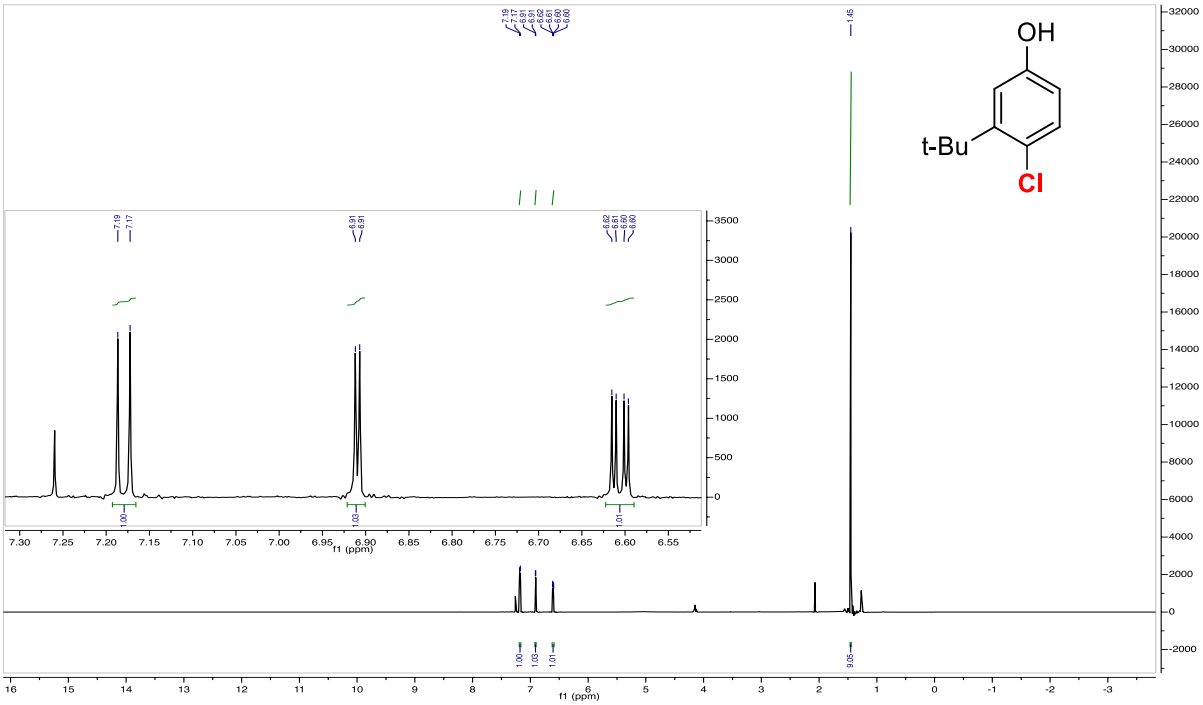

Figure 1.9.76 599 MHz ^{1}H NMR Spectrum of 1.16b

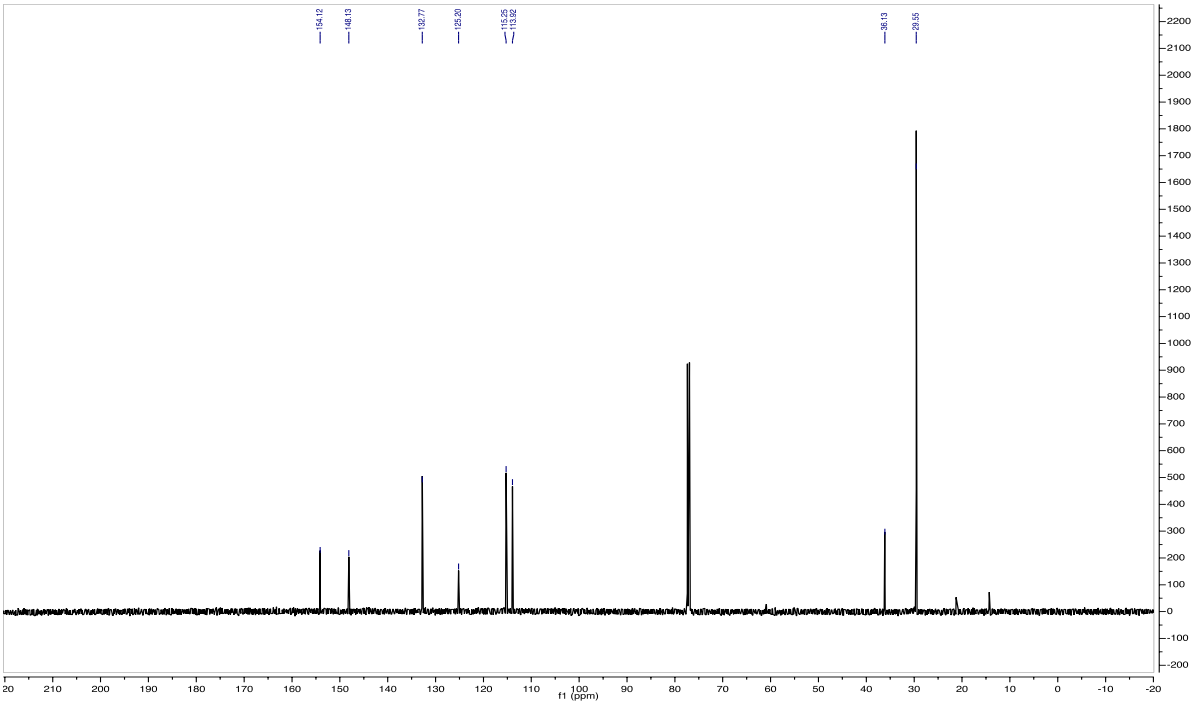

Figure 1.9.77 151 MHz ^{13}C NMR Spectrum of 1.16b

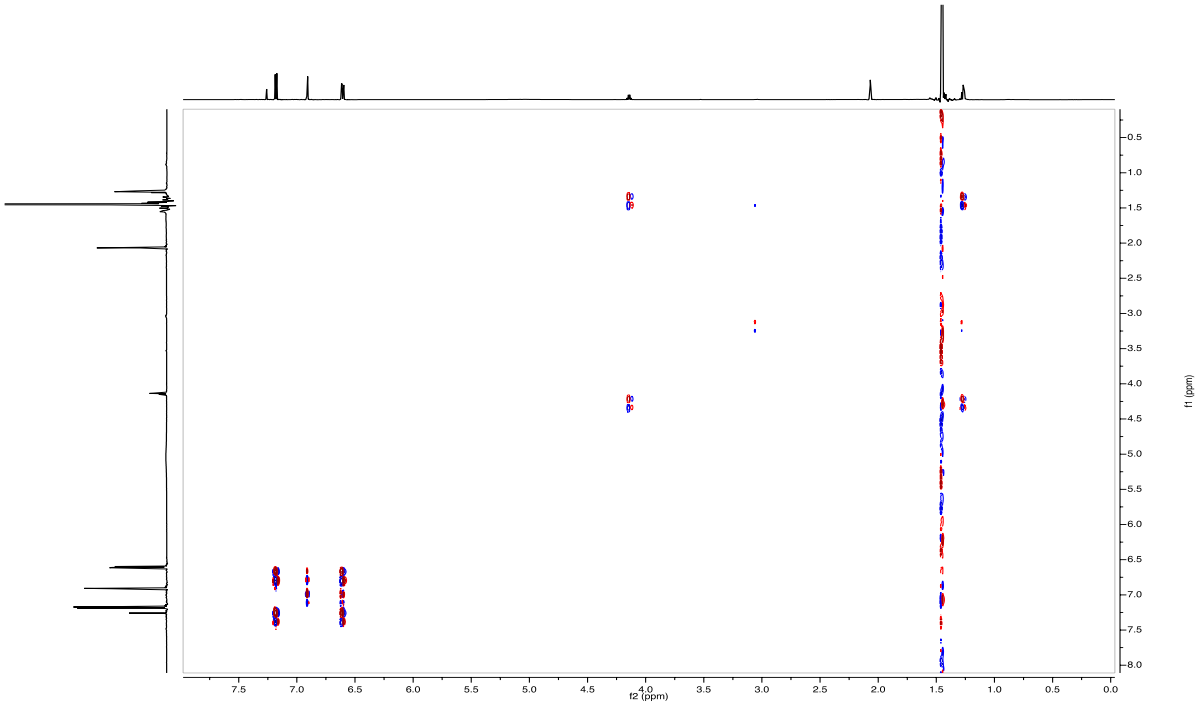

Figure 1.9.78 COSY ($^{1}H/^{1}H$) Spectrum of 1.16b

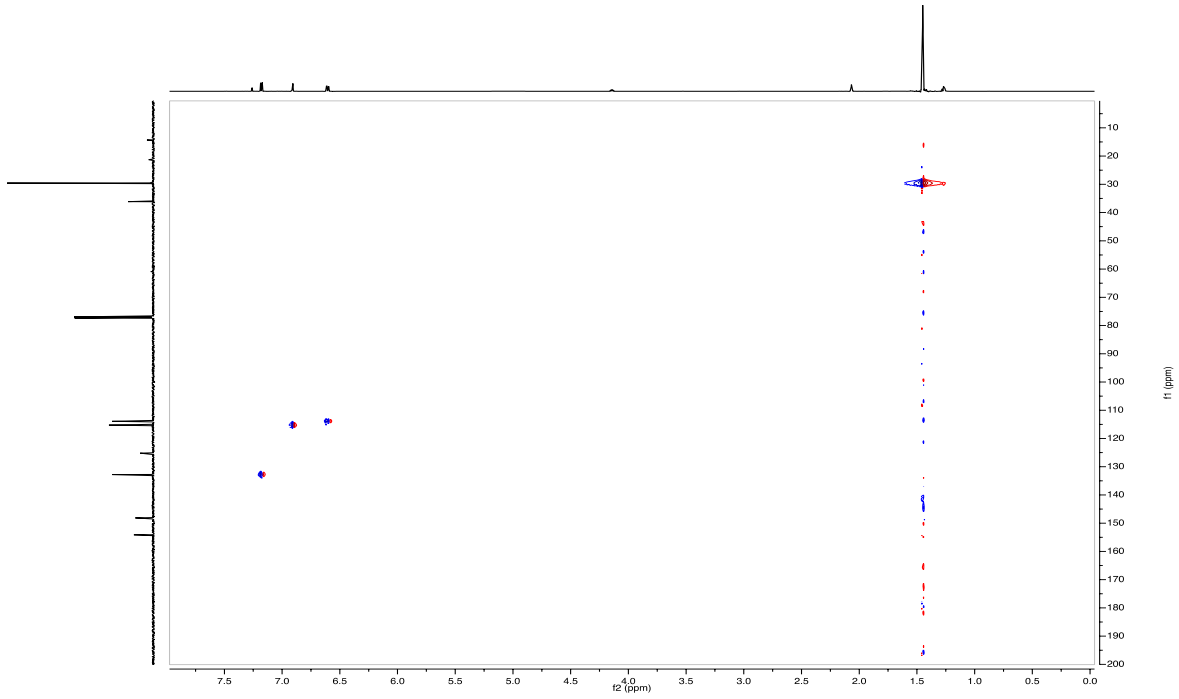

Figure 1.9.79 HSQC ($^{1}H/^{13}C$) Spectrum of 1.16b

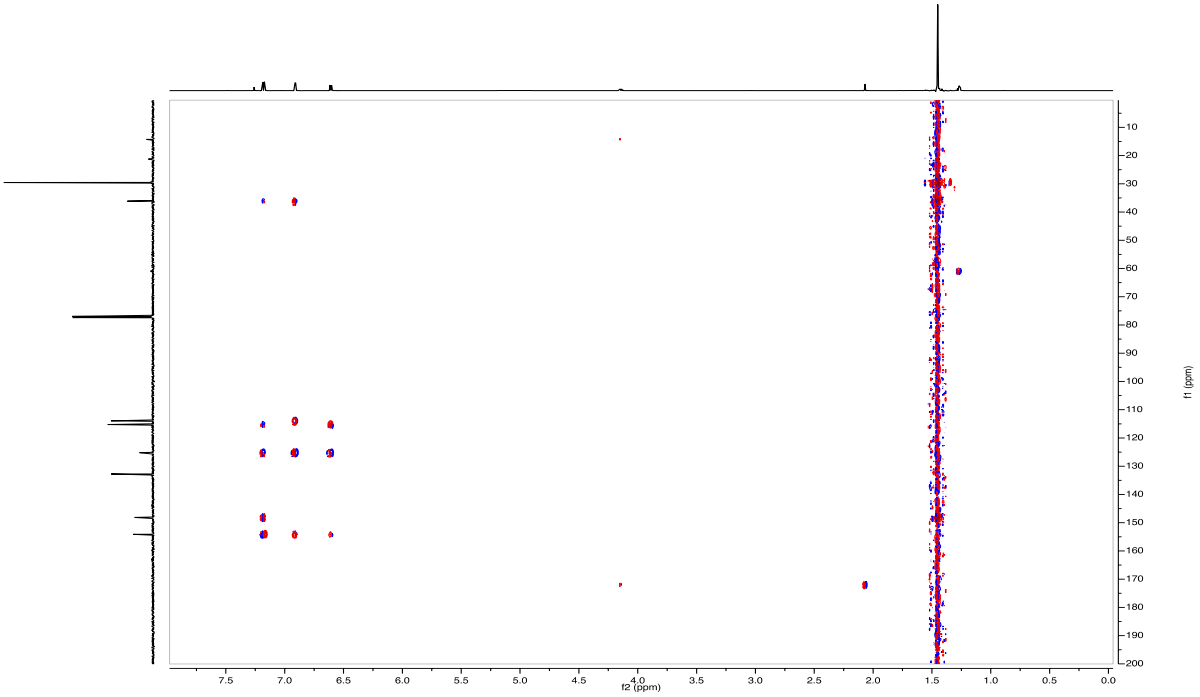

Figure 1.9.80 HMBC ($^{1}H/^{13}C$) Spectrum of 1.16b

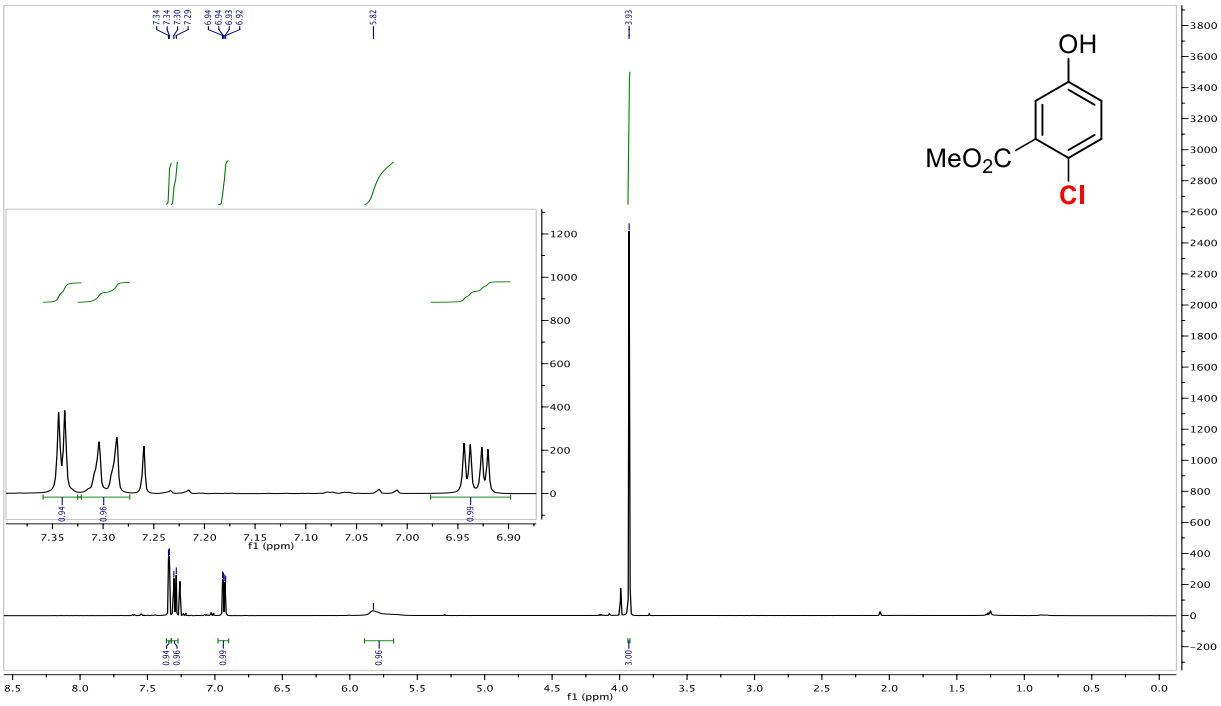

Figure 1.9.81 500 MHz ^{1}H NMR Spectrum of 1.17b

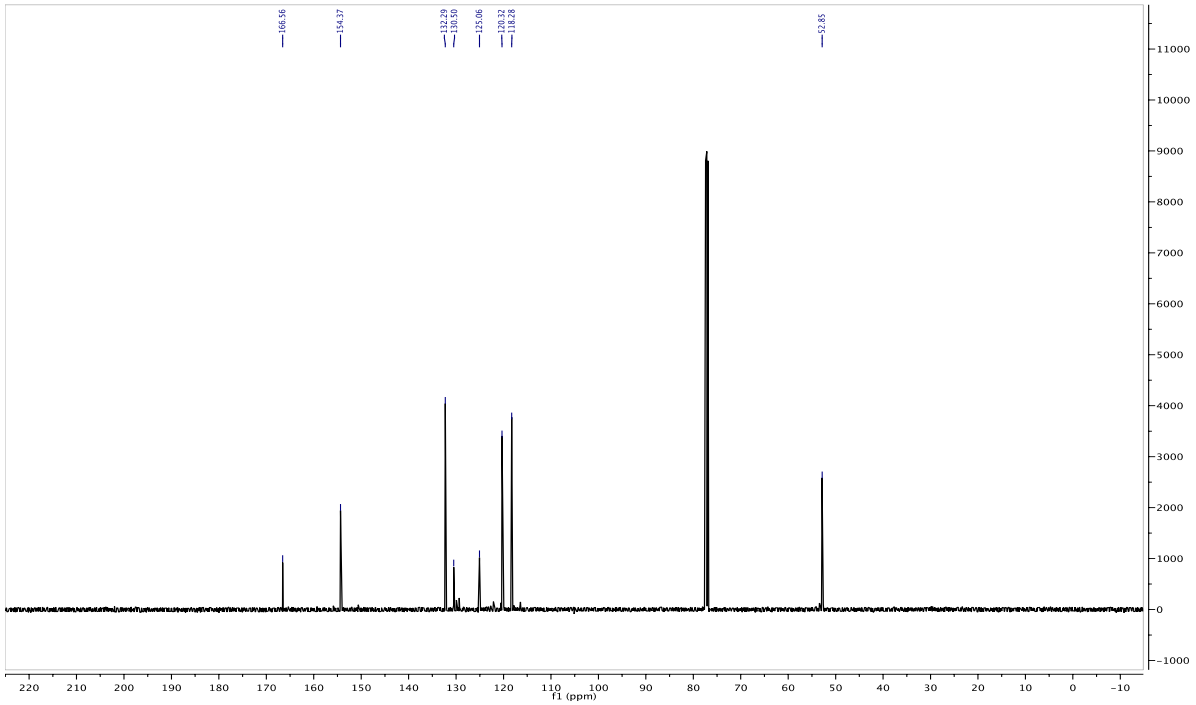

Figure 1.9.82 126 MHz ^{13}C NMR Spectrum of 1.17b

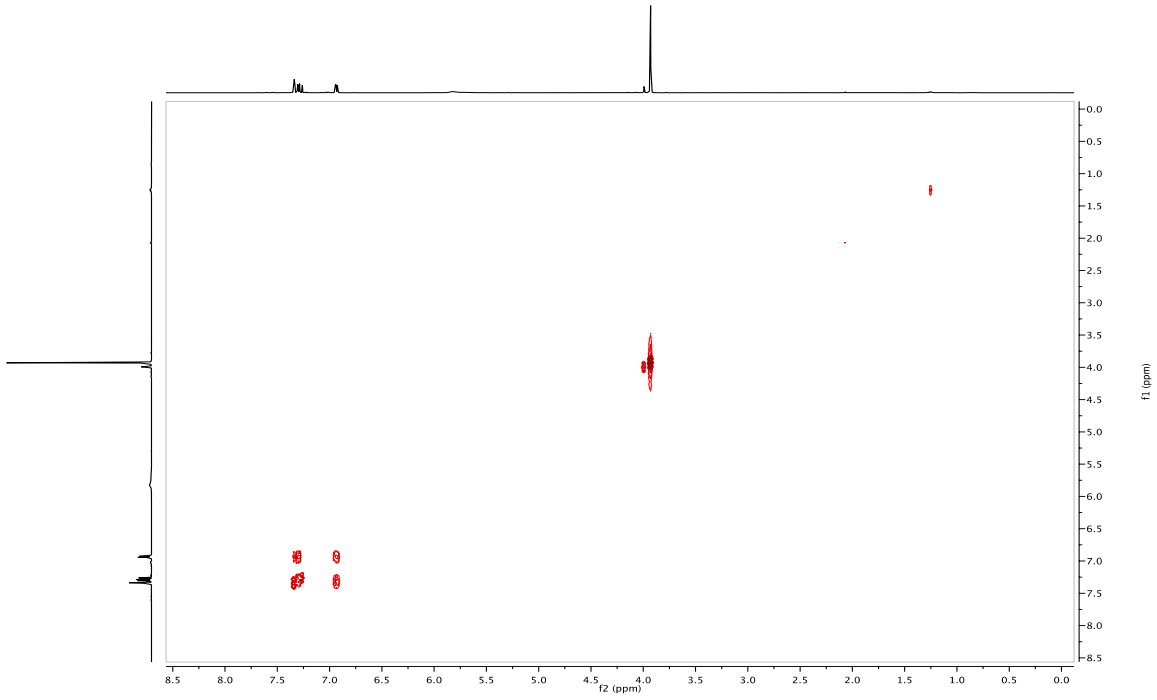

Figure 1.9.83 COSY (^{1}H/^{1}H) Spectrum of 1.17b

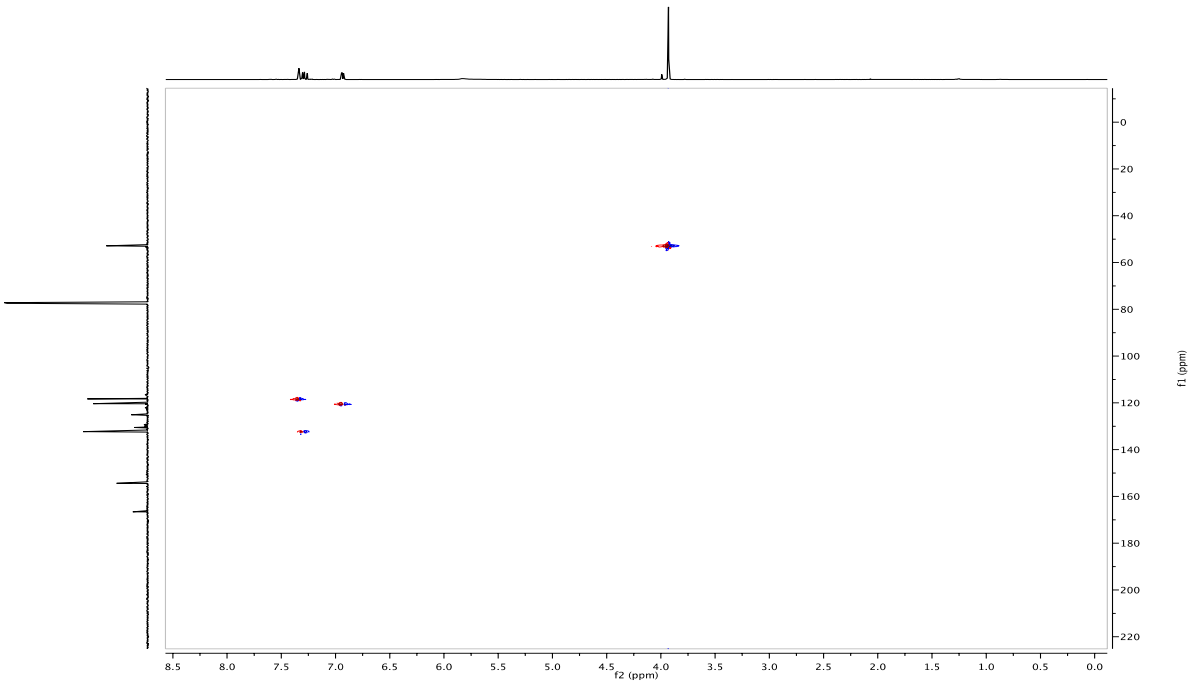

Figure 1.9.84 HSQC ($^{1}H/^{13}C$) Spectrum of 1.17b

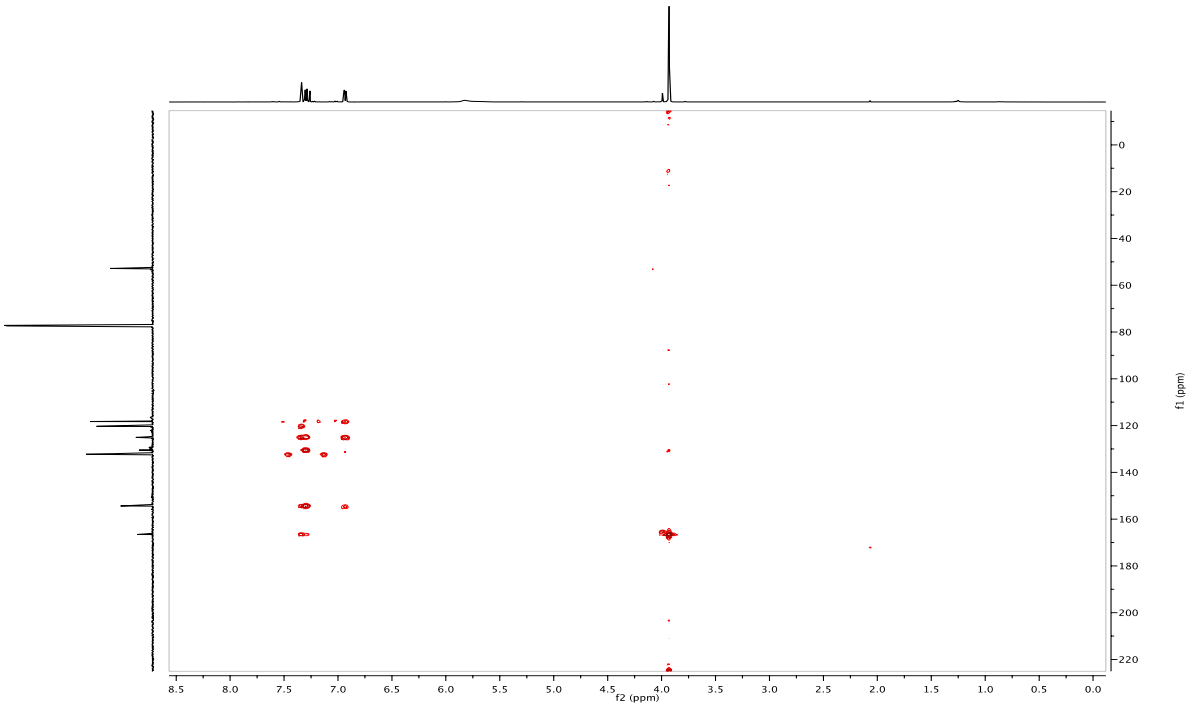

Figure 1.9.85 HMBC ($^{1}H/^{13}C$) Spectrum of 1.17b

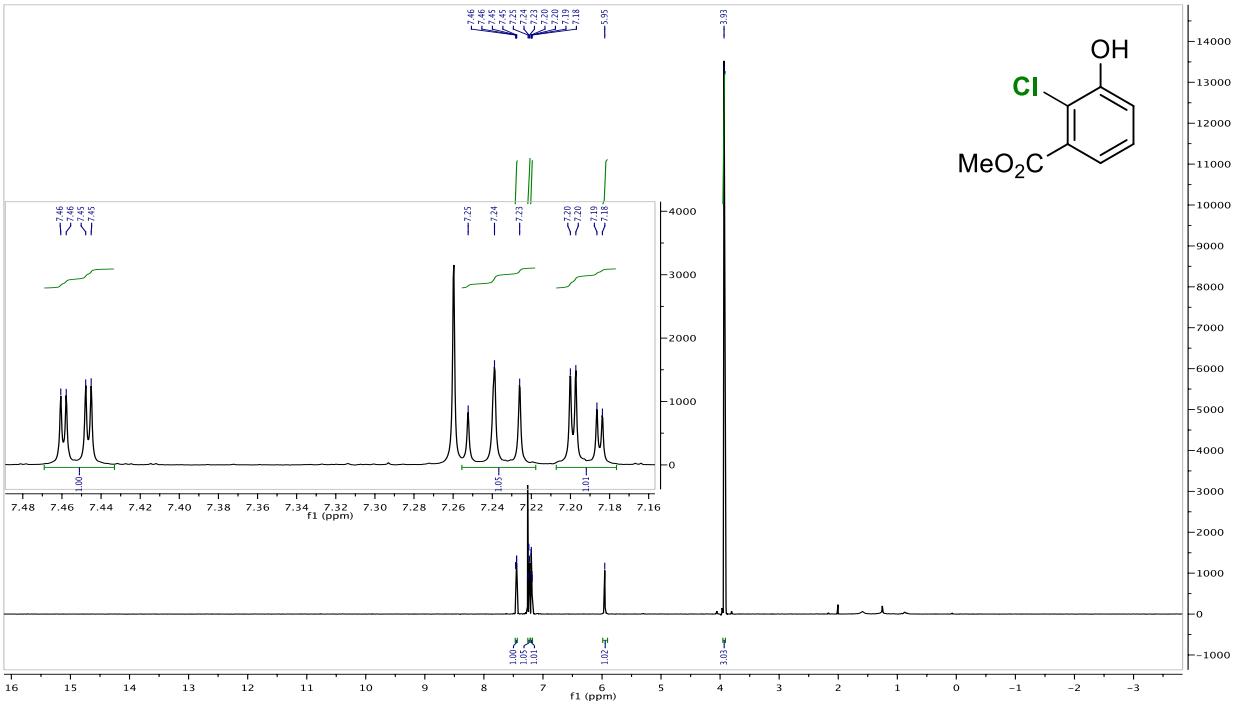

Figure 1.9.86 599 MHz ^{1}H NMR Spectrum of 1.17c

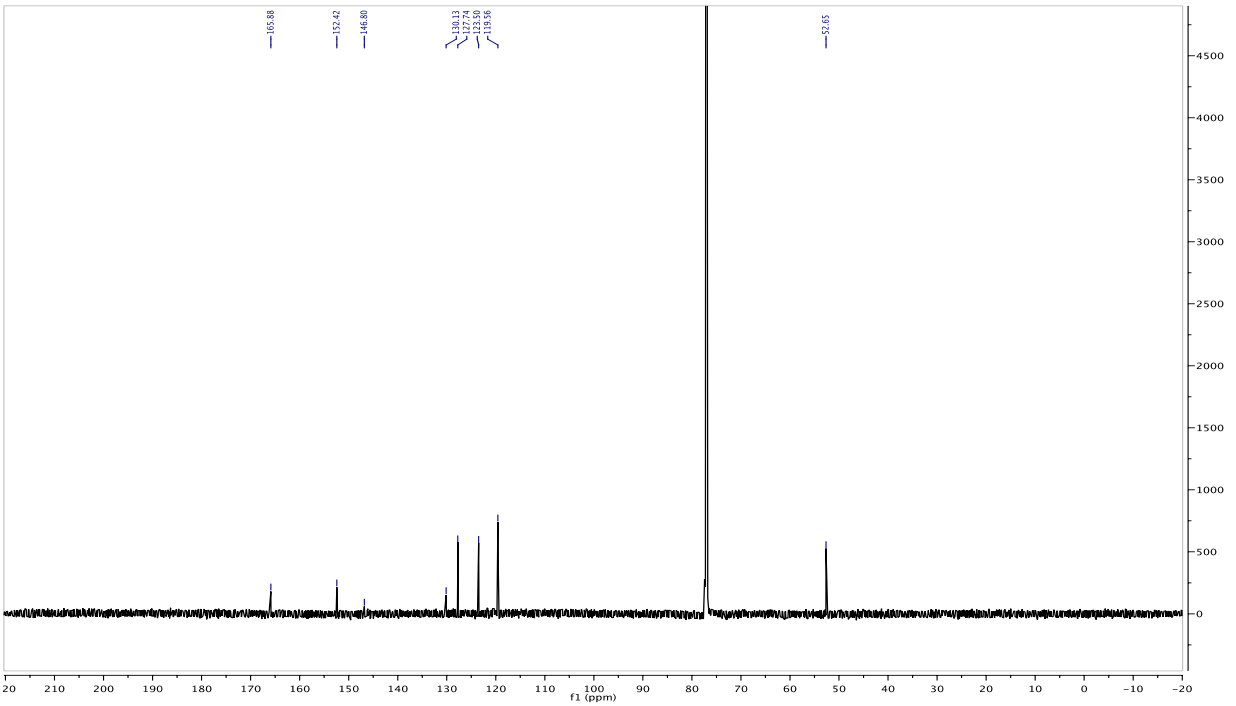

Figure 1.9.87 151 MHz ^{13}C NMR Spectrum of 1.17c

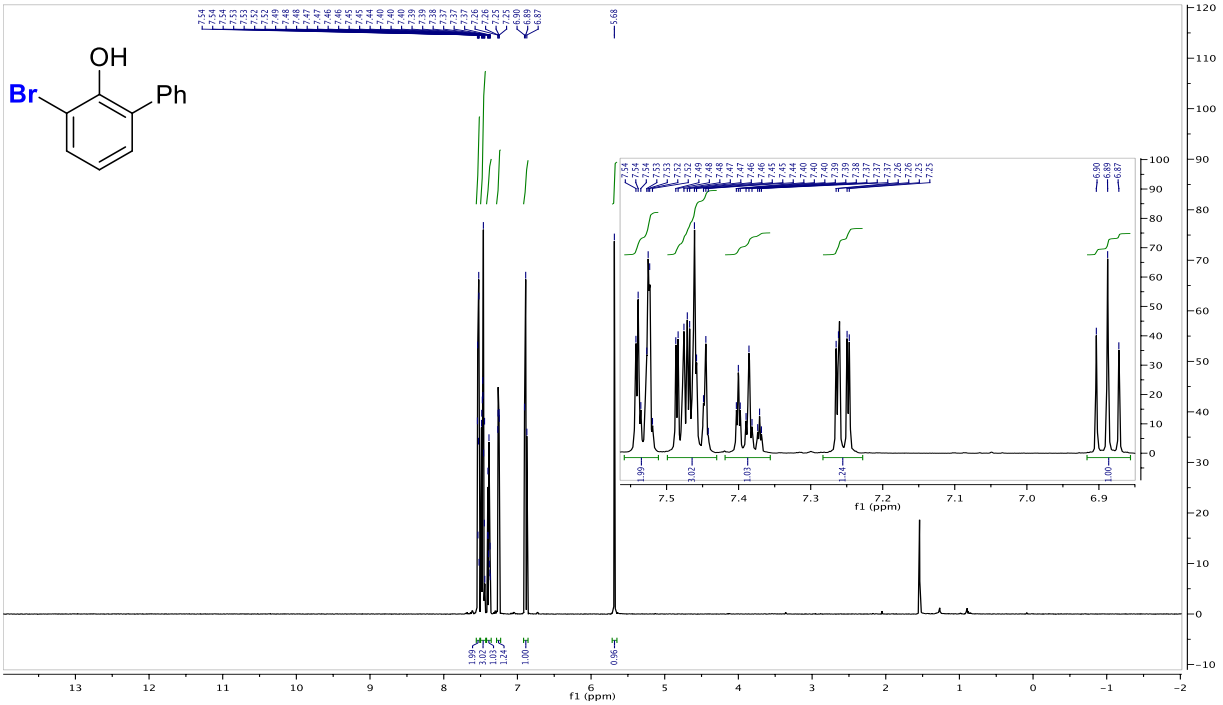

Figure 1.9.88 500 MHz ^{1}H NMR Spectrum of 1.8c

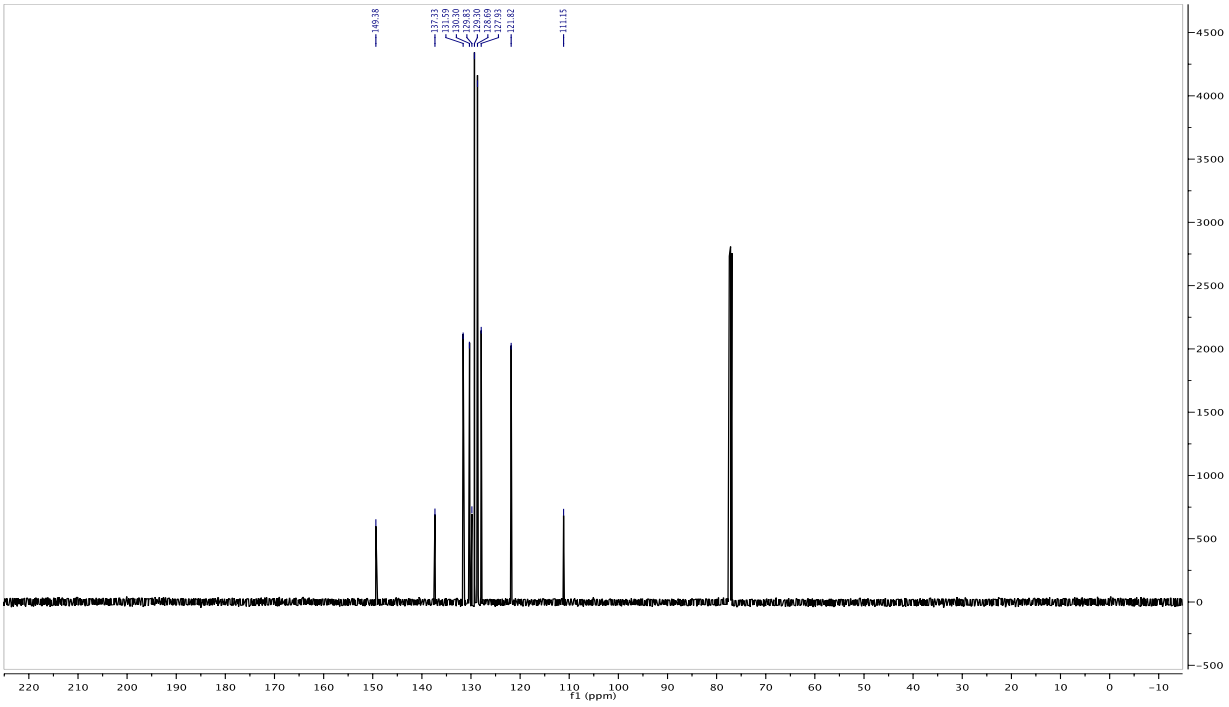

Figure 1.9.89 126 MHz ^{13}C NMR Spectrum of 1.8c

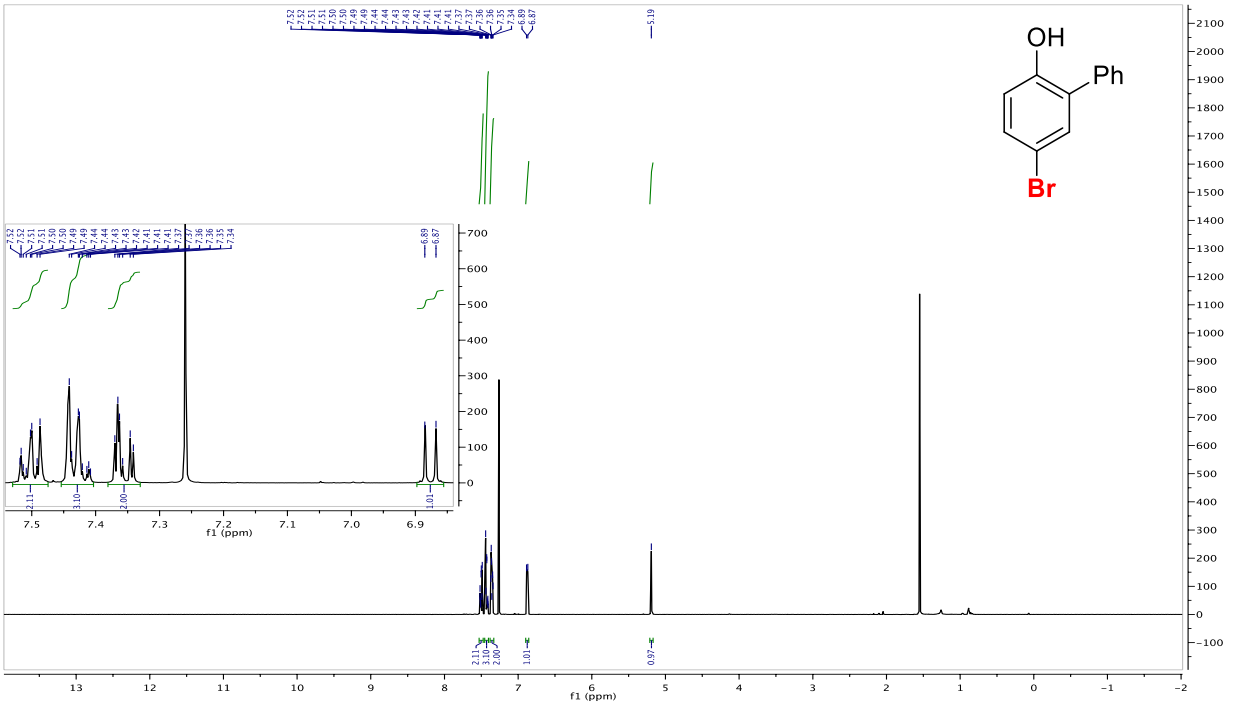

Figure 1.9.90 500 MHz ^{1}H NMR Spectrum of 1.8d

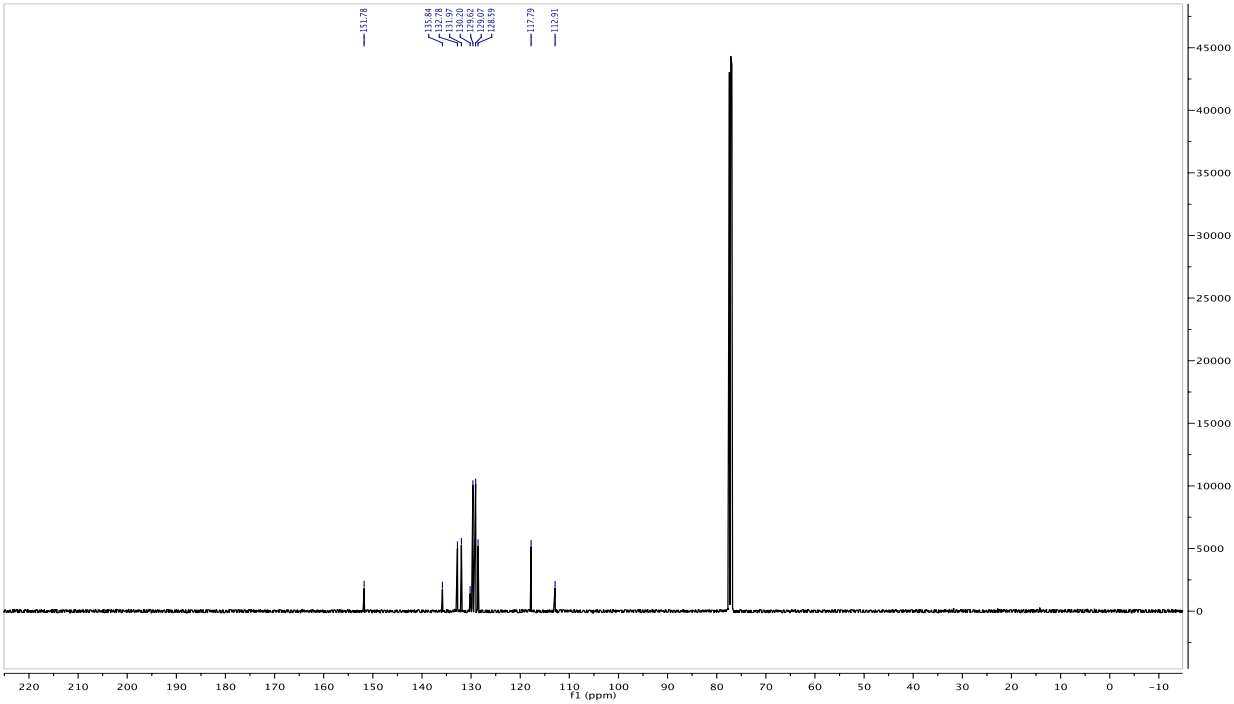

Figure 1.9.91 126 MHz ^{13}C NMR Spectrum of 1.8d

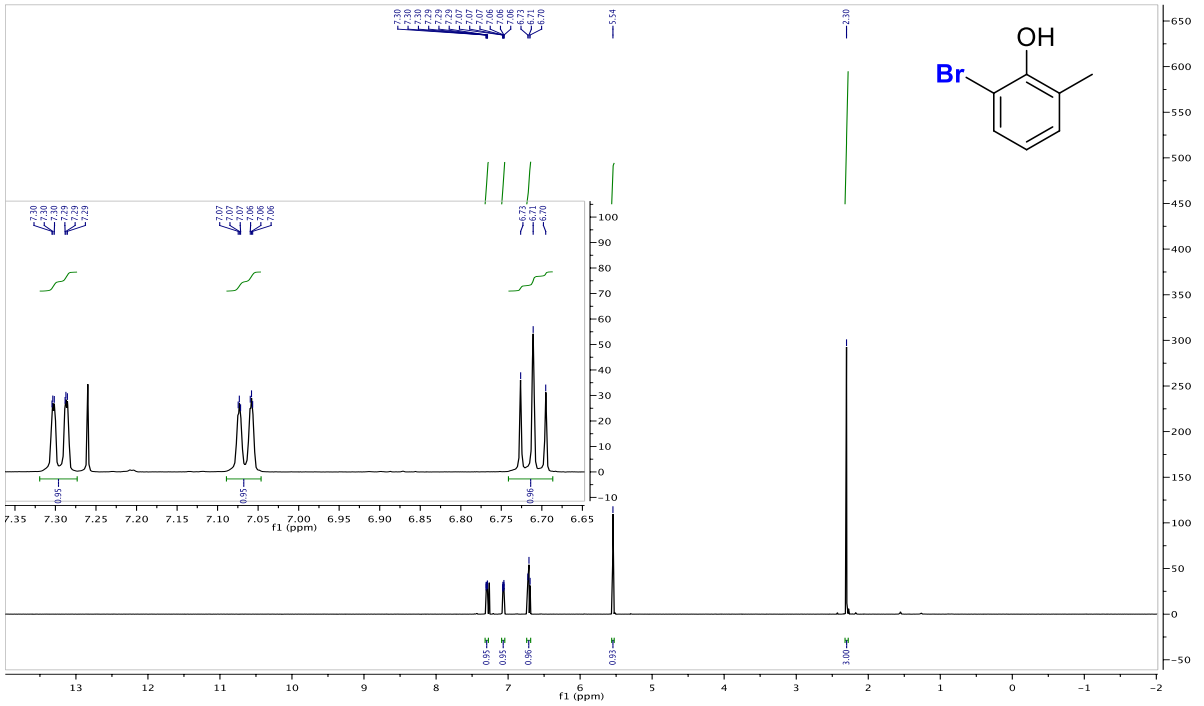

Figure 1.9.92 500 MHz ^{1}H NMR Spectrum of 1.18a

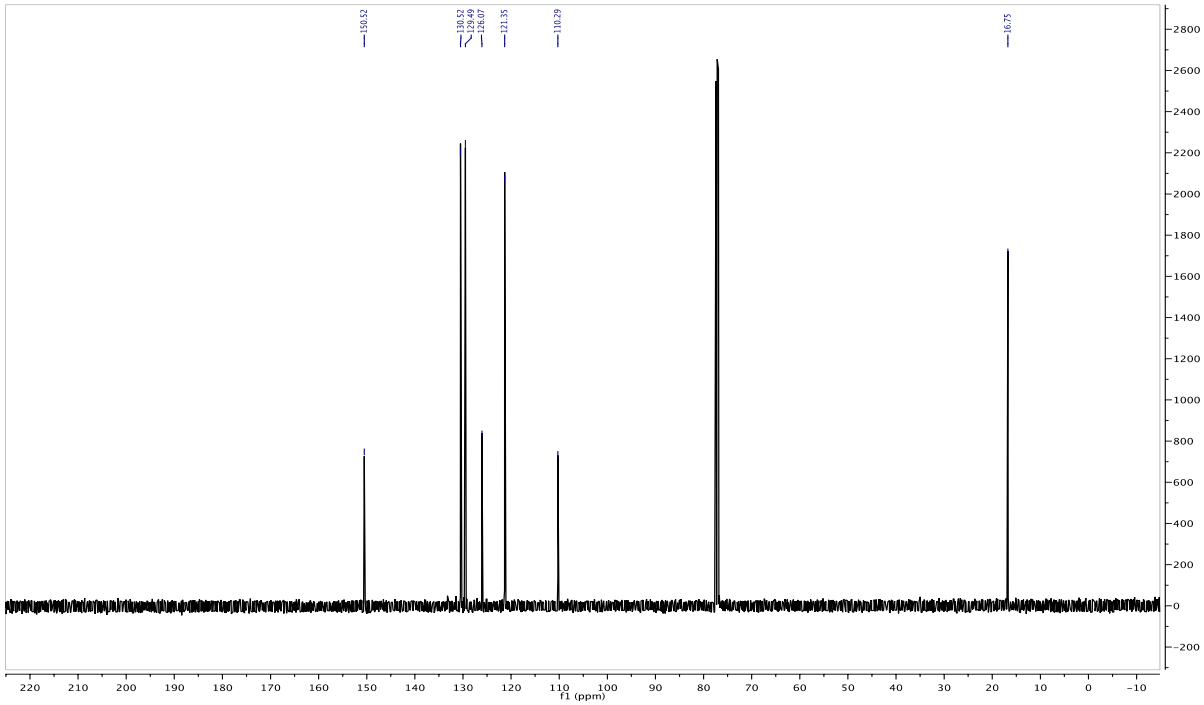

Figure 1.9.93 126 MHz ^{13}C NMR Spectrum of 1.8a

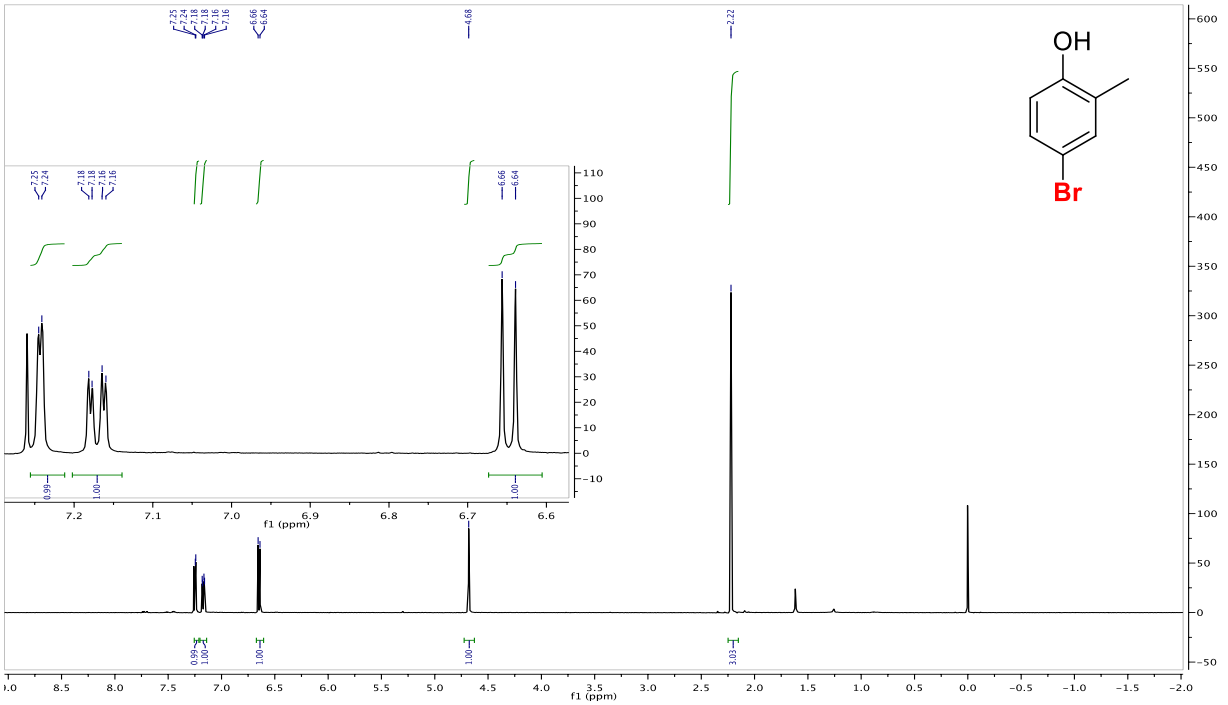

Figure 1.9.94 500 MHz ^{1}H NMR Spectrum of 1.18b

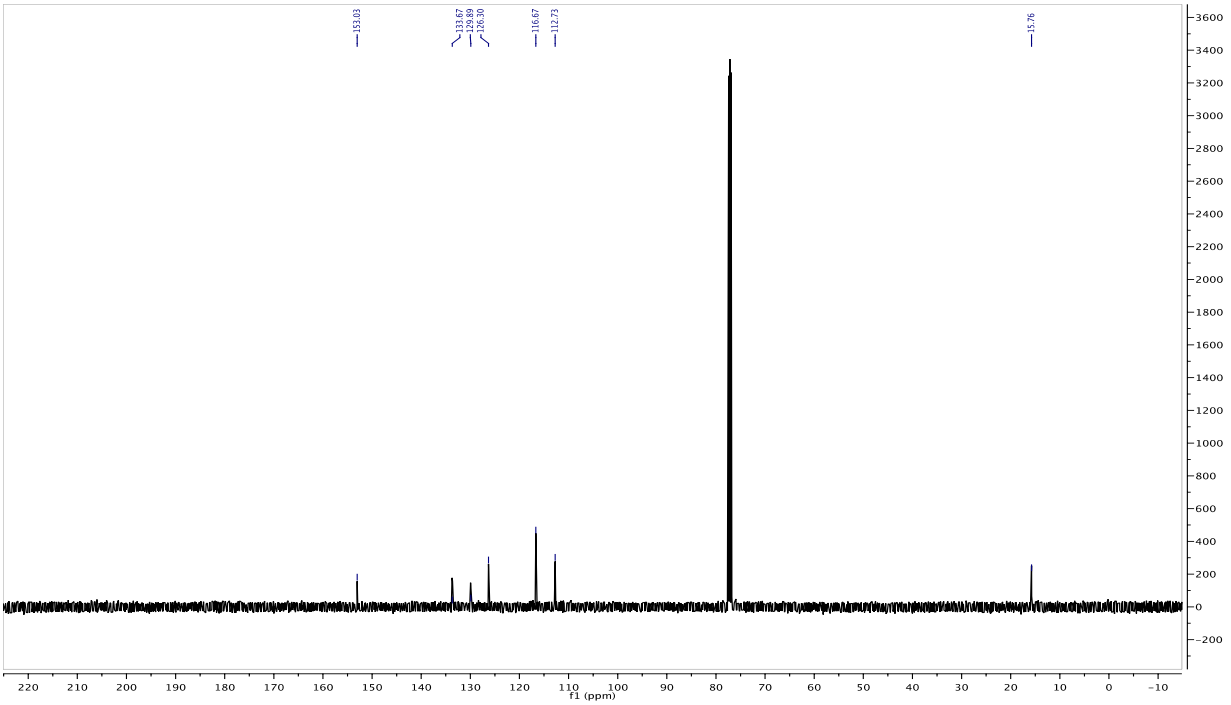

Figure 1.9.95 126 MHz ^{13}C NMR Spectrum of 1.18b

1.9.6 Spectral Data Examples for Determination of Ratios for Table 1.8.1

Spectral data examples represent one trial selected from the three trials performed. In the case of phenol exclusively, adding precise equivalents of NCS was crucial, due to over-chlorination. For *ortho*-selective catalyst **1.6**, adding too much NCS resulted in degraded *ortho*-selectivity, and adding too little NCS resulted in improved *ortho*-selectivity. The ratios for all three trials are reported below each of the example NMR spectra.

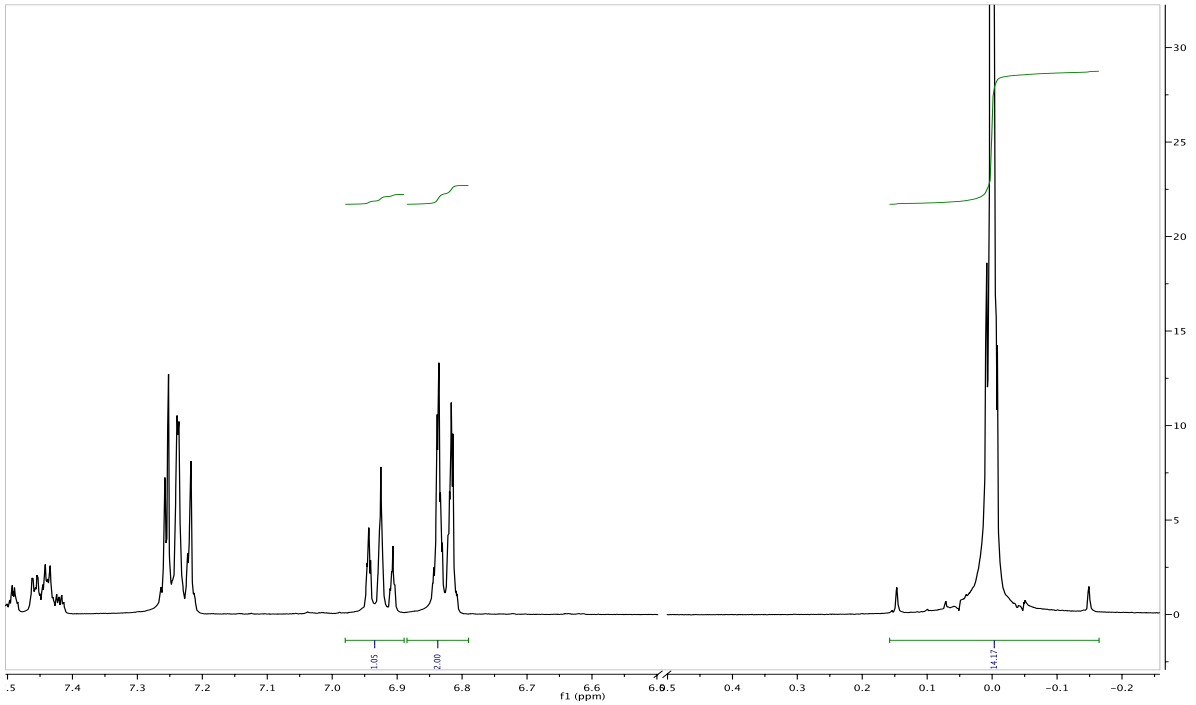

Figure 1.9.96 Example of 500 MHz ^{1}H NMR Spectrum for Table 1.8.1, Entry 1; t = 0 h

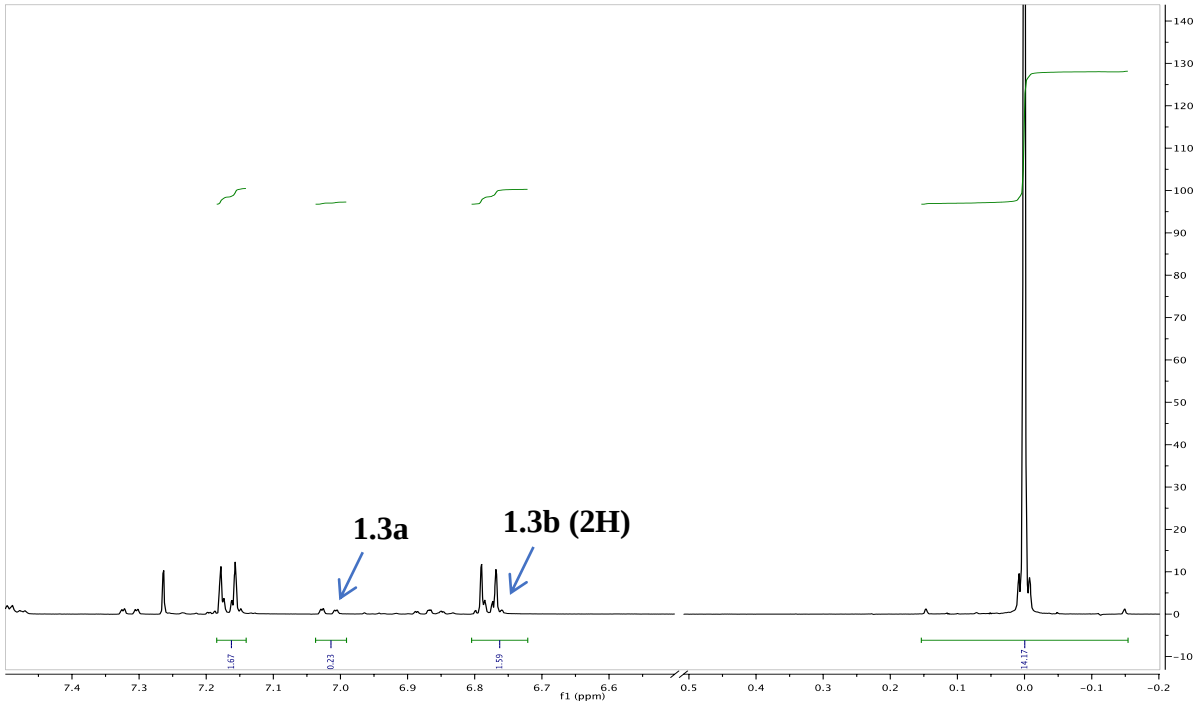

Figure 1.9.97 Example of 500 MHz ^{1}H NMR Spectrum for Table 1.8.1, Entry 1; t = 3 h

Trial 1: **1.3a**:**1.3b** as 1.0:5.4
Trial 2: **1.3a**:**1.3b** as 1.0:3.5
Trial 3: **1.3a**:**1.3b** as 1.0:3.1

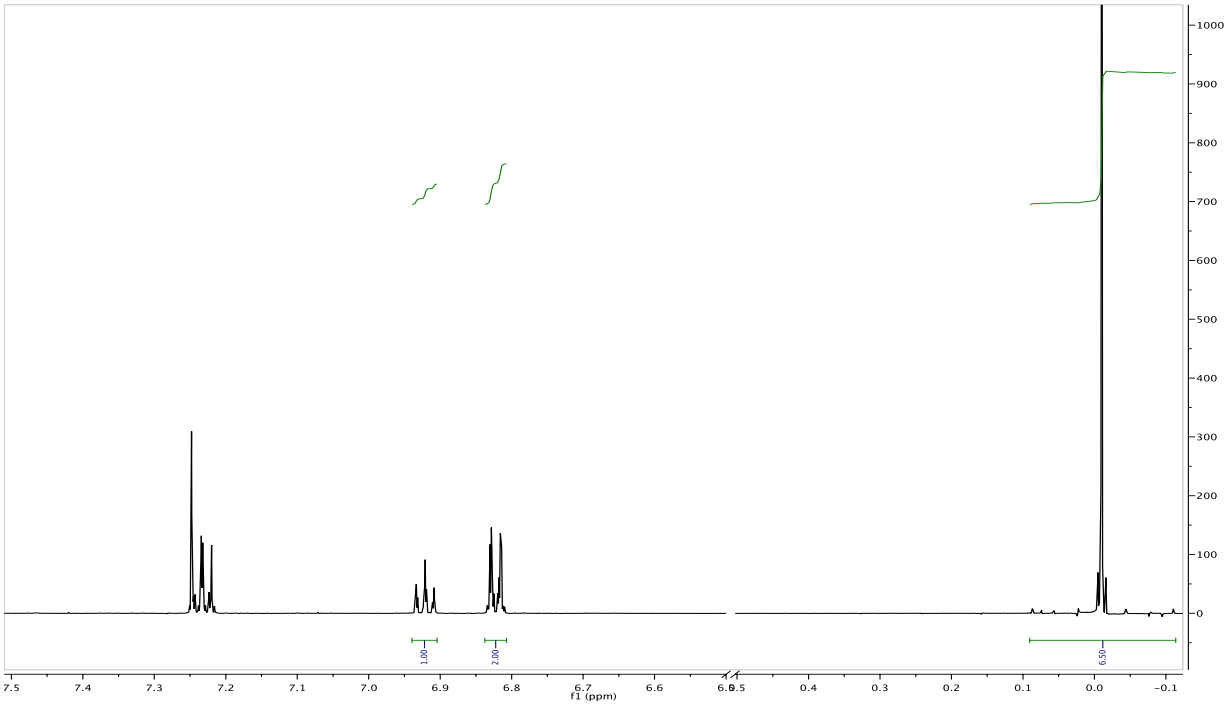

Figure 1.9.98 Example of 500 MHz ^{1}H NMR Spectrum for Table 1.8.1, Entry 7; t = 0 h

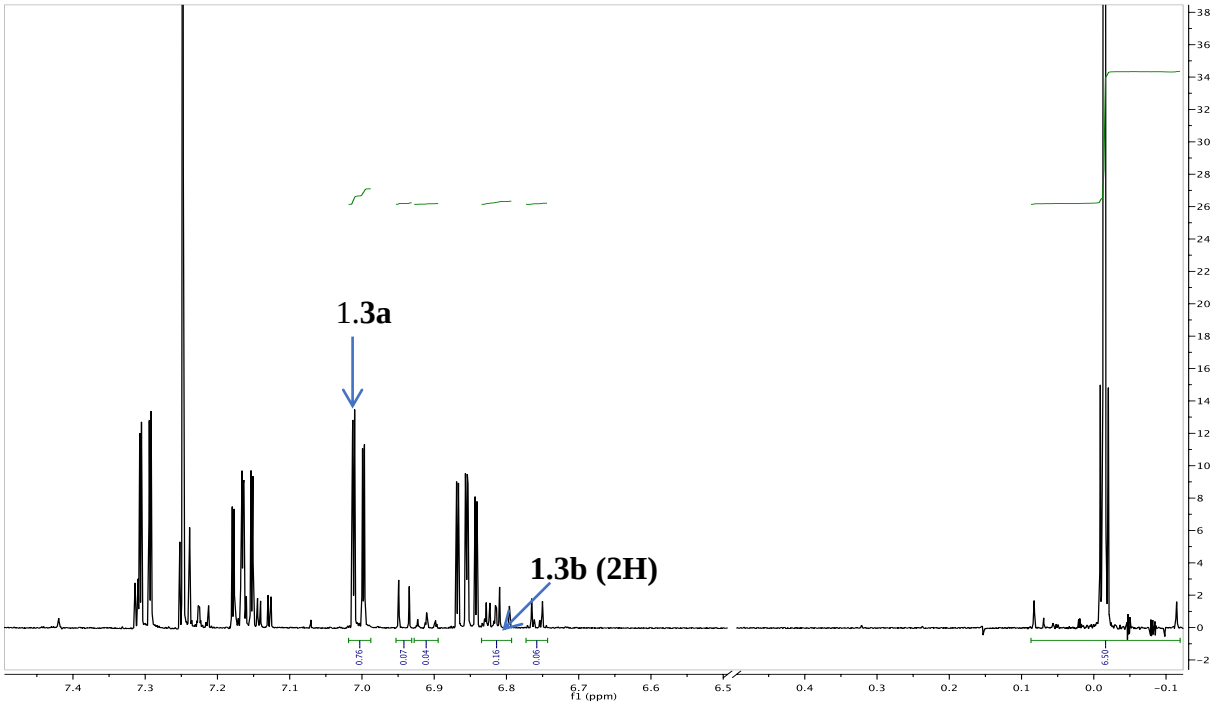

Figure 1.9.99 Example of 500 MHz ^{1}H NMR Spectrum for Table 1.8.1, Entry 7; t = 3 h

Trial 1: **1.3a**:**1.3b** as 25:1.0
Trial 2: **1.3a**:**1.3b** as 18:1.0
Trial 3: **1.3a**:**1.3b** as 38:1.0

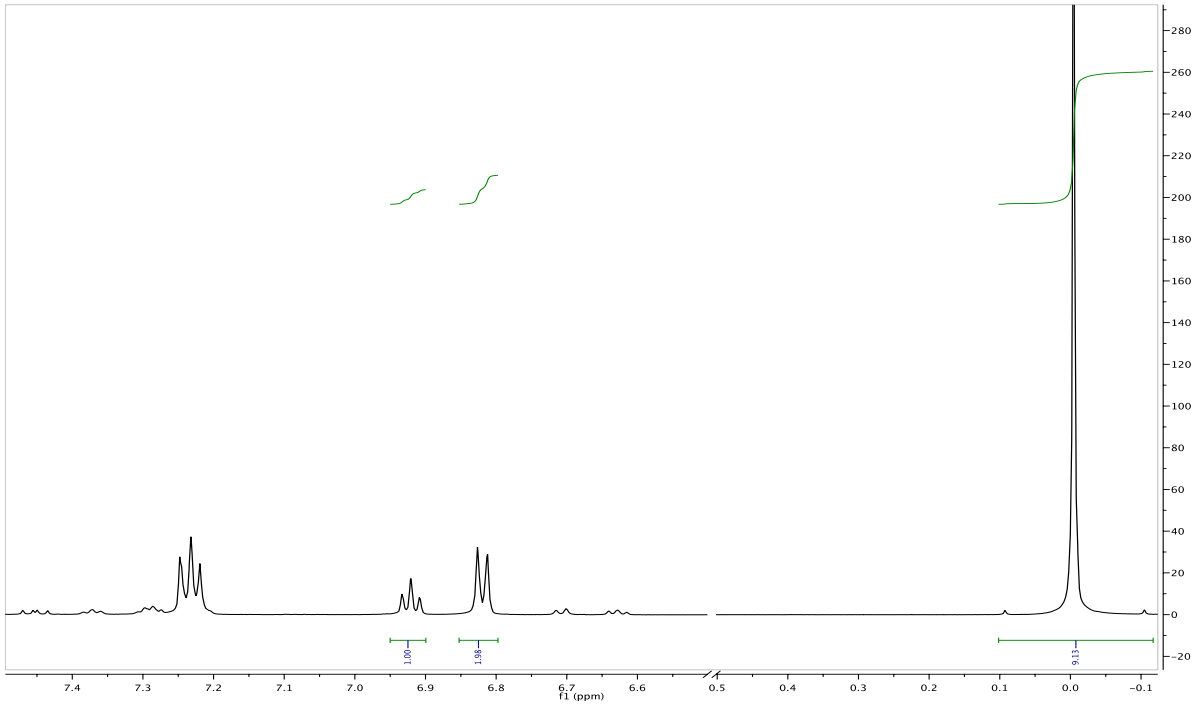

Figure 1.9.100 Example of 500 MHz ^{1}H NMR Spectrum for Table 1.8.1, Entry 10; t = 0 h

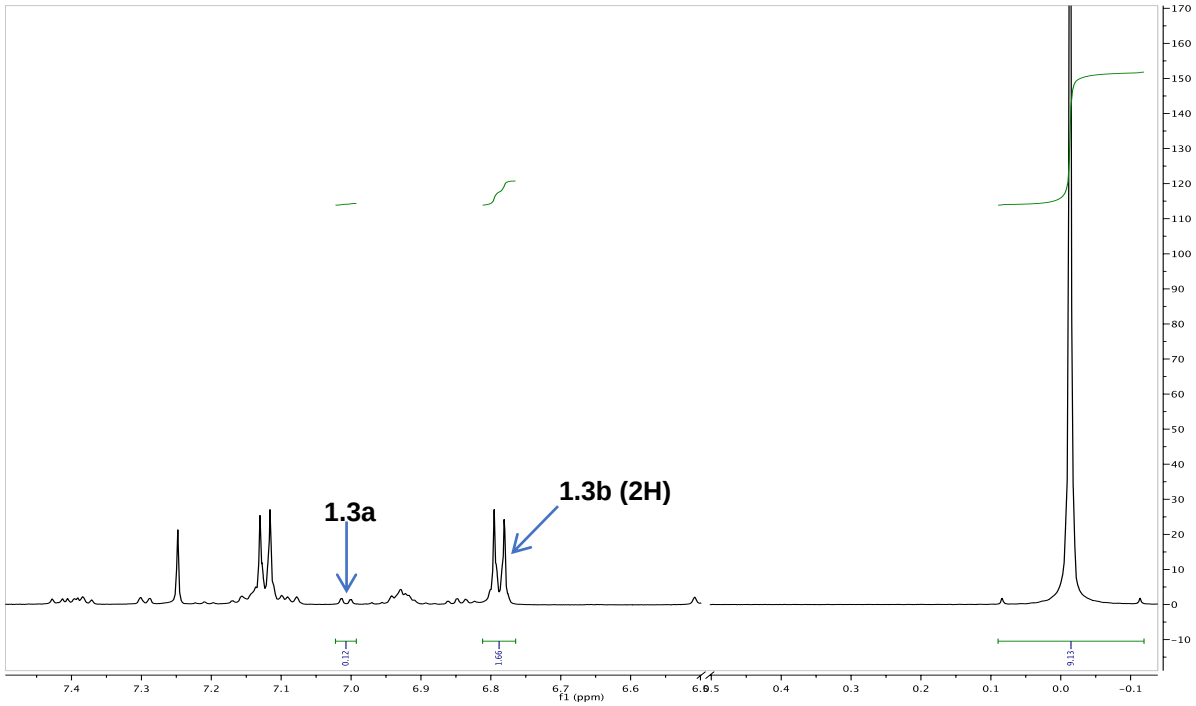

Figure 1.9.101 Example of 500 MHz ^{1}H NMR Spectrum for Table 1.8.1, Entry 10; t = 3 h

Trial 1: **1.3a**:**1.3b** as 1.0:6.9
Trial 2: **1.3a**:**1.3b** as 1.0:7.1
Trial 3: **1.3a**:**1.3b** as 1.0:7.4

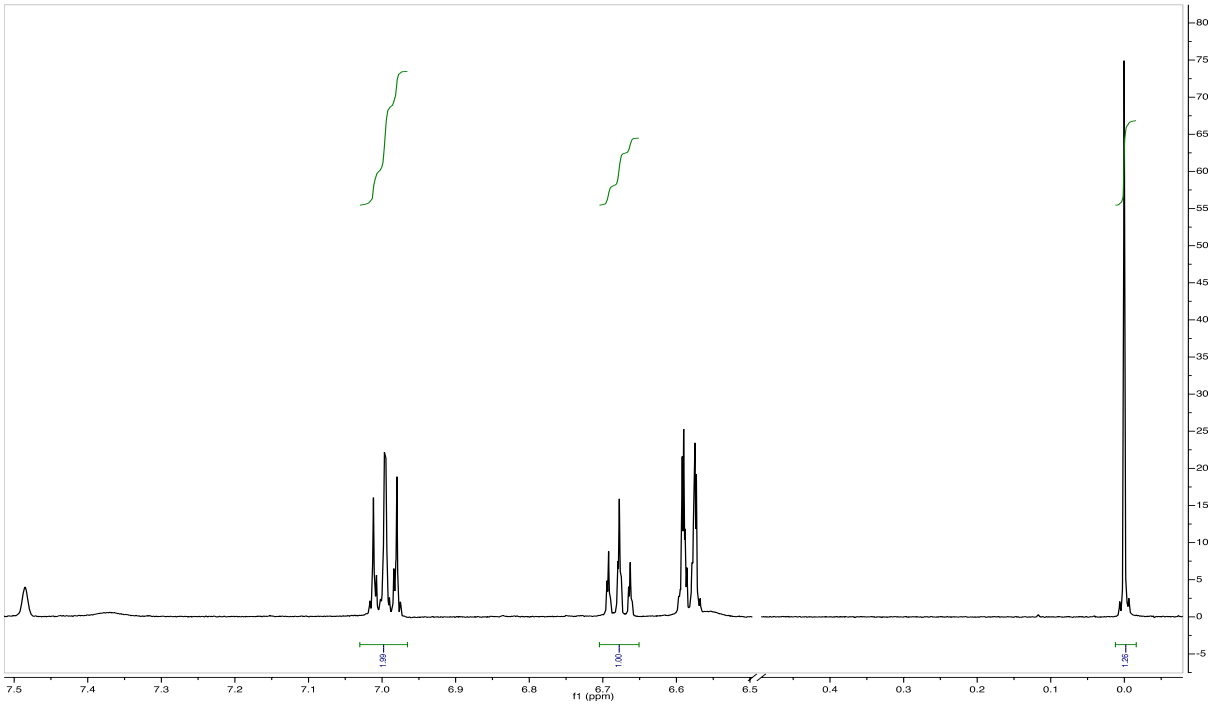

Figure 1.9.102 Example of 500 MHz ^{1}H NMR Spectrum for Table 1.8.1, Entry 11; t = 0 h

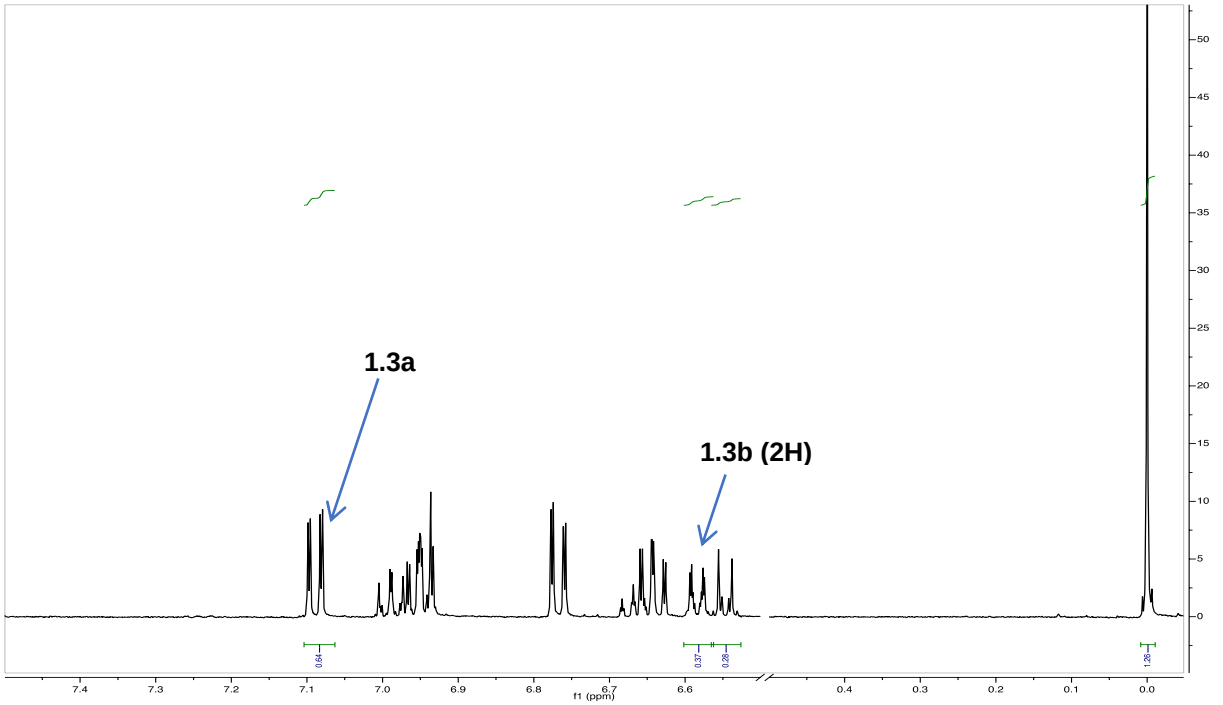

Figure 1.9.103 Example of 500 MHz ^{1}H NMR Spectrum for Table 1.8.1, Entry 11; t = 3 h

Trial 1: **3.3a**:**3.3b** as 1.0:4.6
Trial 2: **3.3a**:**3.3b** as 1.0:4.6
Trial 3: **3.3a**:**3.3b** as 1.0:4.8

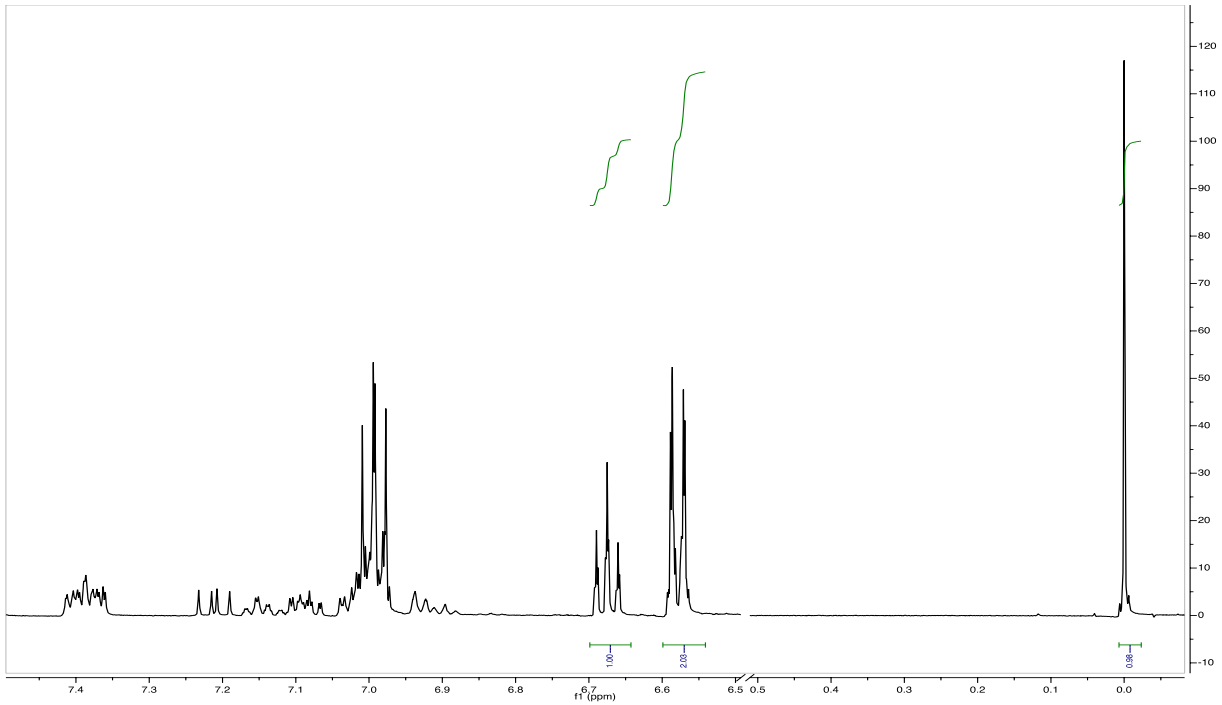

Figure 1.9.104 Example of 500 MHz ^{1}H NMR Spectrum for Table 1.8.1, Entry 12; t = 0 h

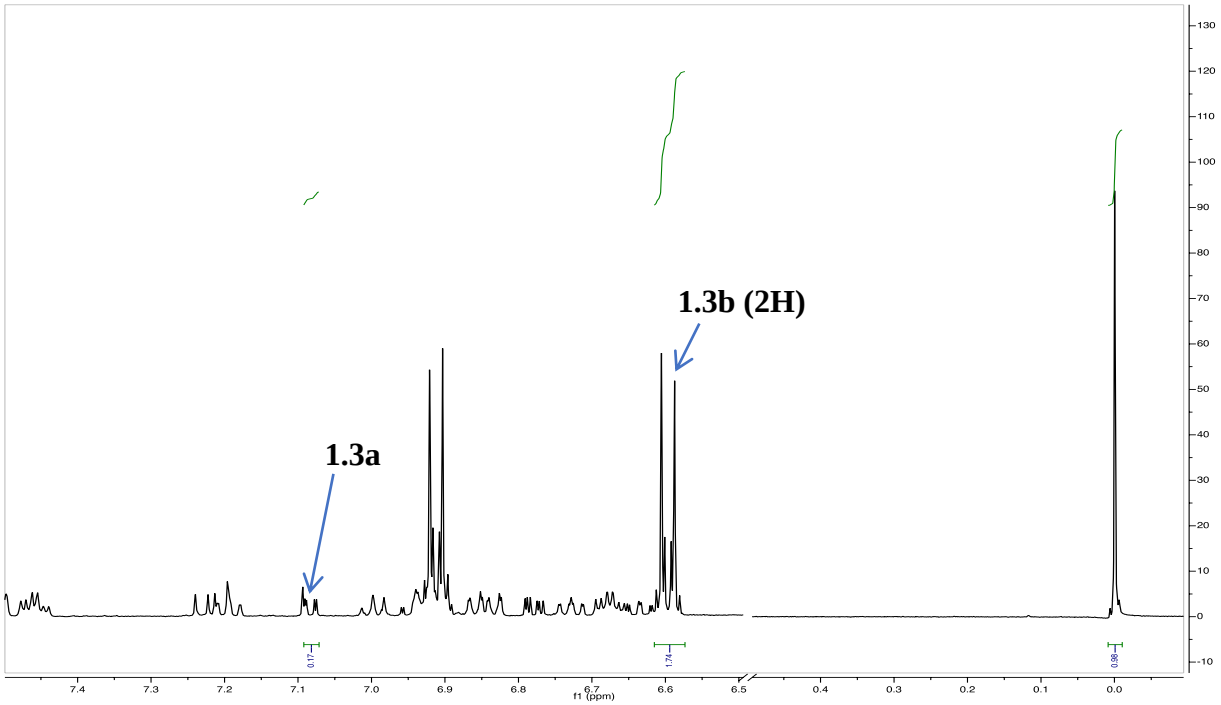

Figure 1.9.105 Example of 500 MHz ^{1}H NMR Spectrum for Table 1.8.1, Entry 12; t = 3 h

Trial 1: **3.3a**:**3.3b** as 1.0:5.1
Trial 2: **3.3a**:**3.3b** as 1.0:6.9
Trial 3: **3.3a**:**3.3b** as 1.0:2.9

1.9.7 Example Spectral Data for Determination of Ratios

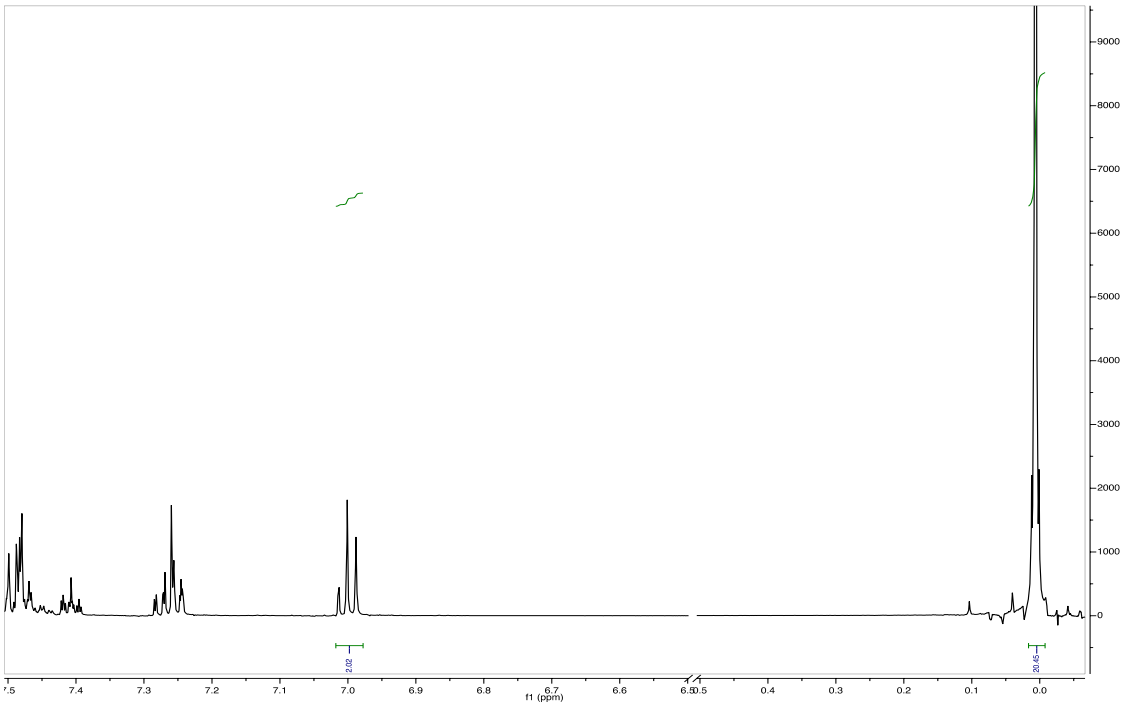

Figure 1.9.106 Example of 400 MHz ^{1}H NMR Spectrum for 1.8 + 1.1; t = 0 h

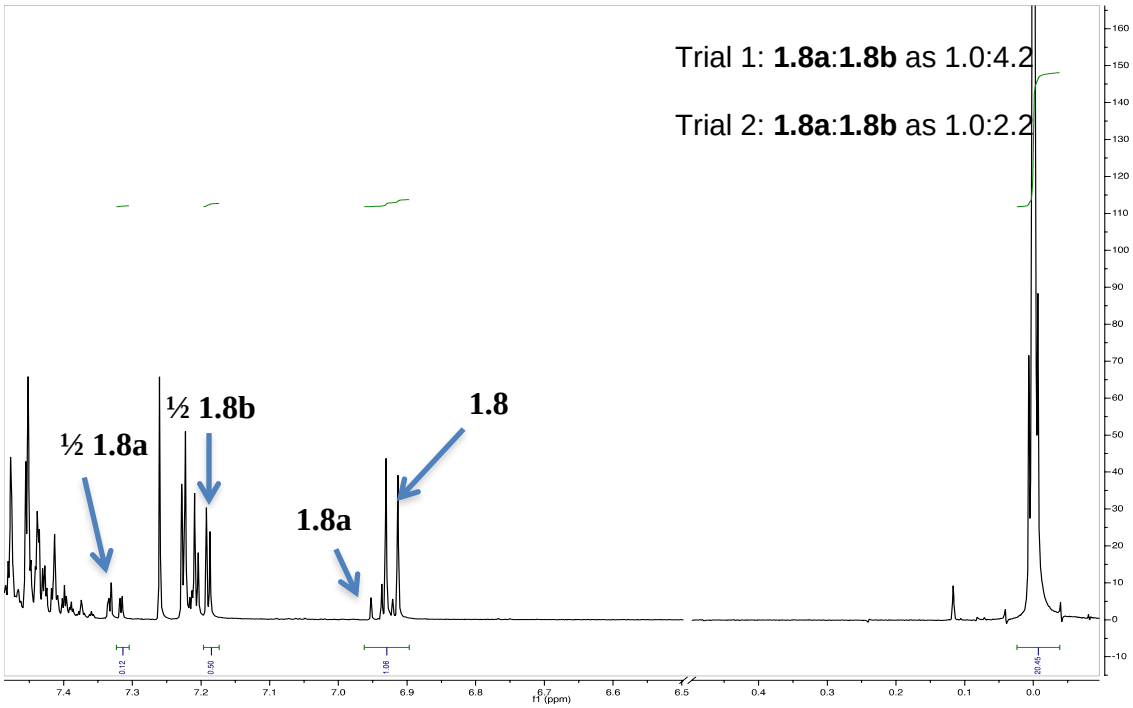

Figure 1.9.107 Example of 400 MHz ^{1}H NMR Spectrum for 1.8a + 1.8b + 1.1; t = 4 h

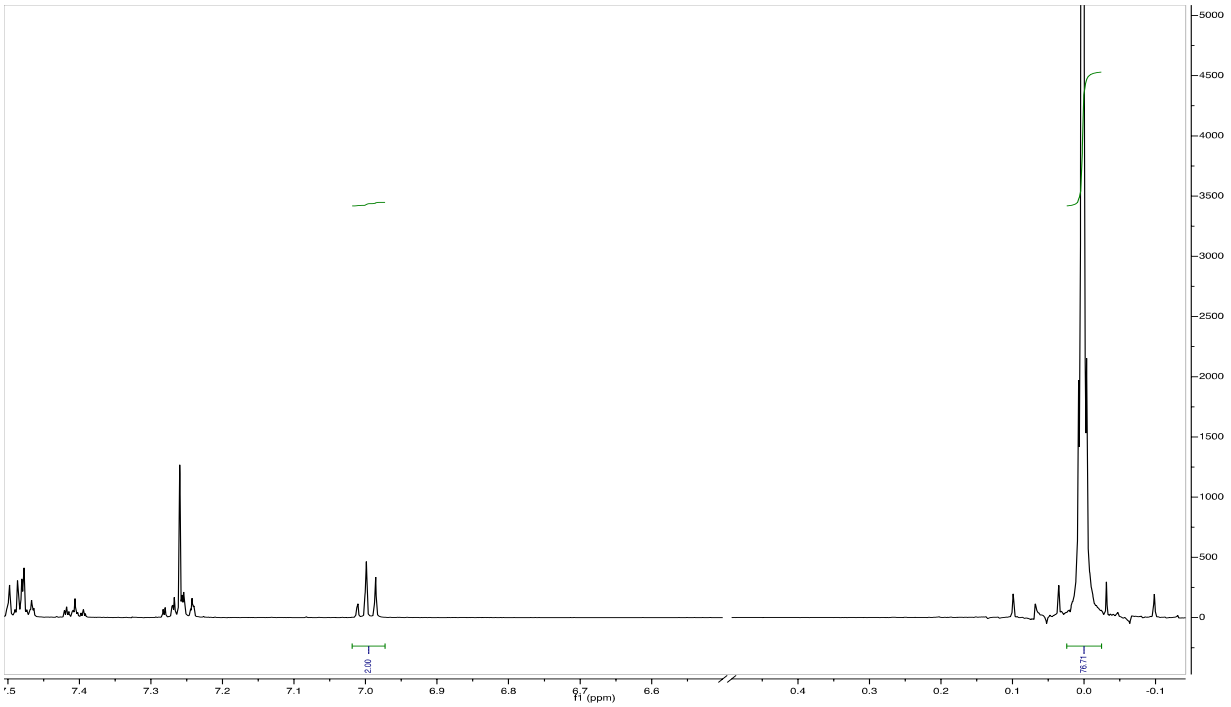

Figure 1.9.108 Example of 400 MHz ^{1}H NMR Spectrum for 1.8 + 1.6; t = 0 h

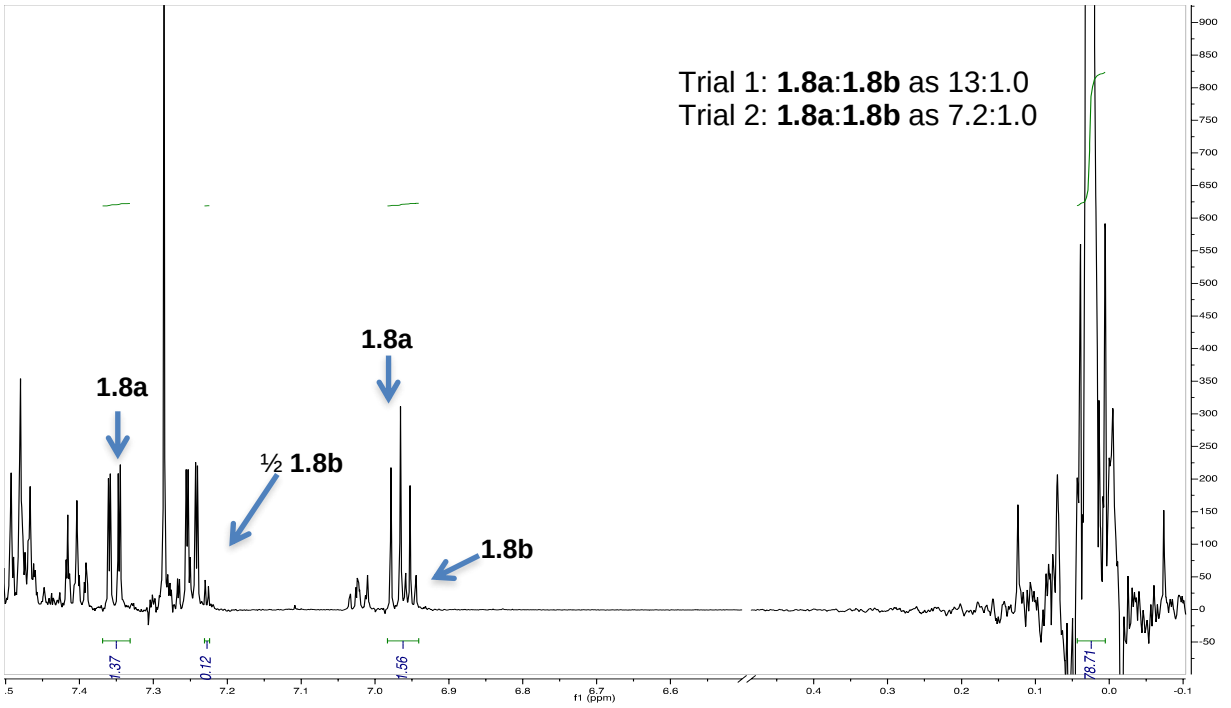

Figure 1.9.109 Example of 400 MHz ^{1}H NMR Spectrum for 1.8a + 1.8b + 1.6; t = 4 h

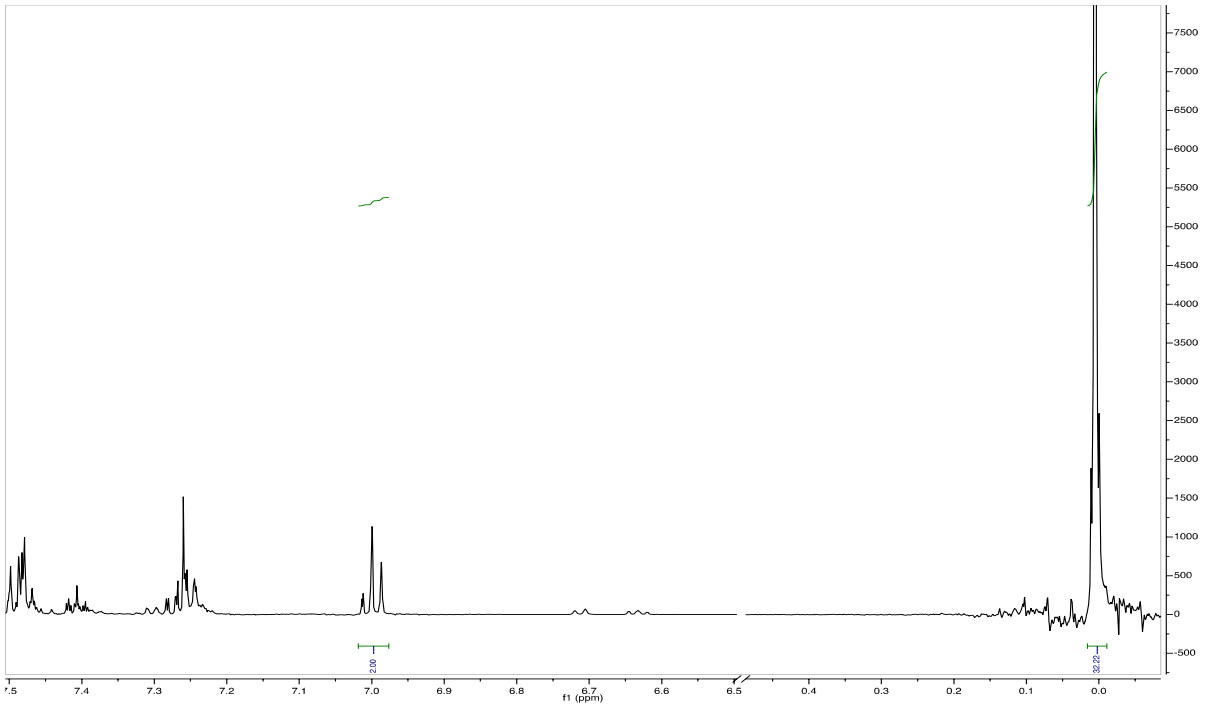

Figure 1.9.110 Example of 500 MHz ^{1}H NMR Spectrum for 1.8 + 1.7; t = 0 h

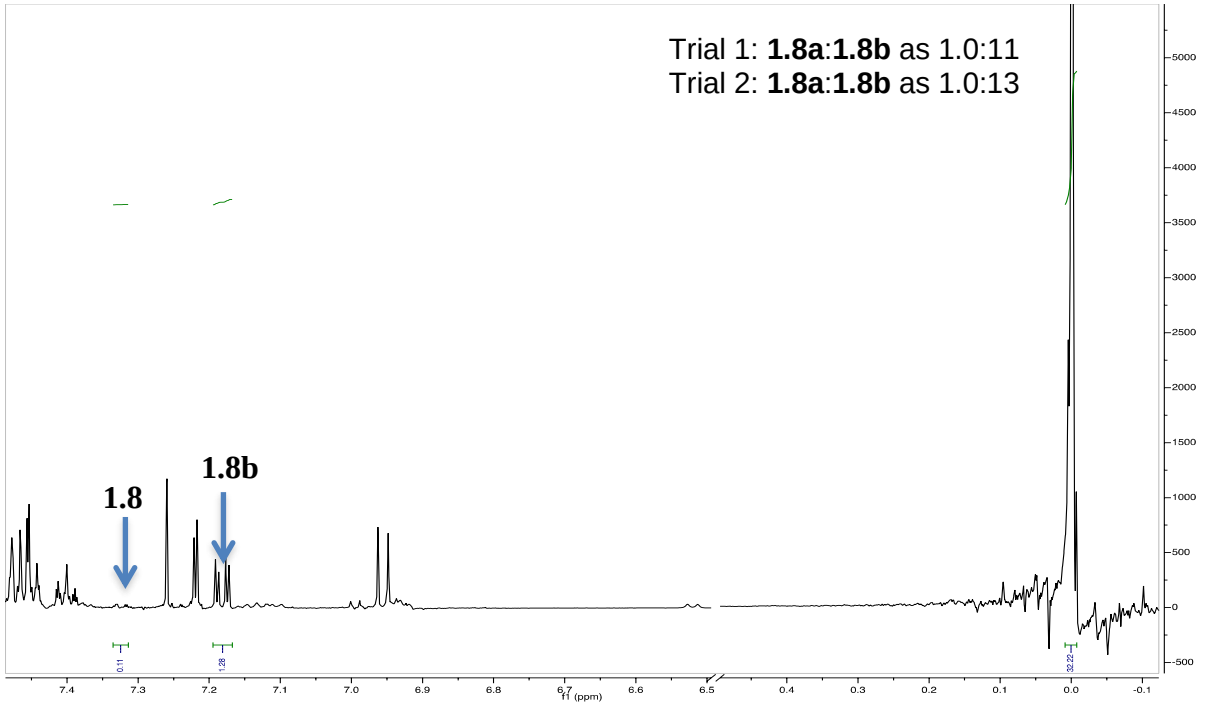

Figure 1.9.111 Example of 500 MHz ^{1}H NMR Spectrum for 1.8a + 1.8b + 1.7; t = 4 h

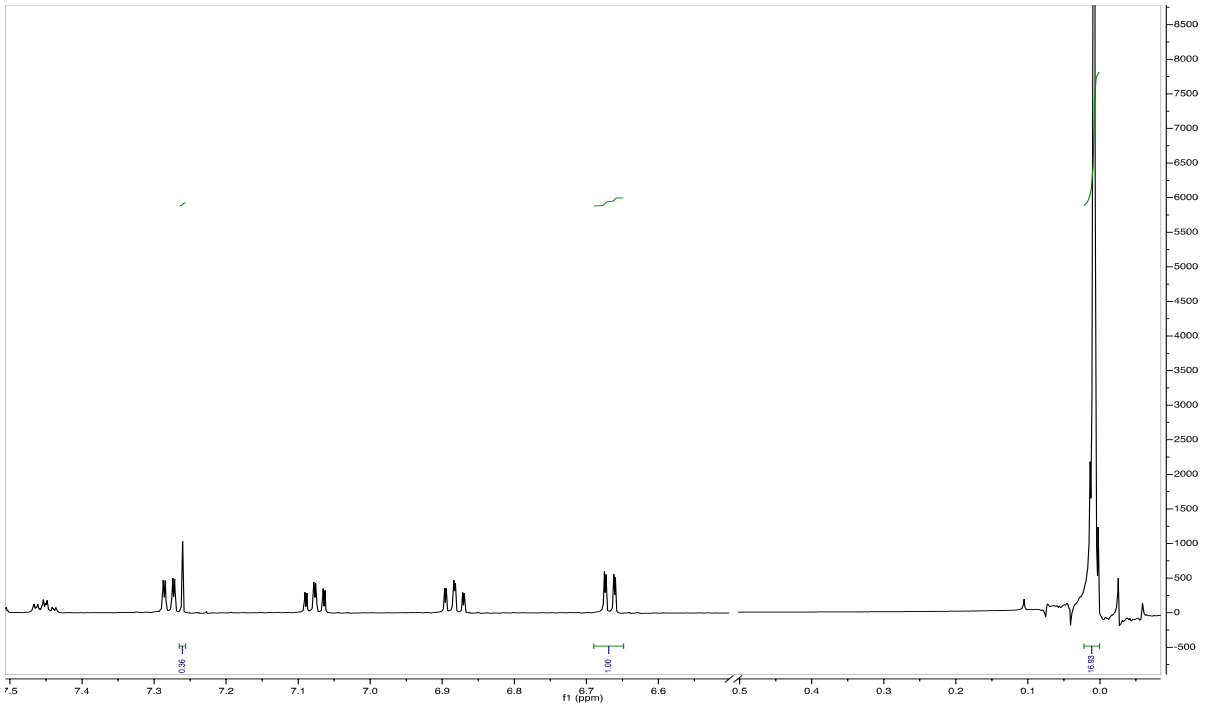

Figure 1.9.112 Example of 500 MHz ^{1}H NMR Spectrum for 1.9 + 1.1; t = 0 h

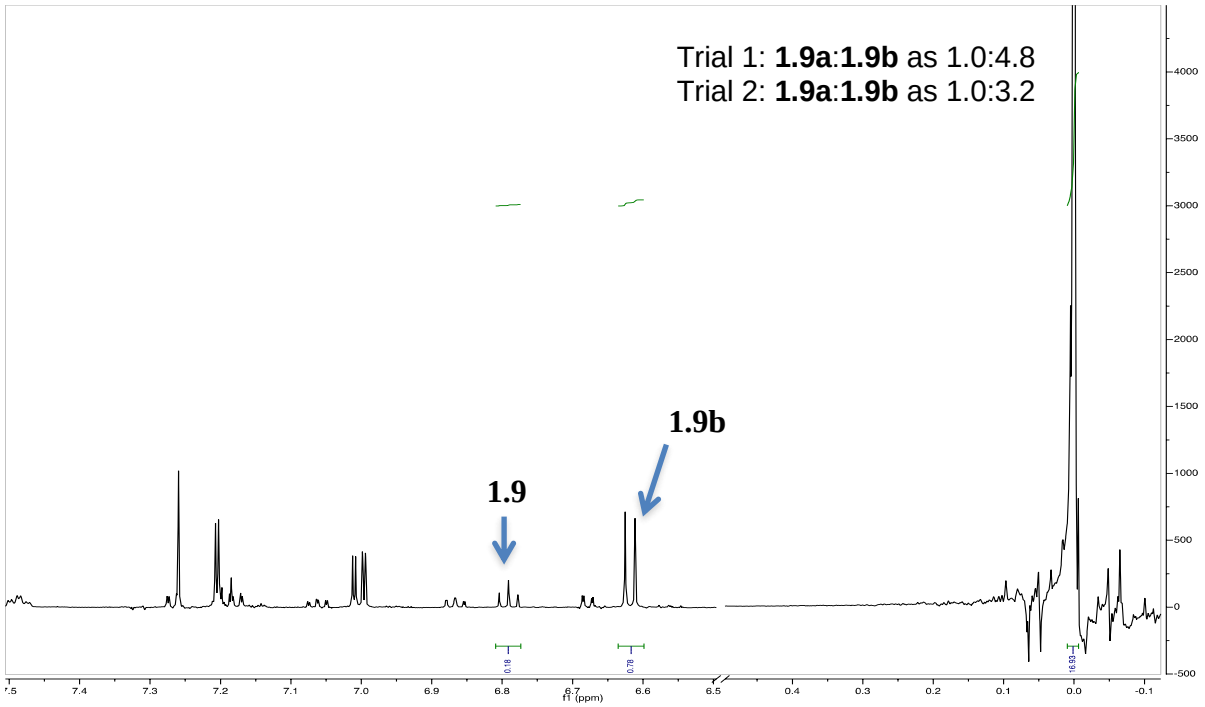

Figure 1.9.113 Example of 500 MHz ^{1}H NMR Spectrum for 1.9a + 1.9b + 1.1; t = 12 h

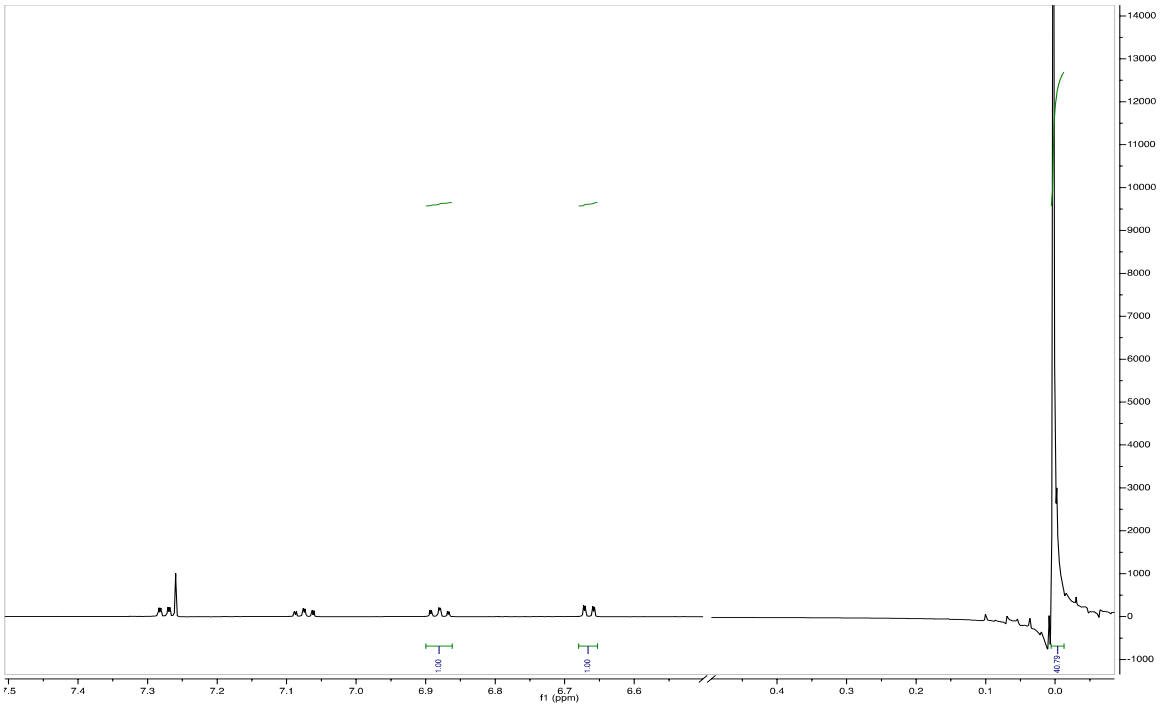

Figure 1.9.114 Example of 500 MHz ^{1}H NMR Spectrum for 1.9 + 1.6; t = 0 h

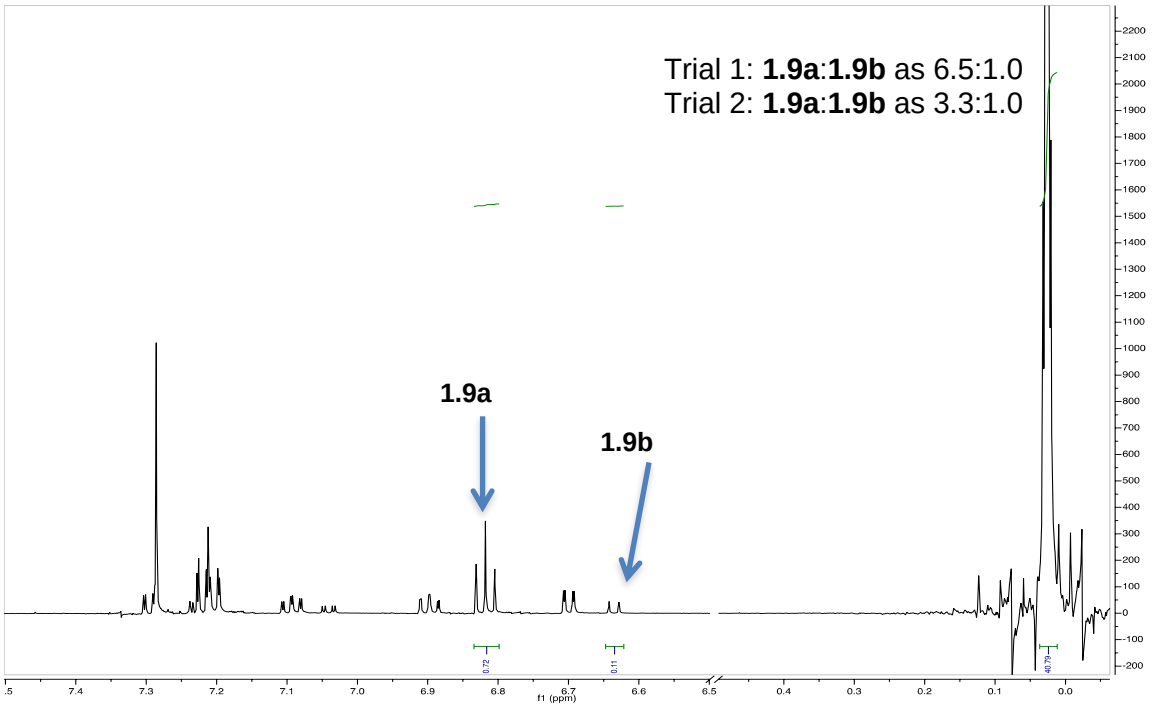

Figure 1.9.115 Example of 500 MHz ^{1}H NMR Spectrum for 1.9a + 1.9b + 1.6; t = 12 h

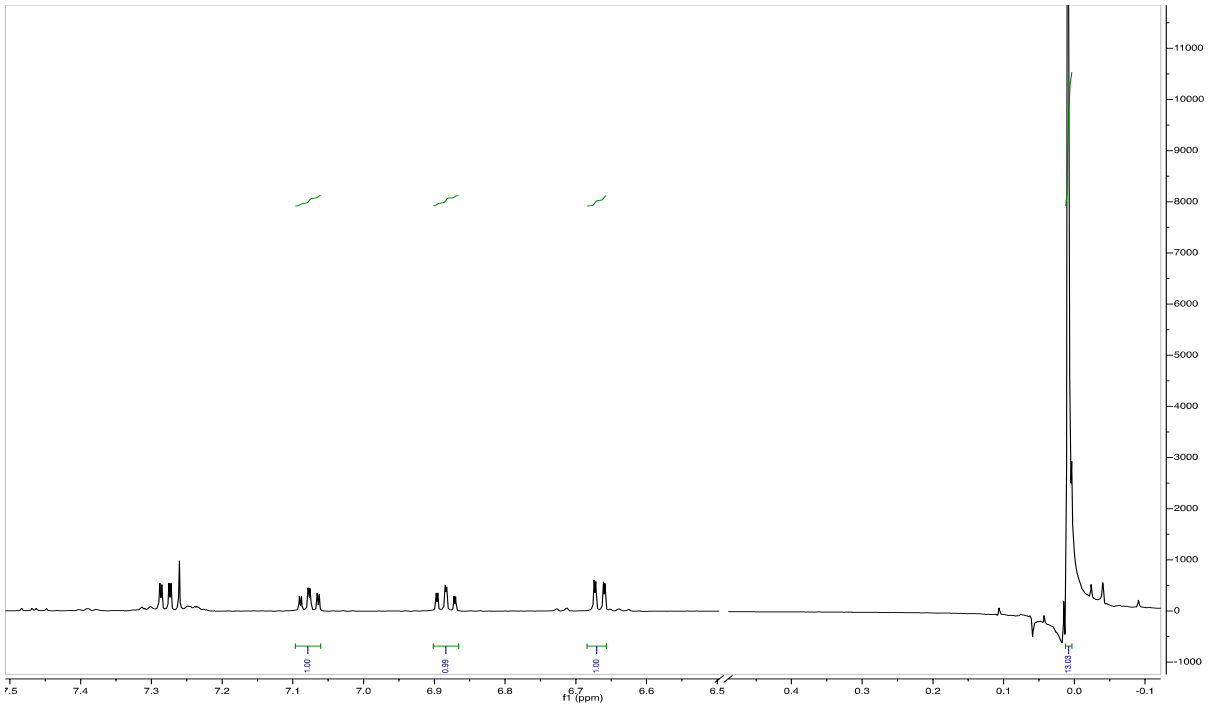

Figure 1.9.116 Example of 500 MHz ^{1}H NMR Spectrum for 1.9 + 1.7; t = 0 h

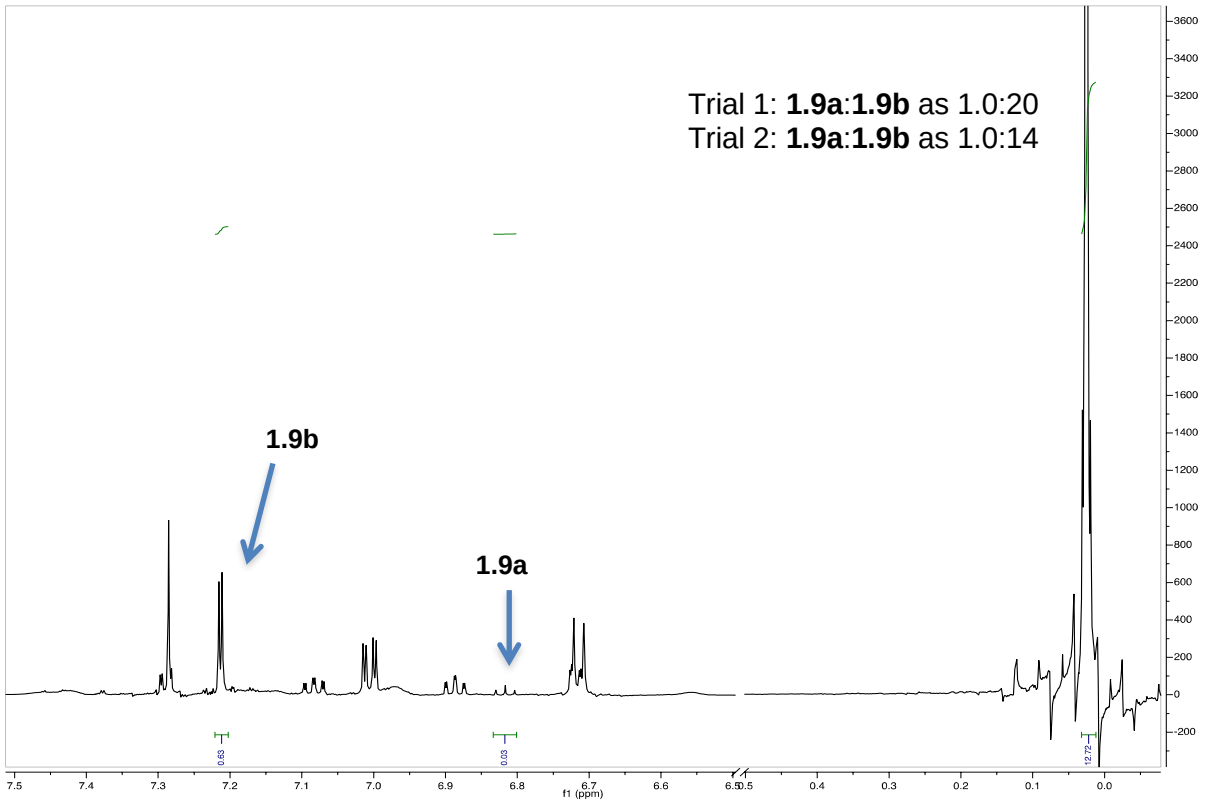

Figure 1.9.117 Example of 500 MHz ^{1}H NMR Spectrum for 1.9a + 1.9b + 1.7; t = 12 h

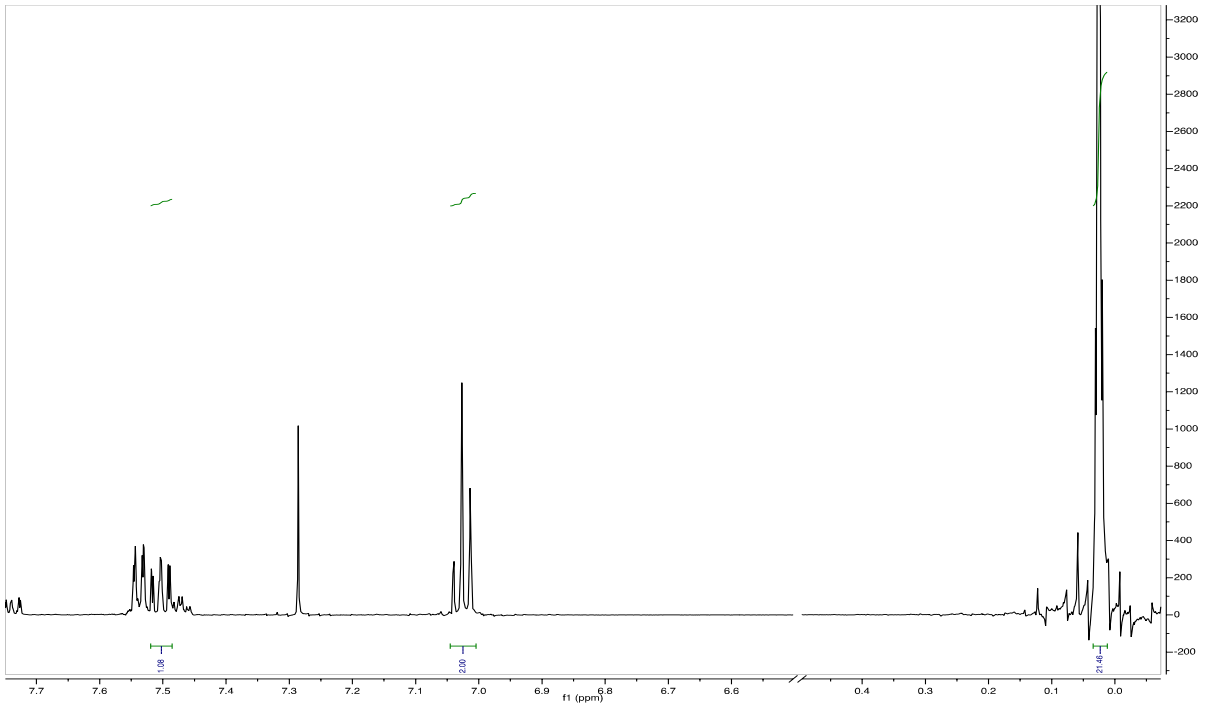

Figure 1.9.118 Example of 400 MHz ^{1}H NMR Spectrum for 1.10 + 1.1; t = 0 h

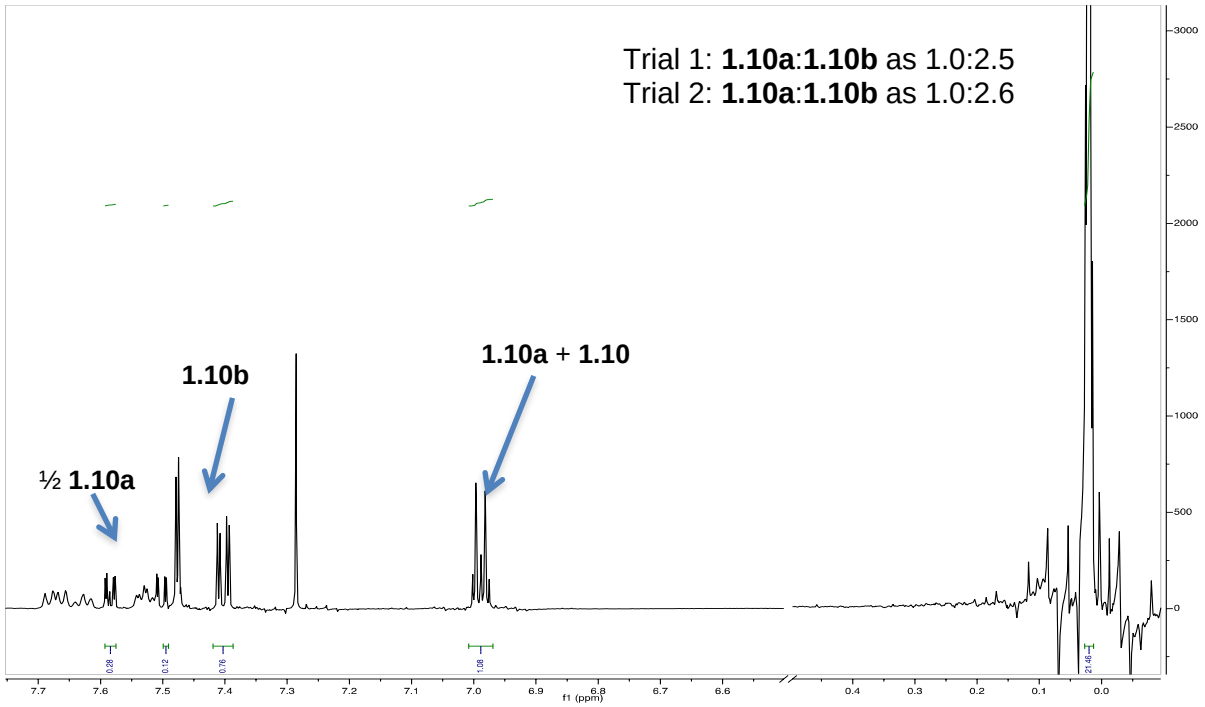

Figure 1.9.119 Example of 400 MHz ^{1}H NMR Spectrum for 1.10a + 1.10b + 1.1; t = 12 h

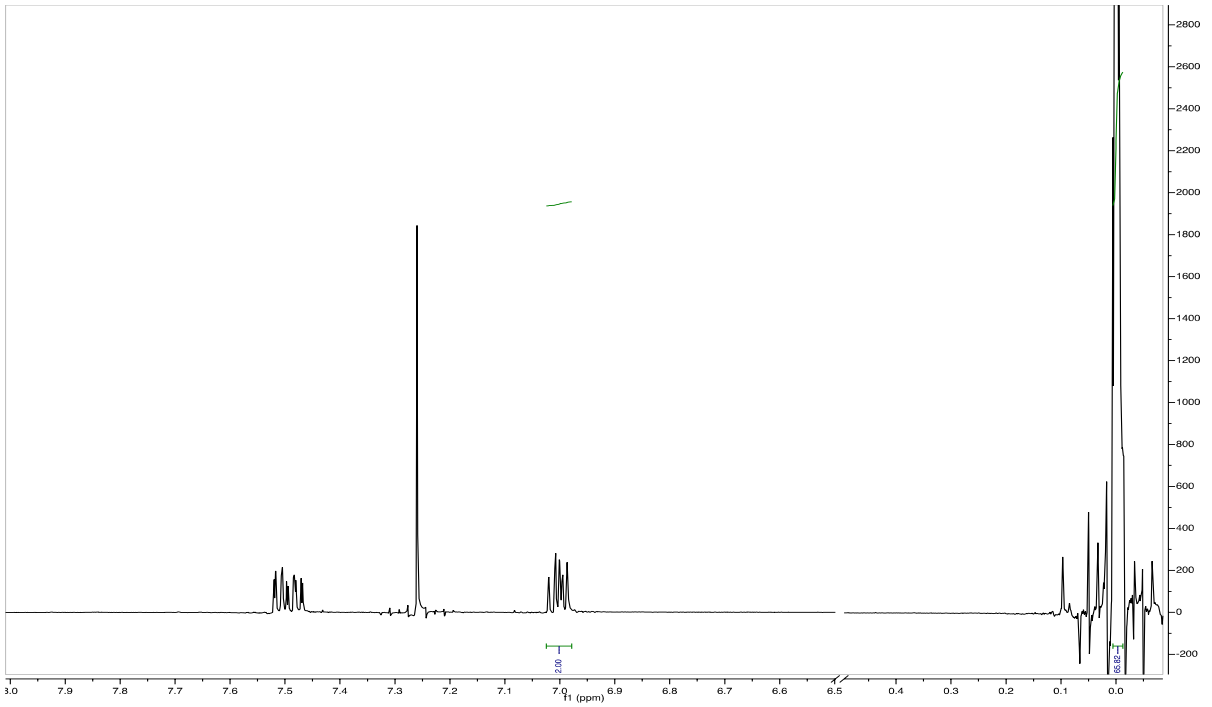

Figure 1.9.120 Example of 400 MHz ^{1}H NMR Spectrum for 1.10 + 1.6; t = 0 h

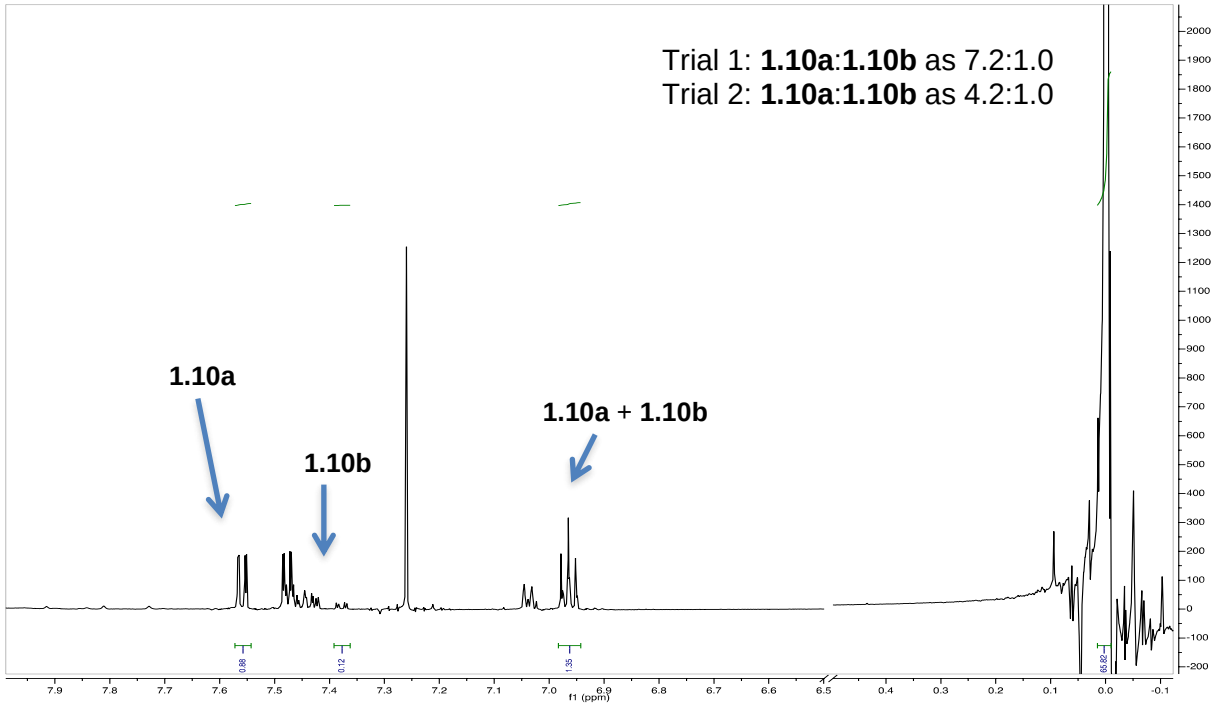

Figure 1.9.121 Example of 400 MHz ^{1}H NMR Spectrum for 1.10a + 1.10b + 1.6; t = 12 h

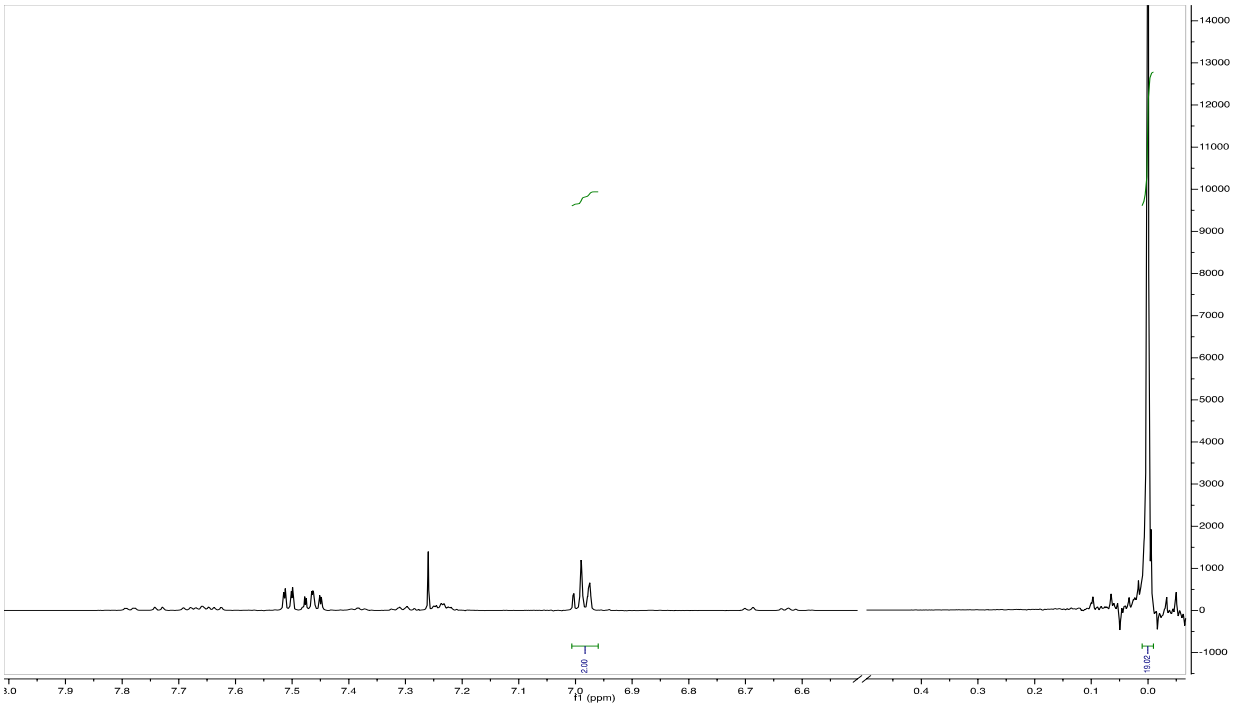

Figure 1.9.122 Example of 400 MHz ^{1}H NMR Spectrum for 1.10 + 1.7; t = 0 h

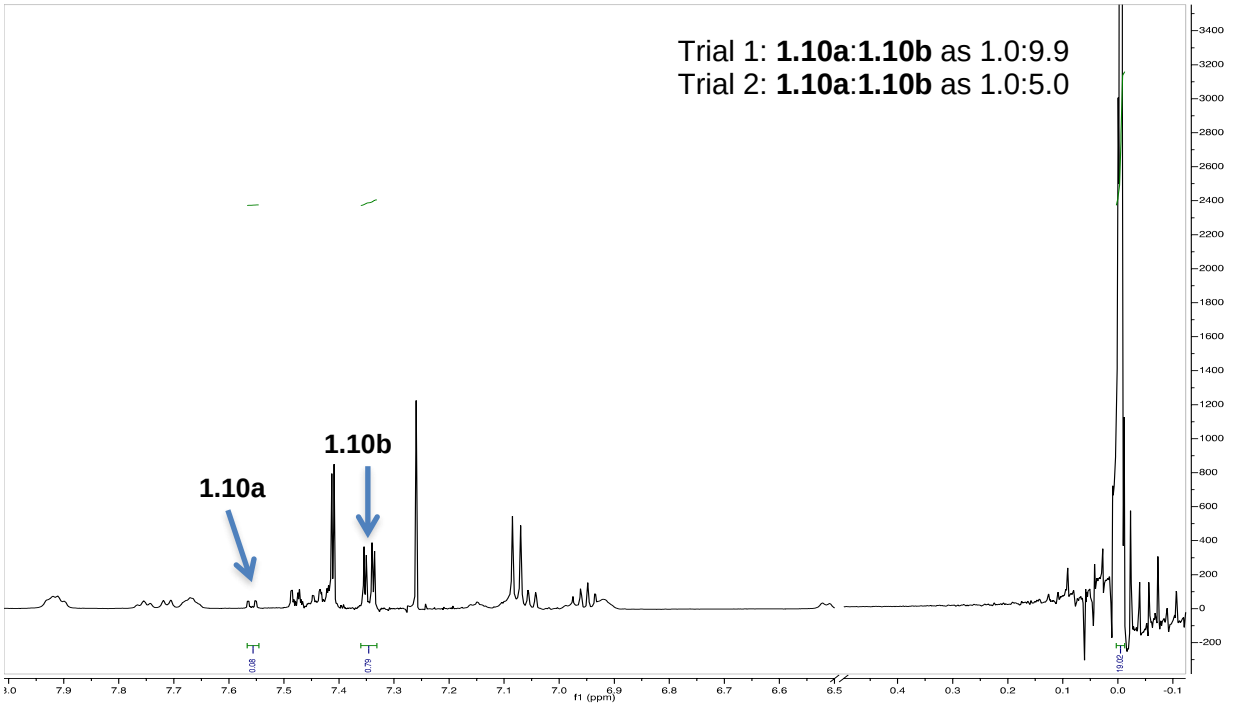

Figure 1.9.123 Example of 400 MHz ^{1}H NMR Spectrum for 1.10a + 1.10b + 1.7; t = 12 h

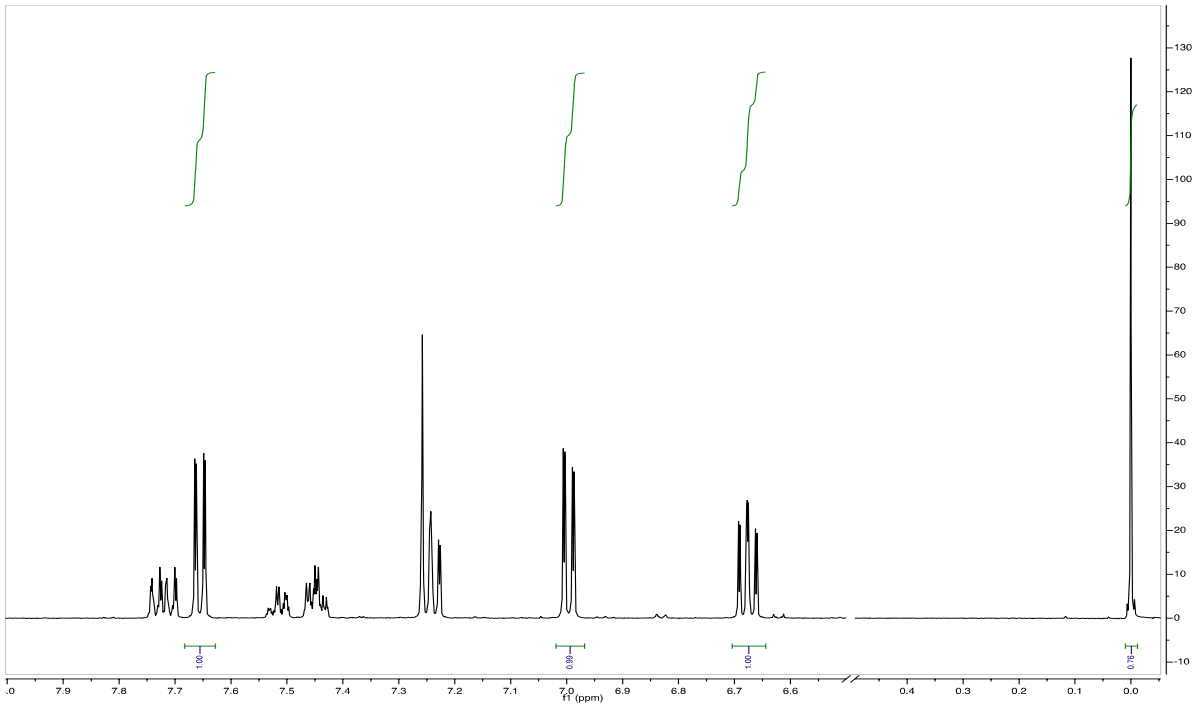

Figure 1.9.124 Example of 400 MHz ^{1}H NMR Spectrum for 1.11 + 1.1; t = 0 h

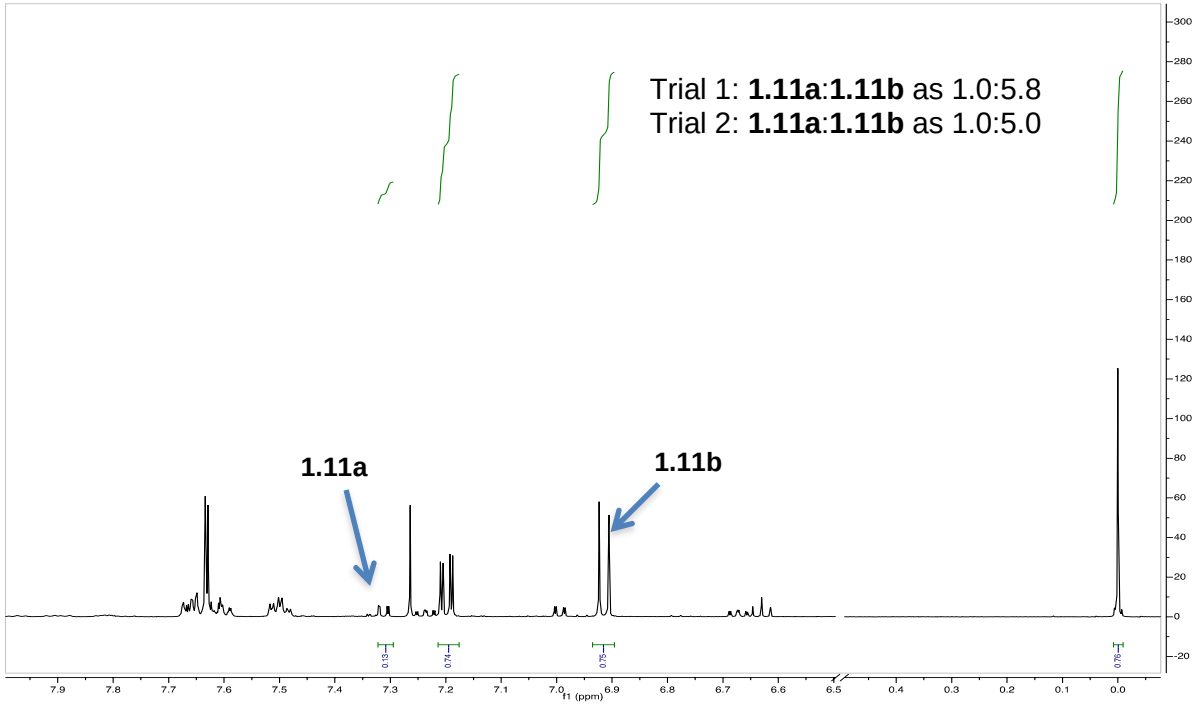

Figure 1.9.125 Example of 400 MHz ^{1}H NMR Spectrum for 1.11a + 1.11b + 1.1; t = 12 h

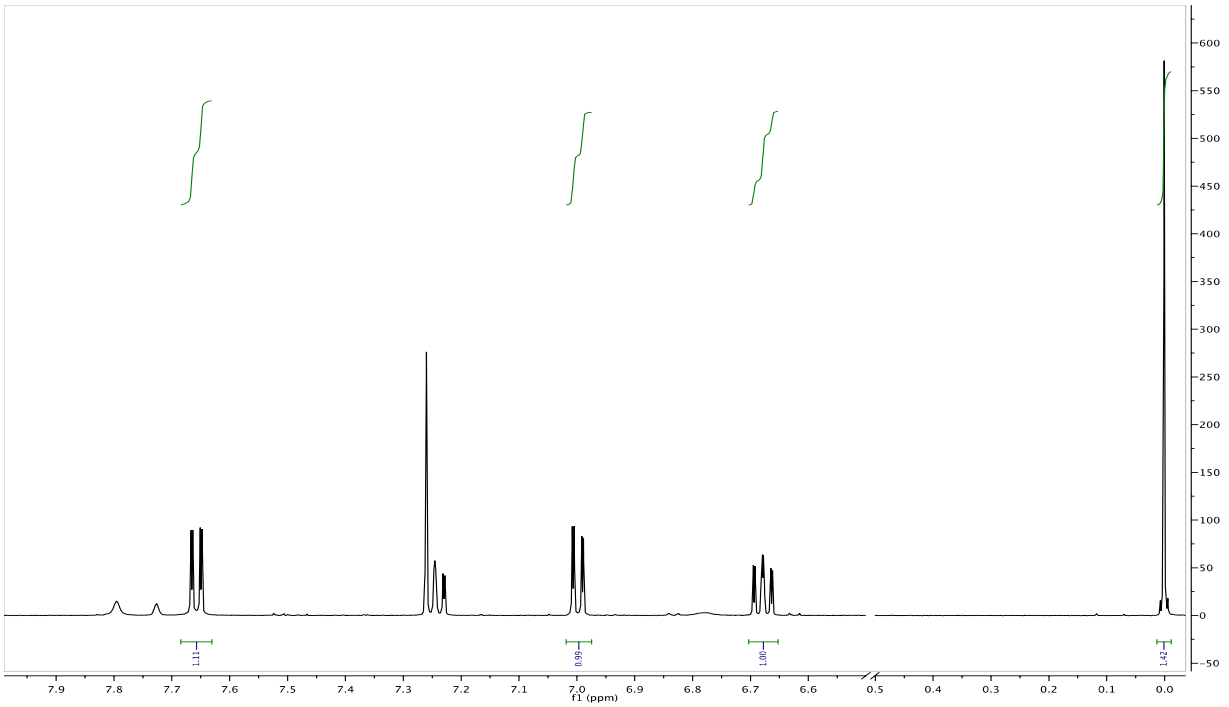

Figure 1.9.126 Example of 400 MHz ^{1}H NMR Spectrum for 1.11 + 1.6; t = 0 h

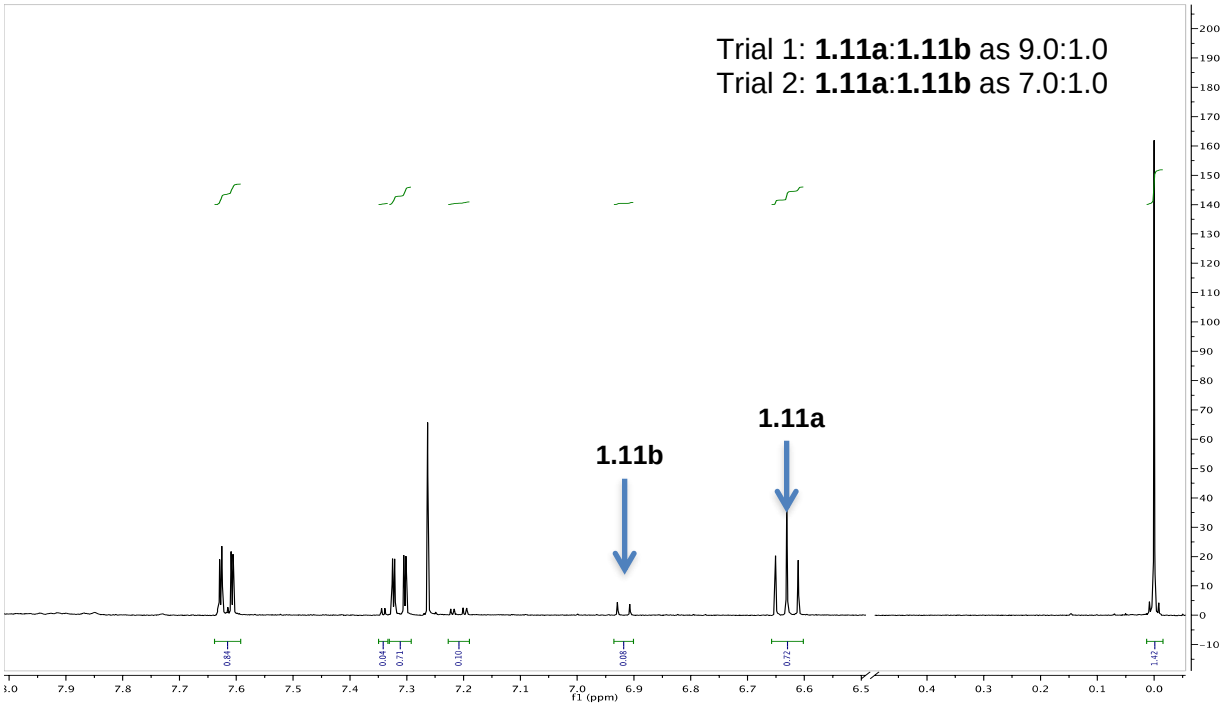

Figure 1.9.127 Example of 400 MHz ^{1}H NMR Spectrum for 1.11a + 1.11b + 1.6; t = 12 h

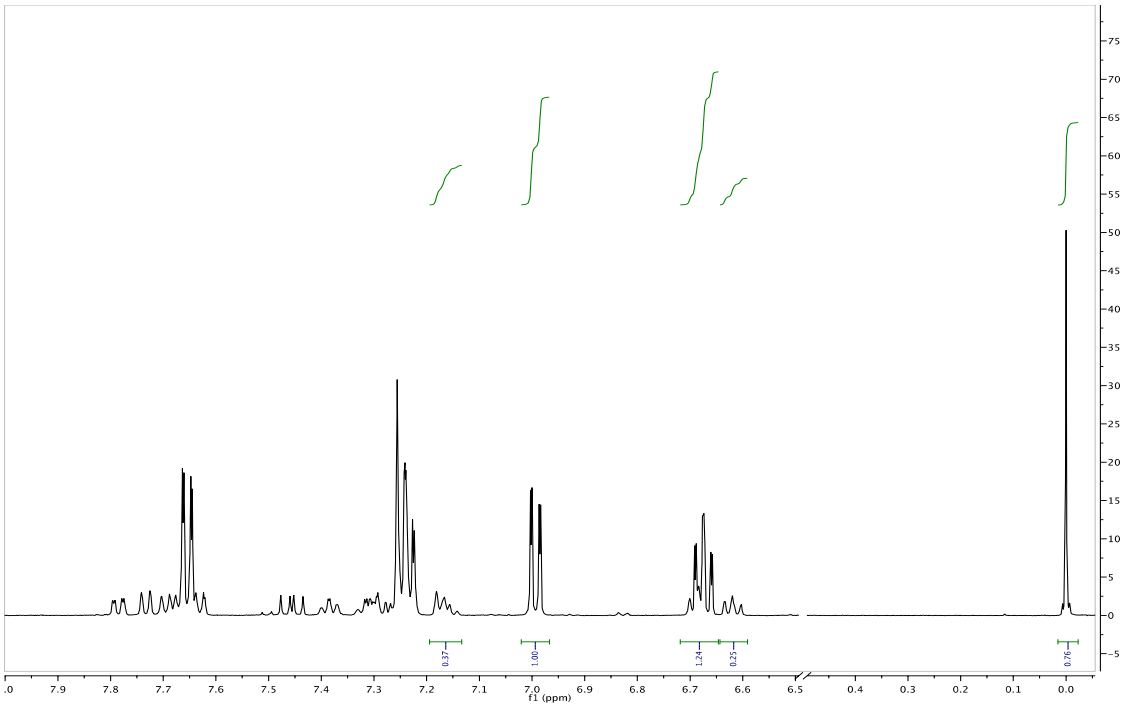

Figure 1.9.128 Example of 400 MHz ^{1}H NMR Spectrum for 1.11 + 1.7; t = 0 h

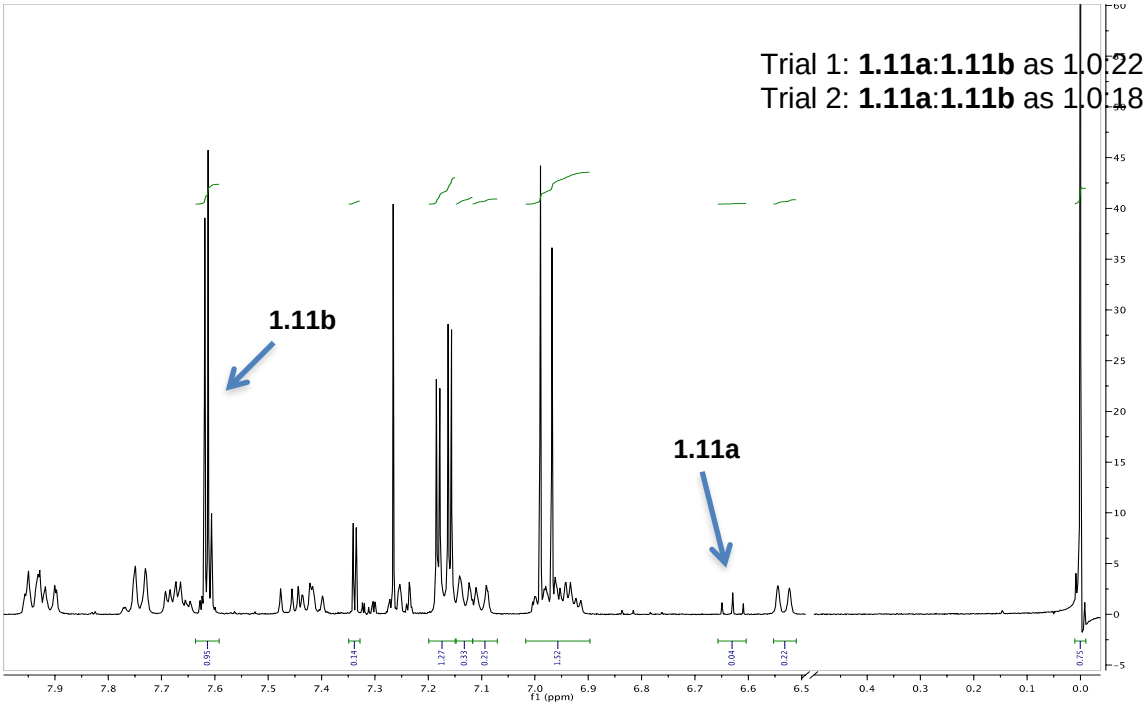

Figure 1.9.129 Example of 400 MHz ^{1}H NMR Spectrum for 1.11a + 1.11b + 1.7; t = 12 h

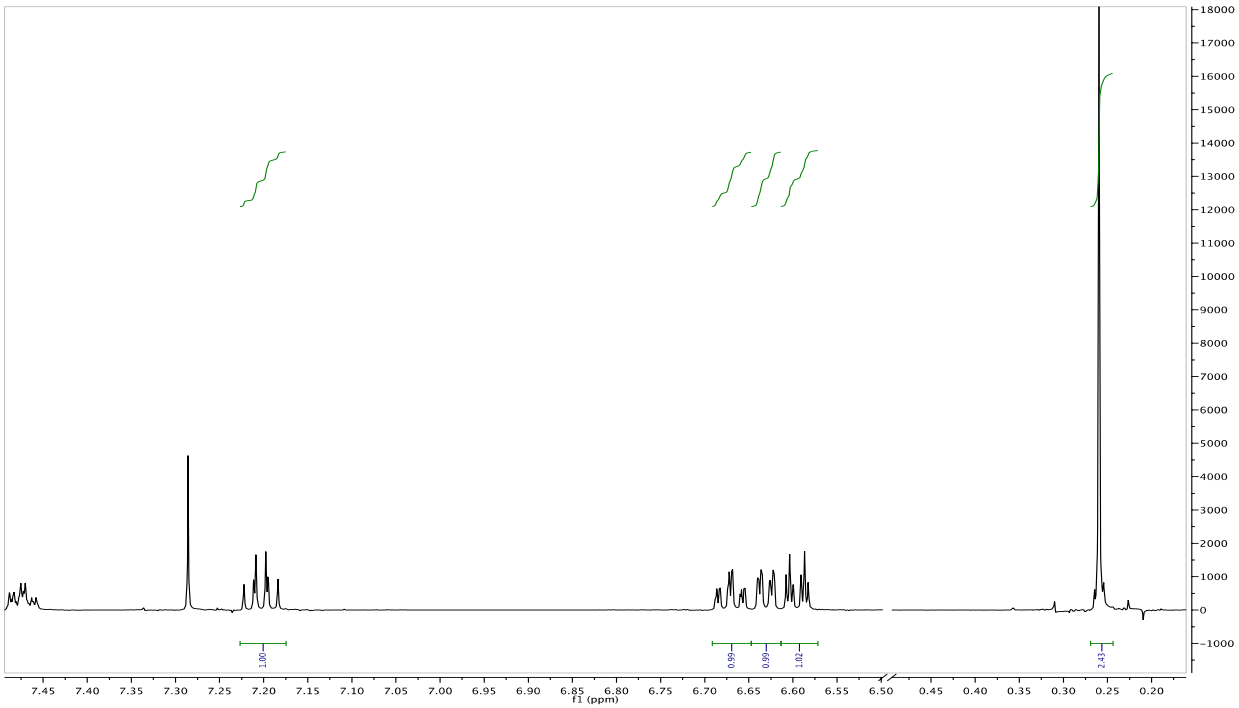

Figure 1.9.130 Example of 400 MHz ^{1}H NMR Spectrum for 1.12 + 1.1; t = 0 h

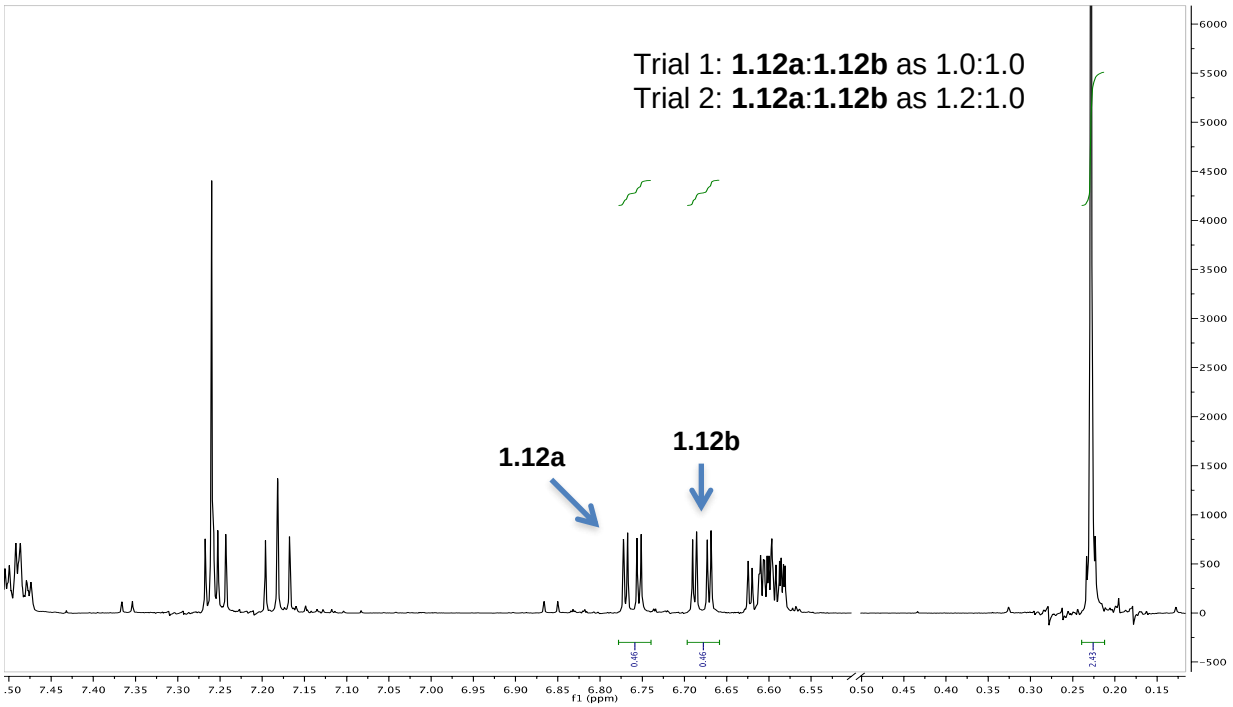

Figure 1.9.131 Example of 400 MHz ^{1}H NMR Spectrum for 1.12a + 1.12b + 1.12c + 1.1; t = 12 h

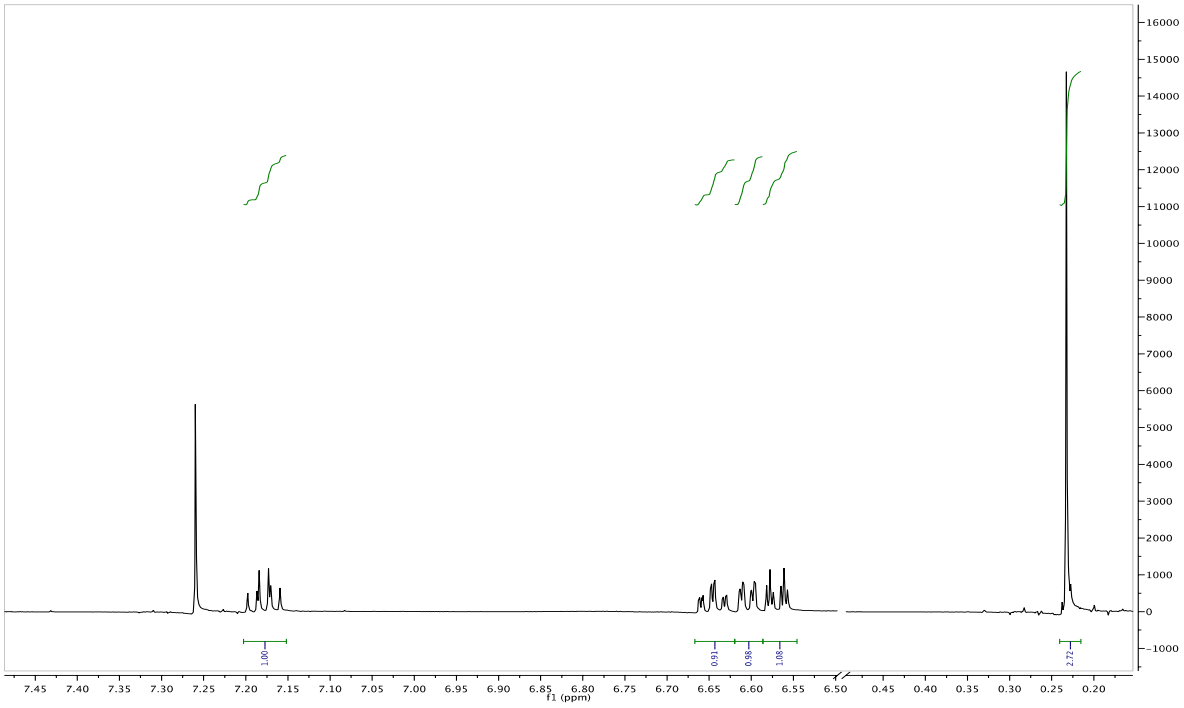

Figure 1.9.132 Example of 400 MHz ^{1}H NMR Spectrum for 1.12 + 1.6; t = 0 h

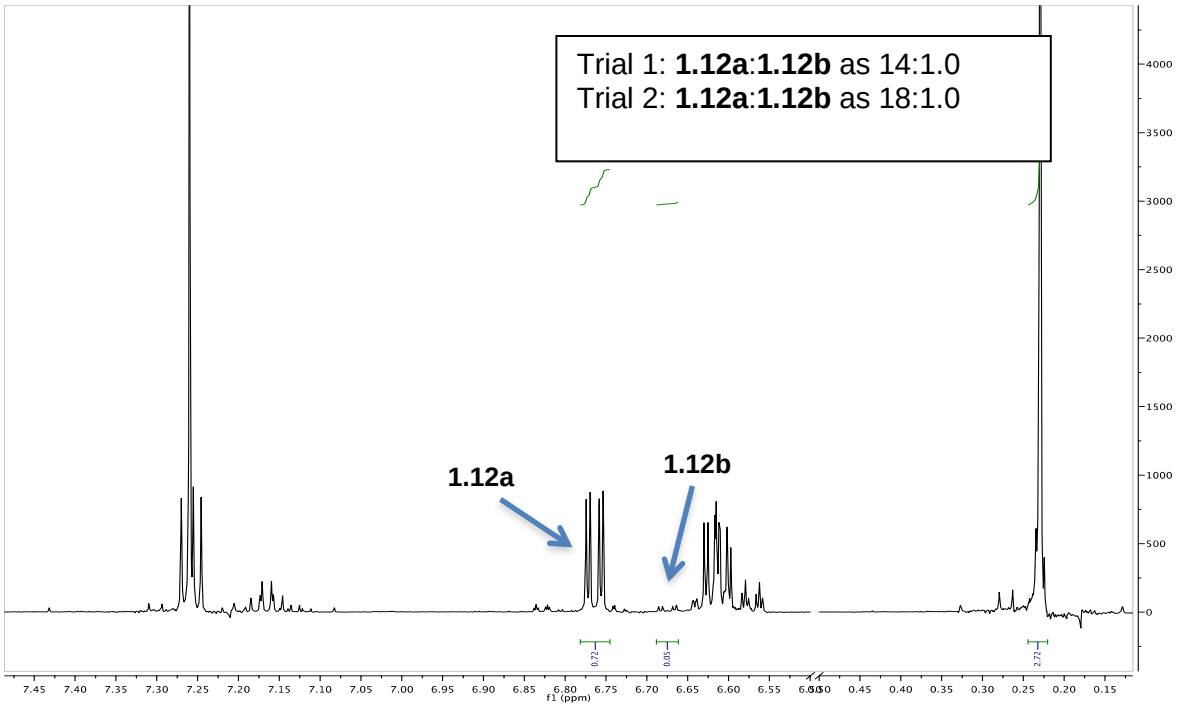

Figure 1.9.133 Example of 400 MHz ^{1}H NMR Spectrum for 1.12a + 1.12b +1.12c + 1.6; t = 9 h

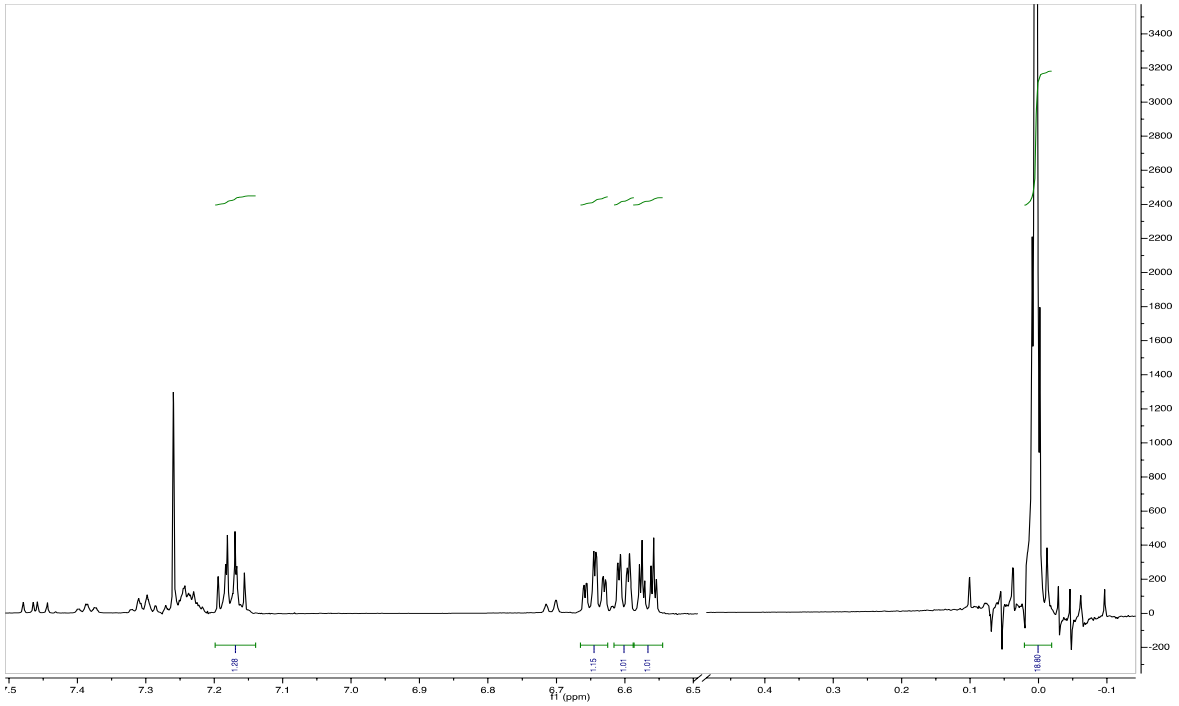

Figure 1.9.134 Example of 400 MHz ^{1}H NMR Spectrum for 1.12 + 1.7; t = 0 h

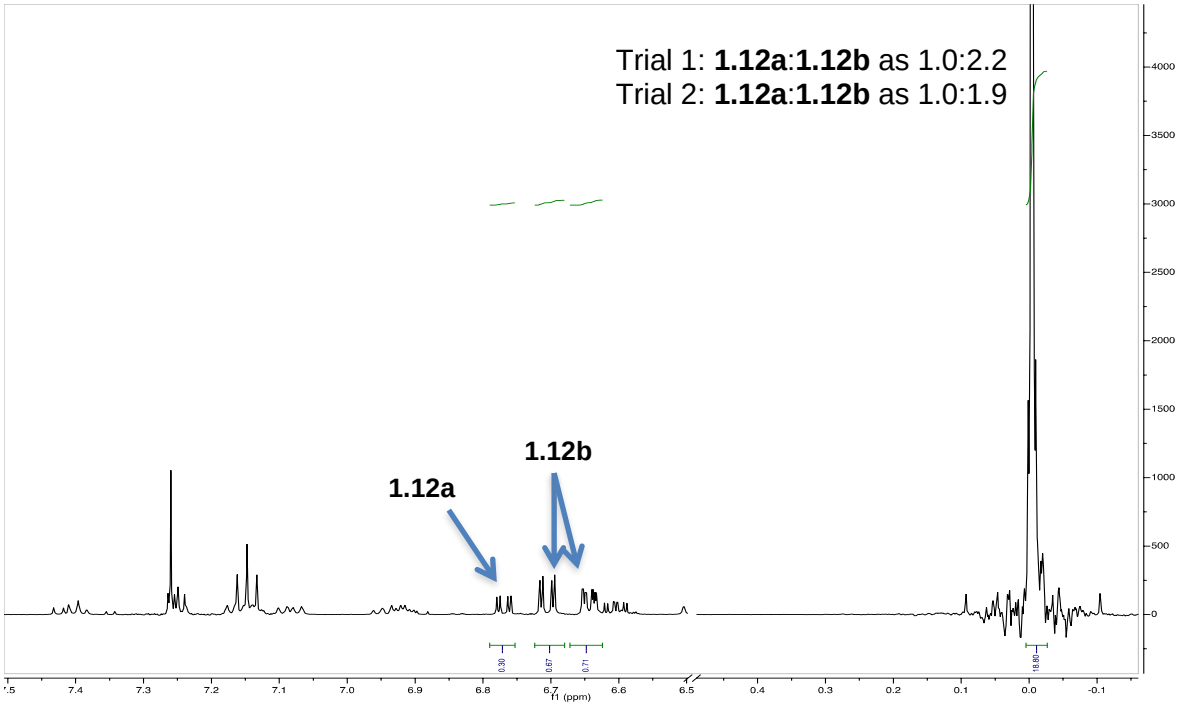

Figure 1.9.135 Example of 400 MHz ^{1}H NMR Spectrum for 1.12a + 1.12b +1.12c + 1.7; t = 6 h

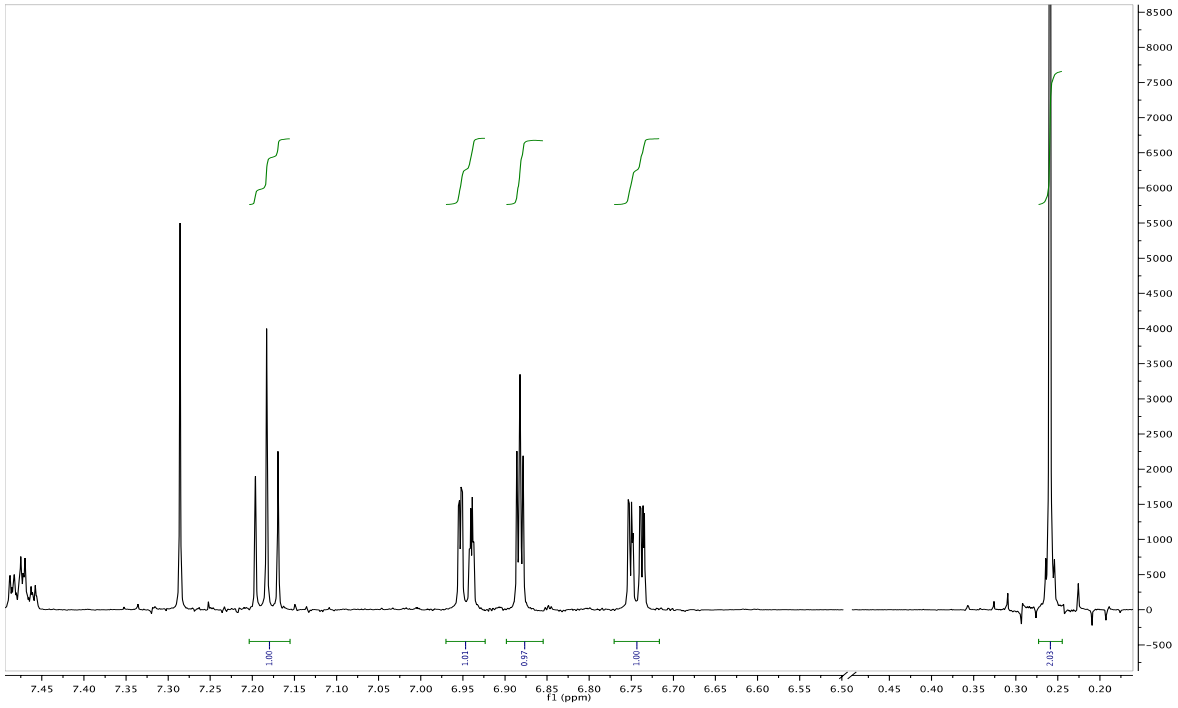

Figure 1.9.136 Example of 500 MHz ^{1}H NMR Spectrum for 1.13 + 1.1; t = 0 h

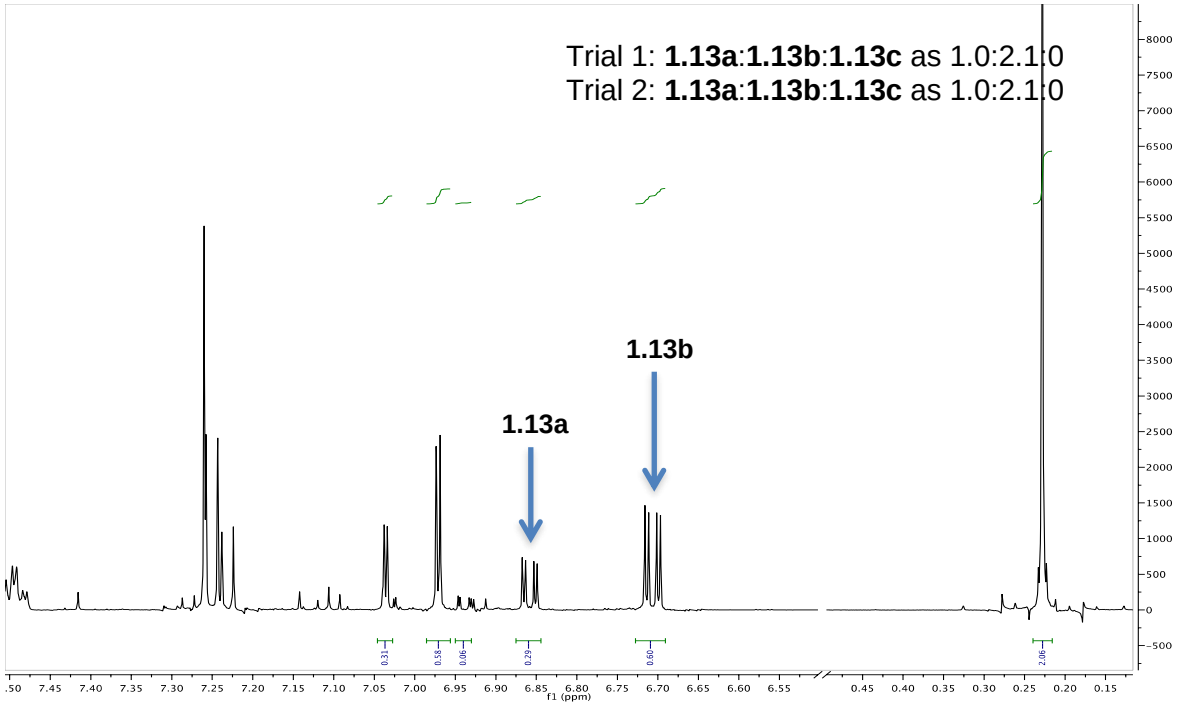

Figure 1.9.137 Example of 500 MHz ^{1}H NMR Spectrum for 1.13a + 1.13b +1.13c + 1.1; t = 5 h

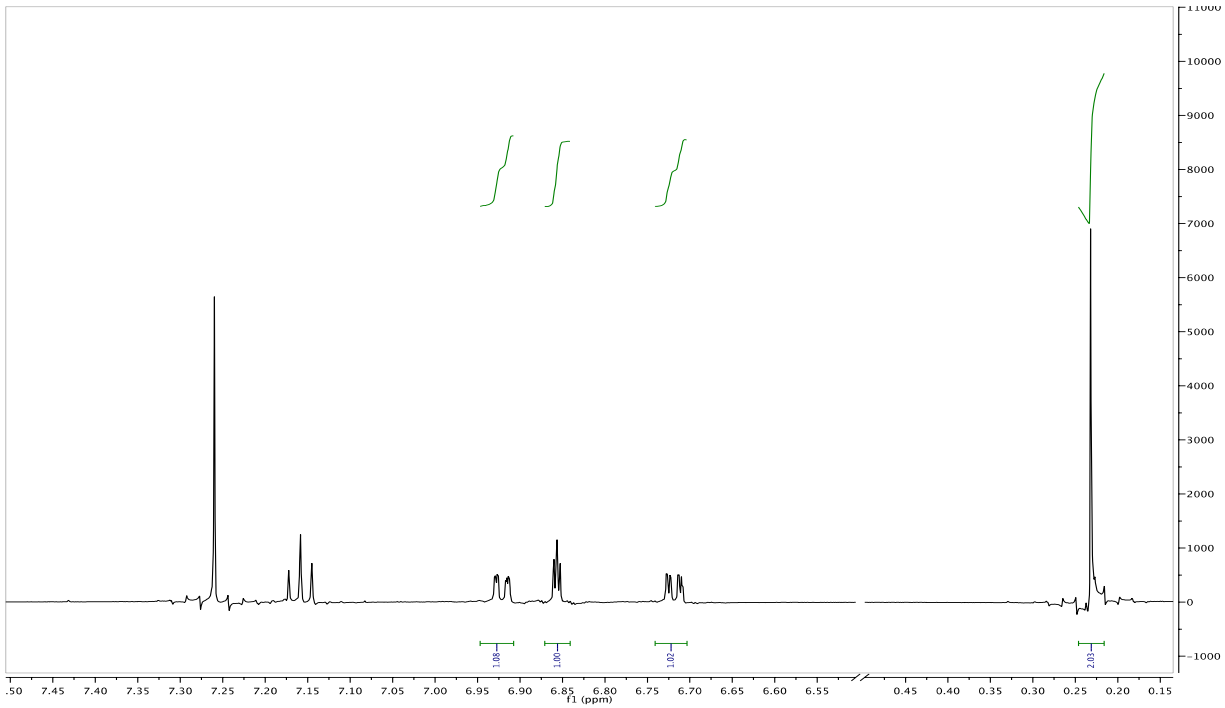

Figure 1.9.138 Example of 500 MHz ^{1}H NMR Spectrum for 1.13 + 1.6; t = 0 h

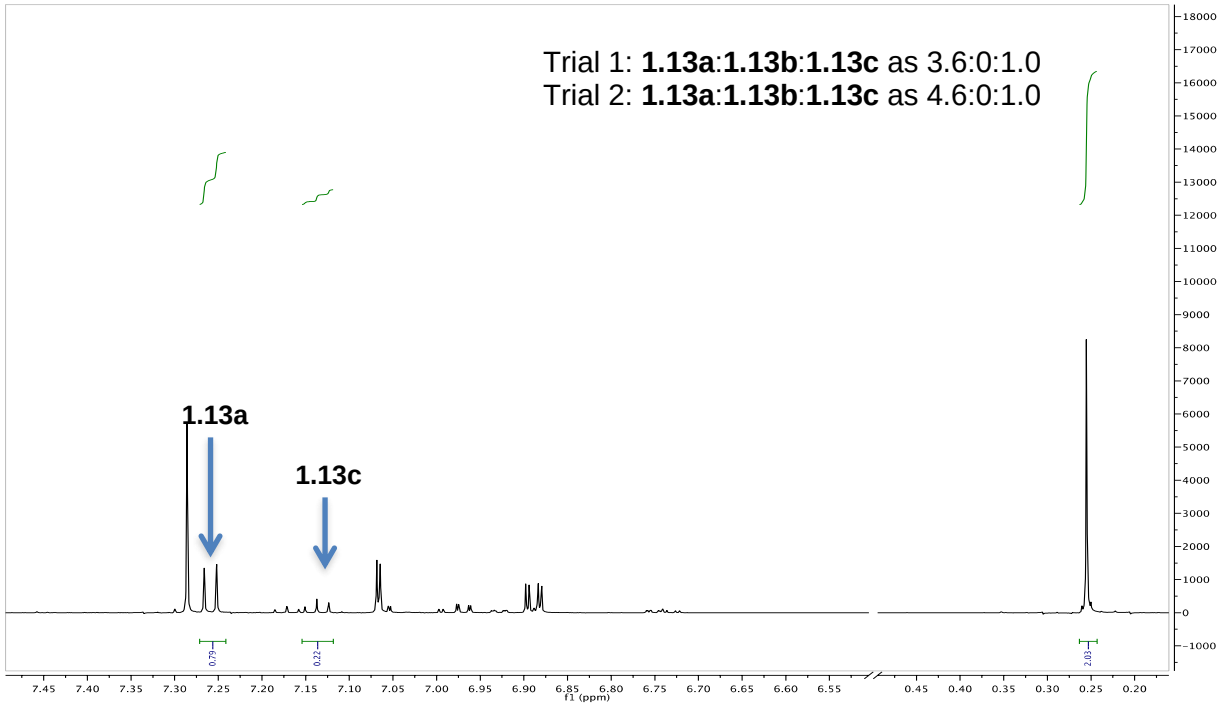

Figure 1.9.139 Example of 500 MHz ^{1}H NMR Spectrum for 1.13a + 1.13b +1.13c + 1.6; t = 5 h

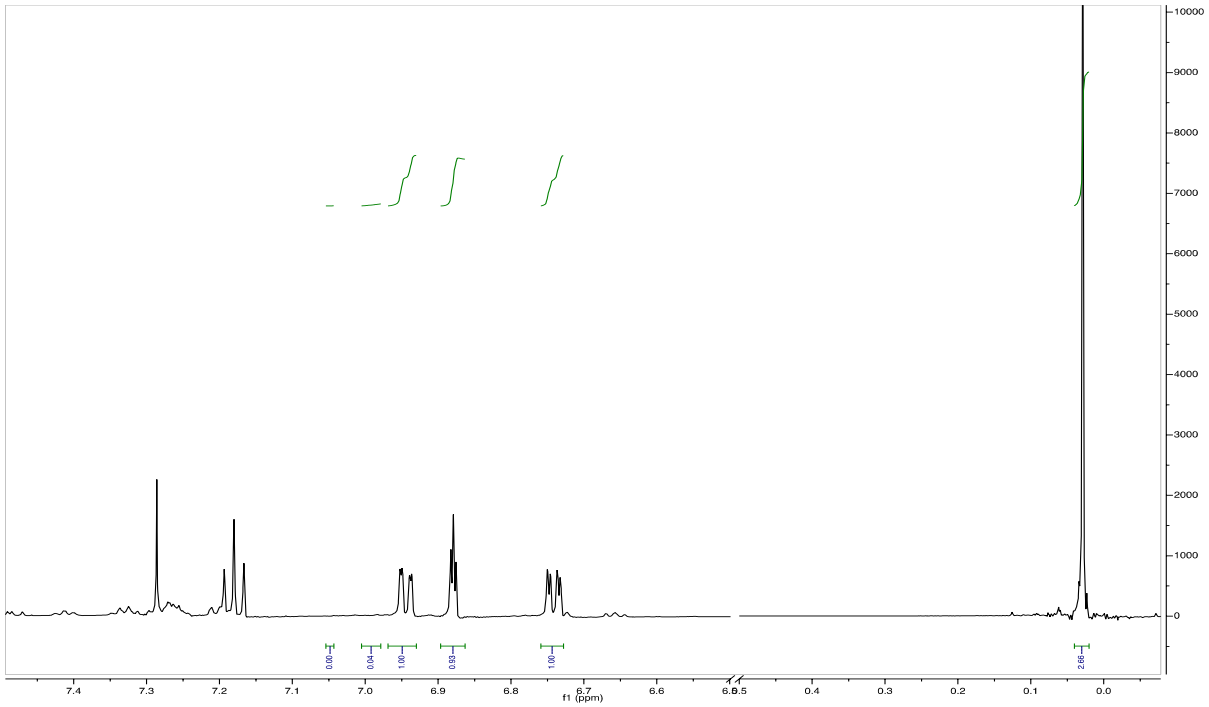

Figure 1.9.140 Example of 500 MHz ^{1}H NMR Spectrum for 1.13 + 1.7; t = 0 h

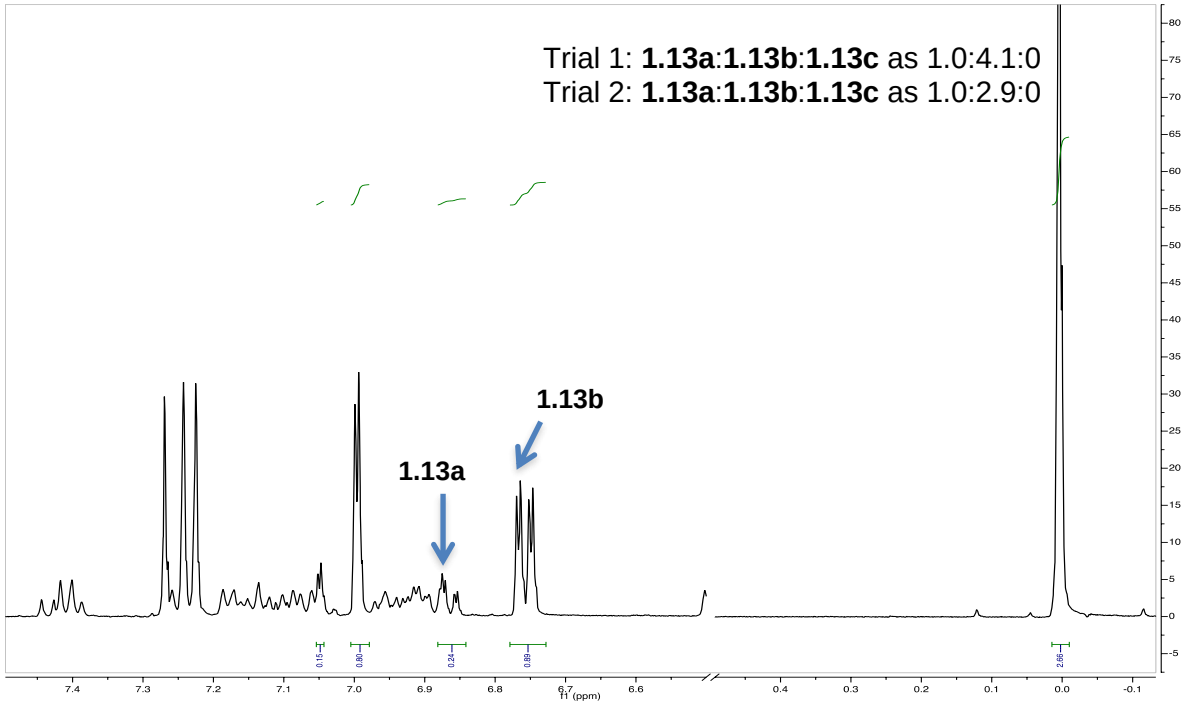

Figure 1.9.141 Example of 500 MHz ^{1}H NMR Spectrum for 1.13a + 1.13b +1.13c + 1.7; t = 5 h

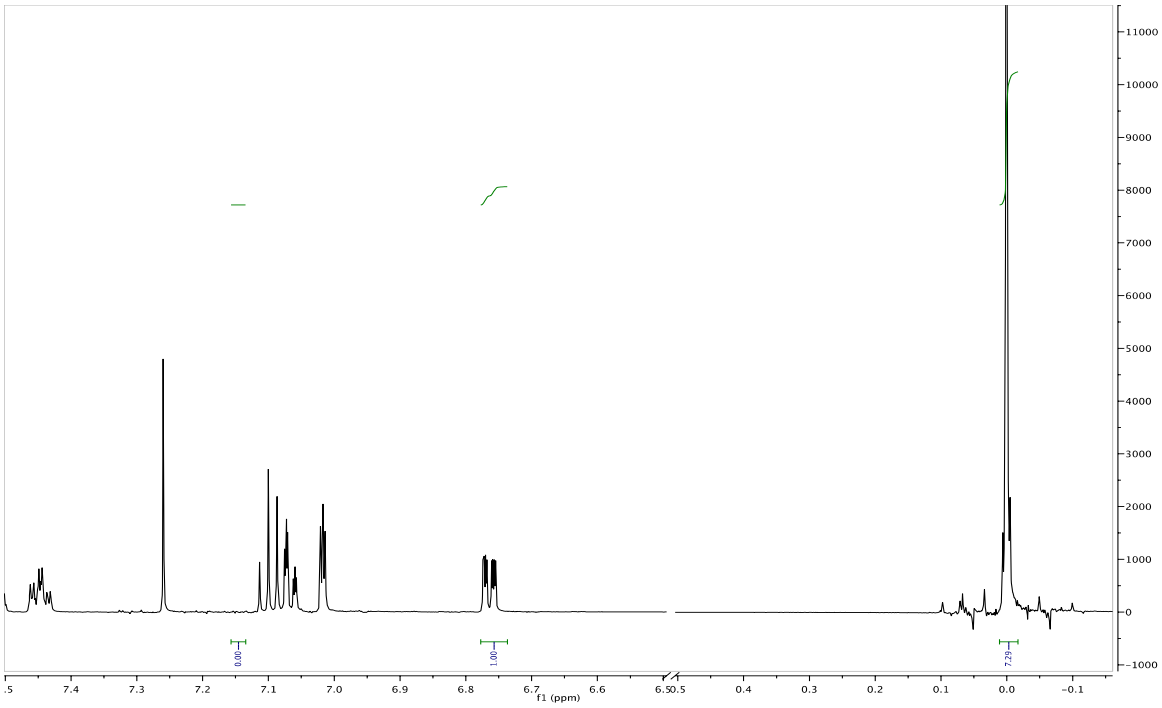

Figure 1.9.142 Example of 500 MHz ^{1}H NMR Spectrum for 1.14 + 1.1; t = 0 h

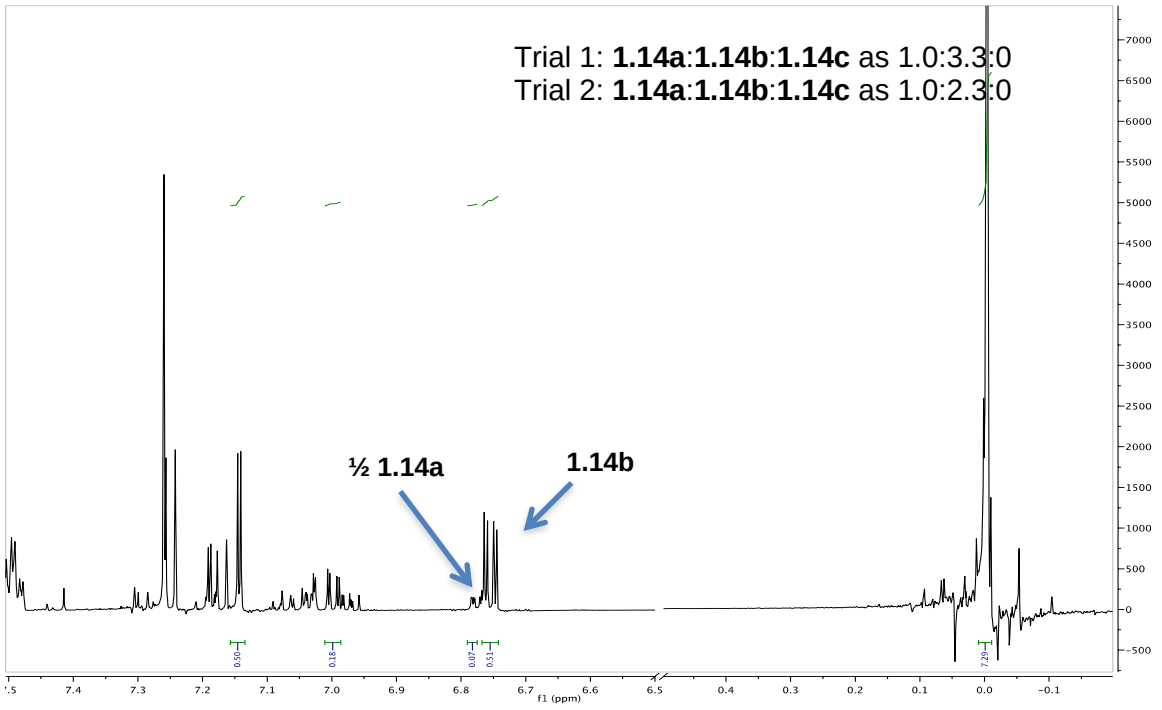

Figure 1.9.143 Example of 500 MHz ^{1}H NMR Spectrum for 1.14a + 1.14b +1.14c + 1.1; t = 3 h

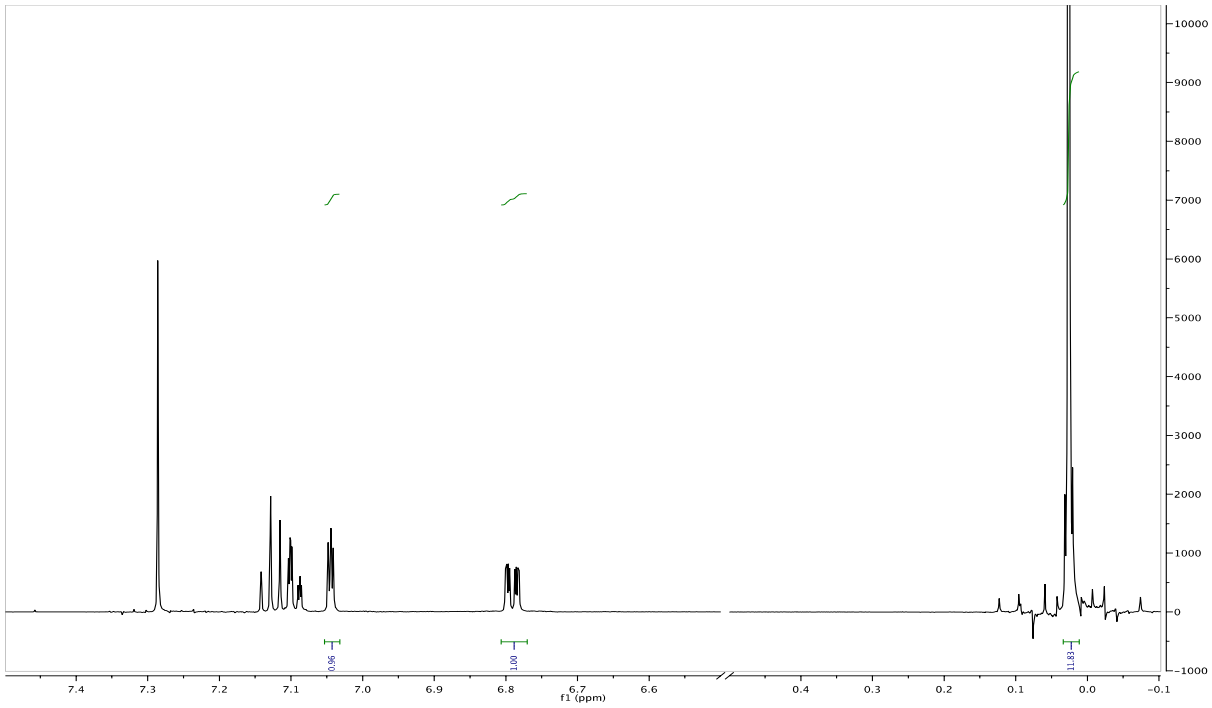

Figure 1.9.144 Example of 500 MHz ^{1}H NMR Spectrum for 1.14 + 1.6; t = 0 h

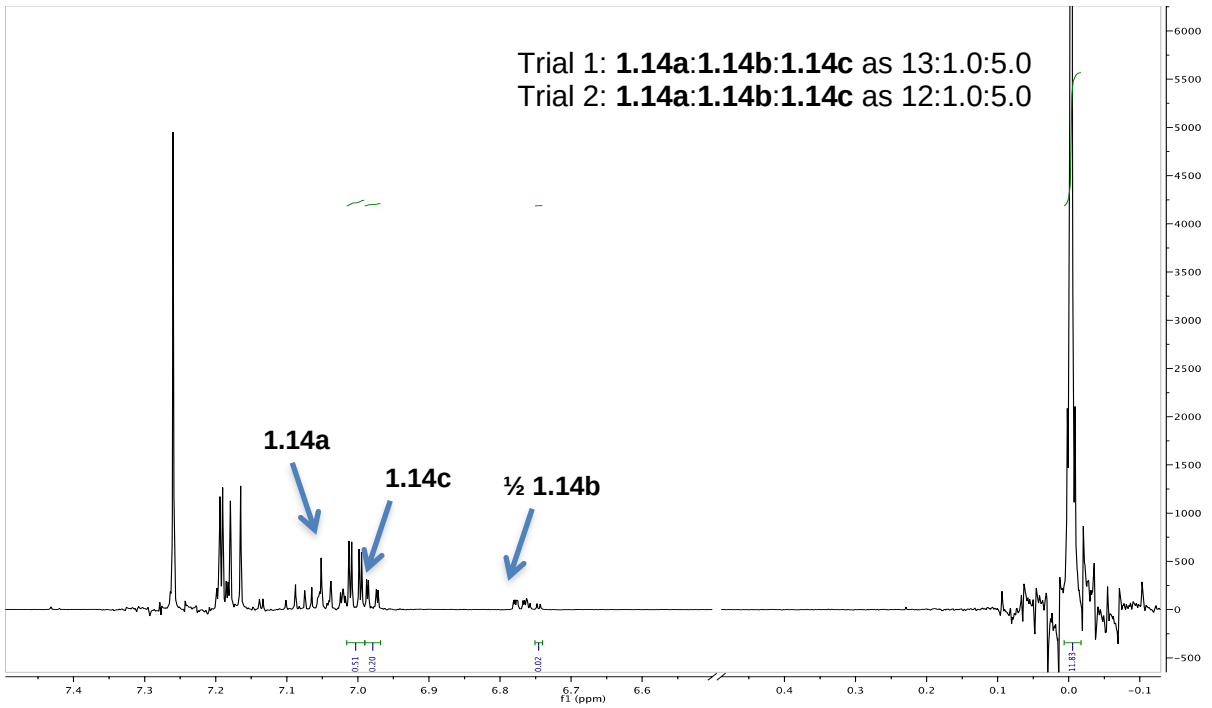

Figure 1.9.145 Example of 500 MHz ^{1}H NMR Spectrum for 1.14a + 1.14b +1.14c + 1.6; t = 3 h

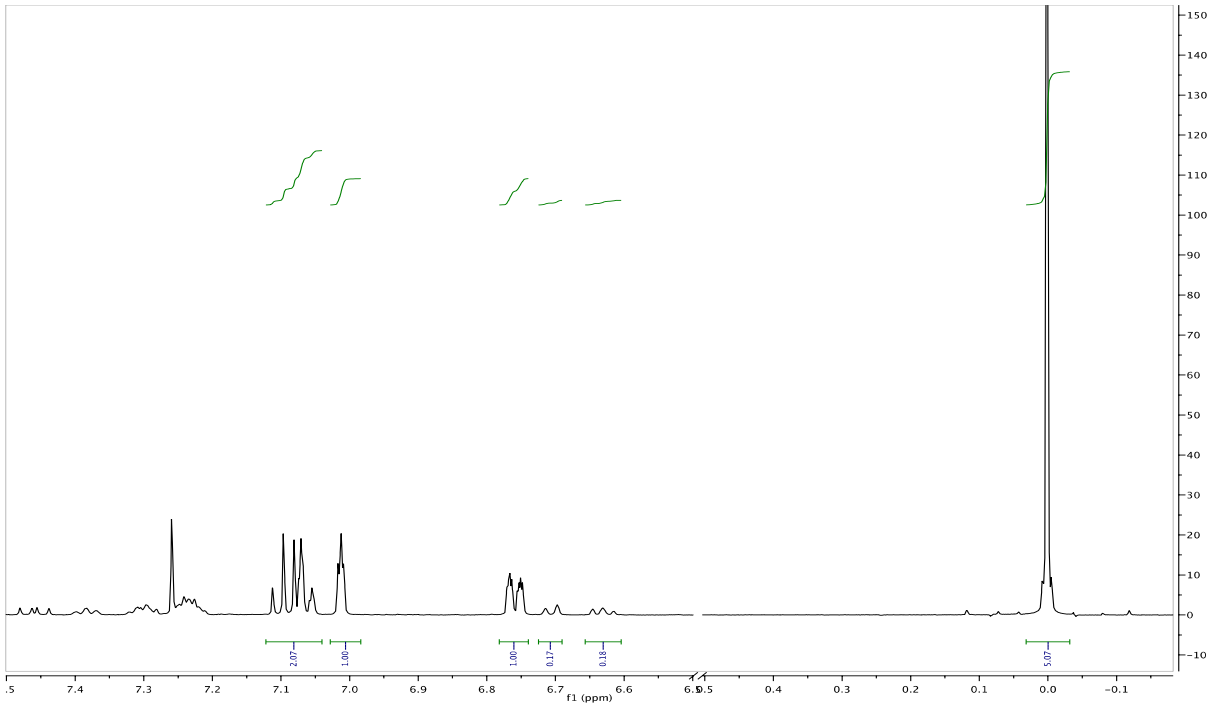

Figure 1.9.146 Example of 500 MHz ^{1}H NMR Spectrum for 1.14 + 1.7; t = 0 h

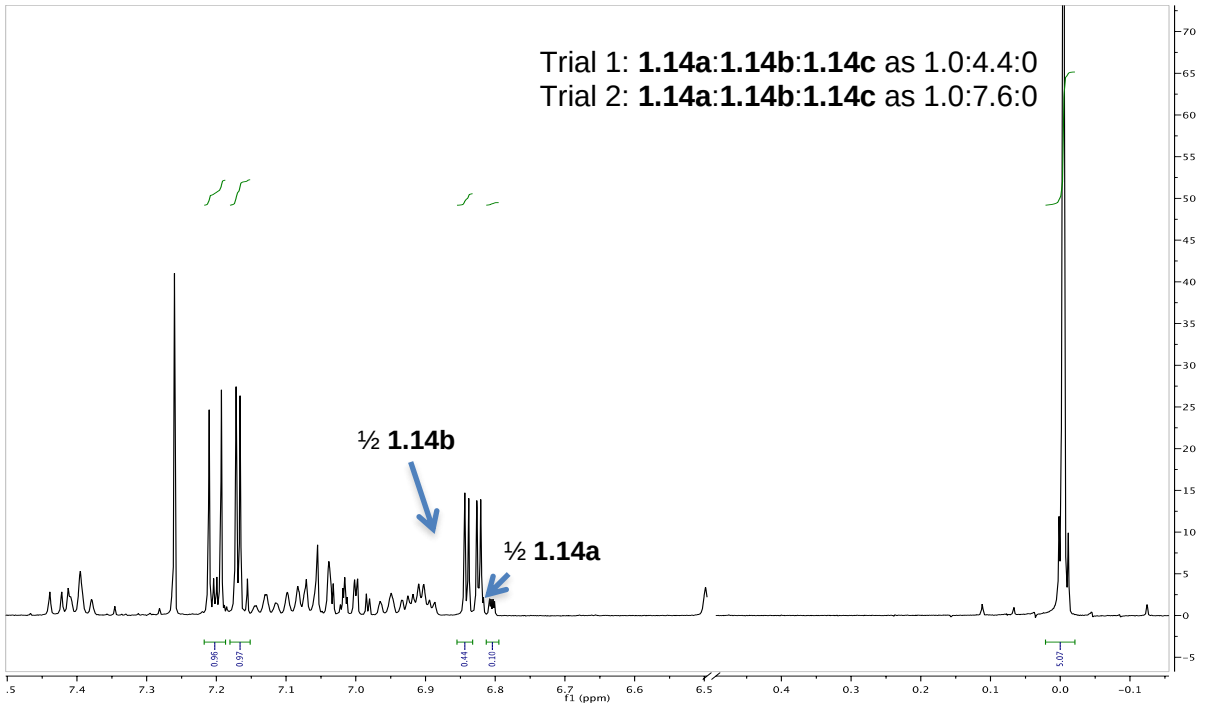

Figure 1.9.147 Example of 500 MHz ^{1}H NMR Spectrum for 1.14a + 1.14b +1.14c + 1.7; t = 2 h

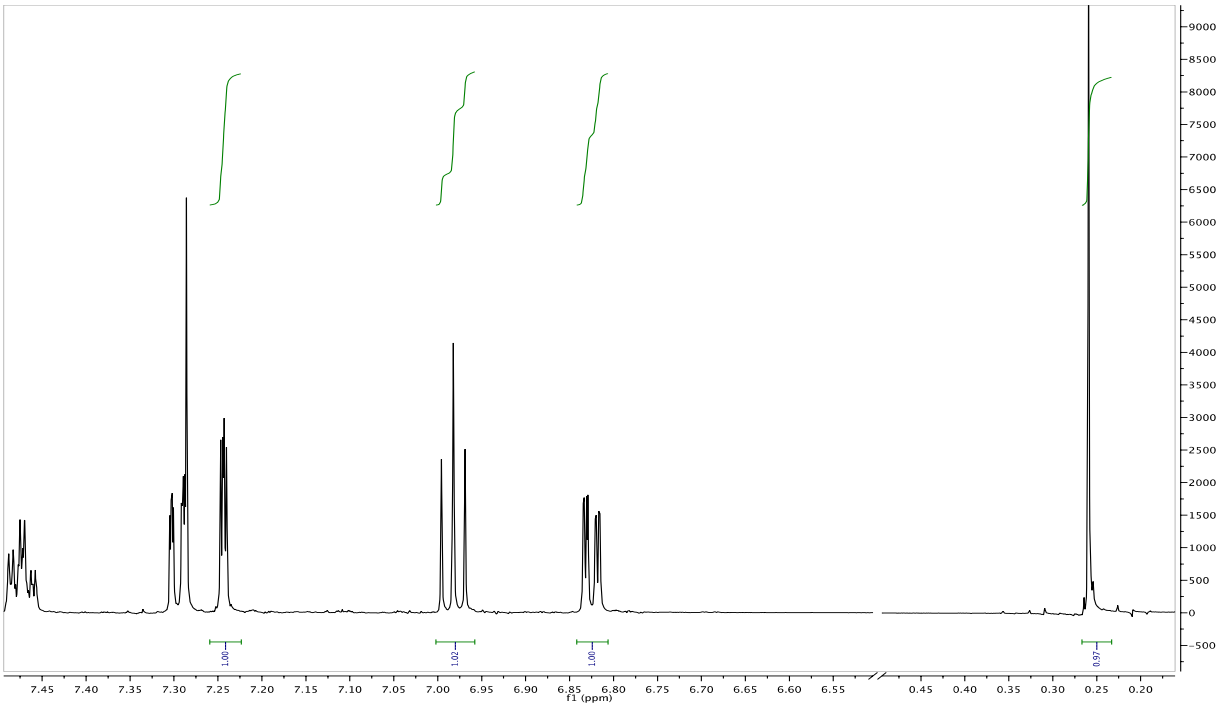

Figure 1.9.148 Example of 400 MHz ^{1}H NMR Spectrum for 1.15 + 1.1; t = 0 h

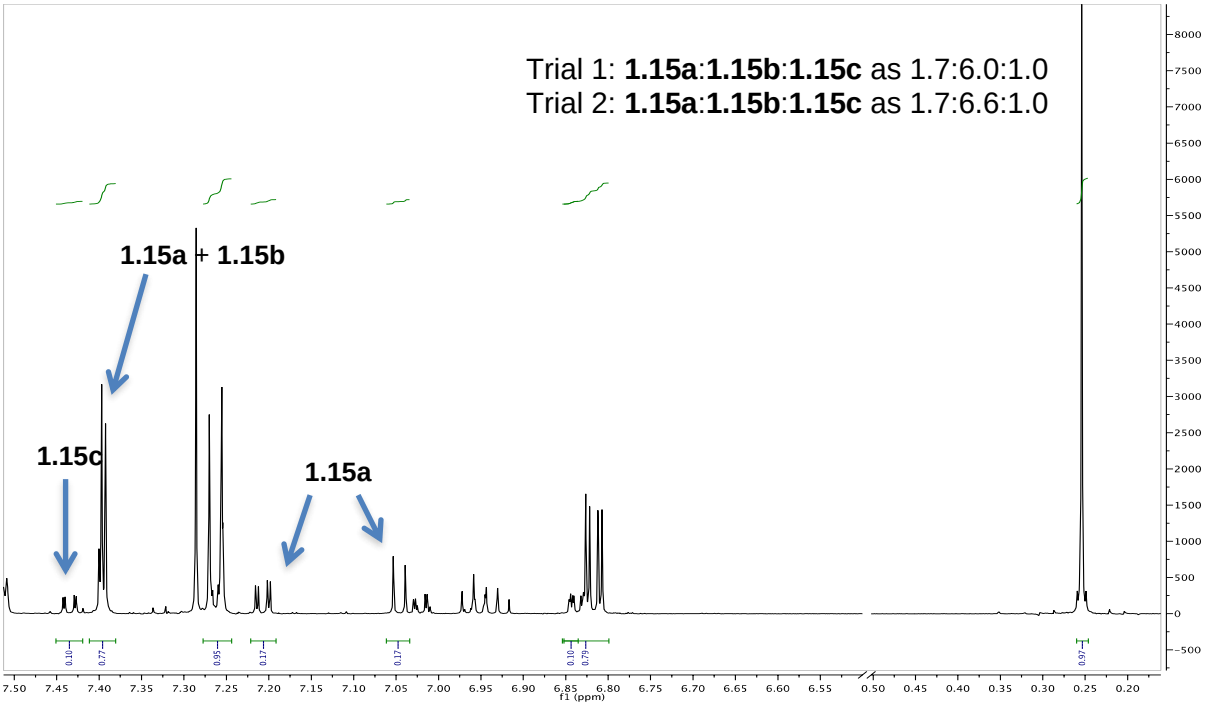

Figure 1.9.149 Example of 400 MHz ^{1}H NMR Spectrum for 1.15a + 1.15b +1.15c + 1.1; t = 5 h

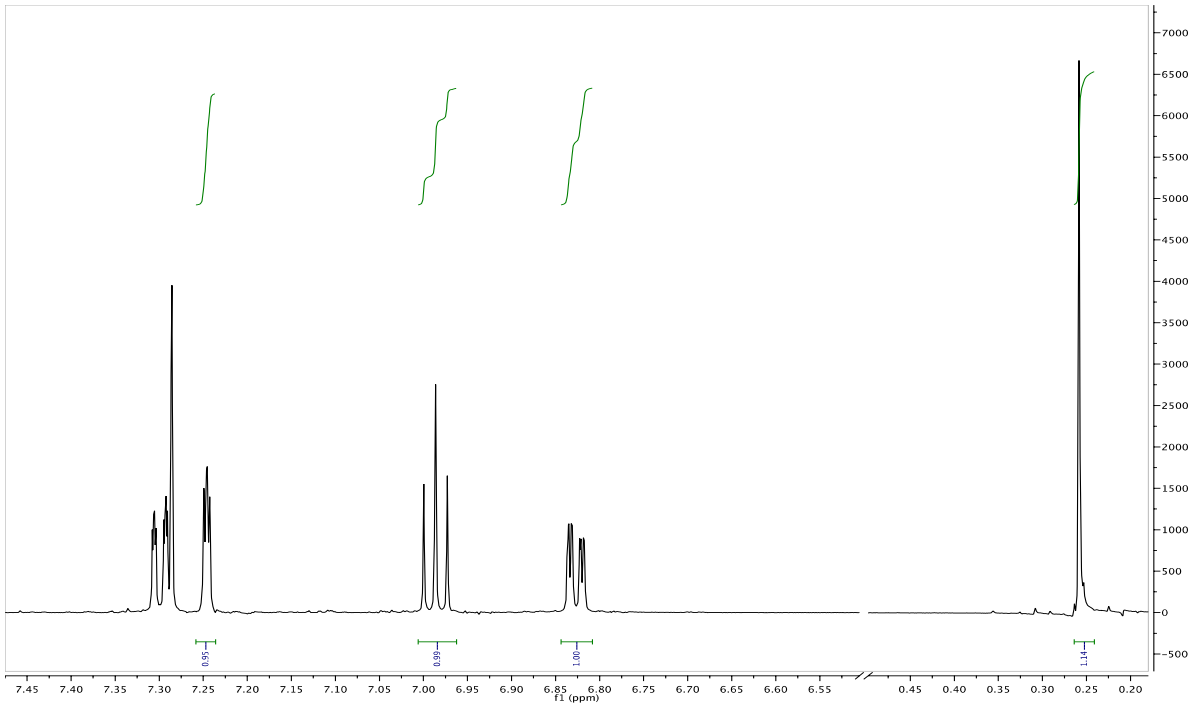

Figure 1.9.150 Example of 400 MHz ^{1}H NMR Spectrum for 1.15 + 1.6; t = 0 h

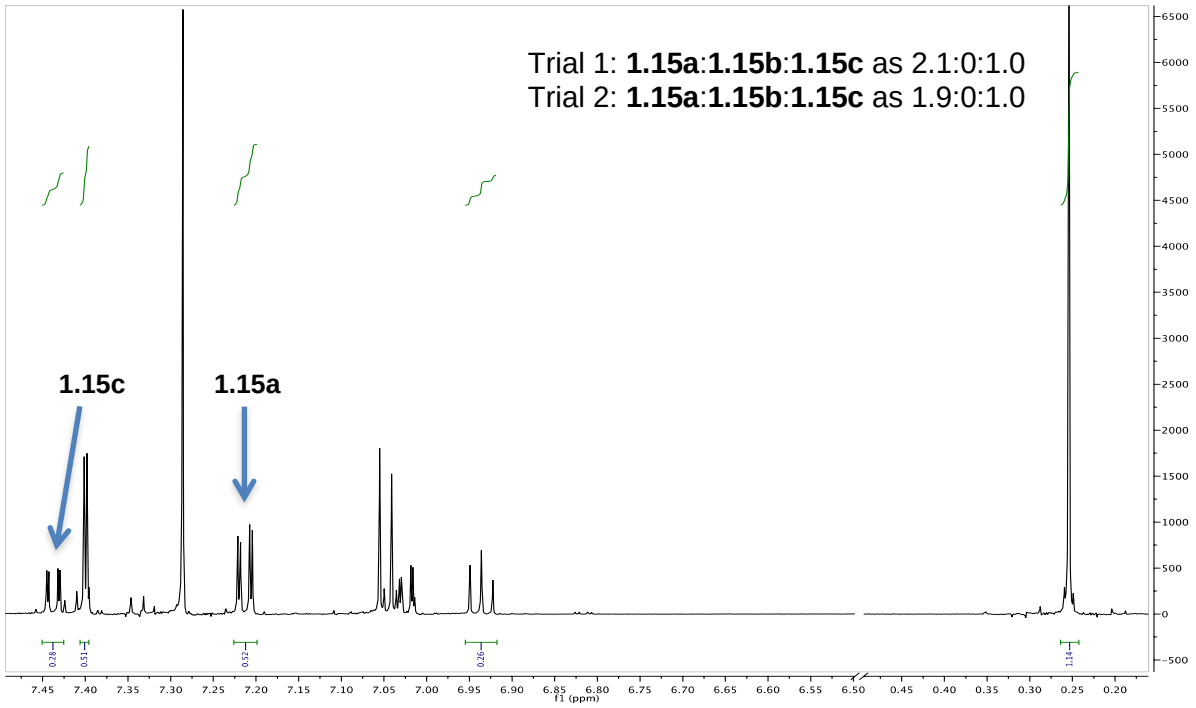

Figure 1.9.151 Example of 400 MHz ^{1}H NMR Spectrum for 1.15a + 1.15b +1.15c + 1.6; t = 5 h

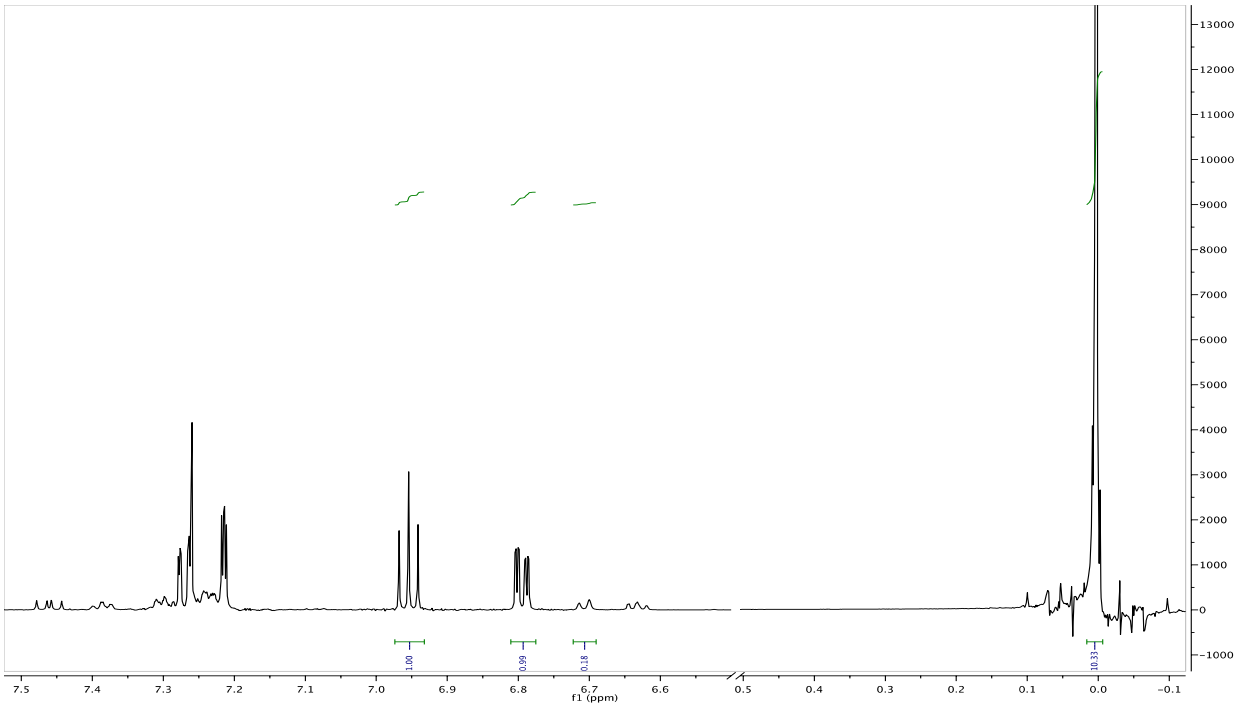

Figure 1.9.152 Example of 400 MHz ^{1}H NMR Spectrum for 1.15 + 1.7; t = 0 h

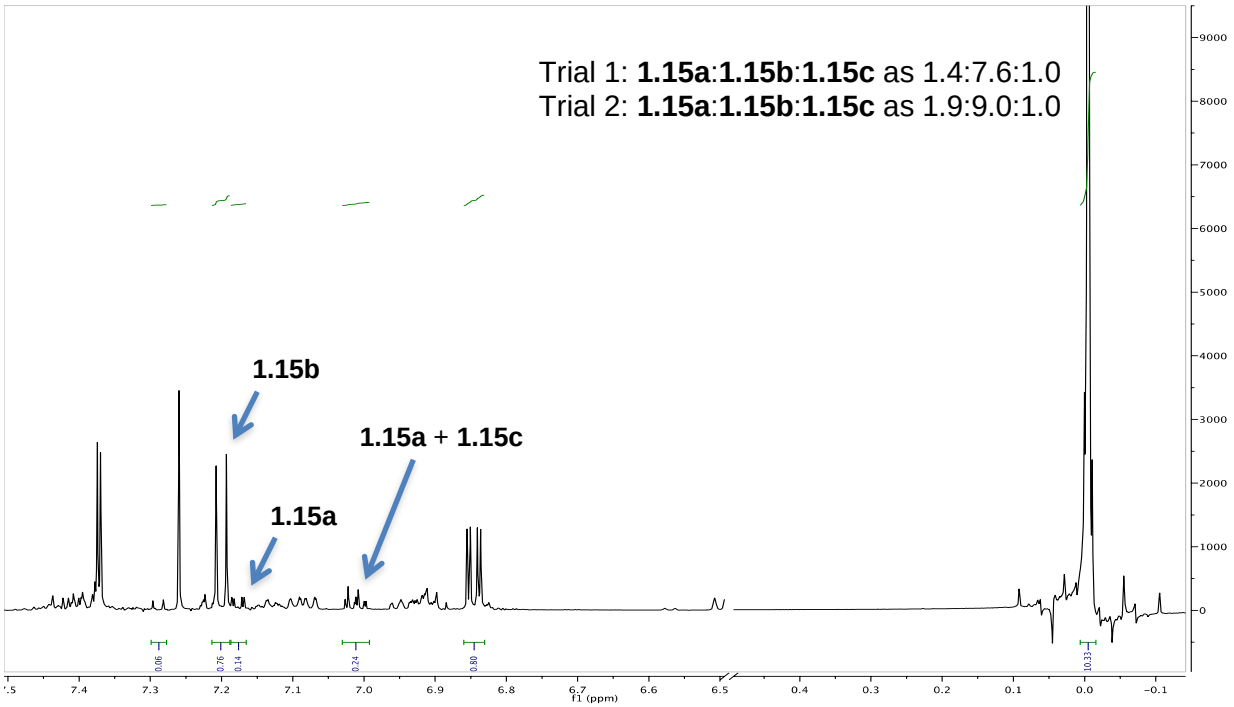

Figure 1.9.153 Example of 400 MHz ^{1}H NMR Spectrum for 1.15a + 1.15b +1.15c + 1.7; t = 1 h

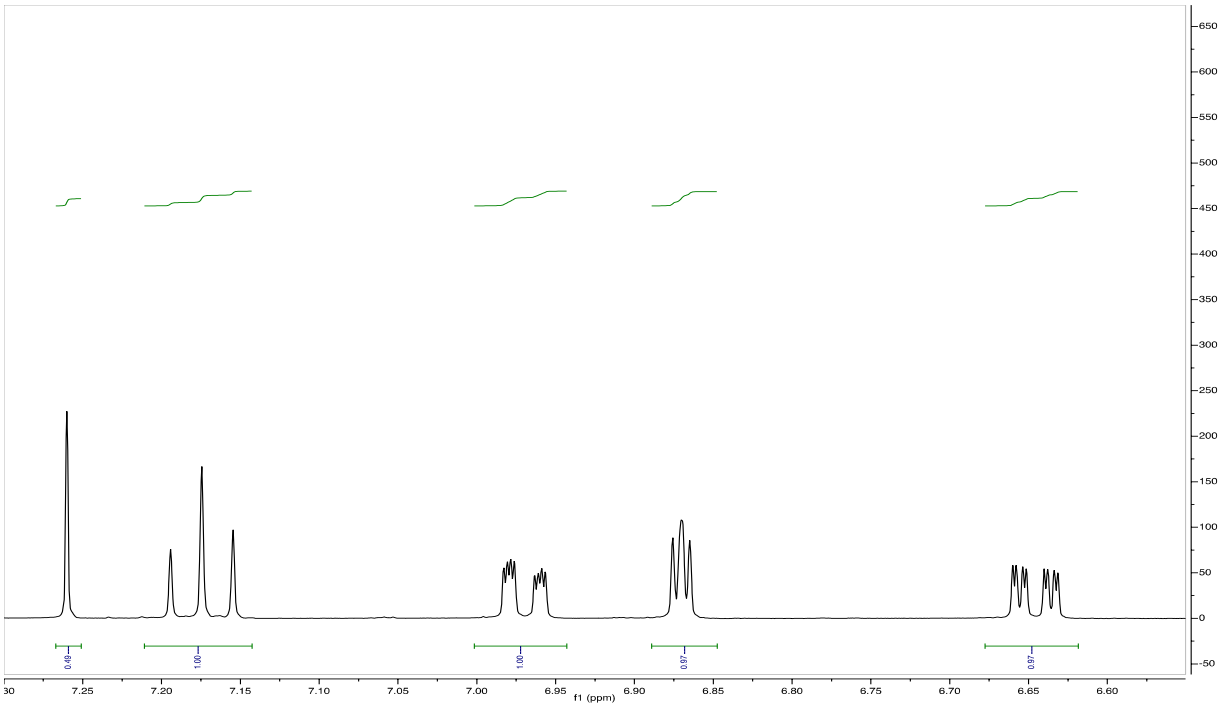

Figure 1.9.154 Example of 400 MHz ^{1}H NMR spectrum for 1.16 + 1.1; t = 0 h

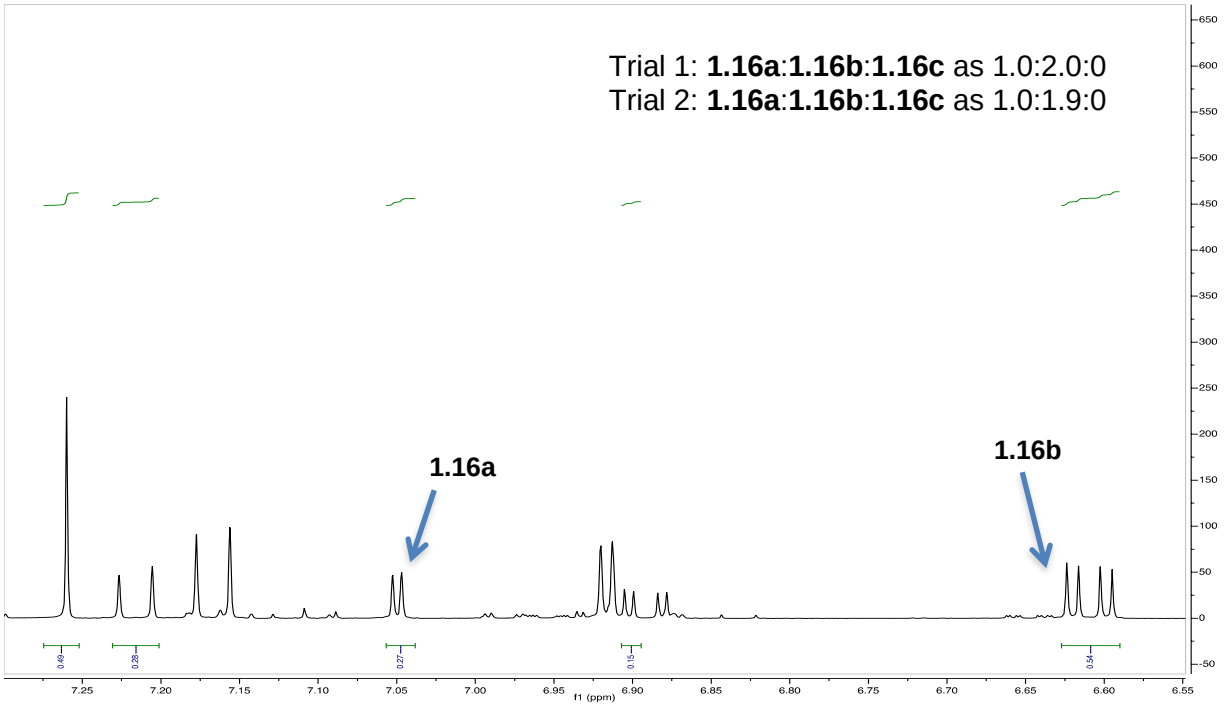

Figure 1.9.155 Example of 400 MHz ^{1}H NMR spectrum for 1.16a + 1.16b +1.16c + 1.1; t = 12 h

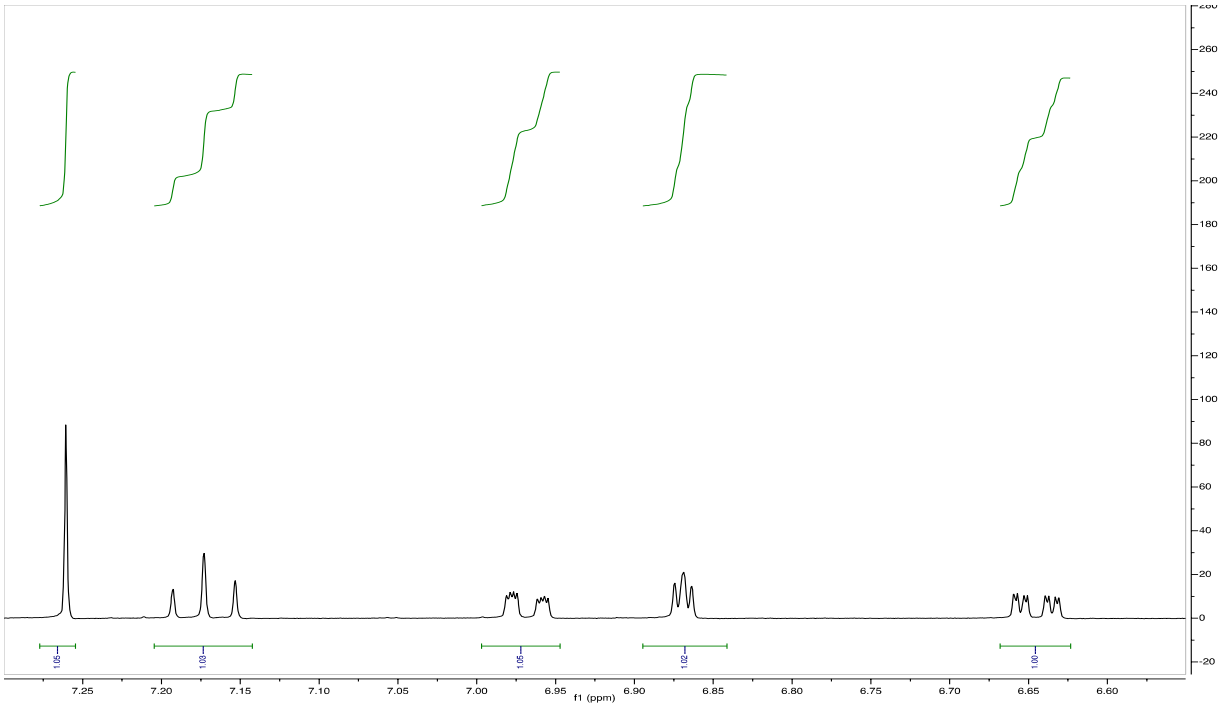

Figure 1.9.156 Example of 400 MHz ^{1}H NMR spectrum for 1.16 + 1.6; t = 0 h

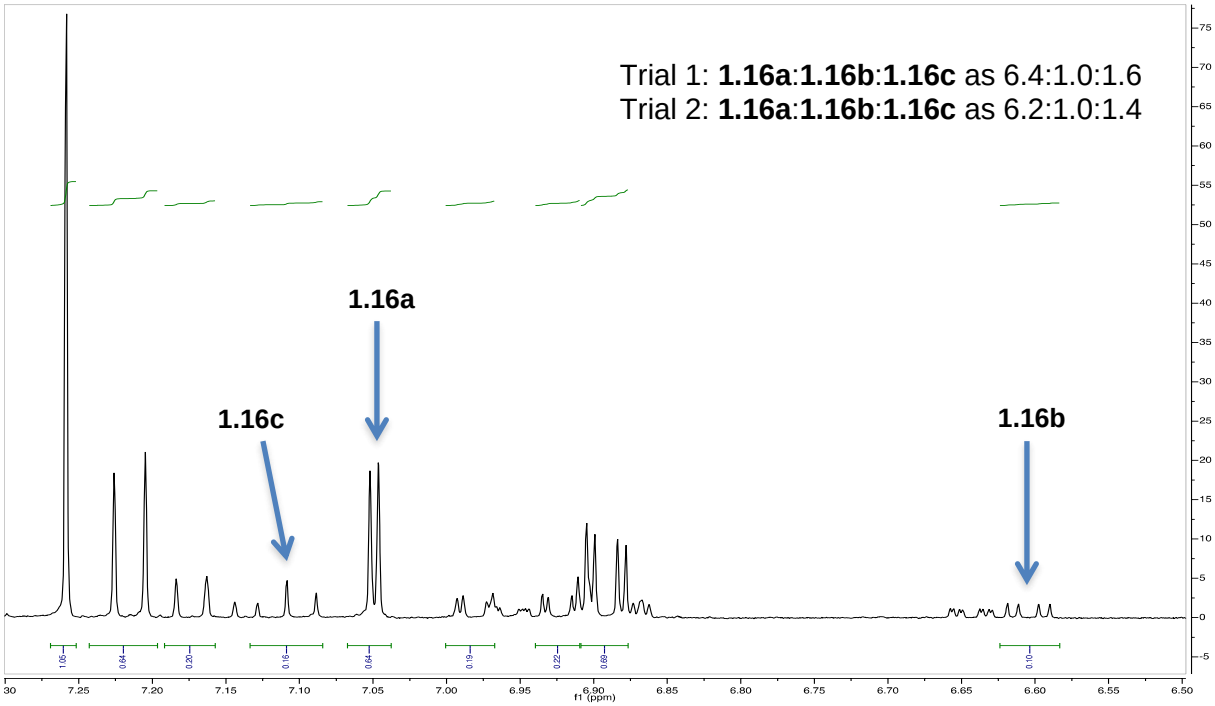

Figure 1.9.157 Example of 400 MHz ^{1}H NMR spectrum for 1.16a + 1.16b +1.16c + 1.6; t = 12 h

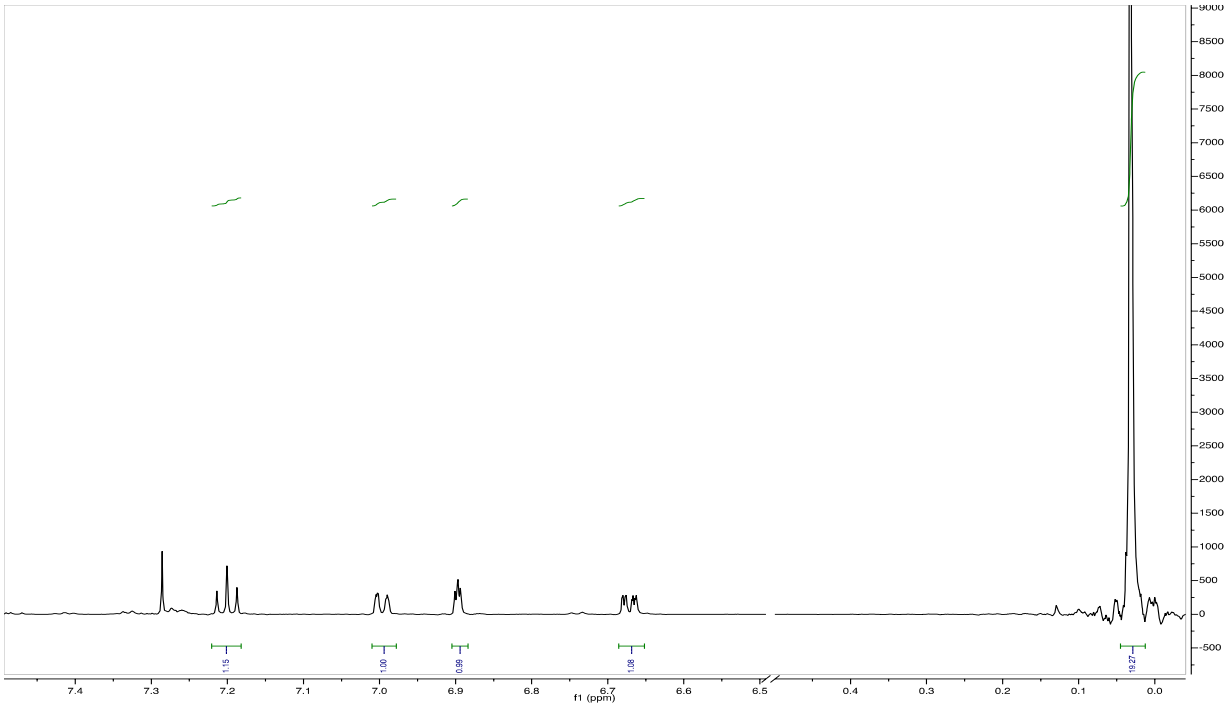

Figure 1.9.158 Example of 400 MHz ^{1}H NMR spectrum for 1.16 + 1.7; t = 0 h

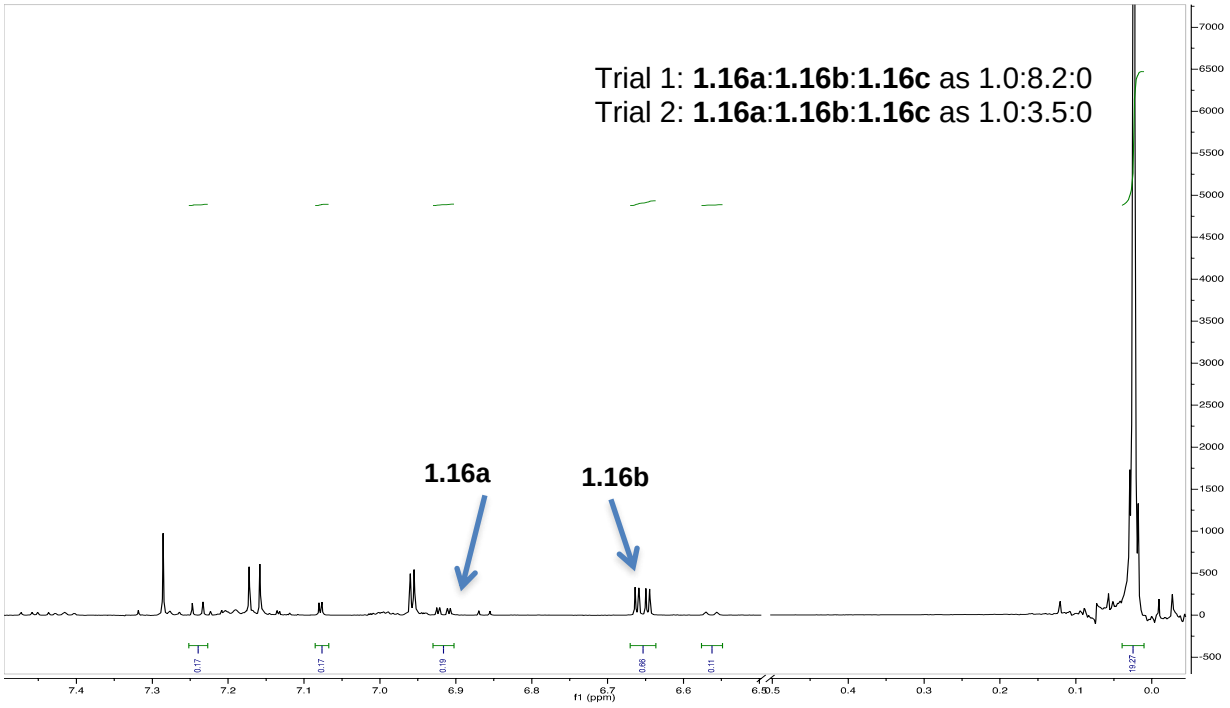

Figure 1.9.159 Example of 400 MHz ^{1}H NMR spectrum for 1.16a + 1.16b +1.16c + 1.7; t = 12 h

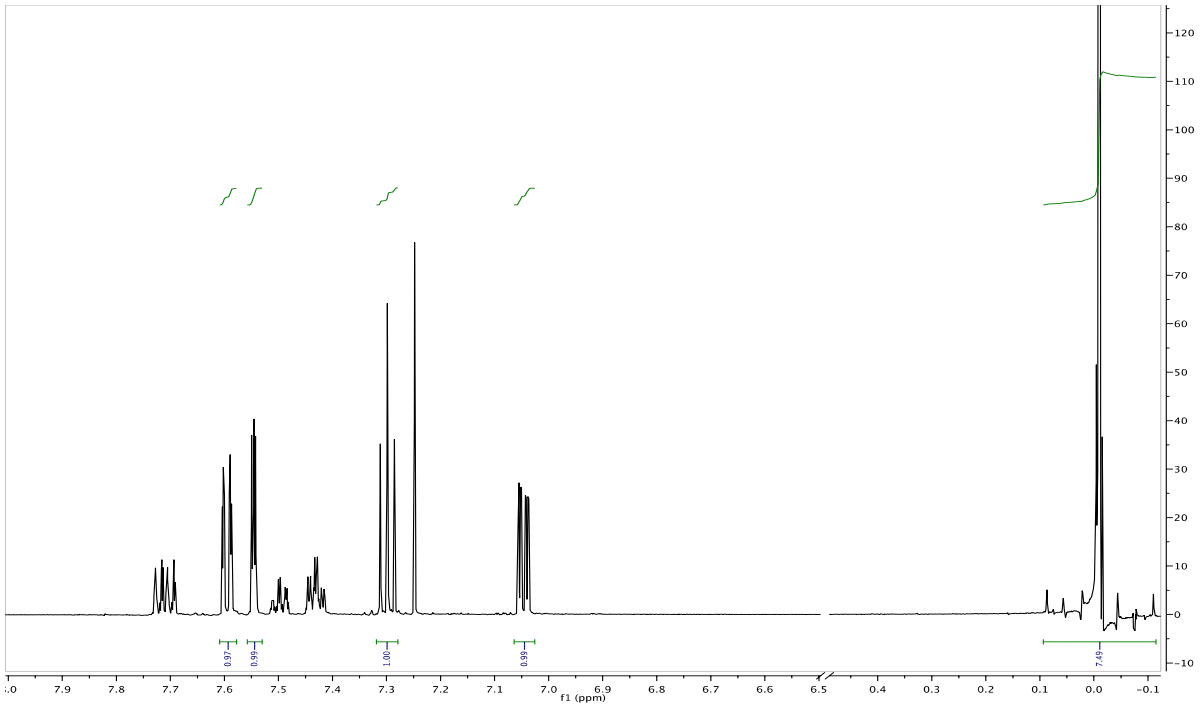

Figure 1.9.160 Example of 400 MHz ^{1}H NMR spectrum for 1.17 + 1.1; t = 0 h

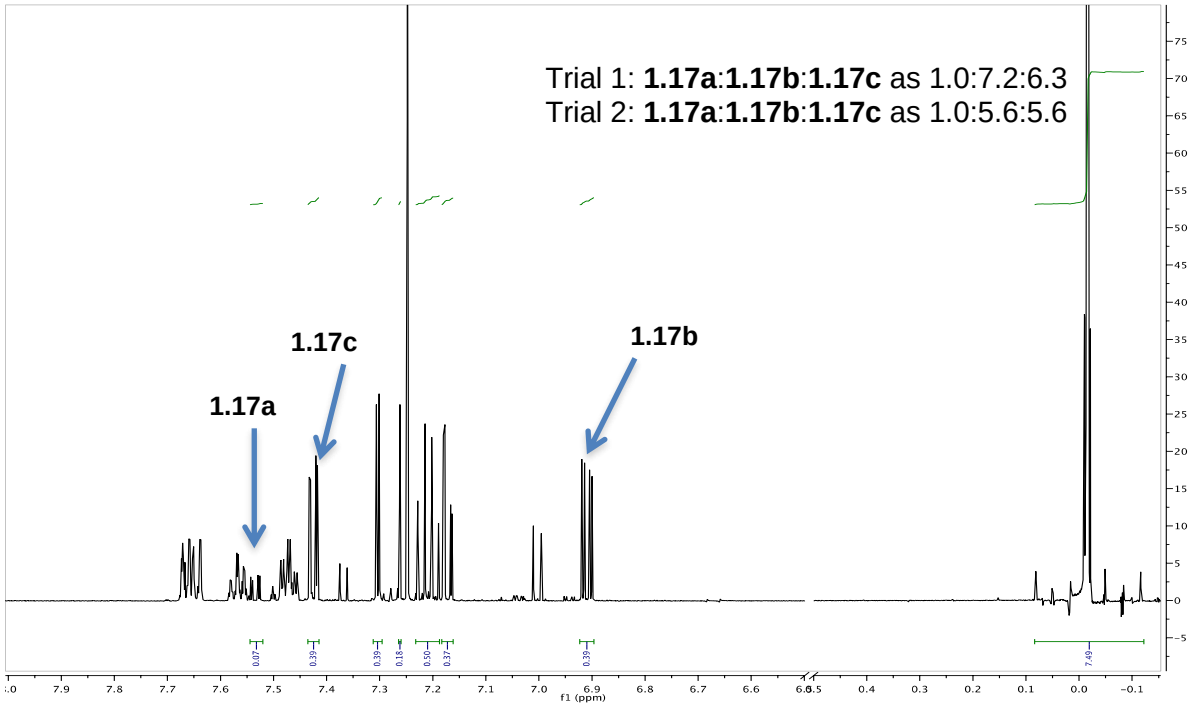

Figure 1.9.161 Example of 400 MHz ^{1}H NMR spectrum for 1.17a + 1.17b +1.17c + 1.1; t = 20 h

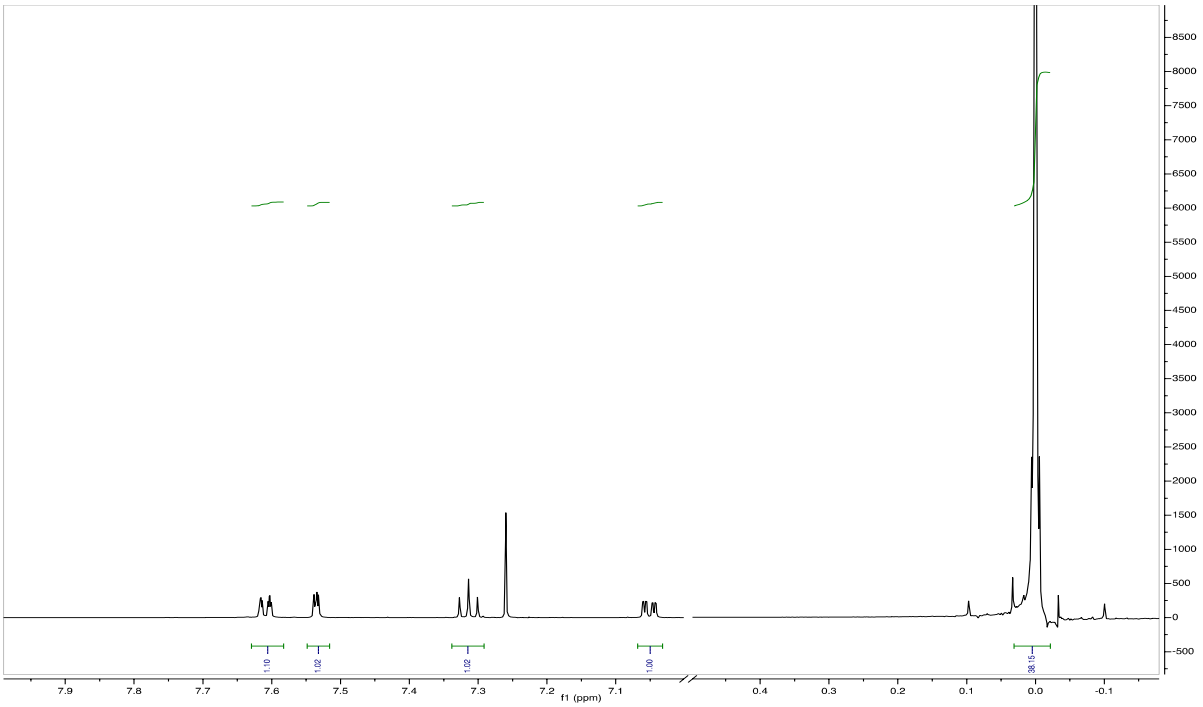

Figure 1.9.162 Example of 400 MHz ^{1}H NMR spectrum for 1.17 + 1.6; t = 0 h

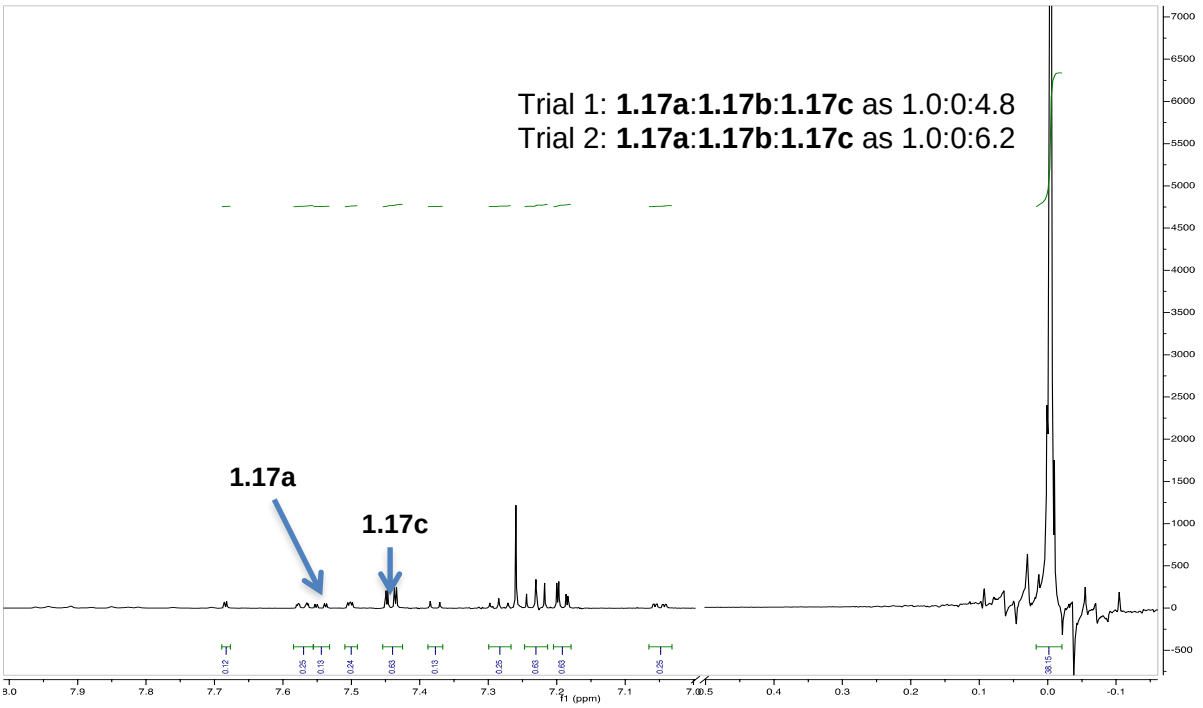

Figure 1.9.163 Example of 400 MHz ^{1}H NMR spectrum for 1.17a + 1.17b +1.17c + 1.6; t = 20 h

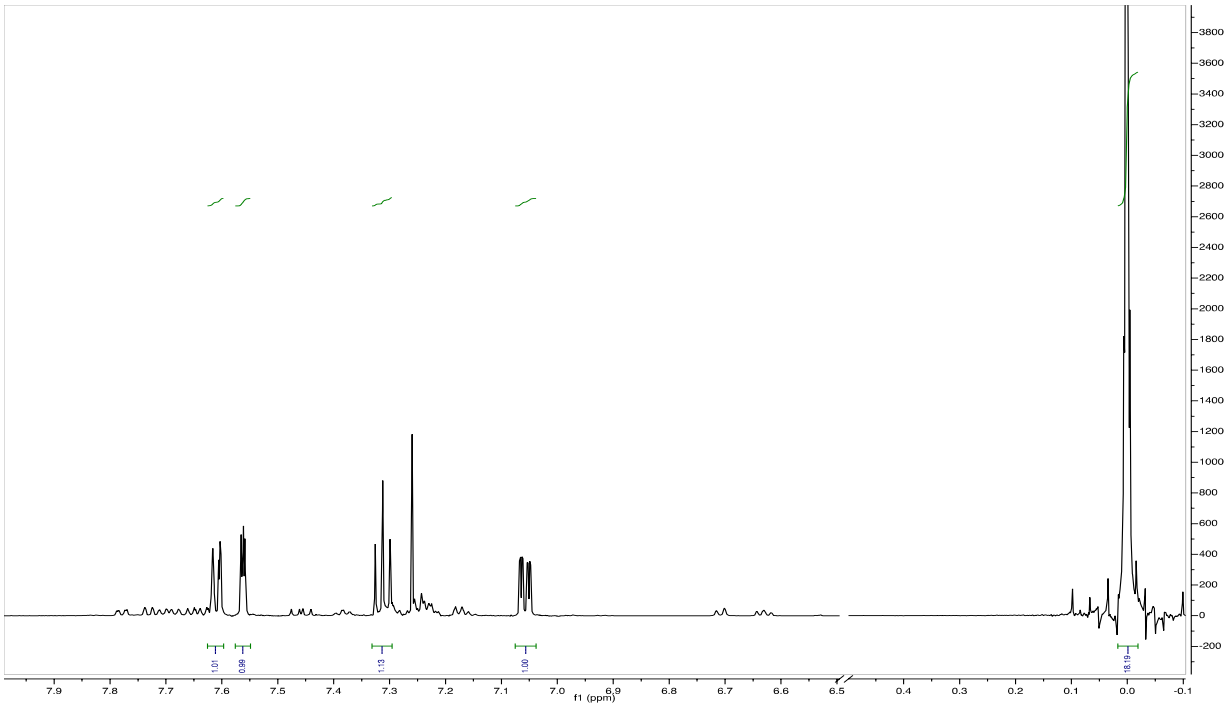

Figure 1.9.164 Example of 400 MHz ^{1}H NMR spectrum for 1.17 + 1.7; t = 0 h

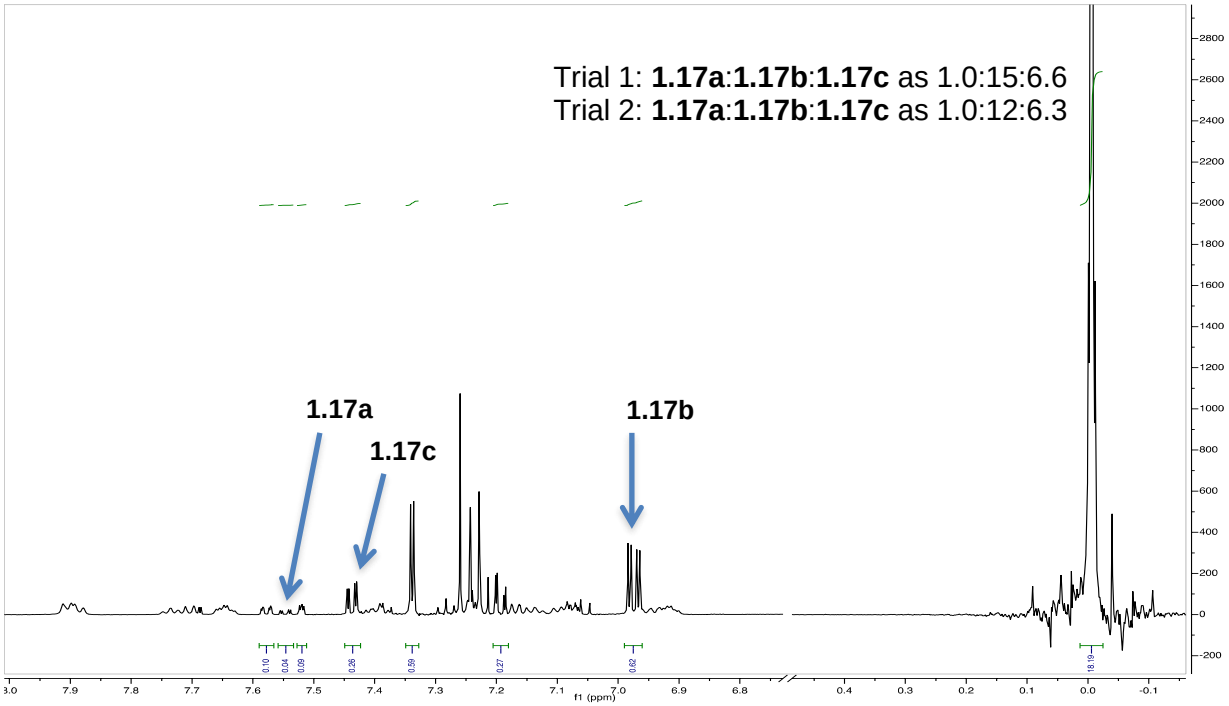

Figure 1.9.165 Example of 400 MHz ^{1}H NMR spectrum for 1.17a + 1.17b +1.17c + 1.7; t = 2 h

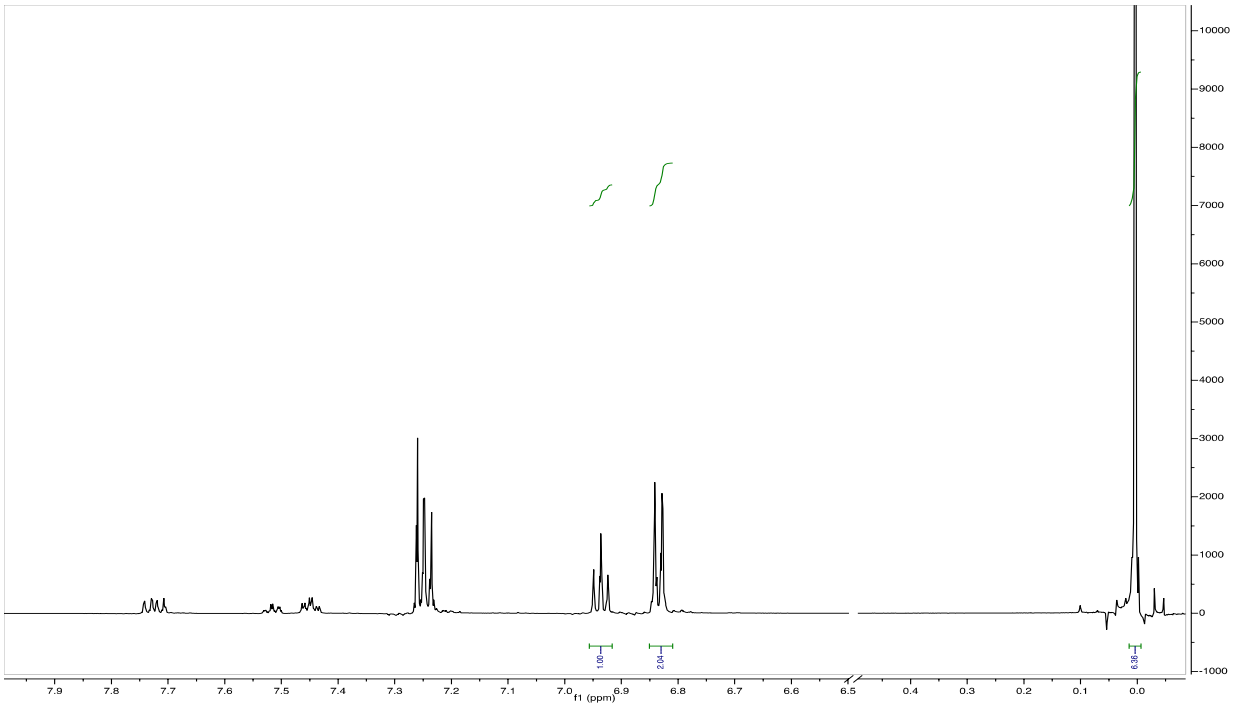

Figure 1.9.166 Example of 500 MHz ^{1}H NMR spectrum for 1.3 + 1.1; t = 0 h

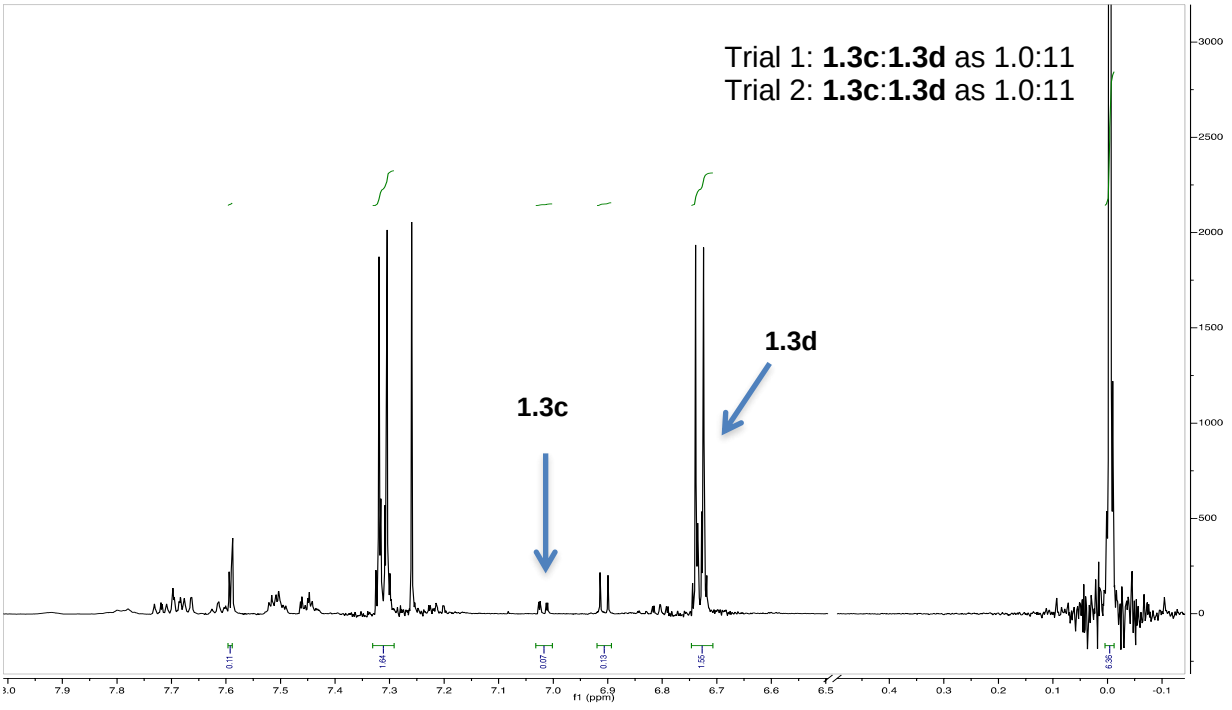

Figure 1.9.167 Example of 500 MHz ^{1}H NMR spectrum for 1.3c + 1.3d + 1.1; t = 30 min

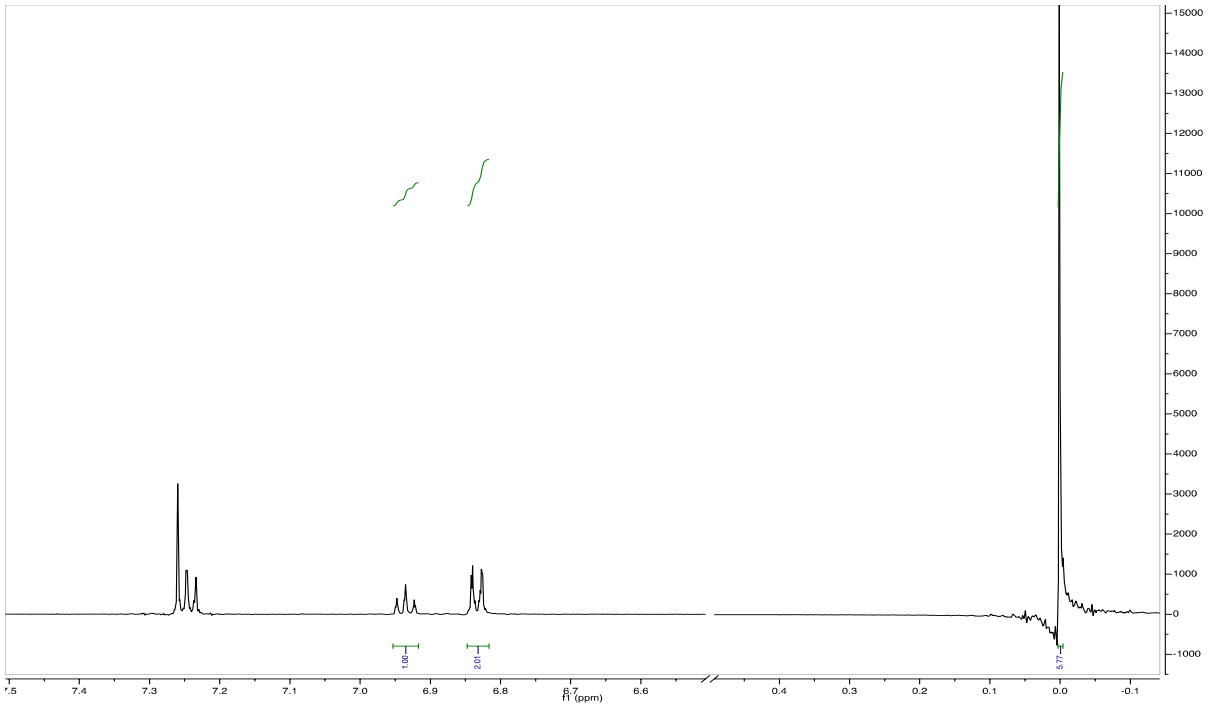

Figure 1.9.168 Example of 500 MHz ^{1}H NMR spectrum for 1.3 + 1.6; t = 0 h

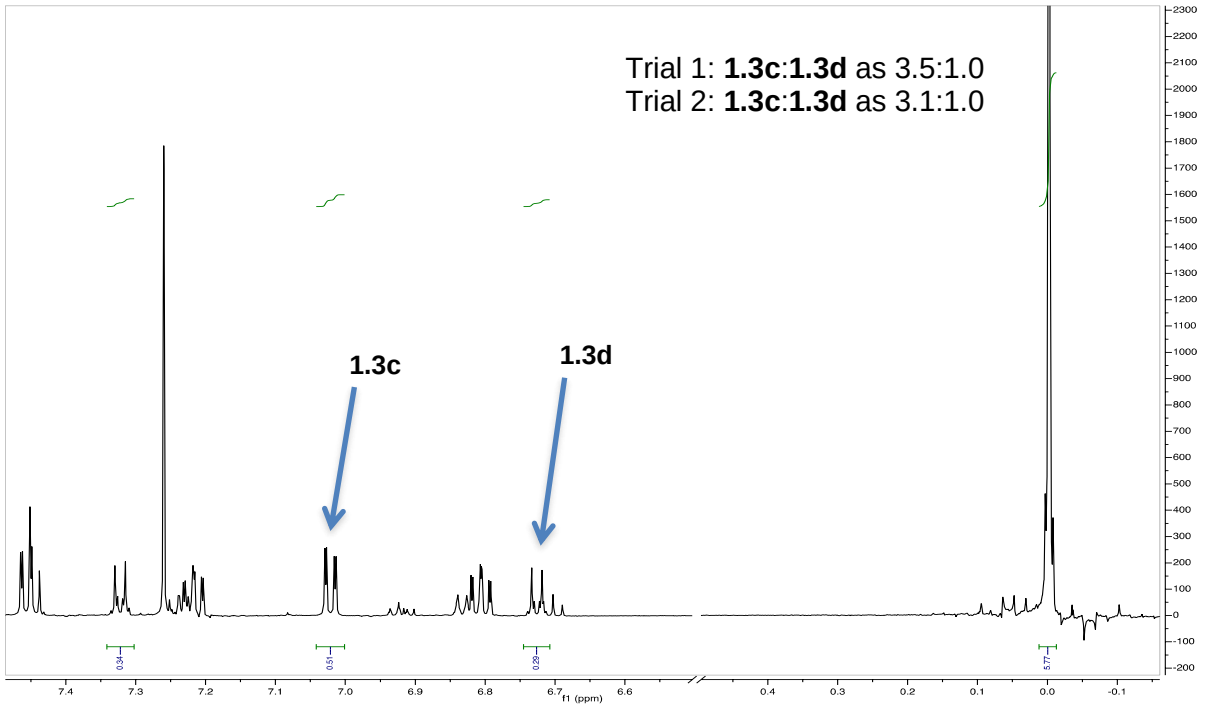

Figure 1.9.169 Example of 500 MHz ^{1}H NMR spectrum for 1.3c + 1.3d + 1.6; t = 30 min

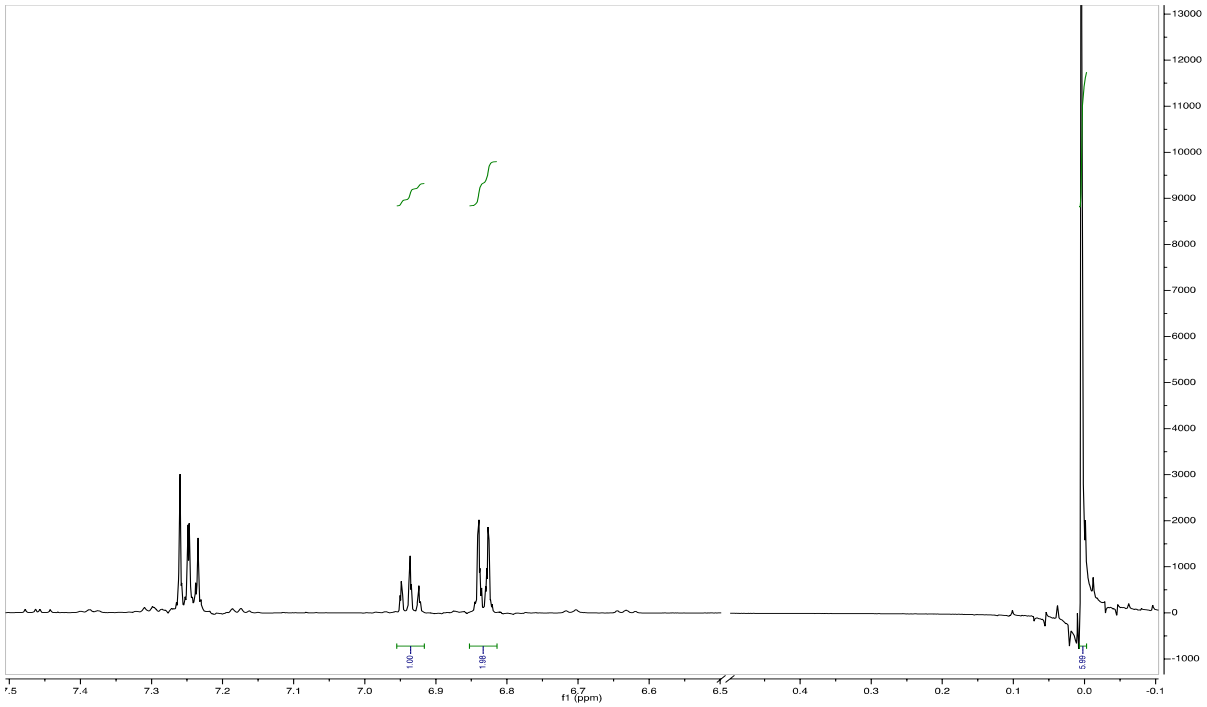

Figure 1.9.170 Example of 500 MHz ^{1}H NMR spectrum for 1.3 + 1.7; t = 0 h

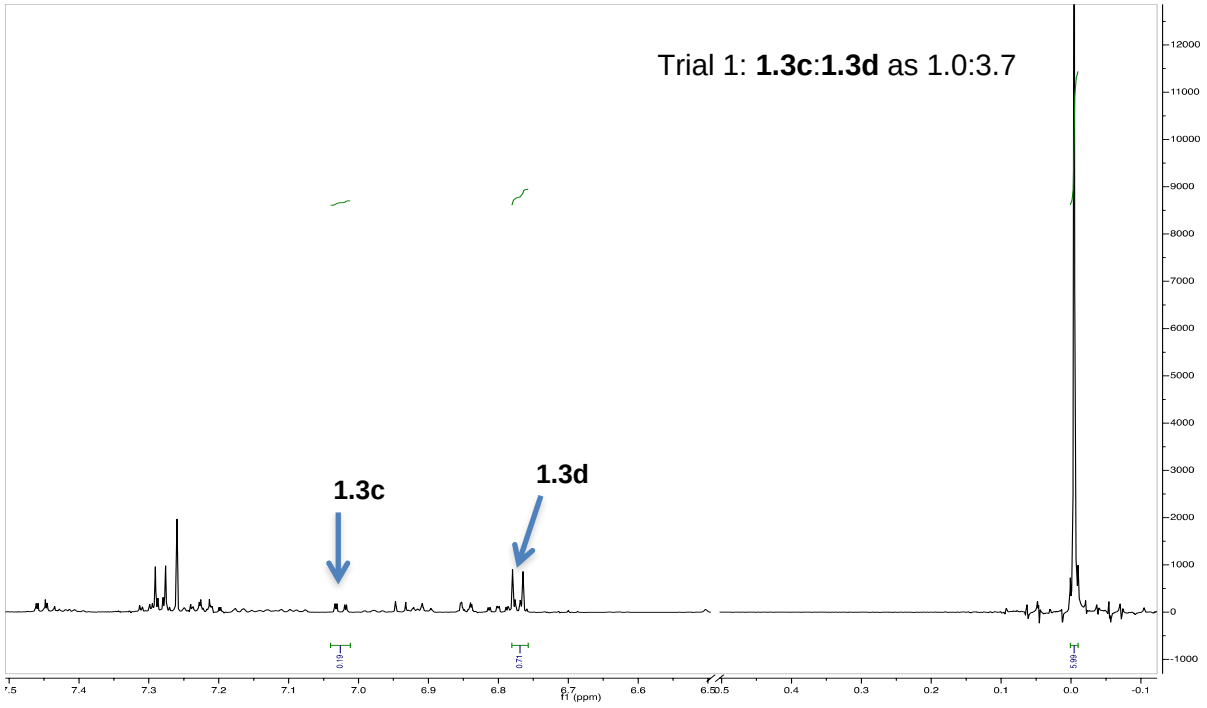

Figure 1.9.171 Example of 500 MHz ^{1}H NMR spectrum for 1.3c + 1.3d + 1.7; t = 30 min

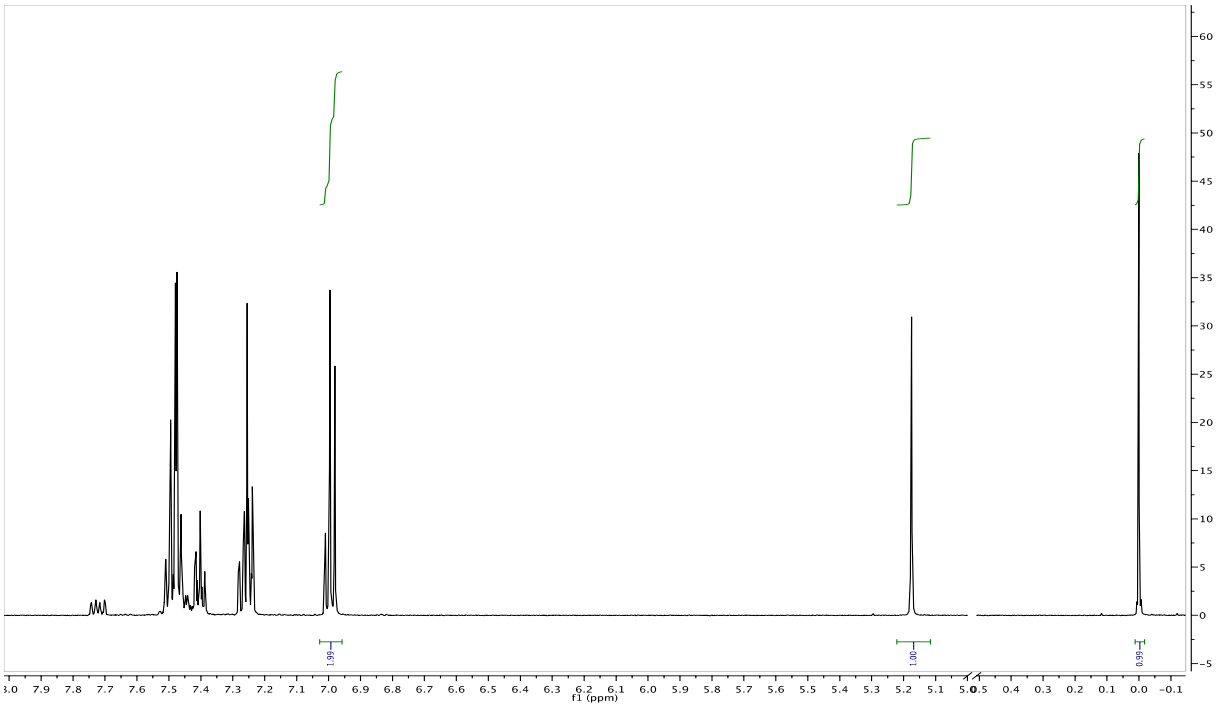

Figure 1.9.172 Example of 500 MHz ^{1}H NMR spectrum for 1.8 + 1.1; t = 0 h

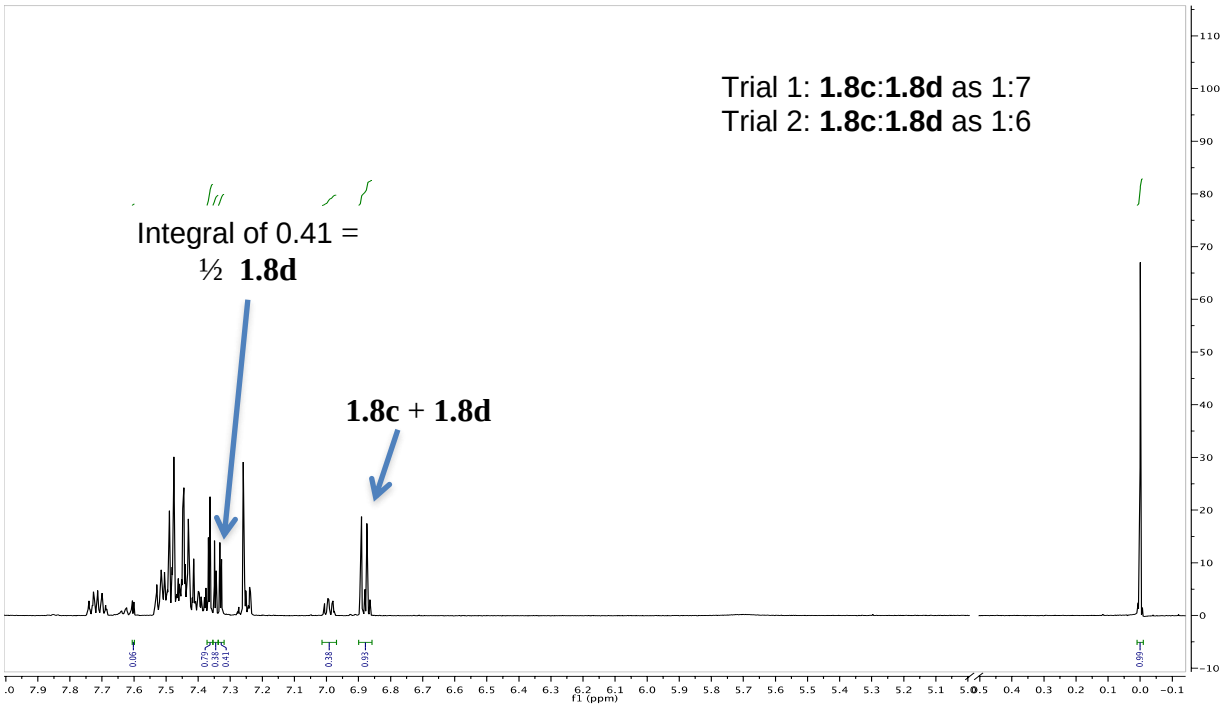

Figure 1.9.173 Example of 500 MHz ^{1}H NMR spectrum for 1.8c + 1.8d + 1.1; t = 12 h

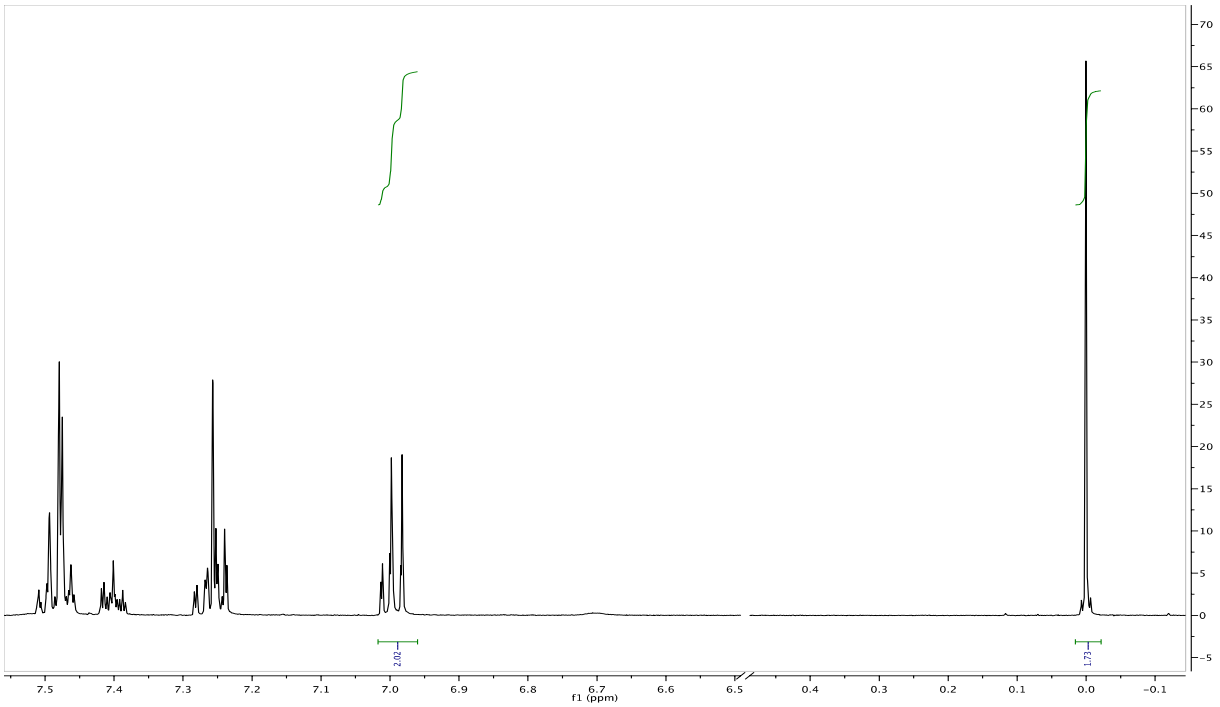

Figure 1.9.174 Example of 500 MHz ^{1}H NMR spectrum for 1.8 + 1.6; t = 0 h

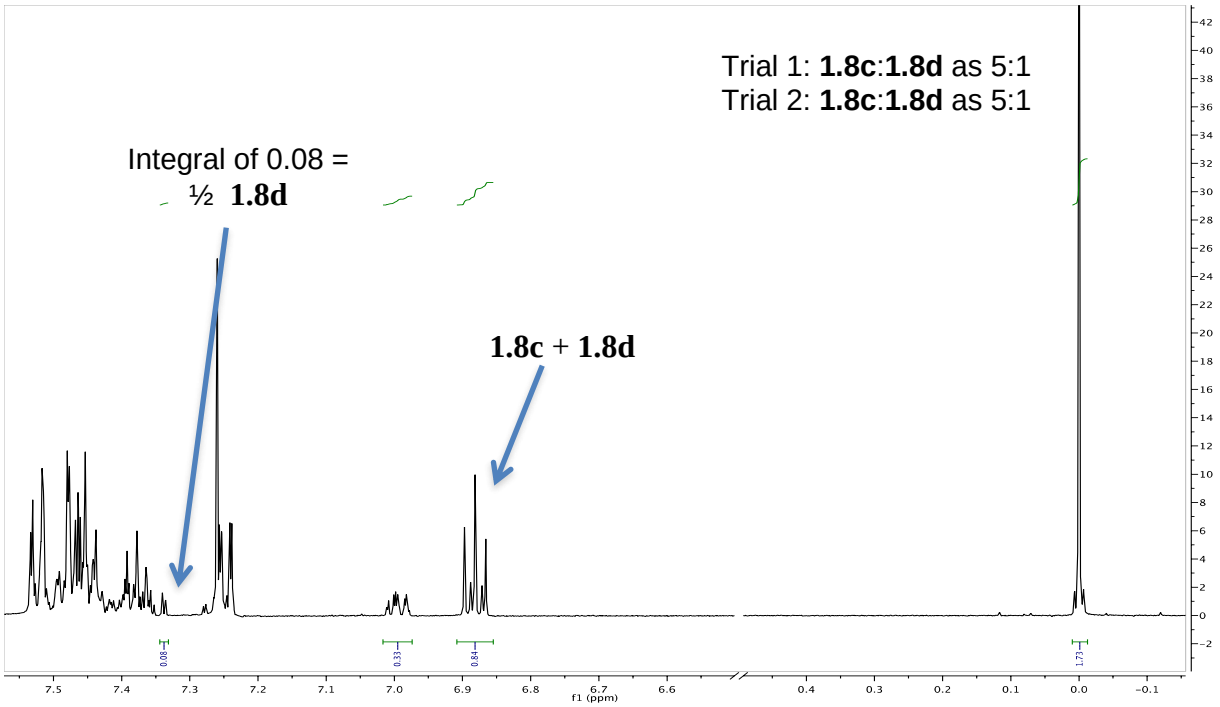

Figure 1.9.175 Example of 500 MHz ^{1}H NMR spectrum for 1.8c + 1.8d + 1.6; t = 12 h

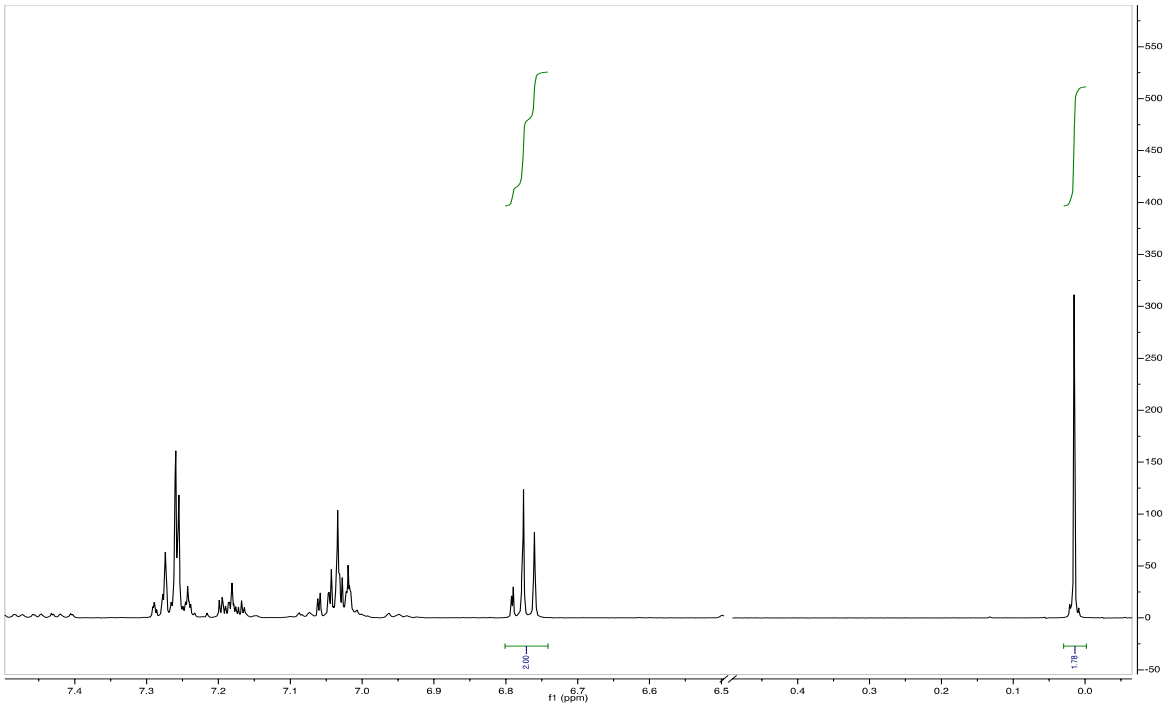

Figure 1.9.176 Example of 500 MHz ^{1}H NMR spectrum for 1.8 + 1.7; t = 0 h

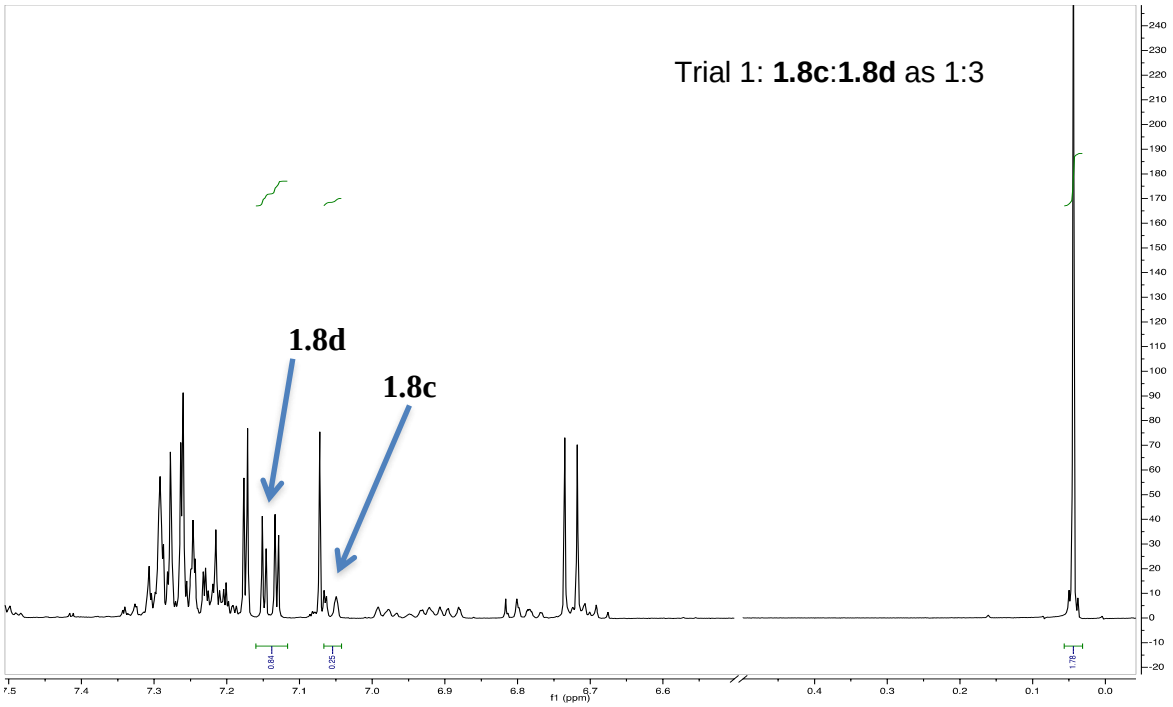

Figure 1.9.177 Example of 500 MHz ^{1}H NMR spectrum for 1.8c + 1.8d + 1.7; t = 12 h

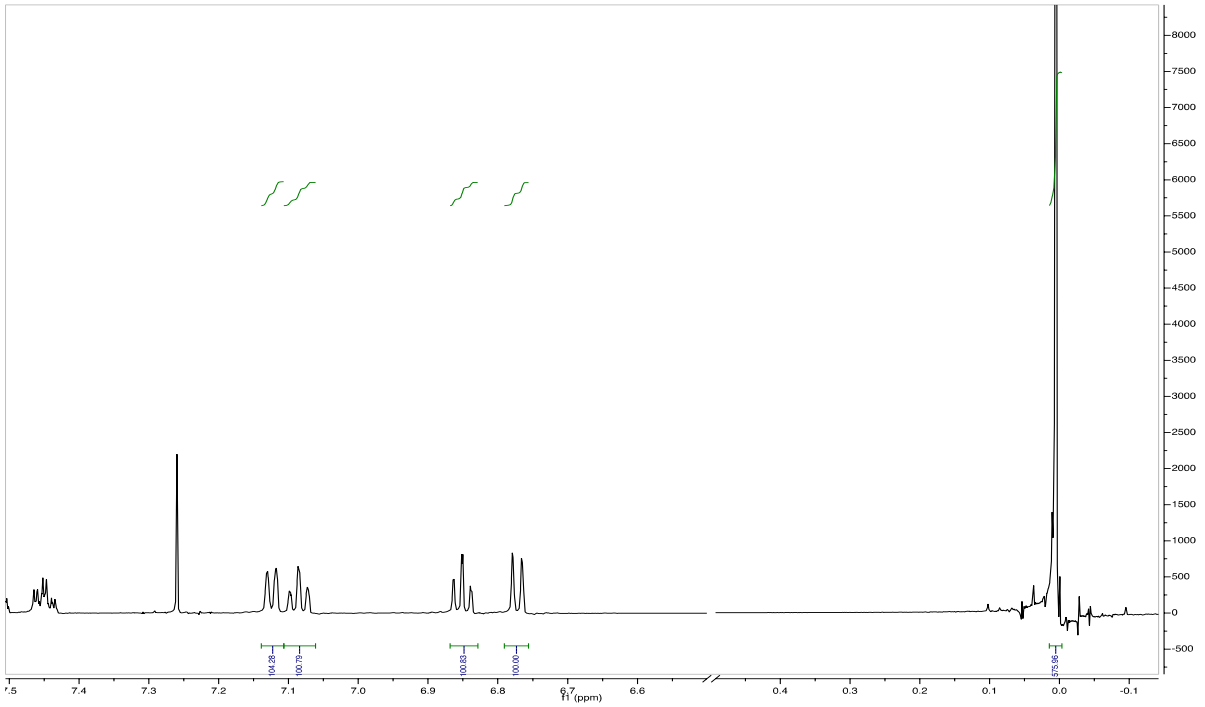

Figure 1.9.178 Example of 500 MHz ^{1}H NMR spectrum for 1.18 + 1.1; t = 0 h

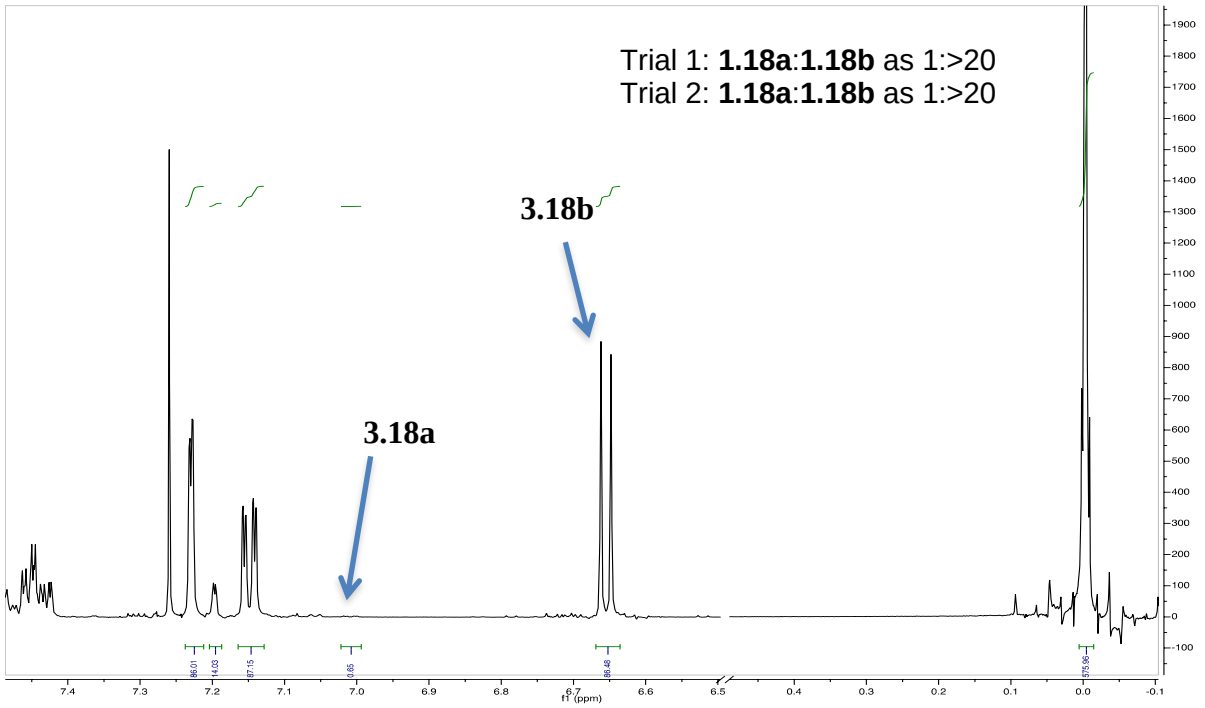

Figure 1.9.179 Example of 500 MHz ^{1}H NMR spectrum for 1.18c + 1.18d + 1.1; t = 30 min

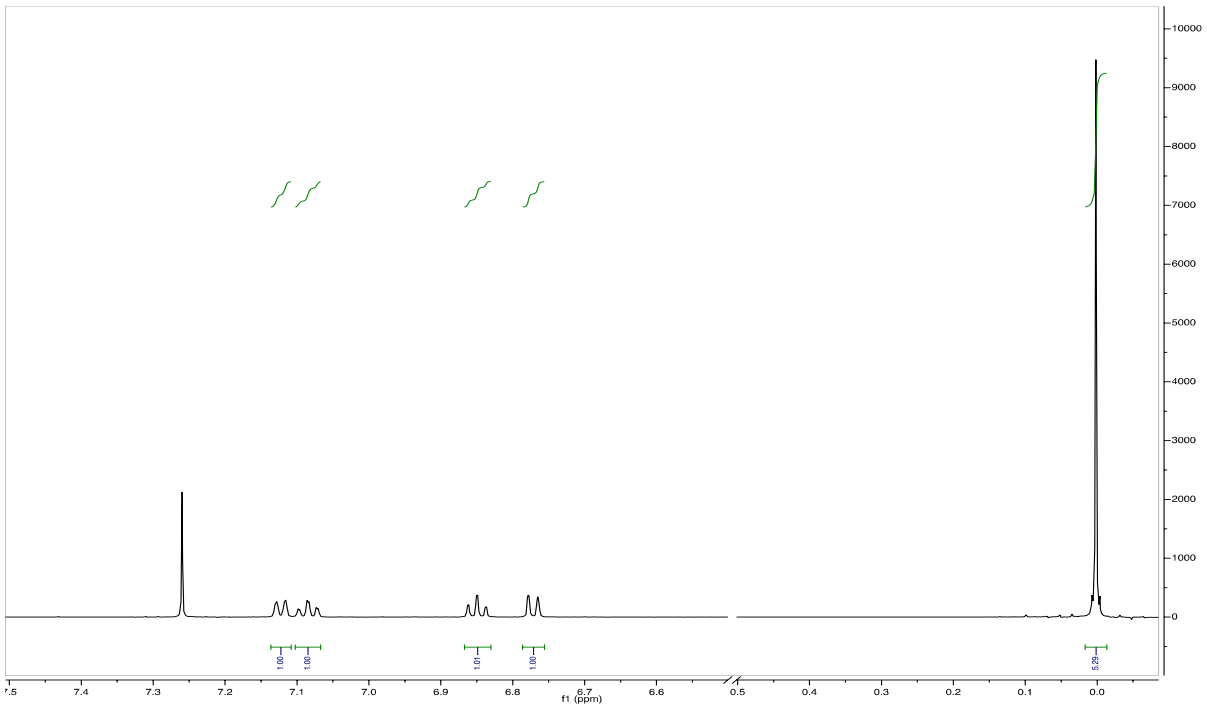

Figure 1.9.180 Example of 500 MHz ^{1}H NMR spectrum for 1.18 + 1.6; t = 0 h

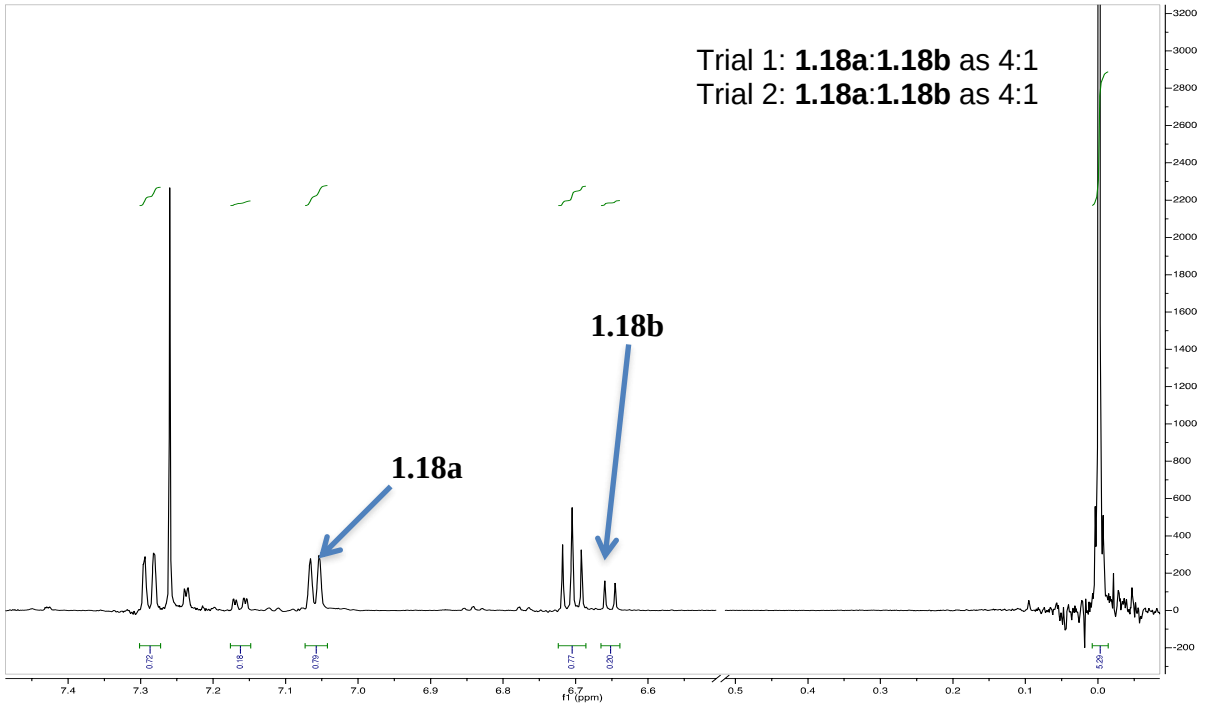

Figure 1.9.181 Example of 500 MHz ^{1}H NMR spectrum for 1.18a + 1.18b + 1.6; t = 30 min

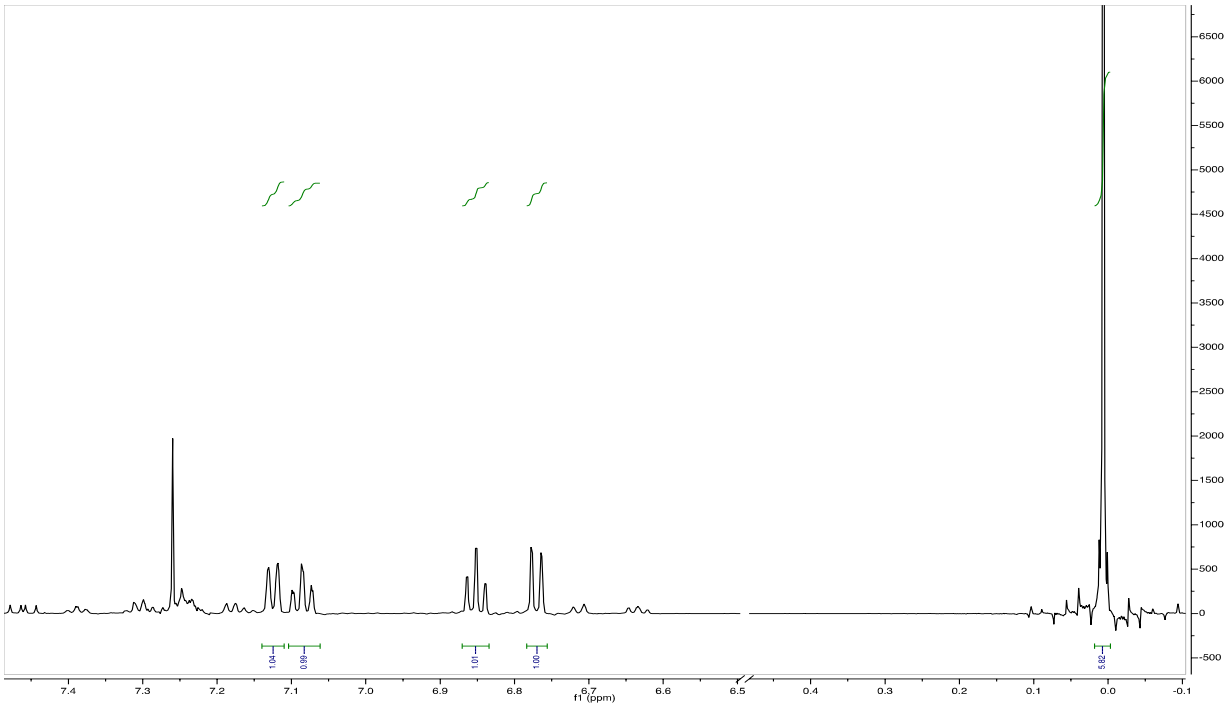

Figure 1.9.182 Example of 500 MHz ^{1}H NMR spectrum for 1.18 + 1.7; t = 0 h

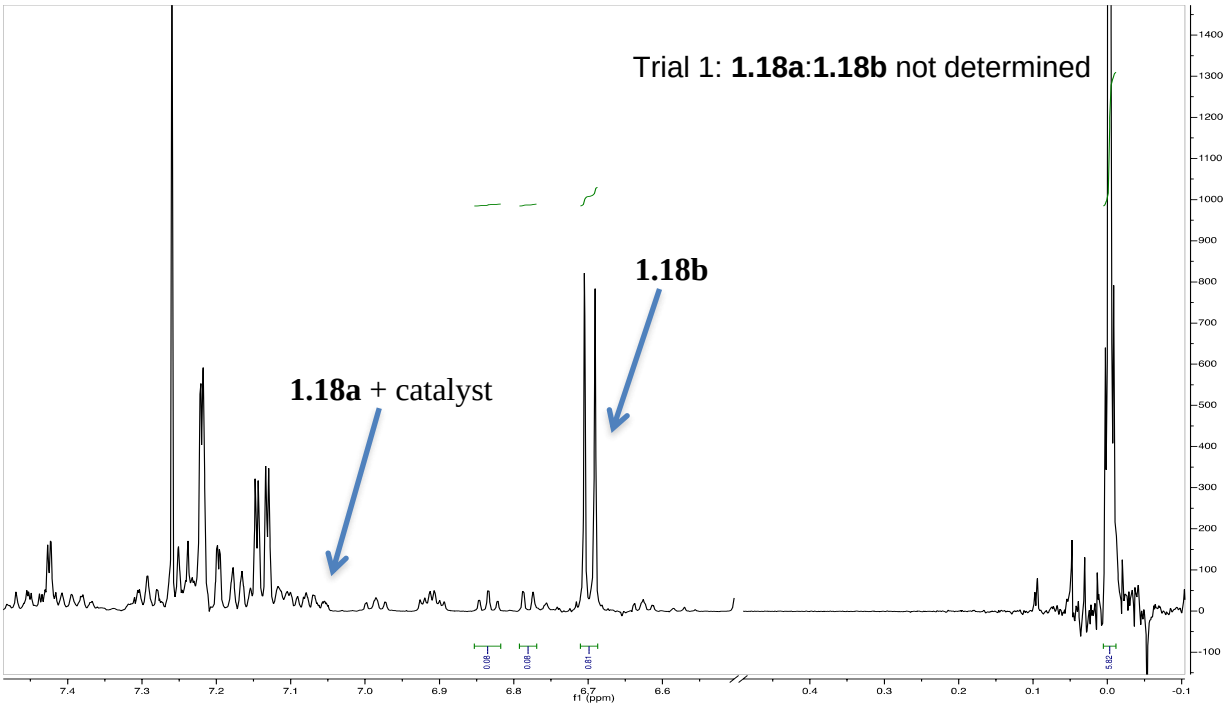

Figure 1.9.183 Example of 500 MHz ^{1}H NMR spectrum for 1.18a + 1.18b + 1.7; t = 30 min

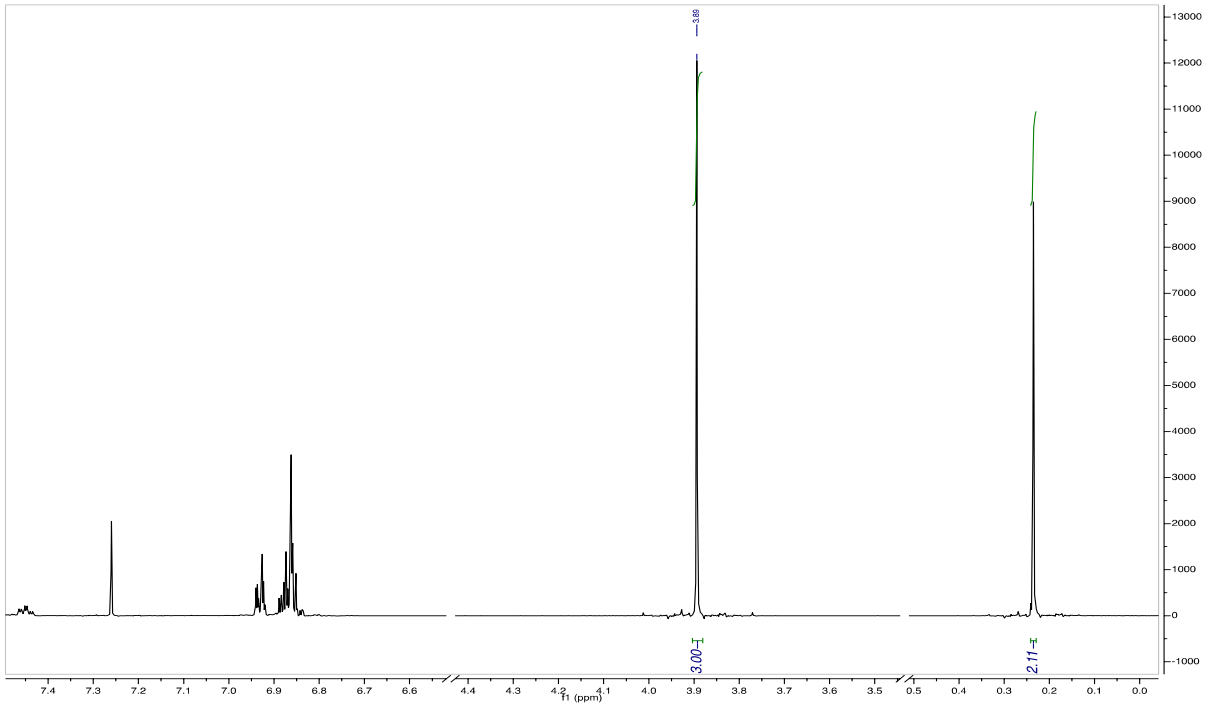

Figure 1.9.184 Example of 400 MHz ^{1}H NMR spectrum for 1.19 + 1.1; t = 0 h

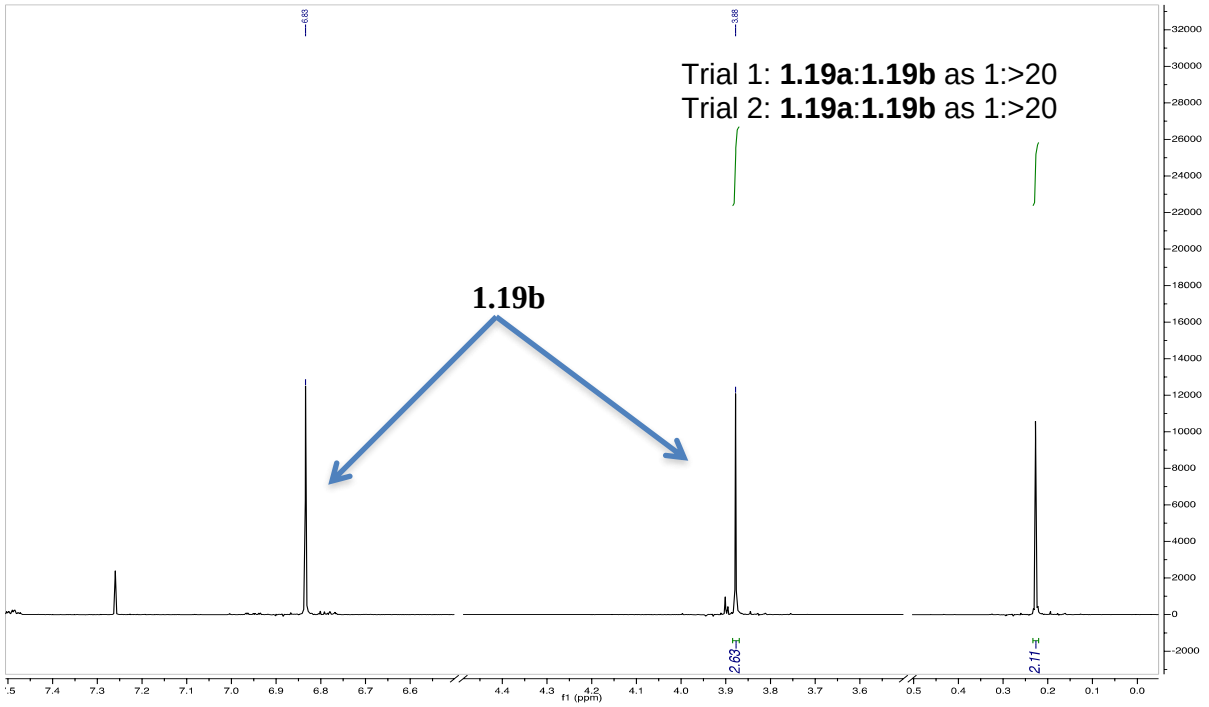

Figure 1.9.185 Example of 400 MHz ^{1}H NMR spectrum for 1.19a + 1.19b + 1.1; t = 1 h

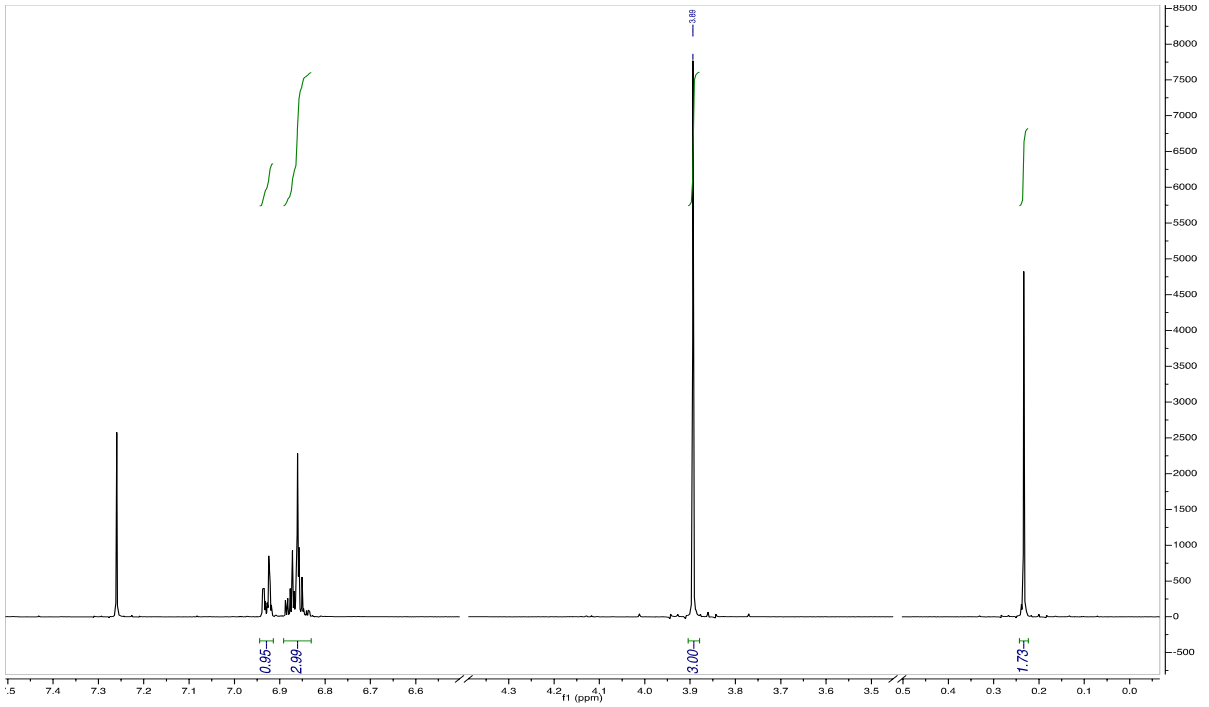

Figure 1.9.186 Example of 400 MHz ^{1}H NMR spectrum for 1.19 + 1.6; t = 0 h

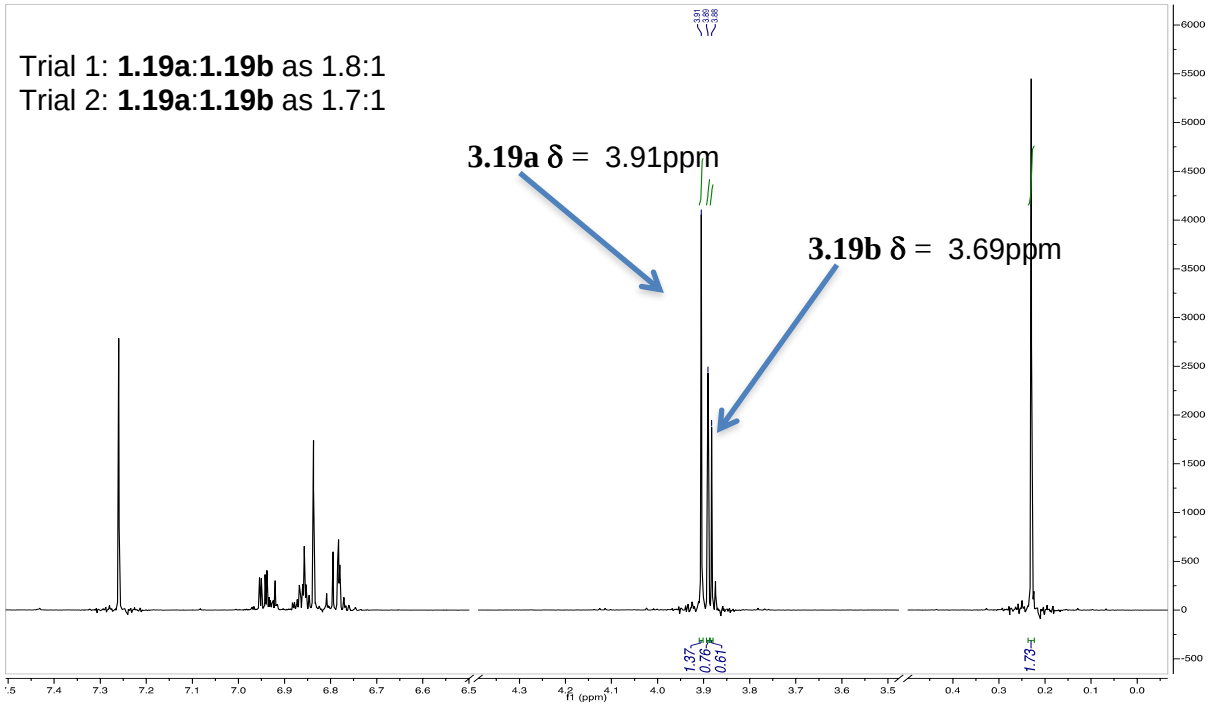

Figure 1.9.187 Example of 400 MHz ^{1}H NMR spectrum for 1.19a + 1.19b + 1.6; t = 2 h

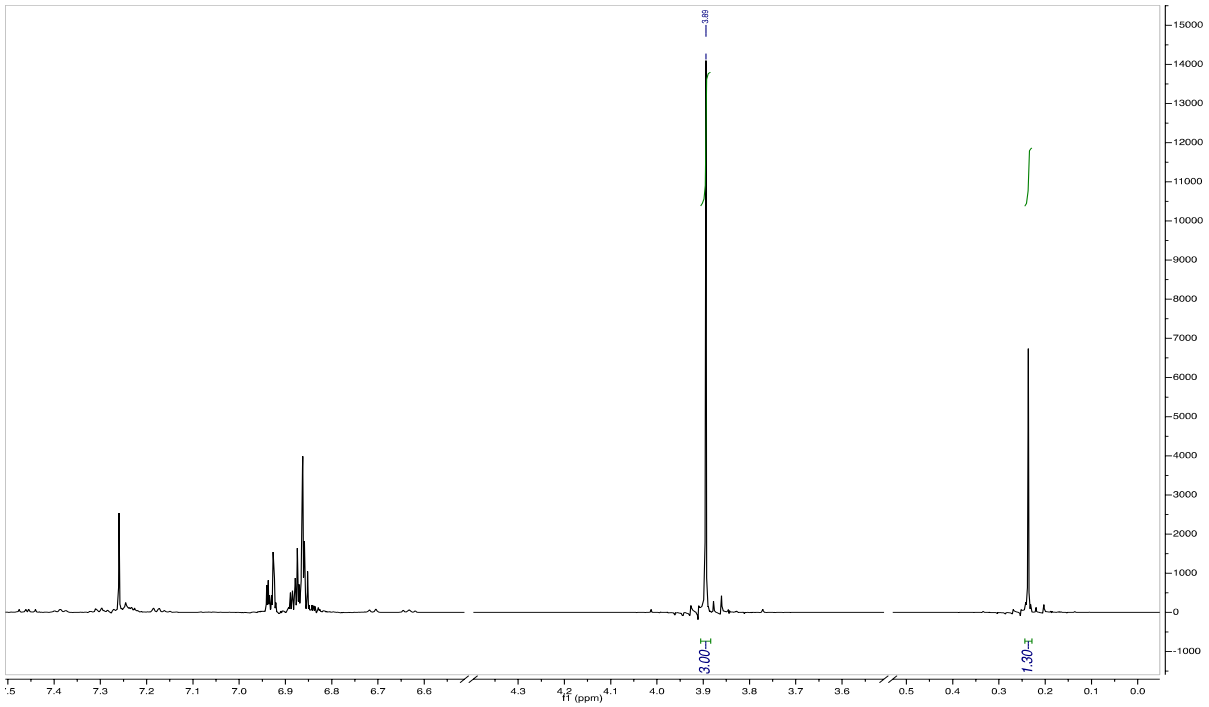

Figure 1.9.188 Example of 400 MHz ^{1}H NMR spectrum for 1.19 + 1.7; t = 0 h

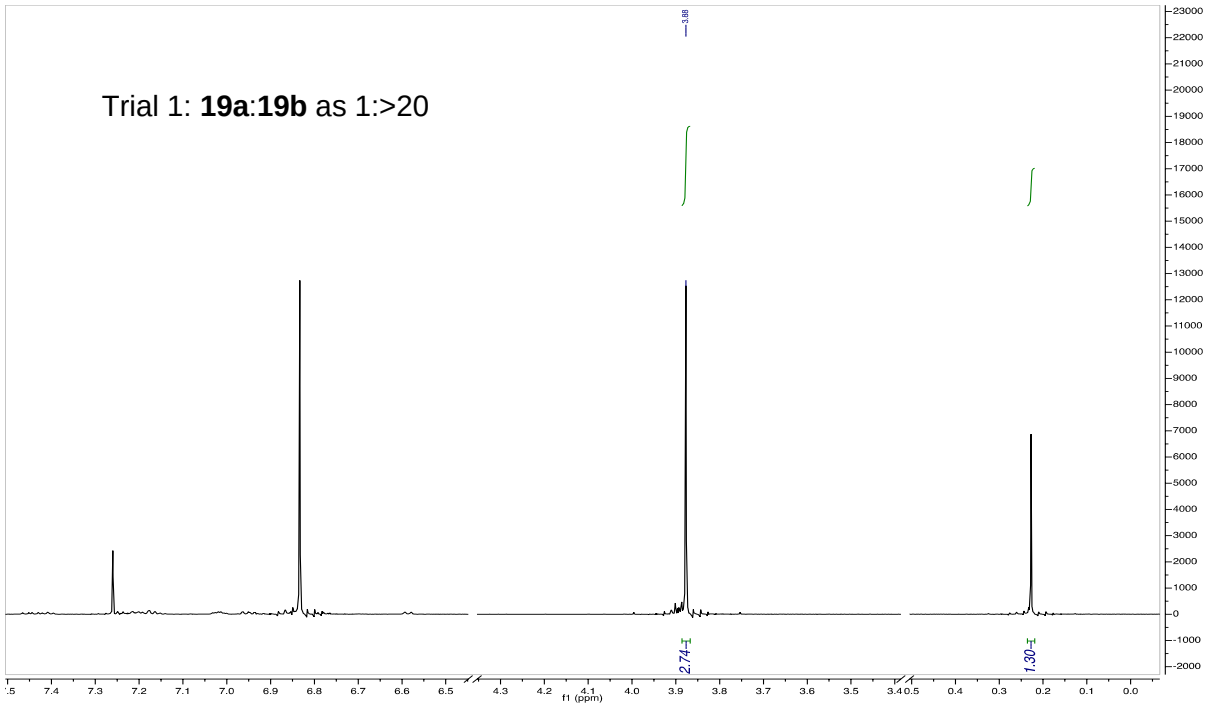

Figure 1.9.189 Example of 400 MHz ^{1}H NMR spectrum for 1.19a + 1.19b + 1.7; t = 1 h

1.10 Acknowledgements

The contents in Chapter 1 are in part a reformatted reprint of the following manuscript, with permission from the American Chemical Society: Maddox, S. M.; Dinh, A. N.; Armenta, F.; Um, J.; Gustafson, J. L. "The Catalyst-Controlled Regiodivergent Chlorination of Phenols." *Org. Lett.* **2016**, *18*, 5476. Both Sean Maddox and I are co-authors for the manuscript; Sean initially developed the proof-of-concept and optimization of regioselective Lewis base catalysts, and both of us provided equal effort to the substrate scope of phenols. Felipe Armenta and Joann Um worked on *in silico* studies to predict the relative energy levels for catalyst-substrate transition states. Support of this work by San Diego State University and the SDSU Presidential Leadership Fund is acknowledged. The dissertation author was a primary researcher for the data presented. Support of this work by the National Science Foundation is acknowledged (CHE-1664565).

CHAPTER 2: Catalyst-Controlled Regioselective Chlorination of Phenols and Anilines Through a Lewis Basic Selenoether Catalyst

2.0 ACS Copyright

Chapter 2 is a reformatted section for a future manuscript that will be submitted to an ACS journal, most likely *Organic Letters* or *Journal of Organic Chemistry*.

2.1 Revisiting *ortho*-Chlorination: Degradation of Nagasawa's Catalyst

As mentioned in the previous chapter, I reported a regiodivergent electrophilic chlorination of phenol through Lewis base catalysis where utilization of Nagasawa's bis-thiourea **1.6** provided high *ortho*-selectivity. To better understand the mechanism of action for catalyst **1.6**, I synthesized isotopically labeled catalyst analogs and followed the reaction under optimal conditions via ^{15}N and ^{13}C NMR (see experimental section). I was somewhat surprised to observe that **1.6** converted to a new species during the reaction. Isolation of the observed byproduct led us to identify it as guanidine **1.6a** (Scheme 2.1.1, see experimental section for plausible mechanism of formation)[81] which I found to be catalytically inactive. Because of the cyclohexyl scaffold and the electrophilic nature of the thiourea, one possible mechanism is that the adjacent amide can attack the thiourea, followed by elimination of sulfur. This is supported by S_8 as a byproduct of the reaction. I hypothesized that this catalyst degradation attenuated the observed catalyst activities, perhaps limiting the scope of chemistry that could be affected. This led us to explore the development of a

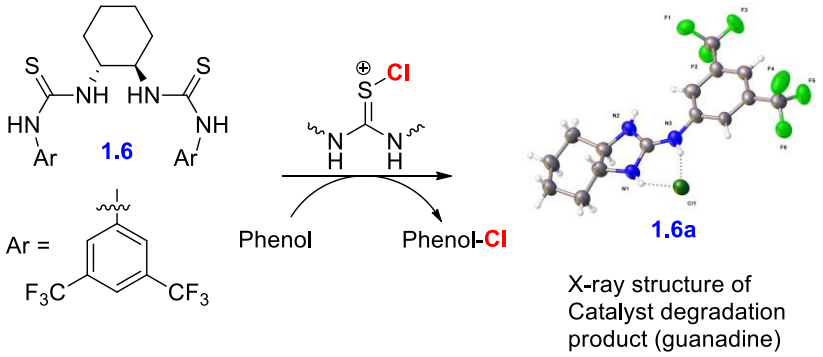

Scheme 2.1.1 Degradation of Nagasawa's Catalyst

2nd generation *ortho*-selective catalyst. I hypothesized that replacing one of the thioureas with another Lewis basic moiety such as a thioether would lead to a longer-lived catalyst that would not undergo the intramolecular cyclization I observed with **1.6**.

2.2 Discussion

Zhao and coworkers have developed a series of chiral bifunctional Lewis base chalcogenides derived from the 1-amino indanol scaffold and have successfully implemented them in the context of diverse electrophilic olefin functionalizations.[82–87] Inspired by this work, I initially synthesized and evaluated a series of thioether catalysts based on Zhao's scaffold that possessed varying directing groups off of the 1-amino group; however these catalysts offered little perturbation from the 'innate' regioselectivity observed with triphenylphosphine sulfide **1.1** (Table 2.1.1, entry 2-6) . Interestingly, 10 mol % indanol catalyst **2.4**, which possesses an electron poor thiourea, and is perhaps a direct analog of our original *ortho*-selective catalyst **1.6**, displayed preliminary levels of *ortho*-selectivity (1.5:1.0 of **1.3a**:**1.3b**), albeit with modest conversion. In order to increase conversion, I kept the thiourea functional group constant and began varying the Lewis base moiety. When the aryl substitution off the thioether was made more electron rich as in catalyst **2.5**, I observed increased conversion, albeit with equal amounts of constitutional isomers (85% conversion, 1.0:1.0 of **1.3a**:**1.3b** (entry 7)). Incorporating a sterically bulky 2,4,6-trimethyl

substitution off the thioether aryl, as in catalyst **2.6**, increased *ortho*-selectivity to 2.5:1.0 **1.3a:1.3b**, albeit with a decrease in conversion to 49%. (entry 8).

Table 2.2.1 Optimization of *ortho*-chlorination with Indanol Lewis base Catalysts

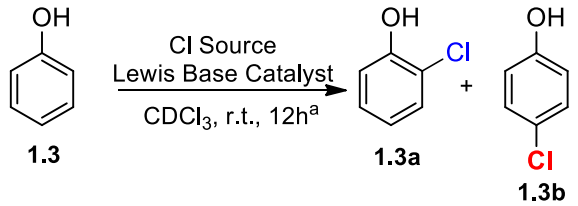

1.3 **1.3a** **1.3b**

Entry	Cat (%)	Cl Source	Conv.(%)[b]	1.3a:1.3b[c]	ΔΔG‡(kcal/mol)[d]
1	None	NCS	0	N/A	N/A
2	PPh_3=S **1.1** (10%)	NCS	85	1.0:4.0	0
3	**2.1** (10%)	NCS	40	1.0:3.0	.17
4	**2.2** (10%)	NCS	46	1.0:3.5	.07
5	**2.3** (10%)	NCS	56	1.0:2.7	.23
6	**2.4** (10%)	NCS	51	1.5:1.0	1.05
7	**2.5** (10%)	NCS	85	1.0:1.0	.81
8	**2.6** (10%)	NCS	49	2.5:1.0	1.35
9	**2.7** (10%)	NCS	72	4.5:1.0	1.71
10	**2.7** (1%)	NCS	70	>20:1.0	2.59
11	**2.7** (1%)	DCDMH	90	2.0:1.0	1.22

Lewis Base Catalyst:

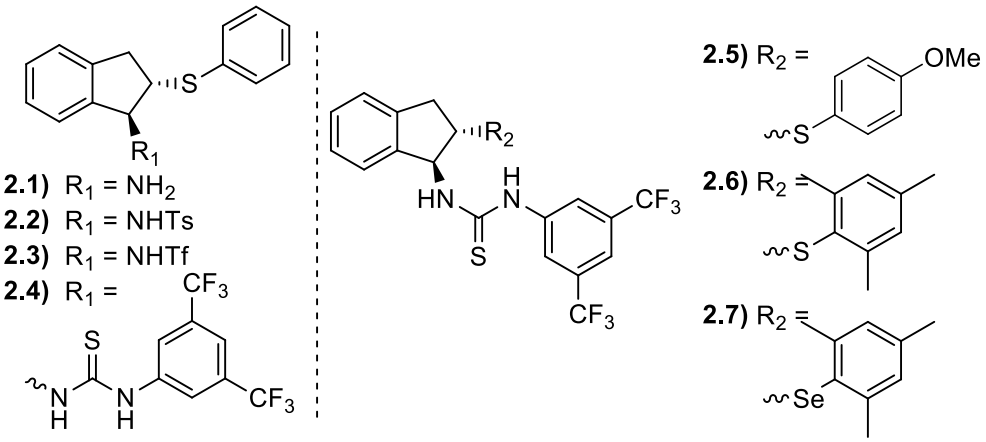

[a]All reactions were performed with 0.03mmol of **1.3**, stirred with $CDCl_3$ and catalyst, followed by 0.036 mmol of NCS. [b]Conversion is the sum of both regioisomers **1.3a** and **1.3b** and represents an average of three trials using tetramethylsilane as an internal standard. [c]Regioisomeric ratios were determined by ^1H NMR and represent an average of three trials. [d]$\Delta\Delta G^{\ddagger} = \Delta\Delta G^{\ddagger}_{entry\#} - \Delta\Delta G^{\ddagger}_{entry\ 1}$, with *ortho*-selectivity defined as ΔΔG and *para*-selectivity defined as negative $\Delta\Delta G^{\ddagger}$.

Guided by Zhao's recent work on activation of a weakly electrophilic SCF_3 reagent with selenoethers[83], I replaced the thioether with a selenoether in catalyst **2.7**, observing a notable increase in *ortho*-selectivity and conversion (entry 9). Finally, lowering the catalyst loading of **2.7** from 10 mol% to 1 mol% yielded significantly improved conversion and regioselectivity (90% conversion; **1.3a**: **1.3b**>20:1; entry 10). This is in line with observations from the Seidel group[74], wherein they observed that at higher concentrations thioureas can aggregate, attenuating their catalytic efficiency. To put these selectivities in perspective, the difference in energy between a catalyst such as 3 that yields 1:4 *ortho*:*para* and a catalyst that yields 20:1 *ortho*:*para* (defined as $\Delta\Delta\Delta G^{\ddagger}$, see Table 1, footnoted for definition) is 2.58 kcal/mol, which would correspond to greater than 97% ee in the realm of enantioselectivity.

I next sought to define the substrate scope of this chemistry across simple phenols. Electron-poor substituted phenols yielded excellent *ortho* selectivities in line with phenol. For example, **2.7** effected the chlorination of 2-phenyl and 2-cyano substituted phenols (**2.8** and **2.9)** exclusively at the *ortho*-position to provide **2.8a** and **2.9a** in isolated yields of 44% and 38% respectively, significantly overriding the *para* selectivity observed with triphenylphosphine sulfide **1.1**. On the other hand, I observed a decrease in *ortho* selectivities once I introduced bulkier substituents at the 2-position; nonetheless there was still a significant overriding of the innate *para* selectivity. For example, 2-bromophenol (**2.10**) and 2-iodophenol (**2.11)** all provided the *ortho*-substituted regioisomers as the major product (**2.10a** & **2.11a**), affording *ortho*:*para* ratios between 2.0:1.0 and 4.0:1.0. One possible explanation for this decrease may be due to steric hindrance of the bulky substituents, interfering with the substrate-catalyst interaction.

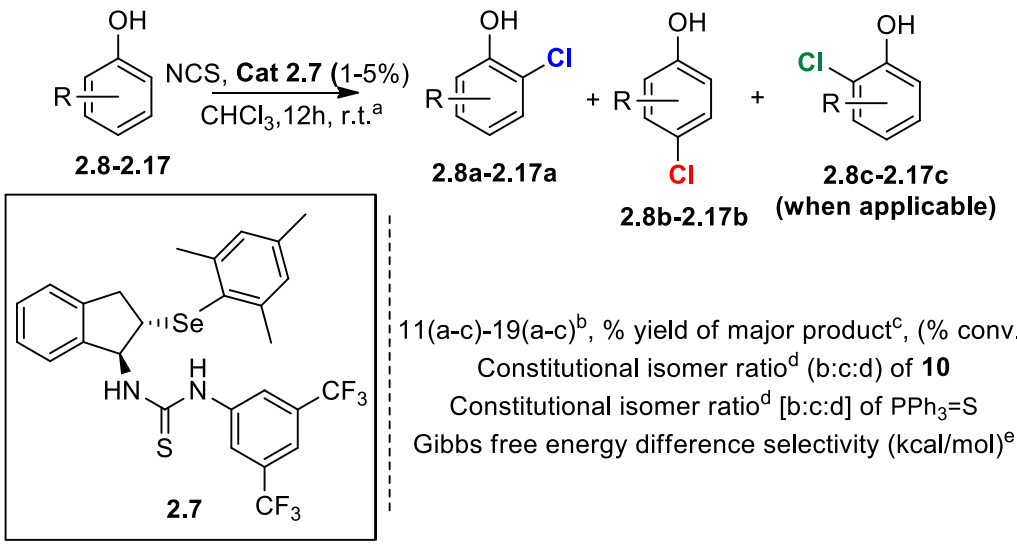

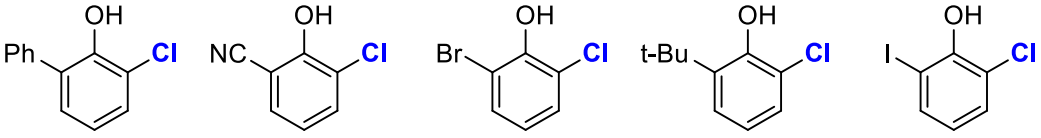

2.8a:44% (56%) (>20:1.0) [1.0:3.2] ΔΔΔG‡: 2.45

2.9af: 38% (53%) (>20:1.0) [1.0: 3.1] ΔΔΔG‡: 2.31

2.10af 43% (54%) (6.9:1.0) [1.0:4.7] ΔΔΔG‡:2.06

2.11a: 56% (73%) (2.0:1.0) [1.0:4.1] ΔΔΔG‡: 1.24

2.12a:75% (93%) (4.0:1.0) [1.0:5.4] ΔΔΔG‡: 1.84

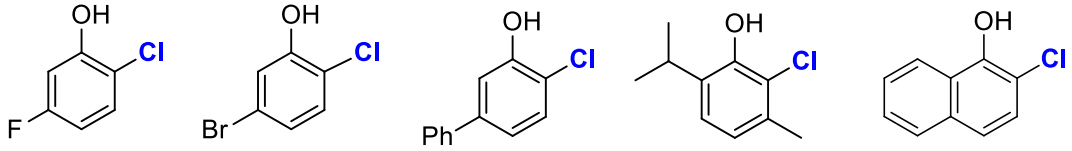

2.13af: 70% (70%) (>20:1.0:1.0) [1.1:1.0:0.0] ΔΔΔG‡: 1.83

2.14af: 60% (80%) (3.0:1.0:0.0) [1.0:2.8:0.0] ΔΔΔG‡: 1.26

2.15af: 55% (74%) (5.6:1.0:2.0) [1.0:3.9:0.0] ΔΔΔG‡:1.83

2.16a: 47% (56%) (5.2:1.0) [1.0:8.0] ΔΔΔG‡: 2.21

2.17a: 50% (55%) (9.5:1.0) [1.0:5.0] ΔΔΔG‡: 2.28

[a]Optimized reaction conditions were used with respect to the catalyst. [b]Only the major product is shown. [c]Isolated yields were determined a .1mmol scale, using $CHCl_3$ as the solvent, and represent an average of two trials. [d]Isomeric ratios were determined by ^1H NMR and represent an average of two trials. [e]$\Delta\Delta\Delta G^{\ddagger} = \Delta\Delta G^{\ddagger}_{entry\#} - \Delta\Delta G^{\ddagger}_{entry\ 2}$, with *ortho*-selectivity defined as ΔΔG and *para*-selectivity defined as negative $\Delta\Delta G^{\ddagger}$. [f]The following substrates required 5% catalyst loading for higher yield. [g]Substrate provided exclusively the *ortho* regioisomer. 20:1.0 is the estimated ratio used to calculate the $\Delta\Delta\Delta G^{\ddagger}$value.

Scheme 2.2.1 Substrate Scope of *ortho*-chlorination of Phenols with Selenoether Catalyst

Catalyst **2.7** also directed chlorination to the least hindered *ortho* (6)-position of 3-substituted phenols. For example, the chlorination of 3-fluorophenol (**2.13)** yielded exclusive

ortho-selectivity at the 6-position to give **2.13a** in 70% yield. 3-bromophenol **2.14** resulted in lower *ortho* selectivities with 1 mol% **2.7** (3.0:1.0 **2.14a**:**2.14b**); nonetheless **2.14a** was furnished as the major products in good isolated yields. Phenyl substituted **2.15** was also predominantly chlorinated at the least hindered position (5.6:1.0:2.0 **2.15a:2.15b:2.15c**), however in this case some halogenation at the more hindered position was also observed. The terpenoid thymol (**2.16)** also provided *ortho*-selectivity (5.2:1.0 **2.16a**:**2.16b**). Finally, *α*-naphthol **2.17** afforded high *ortho*-selectivity to give **2.17a** with a moderate yield of 50%. Overall, we show this chemistry can be applied for a diversity of substituted phenols.

I next evaluated whether **2.7** could affect *ortho*-selective chlorination on anilines. Anilines are typically more reactive, but less selective substrates for S_EAr than phenols; indeed no catalyst is needed to affect the chlorination of anilines. Furthermore, anilines typically display innate *para* selectivities on par or greater than that of phenols. To overcome these issues, the Yeung group has studied *ortho*-selective halogenation on protected anilines[37], however unprotected anilines have proven recalcitrant to catalyst-controlled regioselectivity.

The increased reactivity of **2.7** compared to **1.1** led us to hypothesize that it could outcompete the innate reactivity of anilines. Indeed, chlorination of several simple anilines in the presence of 1 mol% **2.7** resulted in nearly exclusive *ortho*-chlorination. For example, alkyl substituted anilines such as 2-methylaniline and 2-isopropyl aniline (**2.18** and **2.19**) gave significant *ortho*-selectivities at greater than 20:1 allowing for isolation of the product in good yields. For comparison, each of these substrates yielded primarily *para* chlorinated products in the absence of catalyst (1.0:5.6 and 1.0:5.9 *o*:*p* respectively). As with phenols, *ortho tert*-butyl substitution (**2.20**) is met by a decrease in the *ortho* selectivity at 2.0:1.0 *o*:*p* (compared to 1.0:3.5 *o*:*p* in the absence of catalyst). 2-Bromoaniline (**2.21**) provided moderate *ortho*-selectivity despite

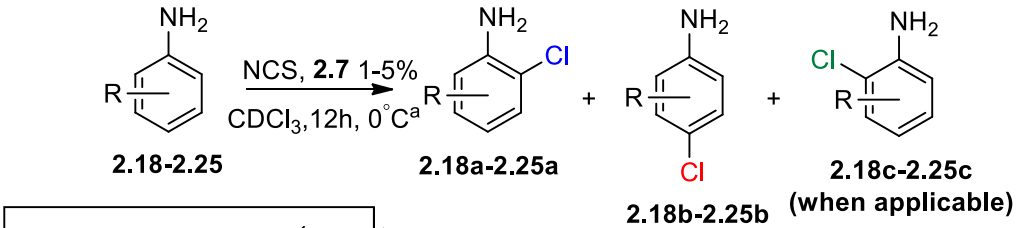

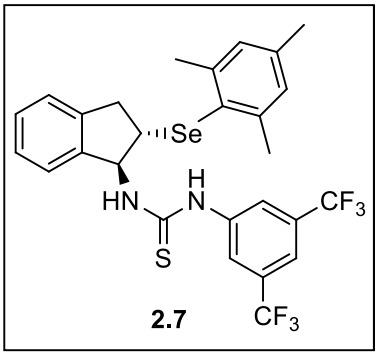

20(a-c)-29(a-c)[b], time, % yield of major product[c], (% conv.)
(Constitutional isomer ratio[d] (b:c:d)) of **2.7**
Constitutional isomer ratio[d] [b:c:d], no catalyst
Gibbs free energy difference selectivity (kcal/mol)[e]

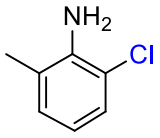

2.18a: 12h, 80% (80%)
(>20:1.0)
[1.0:5.6]
ΔΔΔG‡: 2.79

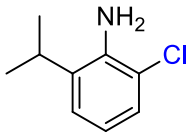

2.19a: 12h, 66% (66%)
(>20:1.0)
[1.0:5.9]
ΔΔΔG‡: 2.82

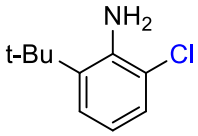

2.20a: 12h, 64% (96%)
(2.0:1.0)
[1.0:3.5]
ΔΔΔG‡: 1.15

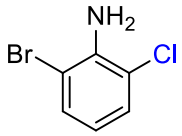

2.21a[f]: 6h, 33% (42%)
(3.6:1.0)
[1.0:4.5]
ΔΔΔG‡:1.64

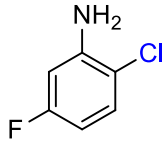

2.22b[f]: 12h, 70% (75%)
(20:1.0:1.0)
[1.0:2.1:0.0]
ΔΔΔG‡: 2.21

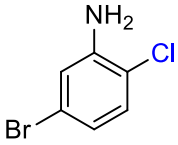

2.23b[f]: 12h, 30% (55%)
(3.0:1.5:1.0)
[1.0:3.1:1.0]
ΔΔΔG‡:1.07

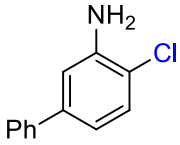

2.24a[f]: 24h, 43% (58%)
(5.6:1.0:1.0)
[1.0:3.9:0.0]
ΔΔΔG‡: 1.82

[a]Optimized reaction conditions were used with respect to the catalyst. Reactions were quenched with vinyl ether after completion to prevent aniline degradation. [b]Only themajor product is shown. [c]Isolated yields were determined a .1mmol scale, using $CHCl_3$ as the solvent, and represent an average of two trials. [d]Isomeric ratios were determined by ^1H NMR and represent an average of two trials. [e]$\Delta\Delta\Delta G = \Delta\Delta G_{\text{entry\#}} - \Delta\Delta G_{\text{entry 1}}$, with *ortho*-selectivity defined as ΔΔG and *para*-selectivitydefined as negative ΔΔG . [f]5% catalyst loading was used.

Scheme 2.2.2 Substrate Scope of *ortho*-chlorination of Anilines with Selenoether Catalyst

its relatively large steric hindrance, giving an *o*:*p* ratio of 3.6:1.0 albeit at a moderate conversion of 42%. 3-fluoroaniline (**2.22**) provided excellent *ortho*-selectivities for **2.22a** with trace amounts of the other two regioisomers in 70% yield. However, 3-bromoaniline and 3-phenylaniline (**2.23**

and **2.24)** resulted in lower yields and selectivity for the less hindered *ortho*-substituted product (**2.23a** and **2.24a**). Overall, the *ortho* bias demonstrated by **2.7** for substituted anilines (compared to the *para* innate selectivity in the absence of catalyst) is like that observed for phenols, with $\Delta\Delta\Delta G^{\ddagger}$, ranging from 1.07 to 2.82 kcal/mol.

I have demonstrated a second generation Lewis basic methodology for regioselective *ortho* chlorination of phenols and anilines. Mechanistic studies are currently being processed but have been slightly delayed due to the current global health situation. This discussion portion of Chapter 2 will be updated upon final revisions of this thesis.

2.3 Experimental Section

2.3.1 General Information

^{1}H and ^{13}C NMR spectra were recorded on Varian VNMRS 400 MHz, Varian Inova 500 MHz and Varian VNMRS 600 MHz at room temperature. All chemical shifts were reported in parts per million (δ) and were internally referenced to residual protio solvents, unless otherwise noted. All spectral data were reported as follows: chemical shift (multiplicity [singlet (*s*), doublet (*d*), triplet (*t*), quartet (*q*), and multiplet (*m*)], coupling constants [Hz], integration). Carbon spectra were recorded with complete proton decoupling. Most fluorine spectra were recorded with internal fluorine standards (i.e. trifluoroacetic acid, trifluorotoluene). Conventional mass spectra were obtained using Advion expression^{s} CMS APCI/ASAP. For the chlorination of substrates, purchased (*N*)-chlorosuccinimide was recrystallized from water before use. All other chemicals used were purchased from Sigma Aldrich, TCI, Frontier Scientific, Acros Organics, Strem, Oakwood, Cambridge Isotope Laboratories, or Fisher and were used as received without further purification or recrystallization. All flash column chromatography (FCC) was performed using

Grade 60 Silica gel (230-400 mesh) purchased from Fisher Scientific. All TLC preparatory plates were performed using Grade 60 Silica gel with fluorescent indicator F_{254} and were purchased from Fischer Scientific.

2.3.2 Abbreviations

MeCN: acetonitrile

NH_4Cl: Ammonium Chloride

Boc_2O: Di-*tert*-butyl decarbonate

Conc.: Concentration (M)

DCM: dichloromethane

DIPEA: N,N-Diisopropylethylamine

EtOAc: Ethyl Acetate

Equiv.: Equivalents

HCl: hydrochloric acid

MsCl: methanesulfonyl chloride

MeOH: methanol

NXS: N-(halogen)-succinimide

K_2CO_3: Potassium Carbonate

r.t.: Room Temperature

Et_3N: triethylamine

H_2O: water

THF: tetrahydrofuran

2.3.3 Selenoether Catalyst Synthesis

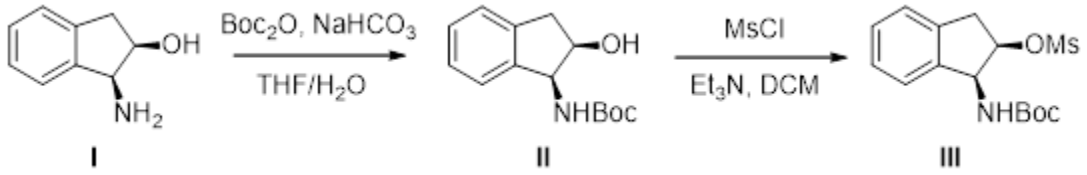

I II III

Scheme 2.3.1 General Synthetic Pathway to Indanol Catalyst Precursor

The following is based on a general procedure from published literature.[88] To a round bottom flask and dry stir bar was added 5 g of **(*1S,2R*)-1-amino-2,3-dihydro-1H-inden-2-ol, I** (5 g, 33.5 mmol, 1.0 equiv.) into a solution of THF/H_2O (~70 mL of both, 0.5M). $NaHCO_3$ (4.2 g ,50.3 mmol, 1.5 equiv.) was added to the solution and stirred for five minutes. Boc_2O (8.0 g, 36.8 mmol, 1.1 equiv.) was then added to the solution. The reaction was then stirred at room temperature for 24 h and then diluted with EtOAc (2 x 30 mL). The organic layer was separated, washed with brine and dried with Na_2SO_4, filtered and concentrated under reduced pressure to give **tert-butyl ((*1S,2R*)-2-hydroxy-2,3-dihydro-1H-inden-1-yl) carbamate, II** as a viscous brown oil. No further purification was needed. The NMR spectra match literature precedence.

The following synthesis is adapted from a general procedure from published literature.[89] **II** (5.7 g, 23 mmol, 1.0 equiv.) was dissolved in anhydrous DCM (~50 mL, 0.5M). Et_3N was syringed (4.8 mL, 34.5 mmol, 1.5 equiv.) into the solution and the reaction was cooled down to 0 ˚C. MsCl (1.96 mL, 25.3 mmol, 1.1 equiv.) was syringed slowly into the reaction. The reaction was then warmed to r.t. and let stirred for 12 h. The reaction was quenched with 1M $NaHCO_3$ solution and then extracted with DCM (2 x 30 mL), dried with Na_2SO_4, filtered and concentrated under reduced pressure to give **(*1S,2R*)-1-((tert-butoxycarbonyl)amino)-2,3-dihydro-1H-inden-2-yl**

methanesulfonate, **III** as a white solid. No further purification was needed. The NMR spectra match literature precedence.

I. Synthesis of Diaryl Diselenides

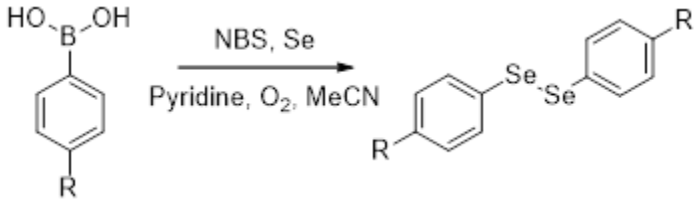

Scheme 2.3.2 General Synthesis of Diaryl Diselenides

The following synthesis is adapted from a general procedure from published literature. *N*-bromosuccinimide (1 equiv.) and selenium metal powder (1.2 equiv.) was added to a round bottom flask, then MeCN (0.2M) was added to the mixture and stirred at 60 ˚C for ten minutes. Boronic acid (1 equiv.) was added followed by addition of pyridine (2.5 equiv). The reaction turns into an orange color immediately after addition. The reaction was left stirring in open air at 60˚C for 12 h. The reaction was concentrated under reduced pressure and dissolved in EtOAc, washed with 1M HCl (30 mL x 3) and brine (30 mL x 3) and dried with Na_2SO_4, filtered and concentrated under reduced pressure. Purification through flash column chromatography (hexanes:EtOAc::100:0 to 99:1) afforded the desired product.

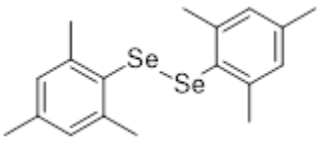

Figure 2.3.1 1,2-dimesityldiselane

Prepared and purified according to the general procedure: *N*-bromosuccinimide (2.1 g, 12.2 mmol, 1 equiv.) and selenium metal powder (1.16 g, 14.6 mmol, 1.2 equiv.) was added to a round bottom flask, then ~60mL of MeCN (0.2M) was added to the mixture and stirred at 60 ˚C for ten minutes. Boronic acid (2 g, 12.2 mmol, 1.0 equiv.) was added followed by addition of pyridine (2.45 mL, 30.5 mmol, 2.5 equiv). **^{1}H NMR (500 MHz, $CDCl_3$)** δ 6.85 (s, 4H), 2.27 (s, 6H), 2.25

(s, 12H). **^{13}C NMR (126 MHz, $CDCl_3$)** δ 143.35, 138.83, 128.08, 128.00, 23.87, 20.83. **MS (APCI): Calculated for $C_{18}H_{22}Se_2$** $[M+H]^+$ = 399.01. Found 399 m/z plus multiplets from selenium isotopes.

II. General Synthesis of Lewis Base Substitution

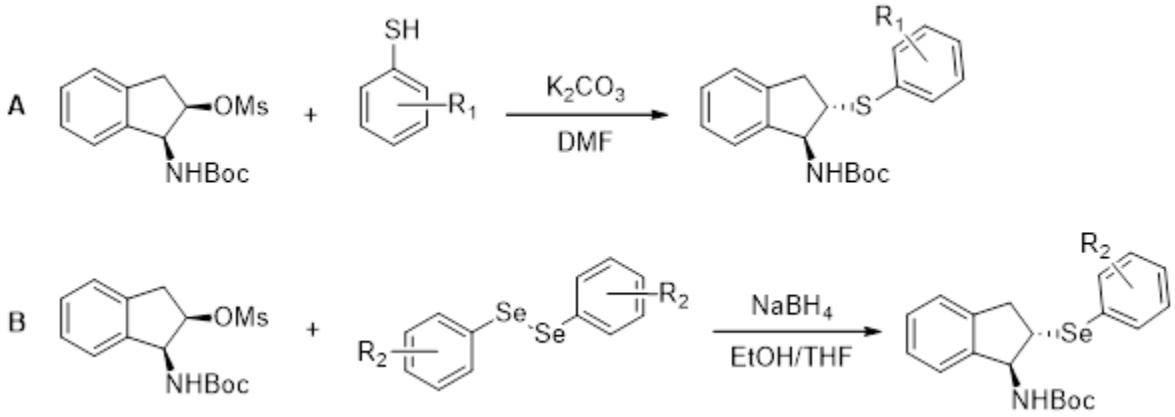

Scheme 2.3.3 General Synthesis of Lewis Base Substitution Scaffold

A. The following synthesis is adapted from a general procedure from published literature.[87] To an oven-dried round bottom flask with a stir bar was added **(*1S,2R*)-1-((*tert*-butoxycarbonyl)amino)-2,3-dihydro-1H-inden-2-yl methanesulfonate** (1 equiv) and K_2CO_3 (3 equiv). The flask was sealed with a rubber stopper, evacuated and back-filled with inert nitrogen gas. Then anhydrous DMF (0.2M) was syringed into the flask and stirred for 10 minutes. Benzenethiol was added to the flask and the reaction was stirred at 100 ˚C for 12h. The reaction was cooled to r.t., quenched with 1M HCl, extracted with EtOAc (20 mL x 3), dried with Na_2SO_4, filtered and concentrated under reduced pressure. Purification through flash column chromatography (hexanes:EtOAc::100:0 to 85:15) afforded the desired product.

B. The following synthesis is adapted from a general procedure from published literature.[85] To an oven-dried round bottom flask with a stir bar was added to a solution of diselenide (0.5

equiv) in EtOH (0.15M) under an inert atmosphere. $NaBH_4$ (2.0 equiv) was added and the mixture was stirred at r.t. for 10 minutes. Then a solution of **(*1S,2R*)-1-((*tert*-butoxycarbonyl)amino)-2,3-dihydro-1H-inden-2-yl methanesulfonate** (1 equiv) in anhydrous THF (0.6M) was slowly added. The resulting mixture was stirred at reflux for 12h. The reaction was quenched with aqueous saturated NH_4Cl. The organic phase was extracted with DCM (20 mL x 2). The combined organic layers were dried over Na_2SO_4, filtered and concentrated under reduced pressure. Purification through flash column chromatography (hexanes:EtOAc::100:0 to 85:15) afforded the desired product.

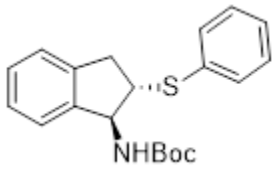

Figure 2.3.2 *tert*-butyl ((*1S,2S*)-2-(phenylthio)-2,3-dihydro-1H-inden-1-yl)carbamate

Prepared and purified according to the general procedure A: To an oven-dried round bottom flask with a stir bar was added 300 mg of (*1S,2R*)-1-((tert-butoxycarbonyl)amino)-2,3-dihydro-1H-inden-2-yl methanesulfonate and 379 mg of K_2CO_3. The flask was sealed with a rubber stopper, evacuated and back-filled with inert nitrogen gas. Then 4.5 mL of anhydrous DMF was syringed into the flask and stirred for 10 minutes. 93 μL of thiophenol was added to the flask and the reaction was stirred at 100 ˚C for 12 h. The synthesis and spectral data are in agreeance with the literature.

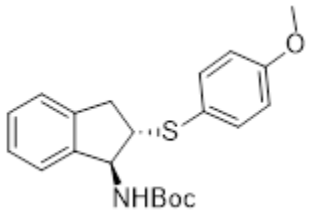

Figure 2.3.3 *tert*-butyl ((*1S,2S*)-2-((4-methoxyphenyl)thio)-2,3-dihydro-1H-inden-1-yl)carbamate

Prepared and purified according to the general procedure A: To an oven-dried round bottom flask with a stir bar was added 300 mg of **(*1S,2R*)-1-((*tert*-butoxycarbonyl)amino)-2,3-dihydro-1H-inden-2-yl methanesulfonate** and 379 mg of K_2CO_3. The flask was sealed with a rubber stopper, evacuated and back-filled with inert nitrogen gas. Then 4.5 mL of anhydrous DMF was syringed into the flask and stirred for 10 minutes. 112 μL of 4-methoxybenzenethiol was added to the flask and the reaction was stirred at 100 ˚C for 12 h. The synthesis and spectral data are in agreeance with the literature.

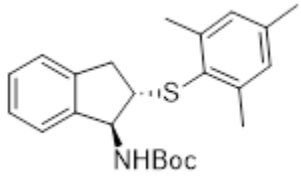

Figure 2.3.4 *tert*-butyl ((*1S,2S*)-2-(mesitylthio)-2,3-dihydro-1H-inden-1-yl)carbamate

Prepared and purified according to the general procedure A: To an oven-dried round bottom flask with a stir bar was added 300 mg of **(*1S,2R*)-1-((*tert*-butoxycarbonyl)amino)-2,3-dihydro-1H-inden-2-yl methanesulfonate** and 379 mg of K_2CO_3. The flask was sealed with a rubber stopper, evacuated and back-filled with inert nitrogen gas. Then 4.5 mL of anhydrous DMF was syringed into the flask and stirred for 10 minutes. 112 mg of 4-methoxybenzenethiol was added to the flask and the reaction was stirred at 100 ˚C for 12 h. **^{1}H NMR (500 MHz, $CDCl_3$)** δ 7.21-7.11 (m, 4H), 6.94 (s, 2H), 5.06 (t, *J* = 7.8 Hz, 1H), 4.60 (d, *J* = 7.8 Hz, 1H), 3.42 (q, *J* =7.8 Hz, 1H), 3.15 (dd, *J* = 7.8, 7.5 Hz, 1H), 2.90-2.84 (m, 1H), 2.51 (s, 6H), 2.27 (s, 3H), 1.47 (s, 9H). **^{13}C NMR (126 MHz, $CDCl_3$)** δ 155.36, 143.16, 129.02, 128.02, 127.05, 124.39, 123.97, 61.93, 54.36, 37.89, 28.33, 22.11, 20.99. **MS (APCI): Calculated for $C_{23}H_{29}NO_2S$**: $[M+H]^+$ = 384.55. Found 384.55 m/z

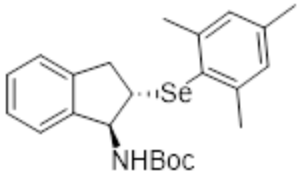

Figure 2.3.5 *tert*-butyl ((*1S,2S*)-2-(mesitylselanyl)-2,3-dihydro-1H-inden-1-yl)carbamate

Prepared and purified according to the general procedure B: To an oven-dried round bottom flask with a stir bar was added 589 mg (1.37 mmol) of **1,2-dimesityldiselane** in 9 mL (0.15M) of EtOH under an inert atmosphere. 104 mg of $NaBH_4$ (2.74 mmol) was added and the mixture was stirred at r.t. for 10 minutes. Then a solution of 900 mg (2.74 mmol) of **(*1S,2R*)-1-((tert-butoxycarbonyl)amino)-2,3-dihydro-1H-inden-2-yl methanesulfonate** in 6 mL anhydrous THF (0.6M) was slowly added. **^{1}H NMR (500 MHz, $CDCl_3$)** δ 7.26-7.12 (m, 4H), 6.94 (s, 2H), 5.11 (t, *J* = 7.8 Hz, 1H), 4.61 (d, *J* = 7.8 Hz, 1H), 3.48 (q, *J* = 7.8 Hz, 1H), 3.18 (dd, *J* = 7.8, 7.5 Hz, 1H), 2.89-2.84 (m, 1H), 2.54 (s, 6H), 2.27 (s, 3H), 1.47 (s, 9H). **^{13}C NMR (126 MHz, $CDCl_3$)** δ 155.35, 143.46, 141.30, 128.47, 127.98, 127.00, 124.28, 123.89, 47.33, 38.29, 28.33, 24.67, 20.92. **MS (APCI): Calculated for $C_{23}H_{29}NO_2Se$**: $[M+H]^+$ = 431.44. Found 431.44 m/z plus multiplets from selenium isotopes.

III. General Synthesis of Boc-deprotection

Scheme 2.3.4 General Synthesis of Boc-deprotection

The following synthesis is adapted from a general procedure from published literature.[5] A solution of 6 M HCl (10 equiv) was added to a solution of dioxane (0.1M) and Boc-protected reagent. The mixture was stirred at 60 ˚C for 6 h, then quenched with 1M NaOH solution until pH 14. Then the solution was extracted with EtOAc (20 mL x 3). The combined organic layers were

dried over Na_2SO_4, filtered and concentrated under reduced pressure. Purification through flash column chromatography (DCM:MeOH::100:0 to 80:20) afforded the desired product.

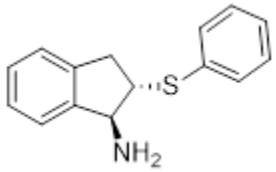

Figure 2.3.6 (*1S,2S*)-2-(phenylthio)-2,3-dihydro-1H-inden-1-amine (Catalyst 2.1)

A solution of 6 M HCl (480 μL was added to a solution of 2.9 mL dioxane and 100 mg (0.29 mmol) of ***tert*-butyl ((*1S,2S*)-2-(phenylthio)-2,3-dihydro-1H-inden-1-yl)carbamate.** The mixture was stirred at 60 ˚C for 6 h. The synthesis and spectral data are in agreeance with the literature.

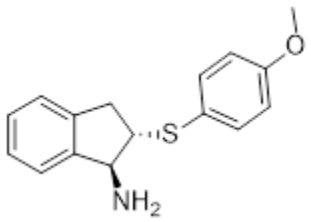

Figure 2.3.7 (*1S,2S*)-2-((4-methoxyphenyl)thio)-2,3-dihydro-1H-inden-1-amine

A solution of 6 M HCl (450 μL was added to a solution of 2.7 mL dioxane and 100 mg (0.27 mmol) of ***tert*-butyl ((*1S,2S*)-2-((4-methoxyphenyl)thio)-2,3-dihydro-1H-inden-1-yl)carbamate.** The mixture was stirred at 60 ˚C for 6 h. The synthesis and spectral data are in agreeance with the literature.

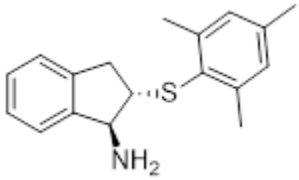

Figure 2.3.8 (*1S,2S*)-2-(mesitylthio)-2,3-dihydro-1H-inden-1-amine

A solution of 6 M HCl (650 μL) was added to a solution of 3.9 mL dioxane and 150 mg (0.39 mmol) of ***tert*-butyl ((*1S,2S*)-2-(mesitylthio)-2,3-dihydro-1H-inden-1-yl)carbamate.** The

mixture was stirred at 60 ˚C for 6 h. **^{1}H NMR (400 MHz, $CDCl_3$)** δ 7.31 (d, *J* = 7.0 Hz, 1H), 7.24-7.17 (m, 2H), 7.13 (d, *J* = 6.6 Hz, 1H), 6.96 (s, 2H), 4.24 (d, *J* = 7.8 Hz, 1H), 3.24 (dd, *J* = 16.7, 7.5Hz, 1H), 3.15 (dd, *J* = 15.5, 7.5Hz, 1H), 2.85 (dd, *J* = 15.5, 9.0 Hz, 1H), 2.56 (s, 6H), 2.27 (s, 3H). **^{13}C NMR (126 MHz, $CDCl_3$)** δ 145.16, 143.08, 140.58, 138.37, 129.14, 128.96, 127.58, 126.91, 124.22, 123.44, 63.62, 58.48, 37.98, 22.23, 21.00. **MS (APCI): Calculated for $C_{18}H_{21}NS$**: 284.43. Found 284.43 m/z.

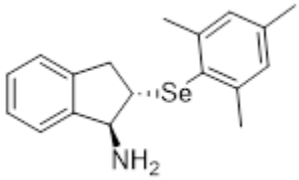

Figure 2.3.9 (*1S,2S*)-2-(mesitylselanyl)-2,3-dihydro-1H-inden-1-amine

A solution of 6 M HCl (940 μL) was added to a solution of 5.6 mL dioxane with 244 mg (0.56 mmol) of ***tert*-butyl ((*1S,2S*)-2-(mesitylselanyl)-2,3-dihydro-1H-inden-1-yl)carbamate.** The mixture was stirred at 60 ˚C for 6 h. **^{1}H NMR (500 MHz, $CDCl_3$)** δ 7.32 (d, *J* = 7.1 Hz, 1H), 7.23-7.17 (m, 2H), 7.14 (d, *J* = 7.1 Hz, 1H), 6.96 (s, 2H), 4.26 (d, *J* = 7.8 Hz, 1H), 3.30 (dd, *J* = 16.8, 7.6Hz, 1H), 3.21 (dd, *J* = 15.7, 7.6 Hz, 1H), 2.91-2.85 (m, 1H), 2.59 (s, 6H), 2.28 (s, 3H). **^{13}C NMR (126 MHz, $CDCl_3$)** δ 145.38, 143.45, 141.25, 138.50, 128.64, 127.53, 126.90, 126.65, 124.14, 123.40, 64.07, 52.24, 38.20, 24.85, 20.97. **MS (APCI): Calculated for $C_{18}H_{21}NSe$**: 331.33. Found 331.33 m/z plus multiplets from selenium isotopes.

IV. General Synthesis of final Lewis Base catalysts with Substituted amines

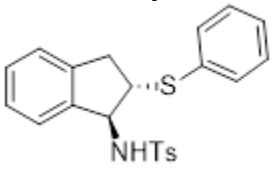

Figure 2.3.10 Catalyst 2.2

The following synthesis is adapted from a general procedure from published literature.[5] To a solution of 250 mg (*1S,2S*)-2-(phenylthio)-2,3-dihydro-1H-inden-1-amine (0.63 mmol, 1 equiv) in 3.1 mL DCM (0.2M) was added 132 μL Et_3N (0.95 mmol, 1.5 equiv) and 136 μL TsCl (0.95 mmol, 1 equiv) at r.t. The solution was stirred for 12 h, then quenched with water and extracted with DCM (10 mL x 3). The combined organic layers were dried over Na_2SO_4, filtered and concentrated under reduced pressure. Purification through flash column chromatography (Hex:EtOAc::100:0 to 90:10) afforded the desired product. The spectral data are in agreeance with the literature.

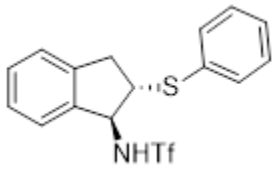

Figure 2.3.11 Catalyst 2.3

The following synthesis is adapted from a general procedure from published literature.[5] DIPEA (250 μL, 1.5 mmol) was added to a solution of **(*1S,2S*)-2-(phenylthio)-2,3-dihydro-1H-inden-1-amine** in 15 mL dry DCM (0.1M) under an inert atmosphere. Then triflic anhydride (185 μL, 1.1 mmol) was added slowly. The reaction was allowed to stir at room temperature for 3 h. Then, 1M HCl solution was added and the solution was extracted with DCM (15 mL x 3). The combined organic layers were dried over Na_2SO_4, filtered and concentrated under reduced pressure. Purification through flash column chromatography (Hex:EtOAc::100:0 to 90:10) afforded the desired product. The spectral data are in agreeance with the literature.

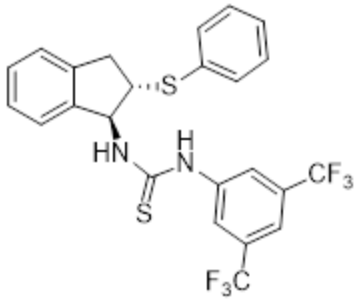

Figure 2.3.12 Catalyst 2.4

The following synthesis is adapted from a general synthesis in published literature. 120 mg (0.50 mmol, 1 equiv) of ***(1S,2S)*-2-(phenylthio)-2,3-dihydro-1H-inden-1-amine** was dissolved in 2.5 mL (0.2M) of anhydrous THF under an inert atmosphere. Then 136 mg (0.50 mmol, 1 equiv) of 3,5-Bis(trifluoromethyl)phenyl isothiocyanate was added to the reaction. The mixture was stirred at r.t. for 4 h, then immediately concentrated under reduced pressure. Purification through flash column chromatography (Hex:EtOAc::100:0 to 85:15) afforded the desired product. **^{1}H NMR (400 MHz, $CDCl_3$)** δ 8.15 (s, 1H), 7.73 (s, 2H), 7.68 (s, 1H), 7.56 (d, J = 7.3 Hz, 2H), 7.40-7.26 (m, 5H), 7.21 (d, J =7.1 Hz, 1H), 6.35 (s, 1H), 3.81 (s, 1H), 3.42 (s, 1H), 3.06-3.01 (m, 1H), 1.60 (s, 1H). **^{13}C NMR (126 MHz, $CDCl_3$)** δ 181.14, 161.62, 140.68, 133.07, 129.40, 128.19, 127.68, 124.89, 124.124, 124.11, 121.40, 119.54, 113.11, 65.79, 54.15, 38.03. **MS (APCI): Calculated for $C_{24}H_{18}F_6N_2S_2$:** 513.53. Found 513.53 m/z.

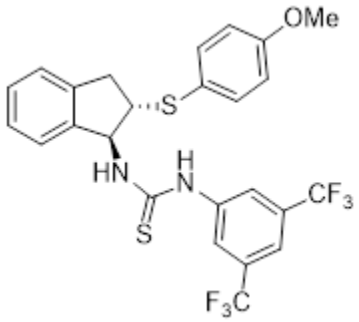

Figure 2.3.13 Catalyst 2.5

The following synthesis is adapted from a general synthesis in published literature. 150 mg (0.28 mmol, 1 equiv) of **(*1S,2S*)-2-((4-methoxyphenyl)thio)-2,3-dihydro-1H-inden-1-amine**

was dissolved in 1.4 mL (0.2M) of anhydrous THF under an inert atmosphere. Then 76 mg (0.28 mmol, 1 equiv) of 3,5-Bis(trifluoromethyl)phenyl isothiocyanate was added to the reaction. The mixture was stirred at r.t. for 4h, then immediately concentrated under reduced pressure. Purification through flash column chromatography (Hex:EtOAc::100:0 to 85:15) afforded the desired product. **^{1}H NMR (400 MHz, $CDCl_3$)** δ 8.24 (s, 1H), 7.79 (s, 2H), 7.69 (s, 1H), 7.55 (d, J = 8.1 Hz, 2H), 7.36-7.15 (m, 4H), 6.84 (d, J = 8.7 Hz, 2H), 3.74 (s, 3H), 3.65 (s, 1H), 3.25 (s, 1H), 3.00-2.95 (s, 1H), 1.66 (s, 1H). **^{13}C NMR (126 MHz, $CDCl_3$)** δ 181.14, 160.30, 140.74, 136.68, 132.52, 129.09, 127.57, 124.83, 124.28, 122.60, 121.43, 119.35, 114.94, 104.99, 65.37, 55.27, 55.07, 37.45. **MS (APCI): Calculated for $C_{25}H_{20}F_6N_2OS_2$:** 543.56. Found 543.56 m/z

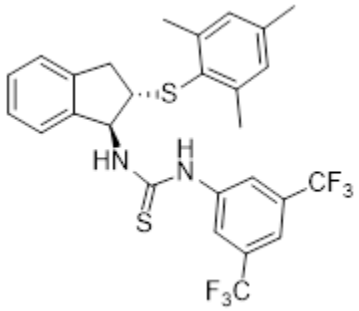

Figure 2.3.14 Catalyst 2.6

The following synthesis is adapted from a general synthesis in published literature. 120mg (0.42 mmol, 1 equiv) of ***(1S,2S)*-2-(mesitylthio)-2,3-dihydro-1H-inden-1-amine** was dissolved in 2.1 mL (0.2M) of anhydrous THF under an inert atmosphere. Then 115 mg (0.42 mmol, 1 equiv) of 3,5-Bis(trifluoromethyl)phenyl isothiocyanate was added to the reaction. The mixture was stirred at r.t. for 4 h, then immediately concentrated under reduced pressure. Purification through flash column chromatography (Hex:EtOAc::100:0 to 85:15) afforded the desired product. **^{1}H NMR (500 MHz, $CDCl_3$)** δ 7.72 (s, 1H), 7.68 (s, 2H), 7.43 (d, *J* = 7.3 Hz, 1H), 7.30-7.26 (m, 4H), 6.87 (s, 2H), 3.74 (s, 1H), 3.43 (s, 1H), 2.94 (d, *J* = 16.5 Hz, 1H), 2.48 (s, 6H), 2.10 (s, 3H). **^{13}C NMR (126 MHz, $CDCl_3$)** δ 180.87, 143.51, 139.58, 129.55, 127.96, 125.17, 123.84, 121.74,

119.81, 109.99, 52.09, 37.42, 22.06, 20.74. **^{19}F NMR (470MHz, $CDCl_3$)** δ -62.87 **MS (APCI): Calculated for $C_{27}H_{24}F_6N_2S_2$:** 555.61. Found 555.61 m/z.

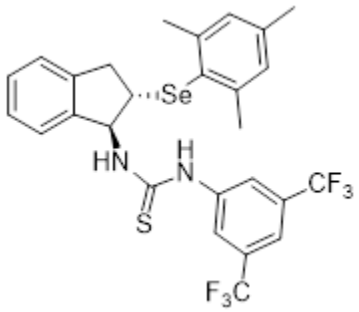

Figure 2.3.15 Catalyst 2.7

The following synthesis is adapted from a general synthesis in published literature. 130 mg (0.33 mmol, 1 equiv) of **(*1S,2S*)-2-(mesitylselanyl)-2,3-dihydro-1H-inden-1-amine** was dissolved in 6.6 mL (0.2M) of anhydrous THF under an inert atmosphere. Then 100 mg (0.37 mmol, 1 equiv) of 3,5-Bis(trifluoromethyl)phenyl isothiocyanate was added to the reaction. The mixture was stirred at r.t. for 4 h, then immediately concentrated under reduced pressure. Purification through flash column chromatography (Hex:EtOAc::100:0 to 85:15) afforded the desired product. **^{1}H NMR (400 MHz, $CDCl_3$)** δ 7.73 (s, 1H), 7.67 (s, 2H), 7.42 (d, J = 7.3 Hz, 1H), 7.29 (bs, 4H), 6.86 (s, 2H), 3.83 (s, 1H), 3.46 (s, 1H), 2.94 (dd, J = 16.9, 4.6 Hz, 1H), 2.51 (s, 6H), 2.09 (s, 3H). **^{13}C NMR (126 MHz, $CDCl_3$)** δ 180.82, 143.70, 142.08, 129.09, 128.98, 127.73, 125.18, 124.16, 121.45, 119.81, 44.97, 37.61, 24.63, 20.66. **^{19}F NMR (470 MHz, $CDCl_3$)** δ -62.92 **MS (APCI): Calculated for $C_{27}H_{24}F_6N_2SSe$:** 602.51. Found 602.51 plus multiplets from selenium isotopes.

V. General *ortho*-halogenation Synthesis for Chlorination of Phenols and Anilines

Substrate (0.030 mmol, 1 equiv.), catalyst (0.00030 mmol, 0.01 equiv. unless specifically mentioned otherwise), and $CDCl_3$ (0.05M) were added to an NMR tube followed by the addition of either tetramethylsilane (TMS) or tetrakis(trimethylsilyl)methane (TTMSM) as an internal

standard (when necessary). A ^{1}H spectrum of the reaction mixture was then obtained with a relaxation delay of 5.00 sec (number of scans = 4), representing the reaction mixture at time = 0. *N*-Halosuccinimide (0.036 mmol, 1.2 equiv.) was then added to the NMR tube, and the reaction was monitored by ^{1}H NMR. The reaction was considered complete once the substrate conversion had ceased. Isomeric ratios were determined via integration of the aromatic peaks of each product. Conversion to mono-Cl products represents the sum of the conversions of all identified mono-chlorinated products, and the value was determined via integration of mono-chlorinated products with respect to either the residual protio solvent or TMS. Isomeric ratios determined by analysis of non-obscure peaks. When necessary, clear coupling patterns were partially integrated, and full integration value was extrapolated from the partial integration. If multiple peaks were clear, the average of those peaks were used to determine the isomeric ratio. Each experiment was performed in duplicate, and the reported ratios are the average of the two trials.

Isolated yields were determined on a 0.1 mmol scale using $CHCl_3$; all reagents and solvent were scaled equally, omitting TMS (or TTMSM). Phenols were stirred at room temperature while anilines were stirred at 0 ˚C. Upon reaction completion, as determined by Thin-Layer Chromatography (TLC), the reaction was filtered through a short normal phase silica plug with DCM to remove succinimide. The solvent was then removed by rotovap, and, for almost all substrates, the resulting crude mixture was purified by Flash Column Chromatography (FCC) on normal phase silica gel, eluting with hexanes and ethyl acetate (hexanes:ethyl acetate::100:0 → 99:1 → 98:2 → 97:3 → 95:5), unless otherwise noted.

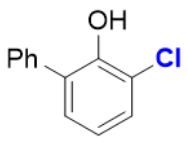

Figure 2.3.16 Product 2.8a

3-chloro-[1,1'-biphenyl]-2-ol (2.8a) was prepared according to the general procedure on a 0.1 mmol scale and obtained as a pale white solid, 44% yield. **^{1}H NMR (500 MHz, $CDCl_3$)** δ 7.57-7.52 (m, 2H), 7.47 (t, J = 7.5 Hz, 2H), 7.41-7.38 (m, 1H), 7.33 (dd, J = 8.0, 1.5 Hz, 1H), 7.23 (d, J = 7.8 Hz, 1H), 6.95 (td, J = 7.8, 2.3 Hz, 1H), 5.71 (s, 1H). **^{13}C NMR (126 MHz, $CDCl_3$)** δ 148.41, 137.06, 129.72, 129.42, 129.15, 128.52, 128.30, 127.75, **MS (APCI)**: **Calculated for** $C_{12}H_{10}ClO$ $[M+H]^+$ 205.0. **Found:** 205.0 m/z.

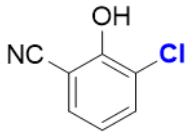

Figure 2.3.17 Product 2.9a

3-chloro-2-hydroxybenzonitrile (2.9a) was prepared according to the general procedure on a 0.1 mmol scale and obtained a white solid. 5% catalyst loading was used, 38% yield. **^{1}H NMR (500 MHz, $CDCl_3$)** δ 7.56 (dq, J = 8.0, 1.3 Hz, 1H), 7.48 (dq, J = 7.9, 1.4 Hz, 1H), 7.02-6.93 (m, 1H), 6.25 (s, 1H). **^{13}C NMR (126 MHz, $CDCl_3$)** δ 153.75, 133.70, 132.08, 121.54, 121.11, 114.99, 101.26. **MS (APCI)**: **Calculated for** C_7H_4ClNO $[M+H]^+$: 154.57. Found 154.57 m/z

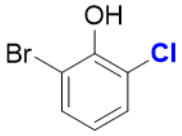

Figure 2.3.18 Product 2.10a

2-bromo-6-chlorophenol (2.10a) was prepared according to the general procedure on a 0.1 mmol scale, and obtained as a clear oil. 5% catalyst loading was used, 43% yield. **^{1}H NMR (500 MHz, $CDCl_3$)** δ 7.41 (dq, J = 8.1, 1.6 Hz, 1H), 7.30 (dq, J = 8.1, 1.6 Hz, 1H), 6.76 (ddd, J = 8.0, 2.0 Hz, 1H), 5.88 (s, 1H). **^{13}C NMR (126MHz, $CDCl_3$)** δ 148.69, 131.38, 128.97, 121.83, 120.82, 110.30. **MS (APCI)**: **Calculated for** C_6H_4BrClO $[M+H]^+$: 208.45. Found 208.45 m/z

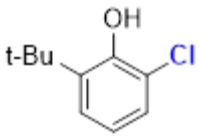

Figure 2.3.19 Product 2.11a

2-(tert-butyl)-6-chlorophenol (2.11a) was prepared according to the general procedure on a .1 mmol scale and obtained as a light orange oil. 56% yield. **^{1}H NMR** (400 MHz, $CDCl_3$) δ 7.19 (t, J = 7.3 Hz, 2H), 6.80 (td, 8.0, 2.2 Hz, 1H), 5.85 (s, 1H), 1.41 (s, 1H). **^{13}C NMR** (126MHz, $CDCl_3$) δ 149.66, 137.60, 126.42, 125.67, 120.88, 120.25, 35.16, 29.30. **MS (APCI)**: **Calculated for** $C_{10}H_{13}ClO$ $[M+H]^+$: 185.66. Found 185.66 m/z

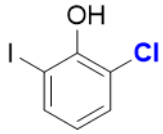

Figure 2.3.20 Product 2.12a

2-chloro-6-iodophenol (2.12a) was prepared according to the general procedure on a 0.1 mmol scale, obtained as a white solid. 75% yield. **^{1}H NMR (400 MHz, $CDCl_3$)** *δ* 7.61 (dd, *J* = 8.0, 2.0 Hz, 1H), 7.31 (dd, *J* = 8.1, 1.8 Hz, 1H), 6.63 (td, *J* = 8.9, 8.5, 1.9 Hz, 1H), 5.94 (s, 1H). **^{13}C NMR (126MHz, $CDCl_3$)** *δ* 150.85, 137.75, 129.63, 122.79, 119.23, 83.47. **MS (APCI)**: **Calculated for** C_6H_4ClIO $[M+H]^+$: 255.45. Found 255.45 m/z

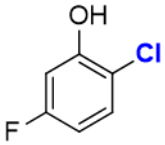

Figure 2.3.21 Product 2.13a

2-chloro-5-fluorophenol (2.13a) was prepared according to the general procedure on a 0.1 mmol scale, obtained as a clear oil. 70% yield. **^{1}H NMR (400 MHz, $CDCl_3$)** *δ* 7.29-7.23 (m, 1H), 6.76 (dd, *J* = 9.6, 2.9 Hz, 1H), 6.61 (ddd, *J* = 8.9, 8.0, 2.9 Hz, 1H), 5.66 (s, 1H). **^{13}C NMR (126 MHz, $CDCl_3$)** *δ* 162.25 (d, *J* = 246 Hz), 152.30 (d, *J* = 12.7 Hz), 129.40 (d, *J* = 9.9 Hz), 115.03,

108.51 (d, J = 23.3 Hz), 103.99 (d, J = 26.6 Hz) **^{19}F NMR (470 MHz, $CDCl_3$)** δ -112.43. **MS (APCI)**: **Calculated for:** C_6H_4ClFO $[M+H]^+$: 147.55. Found 147.55 m/z

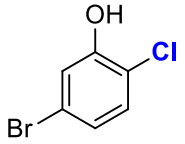

Figure 2.3.22 Product 2.14a

5-bromo-2-chlorophenol (2.14a) was prepared according to the general procedure on a 0.1 mmol scale, obtained as a dark brown oil. 5% catalyst loading was used. 60% yield**. ^{1}H NMR (500 MHz, $CDCl_3$)** δ 7.20-7.17 (m, 2H), 7.01 (dt, J = 8.6, 1.9 Hz, 1H), 5.58 (s, 1H). **^{13}C NMR (126 MHz, $CDCl_3$)** δ 152.03, 129.90, 124.48, 121.27, 119.58, 119.02. **MS (APCI)**: **Calculated for:** C_6H_4BrClO $[M+H]^+$: 208.45. Found 208.45 m/z

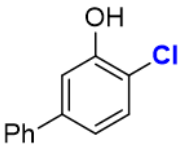

Figure 2.3.23 Product 2.15a

4-chloro-[1,1'-biphenyl]-3-ol (2.15a) was prepared according to the general procedure on a 0.1 mmol scale, obtained as a white solid. 5% catalyst loading was used. 55% yield. **^{1}H NMR (400 MHz, $CDCl_3$)** δ 7.56-7.53 (m, 2H), 7.45-7.41 (m, 4H), 7.38-7.35 (m, 2H), 7.11 (dd, J = 8.3, 2.1 Hz, 1H), 5.59 (s, 1H). **^{13}C NMR (126 MHz, $CDCl_3$)** δ 151.47, 141.90, 139.81, 129.23, 129.12, 128.82, 128.08, 127.73, 126.96, 122.97, 120.13, 114.80. **MS (APCI)**: **Calculated for:** $C_{12}H_9ClO$ $[M+H]^+$: 205.65. Found 205.65 m/z

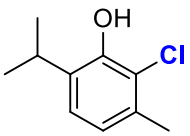

Figure 2.3.24 Product 2.16a

2-chloro-6-isopropyl-3-methylphenol (2.16a) was prepared according to the general procedure on a 0.1 mmol scale, obtained as a brownish-white solid. 47% yield. **^{1}H NMR (400**

MHz, $CDCl_3$) δ 7.01 (d, J = 7.8 Hz, 1H), 6.77 (d, J = 7.8 Hz, 1H), 5.69 (s, 1H), 3.28 (hept, J = 4.2 Hz, 1H), 2.34 (s, 3H), 1.24 (d, J = 9.6 Hz, 6H). **^{13}C NMR (126 MHz, $CDCl_3$)** δ 148.50, 133.43, 133.24, 124.13, 121.85, 120.31, 27.64, 22.41, 19.87. **MS (APCI)**: **Calculated for:** $C_{10}H_{13}ClO$ $[M+H]^+$: 185.66. Found 185.67 m/z

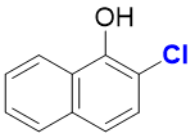

Figure 2.3.25 Product 2.17a

2-chloronaphthalen-1-ol (2.17a) was prepared according to the general procedure on a 0.1 mmol scale, obtained as a white solid. 50% yield. **^{1}H NMR (400 MHz, $CDCl_3$)** δ 8.22 (d, J = 8.7 Hz, 1H), 7.78 (d, J = 7.8 Hz, 1H), 7.55-7.47 (m, 2H), 7.37 (t, J = 1.3 Hz, 2H), 5.99 (s, 1H). **^{13}C NMR (126 MHz, $CDCl_3$)** δ 147.03, 133.21, 127.58, 126.64, 126.06, 125.86, 124.39, 122.05, 120.91, 113.52. **MS (APCI)**: **Calculated for** $C_{10}H_7ClO$ $[M+H]^+$: 179.61. Found 179.61 m/z

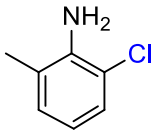

Figure 2.3.26 Product 2.18a

2-chloro-6-methylaniline (2.18a) was prepared according to the general procedure on a 0.1 mmol scale, obtained as a dark brown oil. 80% yield. **^{1}H NMR (400 MHz, $CDCl_3$)** δ 7.14 (d, J = 8.0 Hz, 1H), 6.96 (d, J = 8.0 Hz, 1H), 6.63 (dd, J = 7.9, 2.5 Hz, 1H), 4.01 (bs, 2H), 2.20 (s, 3H). **^{13}C NMR (126 MHz, $CDCl_3$)** δ 141.13, 128.67, 127.04, 123.50, 119.14, 118.28, 17.94. **MS (APCI)**: **Calculated for:** C_7H_8ClN $[M+H]^+$: 142.60. Found 142.61 m/z.

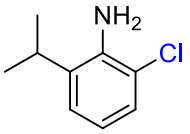

Figure 2.3.27 Product 2.19a

2-chloro-6-isopropylaniline (2.19a) was prepared according to the general procedure on a 0.1 mmol scale, obtained as a dark brown oil. 66% yield. **^{1}H NMR (400 MHz, $CDCl_3$)** δ 7.13 (dd, J = 7.9, 1.5 Hz, 1H), 7.05 (dd, J = 7.9, 1.4 Hz, 1H), 6.70 (t, J = 7.8 Hz, 1H), 4.11 (s, 2H), 2.90 (hept, J = 7.0 Hz, 1H), 1.27 (d, J = 6.8 Hz, 6H). **^{13}C NMR (126 MHz, $CDCl_3$)** δ 139.92, 133.79, 126.67, 123.70, 119.79, 118.56, 28.43, 22.11. **MS (APCI)**: **Calculated for:** $C_9H_{12}ClN$ $[M+H]^+$: 170.65. Found 170.65 m/z.

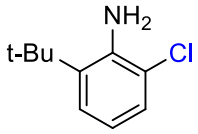

Figure 2.3.28 Product 2.20a

2-(*tert*-butyl)-6-chloroaniline (2.20a) was prepared according to the general procedure on a 0.1 mmol scale, obtained as a dark brown oil. 64% yield. **^{1}H NMR (400 MHz, $CDCl_3$)** δ 7.16 (ddd, J = 10.7, 7.9, 1.4 Hz, 2H), 6.65 (t, J = 7.9 Hz, 1H), 4.35 (s, 2H), 1.43 (s, 9H). **^{13}C NMR (126 MHz, $CDCl_3$)** δ 140.87, 134.92, 127.25, 124.96, 121.17, 117.99, 34.72, 29.50. **MS (APCI)**: **Calculated for:** $C_{10}H_{14}ClN$ $[M+H]^+$: 184.68. Found 184.68 m/z.

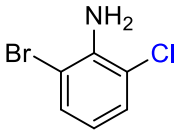

Figure 2.3.29 Product 2.21a

2-bromo-6-chloroaniline (2.21a) was prepared according to the general procedure on a 0.1 mmol scale, obtained as a brownish-white solid. 5% of catalyst was used. 33% yield. **^{1}H NMR (400 MHz, $CDCl_3$)** δ 7.33 (dd, J = 8.0, 1.4 Hz, 1H), 7.21 (dd, J = 8.0, 1.4 Hz, 1H), 4.50 (s, 2H). **^{13}C NMR (126 MHz, $CDCl_3$)** δ 141.09, 130.99, 128.49, 119.31, 118.74, 109.20. **MS (APCI)**: **Calculated for:** C_6H_5BrClN $[M+H]^+$: 206.47. Found 206.47 m/z

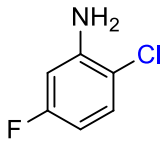

Figure 2.3.30 Product 2.22a

2-chloro-5-fluoroaniline (2.22a) was prepared according to the general procedure on a 0.1 mmol scale, obtained as a brown-orange oil. 5% of catalyst was used. 70% yield. **^{1}H NMR (400 MHz, $CDCl_3$)** δ 7.17 (dd, J = 8.8, 5.7 Hz, 1H), 6.47 (dd, J = 10.1, 2.9 Hz, 1H), 6.40 (td, J = 8.4, 2.9 Hz, 1H), 4.14 (s, 2H). **^{13}C NMR (126 MHz, $CDCl_3$)** δ 162.17 (d, J = 244 Hz), 144.08 (d, J = 11.3 Hz), 130.15 (d, J = 10.0 Hz), 114.14 (d, J = 2.9 Hz), 105.71 (d, J = 23.4 Hz), 102.45 (d, J = 26.4 Hz). **^{19}F NMR (470 MHz, $CDCl_3$)** δ -114.81. **MS (APCI)**: **Calculated for:** C_6H_5ClFN $[M+H]^+$: 145.56 Found 145.56 m/z

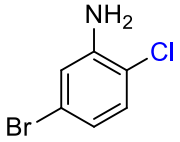

Figure 2.3.31 Product 2.23a

5-bromo-2-chloroaniline (2.23a) was prepared according to the general procedure on a 0.1 mmol scale, obtained as a brown-orange oil. 5% of catalyst was used. 30% yield. **^{1}H NMR (400 MHz, $CDCl_3$)** δ 7.08 (d, J = 8.4, 1H), 6.90 (d, J = 2.3 Hz, 1H), 6.79 (dd, J = 8.5, 2.2, 1H). 4.09 (s, 1H). **^{13}C NMR (126 MHz, $CDCl_3$)** δ 144.07,130.51, 121.72, 121.69, 118.26, 118.07. **MS (APCI)**: **Calculated for:** C_6H_5BrClN $[M+H]^+$: 207.47 Found 207.47 m/z **MS (APCI)**: **Calculated for:** C_6H_5BrClN $[M+H]^+$: 207.47 Found 207.47 m/z

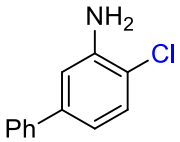

Figure 2.3.32 Product 2.24a

4-chloro-[1,1'-biphenyl]-3-amine (2.24a) was prepared according to the general procedure on a .1 mmol scale, obtained as a brown-orange oil. 5% of catalyst was used. 43% yield. **^{1}H NMR (400 MHz, $CDCl_3$)** δ 7.47-7.38 (m, 5H), 7.30 (d, J = 8.2 Hz, 1H), 6.98 (d, J = 2.1 Hz, 1H), 6.92 (dd, J = 8.2, 2.1 Hz, 1H), 4.12 (s, 2H). **^{13}C NMR (126 MHz, $CDCl_3$)** δ 142.99, 140.99, 140.44, 129.62, 129.31, 128.71, 127.90, 127.44, 126.95, 120.83, 117.99, 114.42. **MS (APCI)**: **Calculated for:** $C_{12}H_{10}ClN$ $[M+H]^+$: 204.67. Found 204.67 m/z

2.3.4: NMR Spectra of Purified Products

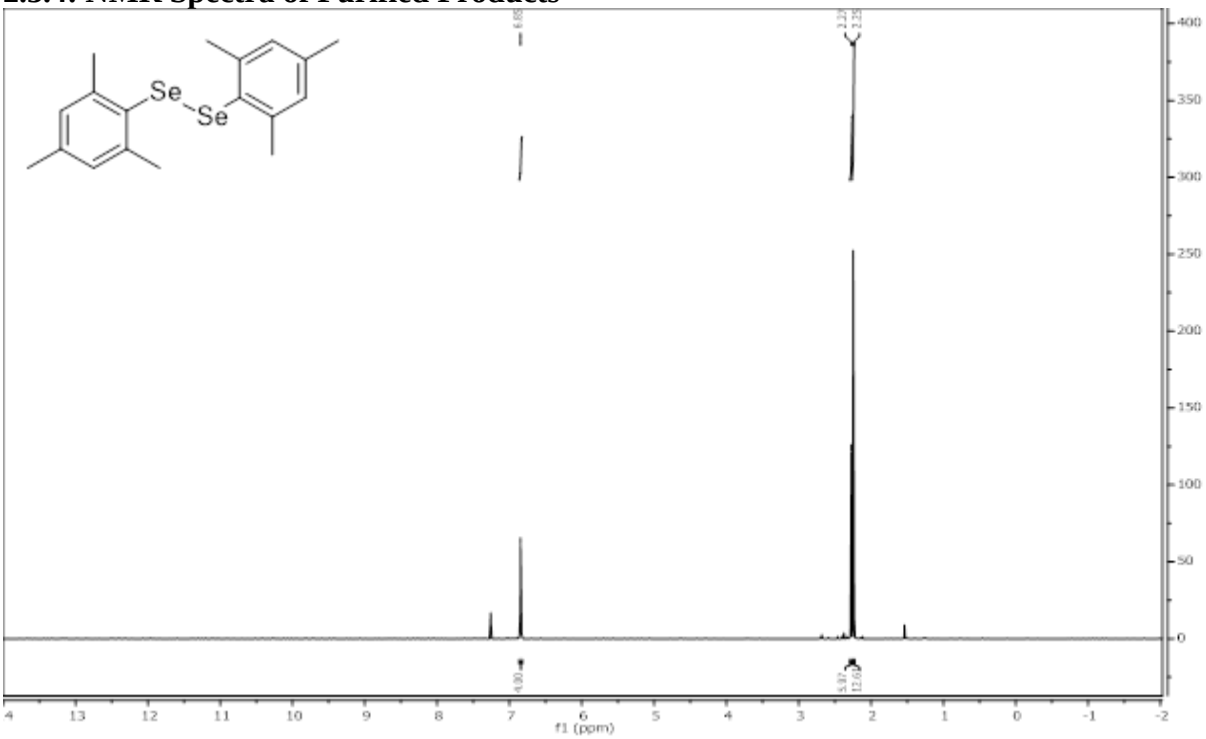

Figure 2.3.33 500 MHz ^{1}H Spectrum of 1,2-dimeityldiselane

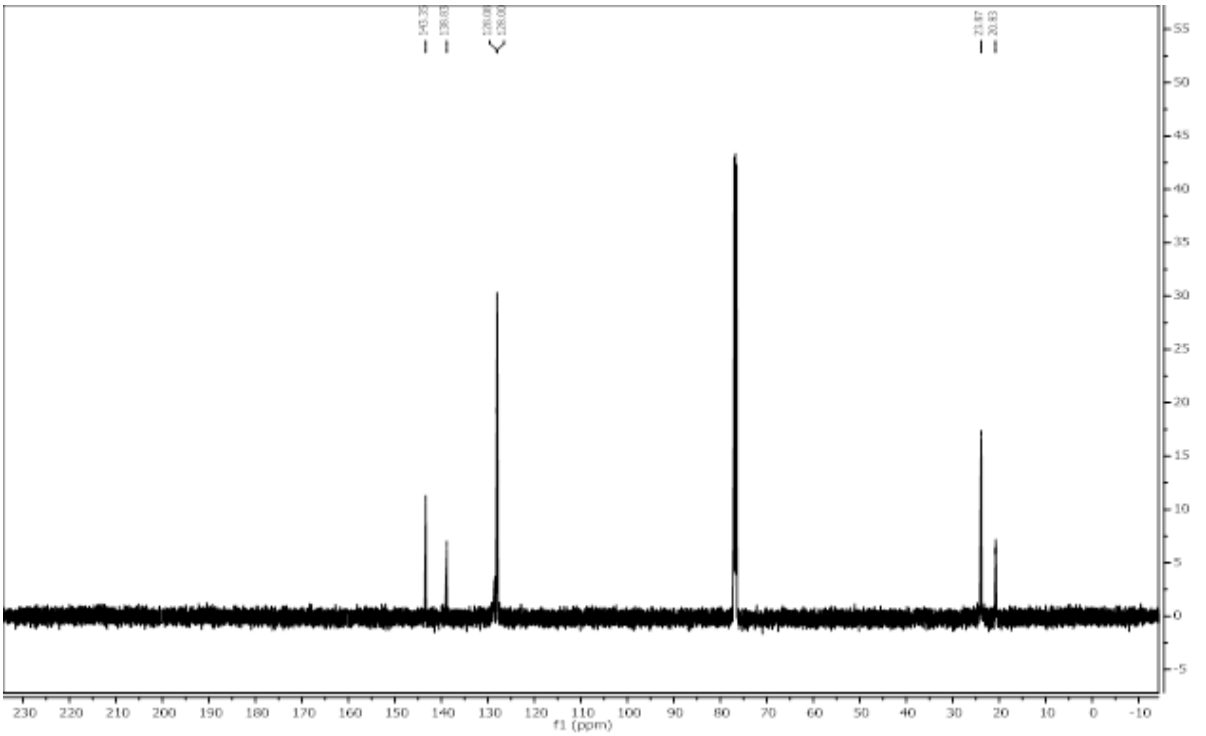

Figure 2.3.34 126 MHz ^{13}C Spectrum of 1,2-dimeityldiselane

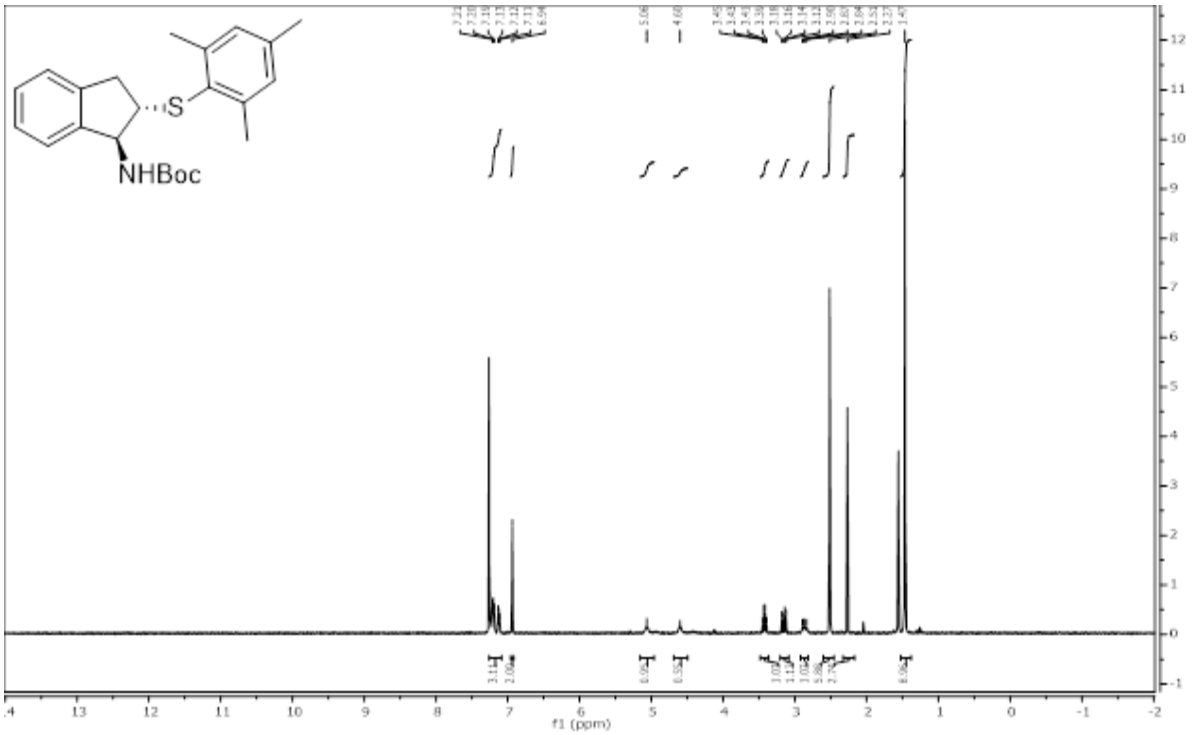

Figure 2.3.35 500 MHz ^{1}H Spectrum of *tert*-butyl ((*1S,2S*)-2-(mesitylthio)-2,3-dihydro-1H-inden-1-yl)carbamate

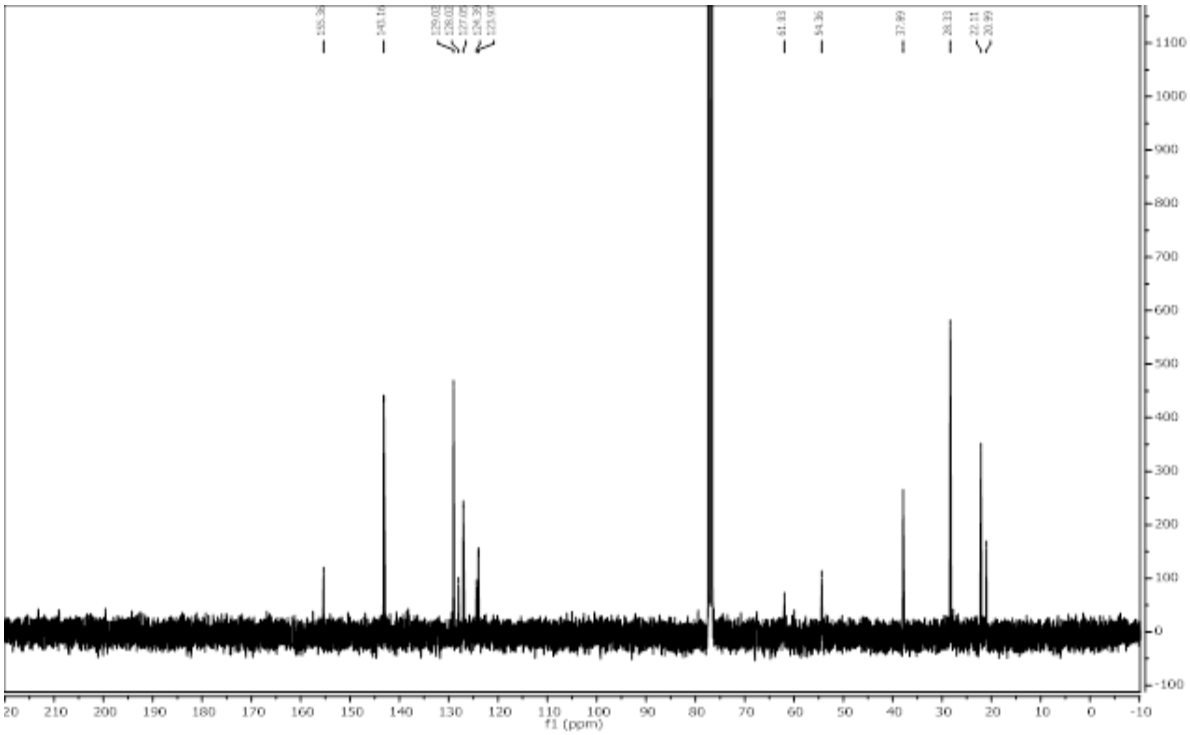

Figure 2.3.36 126 MHz ^{13}C Spectrum of *tert*-butyl ((*1S,2S*)-2-(mesitylthio)-2,3-dihydro-1H-inden-1-yl)carbamate

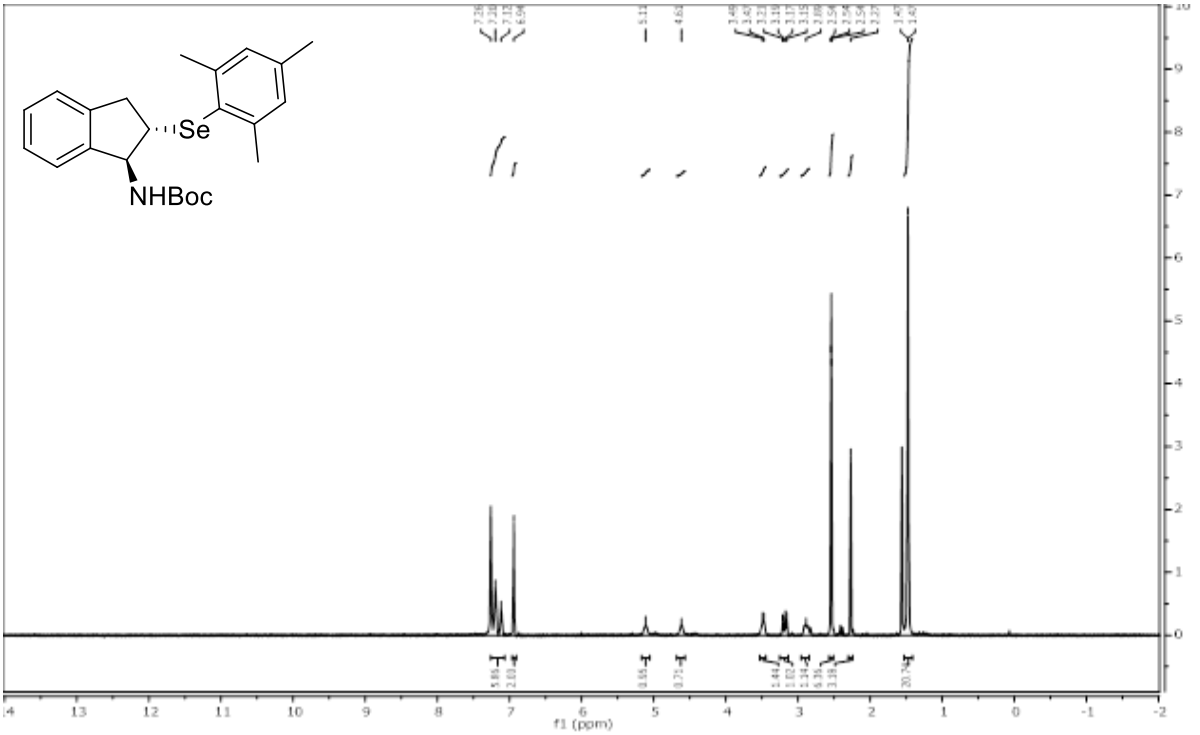

Figure 2.3.37 500 MHz ^{1}H Spectrum of *tert*-butyl ((*1S,2S*)-2-(mesitylselanyl)-2,3-dihydro-1H-inden-1-yl)carbamate

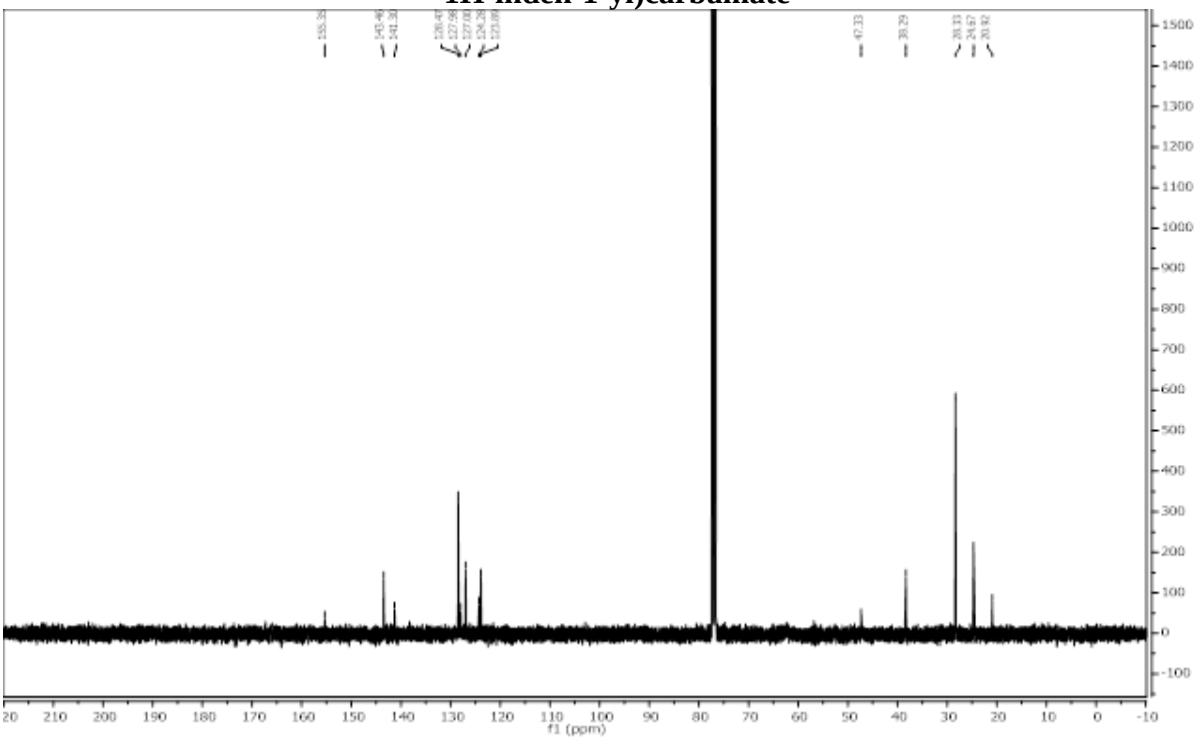

Figure 2.3.38 126 MHz ^{13}C Spectrum of *tert*-butyl ((*1S,2S*)-2-(mesitylselanyl)-2,3-dihydro-1H-inden-1-yl)carbamate

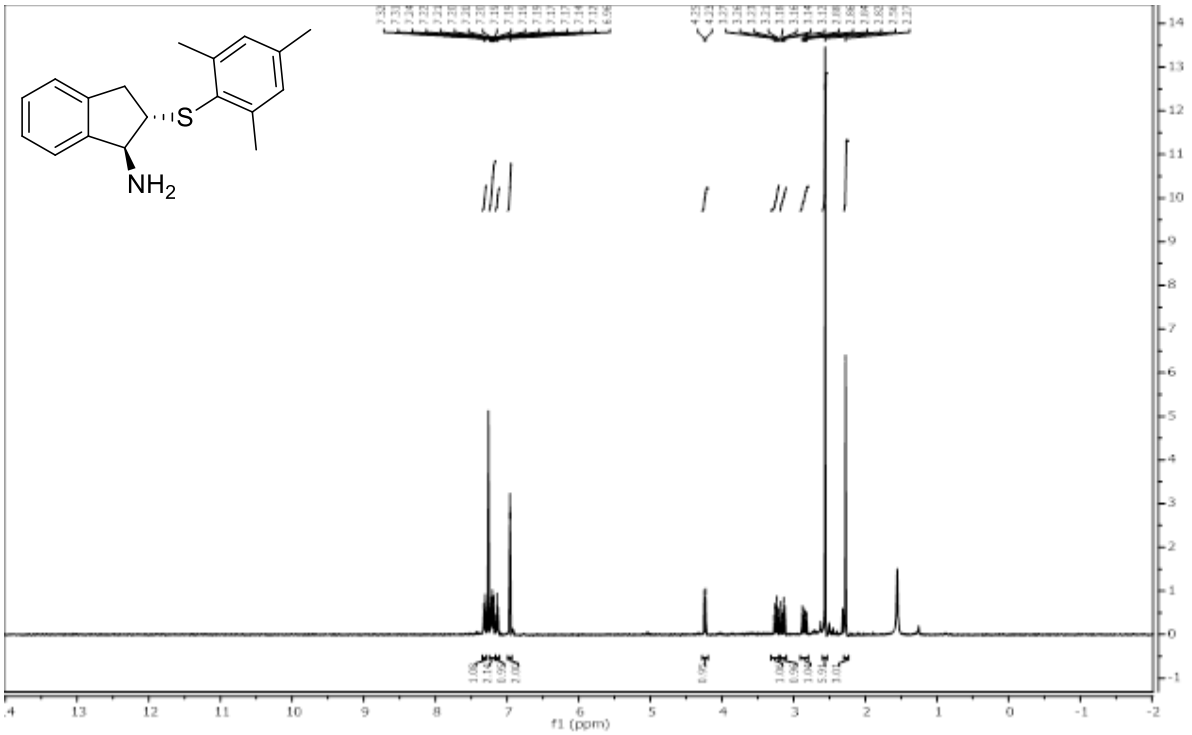

Figure 2.3.39 400 MHz ^{1}H Spectrum of (*1S,2S*)-2-(mesitylthio)-2,3-dihydro-1H-inden-1-amine

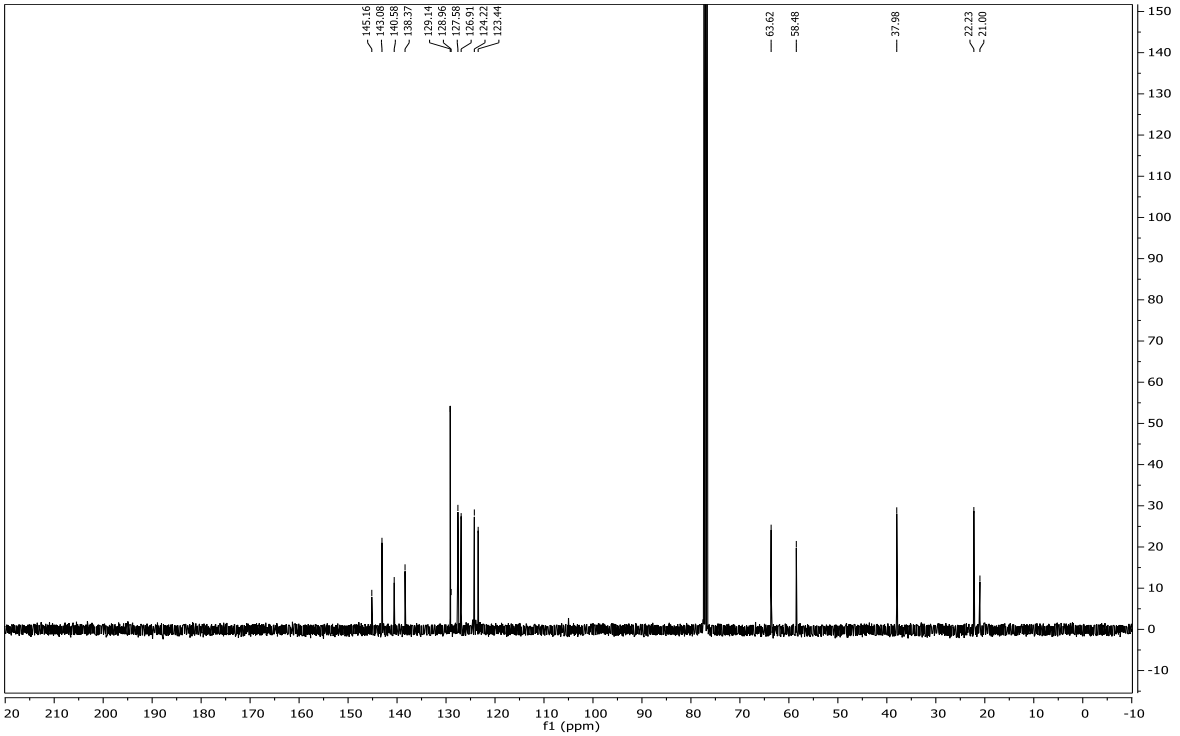

Figure 2.3.40 126 MHz ^{13}C Spectrum of (*1S,2S*)-2-(mesitylthio)-2,3-dihydro-1H-inden-1-amine

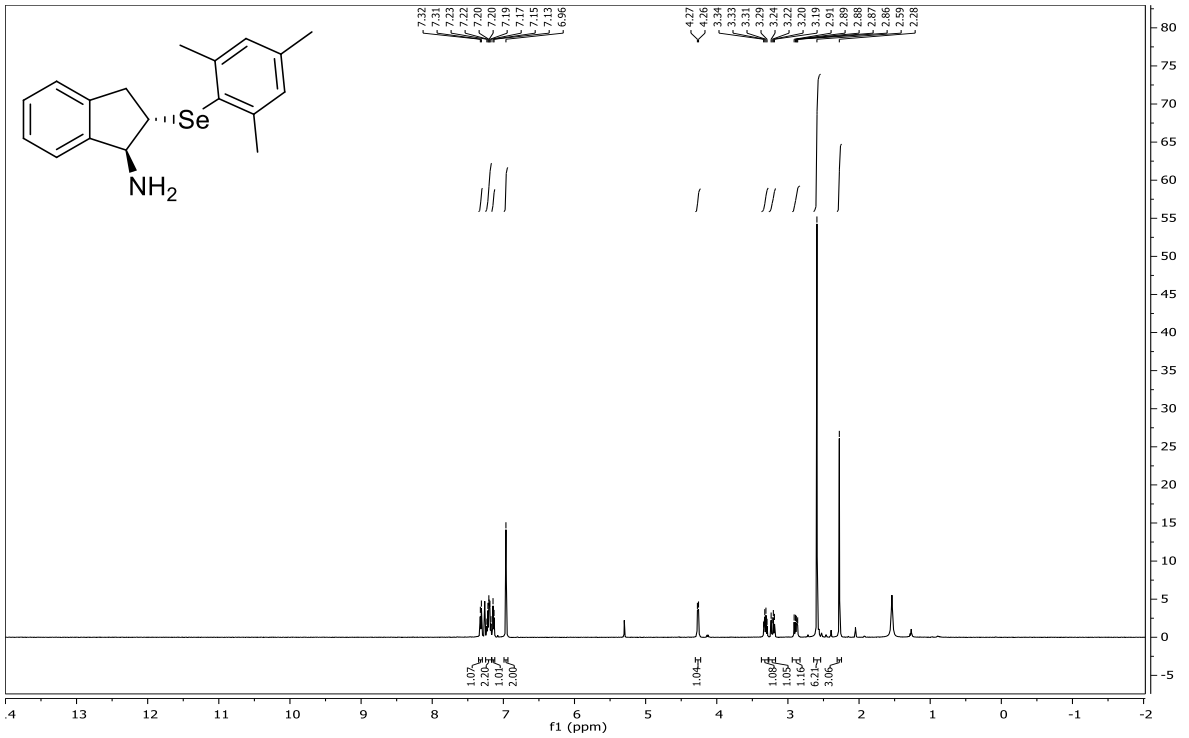

Figure 2.3.41 500 MHz ^{1}H Spectrum of (*1S,2S*)-2-(mesitylselanyl)-2,3-dihydro-1H-inden-1-amine

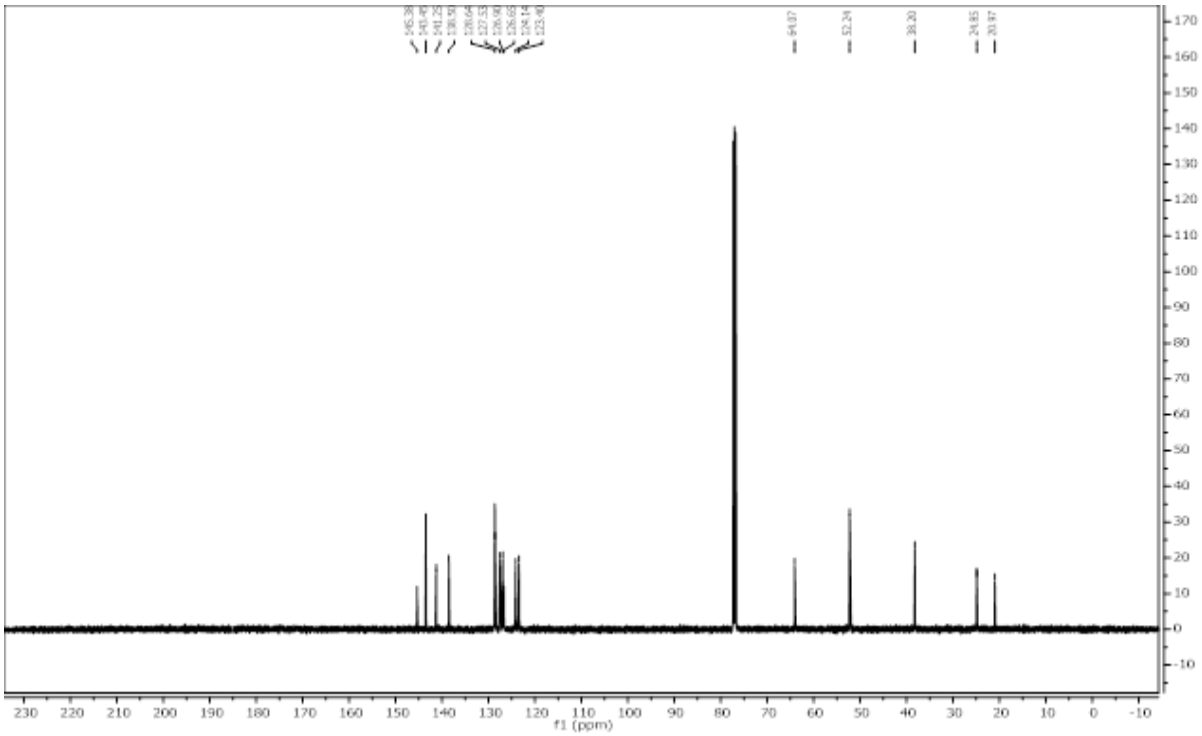

Figure 2.3.42 126 MHz ^{13}C Spectrum of (*1S,2S*)-2-(mesitylselanyl)-2,3-dihydro-1H-inden-1-amine

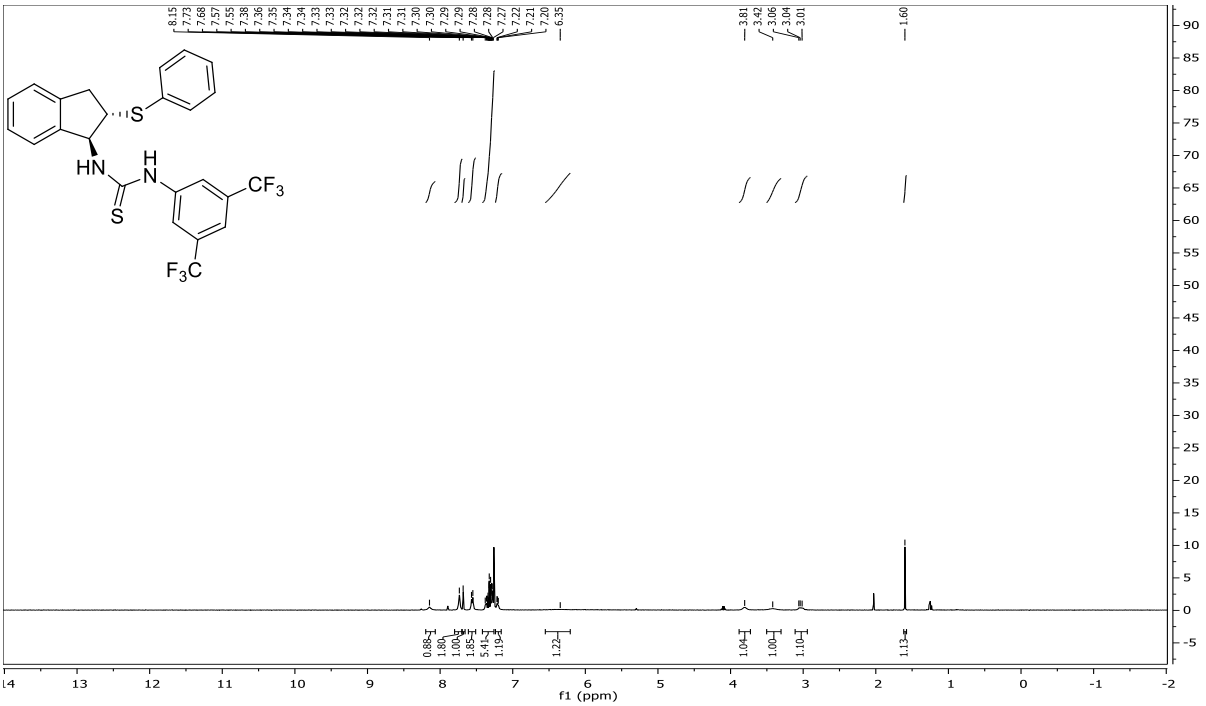

Figure 2.3.43 400 MHz ^{1}H Spectrum of 1-(3,5-bis(trifluoromethyl)phenyl)-3-((*1S,2S*)-2-(phenylthio)-2,3-dihydro-1H-inden-1-yl)thiourea

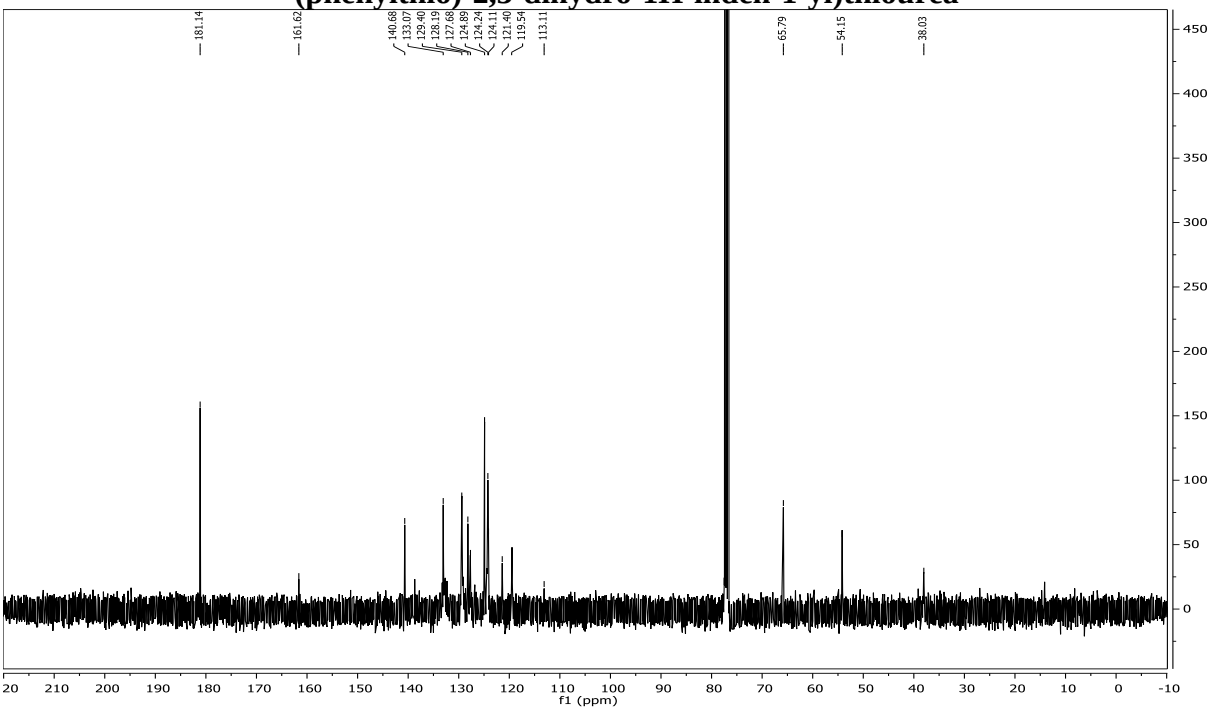

Figure 2.3.44 126 MHz ^{13}C Spectrum of 1-(3,5-bis(trifluoromethyl)phenyl)-3-((*1S,2S*)-2-(phenylthio)-2,3-dihydro-1H-inden-1-yl)thiourea

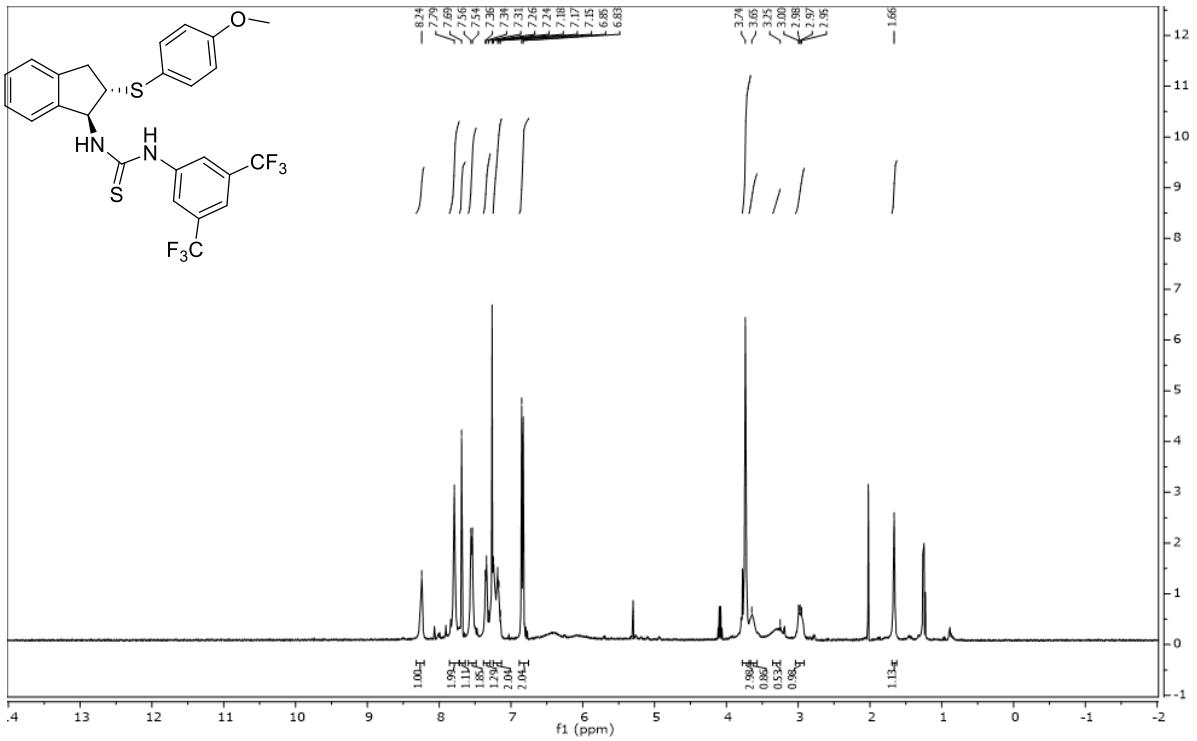

Figure 2.3.45 400 MHz ^{1}H Spectrum of 1-(3,5-bis(trifluoromethyl)phenyl)-3-((*1S,2S*)-2-((4-methoxyphenyl)thio)-2,3-dihydro-1H-inden-1-yl)thiourea

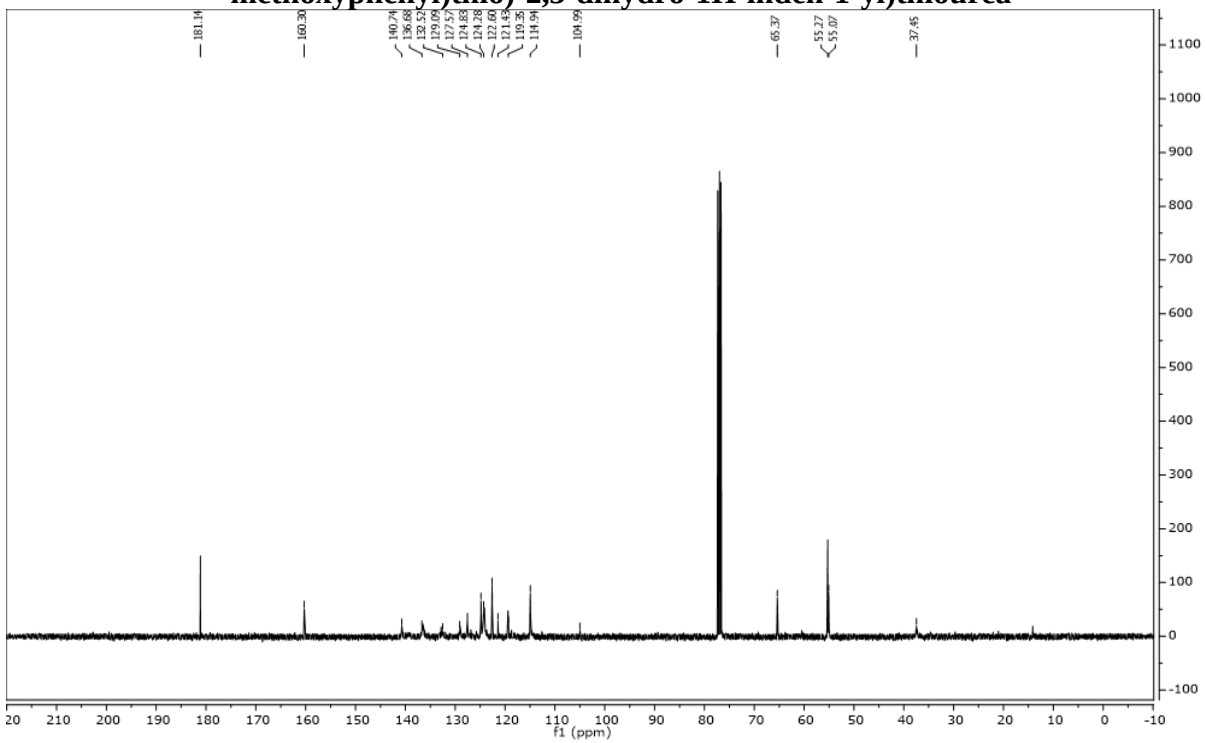

Figure 2.3.46 126 MHz ^{13}C Spectrum of 1-(3,5-bis(trifluoromethyl)phenyl)-3-((*1S,2S*)-2-((4-methoxyphenyl)thio)-2,3-dihydro-1H-inden-1-yl)thiourea

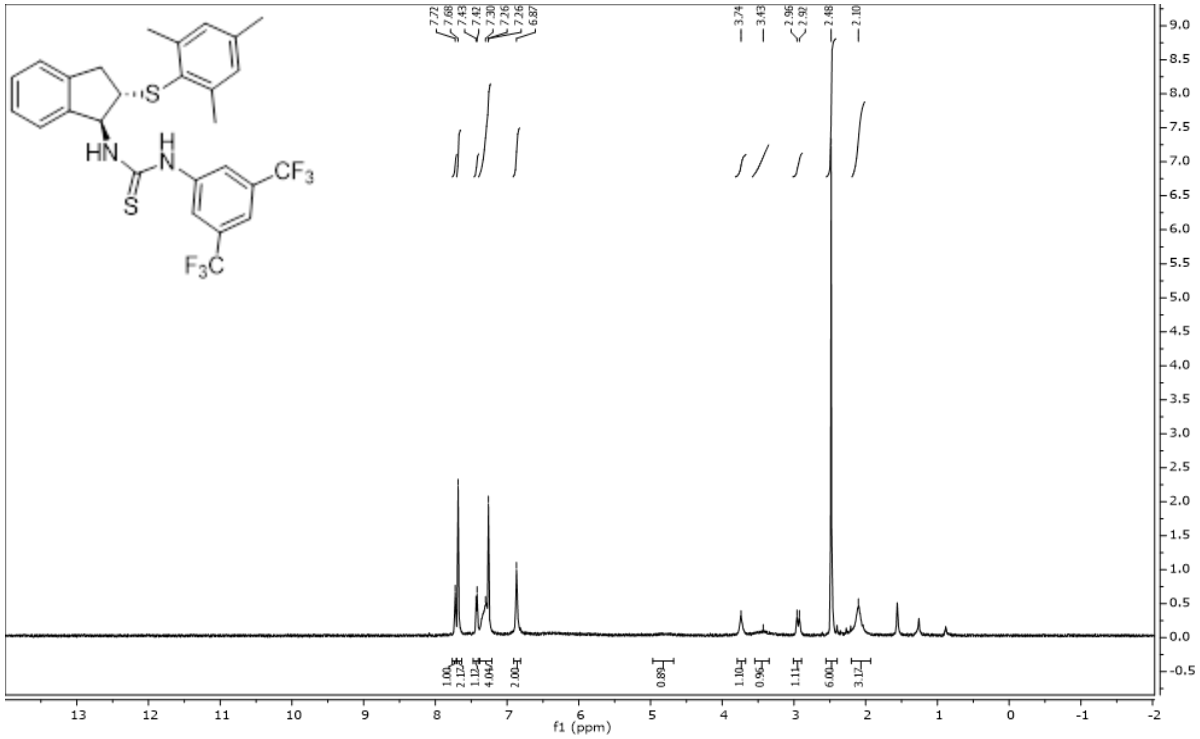

Figure 2.3.47 500 MHz ^{1}H Spectrum of 1-(3,5-bis(trifluoromethyl)phenyl)-3-((*1S,2S*)-2-(mesitylthio)-2,3-dihydro-1H-inden-1-yl)thiourea

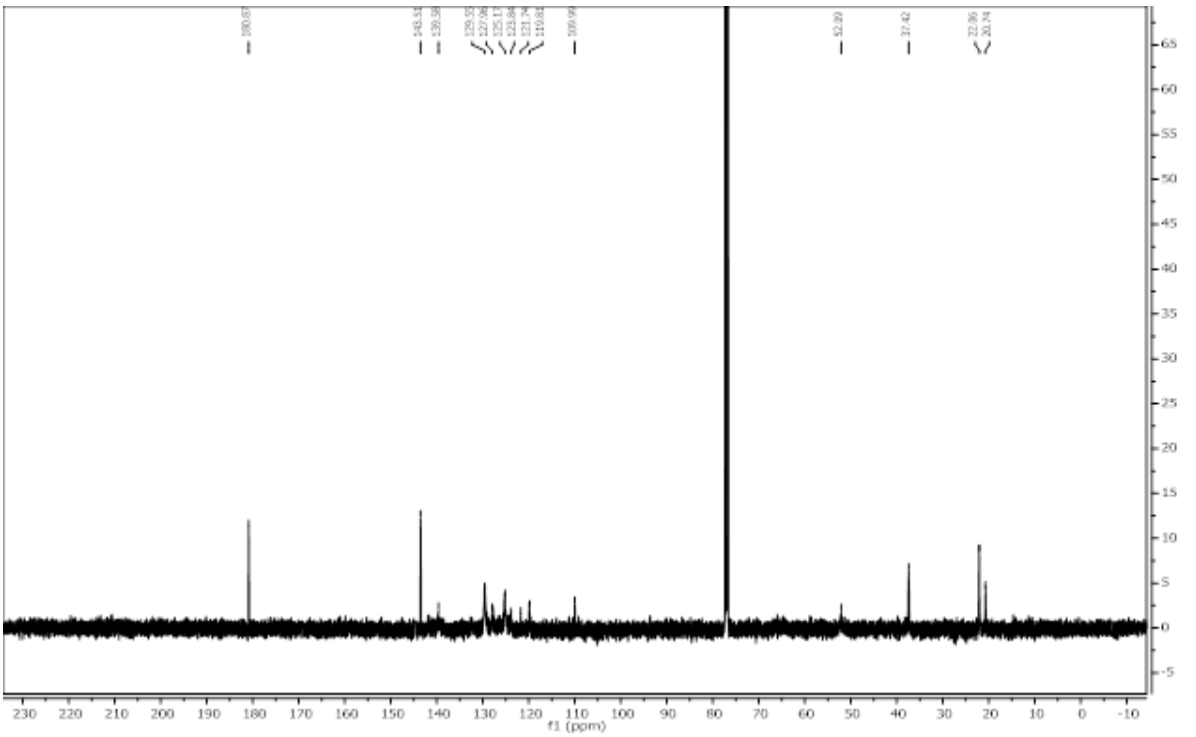

Figure 2.3.48 126 MHz ^{13}C Spectrum of 1-(3,5-bis(trifluoromethyl)phenyl)-3-((*1S,2S*)-2-(mesitylthio)-2,3-dihydro-1H-inden-1-yl)thiourea

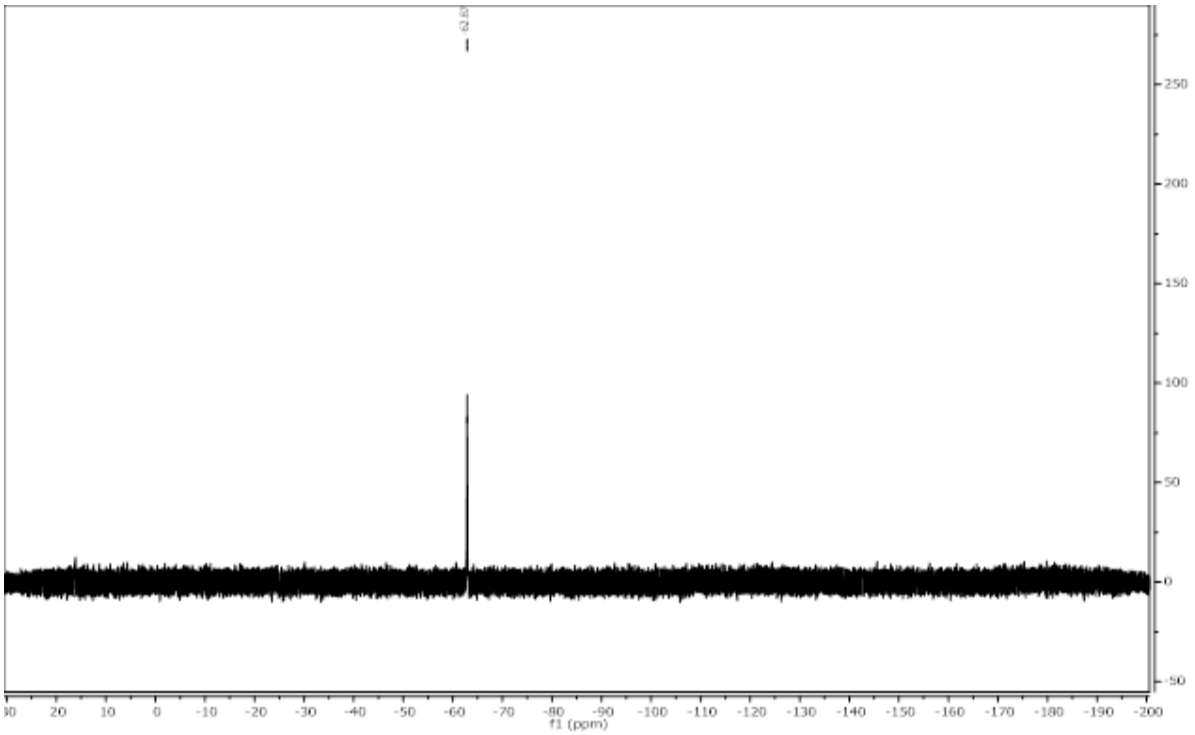

Figure 2.3.49 470 MHz ^{19}F Spectrum of 1-(3,5-bis(trifluoromethyl)phenyl)-3-((*1S,2S)*-2-(mesitylthio)-2,3-dihydro-1H-inden-1-yl)thiourea

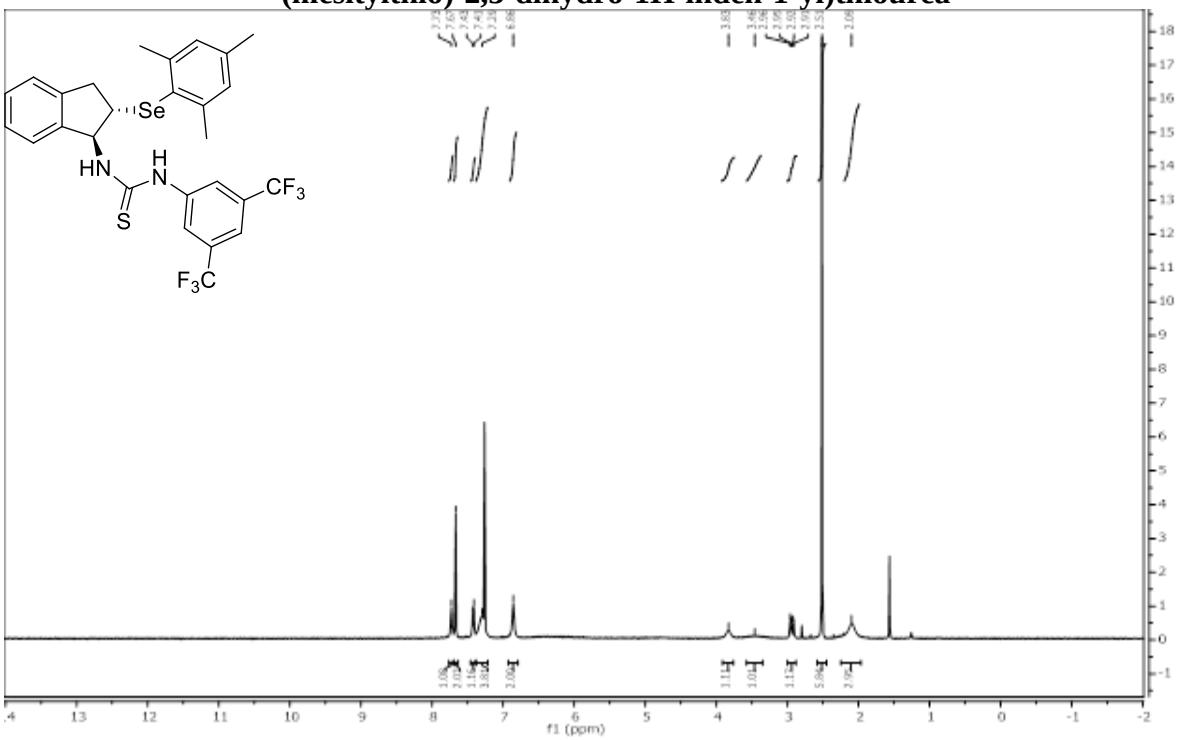

Figure 2.3.50 400 MHz ^{1}H Spectrum of 1-(3,5-bis(trifluoromethyl)phenyl)-3-((*1S,2S*)-2-(mesitylselanyl)-2,3-dihydro-1H-inden-1-yl)thiourea

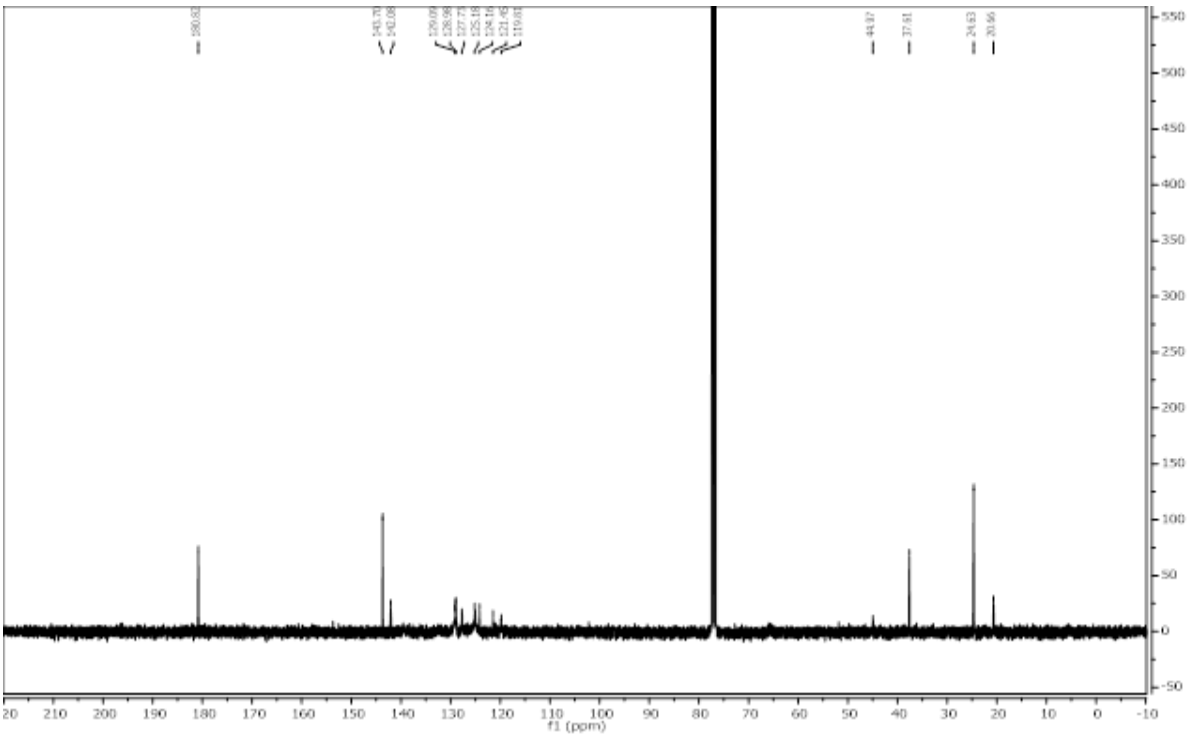

Figure 2.3.51 126 MHz ^{13}C Spectrum of 1-(3,5-bis(trifluoromethyl)phenyl)-3-((*1S,2S*)-2-(mesitylselanyl)-2,3-dihydro-1H-inden-1-yl)thiourea

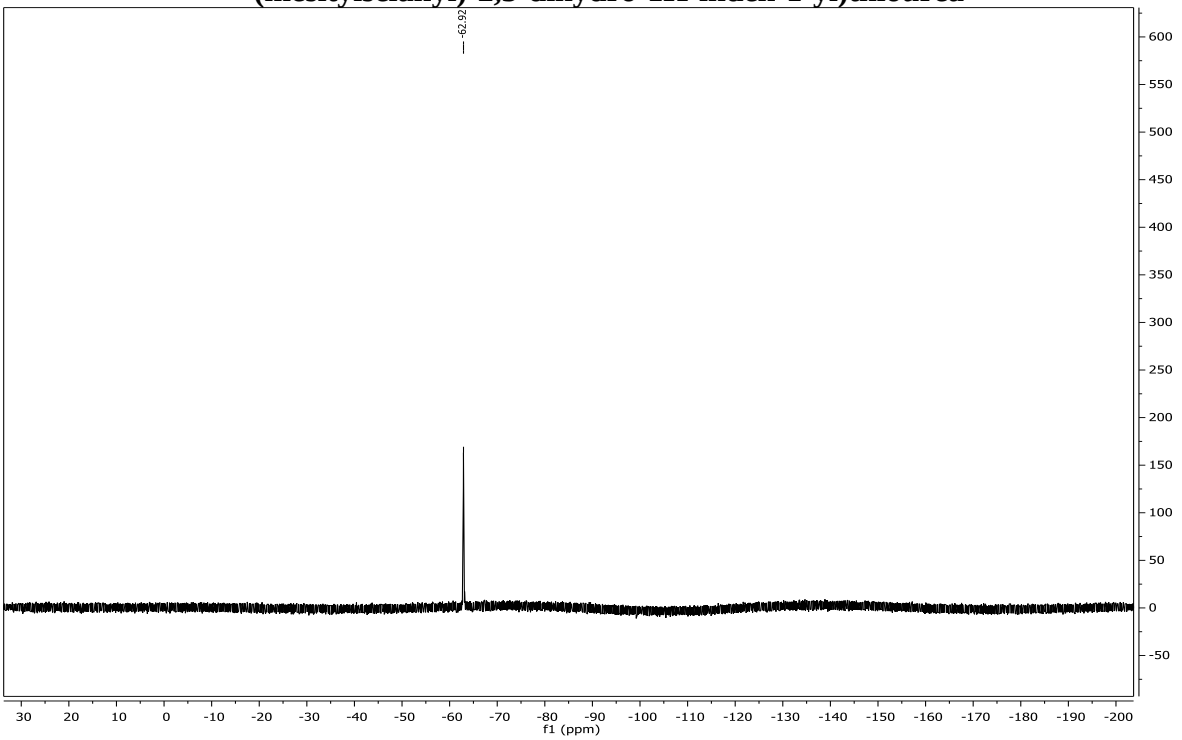

Figure 2.3.52 470 MHz ^{19}F Spectrum of 1-(3,5-bis(trifluoromethyl)phenyl)-3-((*1S,2S*)-2-(mesitylselanyl)-2,3-dihydro-1H-inden-1-yl)thiourea

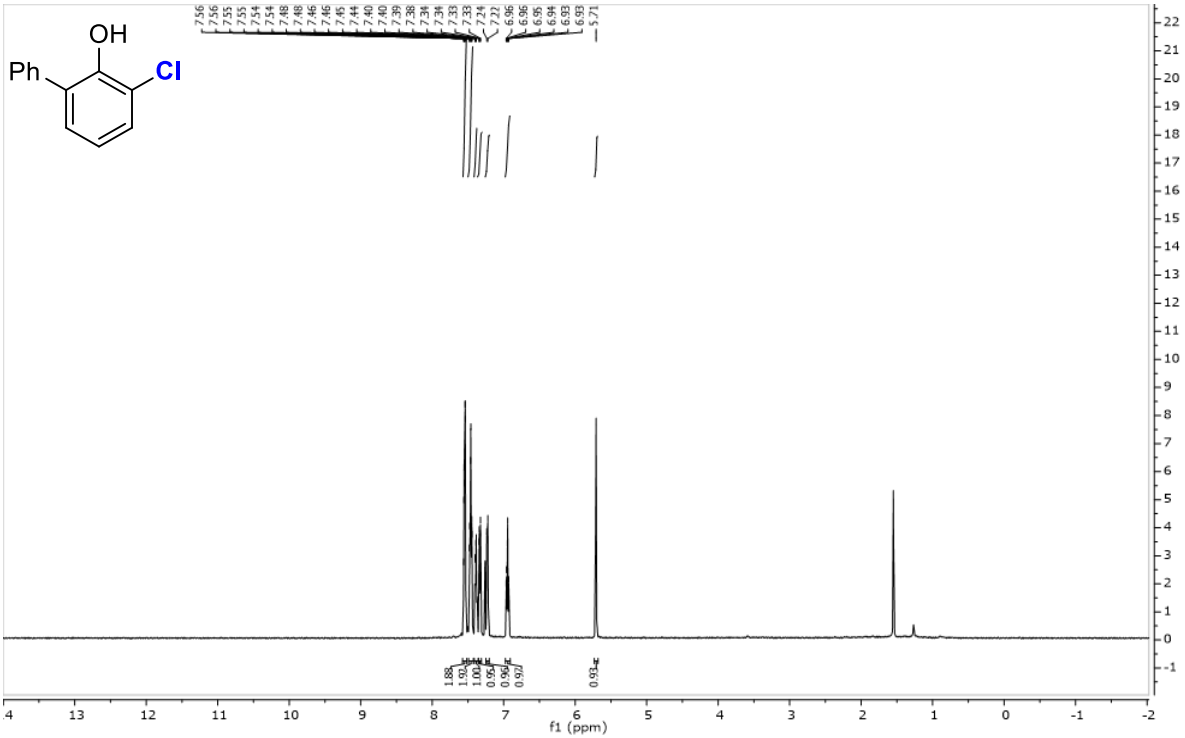

Figure 2.3.53 500 MHz ^{1}H Spectrum of Product 2.8a

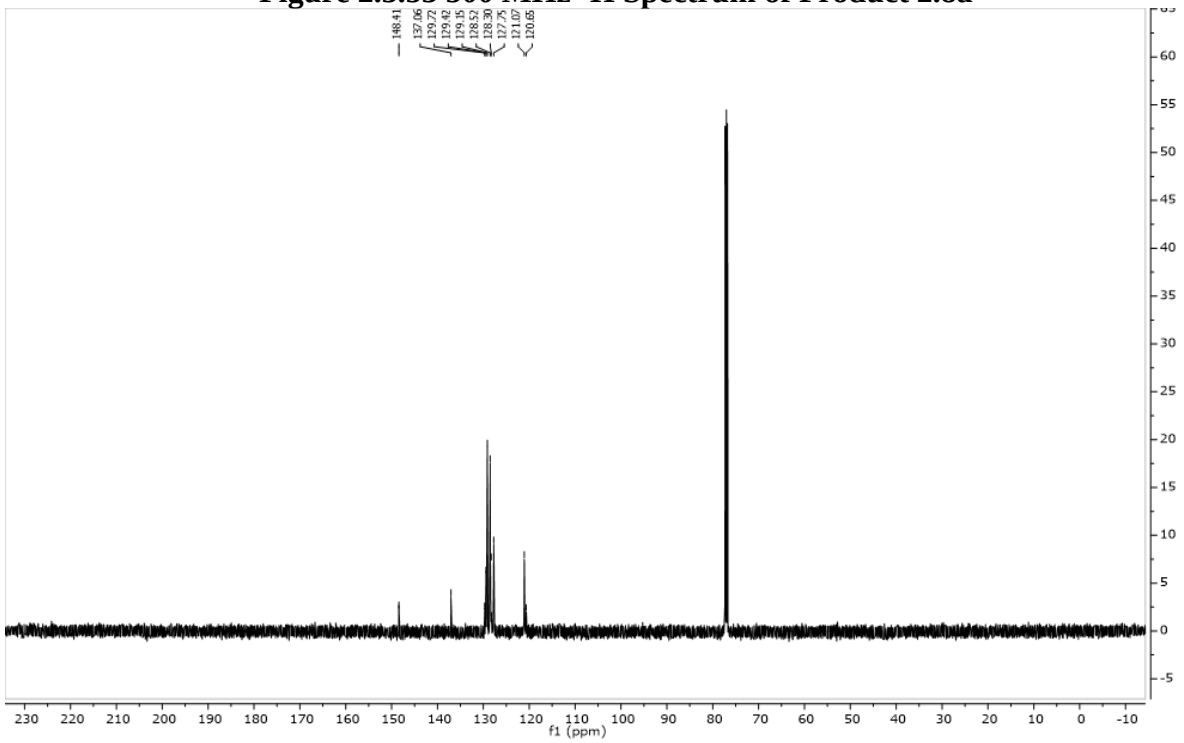

Figure 2.3.54 126 MHz ^{13}C Spectrum of Product 2.8a

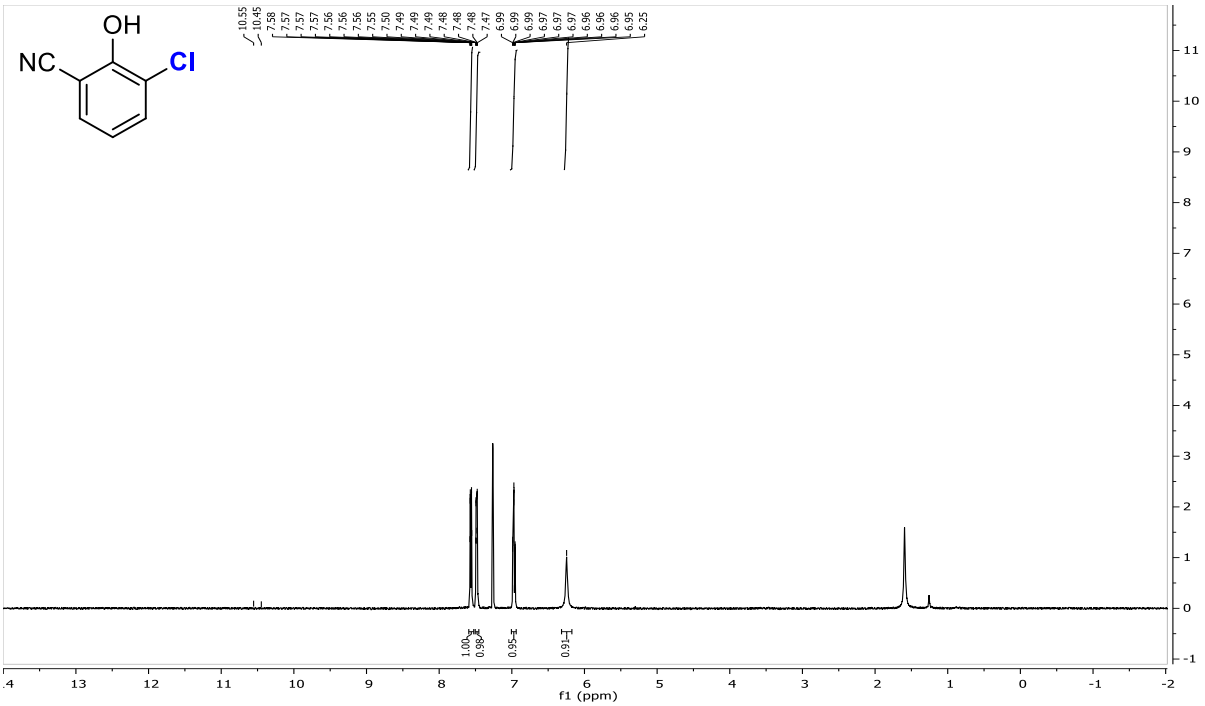

Figure 2.3.55 500 MHz ^{1}H Spectrum of Product 2.9a

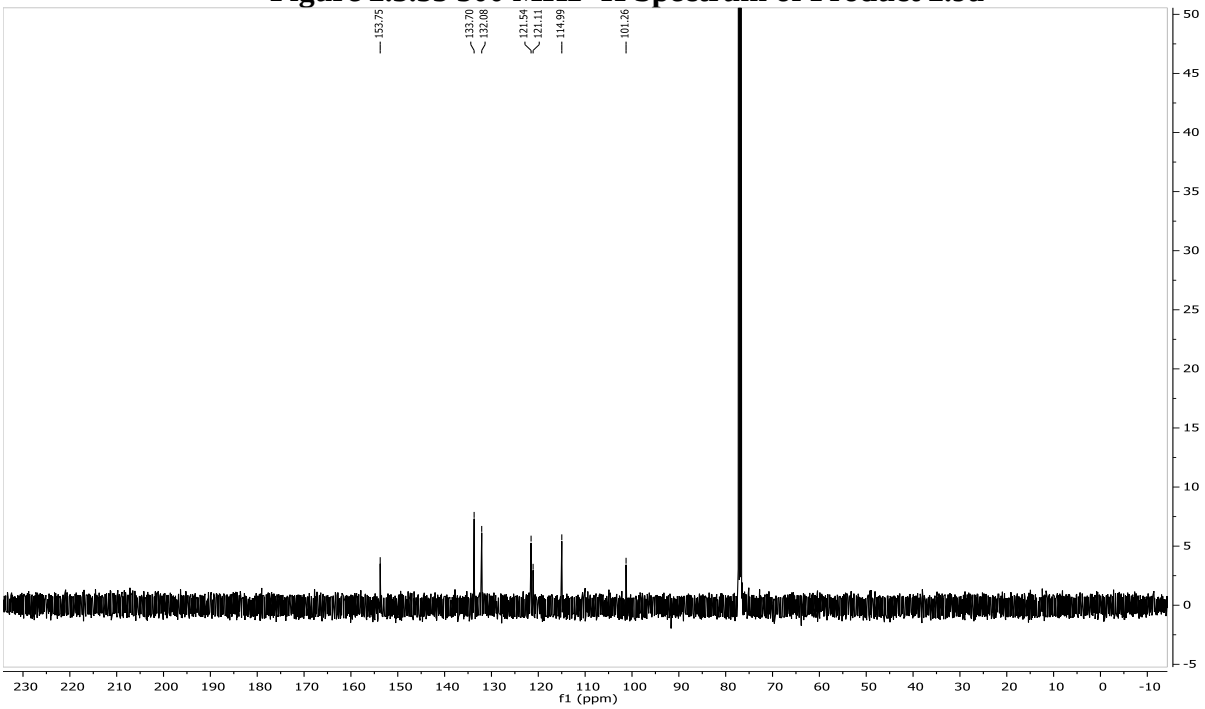

Figure 2.3.56 126 MHz ^{13}C Spectrum of Product 2.9a

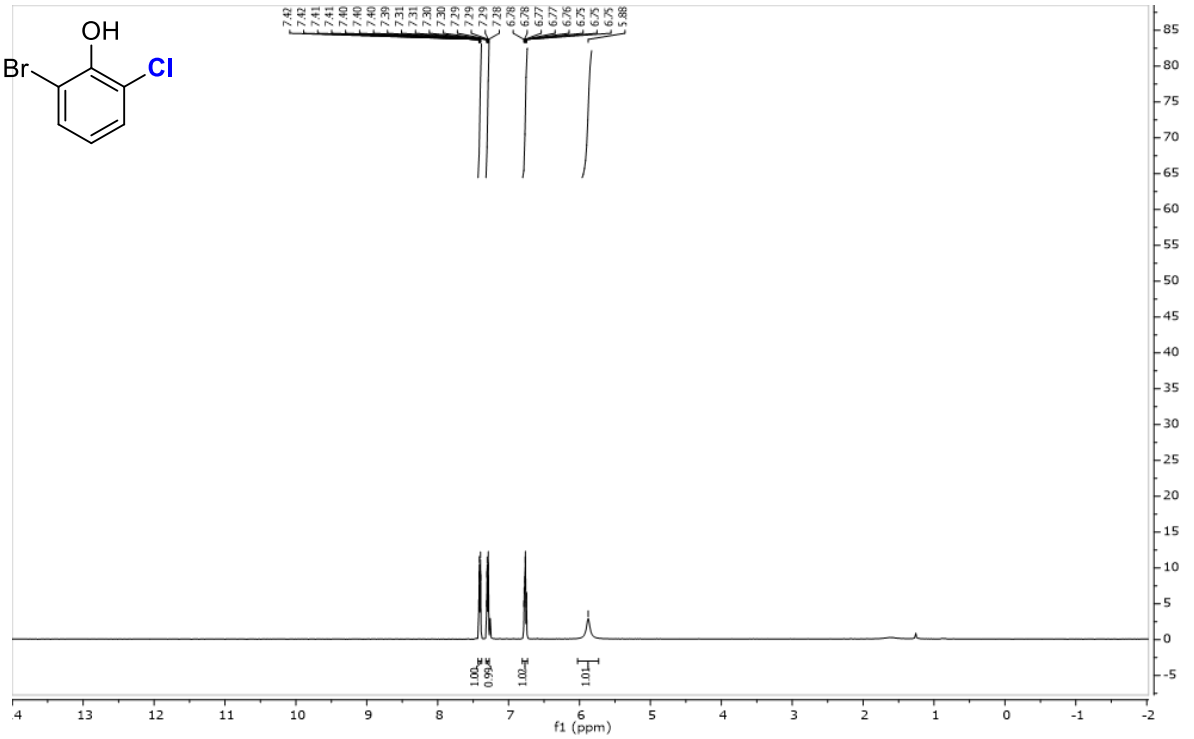

Figure 2.3.57 500 MHz ^{1}H Spectrum of Product 2.10a

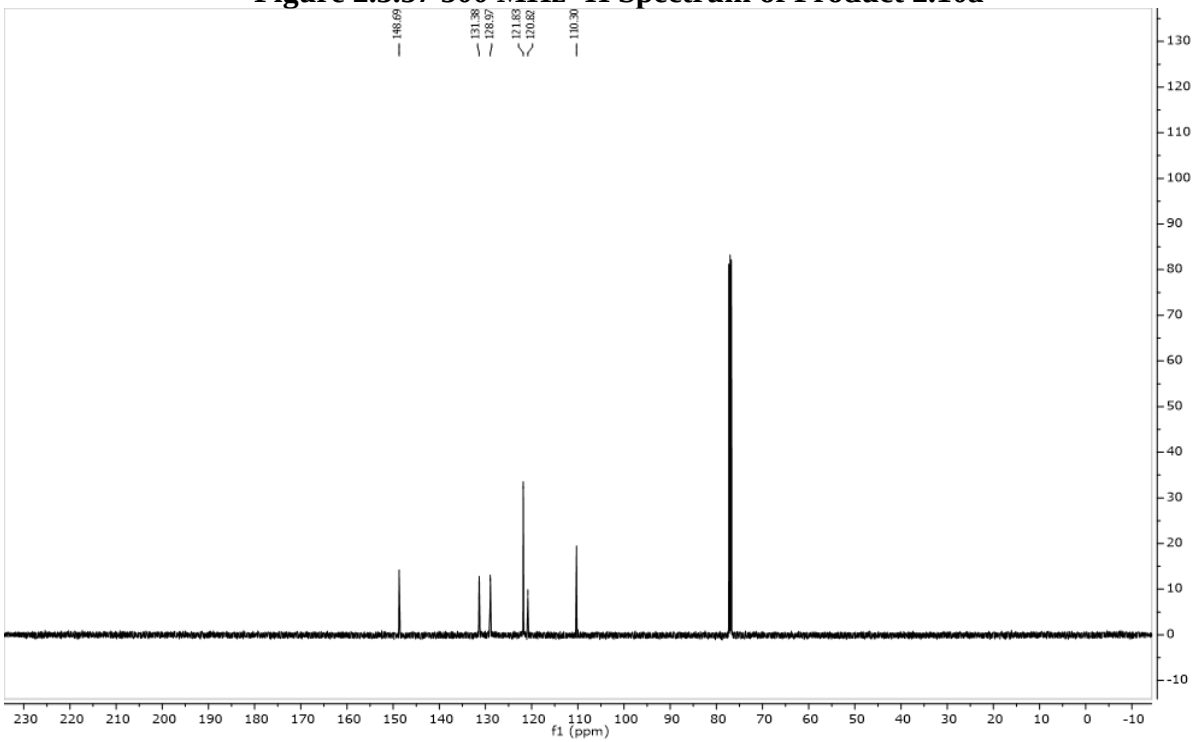

Figure 2.3.58 126 MHz ^{13}C Spectrum of Product 2.10a

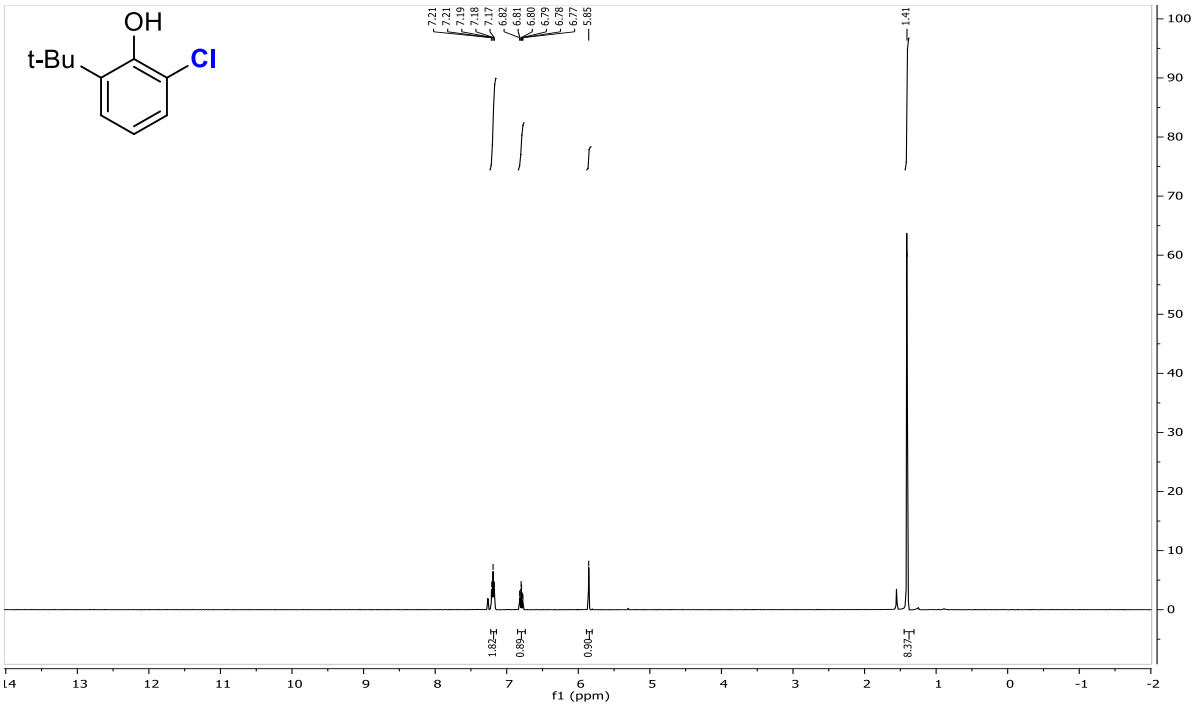

Figure 2.3.59 400 MHz ^{1}H Spectrum of Product 2.11a

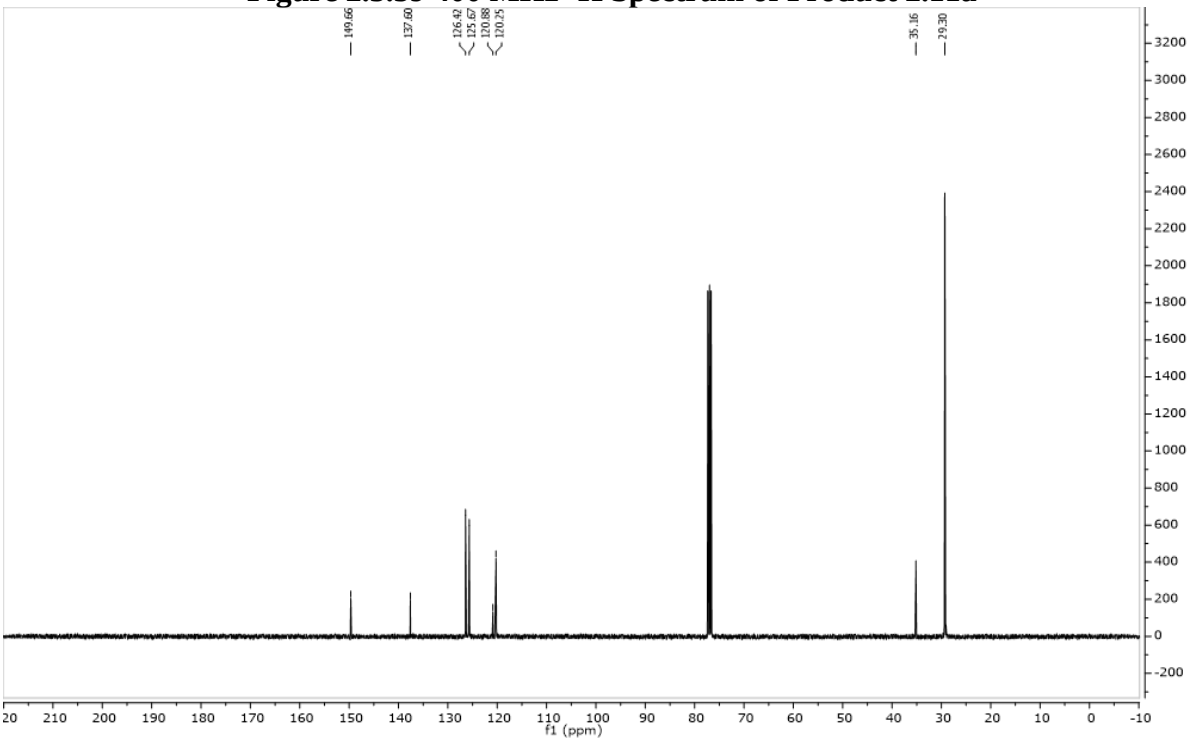

Figure 2.3.60 126 MHz ^{13}C Spectrum of Product 2.11a

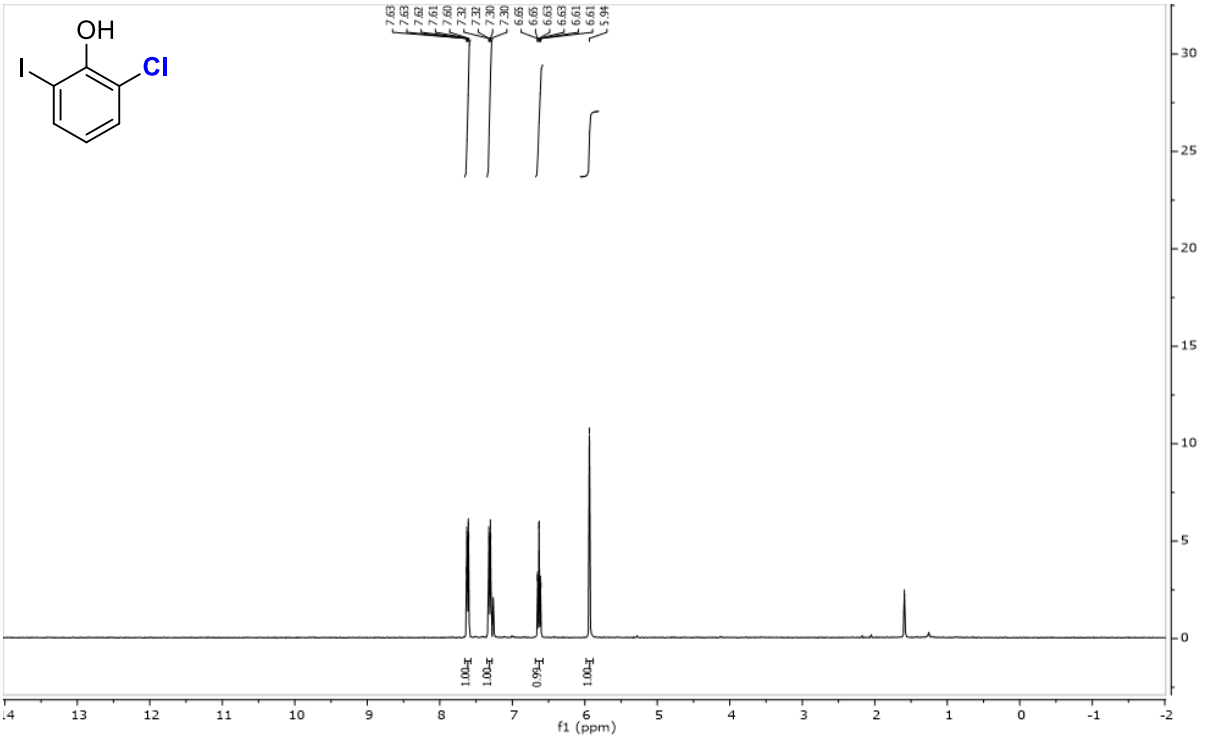

Figure 2.3.61 400 MHz ^{1}H Spectrum of Product 2.12a

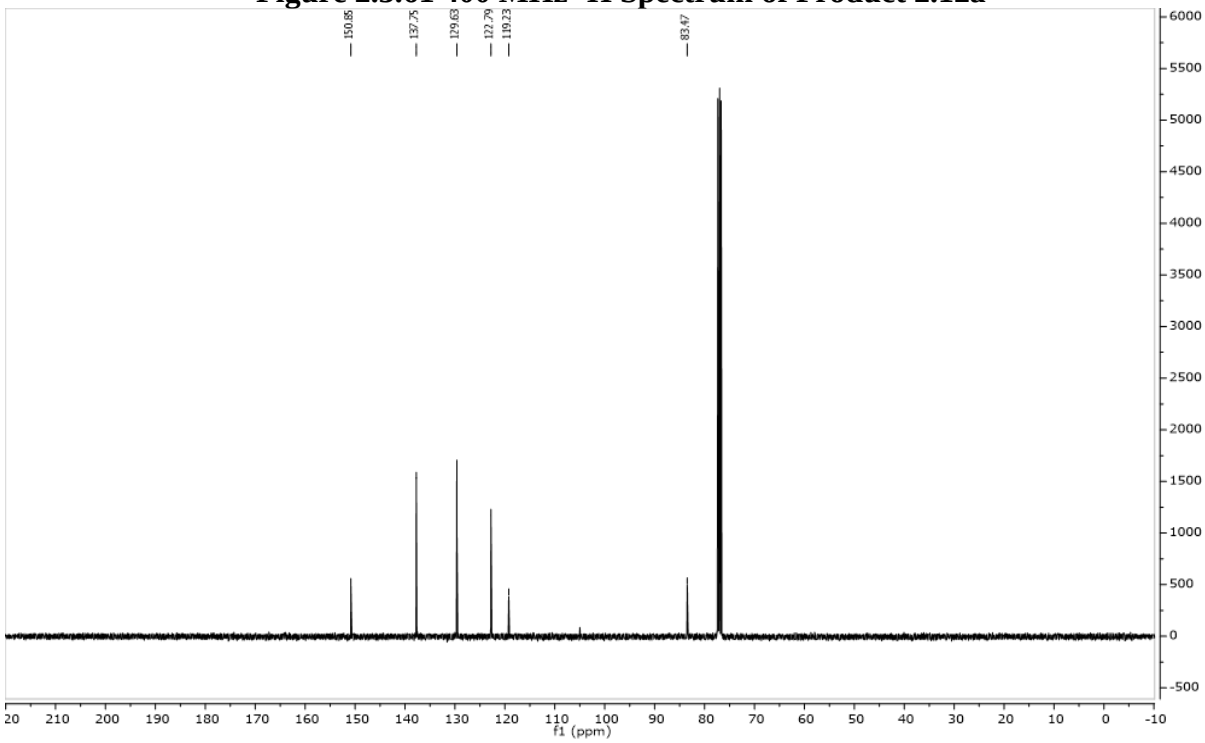

Figure 2.3.62 126 MHz ^{13}C Spectrum of Product 2.12a

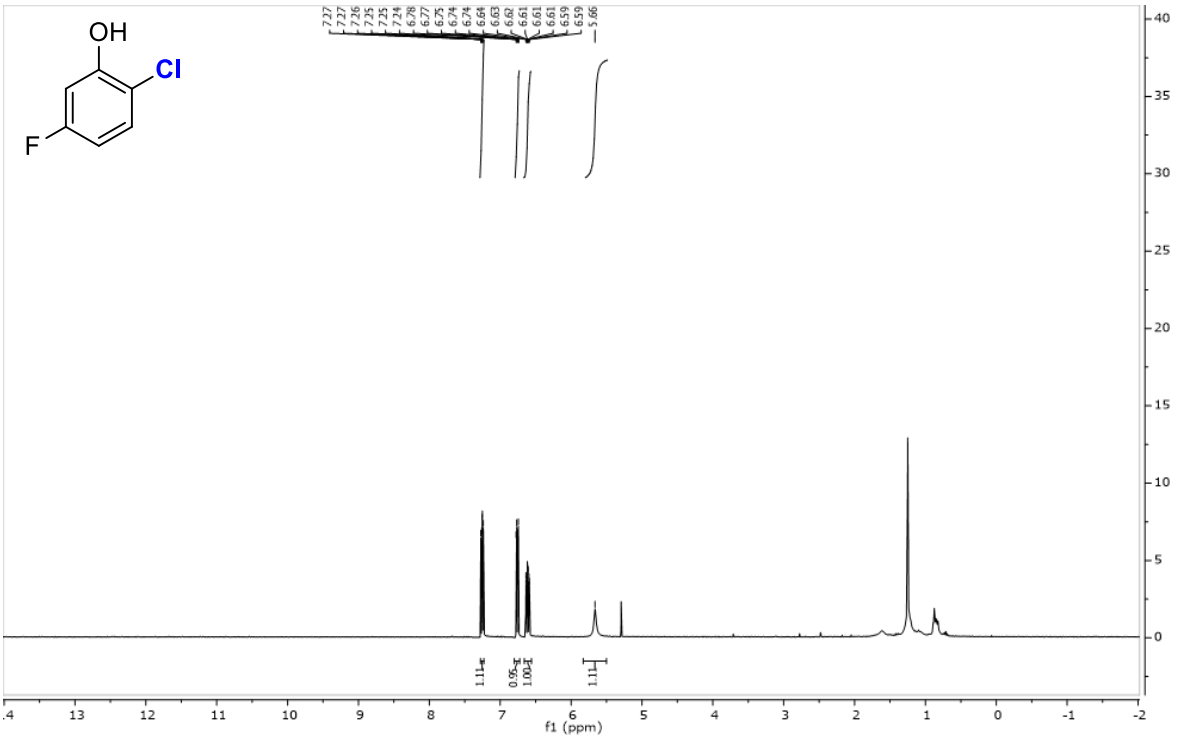

Figure 2.3.63 400 MHz ^{1}H Spectrum of Product 2.13a

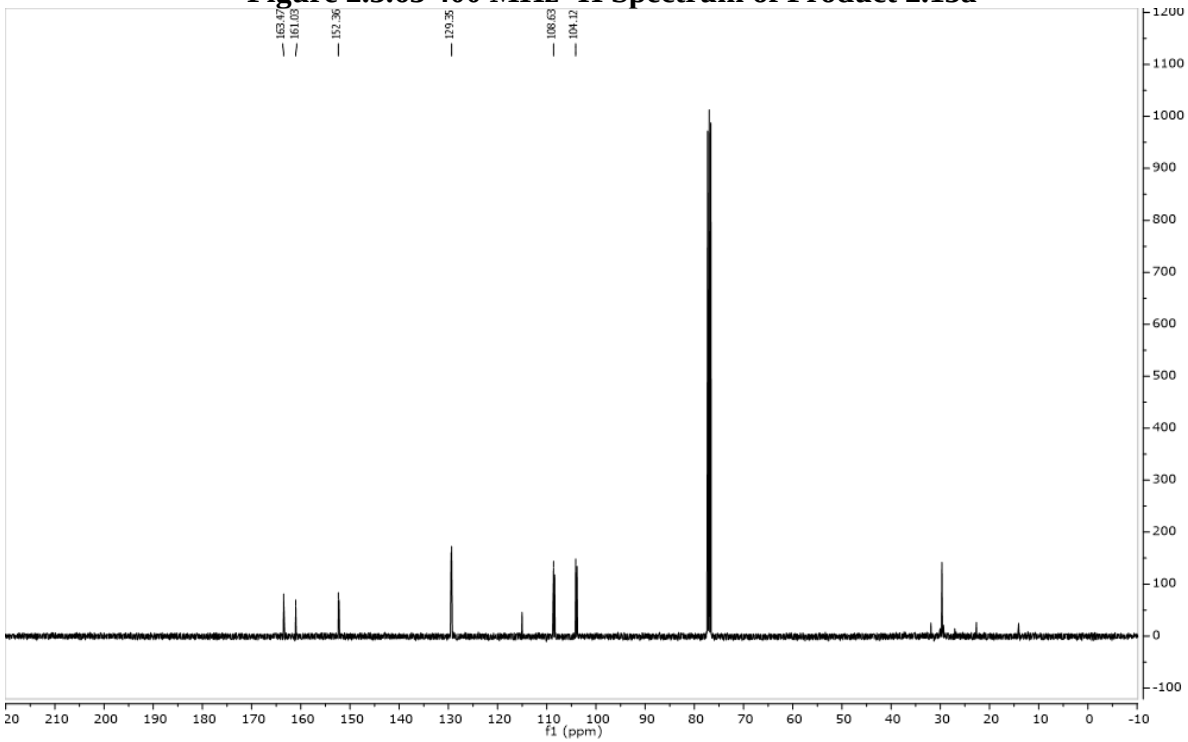

Figure 2.3.64 126 MHz ^{13}C Spectrum of Product 2.13a

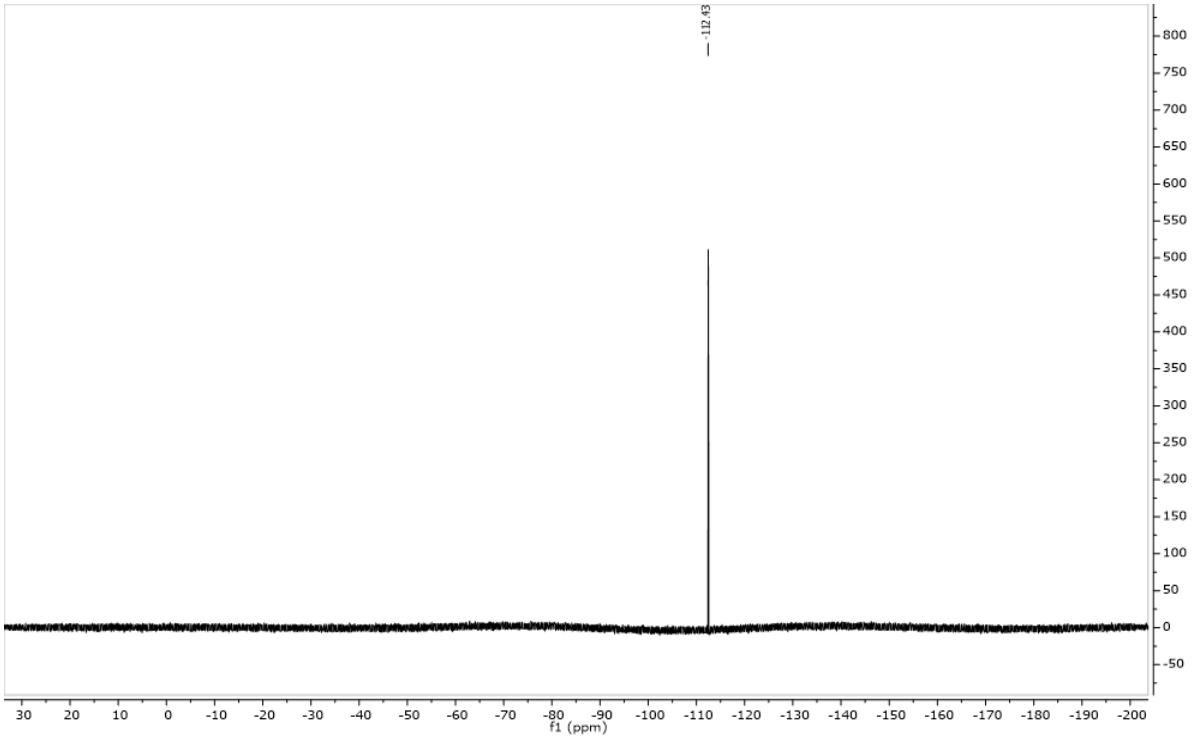

Figure 2.3.65 470 MHz ^{19}F Spectrum of Product 2.13a

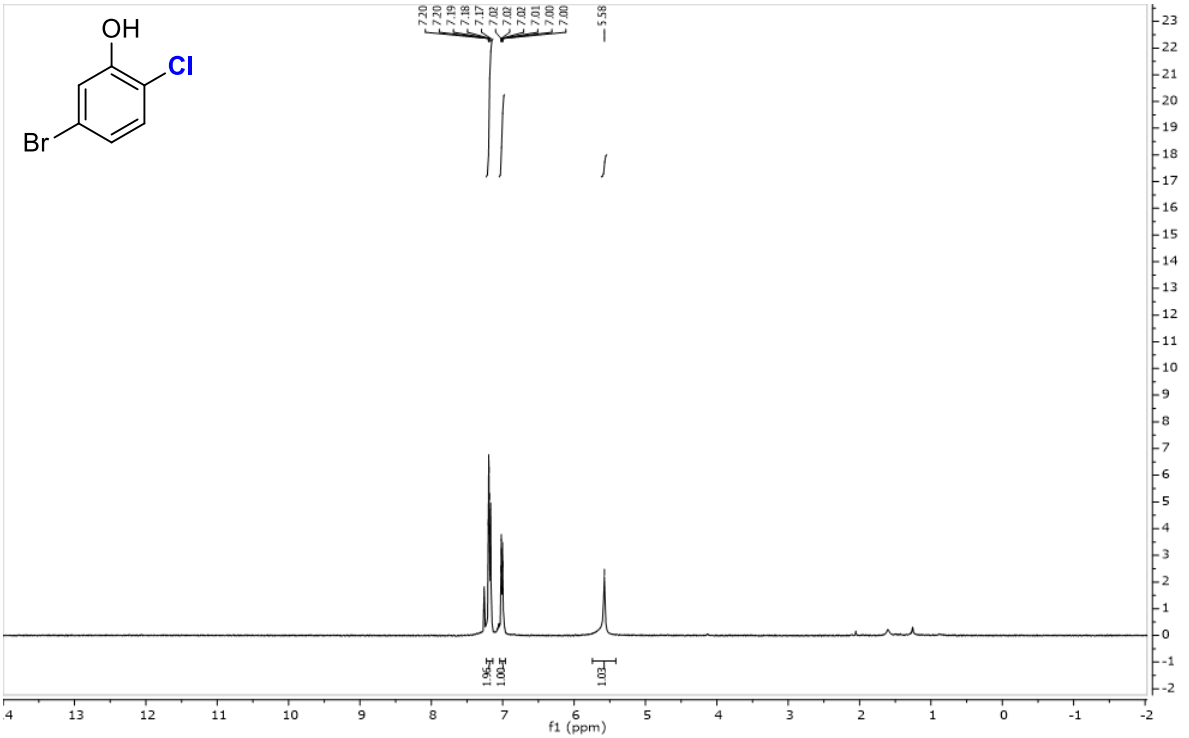

Figure 2.3.66 500 MHz ^{1}H Spectrum of Product 2.14a

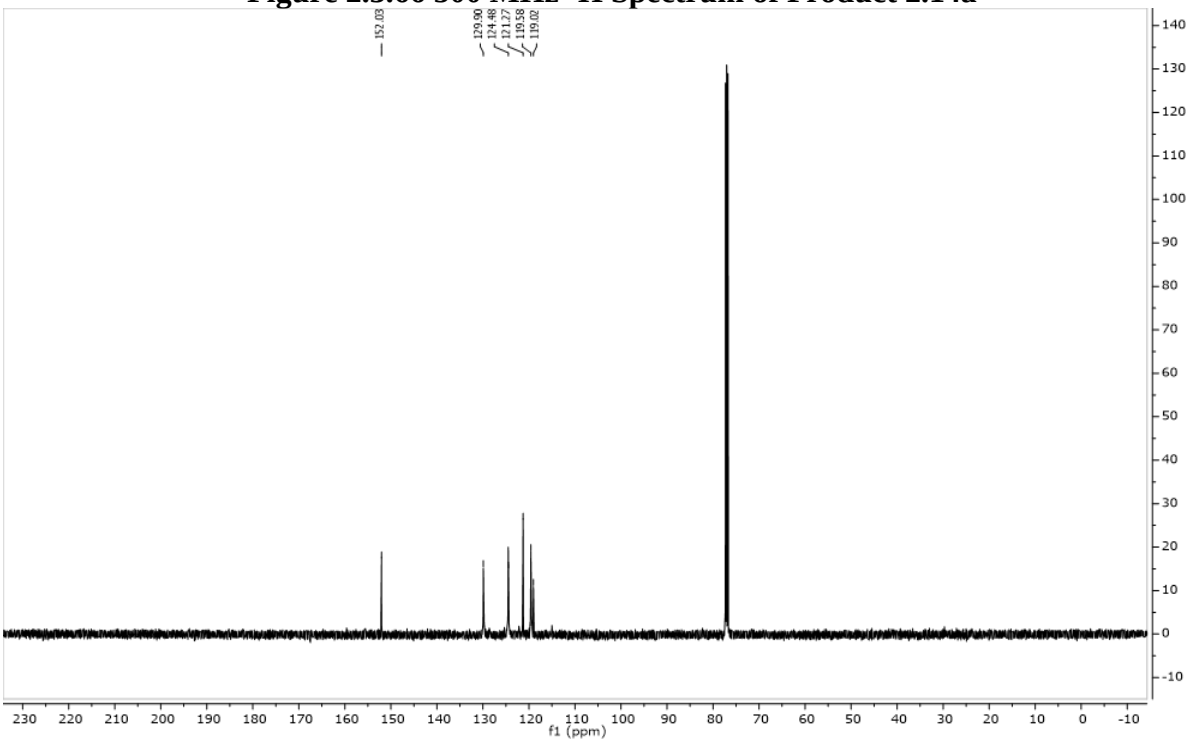

Figure 2.3.67 126 MHz ^{13}C Spectrum of Product 2.14a

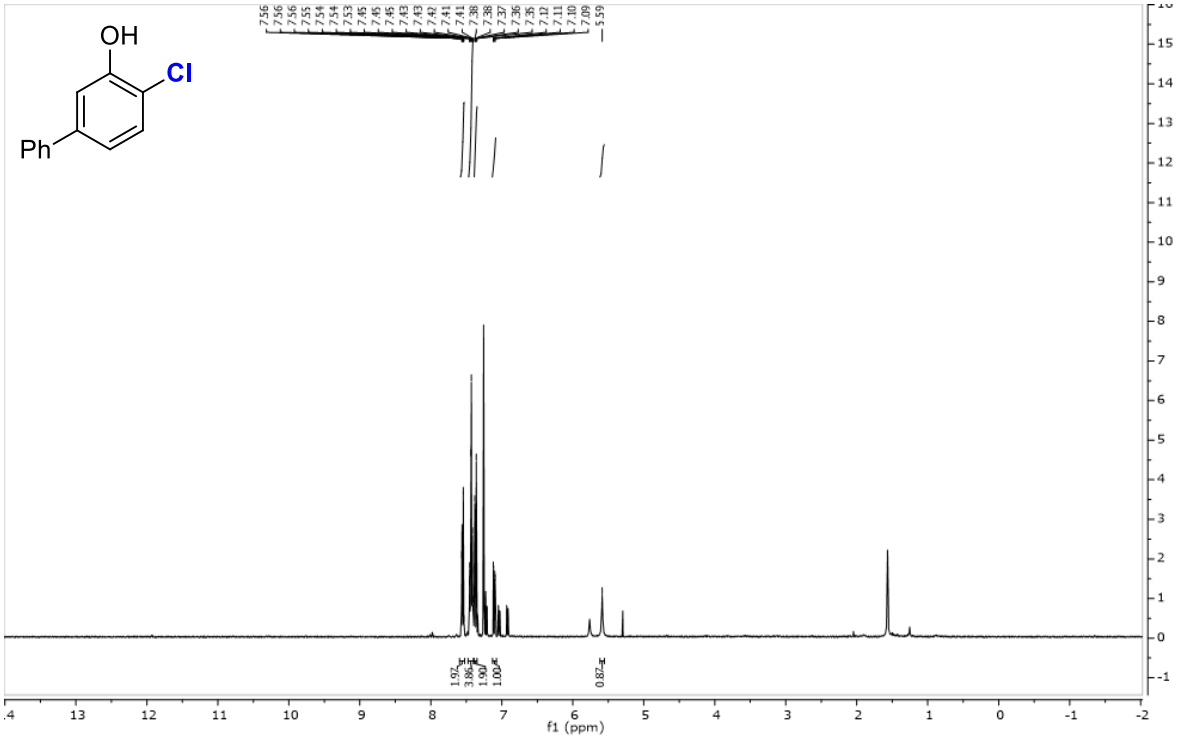

Figure 2.3.68 400 MHz ^{1}H Spectrum of Product 2.15a

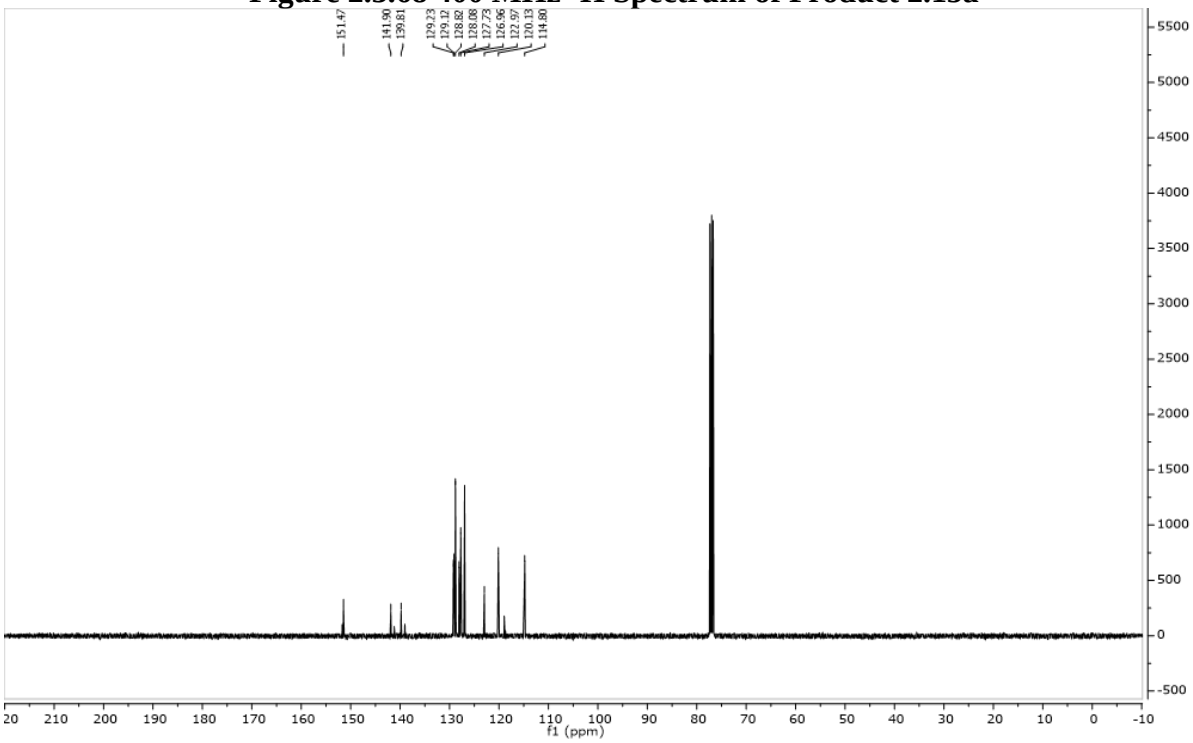

Figure 2.3.69 126 MHz ^{13}C Spectrum of Product 2.15a

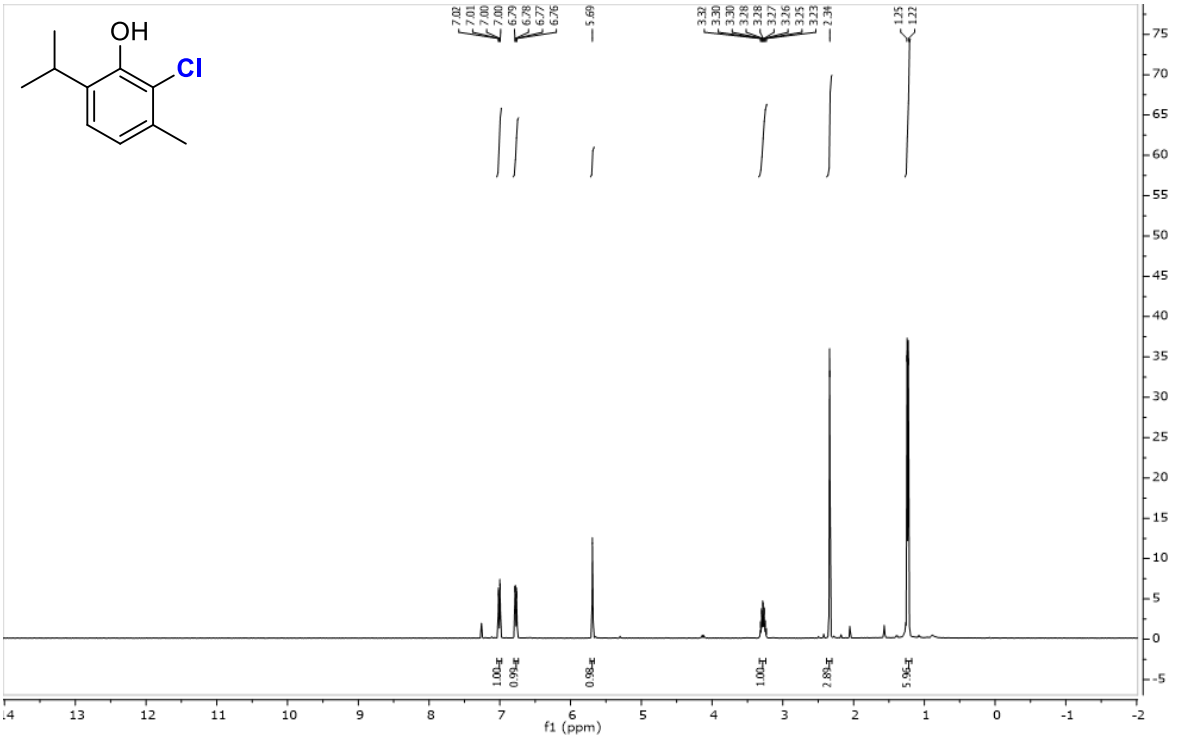

Figure 2.3.70 400 MHz ^{1}H Spectrum of Product 2.16a

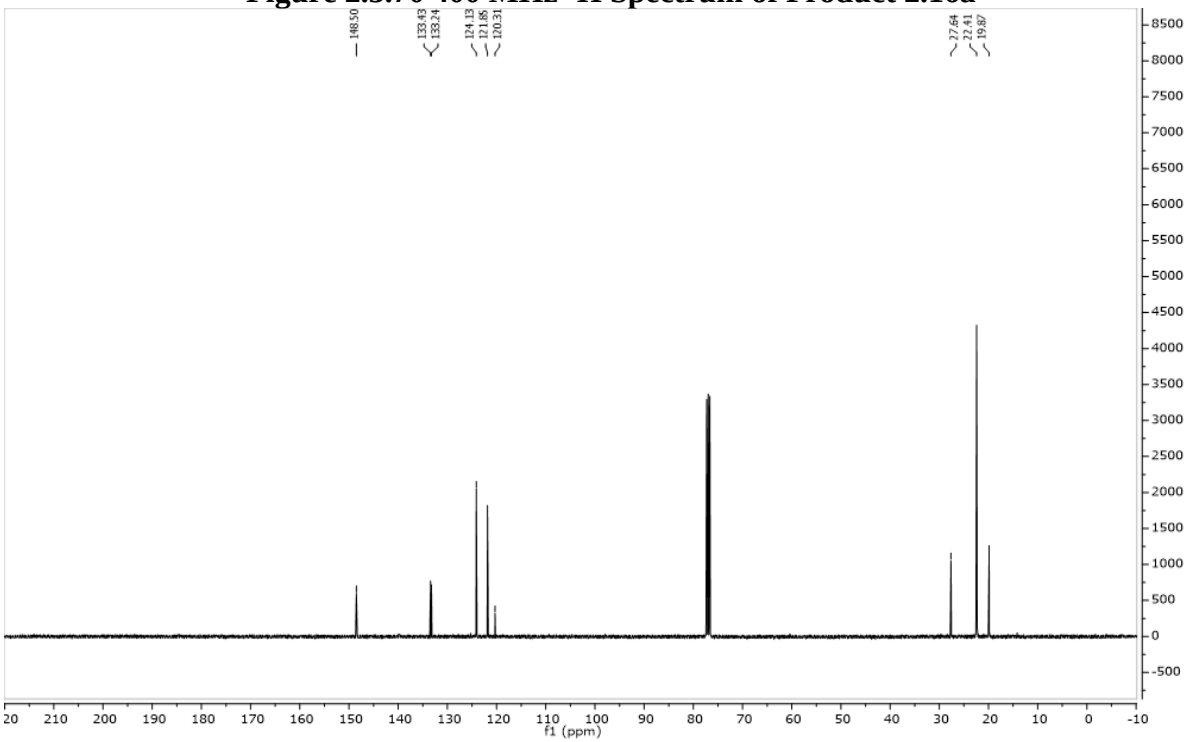

Figure 2.3.71 126 MHz ^{13}C Spectrum of Product 2.16a

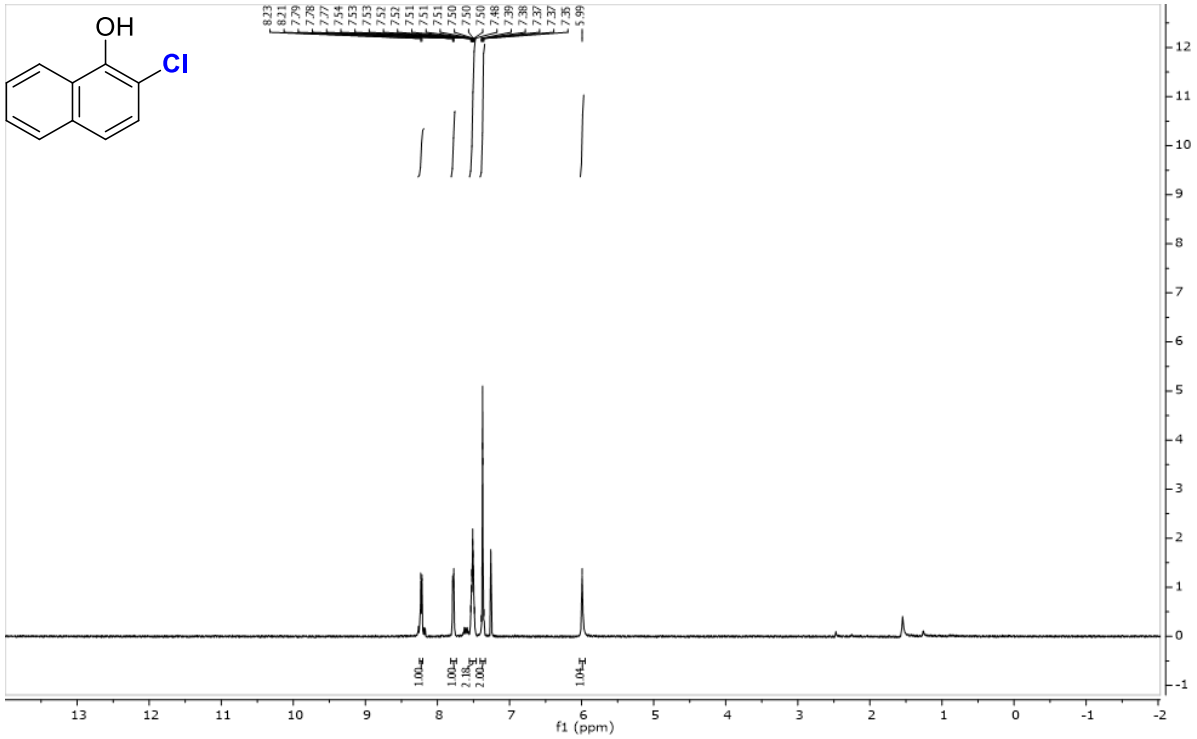

Figure 2.3.72 400 MHz ^{1}H Spectrum of Product 2.17a

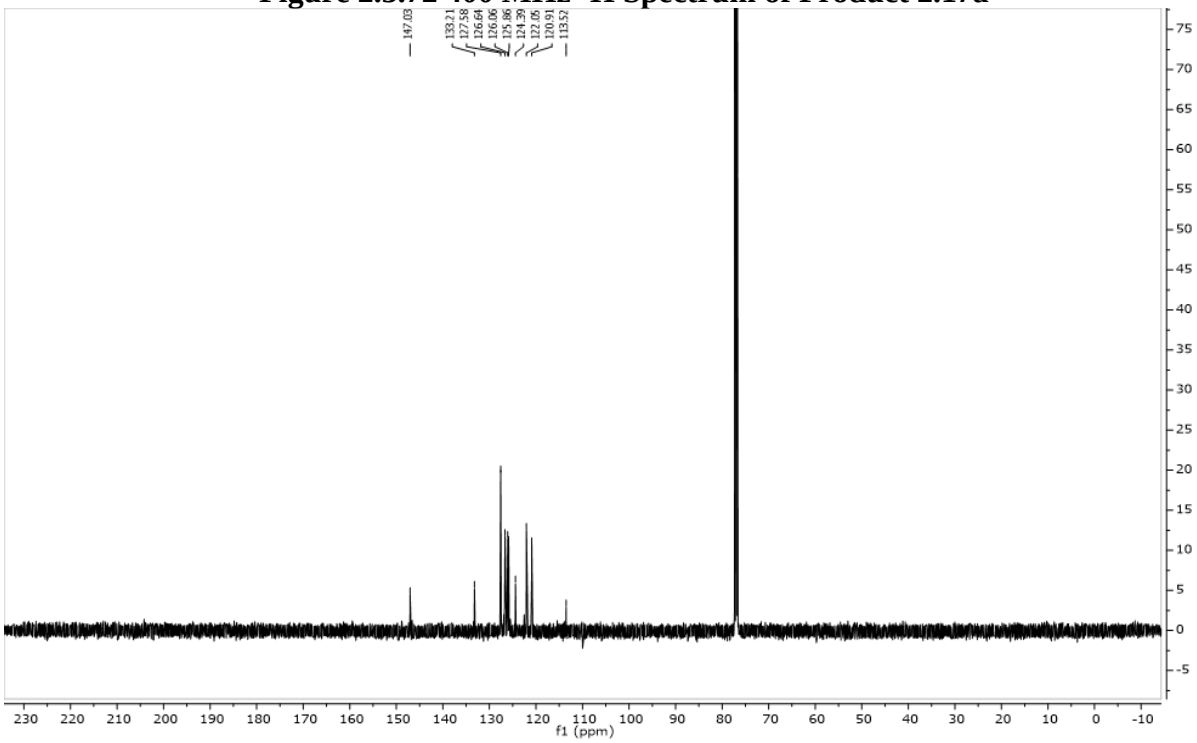

Figure 2.3.73 126 MHz ^{13}C Spectrum of Product 2.17a

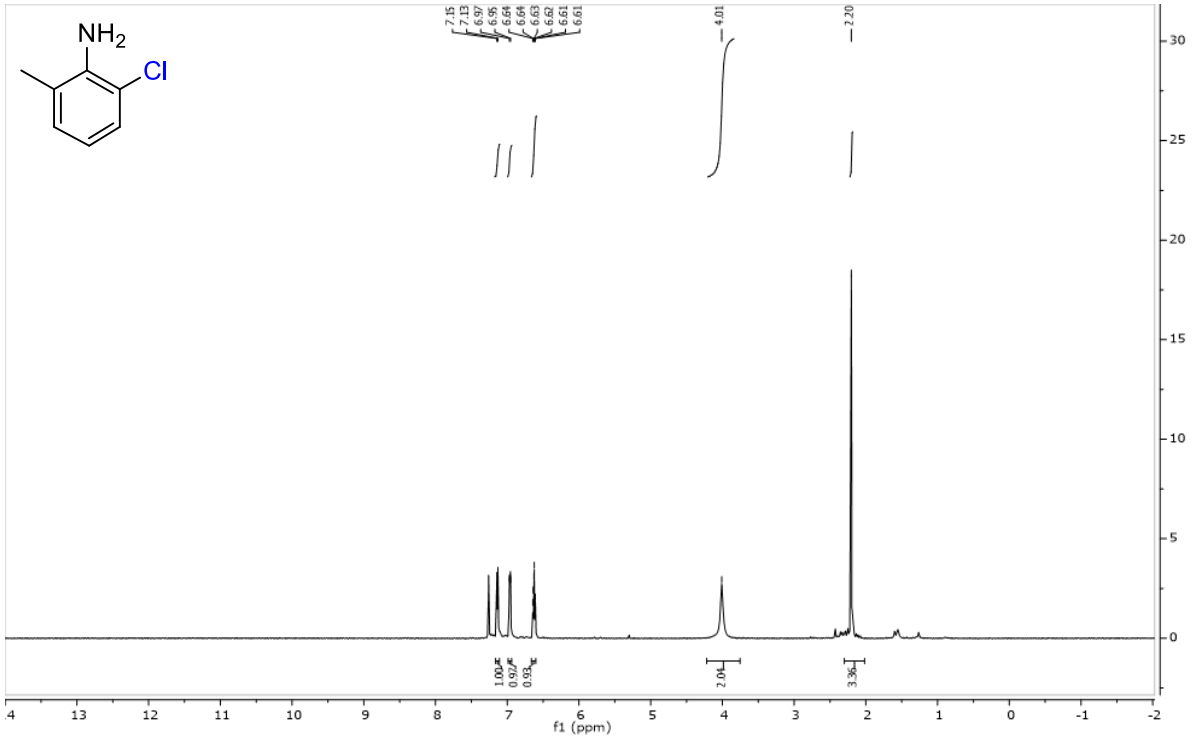

Figure 2.3.74 400 MHz ^{1}H Spectrum of Product 2.18a

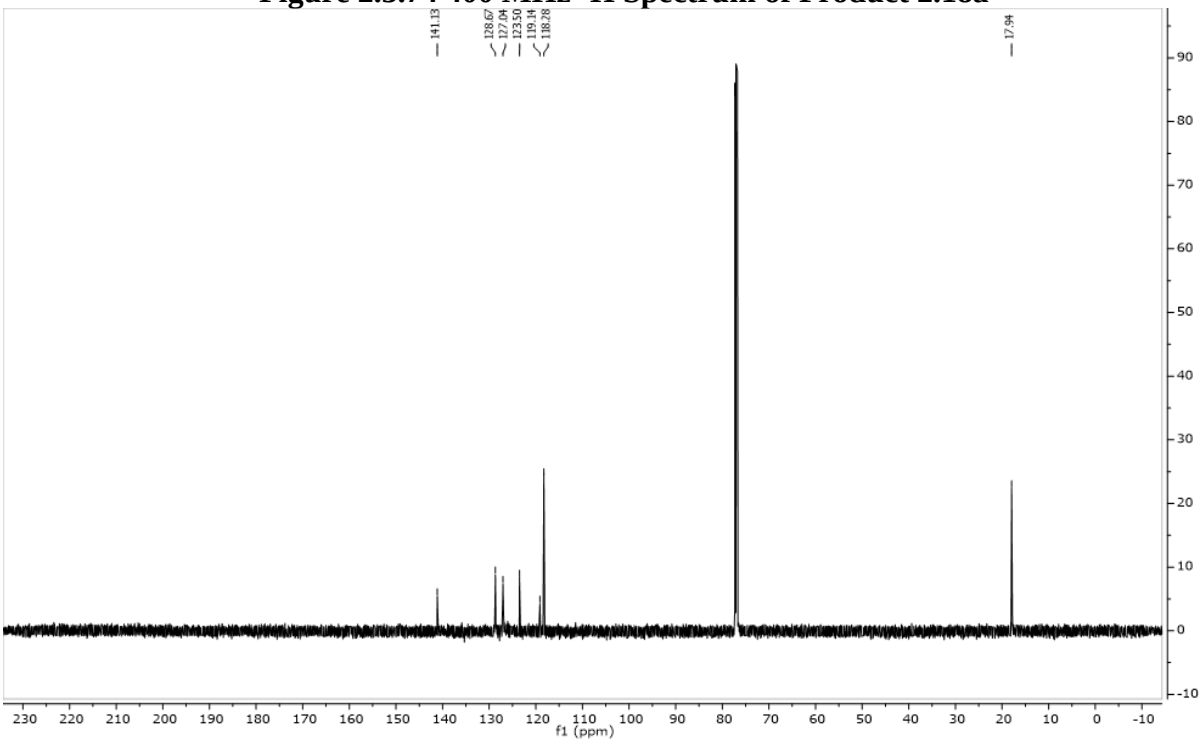

Figure 2.3.75 126 MHz ^{13}C Spectrum of Product 2.18a

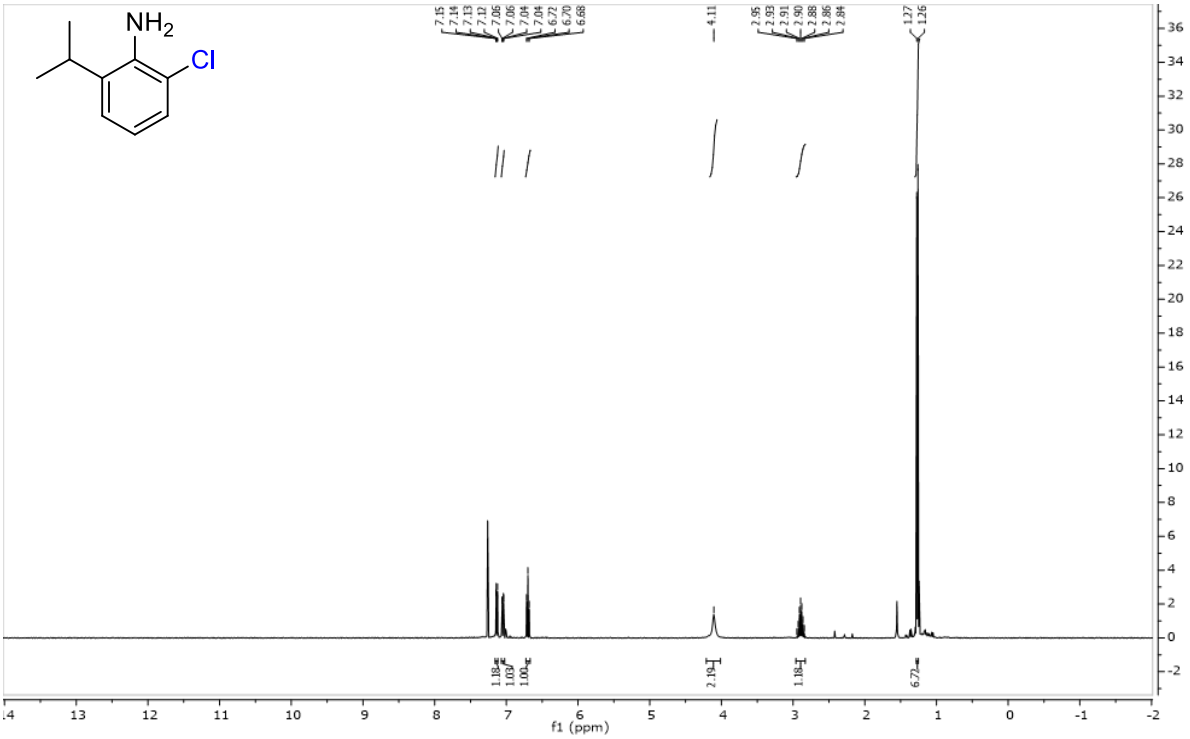

Figure 2.3.76 400 MHz ^{1}H Spectrum of Product 2.19a

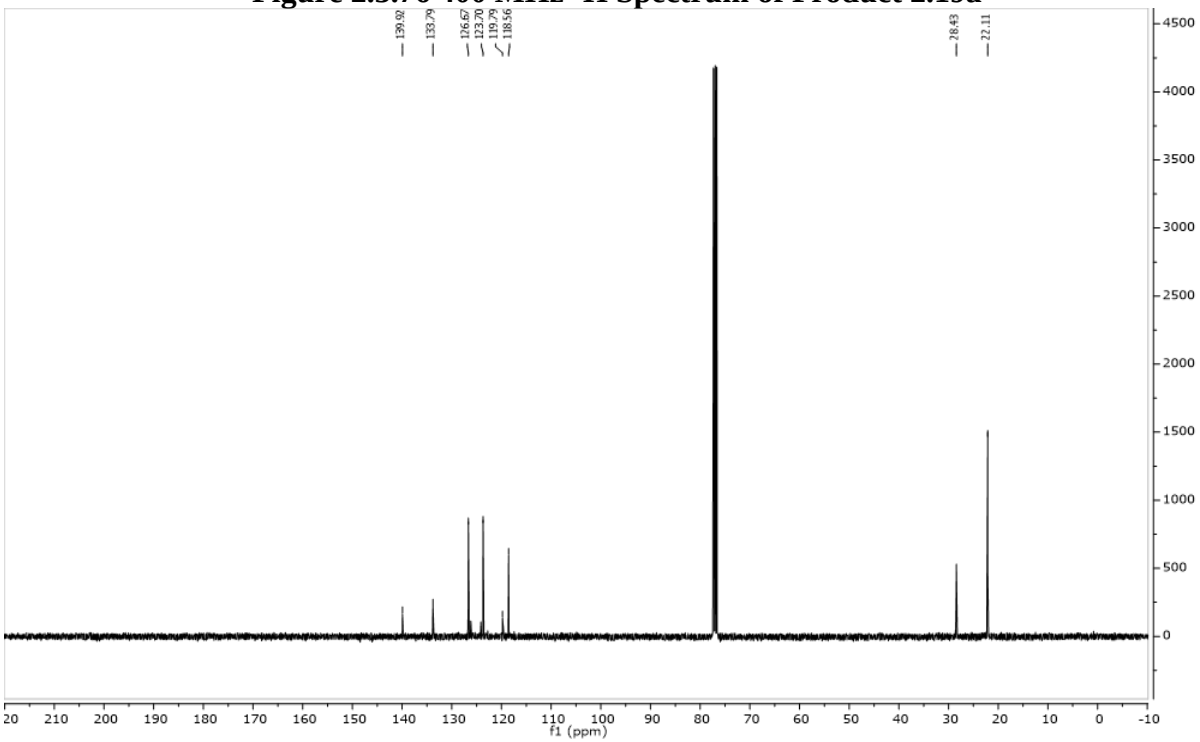

Figure 2.3.77 126 MHz ^{13}C Spectrum of Product 2.19a

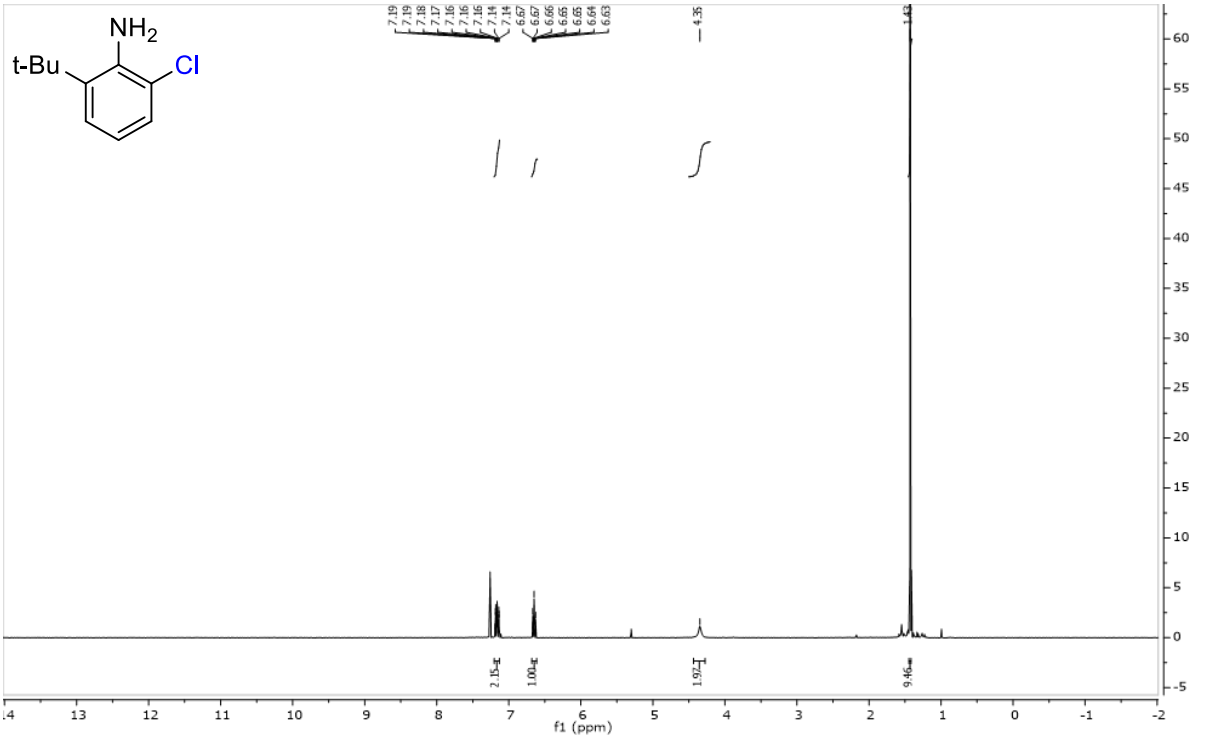

Figure 2.3.78 400 MHz ^{1}H Spectrum of Product 2.20a

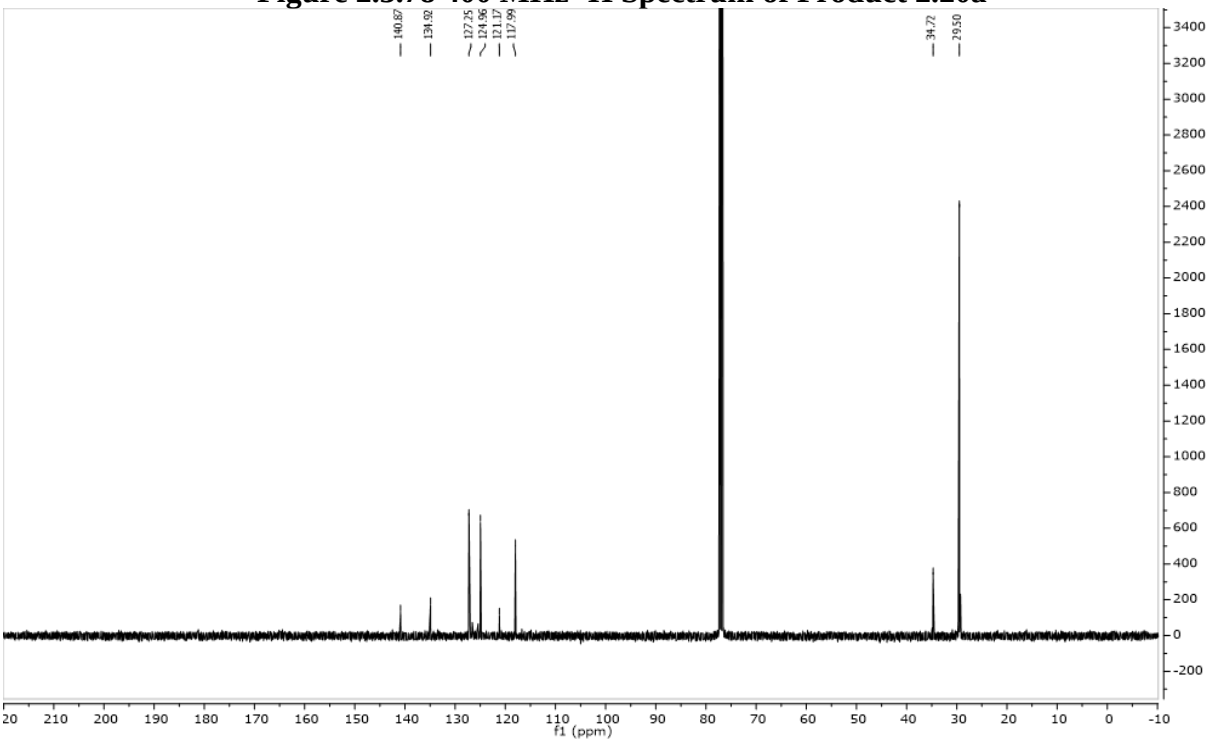

Figure 2.3.79 126 MHz ^{13}C Spectrum of Product 2.20a

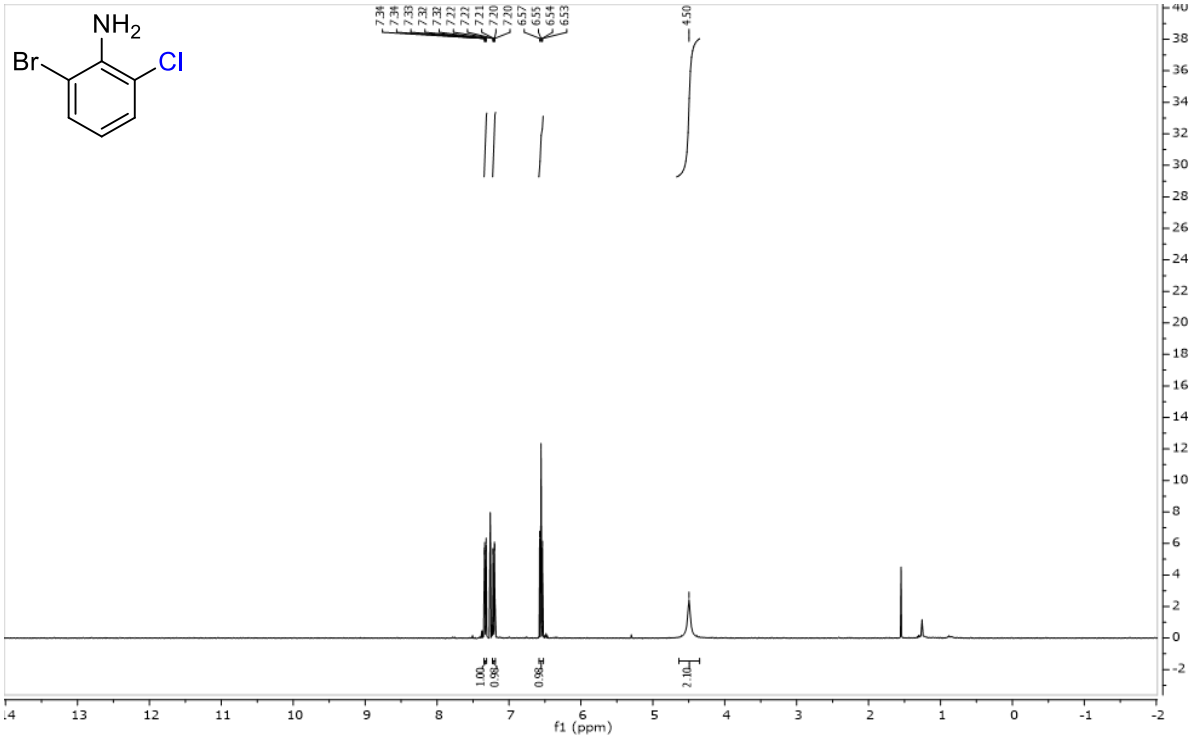

Figure 2.3.80 400 MHz ^{1}H Spectrum of Product 2.21a

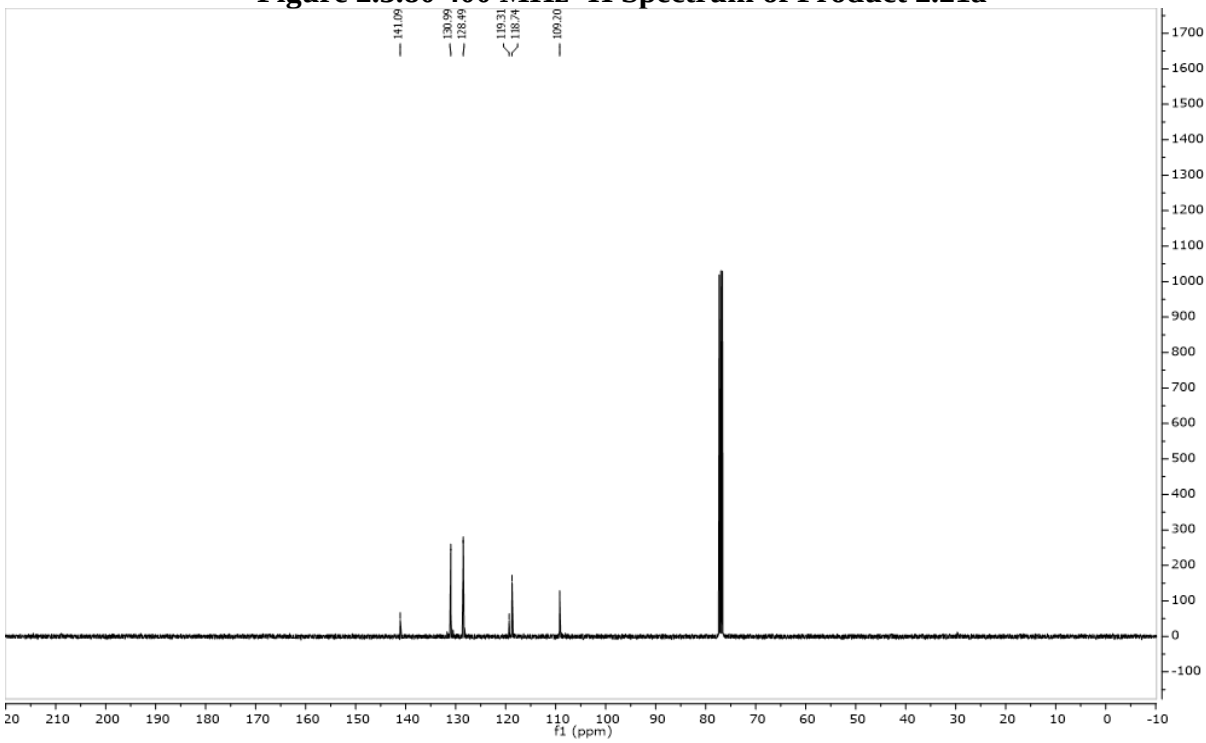

Figure 2.3.81 126 MHz ^{13}C Spectrum of Product 2.21a

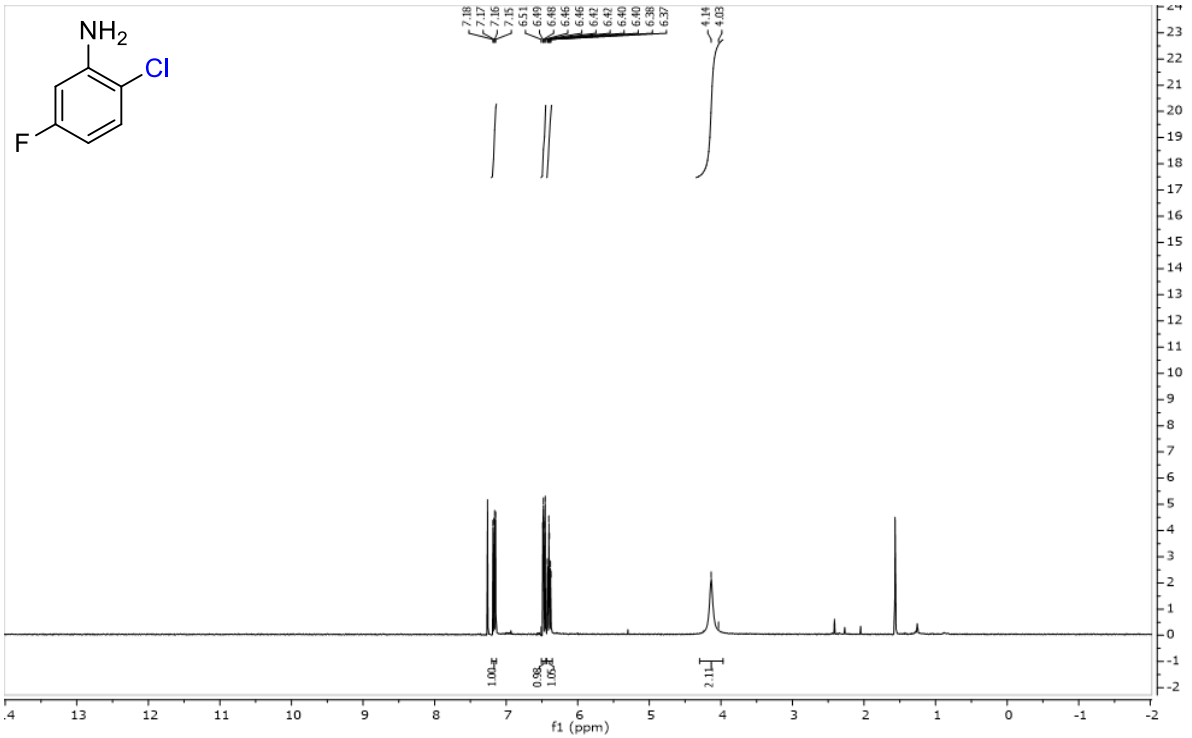

Figure 2.3.82 400 MHz ^{1}H Spectrum of Product 2.22a

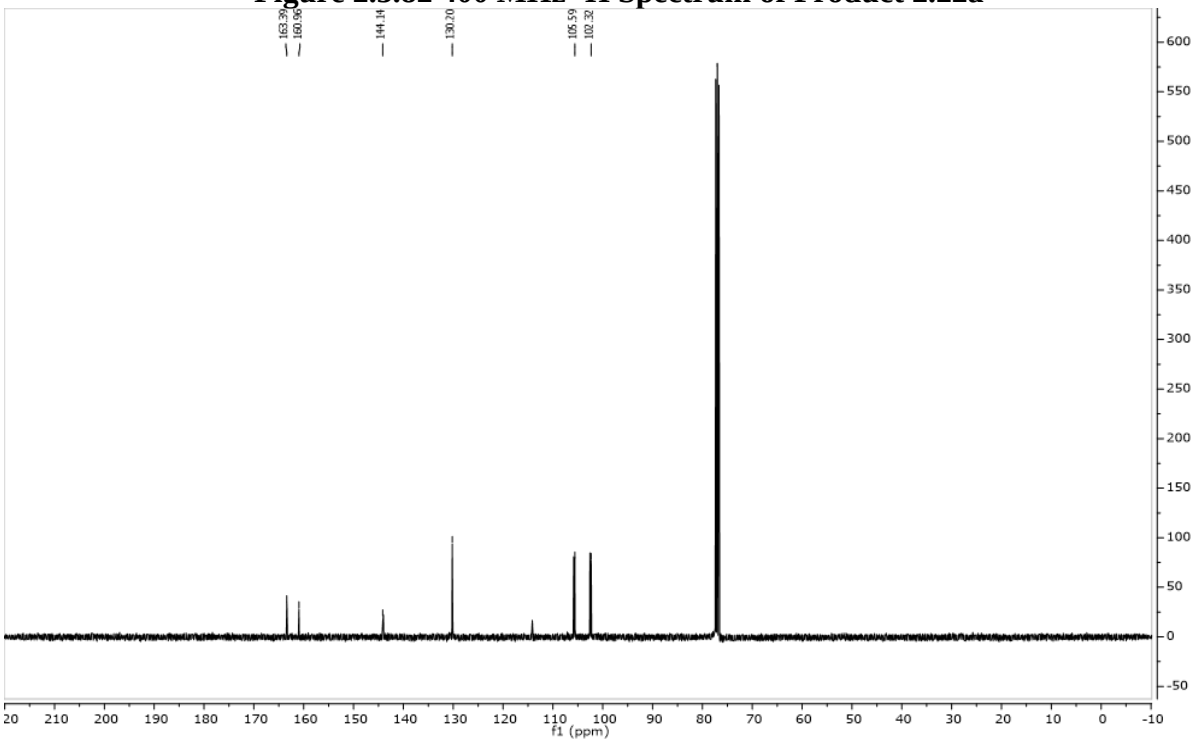

Figure 2.3.83 126 MHz ^{13}C Spectrum of Product 2.22a

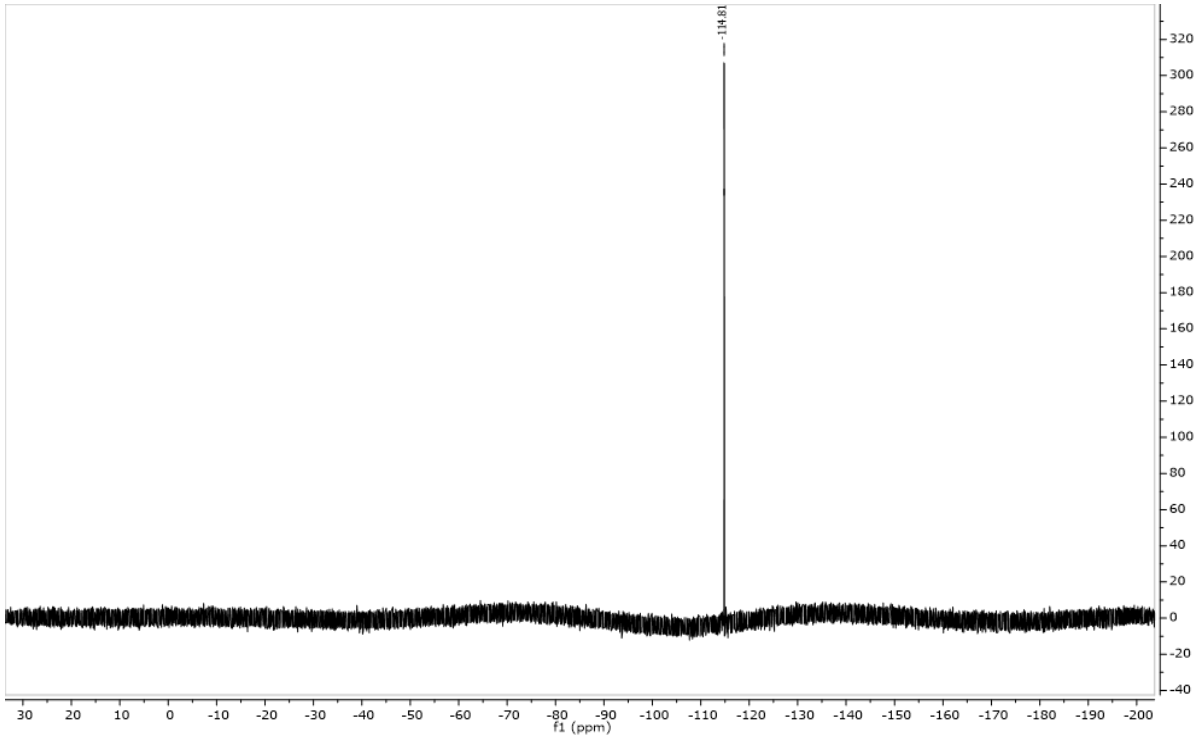

Figure 2.3.84 470 MHz ^{19}F Spectrum of Product 2.22a

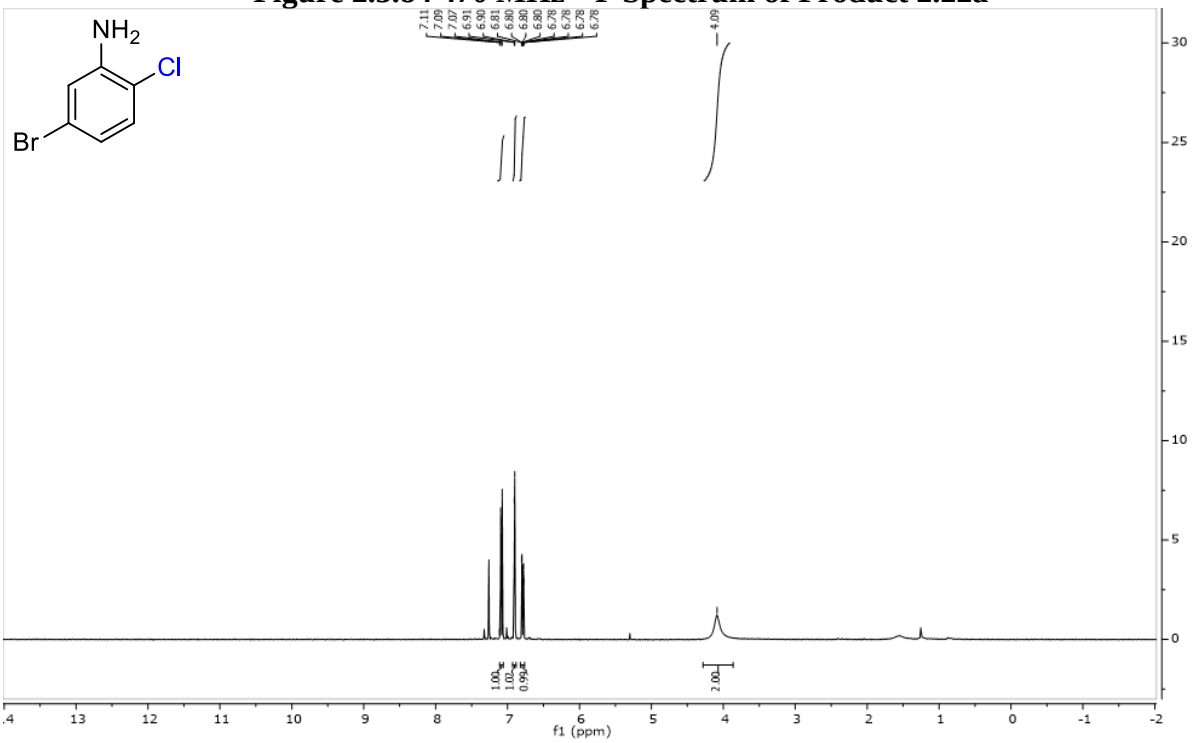

Figure 2.3.85 400 MHz ^{1}H Spectrum of Product 2.23a

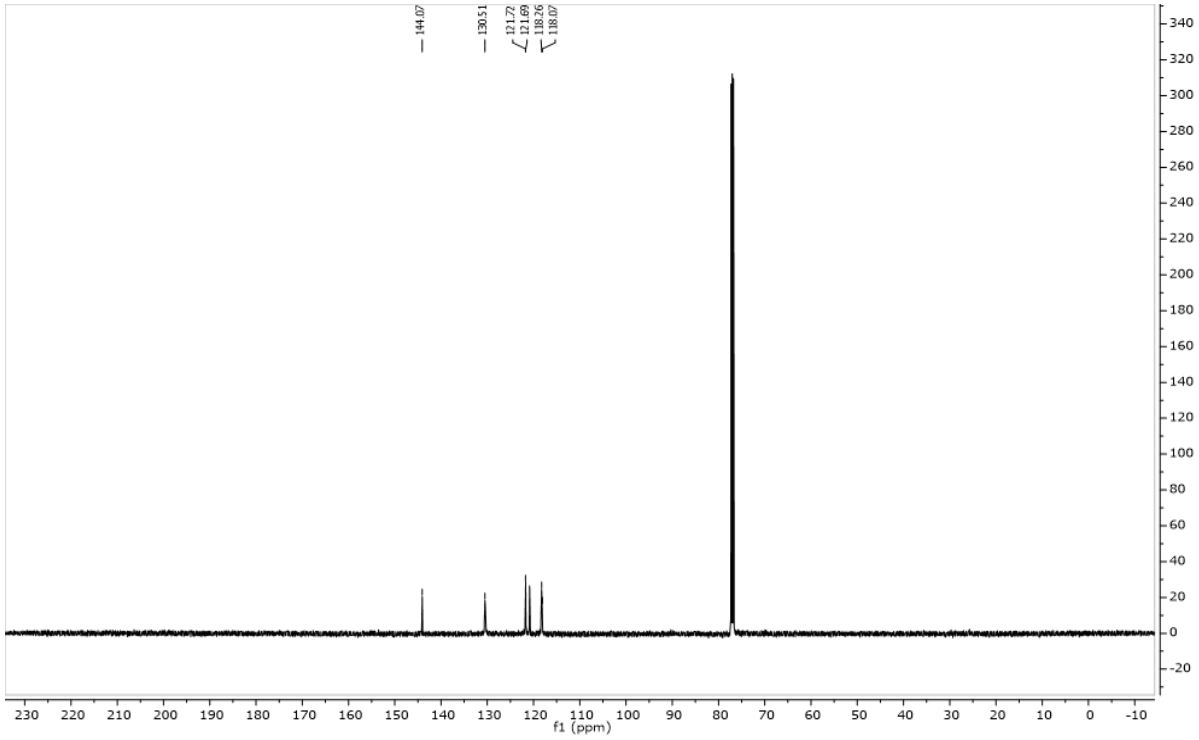

Figure 2.3.86 126 MHz ^{13}C Spectrum of Product 2.23a

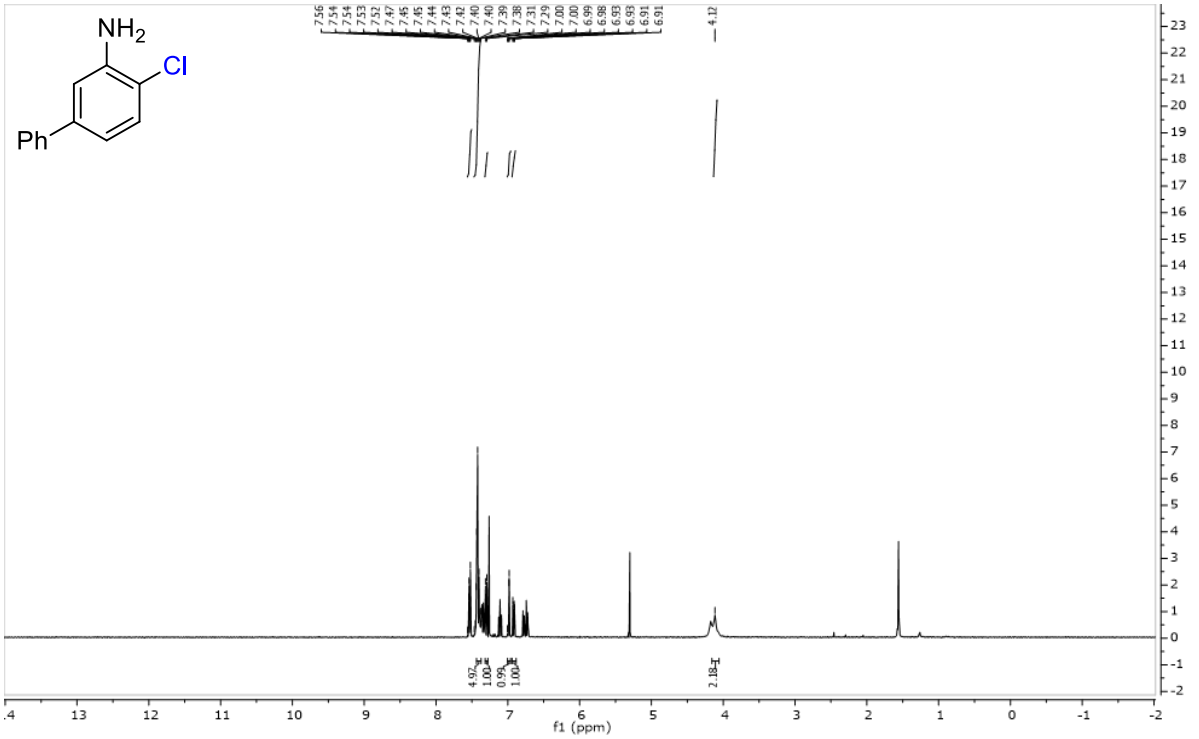

Figure 2.3.87 400 MHz ^{1}H Spectrum of Product 2.24a

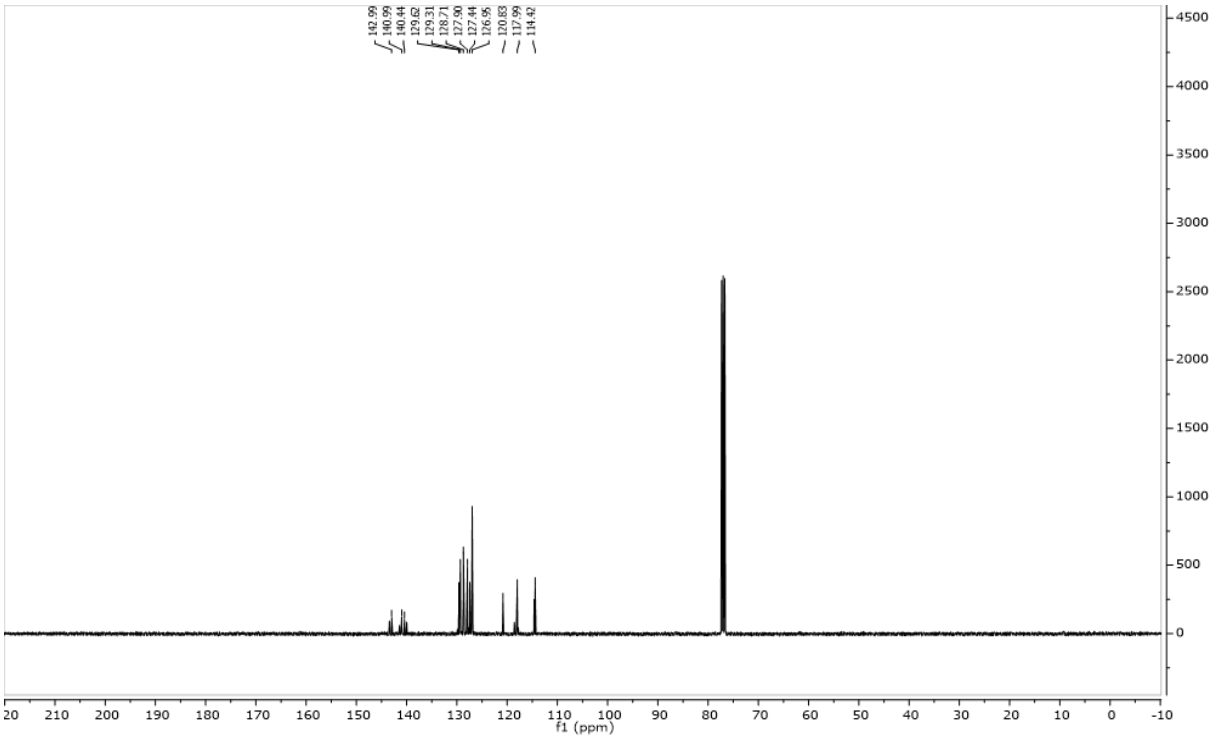

Figure 2.3.88 126 MHz ^{13}C Spectrum of Product 2.24a

2.3.5: Degradation of Nagasawa's Catalyst

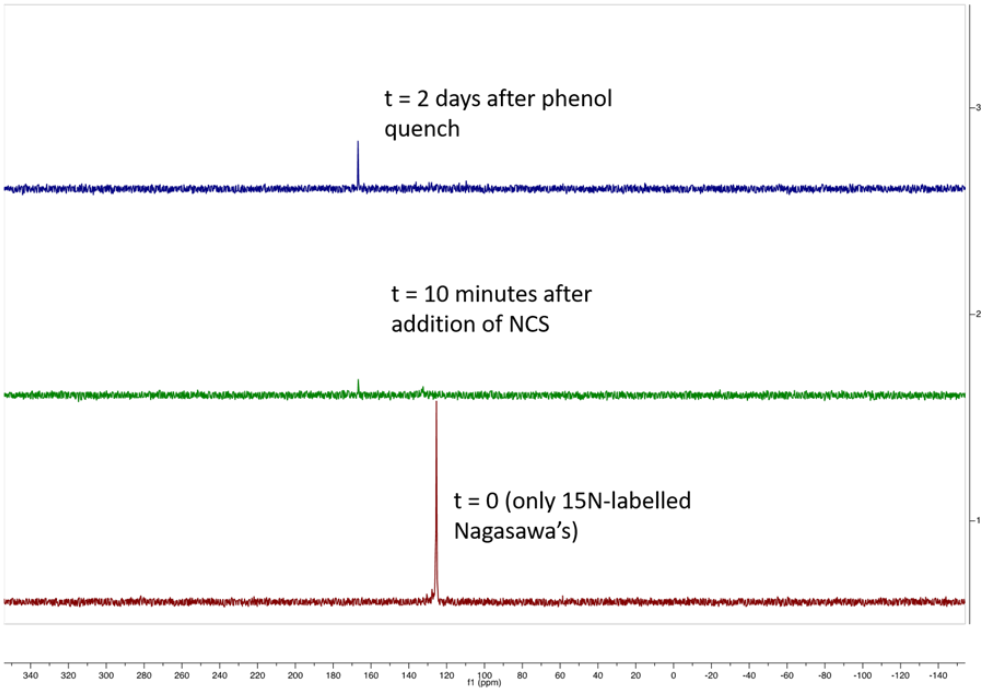

Figure 2.3.89 ^{15}N-labeled Experiments with Nagasawa's Bis-Thiourea Catalyst

2.4 Acknowledgements

The contents in Chapter 2 are in part a reformatted reprint of a future manuscript Dinh A.; Maddox, S.; Vaidya, S.; Saputra, M.; Nalbandian, C; Gustafson, J. “Catalyst-controlled Regioselective Chlorination of Phenols and Anilines through a Lewis basic Selenoether Catalyst”. I provided a majority of the optimization and substrate scope data, and all of the preliminary mechanistic data. While Sean Maddox is no longer in the department, his previous contributions to science have led to the presented data and therefore deserves co-authorship. Sagar Vaidya and Mirza Saputra have contributed equally in obtaining substrate scope data. Chris Nalbandian participated in discussions which inspired the development of the selenoether Lewis base catalyst utilized in the manuscript. The dissertation author was the primary researcher for the data presented. Support of this work by the National Science Foundation is acknowledged (CHE-1664565).

CHAPTER 3: Photocatalytic Oxidative C-H Thiolation: Synthesis of Benzothiazoles and Sulfenylated Indoles

3.0 Thieme Copyright

3.1 Carbon-Sulfur Bond Formation as a Useful Synthetic Transformation

The formation of carbon-sulfur bonds is an important reaction in synthetic chemistry, as this motif is found in numerous natural products, pharmaceuticals, polymers, and semiconductors.[90–97] The most common methods to achieve (C-S) bond formation have utilized transition-metal thiol cross-couplings[98–100]; however, these methods typically involve harsh reaction conditions, high temperatures and require pre-functionalization of the substrate. It would be more desirable to directly functionalize the C-H bond without any intermediate transformation. Direct C-H thiolation has been previously achieved through electrophilic aromatic substitution (S_EAr) utilizing activated sulfenyl sources such as sulfenyl halides or N-thiosuccinimides.[101–105] These reactions are limited primarily to electron rich aromatics and heterocycles such as substituted indoles. Other colleagues in my lab have recently reported methodologies that function via a Lewis base/Bronsted acid dual catalytic system that allow for the C-H sulfenylation of diverse arenes.[106,107] One drawback to this approach is that the formation of activated sulfenyl sources is often cumbersome and require extra synthetic steps to form the necessary reagents; thus, methods that could activate readily available thiols *in situ* would represent a welcome advancement.

3.2 Photocatalysis in Organic Chemistry

Over the past century, light-mediated catalysis has allowed development of a wide variety of bond formations in organic chemistry. In the field of photocatalysis, the photon energy from light can be captured by an absorbing source such as a photocatalyst, and upon excitation, is able to induce a chemical change towards another reagent or substrate, allowing for a plethora of chemical transformations.[108–110] While photoredox catalysis has been utilized in a number of different applications such as carbon dioxide reduction and solar cells materials, it has only recently been applied as a catalyst for organic synthesis in the past decade.[111] One of the biggest contributions to this rapid growth in synthetic methodologies is the number of readily available transition metal polypyridyl complexes and organic dyes that can act as a photocatalyst and facilitate the conversion of light energy into chemical energy.

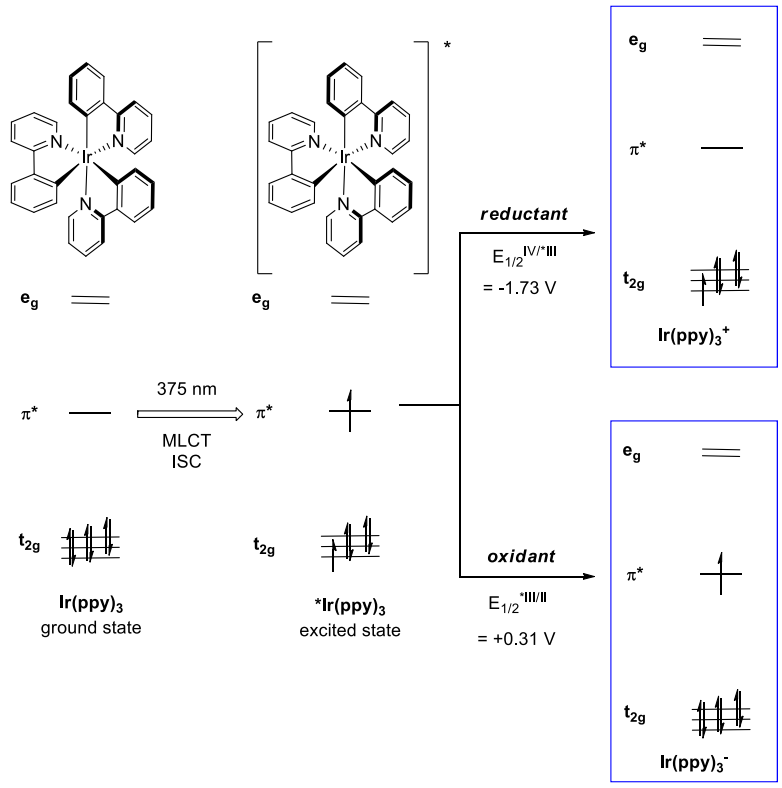

Figure 3.2.1 General Molecular Orbital depiction of $Ir(ppy)_3$ Photocatalyst

Upon excitation, the catalyst can convert this energy into various modes of interactions such as photo-induced electron transfer or single electron transfer (SET), energy transfer (ET) or atom transfer (i.e. hydrogen atom transfer or HAT).[112] For the purposes of this thesis and the following studies, I will be focusing primarily on SET chemical processes. As eloquently described in a review by Macmillan, irraditation with ultraviolet or visible light, at wavelengths where organic molecules usually do not absorb, will selectively activate the photoredox catalyst to its excited state via a metal ligand charge transfer (MLCT). After intersystem crossing (ISC), the resultant excited state is a longer-lived triplet state and now has dual functionality wherein it can act both as a strong oxidant and reductant, providing a unique radical chemical environment (Figure 3.2.1, adapted from review by Macmillan). Traditionally, radical chemistry is taught and introduced in sophomore organic chemistry in the context of chain mechanisms, which are difficult to control and provide limited scope. However, photocatalysis allows for selective C-H functionalization with high energy open-shell intermediates, providing access for making molecules selectivity that could not be achieved using traditional polar pathways.[113,114]

3.3 Previous strategies for C-S bond synthesis Utilizing Photocatalysis

In the past five years, there have been multiple accounts of C-H thiolation employing the use of photoredox catalysis (Scheme 3.3.1). In 2015, Lei showed that benzothiazoles can be synthesized using a $Ru(bpy)_3(PF_6)_2$/Co dual catalytic system.[115] Similarly, Xu reported a similar benzothiazole transformation from thioamides using a TEMPO-catalyzed electrochemical C-H thiolation.[116] Alternatively, Barman and Fan both independently reported the use of Rose Bengal and thiophenol for the sulfenylation of 3-substituted indoles and imidazopyridines, respectively.[117,118] Recently, König and Rehbein showed that electron-rich arenes (such as trimethoxybenzenes) could react with diaryl and dialkyl sulfides with an iridium photocatalyst and

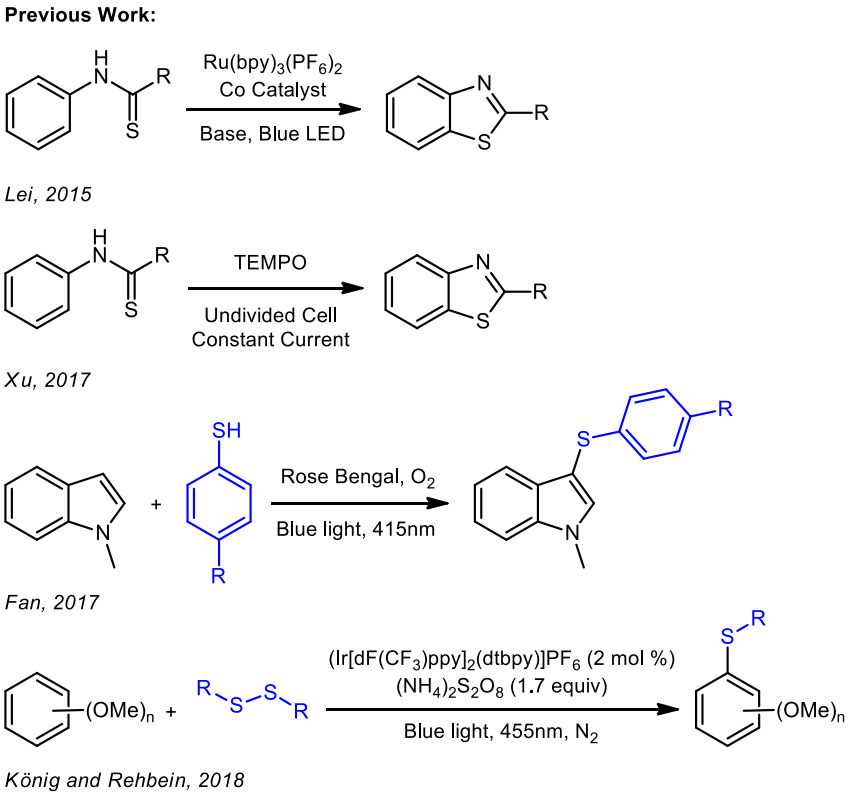

Scheme 3.3.1 Previous Photocatalytic and Electrochemical Methodologies for C-H Thiolation

a persulfate salt to provide arylthiols.[119] Herein, I report an oxidative photocatalytic thiolation to synthesize benzothiazoles through an intramolecular synthesis from thioamides, as well as the intermolecular sulfenylation of substituted indoles (Scheme 3.3.2). Notably, our mechanistic studies via cyclic voltammetry and density functional theory calculations suggest that even though both reactions use similar conditions, they proceed with markedly different roles for the sulfur, with an electrophilic sulfur radical in the benzothiazole formation, and a nucleophilic sulfur radical in the indole sulfenylation.

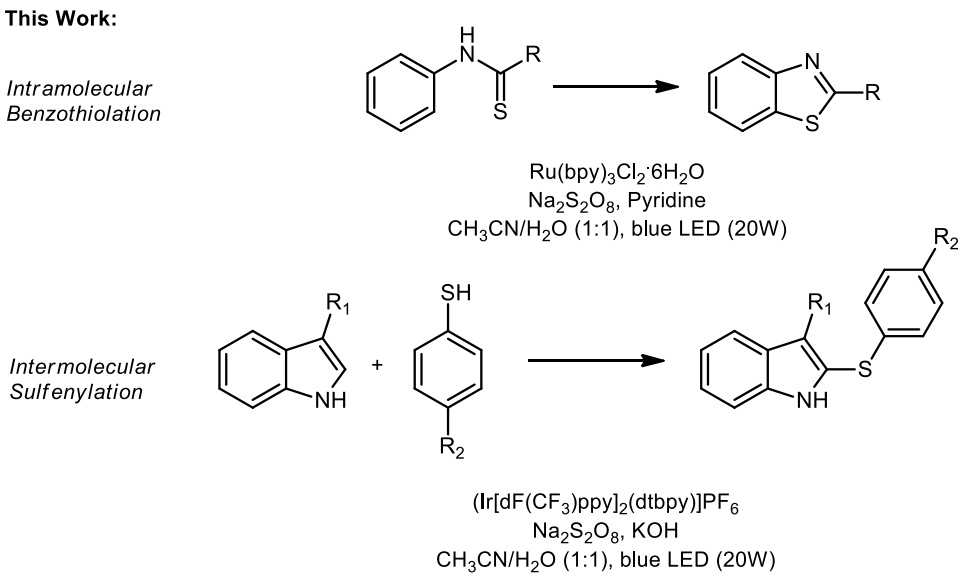

Scheme 3.3.2 Synthesis of Benzothiazoles and Sulfenylated Indoles from Oxidative Conditions

3.4 Discussion

I first discovered the synthesis of benzothiazoles serendipitously. Our lab initially hypothesized that anilines could be selectively functionalized via a Lewis base directing group based on previous work on radical intermediate control[120]; hence I synthesized molecules such as thioamide **3.1** and observed whether *ortho*-chlorination via S_EAr could be observed. When I used Hu's photocatalytic chlorination conditions (see Table 3.4.1), I instead observed a significant amount of benzothiazole **3.1a** (Table 3.4.1, entry 1). Interestingly, removal of the sodium chloride still provided a small increase in conversion of **3.1** to **3.1a**, suggesting this chemistry occurred via a substrate oxidative mechanism rather than sulfur activation through the halogen source (Table 3.4,1, entry 2). Removal of both the $Ru(bpy)_3Cl_2$ (Table 3.4.1, entry 3) and sodium persulfate (Table 3.4.1, entry 4) resulted in a significant decrease in conversion; however, there is a still a small benzothiazole background reaction in the presence of persulfate. I then continued our optimization with an evaluation of other common photocatalysts. Because I utilized a 390nm LED

Table 3.4.1 Optimization of Intramolecular Benzothiazole Synthesis

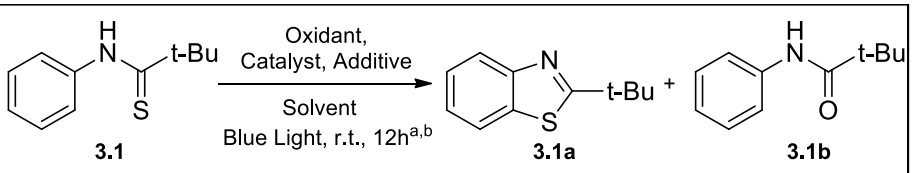

3.1 3.1a 3.1b

Entry	Catalyst	Oxidant (Equiv)	Additive (Equiv)	Solvent	Conversion (%)
1	$Ru(bpy)_3Cl_2$	$Na_2S_2O_8$ (2)	NaCl (3)	CH_3CN/H_2O (1:1)	52%
2	$Ru(bpy)_3Cl_2$	$Na_2S_2O_8$ (2)	None	CH_3CN/H_2O (1:1)	57%
3	$Ru(bpy)_3Cl_2$	None	None	CH_3CN/H_2O (1:1)	0%
4	None	$Na_2S_2O_8$ (2)	None	CH_3CN/H_2O (1:1)	5%
5	$Ru(phen)_3Cl_2$	$Na_2S_2O_8$ (2)	None	CH_3CN/H_2O (1:1)	15%
6	4CzIPN	$Na_2S_2O_8$ (2)	None	CH_3CN/H_2O (1:1)	30%
7	$Ir[dF(CF_3)ppy]_2(dtbpy)]PF_6$	$Na_2S_2O_8$ (2)	None	CH_3CN/H_2O (1:1)	20%
8	$Ru(bpy)_3Cl_2$	$Na_2S_2O_8$ (2)	None	CH_3CN/H_2O (9:1)	34%
9	$Ru(bpy)_3Cl_2$	$Na_2S_2O_8$ (5)	None	CH_3CN/H_2O (1:1)	0% (**1b** obtained)
10	$Ru(bpy)_3Cl_2$	$Na_2S_2O_8$ (10)	None	CH_3CN/H_2O (1:1)	0% (**1b** obtained)
11	$Ru(bpy)_3Cl_2$	$Na_2S_2O_8$ (2)	Pyridine (2)	CH_3CN/H_2O (1:1)	79%

blue light source, I hypothesized that $Ru(phen)_3Cl_2$ (I_{max} = 422nm) would be in a higher absorbance range relative to $Ru(bpy)_3Cl_2$ (I_{max} = 452nm). However, conversion of the benzothiazole was low at only 15% (Table 3.4.1, entry 5). Switching from a transition metal to an organic photocatalyst 4CzIPN also provided no improvement in conversion (Table 3.4.1, entry 6), possibly due to the reaction being performed in a biphasic solvent system. Surprisingly, $(Ir[dF(CF_3)ppy]_2(dtbpy)]PF_6$, which has a higher oxidizing potential in its excited state [(Ir(III)*/Ir(II) = 1.21V versus SCE] relative to $Ru(bpy)_3Cl_2$ [Ru(II)*/Ru(I) =.77V versus SCE] and would be expected to oxidize **3.1** more effectively, proved markedly worse than the ruthenium catalyst (Table 3.4.1, entry 7). Mechanistically, this implies that while the photocatalyst has a significant effect on the overall conversion of the reaction, its excited state does not directly oxidize the thioamide but rather likely activates the persulfate as a better oxidizing agent (see proposed mechanism). Testing solvent conditions, I observed a decrease in conversion when switching to a more organic composition of

9:1 MeCN/H_2O, suggesting aqueous media is necessary to help solubilize the persulfate salt (Table 3.4.1, entry 8). To see if circumventing persulfate activation was a possibility, I added excess amount of sodium persulfate (Table 3.4.1, entry 9 & 10); however, I only obtained the acetanilide side product **3.1b**, which is a common degradation product for thioamides under oxidative conditions. Finally, I observed that benzothiazole conversion could be improved markedly (up to 79%) by the addition of two equivalents of pyridine as a base.

I decided to evaluate our conditions from Table 3.4.1, entry 11 across a variety of substituted thioamide derivatives (Scheme 3.4.1). To confirm our initial hypothesis, I tested the substrates in the absence and presence of pyridine and obtained isolated yields of the benzothiazoles. Varying the electronics at the aryl ring R^1 (**3.2-3.5**) provided minor decreases in yield relative to the unsubstituted **3.1a** (isolating between 49-63% yield for **3.2a-3.5b**). Notably, I observed no effect when adding pyridine for naphthyl based substrate **3.6** (54% with no pyridine, 55% with pyridine for **3.6a**) and substrate **3.7** (32% without, 34% with pyridine for **3.7a**). This lack of pyridine effect held for other substrates that possessed these aryl groups **3.9** (43% no pyridine, 38% with pyridine for **3.9a**), and **3.15** (31% no pyridine, 30% with pyridine for **3.15a**). Replacing the thioamide *tert*-butyl group **3.1** with a phenyl group in **3.8**, resulted in a marked decrease in yield (79% to 32% of **3.8a**); however other phenyl containing thioamides resulted in decent yields (*i.e.* **3.10** resulted in 68% yield **3.10a**). Finally, when I replaced the thioamide substitution with aliphatic groups other than *tert*-butyl (**3.11-3.14**), I isolated the corresponding benzothiazoles in good yield (55% to 73% **3.11a-3.14a**). Surprisingly, when the thioamide substitution was a methyl (**3.16**) we only isolated the corresponding amide. Alternatively, when I evaluated trifluoromethyl containing **3.17**, I observed no reaction of any kind, perhaps due to the

thioamide being significantly more electron poor and possessing a higher redox potential, or a lower innate nucleophilicity.

To explain the subsequent transformation, I propose the following mechanism (Scheme 3.4.2 to 3.4.4), which are supported by several key experiments. Due to the increase in yield upon addition of pyridine, I believe there is a Lewis base effect wherein the pyridine coordinates to the N-H thioamide bond, providing extra stability to the radical cation that forms upon initial oxidation. This hypothesis is substantiated through cyclic voltammetry experiments (Scheme 3.4.2) on substrate **3.1**. In pure acetonitrile without the presence of additive base, I observed two half wave oxidation potentials at 1.5V and 1.9V versus SCE, meaning both values are out of the range of the $Ru(bpy)_3Cl_2$ reduction potential in its excited state [$Ru(II)^*/Ru(I)$ = 0.77V versus SCE]. Upon titration of pyridine, I noticed a distinct shift in the two oxidation potentials to 1.2V

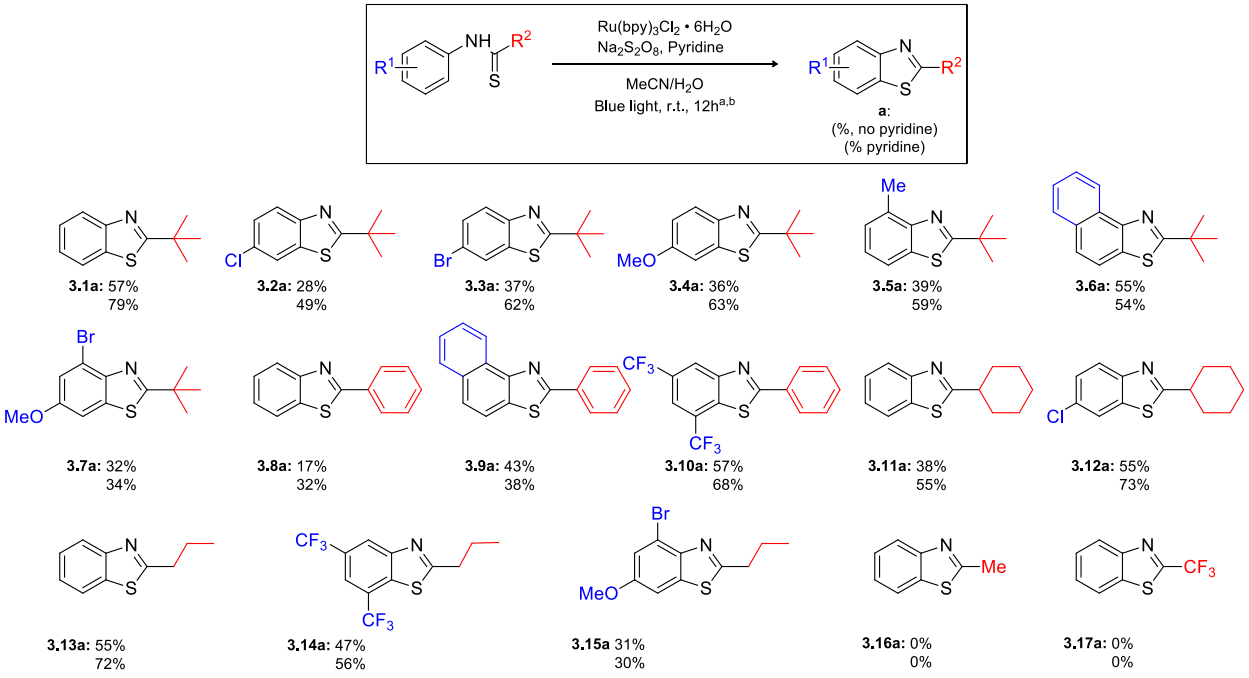

Scheme 3.4.1 Substrate Scope of Benzothiazole Synthesis from Thioamides

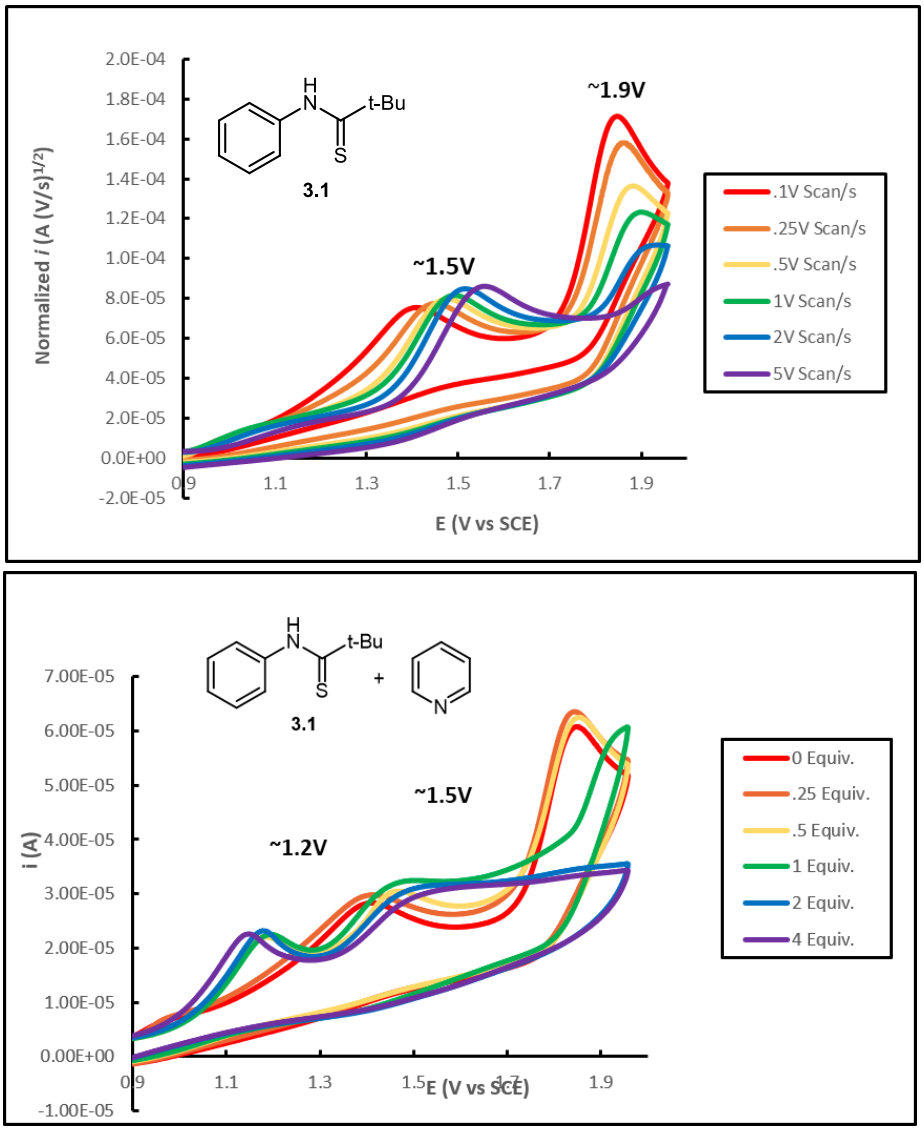

Scheme 3.4.2 Cyclic Voltammetry Measurements for Substrate 3.1

and 1.5V versus SCE. Interestingly, the first oxidation potential of **A** with pyridine is now within the range of the ground state reduction potential of $Ru(bpy)_3Cl_2$ [Ru(III)/Ru(II) = 1.29V versus SCE]. This suggests that, in its excited state, the photocatalyst reduces persulfate to the SO_4^{2-} anion and the $SO_4^{\cdot-}$ anion radical, followed by the resultant Ru^{3+} complex oxidizing the thioamide substrate to radical cation **B**. Additionally, I utilized density functional theory (DFT) calculations to predict the electron density maps for several thioamide intermediates and consequently predict the most favorable sites for oxidation. In the first map, I see a large concentration of electron

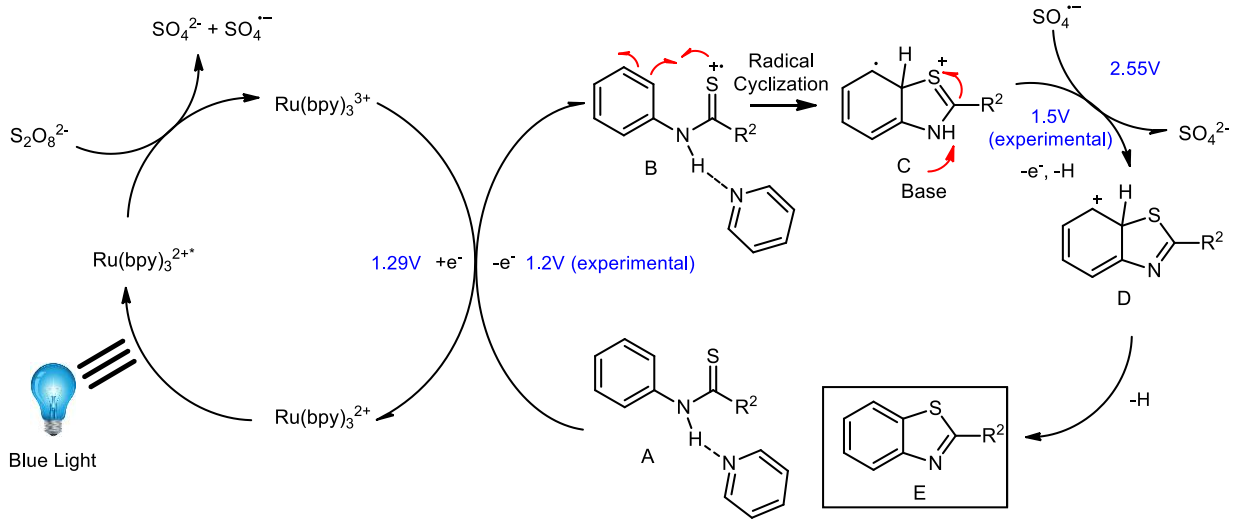

Scheme 3.4.3 Proposed Mechanism for Intramolecular Benzothiazole Synthesis

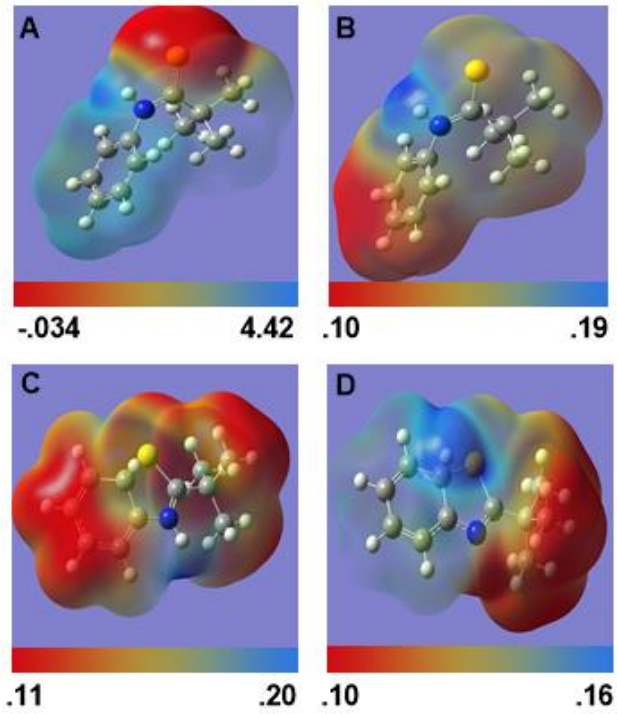

Scheme 3.4.4 Electron Density Maps of Predicted Intermediates

density at the sulfur relative to the rest of the molecule **A**, implying it is the most favorable site for initial oxidation; this pathway is also supported by recently reported work from Nicewicz on allylic thioamides.[121,122]

At this point, **B** will likely undergo radical cyclization to **C**. This is supported by a CV scan rate experiment; as the voltage is increased from 0.1 to 5 V/s, the second half-wave oxidation peak begins to diminish and completely disappears at the highest scan rate. One explanation for this observation is there is a new intermediate reaction between the first and second oxidation (i.e. thioamide cyclization) and that faster voltage sweeps can kinetically outpace the reaction, thereby hindering subsequent oxidation. Additionally, the predicted electron map of **B** (Scheme 3.4.4) suggests that the sulfur is now more electron deficient compared to the aryl ring; thus it is likely that the cyclization will occur via the arene acting as a nucleophile and the sulfur acting as an electrophilic radical. Due to the comparable yields of electron deficient thioamides without the presence of pyridine (i.e **3.10a**), I believe that the additive is beneficial towards initial oxidation but not necessary as persulfate can also promote formation of the thiyl radical cation; it is the subsequent radical cyclization which drives the reaction favorably towards the benzothiazole product. Upon cyclization, the electron density map shows a more electron rich intermediate which should be easily oxidized by the persulfate radical anion to give Wheland arenium ion **D**, which will rapidly undergo aromatization to the final product **E**.

I also explored whether our methodology for intramolecular C-H thiolation could be applied to other arenes for intermolecular functionalization, specifically the sulfenylation of electron rich heterocycles such as indoles. Our initial experiment utilized our optimized conditions for benzothiazole synthesis without pyridine, using **3.18** melatonin as the substrate and 4-methyl thiophenol as the sulfenylating reagent, and obtained 29% yield of **3.18a**. (Table 3.4.2, entry 1). Upon addition of pyridine (entry 2 & 3), I observed a similar trend as the yields increased to 40%. Just like the previous reaction, removal of the photocatalyst diminishes the yield significantly to 8% (entry 4), however there is still a background reaction from just persulfate exclusively.

Table 3.4.2 Optimization of Intermolecular Sulfenylation with Melatonin

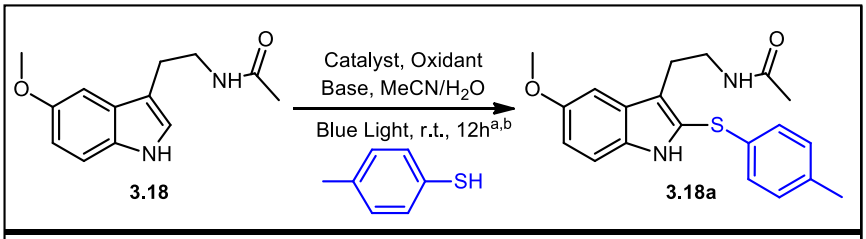

Entry	Catalyst	Oxidant (equiv)	Solvent	Base (equi)	Yield (%)
1	$Ru(bpy)_3Cl_2$	$Na_2S_2O_8$ (2)	CH_3CN/H_2O (1:1)	Pyridine (0)	29
2	$Ru(bpy)_3Cl_2$	$Na_2S_2O_8$ (2)	CH_3CN/H_2O (1:1)	Pyridine (1)	31
3	$Ru(bpy)_3Cl_2$	$Na_2S_2O_8$ (2)	CH_3CN/H_2O (1:1)	Pyridine (2)	40
4	None	$Na_2S_2O_8$ (2)	CH_3CN/H_2O (1:1)	Pyridine (2)	8
5	$Ru(bpy)_3Cl_2$	$Na_2S_2O_8$ (1)	CH_3CN/H_2O (1:1)	Pyridine (2)	5
6	$Ru(bpy)_3Cl_2$	None	CH_3CN/H_2O (1:1)	Pyridine (2)	0
7	$Ru(bpy)_3Cl_2$	$Na_2S_2O_8$ (2)	CH_3CN/H_2O (9:1)	Pyridine (2)	30
8	$Ru(bpy)_3Cl_2$	$Na_2S_2O_8$ (2)	CH_3CN	Pyridine (2)	15
9	CzIPN	$Na_2S_2O_8$ (2)	CH_3CN/H_2O (1:1)	Pyridine (2)	25
10	9-Mesi-Acri	$Na_2S_2O_8$ (2)	CH_3CN/H_2O (1:1)	Pyridine (2)	8
11	Ir{df(CF_3)...	$Na_2S_2O_8$ (2)	CH_3CN/H_2O (1:1)	Pyridine (2)	52
12	Ir{df(CF_3)...	$Na_2S_2O_8$ (2)	CH_3CN/H_2O (1:1)	K_2HPO_4 (2)	61
13	Ir{df(CF_3)...	$Na_2S_2O_8$ (2)	CH_3CN/H_2O (1:1)	K_3PO_4 (2)	28
14	Ir{df(CF_3)...	$Na_2S_2O_8$ (2)	CH_3CN/H_2O (1:1)	KOH (2)	68

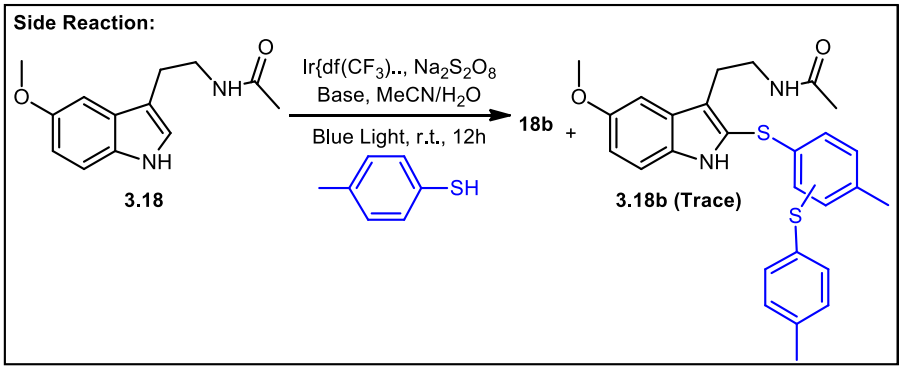

Interestingly, reintroduction of the photocatalyst but cutting the persulfate equivalent in half reduced the overall yield to 5% (entry 5). As expected, complete removal of persulfate provides no reaction (entry 6). Similar trends also hold for changing the ratio of solvents, as I see almost no variation going from 1:1 to 9:1 $MeCN/H_2O$, and a lowering of 15% yield switching to completely

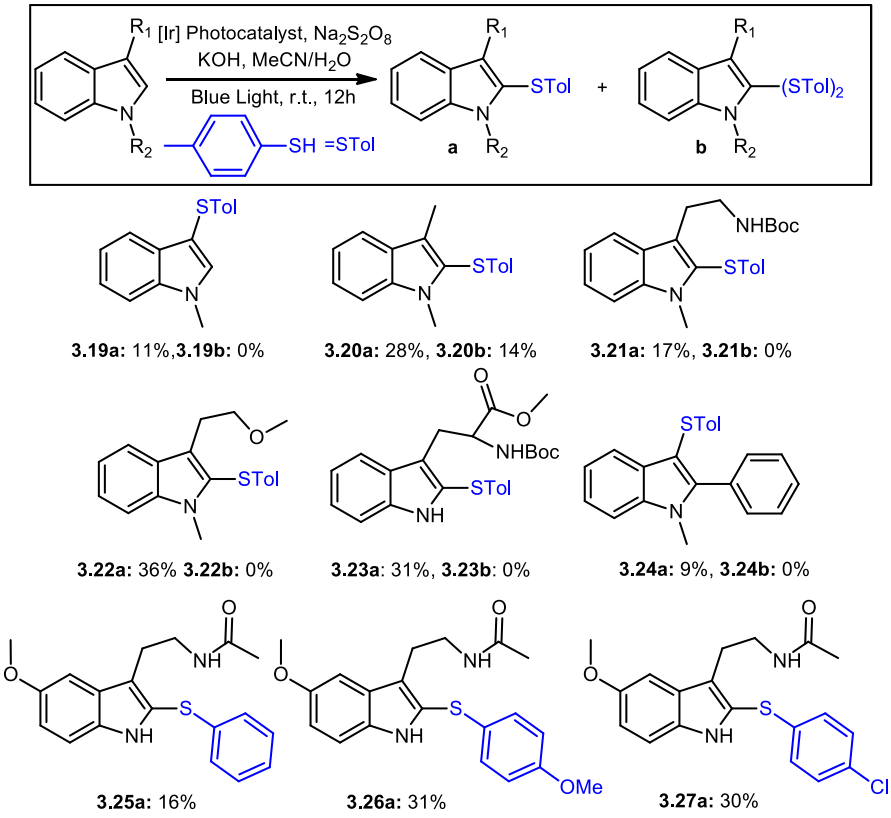

Scheme 3.4.5 Sulfenylation Substrate Scope of Various Indoles

acetonitrile (entry 7 & 8). After evaluating a number of photocatalysts (entry 9-11), I observed that $(Ir[dF(CF_3)ppy]_2(dtbpy)]PF_6$ gave a much higher yield at 52% compared with $Ru(bpy)_3Cl_2$. Finally, variation of the base to potassium hydroxide (12-14) provided an increase of yield to 68%. Interestingly, I noticed a trace amount of a disulfenylated side product **3.18b** when the iridium photocatalyst is used, suggesting that at some point the thiophenol reagent (or product sulfide) is oxidized and reacts with a 2nd equivalent of thiophenol.

With the optimized conditions, I evaluated a number of substituted indoles and report the isolated yields of both the mono and di-sulfenylated product, with a majority of substrates providing exclusively the mono-sulfenylated product between 9 to 36% yield (Scheme 3.4.5, **3.19-3.24**). Similar to melatonin, *N*-methyl 3-methyl indole **3.20** also gave a mixture of mono-sulfenylated **3.20a** and di-sulfenylated **3.20b** (28% and 14%, respectively) Additionally, I tested a

number of benzenethiol reagents (**3.25-3.27**) and varied the electronics off the aryl ring; this gave attenuated yields ranging from 16-31% yield (**3.25a-3.27a**). While these yields are moderate compared to other conditions (both via traditional S_EAr, and photocatalysis), I find it notable that this sulfenylation worked on biologically relevant scaffolds such as melatonin and tryptophan. I also found this transformation mechanistically interesting as the conditions were nearly identical to those of the benzothiazole synthesis and performed a series of mechanistic studies.

I first determined the experimental redox potentials of melatonin and 4-methylbenzenethiol sulfenylating reagent by cyclic voltammetry (see following experimental section). I observed that the melatonin **3.18** has a first half wave oxidation potential of 1.10V versus SCE while the latter has a higher half wave oxidation potential of 1.49V versus SCE (see supplementary information). Consequently, in its excited triplet state, the $(Ir[dF(CF_3)ppy]_2(dtbpy)]PF_6$ photocatalyst would be out of the potential range for oxidation of 4-methylbenzenethiol, and initial oxidation likely occurs at melatonin to form the cation radical **F.** Stern-Volmer quenching studies between the iridium photocatalyst, melatonin and 4-methylbenzenethiol supports this hypothesis as melatonin (K_{sv} = 4.2 $M^{-1}L$) is quenched at a much higher rate than the thiophenol (K_{sv} = 0.1 $M^{-1}L$) (see Scheme 3.4.6 and Experimental Section 3.5.10). Additionally, I ran the photocatalytic reaction in the absence of indole, observing a significant amount of the disulfide byproduct, which is known to undergo homolytic cleavage under UV light to form the thiyl radical.[123] To test whether the disulfide was an intermediate, I evaluated the reaction using phenyl disulfide as the sulfur source, observing comparable yields to that of thiophenol. Stern-Volmer quenching of the photocatalyst with 4-methyl diphenyl disulfide provided a slight increase (K_{sv} = 0.6 $M^{-1}L$) relative to the thiophenol but still significantly less than melatonin. To confirm our findings, I ran a sulfenylation

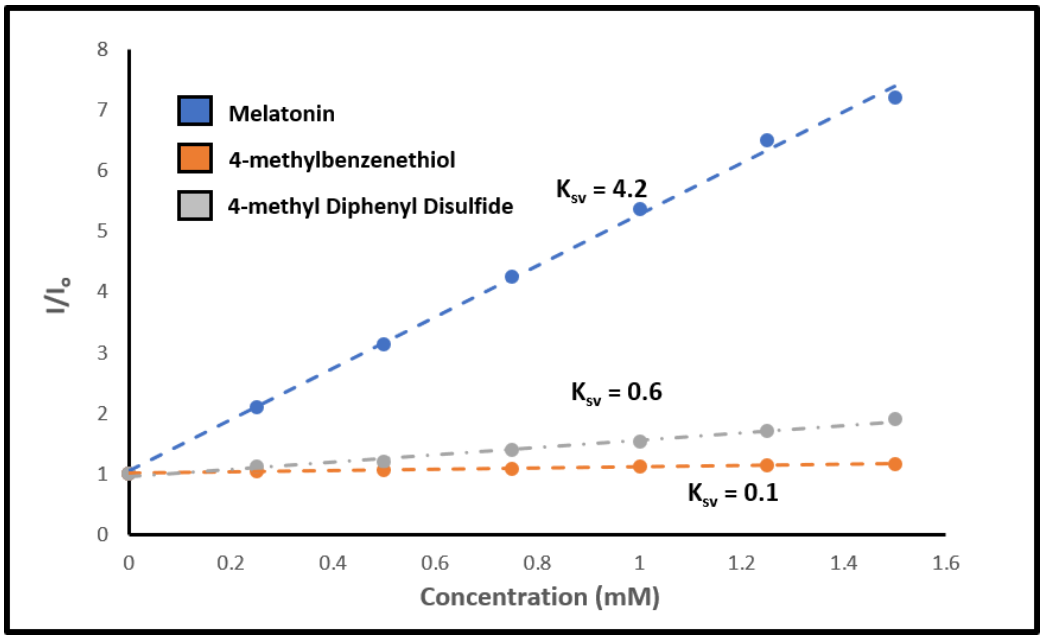

Scheme 3.4.6 Stern-Vollmer Quenching Studies of [Ir[df(CF$_3$)ppy]$_2$(dtbpy)]PF$_6$ with Melatonin, 4-methylbenzenethiol, and 4-methyl Diphenyl Sulfide

cross experiment using both 4-methylbenzenethiol and phenyl sulfide, observing the methylated indole as the main product via mass spectrometry (see Experimental Section 3.5.11). Based on these experiments, two plausible simultaneous mechanisms can occur. Once indole cation radical **F** is formed, deprotonated thiophenol can nucleophilically attack **F** to form radical intermediate **G**, which will be oxidized by persulfate and aromatize to form the sulfenylated product **3.18a** (Scheme 6, pathway 1). Alternatively, under photocatalytic conditions, thiophenol can beconverted to disulfide which can homolytically disassociate to form the thiyl radical. The radical can undergo radical coupling with **F** to form Wheland intermediate **I**, followed by aromatization to form product **3.18a**. Both pathways can occur simultaneously; however, I believe that the nucleophilic pathway is predominant as shown by Stern-Volmer quenching studies and sulfenylation cross experiment.

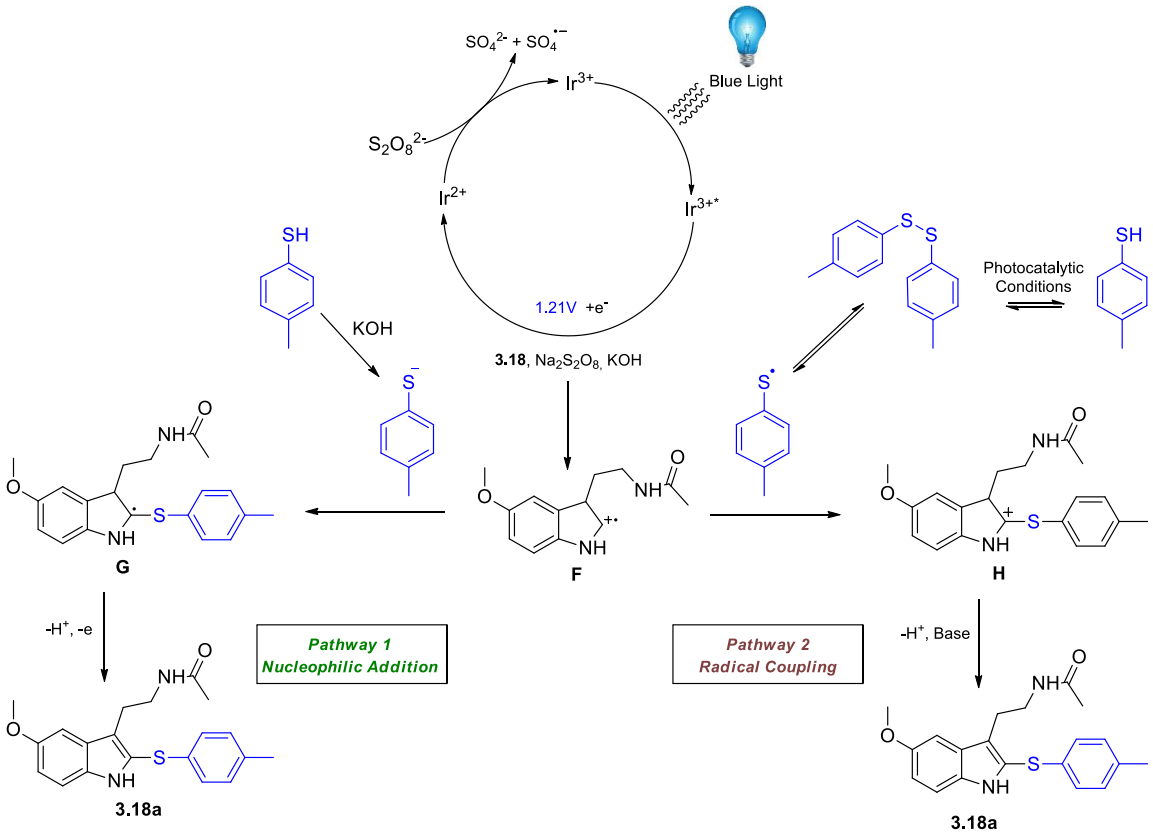

Scheme 3.4.7 Proposed Mechanisms for the Intermolecular Sulfenylation of Indoles.

In conclusion I have developed an operationally simple and economical method to synthesize benzothiazoles via photocatalytic C-H thiolation and have extended these conditions to indole sulfenylation. I performed mechanistic studies that suggest that the sulfur displays divergent activities (nucleophilic or electrophilic radical) in the two reactions.

3.5 Experimental Section

3.5.1 General Information

All ^{1}H, ^{13}C and ^{19}F NMR Spectra were recorded on Varian VNMRS 400 MHz, Bruker Avance AV_1 400MHz, Varian Inova 500 MHz, and Bruker Avance III HD 600MHz at room temperature. All chemical shifts were reported in parts per million (δ) and internally referenced to residual solvent proton signals unless otherwise noted. All spectral data were reported as follows: (multiplicity [singlet (s), doublet (d), doublet of doublets (dd), doublet of doublet of doublets (ddd), doublet of triplets (dt), triplet (t), triplet of triplets (tt), quartet (q), quintet (qn), and multiplet (m), heptet (h)], coupling constants [Hz], integration). Carbon spectra were recorded with complete decoupling. Conventional mass spectra were obtained using Advion Expression^{s} CMS APCI/ASAP. All chemicals and catalysts were purchased from Acros Organics, Cambridge Isotope Laboratories, Fisher Scientific, Frontier Scientific, Oakwood Chemicals, Sigma Aldrich, or TCI America. All normal phase flash column chromatography (FCC) was performed using Grade 60 Silica Gel (230-400 mesh) purchased from Fisher Scientific. Preparative Thin Layer Chromatography (TLC) plates contained grade 60 silica gel coated with fluorescent indicator F_{254} and were purchased from Fisher Scientific. Reflux conditions were done using an Anton Paar Monowave 400, G10, and G30 vials.

3.5.2 Abbreviations

Conc.: Concentration (M)

DCM: Methylene Chloride

Eq.: Equivalent

Et_3N: Triethylamine

EtOAc: Ethyl Acetate

FCC: Flash Column Chromatography

Hex: Hexanes

H_2O: Water

HCl: Hydrochloric Acid

HSPh: Thiophenol

Ir[dF(CF_3)ppy]$_2$(dtbpy)]PF_6: [4,4′-*Bis*(1,1-dimethylethyl)-2,2′-bipyridine-*N*1,*N*1′]*bis*[3,5-difluoro-2-[5-(trifluoromethyl)-2-pyridinyl-*N*]phenyl-C]Iridium(III) hexafluorophosphate

MeCN: Acetonitrile

Na_2SO_4: Sodium Sulfate

r.t: Room Temperature

$Ru(bpy)_3Cl_2 \cdot 6H_2O$: Tris(2,2'-bipyridyl)dichlororuthenium (II) hexahydrate

SM - Starting Material

3.5.3 Experimental Procedures

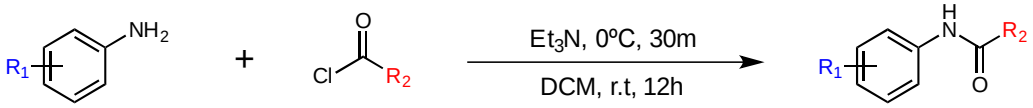

Scheme 3.5.1 Preparation of Substituted Benzamides

A solution of substituted aniline (1.0 eq.) and Et_3N (1.5 eq.) in DCM (0.1M) was prepared and stirred at 0 ºC for 30 minutes. Acyl chloride (1.0 eq.) was then added drop wise. The mixture was warmed to room temperature and stirred for 12 hours. The resulting solution was then quenched with 2M HCl and extracted with two equal volumes of DCM before being dried over Na_2SO_4. Evaporation of solvent gave crude product that was purified by FCC using a 4:1 Hex: EtOAc gradient.

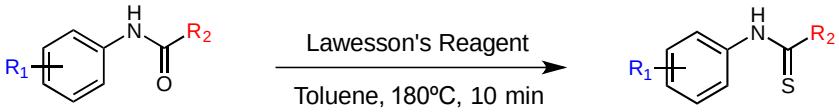

Scheme 3.5.2 Preparation of Substituted Thiobenzamides

A solution of benzamide (1.0 eq.), Lawesson's reagent (0.6 eq.), and toluene (0.1 M) were added to either a G10 or G30 microwave vial and was heated to 180 ºC for 10 minutes in the microwave. The resulting solution was then concentrated down and purified by FCC using a 4:1 Hex:EtOAc gradient.

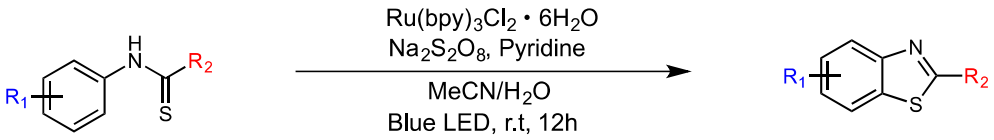

Scheme 3.5.3 Preparation of Substituted Benzothiazoles

In a 2 dram vial, substituted thiobenzamide (1.0 eq.), $Ru(bpy)_3Cl_2$ (2.0 mg, 0.05 eq.), sodium persulfate (2.0 eq.), and pyridine (2.0 eq.) were added to a solution of 1:1 MeCN:H_2O (25 mg/1 mL). The reaction was left to stir under blue LEDs for 12 hours at room temperature. The resulting solution was then quenched with H_2O, extracted with EtOAc and dried over Na_2SO_4. Evaporation of solvent gave crude product that was purified by prep TLC with a gradient from hexanes to 8:2 Hex: EtOAc.

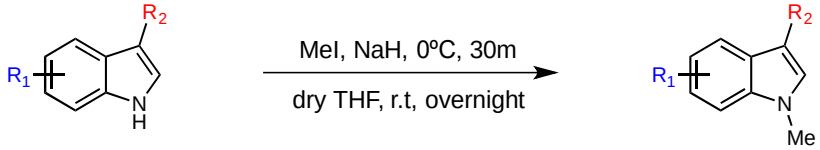

Scheme 3.5.4 Preparation of *N*-methylated Indoles

NaH (2.0 eq.) was added in a round bottom flask with anhydrous THF (1M) under inert atmosphere at 0ºC. A solution of substituted indole (1.0 eq.) and anhydrous THF was then added to the mixture, and the reaction was warmed to room temperature and stirred overnight. The resulting solution was then quenched with 2M HCl, washed with EtOAc, and dried over Na_2SO_4. Evaporation of solvent gave crude *N*-methylated indole that was purified by FCC.

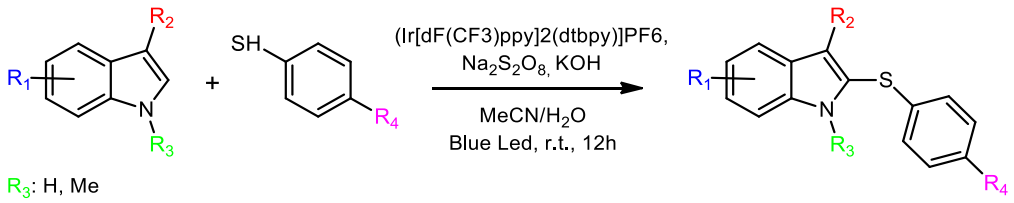

Scheme 3.5.5 Preparation of Sulfenyated Indoles

In a 10mL vial, substituted indole (1.0 eq.), (Ir[dF(CF_3)ppy]$_2$(dtbpy)]PF_6 (0.01 eq.), sodium persulfate (2.0 eq.), KOH (2.0 eq.), and 4-methylthiophenol (<1.0 eq.) were added to a solution of 1:1 MeCN: H_2O (25 mg/1 mL). The reaction was left to stir under blue LEDs for 12 hours at room temperature. The resulting solution was then quenched with H_2O and extracted with DCM before being dried over Na_2SO_4. Evaporation of solvent gave crude product that was purified by prep TLC (9:1 Hex: EtOAc (**3.19a, 3.21a-3.23a**), 9:1 Hex: DCM (**3.20a**), or 10:0 Hex (**3.24a**)). Melatonin substrates (**3.25a-3.27a)** were purified via FCC (8:2 EtOAc: Hex).

3.5.4 Characterization of Substituted Benzothiazoles

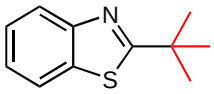

Figure 3.5.1 Product 3.1a

2-(*tert*-butyl)benzo[*d*]thiazole: Compound was synthesized using the general procedures for synthesizing the substituted benzamide, substituted thiobenzamide, and substituted benzothiazole. **Yields** (0.129 mmol scale): No Pyridine- 14.2 mg, 57% & Pyridine- 19.8 mg, 79%, off white solid. **^{1}H NMR (500 MHz, $CDCl_3$)** δ = 8.00 (dt, J = 8.2, 0.9 Hz, 1H), 7.85 (dd, J = 8.0, 0.45 Hz, 1H), 7.44 (ddd, J = 8.3, 7.2, 1.3 Hz, 1H), 7.34 (ddd, J = 8.2, 7.2, 1.2 Hz, 1H), 1.53 (s, 9H). The spectral data is in agreement with the reported literature: Zhang, G.; Liu, C.; Yi, H.; Meng, Q.; Bian, C.; Chen, H.; Jian, J. X.; Wu, L. Z.; Lei, A. *J. Am. Chem. Soc.* 2015, *137*, 9273-9280 **MS-APCI Calculated:** $C_{11}H_{13}NS$ $[M+H]^+$ 192.3, Found: 192.1 m/z

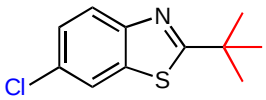

Figure 3.5.2 Product 3.2a

2-(*tert*-butyl)-6-chlorobenzo[*d*]thiazole: Compound was synthesized using the general procedures for synthesizing the substituted benzamide, substituted thiobenzamide, and substituted benzothiazole. **Yields** (0.110 mmol scale): No Pyridine- 7.0 mg, 28% & Pyridine- 12.2 mg, 49%, off white solid. **^{1}H NMR (500 MHz, CDCl$_3$)** δ = 7.88 (dd, J = 8.7, 0.5 Hz, 1H), 7.82 (dd, J = 2.1, 0.5, 1H), 7.44 (dd, J = 8.7, 2.1 Hz, 1H), 1.51 (s, 9H) The spectral data is in agreement with the reported literature: Zhang, G.; Liu, C.; Yi, H.; Meng, Q.; Bian, C.; Chen, H.; Jian, J. X.; Wu, L. Z.; Lei, A. *J. Am. Chem. Soc.* **2015**, *137*, 9273-9280 **MS-APCI Calculated:** $C_{11}H_{12}ClNS$ $[M+H]^+$ 226.7, Found: 226.2, 226.4 m/z

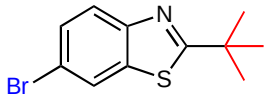

Figure 3.5.3 Product 3.3a

6-bromo-2-(*tert*-butyl)benzo[*d*]thiazole: Compound was synthesized using the general procedures for synthesizing the substituted benzamide, substituted thiobenzamide, and substituted benzothiazole. **Yields** (0.092 mmol scale): No pyridine- 9.2mg, 37% & Pyridine- 15.5mg, 62%, off white solid. **^{1}H NMR (500 MHz, CDCl$_3$)** δ = 7.98 (dd, J = 2.0, 0.5 Hz, 1H), 7.83 (dd, J = 8.7, 0.5 Hz, 1H), 7.54 (dd, J = 8.7, 2.0 Hz, 1H), 1.51 (s, 9H) The spectral data is in agreement with the reported literature: Zhang, G.; Liu, C.; Yi, H.; Meng, Q.; Bian, C.; Chen, H.; Jian, J. X.; Wu, L. Z.; Lei, A. *J. Am. Chem. Soc.* **2015**, *137*, 9273-9280 **MS-APCI Calculated:** $C_{11}H_{12}BrNS$ $[M+H]^+$ 271.2, Found: 271.0, 271.2, 271.3 m/z

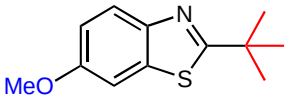

Figure 3.5.4 Product 3.4a

(2-(*tert*-butyl)-6-methoxybenzo[*d*]thiazole: Compound was synthesized using the general procedures for synthesizing the substituted benzamide, substituted thiobenzamide, and substituted benzothiazole. **Yields** (0.112 mmol scale): No pyridine- 9.0 mg, 36% & Pyridine- 15.8 mg, 63%, off white solid. **^{1}H NMR (500 MHz, $CDCl_3$)** δ = 7.86 (dd, *J* = 8.9, 0.5 Hz, 1H), 7.31 (d, *J* = 2.6 Hz, 1H), 7.04 (dd, *J* = 8.9, 2.6 Hz, 1H), 3.87 (s, 3H), 1.50 (s, 9H). The spectral data is in agreement with the reported literature: Zhang, G.; Liu, C.; Yi, H.; Meng, Q.; Bian, C.; Chen, H.; Jian, J. X.; Wu, L. Z.; Lei, A. *J. Am. Chem. Soc.* **2015**, *137*, 9273-9280 **MS-APCI Calculated**: $C_{12}H_{15}NOS$ $[M+H]^+$ 222.3, Found: 222.0 m/z

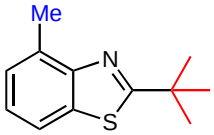

Figure 3.5.5 Product 3.5a

2-(*tert*-butyl)-4-methylbenzo[*d*]thiazole: Compound was synthesized using the general procedures for synthesizing the substituted benzamide, substituted thiobenzamide, and substituted benzothiazole. **Yields** (0.121 mmol scale): No pyridine- 9.8 mg, 39% & Pyridine- 14.8 mg, 59%, slight pink solid. **^{1}H NMR (500 MHz, $CDCl_3$)** δ = 7.69-7.66 (m, 1H), 7.25-7.20 (m, 2H), 2.75 (s, 3H), 1.52 (s, 9H) The spectral data is in agreement with the reported literature: Zhang, G.; Liu, C.; Yi, H.; Meng, Q.; Bian, C.; Chen, H.; Jian, J. X.; Wu, L. Z.; Lei, A. *J. Am. Chem. Soc.* **2015**, *137*, 9273-9280. **MS-APCI Calculated:** $C_{12}H_{15}NS$ $[M+H]^+$ 206.3, Found: 206.2

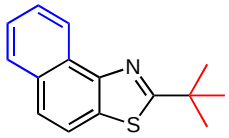

Figure 3.5.6 Product 3.6a

2-(*tert*-butyl)napthol[1,2-*d*]thiazole: Compound was synthesized using the general procedures for synthesizing the substituted benzamide, substituted thiobenzamide, and substituted benzothiazole. **Yields** (0.103 mmol scale): No pyridine- 13.8 mg, 55% & Pyridine- 13.5 mg, 54%,

yellow-green solid. **^{1}H NMR (500 MHz, $CDCl_3$)** δ = 8.82 (dt, *J* = 8.0, 0.8 Hz, 1H), 7.93 (d, *J* = 8.1 Hz, 1H), 7.87 (d, *J* = 8.7 Hz, 1H), 7.75 (d, *J* = 8.7 Hz, 1H), 7.65 (ddd, *J* = 8.2, 6.9, 1.3 Hz, 1H), 7.55 (ddd, *J* =8.2, 6.9, 1.3 Hz, 1H), 1.59 (s, 9H) **^{13}C NMR (101 MHz, $CDCl_3$)** δ = 180.7, 149.2, 131.8, 131.2, 128.6, 127.9, 126.6, 125.7, 125.0, 124.0, 119.0, 38.4, 31.0 **MS-APCI Calculated:** $C_{15}H_{15}NS$ $[M+H]^+$: 242.4 Found: 242.1 m/z

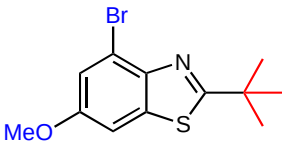

Figure 3.5.7 Product 3.7a

4-bromo-2-(*tert*-butyl)-6-methoxybenzo[*d*]thiazole: Compound was synthesized using the general procedures for synthesizing the substituted benzamide, substituted thiobenzamide, and substituted benzothiazole. **Yields** (0.083 mmol scale): No pyridine- 8.0 mg, 32% & Pyridine- 8.5 mg, 34%, slight pink solid. **^{1}H NMR (500 MHz, $CDCl_3$)** δ = 7.87 (d, *J* = 8.8 Hz, 1H), 7.07 (d, *J* = 8.9 Hz, 1H), 3.97 (s, 3H), 1.51 (s, 9H) **^{13}C NMR (101 MHz, $CDCl_3$)** δ = 170.59, 157.34, 146.03, 136.69, 118.13, 115.79, 103.88, 56.02, 36.22, 29.68, 23.34, 13.74 **MS-APCI Calculated**: $C_{12}H_{14}BrNOS$ $[M+H]^+$: 301.2, Found: 301.0, 301.2, 300.5 m/z

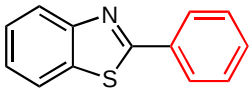

Figure 3.5.8 Product 3.8a

2-phenylbenzo[*d*]thiazole: Compound was synthesized using the general procedures for synthesizing the substituted benzamide, substituted thiobenzamide, and substituted benzothiazole. **Yields** (0.117 mmol scale): No pyridine- 4.3 mg, 17% & Pyridine- 8.0 mg, 32%, yellow-green solid. **^{1}H NMR (500 MHz, $CDCl_3$)** δ = 8.13-8.07 (m, 3H), 7.92 (d, *J* = 8.0 Hz. 1H), 7.53-7.46 (m, 4H), 7.39 (ddd, *J* = 8.3, 7.1, 1.2 Hz, 1H). The spectral data is in agreement with the reported literature: Zhang, G.; Liu, C.; Yi, H.; Meng, Q.; Bian, C.; Chen, H.; Jian, J. X.; Wu, L. Z.; Lei, A.

J. Am. Chem. Soc. **2015**, *137*, 9273-9280 **MS-APCI Calculated:** $C_{13}H_9NS$ $[M+H]^+$: 212.3, Found: 212.1 m/z

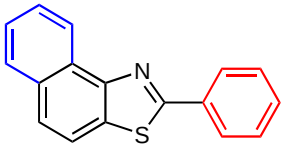

Figure 3.5.9 Product 3.9a

2-phenylnaptho[1,2-*d*]thiazole: Compound was synthesized using the general procedures for synthesizing the substituted benzamide, substituted thiobenzamide, and substituted benzothiazole. **Yields** (0.095 mmol scale): No pyridine- 13.8 mg, 55% & Pyridine- 13.5 mg, 54%, dark green solid. **^{1}H NMR (400 MHz, $CDCl_3$)** δ = 8.93 (ddt, *J* =8.3, 1.4, 0.7 Hz, 1H), 8.24-8.18 (m, 2H), 7.99-7.90 (m, 2H), 7.82 (dt, *J* = 8.7, 0.6 Hz, 1H), 7.70 (ddd, *J* = 8.2, 6.9, 1.3 Hz, 1H), 7.60 (ddd, *J* = 8.2, 6.9, 1.3Hz, 1H), 7.57-7.46 (m, 3H) The spectral data is in agreement with the reported literature: Zhang, G.; Liu, C.; Yi, H.; Meng, Q.; Bian, C.; Chen, H.; Jian, J. X.; Wu, L. Z.; Lei, A. *J. Am. Chem. Soc.* **2015**, *137*, 9273-9280 **MS-APCI Calculated**: $C_{17}H_{11}NS$ $[M+H]^+$: 262.3, Found: 262.2 m/z

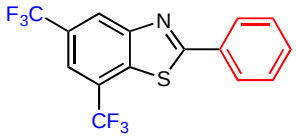

Figure 3.5.10 Product 3.10a

2-phenyl-5,7-bis(trifluoromethyl)benzo[*d*]thiazole: Compound was synthesized using the general procedures for synthesizing the substituted benzamide, substituted thiobenzamide, and substituted benzothiazole. **Yields** (0.072 mmol scale): No pyridine- 14.3 mg, 57% & Pyridine- 17.0 mg, 68%, yellow solid **^{1}H NMR (400 MHz, $CDCl_3$)** δ = 8.5 (s, 1H), 8.16-8.12 (m, 2H), 7.91 (s, 1H), 7.59-7.52 (m, 3H). The spectral data is in agreement with the reported literature: Folgueiras-Amador, A. A.; Qian, X. Y.; Xu, H. C.; Wirth, T. *Chem. Eur. J.* **2018**, *24*, 487-491 **MS-APCI Calculated**: $C_{15}H_7F_6NS$ $[M+H]^+$: 348.3, Found: 348.1 m/z

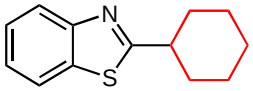

Figure 3.5.11 Product 3.11a

2-cylcohexylbenzo[*d*]thiazole: Compound was synthesized using the general procedures for synthesizing the substituted benzamide, substituted thiobenzamide, and substituted benzothiazole. **Yields** (0.114 mmol scale): No pyridine- 9.5 mg, 38% & Pyridine- 13.8 mg, 55%, off white solid **^{1}H NMR (500 MHz, CDCl$_3$)** δ = 7.99-7.96 (m, 1H), 7.85 (ddd, *J* = 8.0, 1.3, 0.6 Hz, 1H), 7.44 (ddd, *J* = 8.2, 7.2, 1.2 Hz, 1H), 7.34 (ddd, *J* = 8.3, 7.2, 1.2 Hz, 1H), 3.11 (tt, *J* = 11.7, 3.6 Hz, 1H), 2.25-2.17 (m, 2H), 1.89 (dt, *J* = 12.8, 3.5 Hz, 2H), 1.77 (dd, *J* = 12.7, 3.2, 1.6 Hz, 1H), 1.70-1.58 (m, 2H), 1.45 (qt, *J* = 12.4, 3.3 Hz, 2H), 1.34 (tt, *J* = 12.4, 3.2 Hz, 1H) The spectral data is in agreement with the reported literature: Zhang, G.; Liu, C.; Yi, H.; Meng, Q.; Bian, C.; Chen, H.; Jian, J. X.; Wu, L. Z.; Lei, A. *J. Am. Chem. Soc.* **2015**, *137*, 9273-9280 **MS-APCI Calculated:** $C_{13}H_{15}NS$ $[M+H]^+$: 218.3, Found: 218.3 m/z

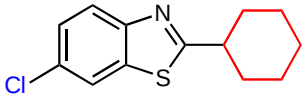

Figure 3.5.12 Product 3.12a

6-chloro-2-cyclohexylbenzo[*d*]thiazole: Compound was synthesized using the general procedures for synthesizing the substituted benzamide, substituted thiobenzamide, and substituted benzothiazole. **Yields** (0.099 mmol scale): No pyridine- 13.8 mg, 55% & Pyridine- 18.3 mg, 73%, off white solid. **^{1}H NMR (500 MHz, CDCl$_3$)** δ = 7.87 (d, *J* = 8.7 Hz, 1H), 7.82 (d, *J* = 1.9 Hz, 1H), 7.40 (d, *J* = 13.3, 3.5 Hz, 2H), 3.09 (tt, *J* = 11.6, 3.6 Hz, 1H), 2.23-2.16 (m, 2H), 1.89 (dt, *J* = 13.3, 3.5 Hz, 2H), 1.77 (dtt, *J* = 12.8, 3.2, 1.5 Hz, 1H), 1.68-1.57 (m, 2H), 1.44 (qt, *J* = 12.7, 3.4 Hz, 2H), 1.33 (tt, *J* =12.4, 3.4 Hz, 1H) **^{13}C NMR (101 MHz, CDCl$_3$)** δ = 178.11, 151.65, 135.75,

130.34, 126.53, 123.25, 121.13, 43.36, 33.30, 25.97, 25.70 **MS-APCI Calculated:** $C_{13}H_{14}ClNS$ $[M+H]^+$: 252.8, Found: 252.3, 252.5 m/z

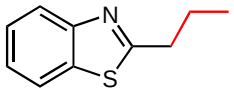

Figure 3.5.13 Product 3.13a

(2-propylbenzo[*d*]thiazole: Compound was synthesized using the general procedures for synthesizing the substituted benzamide, substituted thiobenzamide, and substituted benzothiazole. **Yields** (0.129 mmol scale): No pyridine- 13.8 mg, 55% & Pyridine- 18.0 mg, 72%, orange oil. **^{1}H NMR (500 MHz, $CDCl_3$)** δ= 7.99-7.95 (m, 1H), 7.86-7.82 (m, 1H), 7.45 (ddd, *J* = 8.2, 7.3, 1.3 Hz, 1H), 7.37-7.32 (m, 1H), 3.13-3.06 (m, 2H), 1.92 (m, 2H), 1.06 (t, J= 7.4, 3H) The spectral data is in agreement with the reported literature: Vechorkin, O.; Proust, V.; Hu, X. *Angew. Chem. Int. Ed.* **2010**, *49*. 3061-3064. **MS-APCI Calculated:** $C_{11}H_{13}NS$ $[M+H]^+$: 192.3, Found: 192.2 m/z

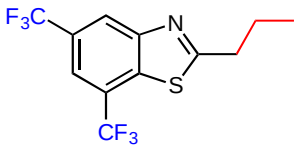

Figure 3.5.14 Product 3.14a

2-propyl-5,7-bis(trifluoromethyl)benzo[*d*]thiazole: Compound was synthesized using the general procedures for synthesizing the substituted benzamide, substituted thiobenzamide, and substituted benzothiazole. **Yields** (0.076 mmol scale): No pyridine- 11.8 mg, 47% & Pyridine- 14.0 mg, 56%, orange solid. **^{1}H NMR (500 MHz, $CDCl_3$)** *δ* = 8.40 (s, 1H), 7.88 (s, 1H), 3.19-3.13 (m, 2H), 1.96 (m, 2H, 1.09 (t, *J* = 7.4 Hz, 3H) **^{13}C NMR (126 MHz, $CDCl_3$)** *δ* = 176.06, 154.58, 135.41, 128.85 (q, *J* = 33.9), 125.36 (q, *J* = 35.1), 124.34 (d, *J* = 60.7), 123.03 (m), 122.18 (d, *J* = 61.1), 118.75 (h), 36.08, 22.81, 13.65 **^{19}F NMR (470 MHz, $CDCl_3$)** *δ* = -61.11, -62.78 **MS-APCI Calculated:** $C_{13}H_{11}F_6NS$ $[M+H]^+$: 328.3, Found: 328.3 m/z

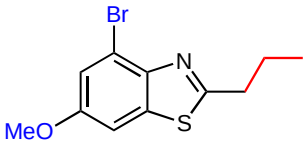

Figure 3.5.15 Product 3.15a

4-bromo-6-methoxy-2-propylbenzo[*d*]thiazole: Compound was synthesized using the general procedures for synthesizing the substituted benzamide, substituted thiobenzamide, and substituted benzothiazole. **Yields** (0.083 mmol scale): No pyridine- 7.8 mg, 31% & Pyridine- 7.5 mg, 30%, off white oil **^{1}H NMR (500 MHz, CDCl$_3$)** δ = 7.27 (d, J = 2.4 Hz, 1H), 7.24 (d, J = 2.4 Hz, 1H), 3.85 (s, 3H), 3.13-3.00 (m, 3H), 1.88 (m, 3H), 1.06 (t, J = 7.4Hz, 4H) **^{13}C NMR (126 MHz, CDCl$_3$)** δ = 179.65, 157.23, 146.03, 136. 68, 118.03, 116.21, 103.85, 56.03 (d, J = 5.0) 38.51, 30.71 **MS-APCI Calculated:** $C_{12}H_{14}BrNOS$ $[M+H]^+$: 301.2, Found: 301.2, 301.3 m/z

3.5.5 Characterization of Substituted Indoles

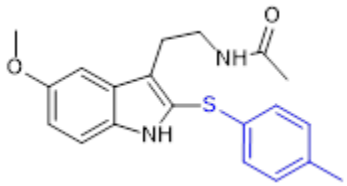

Figure 3.5.16 Product 3.18a

N-(2-(5-methoxy-2-(p-tolylthio)-1H-indol-3-yl)ethyl)acetamide: Compound was synthesized using the general procedures for the synthesis of substituted indoles. **Yields** (.107 mmol scale): 52%, pale tan solid. **^{1}H NMR (400 MHz, CDCl$_3$)** δ = 8.12 (s, 1H), 7.22 (d, J = 8.8 Hz, 1H), 7.02-7.06 (m, 3H), 6.98 (d, J = 8.3 Hz, 2H), 6.91 (dd, J = 8.8, 2.4 Hz, 1H), 5.50 (s, 1H), 3.86 (s, 3H), 3.52 (q, J = 6.4 Hz, 2H), 3.05 (t, J = 6.5 Hz, 2H), 2.27 (s, 3H), 1.78 (s, 3H). **^{13}C NMR (126 MHz, CDCl$_3$)** δ = 170.28, 154.36, 136.17, 133.22, 132.07, 130.04, 128.13, 127.00, 123.50, 119.64, 114.32, 111.93, 100.32, 55.87, 40.01, 24.75, 23.13, 20.89 **MS-APCI Calculated:** $C_{20}H_{22}N_2O_2S$ $[M+H]^+$: 355.5, Found: 355.5 m/z

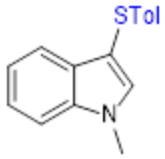

Figure 3.5.17 Product 3.19a

(19b) 1-methyl-3-(p-tolylthio)-1H-indole: Compound was synthesized using the general procedures **V** for the synthesis of substituted indoles. **Yields** (.098 mmol scale): 10.67 mg, 11%, white solid. **^{1}H NMR (400 MHz, $CDCl_3$)** δ = 7.62 (td, *J* = 7.8, 1.0 Hz, 1H), 7.38 (td, *J* = 7.9, 1.0 Hz, 1H), 7.33 (s, 1H), 7.29 (ddd, *J* = 7.1, 6.9, 1.0 Hz, 1H), 7.17 (ddd, *J* = 7.0, 6.9, 1.0 Hz, 1H), 7.03 (d, *J* = 8.6 Hz, 2H), 6.97 (d, *J* = 8.6 Hz, 2H), 3.84 (s, 3H), 2.25 (s, 3H). **^{13}C NMR (126 MHz, $CDCl_3$)** δ = 137.48, 135.92, 134.83, 134.49, 129.82, 129.42, 126.08, 122.46, 120.39, 119.75, 109.64, 101.16, 33.10, 20.86. **MS-APCI Calculated:** $C_{16}H_{15}NS$ $[M+H]^+$: 254.4, Found: 254.4 m/z

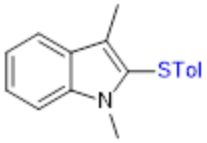

Figure 3.5.18 Product 3.20a

1,3-dimethyl-2-(p-tolylthio)-1H-indole: Compound was synthesized using the general procedures **V** for the synthesis of substituted indoles. **Yields** (.172mmol scale): 26.2 mg, 28%, white solid. **^{1}H NMR (400 MHz, $CDCl_3$)** δ = 7.63 (ddd, *J* = 7.9, 1.0, 0.9 Hz, 1H) 7.28-7.33 (m, 2H), 7.15 (ddd, *J* = 8.0, 1.0, 0.9 Hz, 1H), 7.01 (d, *J* = 8.3 Hz, 2H), 6.88 (d, *J* = 8.2 Hz, 2H), 3.70 (s, 3H), 2.45 (s, 3H), 2.27 (s, 3H). **^{13}C NMR (126 MHz, $CDCl_3$)** δ = 137.98, 135.30, 133.70, 132.61, 129.82, 127.41, 126.14, 124.62, 123.05, 119.44, 119.07, 109.58, 29.98, 20.96, 9.97. **MS-APCI Calculated:** $C_{23}H_{21}NS_2$ $[M+H]^+$: 268.4, Found: 268.4 m/z

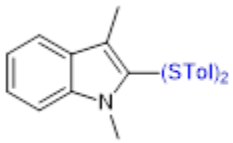

Figure 3.5.19 Product 3.20b

1,3-dimethyl-2-((4-methyl-2-(p-tolylthio)phenyl)thio)-1H-indole: Compound was synthesized using the general procedures **V** for the synthesis of substituted indoles. There is the presence of rotamers in both ^{1}H and ^{13}C NMR. The peaks for the major rotamer is reported. **Yields** (.172mmol scale): 13.1 mg, 14%, white solid. **^{1}H NMR (400 MHz, $CDCl_3$)** δ = 7.63 (d, *J* = 7.9 Hz, 1H), 7.26-7.32 (m, 2H), 7.24 (broad singlet, 1H), 7.12-7.18 (m, 4H), 7.04 (dd, *J* = 8.2, 2.2 Hz, 1H), 6.82 (dd, *J* = 8.2, 2.0 Hz) 6.32 (d, *J* = 8.2 Hz, 1H), 3.62 (s, 3H), 2.39 (s, 3H), 2.35 (s, 3H), 2.20 (s, 3H). **^{13}C NMR (126 MHz, $CDCl_3$)** δ = 138.17, 137.90, 136.71, 136.75, 134.49, 131.98, 130.74, 130.02, 129.95, 129.90, 129.67, 129.64, 128.50, 125.92, 123.08, 119.44, 119.09, 109.63, 29.85, 21.10, 20.64, 9.88. **MS-APCI Calculated**: $C_{24}H_{23}NS_2$ $[M+H]^+$: 390.6, Found: 390.6 m/z

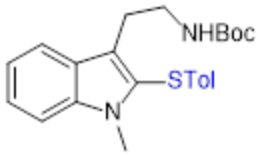

Figure 3.5.20 Product 3.21a

tert-butyl (2-(1-methyl-2-(p-tolylthio)-1H-indol-3-yl)ethyl)carbamate: Compound was synthesized using the general procedures **V** for the synthesis of substituted indoles. **Yields** (.091 mmol scale): 11.7 mg, 17%, white solid. **^{1}H NMR (400 MHz, $CDCl_3$)** δ = 7.71 (d, *J* = 7.0 Hz, 1H), 7.29-7.36 (m, 2H), 7.17 (ddd, *J* = 8.3, 6.0, 1.8 Hz, 1H), 7.02 (d, *J* = 8.3 Hz, 2H), 6.86 (d, *J* = 8.3 Hz, 2H), 4.57 (s, 1H), 3.70 (s, 3H), 3.39 (broad q, 2H), 3.14 (t, *J* = 6.8Hz, 2H), 2.28 (s, 3H), 1.43 (s, 9H). **^{13}C NMR (126 MHz, $CDCl_3$)** δ = 155.90, 138.11, 135.44, 133.60, 132.72, 132.61, 131.61, 129.96, 128.61, 128.48, 126.97, 125.96, 125.37, 123.24, 119.60, 109.76, 30.06, 28.41, 20.89. **MS-APCI Calculated:** $C_{24}H_{23}NS_2$ $[M+H]^+$: 397.6, Found: 397.6 m/z

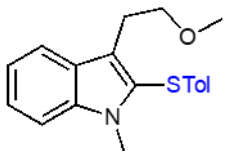

Figure 3.5.21 Product 3.22a

3-(2-methoxyethyl)-1-methyl-2-(p-tolylthio)-1H-indole: Compound was synthesized using the general procedures **V** for the synthesis of substituted indoles. **Yields** (.132 mmol scale): 13.7 mg, 36%, brown oil. **^{1}H NMR (400 MHz, $CDCl_3$)** δ = 7.70 (td, *J* = 7.8, 1.0 Hz, 1H), 7.27-7.34 (m, 2H), 7.16 (ddd, *J* = 7.8, 6.4, 1.1 Hz, 1H), 7.01 (d, *J* = 8.2 Hz, 2H), 6.88 (d, *J* = 8.2 Hz, 2H), 3.69 (s, 3H), 3.58 (t, *J* = 7.6 Hz, 2H), 3.33 (s, 3H), 3.22 (t, *J* = 7.6Hz, 2H), 2.27 (s, 3H). **^{13}C NMR (126 MHz, $CDCl_3$)** δ = 138.07, 135.39, 133.71, 129.83, 126.99, 126.19, 125.43, 123.08, 120.06, 119.54, 119.35, 109.73, 73.01, 58.52, 30.03, 25.96, 20.88. **MS-APCI Calculated**: $C_{19}H_{21}NOS$ $[M+H]^+$: 312.4, Found: 312.4 m/z

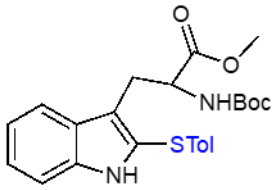

Figure 3.5.22 Product 3.23a

methyl 2-((tert-butoxycarbonyl)amino)-3-(2-(p-tolylthio)-1H-indol-3-yl)propanoate: Compound was synthesized using the general procedures **V** for the synthesis of substituted indoles. **Yields** (.078 mmol scale): 12.1 mg, 31%, white solid. **^{1}H NMR (400 MHz, $CDCl_3$)** δ = 8.33 (d, *J* = 15.4 Hz, 1H) 7.60 (d, *J* = 7.9 Hz, 1H) 7.25 (d, *J* = 7.9 Hz, 1H), 7.21 (td, *J* = 6.9, 1.1 Hz, 1H), 7.13 (td, *J* = 7.0, 1.1 Hz, 1H), 7.02 (q, *J* = 5.9 Hz, 4H), 4.65 (q, *J* = 6.7 Hz, 1H), 3.67 (s, 3H), 3.39 (q, *J* = 5.7 Hz, 2H), 2.28 (s, 3H), 1.40 (s, 9H). **^{13}C NMR (126 MHz, $CDCl_3$)** δ = 172.66, 155.12, 136.92, 136.23, 132.46, 129.98, 127.96, 127.63, 124.55, 123.38, 119.99, 119.21, 116.78, 110.97, 79.71, 54.15, 52.36, 28.30, 27.76, 20.94. **MS-APCI Calculated:** $C_{24}H_{28}N_2O_4S$ $[M+H]^+$: 441.6, Found: 441.6 m/z

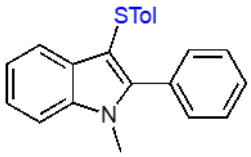

Figure 3.5.23 Product 3.24a

1-methyl-2-phenyl-3-(*p*-tolythio)-1H-indole: Compound was synthesized using the general procedures **V** for the synthesis of substituted indoles. **Yields** (.241 mmol scale): 6.9 mg, 9.0%, white solid. **^{1}H NMR (500 MHz, $CDCl_3$)** δ = 7.65 (dt, *J* = 7.9, 0.9 Hz, 1H), 7.48-7.40 (m, 6H), 7.33 (ddd, *J* = 8.2, 7.1, 1.2 Hz, 1H), 7.20 (ddd, *J* = 7.9, 7.1, 0.9 Hz, 1H), 6.96 (s, 4H), 3.74 (s, 3H), 2.25 (s, 3H). The spectral data is in agreement with the reported literature: Chen, Y.; Cho, C.; Shi, F.; Larock, R. *J. Org. Chem*. **2009**, *74*. 6802-6811 **MS-APCI Calculated:** $C_{22}H_{19}NS$ $[M+H]^+$: 329.5, Found: 330.3 m/z

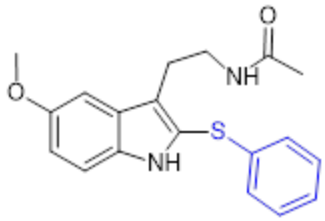

Figure 3.5.24 Product 3.25a

(*N*-(2-(5-methoxy-2-(phenylthio)-1H-indol-3-yl)ethyl)acetamide: Compound was synthesized using the general procedures **V** for the synthesis of substituted indoles. **Yields** (.107 mmol scale): 6.2 mg, 16%, clear oil. **^{1}H NMR (400 MHz, $CDCl_3$)** δ = 8.12 (s, 1H), 7.20-7.25 (m, 3H), 7.13 (ddd, *J* = 7.4, 2.0, 1.9 Hz, 1H) 7.04-7.08 (m, 3H), 6.93 (dd, *J* = 8.8, 2.4 Hz, 1H), 5.47 (s, 1H), 3.87 (s, 1H), 3.50 (q, *J* = 6.3 Hz, 2H) 3.05 (t, *J* = 6.4 Hz, 2H), 1.76 (s, 3H). **^{13}C NMR (126 MHz, $CDCl_3$)** δ = 170.14, 154.41, 137.18, 132.16, 129.28, 128.10, 126.35, 125.99, 122.59, 120.30, 114.56, 112.00, 100.37, 55.86, 39.97, 24.83, 23.17. **MS-APCI Calculated:** $C_{19}H_{20}N_2O_2S$ $[M+H]^+$: 341.4, Found: 341.5 m/z

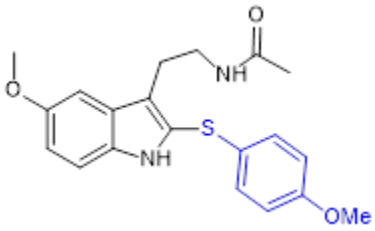

Figure 3.5.25 Product 3.26a

***N*-(2-(5-methoxy-2-((4-methoxyphenyl)thio)-1H-indol-3-yl)ethyl)acetamide:**

Compound was synthesized using the general procedures **V** for the synthesis of substituted indoles. **Yields** (.107 mmol scale): 12.2 mg, 31%, brown solid. **^{1}H NMR (400 MHz, $CDCl_3$)** δ = 8.09 (s, 1H), 7.20 (d, *J* = 8.9 Hz, 1H), 7.11 (dd, *J* = 6.8, 2.3Hz, 2H), 7.03 (d, *J* = 2.5 Hz, 1H), 6.89 (dd, *J* = 8.8, 2.4 Hz, 1H), 6.78 (dd, *J* = 6.7, 2.3 Hz, 2H), 5.52 (s, 1H), 3.86 (s, 3H), 3.75 (s, 3H), 3.51 (q, *J* = 6.5 Hz, 2H), 3.06 (t, *J* = 6.6 Hz, 2H), 1.82 (s, 3H). **^{13}C NMR (126 MHz, $CDCl_3$)** δ = 170.16, 158.73, 154.33, 131.95, 129.76, 128.20, 126.72, 124.80, 118.75, 114.98, 114.06, 111.84, 100.30, 55.85, 55.38, 40.02, 24.76, 23.26. **MS-APCI Calculated**: $C_{20}H_{22}N_2O_3S$ $[M+H]^+$: 370.5, Found: 370.5 m/z

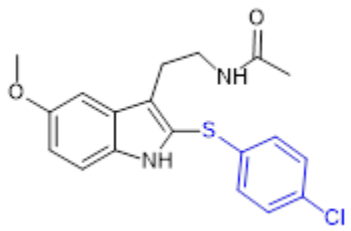

Figure 3.5.26 Product 3.27a

***N*-(2-(2-((4-chlorophenyl)thio)-5-methoxy-1H-indol-3-yl)ethyl)acetamide**: Compound was synthesized using the general procedures **V** for the synthesis of substituted indoles. **Yields** (.107 mmol scale): 11.4 mg, 30%, brown solid. **^{1}H NMR (400 MHz, $CDCl_3$)** δ = 8.03 (s, 1H), 7.24 (d, *J* = 8.1 Hz, 1H), 7.19 (d, *J* = 6.4 Hz, 2H), 7.08 (d, *J* = 2.4 Hz, 1H), 6.93-6.98 (m, 3H), 5.47 (s, 1H), 3.88 (s, 3H), 3.52 (q, *J* = 6.3 Hz, 2H), 3.04 (t, *J* = 6.4 Hz, 2H), 1.84 (s, 3H). **^{13}C NMR (126 MHz, $CDCl_3$)** δ = 155.90, 138.11, 135.44, 133.60, 132.72, 132.61, 129.96, 128.61, 128.48, 126.97, 125.96, 123.24, 119.55, 109.76, 30.06, 28.41, 20.89. **MS-APCI Calculated:** $C_{19}H_{19}ClN_2O_2S$ $[M+H]^+$: 375.9, Found: 376.0 m/z

3.5.6 Spectral data for characterized molecules (^{1}H NMR, ^{13}C NMR, ^{19}F NMR)

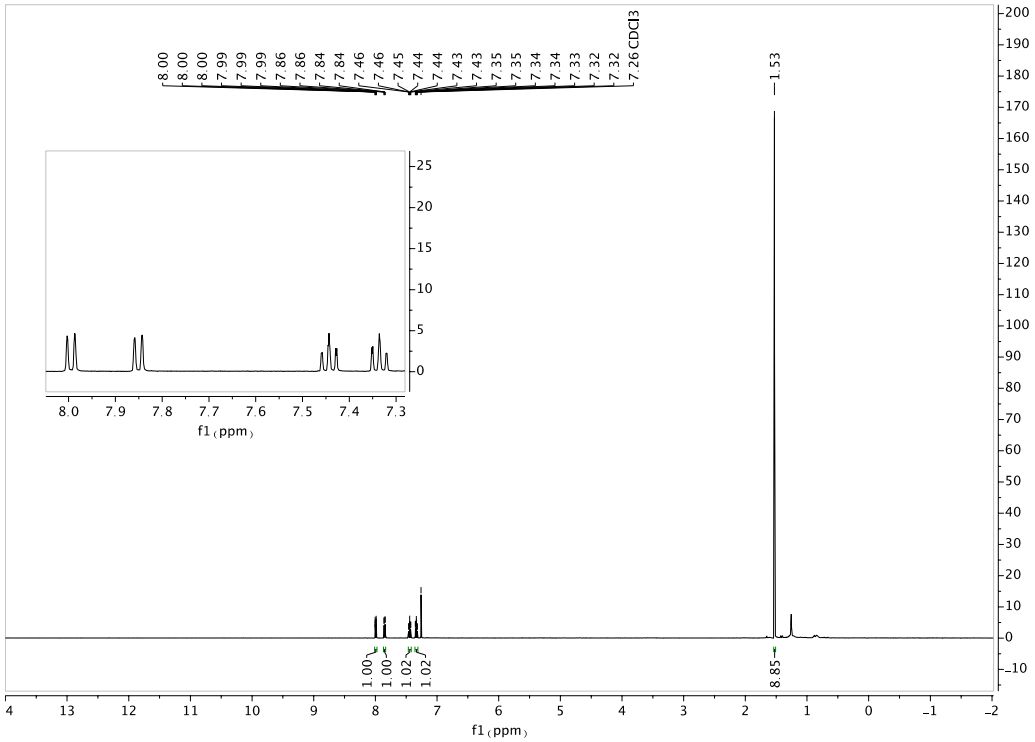

Figure 3.5.27 500 MHz ^{1}H NMR Spectrum of 3.1a

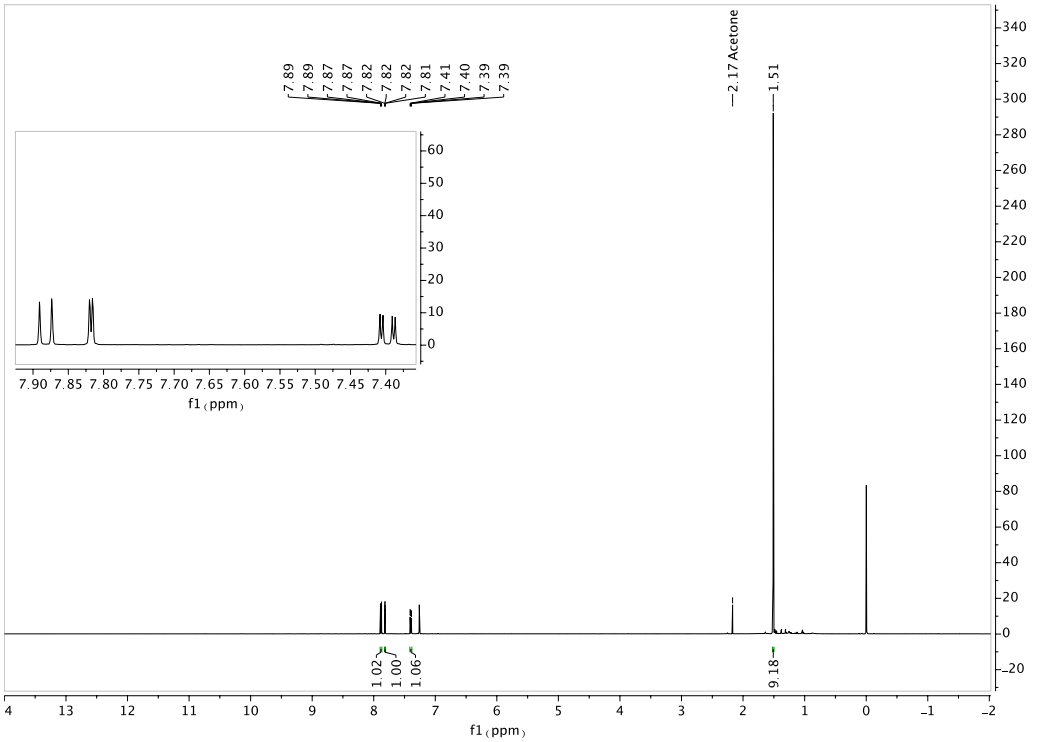

Figure 3.5.28 500 MHz ^{1}H NMR Spectrum of 3.2a

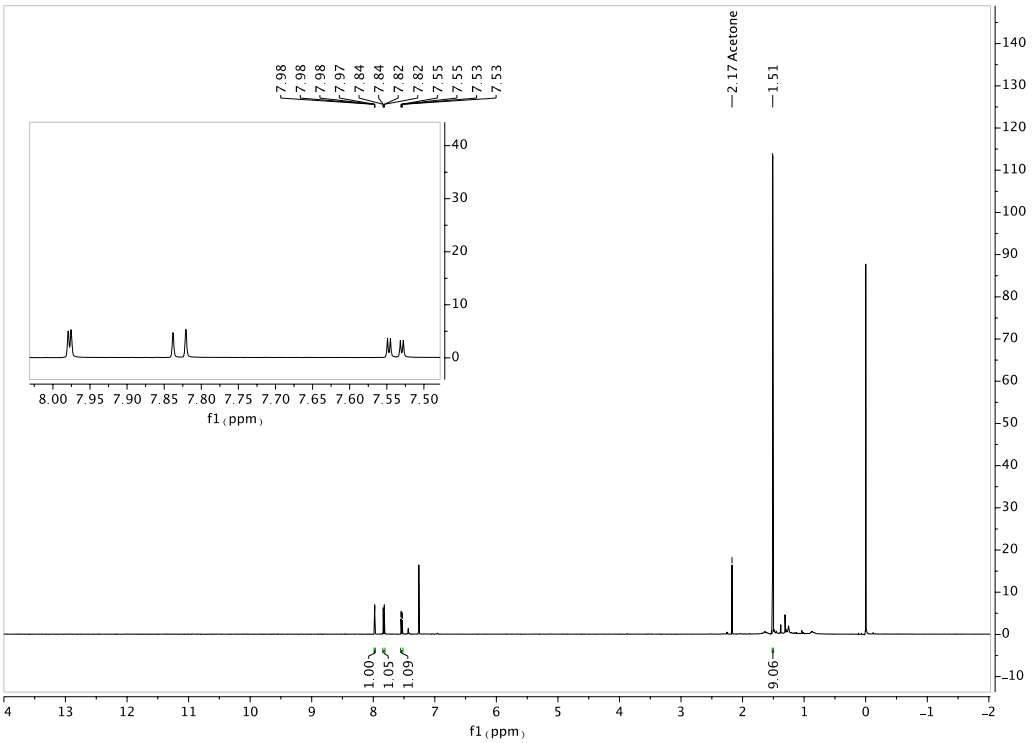

Figure 3.5.29 500 MHz ^{1}H NMR Spectrum of 3.3a

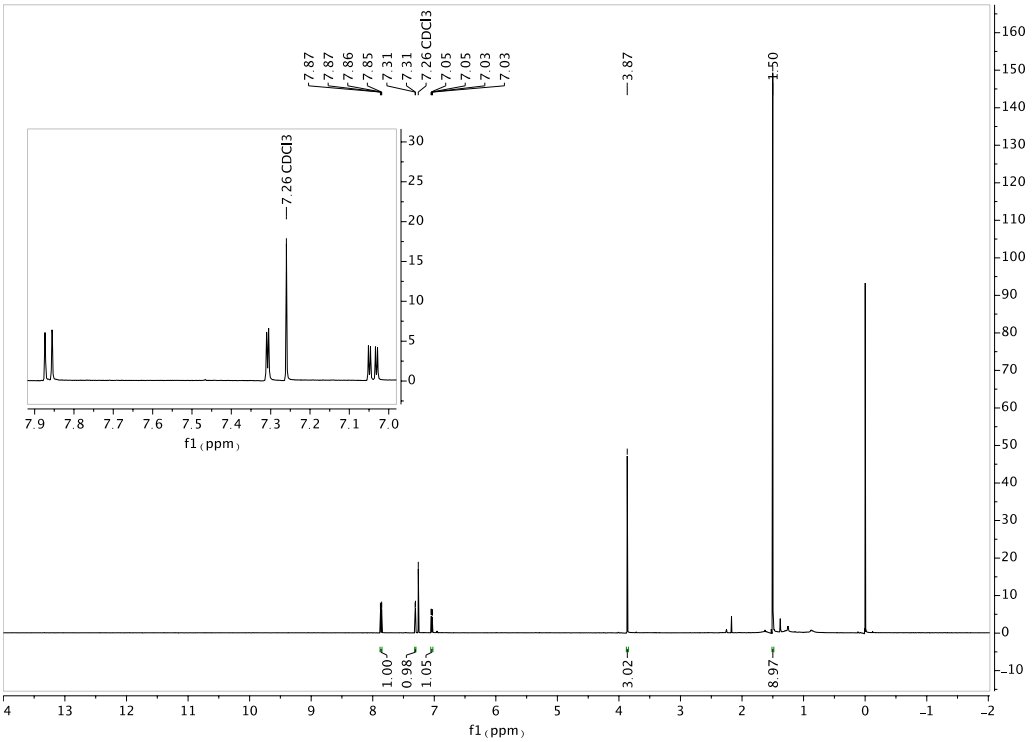

Figure 3.5.30 500 MHz ^{1}H NMR Spectrum of 3.4a

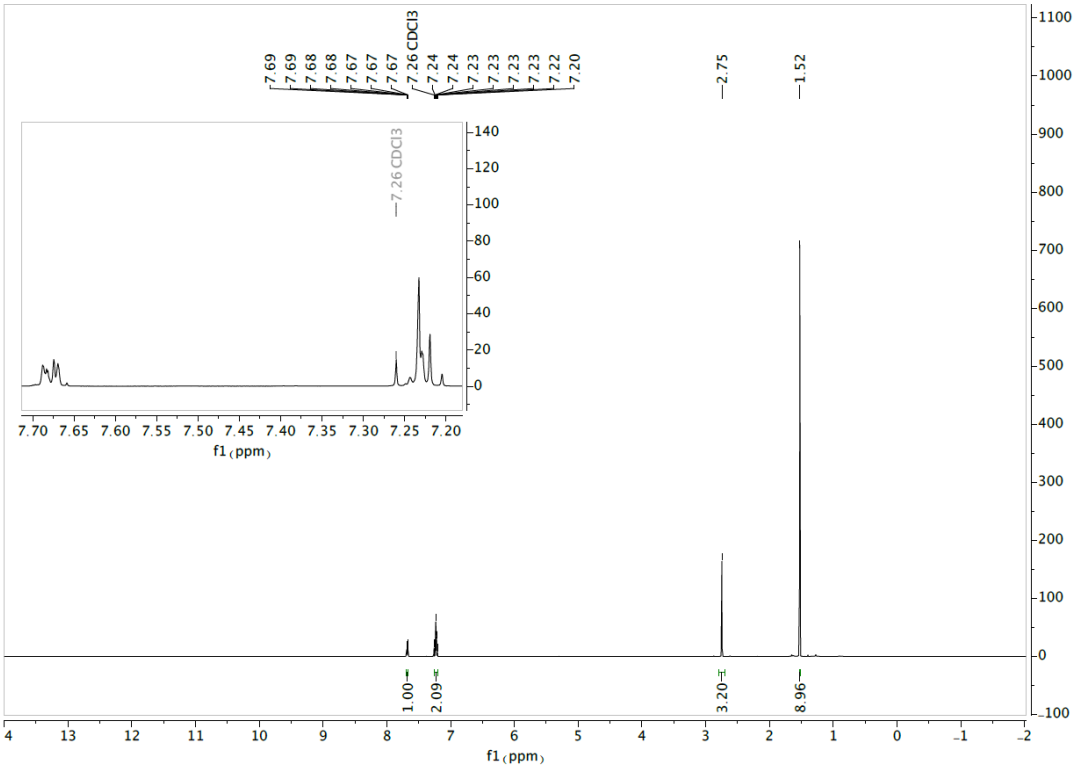

Figure 3.5.31 500 MHz ^{1}H NMR Spectrum of 3.5a

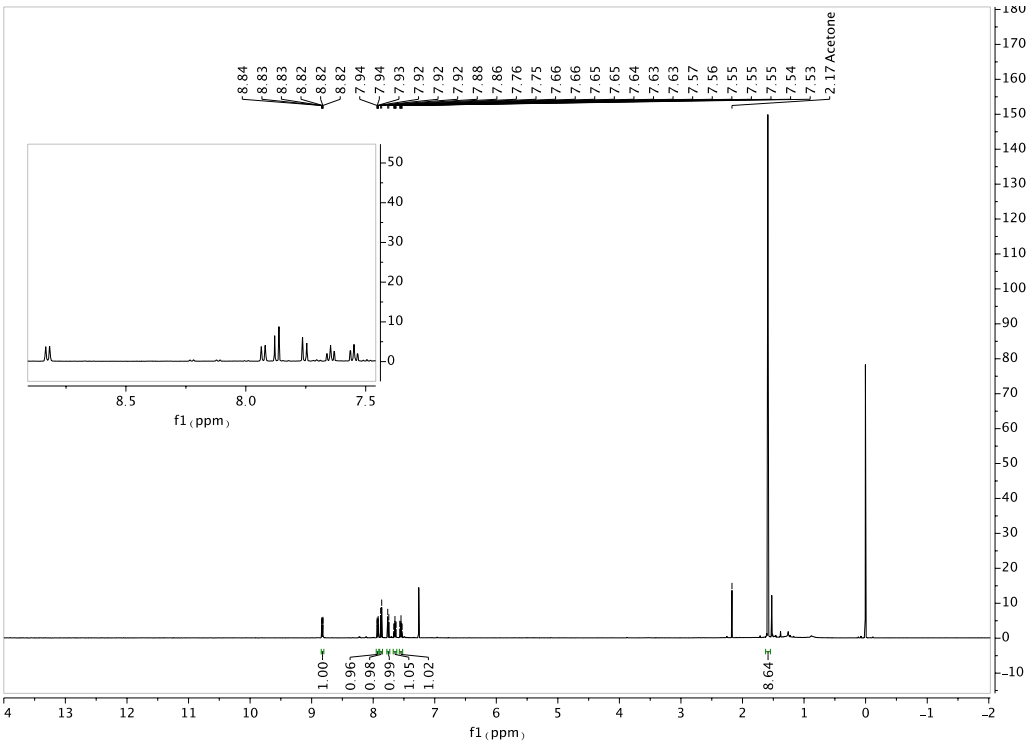

Figure 3.5.32 500 MHz ^{1}H NMR Spectrum of 3.6a

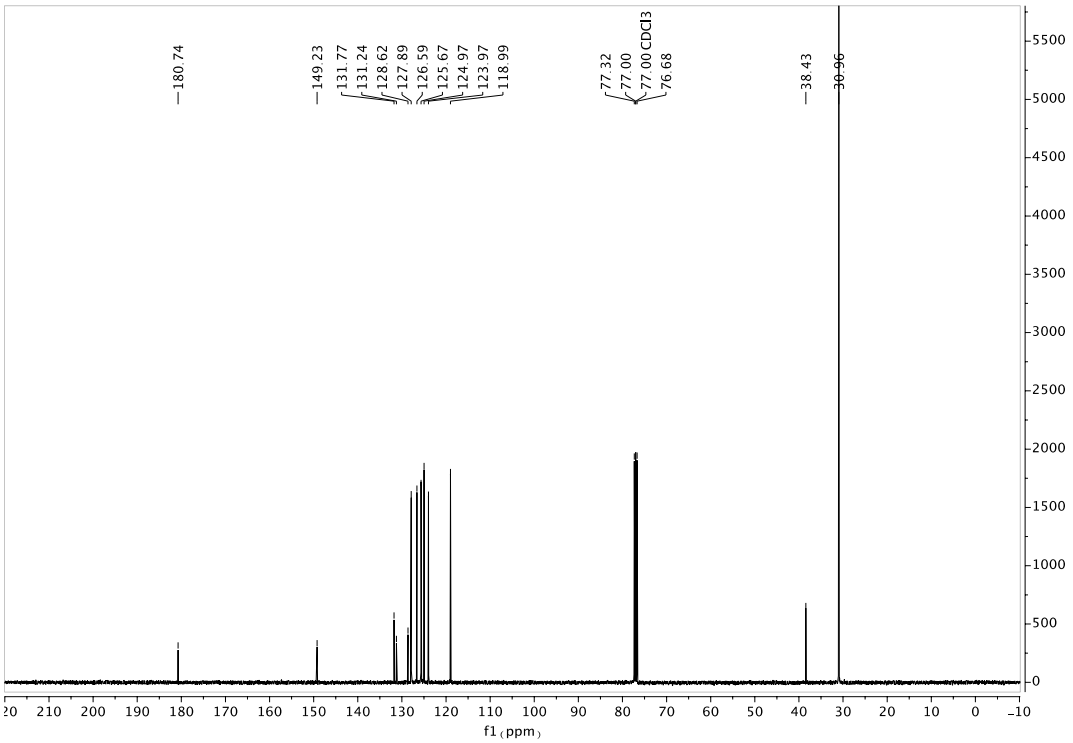

Figure 3.5.33 101 MHz ^{13}C NMR Spectrum of 3.6a

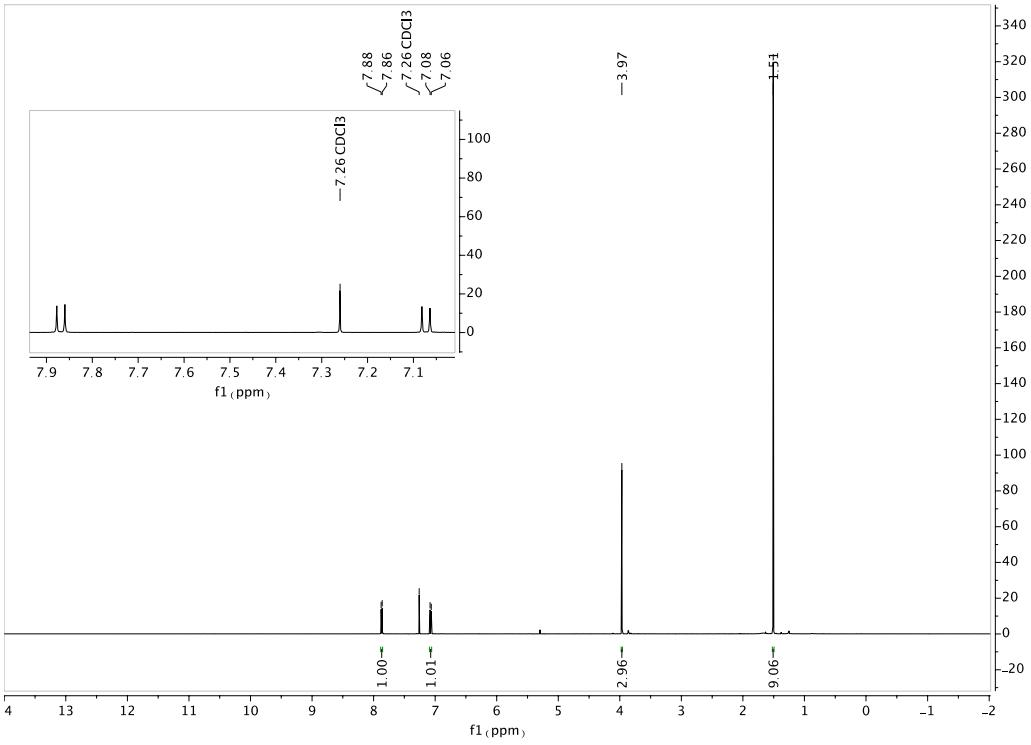

Figure 3.5.34 500 MHz ^{1}H NMR Spectrum of 3.7a

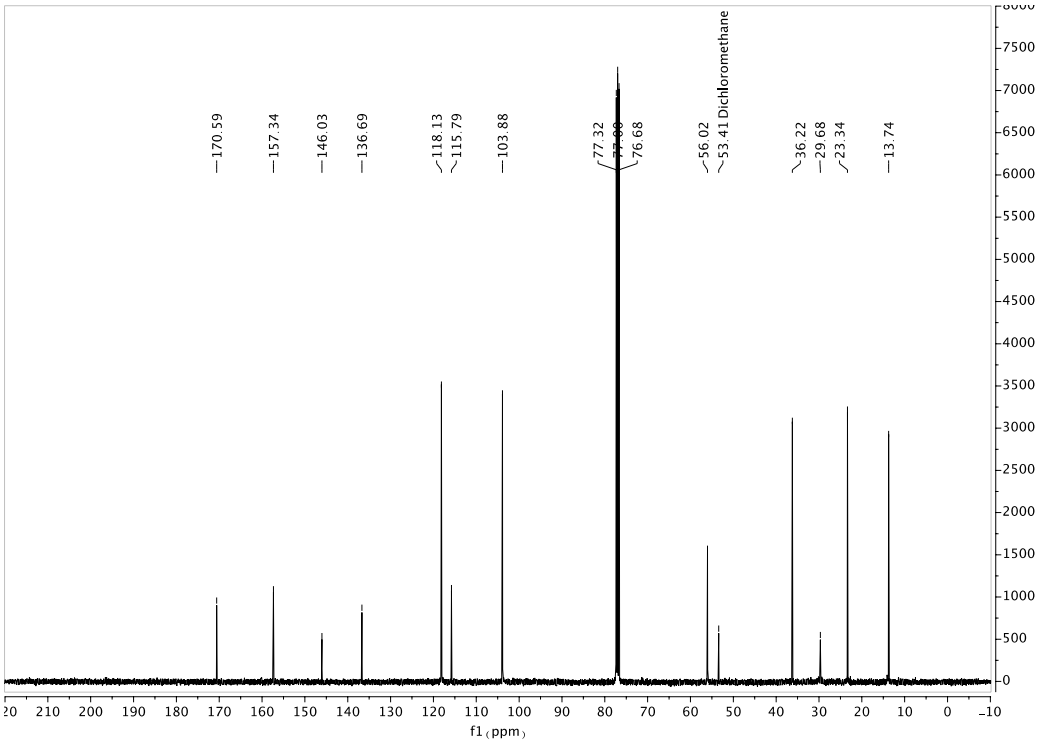

Figure 3.5.35 101 MHz ^{13}C NMR Spectrum of 3.7a

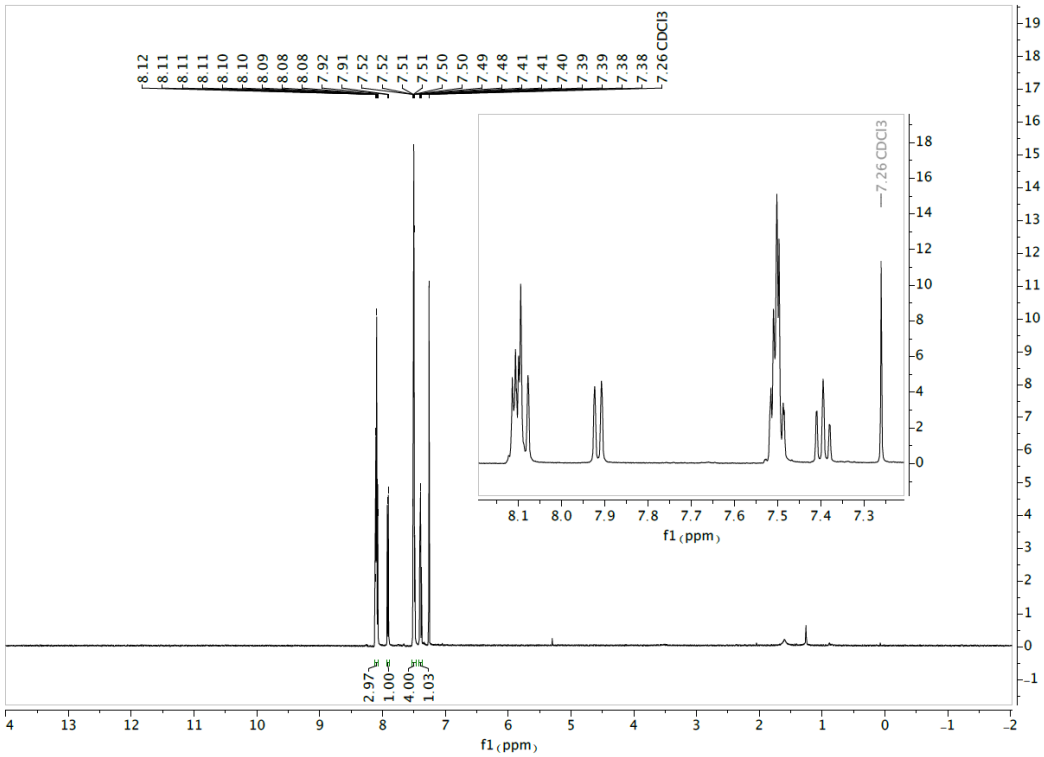

Figure 3.5.36 500 MHz ^{1}H NMR Spectrum of 3.8a

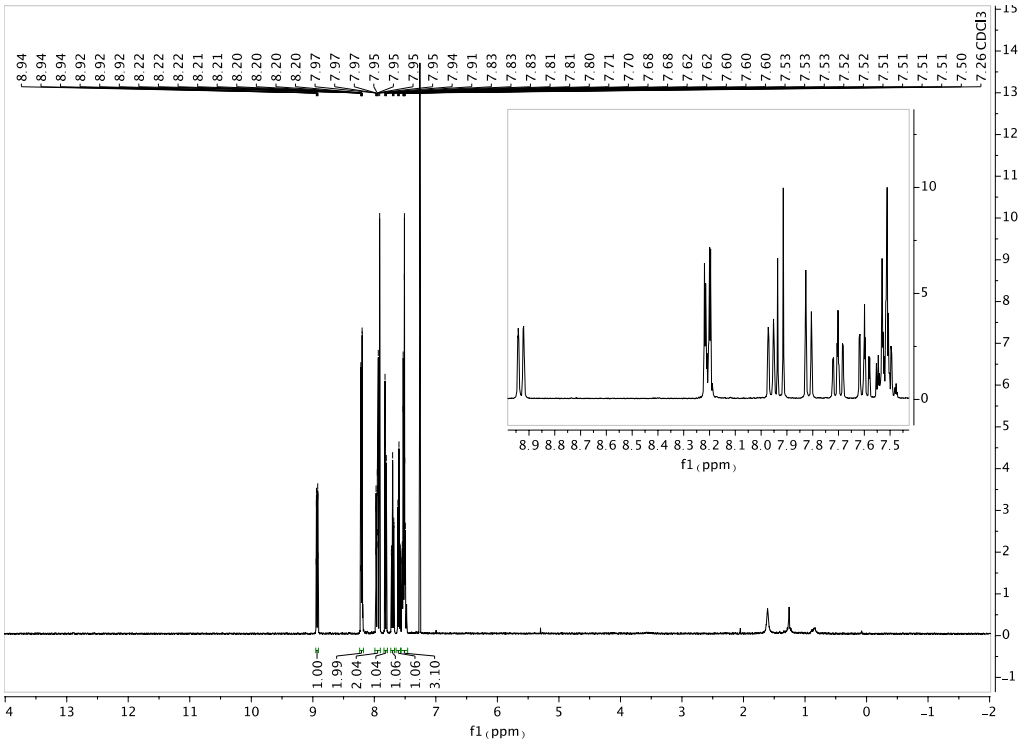

Figure 3.5.37 400 MHz ^{1}H NMR Spectrum of 3.9a

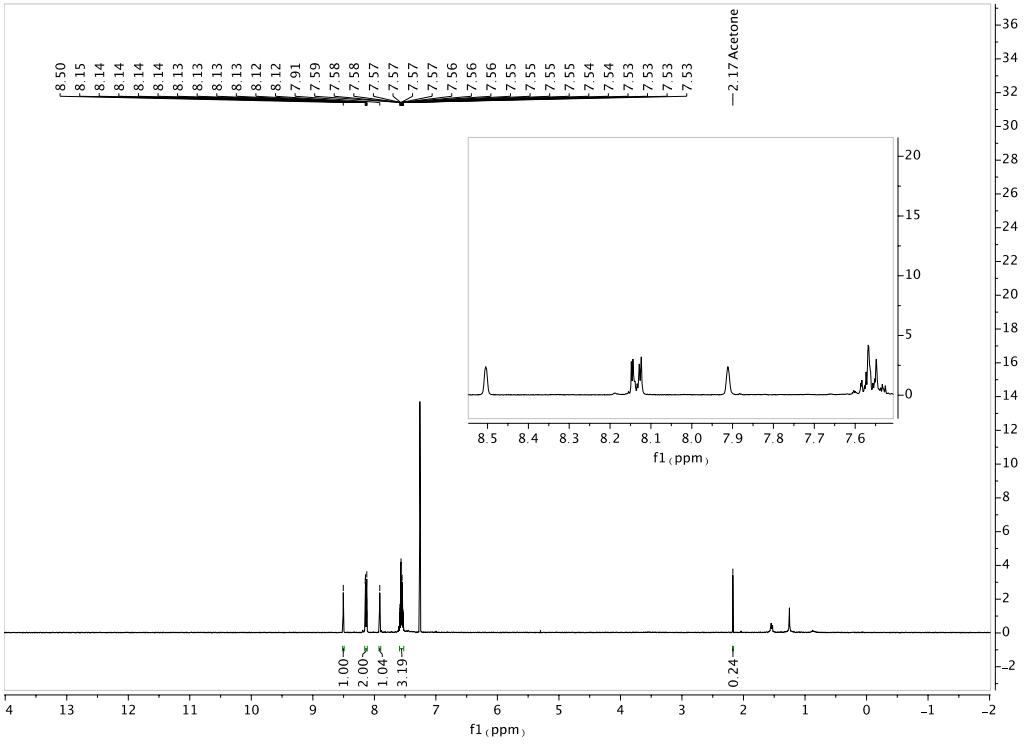

Figure 3.5.38 400 MHz ^{1}H NMR Spectrum of 3.10a

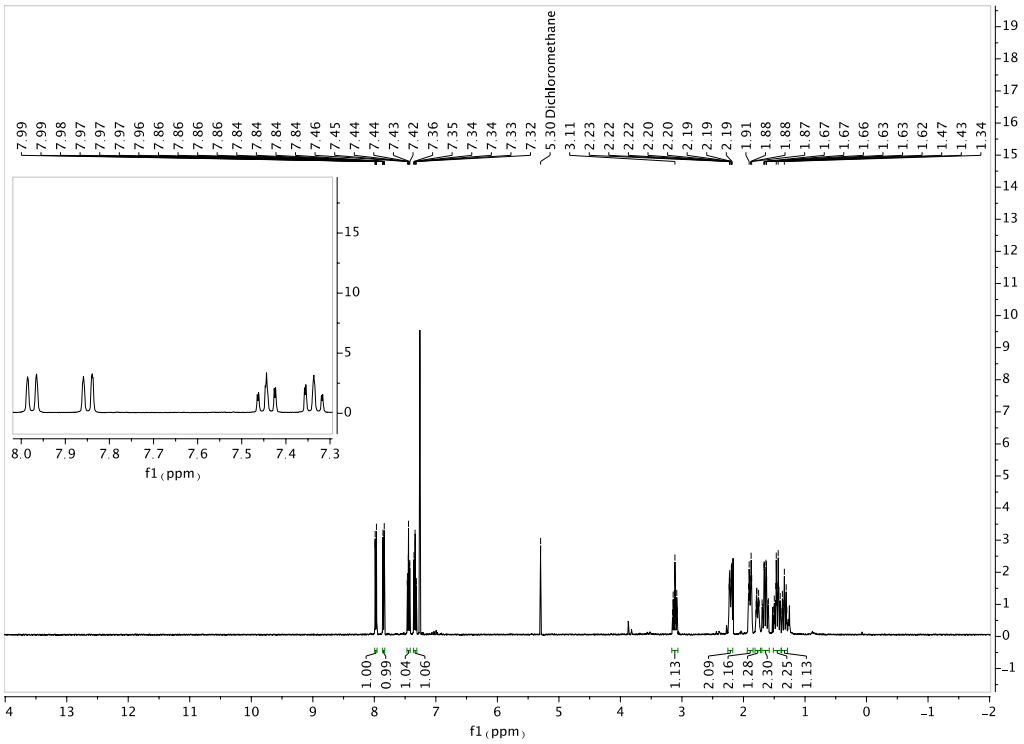

Figure 3.5.39 500 MHz ^{1}H NMR Spectrum of 3.11a

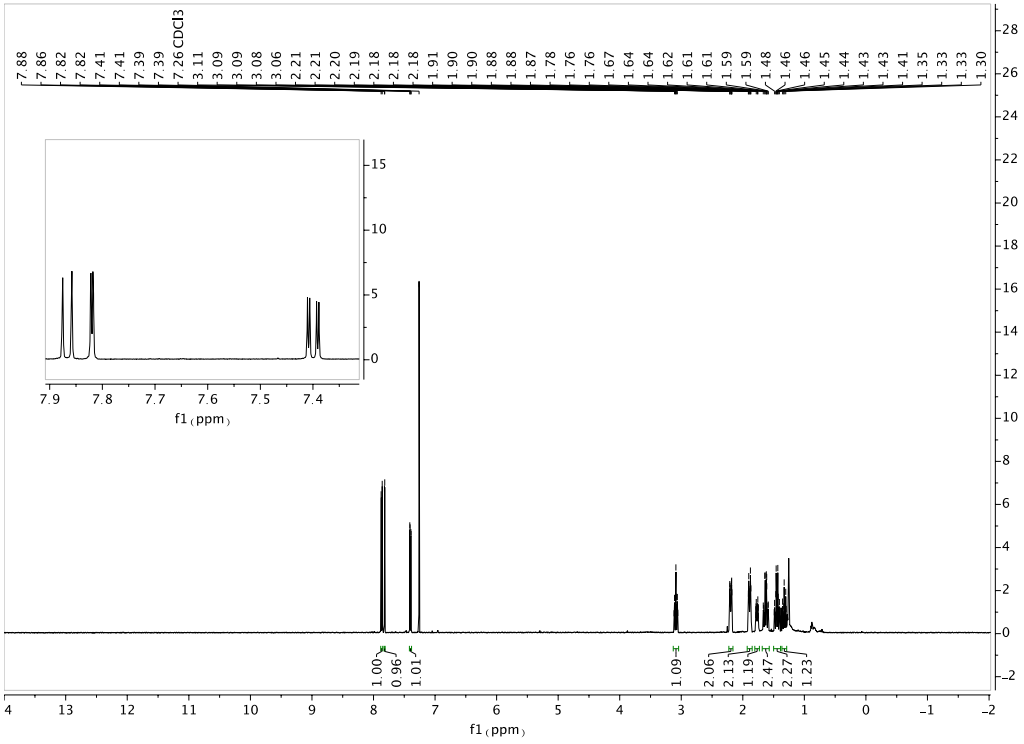

Figure 3.5.40 500 MHz ^{1}H NMR Spectrum of 3.12a

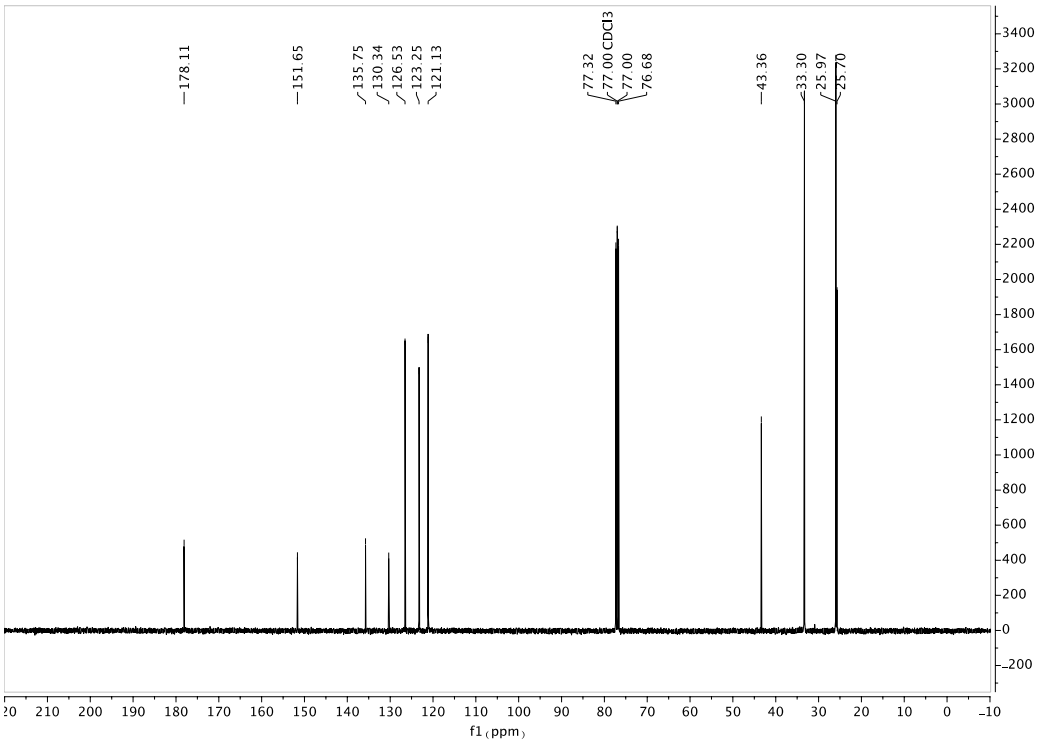

Figure 3.5.41 101 MHz ^{13}C NMR Spectrum of 3.12a

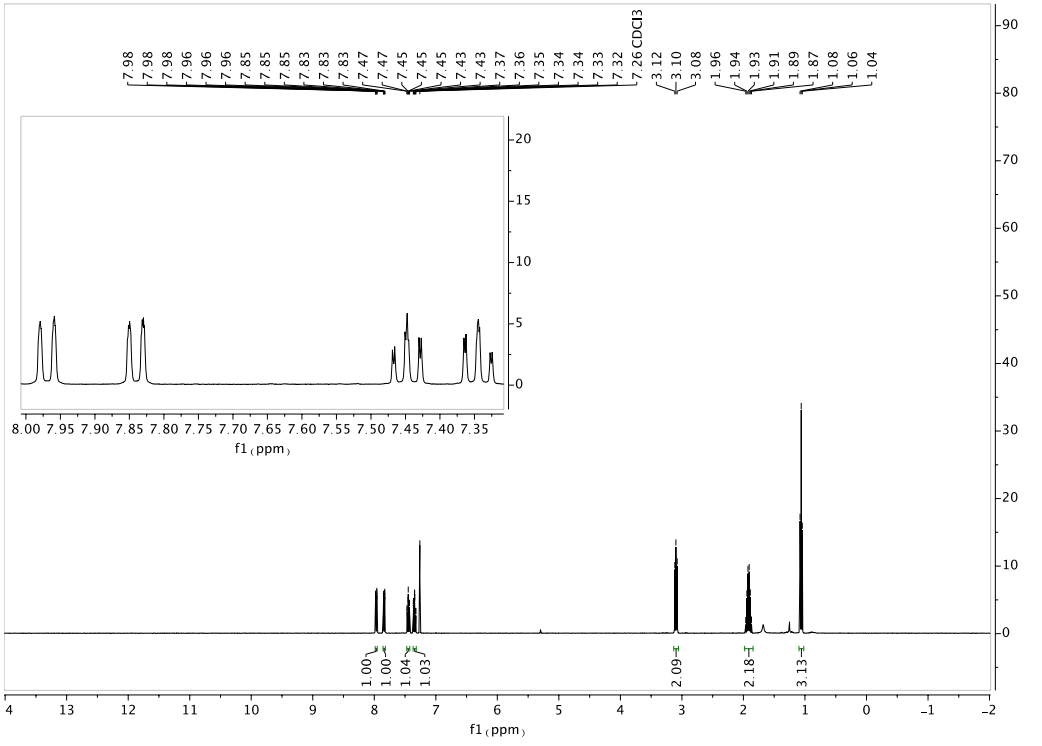

Figure 3.5.42 500 MHz ^{1}H NMR Spectrum of 3.13a

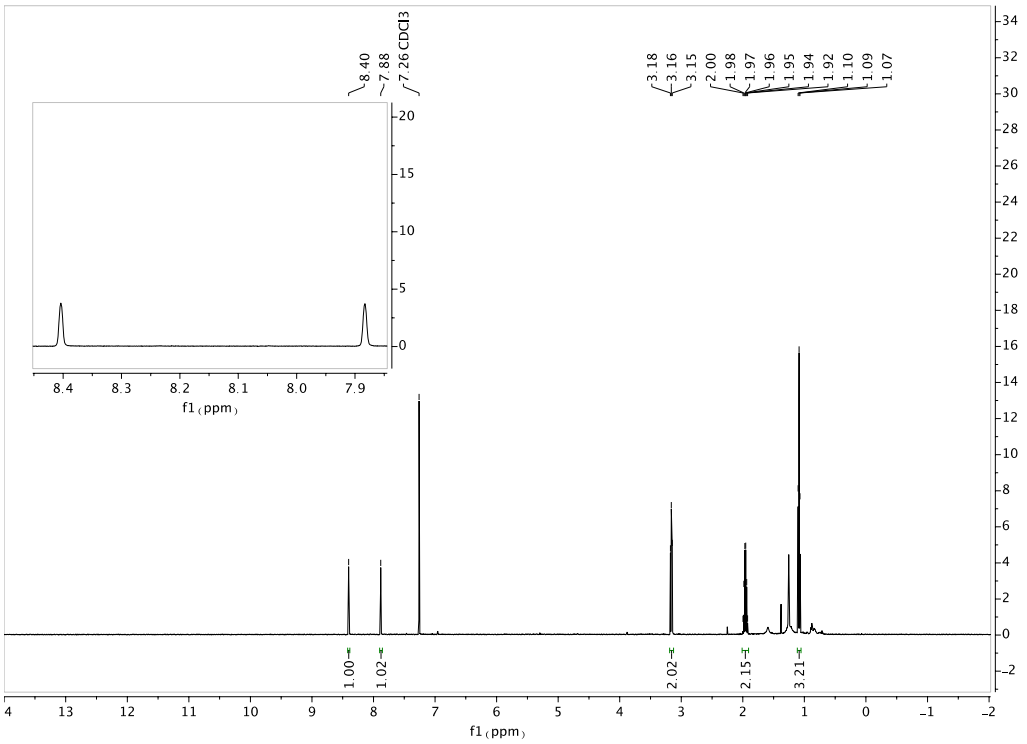

Figure 3.5.43 500 MHz ^{1}H NMR Spectrum of 3.14a

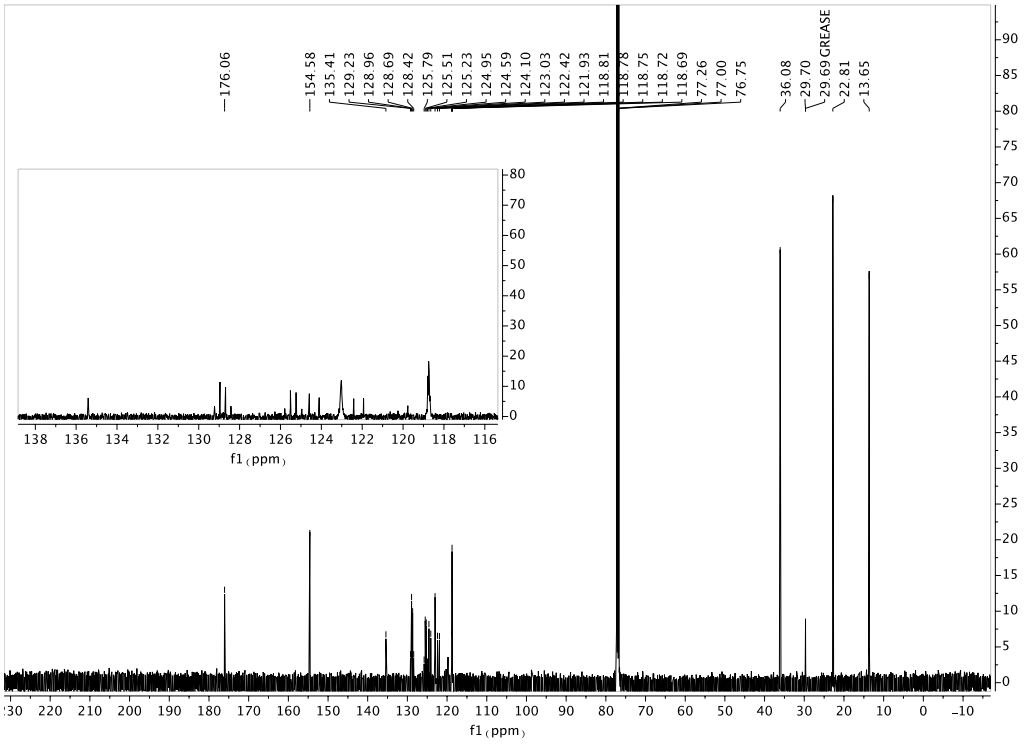

Figure 3.5.44 126 MHz ^{13}C NMR Spectrum of 3.14a

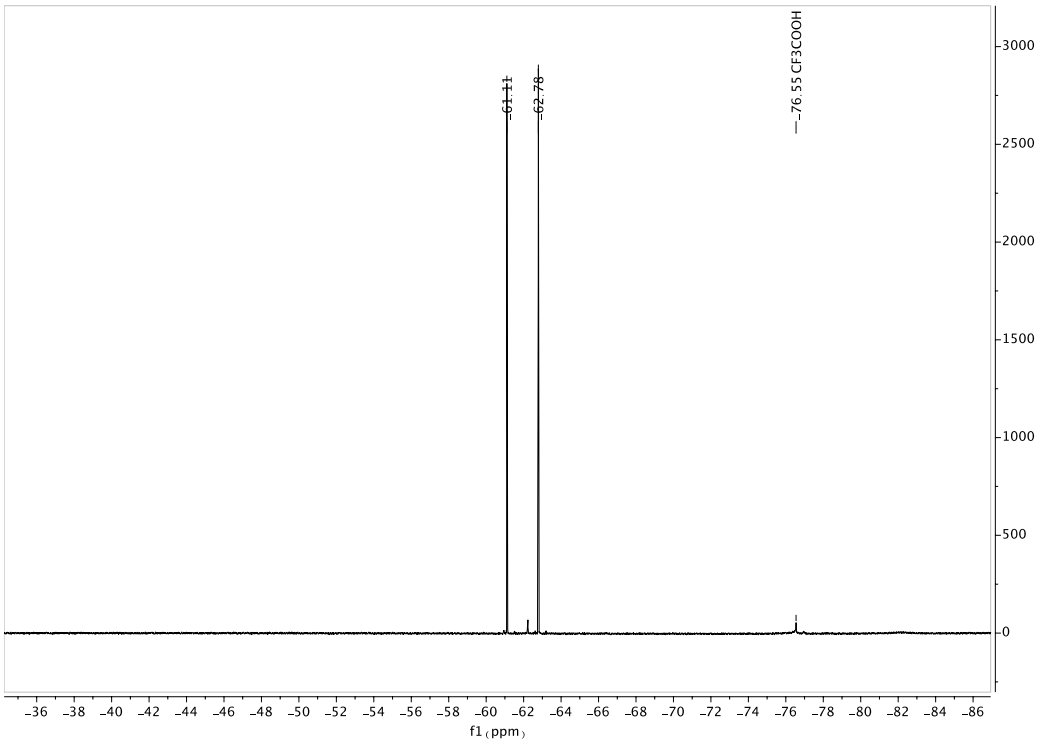

Figure 3.5.45 470 MHz ^{19}F NMR Spectrum of 3.14a

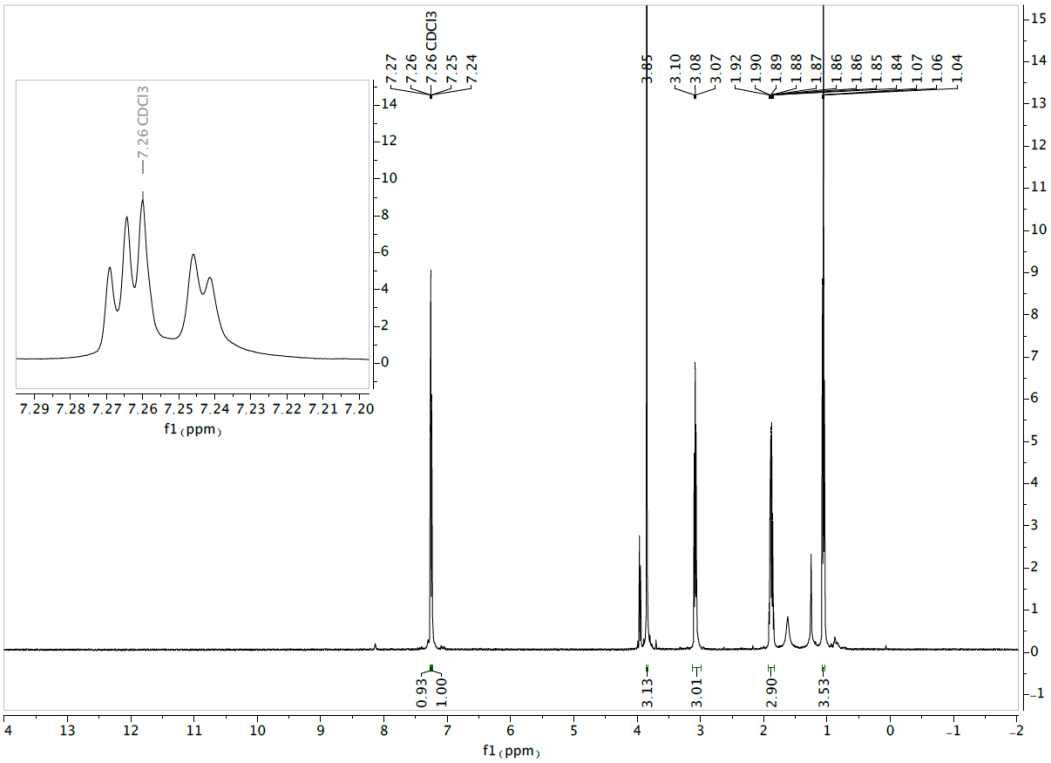

Figure 3.5.46 500 MHz ^{1}H NMR Spectrum of 3.15a

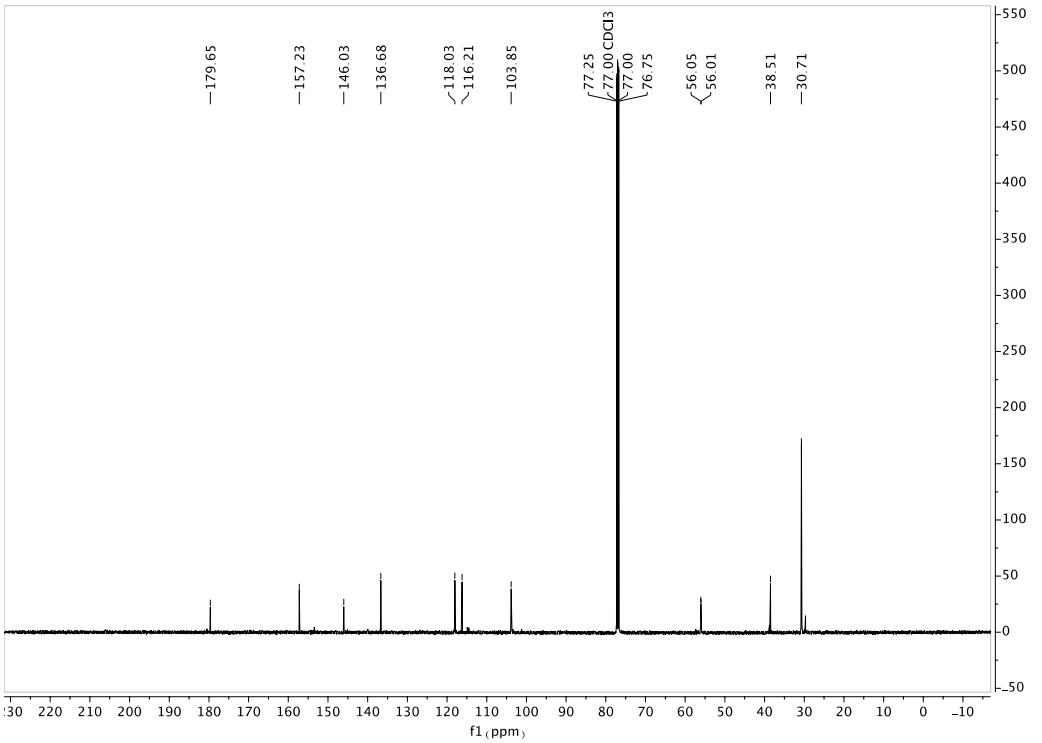

Figure 3.5.47 126 MHz ^{13}C NMR Spectrum of 3.15a

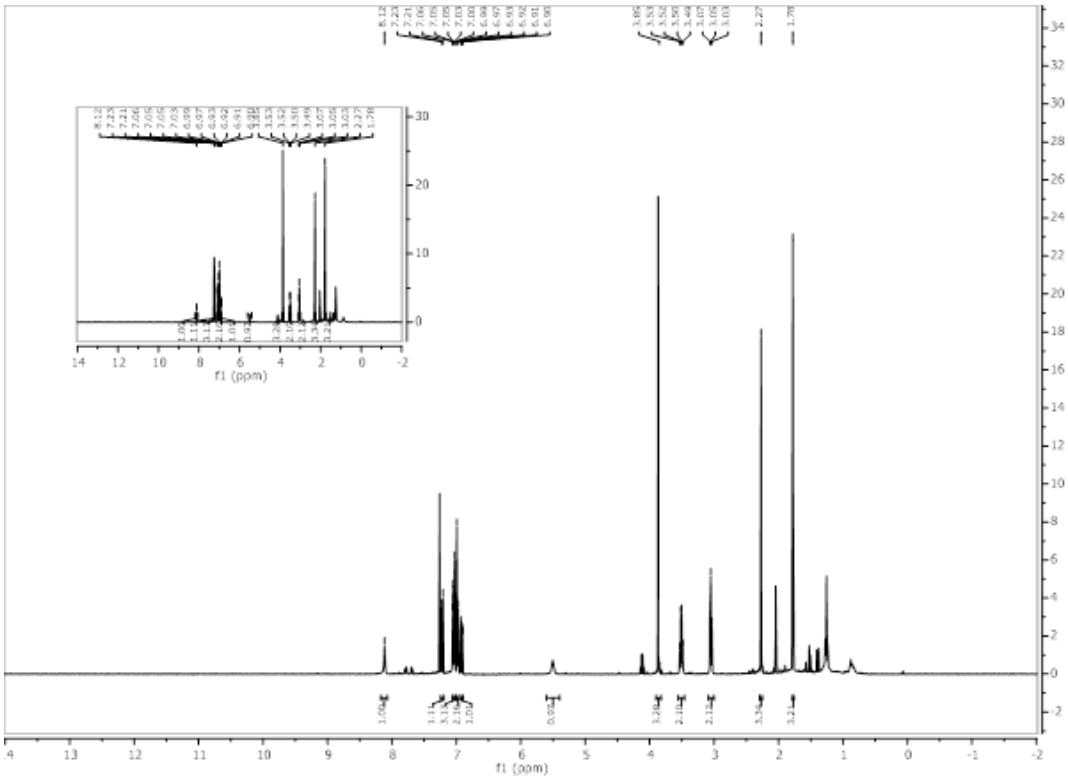

Figure 3.5.48 400 MHz ^{1}H NMR Spectrum of 3.18a

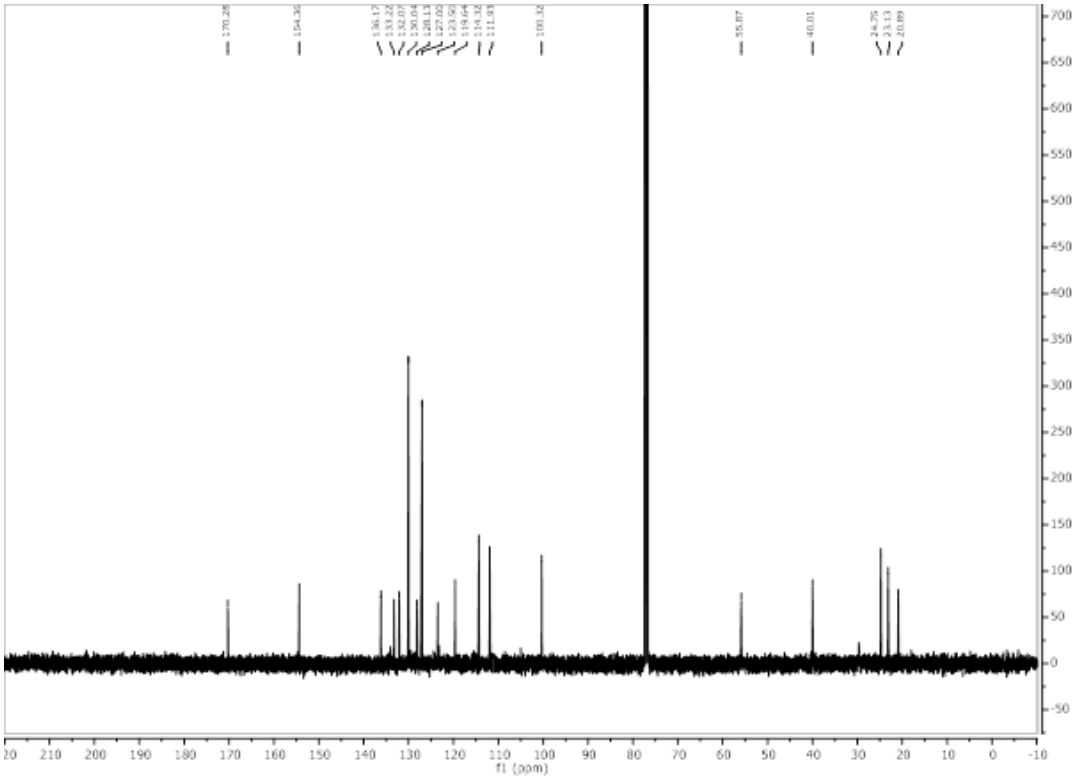

Figure 3.5.49 126 MHz ^{13}C NMR Spectrum of 3.18a

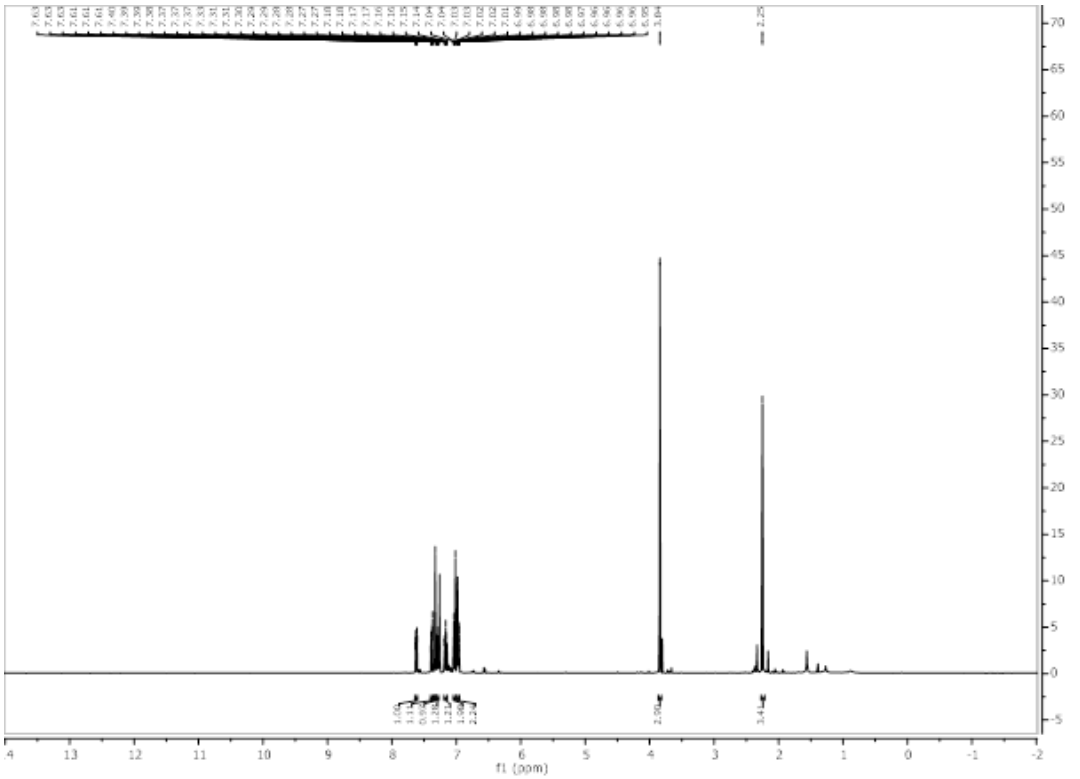

Figure 3.5.50 400 MHz ^{1}H NMR Spectrum of 3.19a

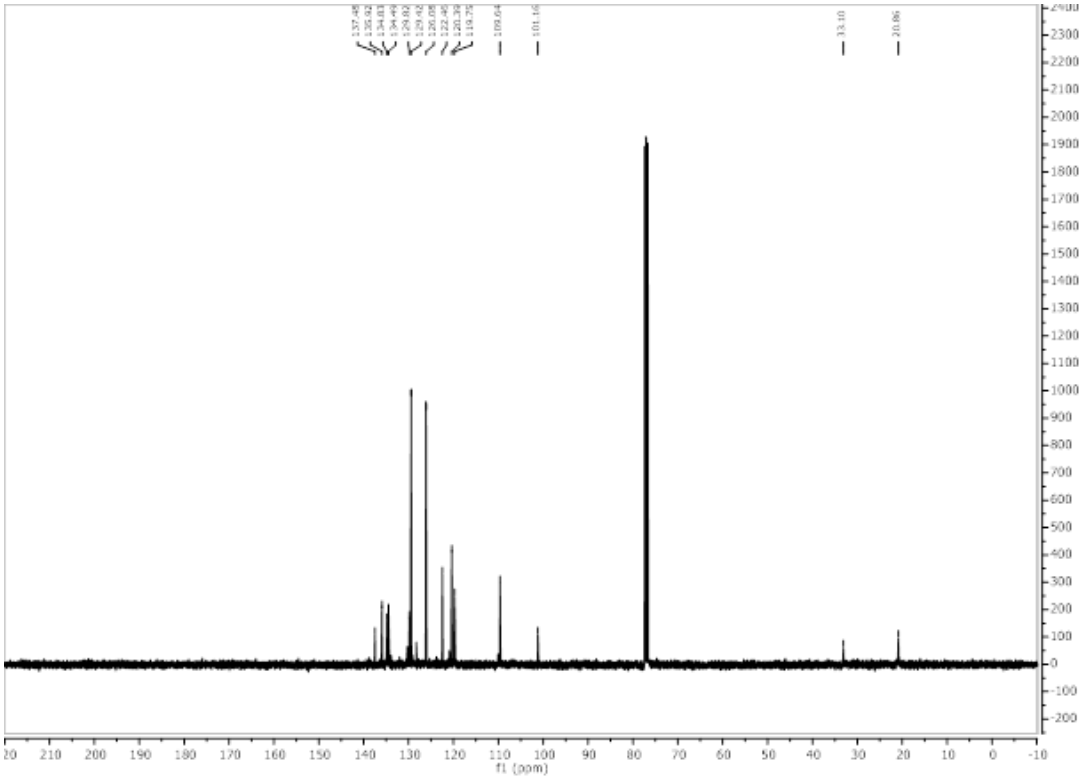

Figure 3.5.51 126 MHz ^{13}C NMR Spectrum of 3.19a

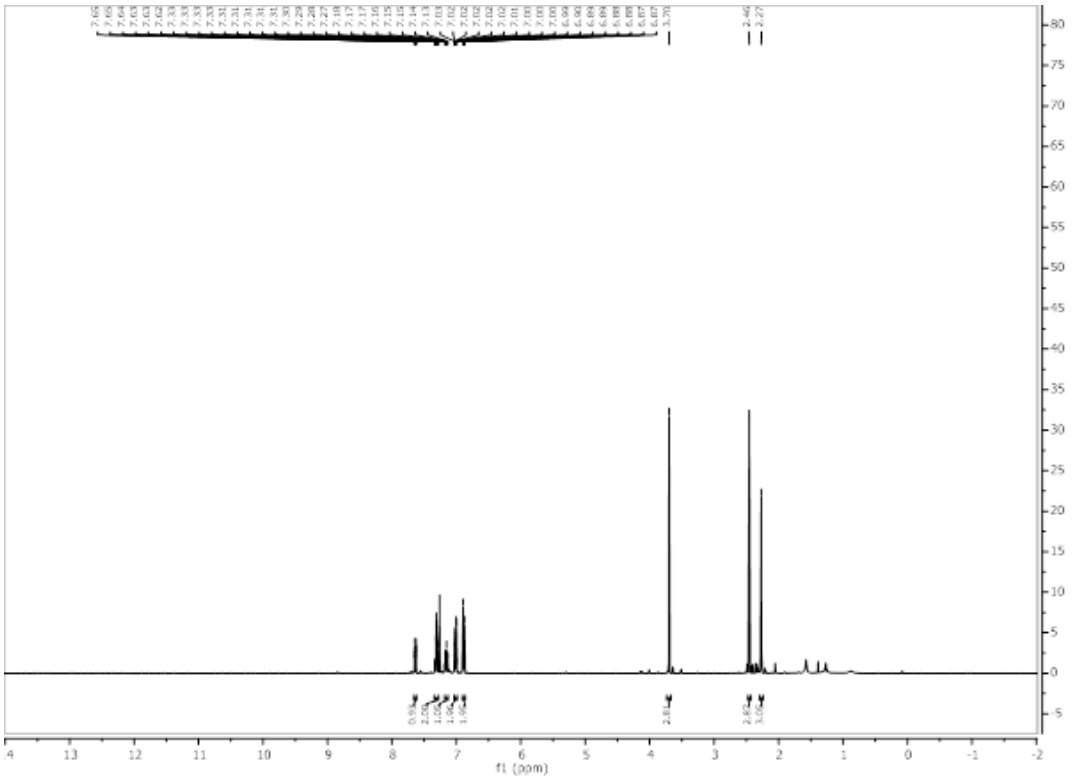

Figure 3.5.52 400 MHz ^{1}H NMR Spectrum of 3.20a

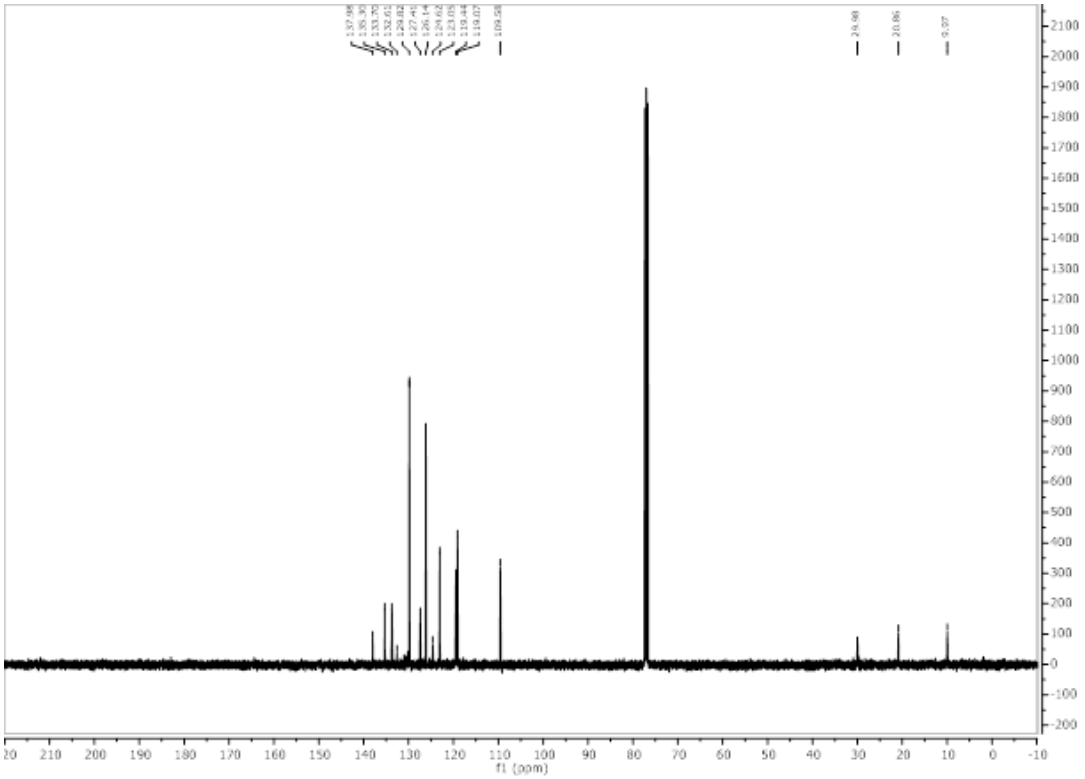

Figure 3.5.53 126 MHz ^{13}C NMR Spectrum of 3.20a

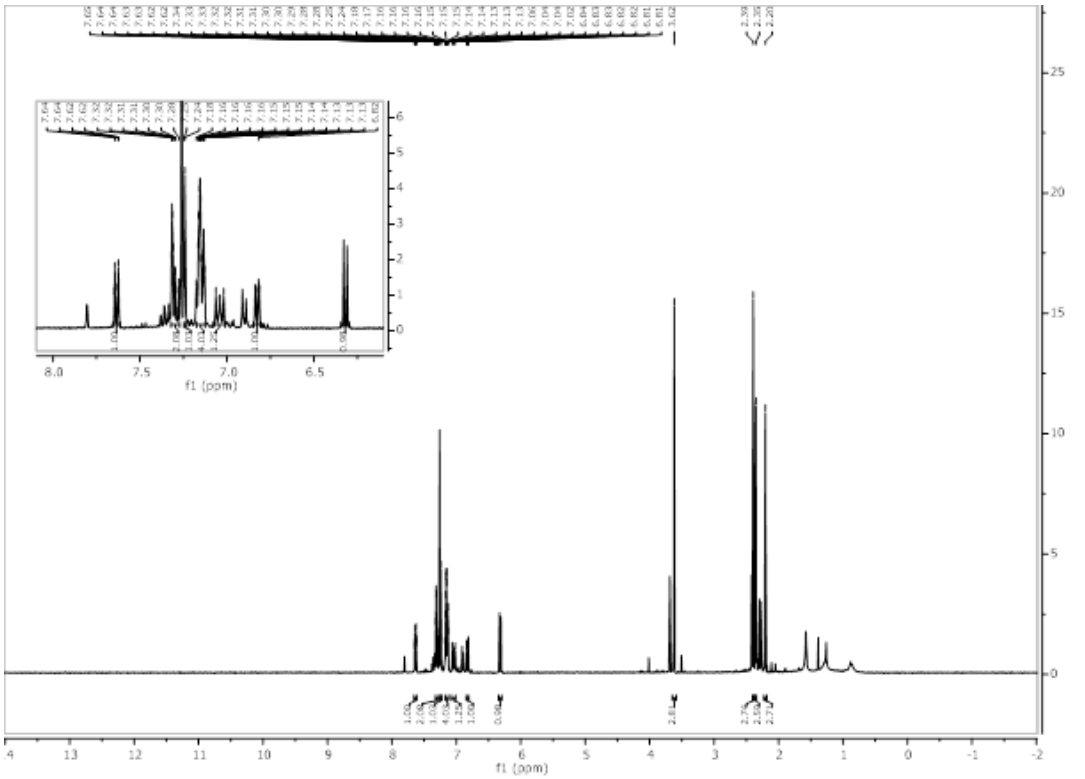

Figure 3.5.54 400 MHz ^{1}H NMR Spectrum of 3.20b

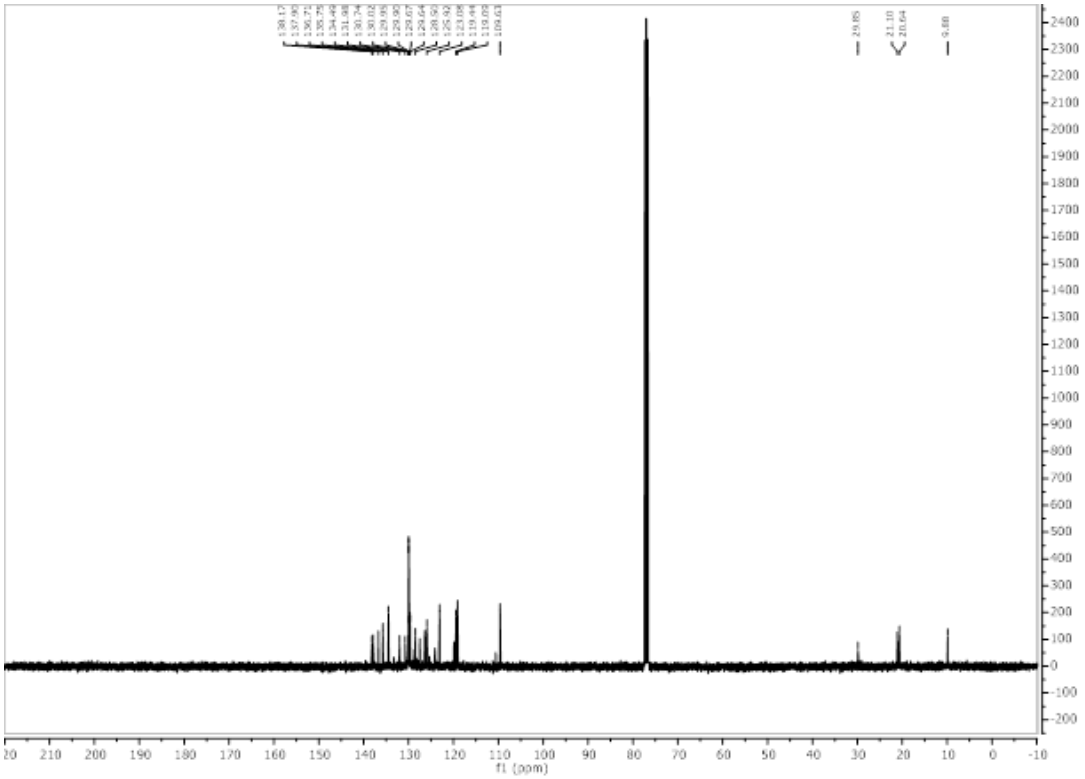

Figure 3.5.55 126 MHz ^{13}C NMR Spectrum of 3.20b

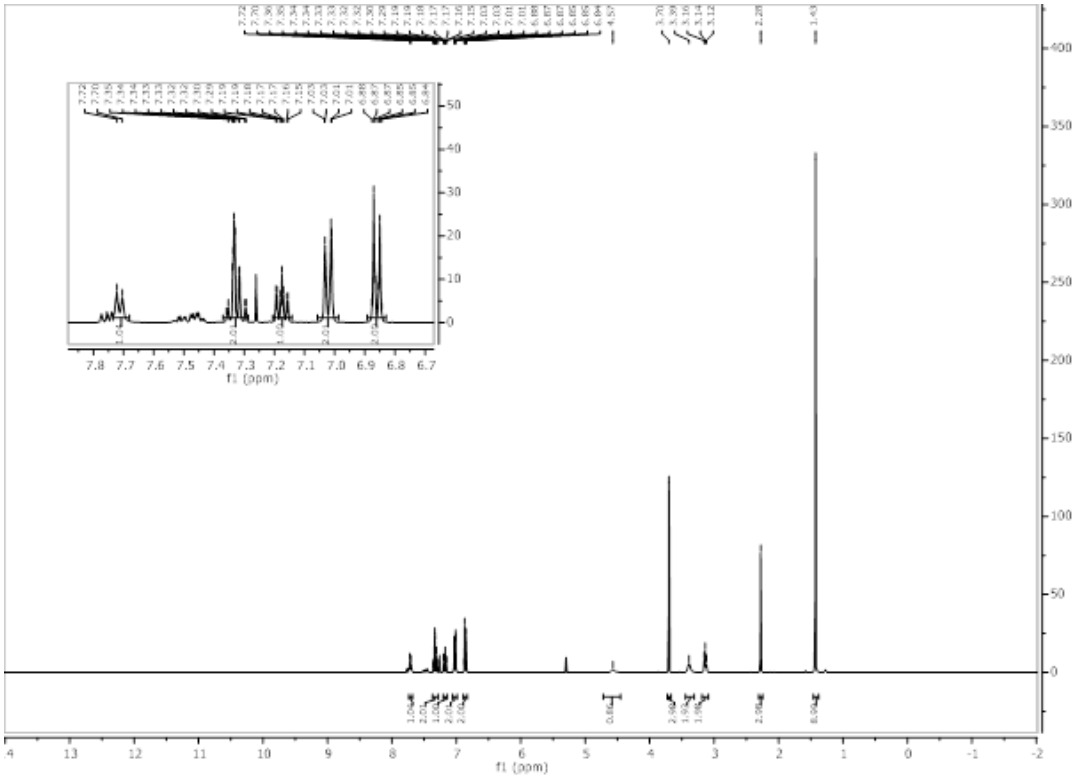

Figure 3.5.56 400 MHz ^{1}H NMR Spectrum of 3.21a

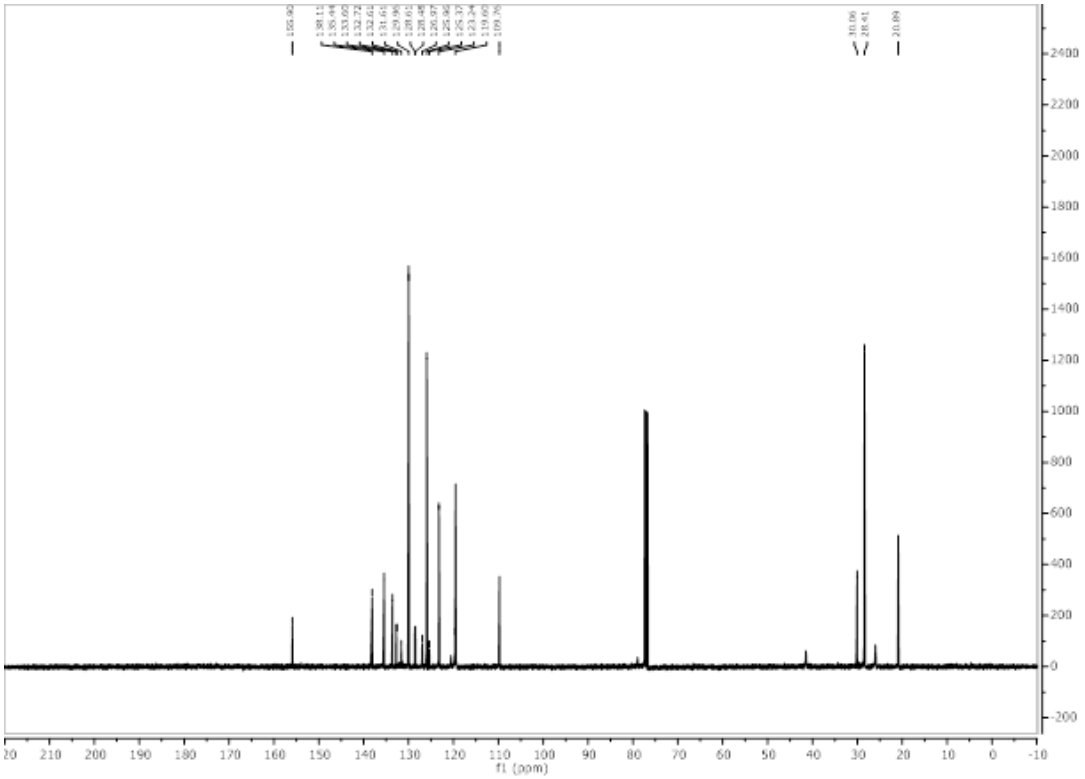

Figure 3.5.57 126 MHz ^{13}C NMR Spectrum of 3.21a

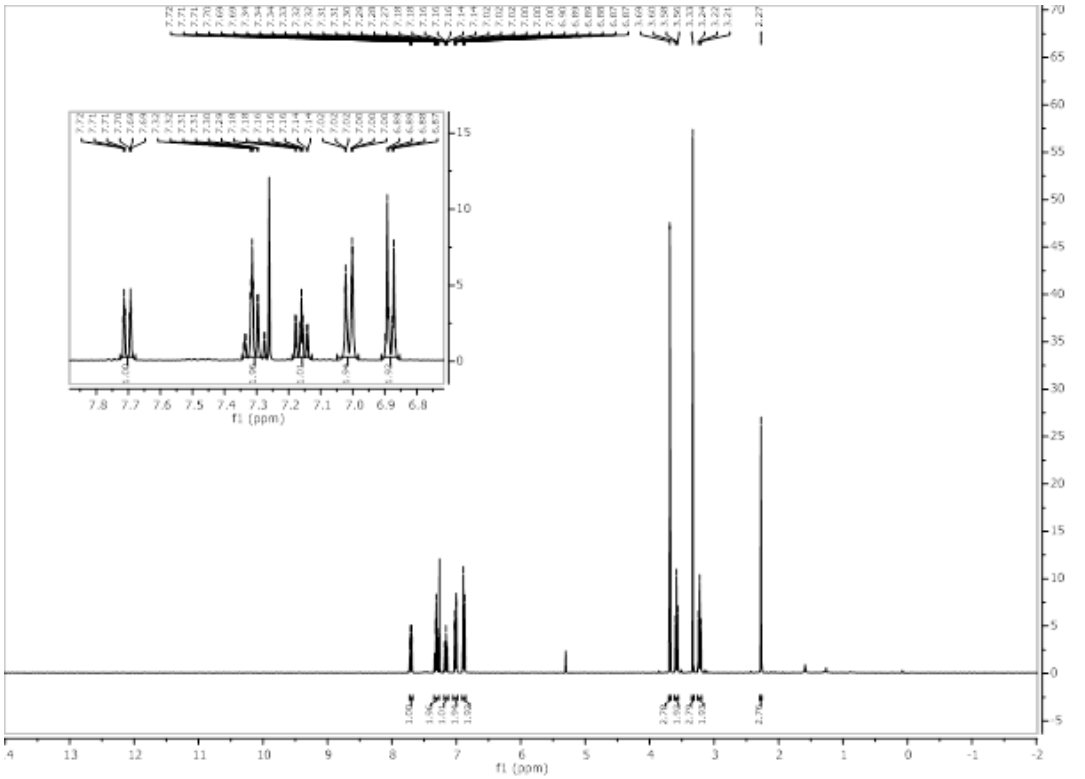

Figure 3.5.58 400 MHz ^{1}H NMR Spectrum of 3.22a

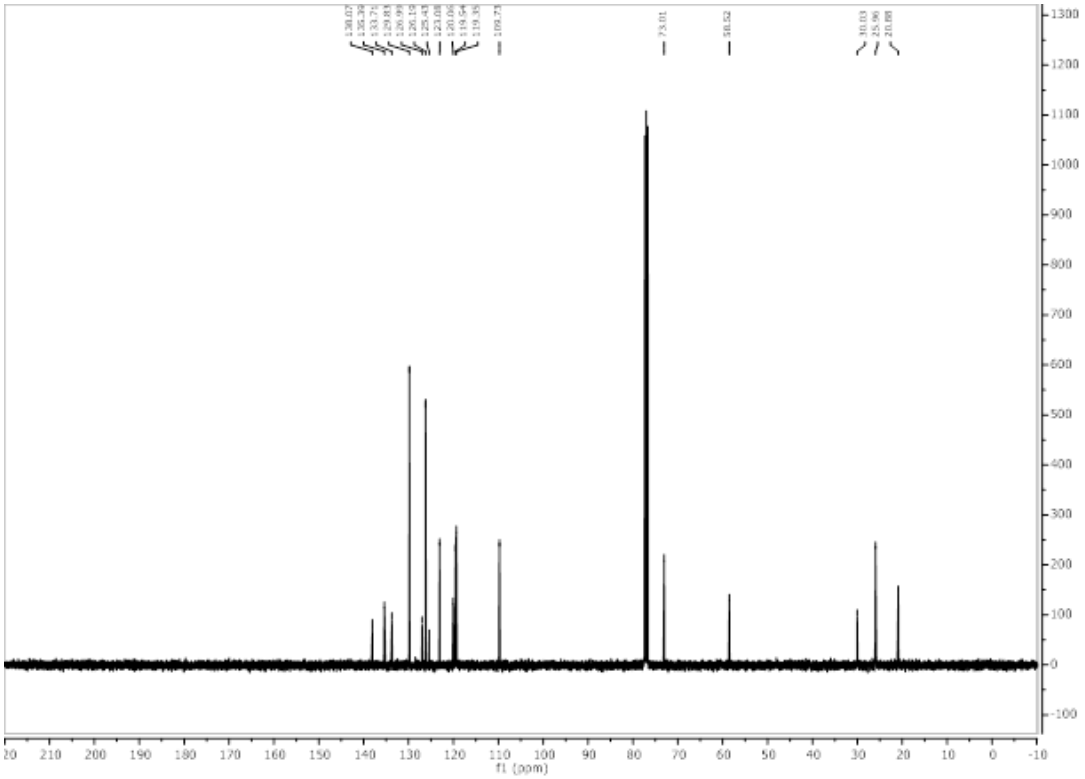

Figure 3.5.59 126 MHz ^{13}C NMR Spectrum of 3.22a

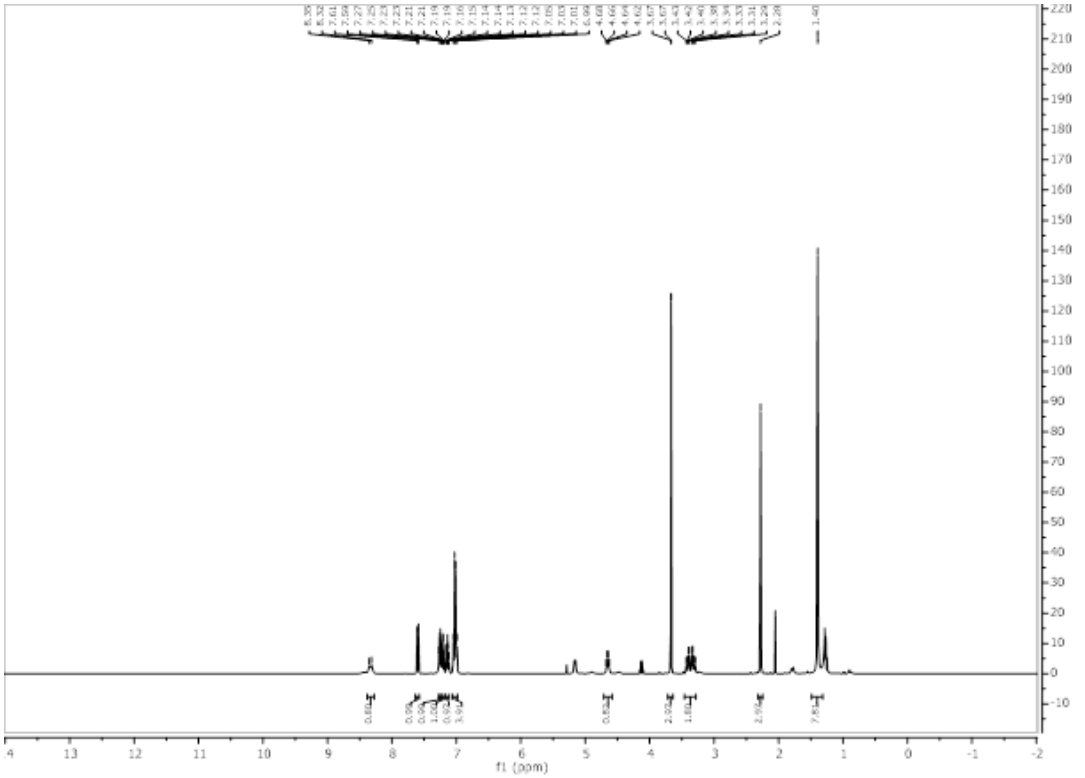

Figure 3.5.60 400 MHz ^{1}H NMR Spectrum of 3.23a

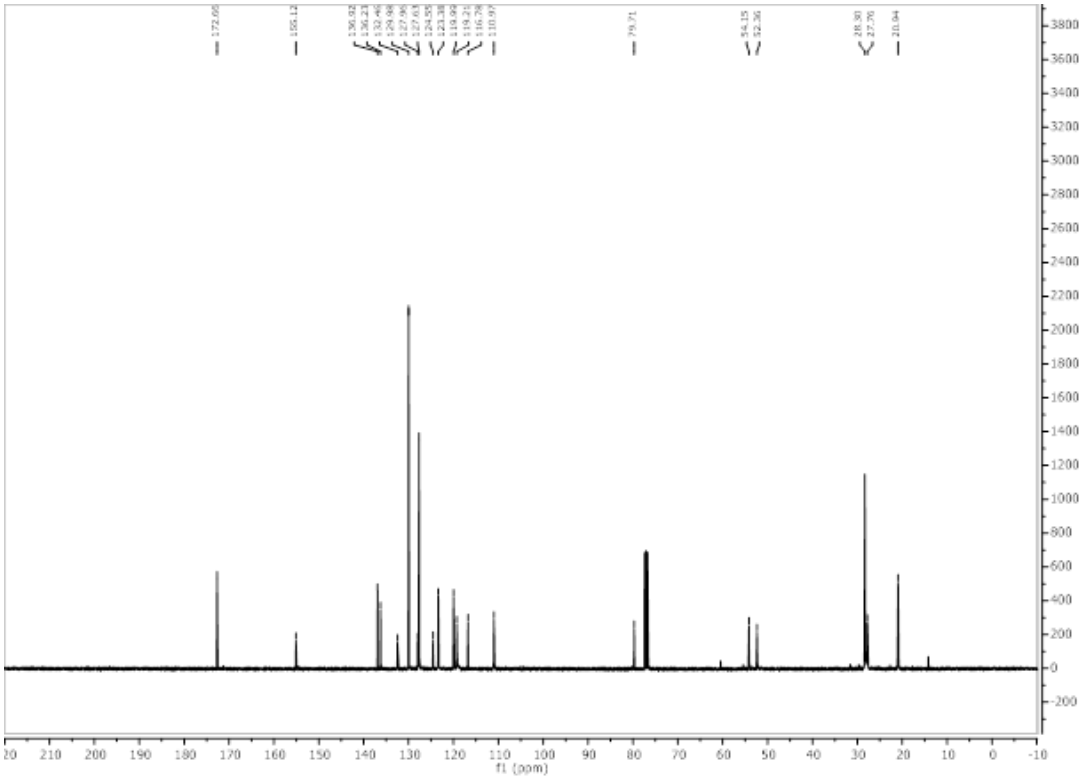

Figure 3.5.61 126 MHz ^{13}C NMR Spectrum of 3.23a

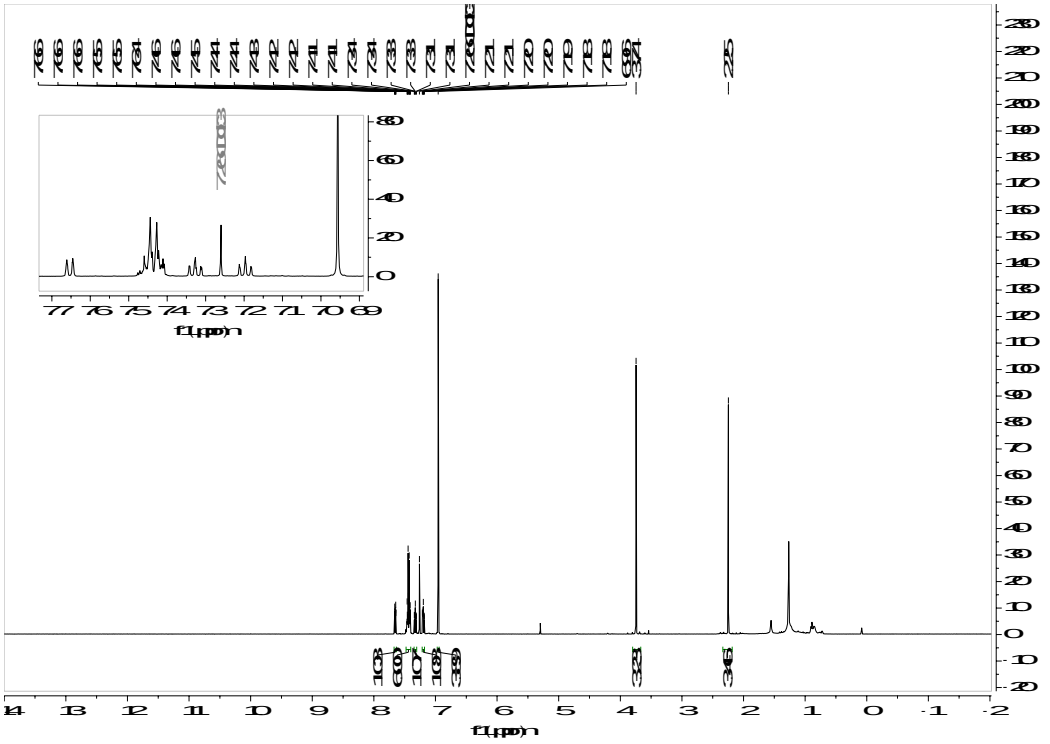

Figure 3.5.62 500 MHz ^{1}H NMR Spectrum of 3.24a

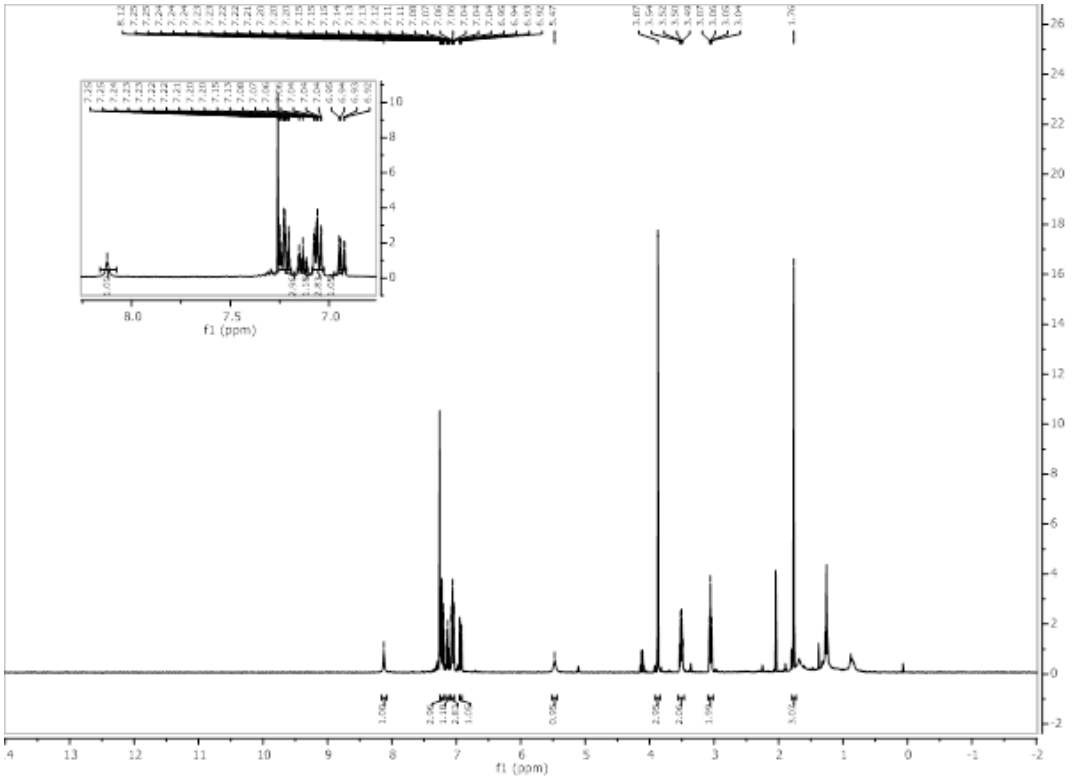

Figure 3.5.63 400 MHz ^{1}H NMR Spectrum of 3.25a

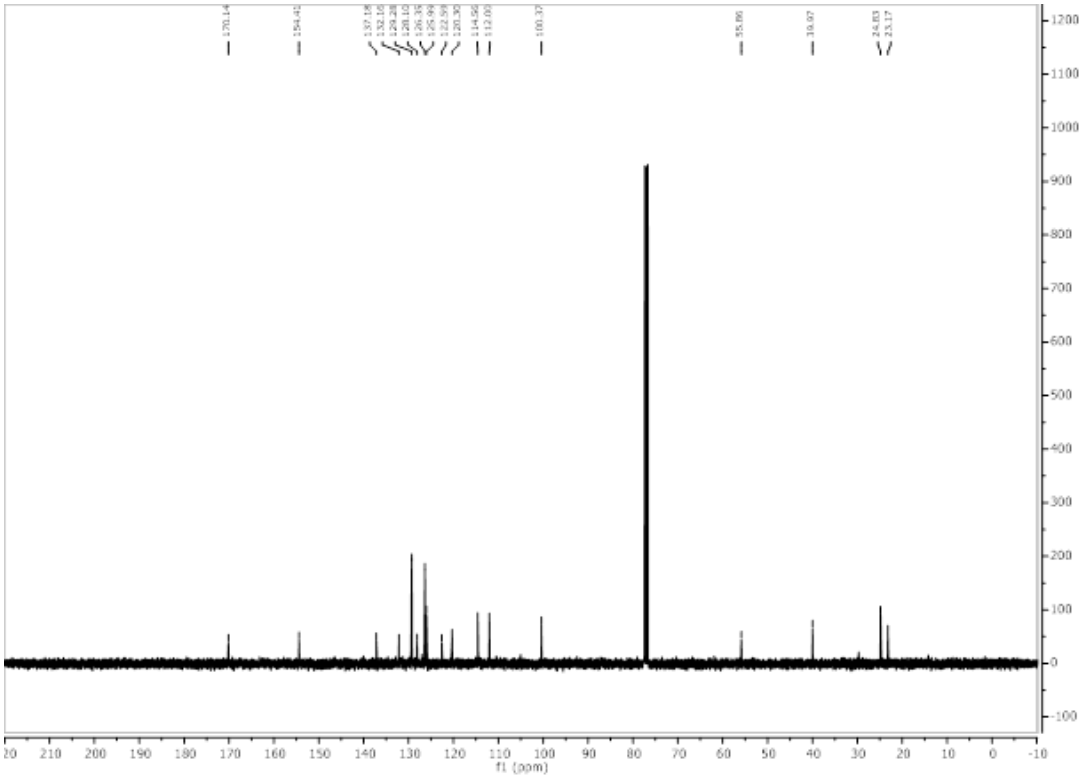

Figure 3.5.64 126 MHz ^{13}C NMR Spectrum of 3.25a

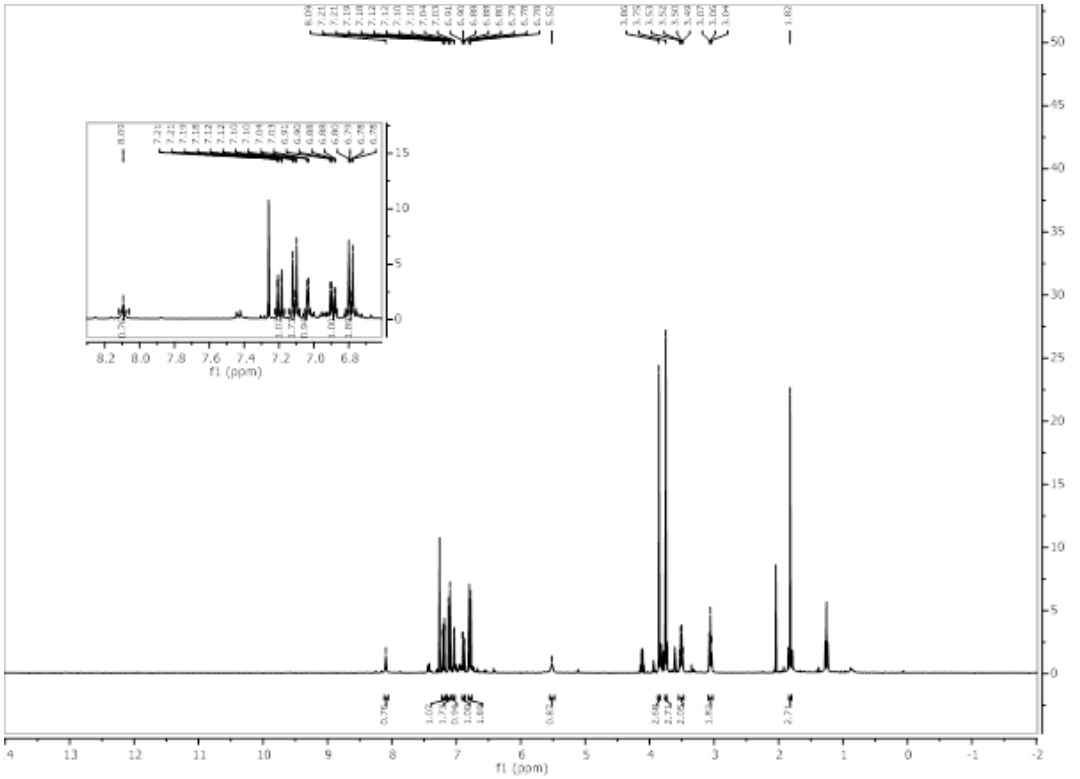

Figure 3.5.65 400 MHz ^{1}H NMR Spectrum of 3.26a

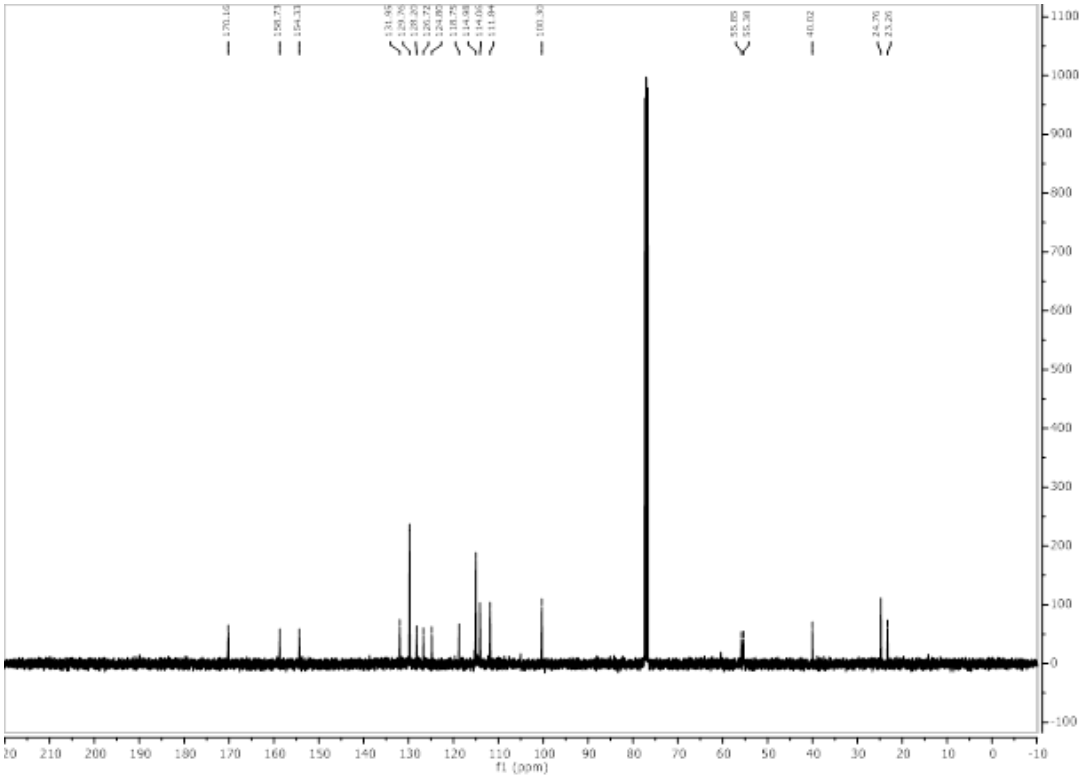

Figure 3.5.66 126 MHz ^{13}C NMR Spectrum of 3.26a

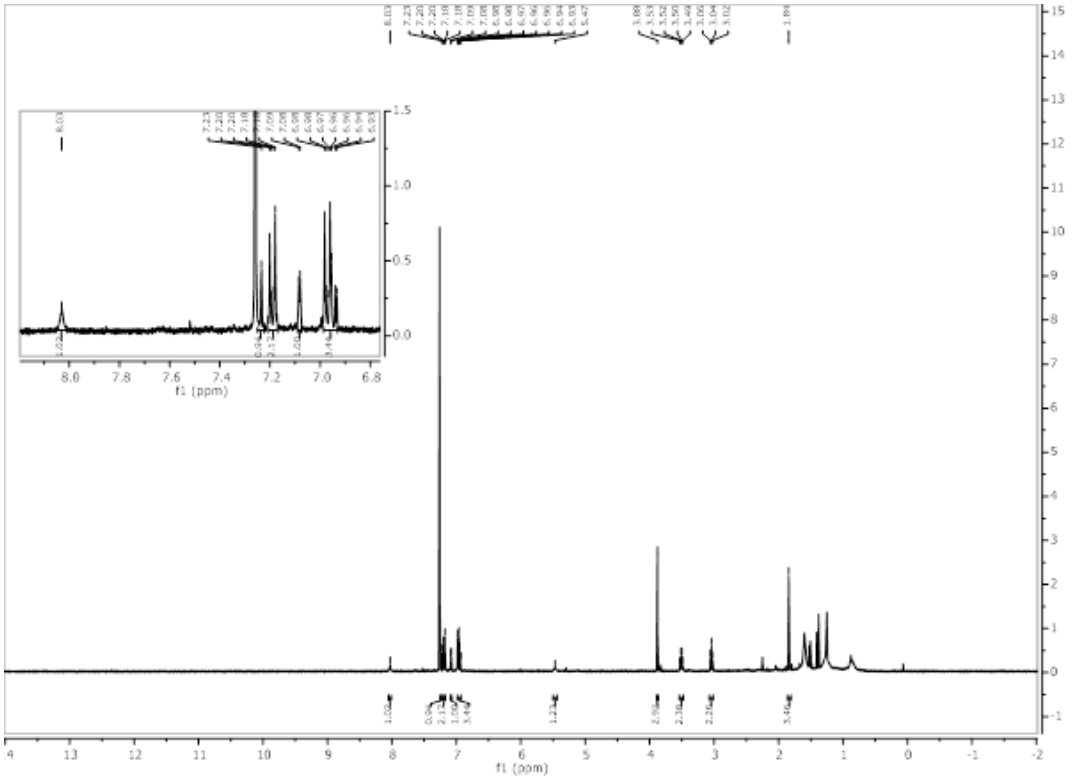

Figure 3.5.67 400 MHz ^{1}H NMR Spectrum of 3.27a

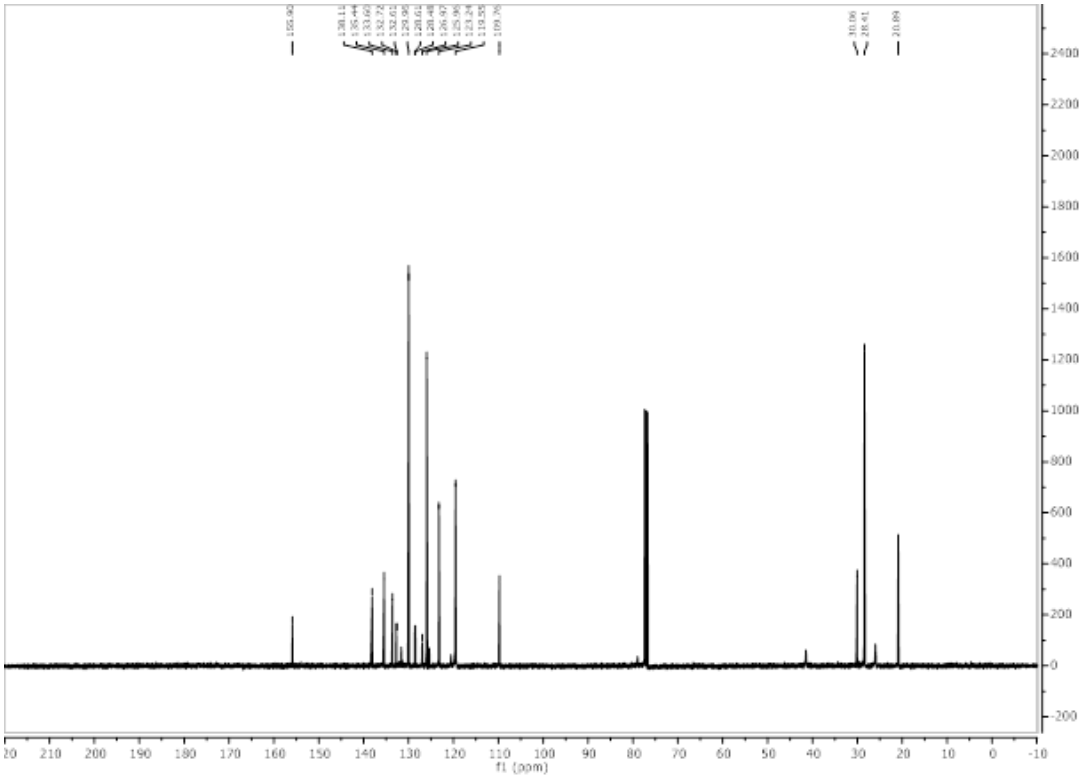

Figure 3.5.68 126 MHz ^{13}C NMR Spectrum of 3.27a

3.5.7 Computational Geometries/Energies for Electron Density Maps

All geometry optimizations and frequency calculations were performed in Gaussian 09 using density functional theory, B3LYP/6-31(d) in gas phase.

Gaussian 09, Revision D.01. M. J. Frisch, G. W. Trucks, H. B. Schlegel, G. E. Scuseria,M. A. Robb, J. R. Cheeseman, G. Scalmani, V. Barone, B. Mennucci, G. A. Petersson,H. Nakatsuji, M. Caricato, X. Li, H. P. Hratchian, A. F. Izmaylov, J. Bloino, G. Zheng, J.L. Sonnenberg, M. Hada, M. Ehara, K. Toyota, R. Fukuda, J. Hasegawa, M. Ishida, T.Nakajima, Y. Honda, O. Kitao, H. Nakai, T. Vreven, J. A. Montgomery, Jr., J. E.Peralta, F. Ogliaro, M. Bearpark, J. J. Heyd, E. Brothers, K. N. Kudin, V. N. Staroverov,T. Keith, R. Kobayashi, J. Normand, K. Raghavachari, A. Rendell, J. C. Burant, S. S.Iyengar, J. Tomasi, M. Cossi, N. Rega, J. M. Millam, M. Klene, J. E. Knox, J. B. Cross,V. Bakken, C. Adamo, J. Jaramillo, R. Gomperts, R. E. Stratmann, O. Yazyev, A. J.Austin, R. Cammi, C. Pomelli, J. W. Ochterski, R. L. Martin, K. Morokuma, V. G.Zakrzewski, G. A. Voth, P. Salvador, J. J. Dannenberg, S. Dapprich, A. D. Daniels, O.Farkas, J. B. Foresman, J. V. Ortiz, J. Cioslowski, and D. J. Fox, Gaussian, Inc.,Wallingford CT, 2013.

(A) Thioamide Starting material

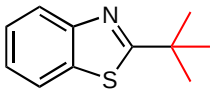

Center Number	Atomic Number	Atomic Type	Coordinates (Angstroms) X	Y	Z
1	6	0	-3.875848	0.246685	0.001251
2	6	0	-3.211295	0.030509	-1.207307
3	6	0	-1.881057	-0.391506	-1.210413
4	6	0	-1.204721	-0.584301	-0.000782
5	6	0	-1.879113	-0.391184	1.209887
6	6	0	-3.209342	0.030875	1.208800
7	1	0	-4.911900	0.573471	0.002038
8	1	0	-3.728637	0.183823	-2.150230
9	1	0	-1.360106	-0.575513	-2.145067
10	1	0	-1.356743	-0.575102	2.143763
11	1	0	-3.725174	0.184425	2.152511
12	7	0	0.129077	-1.126932	-0.001910
13	1	0	0.167375	-2.142991	-0.002203
14	6	0	1.384189	-0.591396	-0.000395
15	16	0	2.662266	-1.676430	0.000870
16	6	0	1.583460	0.943920	-0.000272
17	6	0	3.082302	1.305763	-0.001051
18	1	0	3.593786	0.910919	0.880111
19	1	0	3.592843	0.910939	-0.882779
20	1	0	3.179311	2.398277	-0.001096
21	6	0	0.954010	1.568053	-1.270457
22	1	0	1.358022	1.099897	-2.175160

23	1	0	-0.133753	1.482547	-1.290561
24	1	0	1.203555	2.634618	-1.306249
25	6	0	0.955466	1.567666	1.270842
26	1	0	-0.132300	1.482433	1.292002
27	1	0	1.360300	1.099019	2.174921
28	1	0	1.205329	2.634153	1.306821

Zero-point correction= 0.238571 (Hartree/Particle)
Thermal correction to Energy= 0.251857
Thermal correction to Enthalpy= 0.252801
Thermal correction to Gibbs Free Energy= 0.197414
Sum of electronic and zero-point Energies= -880.903848
Sum of electronic and thermal Energies= -880.890562
Sum of electronic and thermal Enthalpies= -880.889617
Sum of electronic and thermal Free Energies= -880.945005

(B) Radical Cation Intermediate

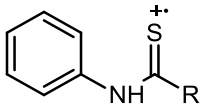

Center Number	Atomic Number	Atomic Type	Coordinates (Angstroms) X	Y	Z
1	6	0	3.867669	0.264444	0.000237
2	6	0	3.209002	0.040502	1.211204
3	6	0	1.884787	-0.400381	1.219324
4	6	0	1.232884	-0.592211	-0.000027
5	6	0	1.884892	-0.399954	-1.219255
6	6	0	3.209106	0.040927	-1.210866
7	1	0	4.898756	0.603816	0.000340
8	1	0	3.724422	0.200923	2.152838
9	1	0	1.370272	-0.593802	2.155534
10	1	0	1.370458	-0.593047	-2.155576
11	1	0	3.724608	0.201677	-2.152399
12	7	0	-0.113084	-1.158594	-0.000184
13	1	0	-0.113400	-2.178513	-0.000344
14	6	0	-1.299722	-0.580512	-0.000161
15	16	0	-2.683681	-1.609290	-0.000410
16	6	0	-1.575023	0.933619	0.000073
17	6	0	-3.100750	1.197995	0.000029
18	1	0	-3.597209	0.809641	-0.897005
19	1	0	-3.597315	0.809324	0.896866

20	1	0	-3.263530	2.281063	0.000210
21	6	0	-0.970707	1.567543	1.278887
22	1	0	-1.364232	1.097141	2.186055
23	1	0	0.118380	1.518483	1.294751
24	1	0	-1.262450	2.622632	1.298100
25	6	0	-0.970560	1.567966	-1.278462
26	1	0	0.118528	1.518908	-1.294219
27	1	0	-1.363983	1.097866	-2.185832
28	1	0	-1.262298	2.623062	-1.297358

Zero-point correction= 0.238132 (Hartree/Particle)
Thermal correction to Energy= 0.250715
Thermal correction to Enthalpy= 0.251659
Thermal correction to Gibbs Free Energy= 0.198722
Sum of electronic and zero-point Energies= -880.629402
Sum of electronic and thermal Energies= -880.616819
Sum of electronic and thermal Enthalpies= -880.615874
Sum of electronic and thermal Free Energies= -880.668812

(C) Cyclized Radical Cation

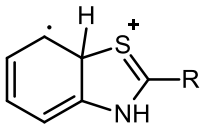

Center Number	Atomic Number	Atomic Type	Coordinates (Angstroms) X	Y	Z
1	6	0	3.747847	-0.330874	-0.304238
2	6	0	2.765790	-1.222761	0.019072
3	6	0	1.246395	0.731463	0.316887
4	6	0	2.263231	1.604990	0.007413
5	6	0	3.538589	1.079171	-0.257508
6	1	0	4.722276	-0.702291	-0.606462
7	1	0	2.949967	-2.292029	0.013776
8	1	0	2.073003	2.669878	-0.096344
9	1	0	4.352061	1.751885	-0.504995
10	16	0	-0.156508	-1.514152	-0.096802
11	6	0	-0.959090	0.014121	0.055166
12	6	0	-2.456219	0.194044	-0.078330
13	6	0	-2.817359	1.680753	-0.278744
14	6	0	-2.962234	-0.634852	-1.283633
15	6	0	-3.113971	-0.329488	1.230399
16	1	0	-2.561443	2.295280	0.593887
17	1	0	-2.347239	2.103417	-1.174290
18	1	0	-3.899289	1.768185	-0.409512

19	1	0	-2.754564	-1.703397	-1.163516
20	1	0	-4.047159	-0.519074	-1.362233
21	1	0	-2.513444	-0.296938	-2.223003
22	1	0	-4.198081	-0.199489	1.154167
23	1	0	-2.907841	-1.392147	1.387224
24	1	0	-2.765574	0.226676	2.106933
25	7	0	-0.119780	1.019835	0.294470
26	1	0	-0.461665	1.977388	0.301564
27	6	0	1.464923	-0.726368	0.547737
28	1	0	1.394175	-0.960958	1.625019

Zero-point correction= 0.237715 (Hartree/Particle)
Thermal correction to Energy= 0.250583
Thermal correction to Enthalpy= 0.251527
Thermal correction to Gibbs Free Energy= 0.197930
Sum of electronic and zero-point Energies= -880.637693
Sum of electronic and thermal Energies= -880.624825
Sum of electronic and thermal Enthalpies= -880.623881
Sum of electronic and thermal Free Energies= -880.677477

(D) Cyclized Cation

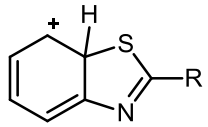

Center Number	Atomic Number	Atomic Type	Coordinates (Angstroms) X	Y	Z
1	6	0	3.737835	0.320718	0.283393
2	6	0	2.746903	1.225990	0.090377
3	6	0	1.155423	-0.731717	-0.218261
4	6	0	2.244795	-1.620706	-0.106218
5	6	0	3.491545	-1.093273	0.153301
6	1	0	4.737035	0.653774	0.544581
7	1	0	2.926346	2.295013	0.146565
8	1	0	2.062413	-2.689754	-0.107952
9	1	0	4.324527	-1.772585	0.312574
10	16	0	-0.178836	1.540375	-0.009532
11	6	0	-0.941201	-0.037975	-0.033076
12	6	0	-2.434295	-0.198602	0.068296
13	6	0	-2.720755	-1.145985	1.266404
14	6	0	-3.151497	1.146566	0.271603
15	6	0	-2.913556	-0.869615	-1.250336
16	1	0	-2.221386	-2.109391	1.140575
17	1	0	-2.397205	-0.700528	2.212875

18	1	0	-3.800547	-1.315684	1.321843
19	1	0	-2.999474	1.827426	-0.573523
20	1	0	-4.227920	0.972172	0.357063
21	1	0	-2.831211	1.646871	1.193414
22	1	0	-3.992859	-1.037577	-1.180896
23	1	0	-2.725518	-0.227755	-2.117492
24	1	0	-2.420600	-1.832261	-1.408088
25	7	0	-0.129387	-1.086128	-0.149117
26	6	0	1.424581	0.734091	-0.385029
27	1	0	1.494810	0.870221	-1.487933

Zero-point correction= 0.226086 (Hartree/Particle)
Thermal correction to Energy= 0.238592
Thermal correction to Enthalpy= 0.239536
Thermal correction to Gibbs Free Energy= 0.187408
Sum of electronic and zero-point Energies= -880.049093
Sum of electronic and thermal Energies= -880.036587
Sum of electronic and thermal Enthalpies= -880.035643
Sum of electronic and thermal Free Energies= -880.087771

3.5.8 Cyclic Voltammetry

General Procedure: A CH Instruments Model 630c Electrochemical Workstation potentiostat was utilized. Experiments were run in a jacketed single compartment cell with a glassy carbon disk working electrode, a platinum wire counter electrode, and a Ag wire pseudo reference electrode. Immediately before use, the working electrode was polished with 0.25 μm diamond polishing paste, rinsed thoroughly with DI water, then polished with 0.25 μm alumina suspension, followed by a thorough rinse with DI water and acetone. The Ag wire pseudo reference electrode was housed in a separate compartment containing 3 M KCl(aq) and was allowed to soak for at least 30 minutes before experiments. The potential of the pseudo-reference was later measured relative to a standard Ag/AgCl(4 M KCl)reference electrode to allow conversion of the data to V vs. SCE. Temperature was controlled during experiments by running 25 °C through the cell jacket using a circulating water bath. The electrolyte solution was 0.10 M NBu_4PF_6 in MeCN, unless noted otherwise. The solution was purged for several minutes with Ar gas prior to running CVs. An analyte

concentration of 0.1 mM in 5 mL of electrolyte was used for voltage experiments and 0.2 mM in mL of electrolyte was used for pyridine titration. Background scans without analyte were taken at each scan rate and subtracted from the analyte scan. All scan experiments were normalized by dividing the measured current by the square root of scan rate. The potentials were converted from AgCl/Ag reference values to SCE by subtraction of 0.045 V.

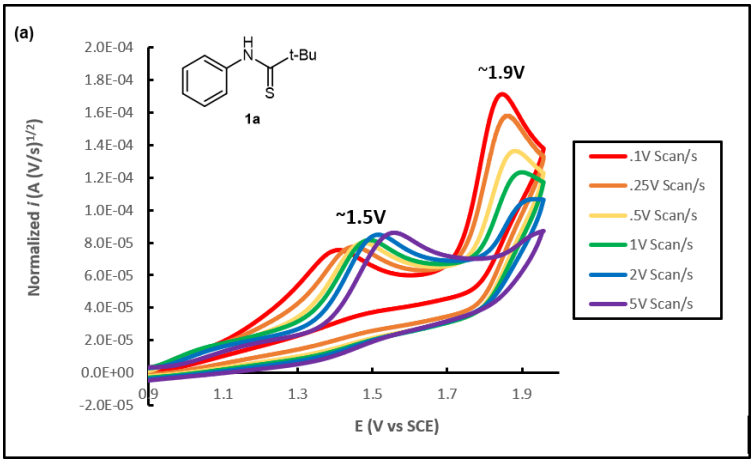

Figure 3.5.69 CV Scan of 3.1

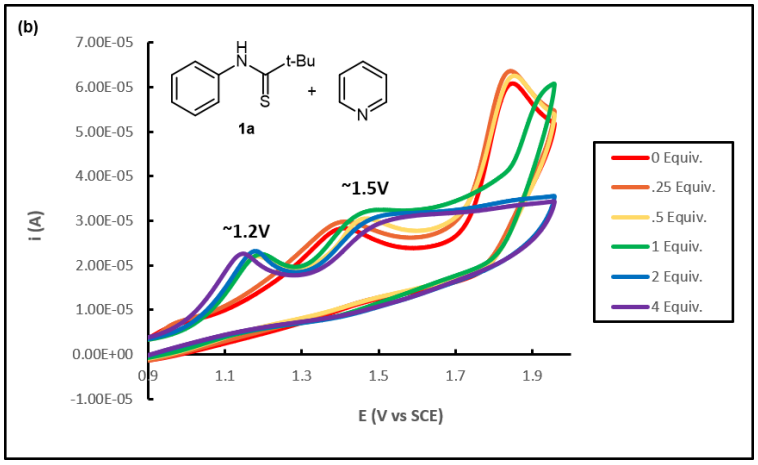

Figure 3.5.70 CV Scan of Pyridine Titration of 3.1

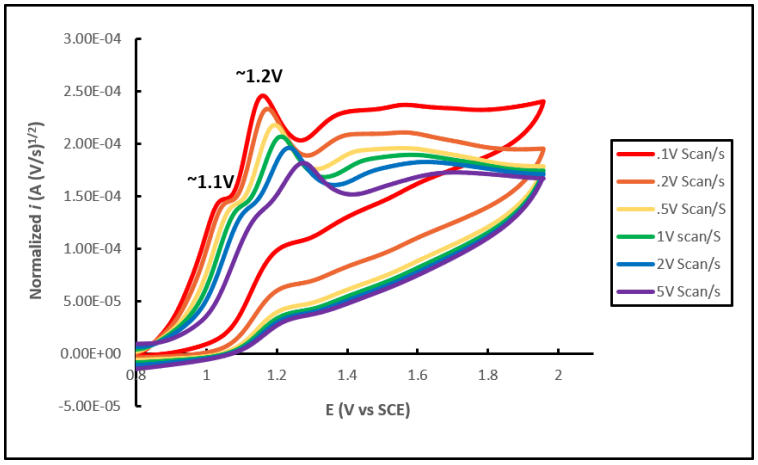

Figure 3.5.71 CV Scan of Melatonin 3.18

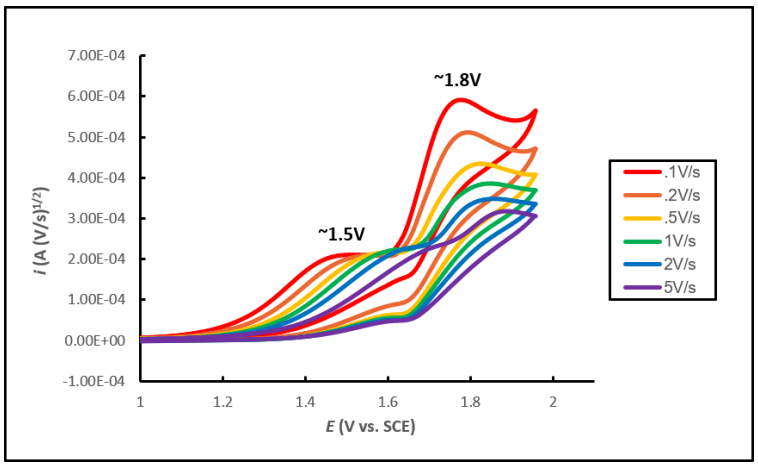

Figure 3.5.72 CV Scan of 4-methylbenzenethiol

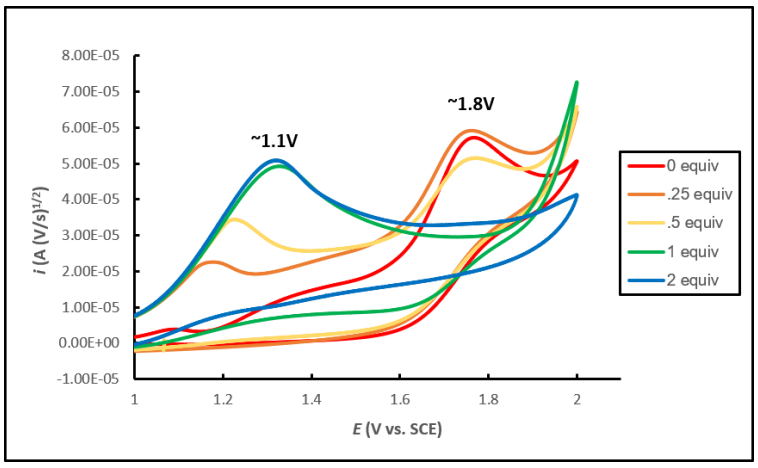

Figure 3.5.73 CV Scan of N-(3,5-bis(trifluoromethyl)phenyl)benzothioamide 3.10

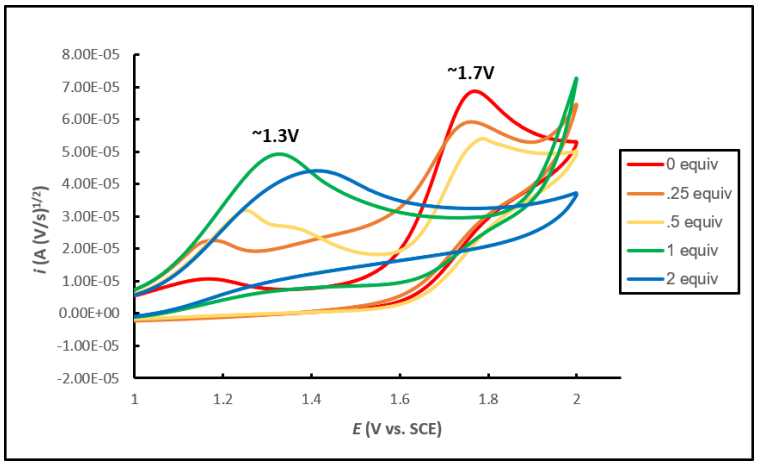

Figure 3.5.74 CV Scan of N-(3,5-bis(trifluoromethyl)phenyl)butanethioamide 3.14

3.10 and **3.14** cyclic voltammograms were taken because the pyridine additive effect was minimal. For both substrates, we observe one oxidation peak at approximately 1.8V and 1.7V respectively. Upon addition of pyridine, we observe a similar downward shift of the oxidation potential to 1.1V and 1.3V. Because the yields are still moderately good in the absence of pyridine, we hypothesize that persulfate can oxidize the thioamide in addition to the ruthenium photocatalyst.

3.5.9 Photochamber Setup

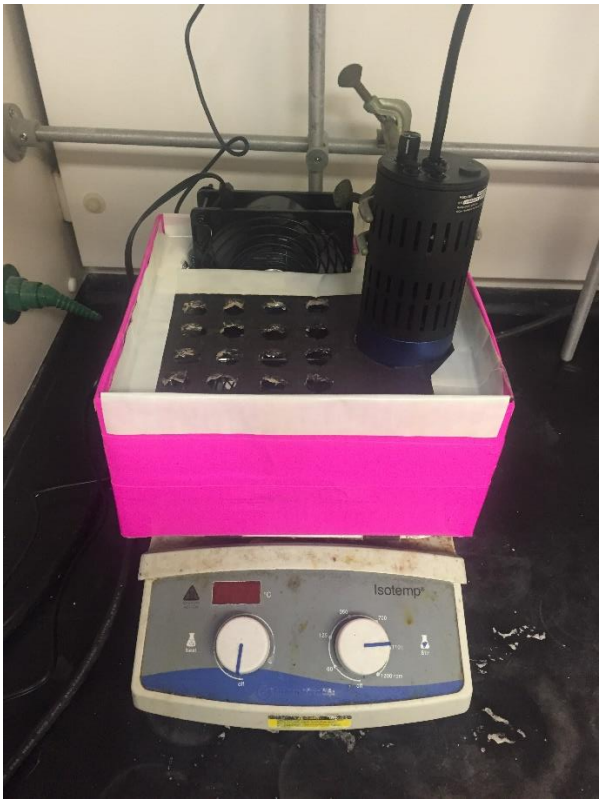

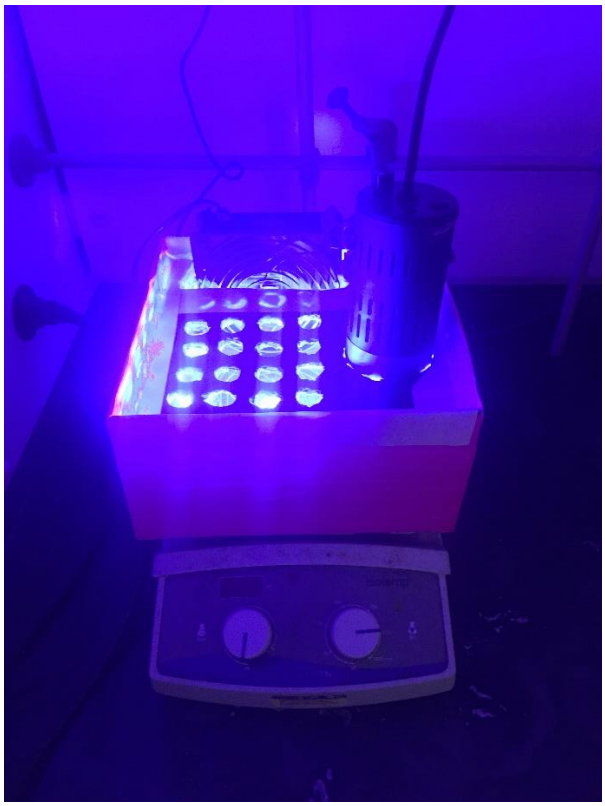

A PR160 LED photoredox Kessil lamp (390nm or 440nm) was inserted into a cutout cardboard box with angled mirrors inside for even distribution of light. A computer fan was used to minimize heat output from the lamp.

3.5.10 Stern-Vollmer Analysis

Stern-Volmer experiments were done at 410nm detection on a Horiba Fluoromax-4 spectrofluorometer. A solution of $(Ir[dF(CF_3)ppy]_2(dtbpy)]PF_6$ photocatalyst in acetonitrile (2.0×10^{-5}M) and a quencher in acetonitrile (.1M) stock solution was prepared. Stern-Volmer analysis was conducted according to the following relationship:

$$\tau_o/\tau = 1 + K_{SV}[Q] = 1 + k_q\tau_o[Q]$$

where τ_o and τ are the fluorescence lifetime in the absence and presence of Q, K_{sv} is the Stern-Volmer constant, k_q is the bimolecular quenching constant, and [Q] is the concentration of quencher.

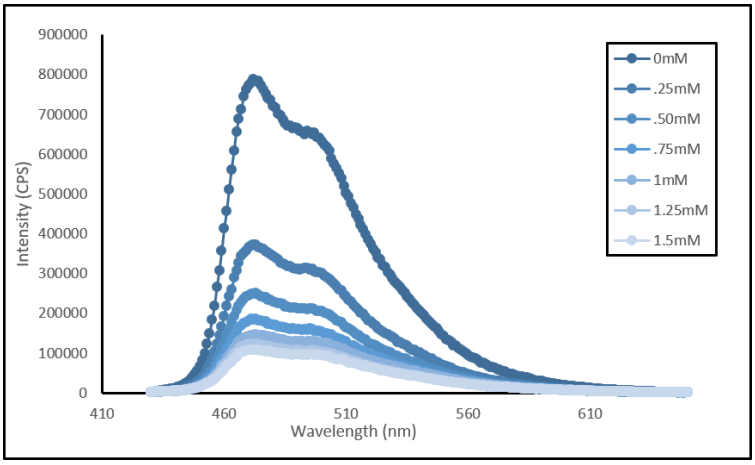

Figure 3.5.75 Stern Vollmer Quenching with Melatonin

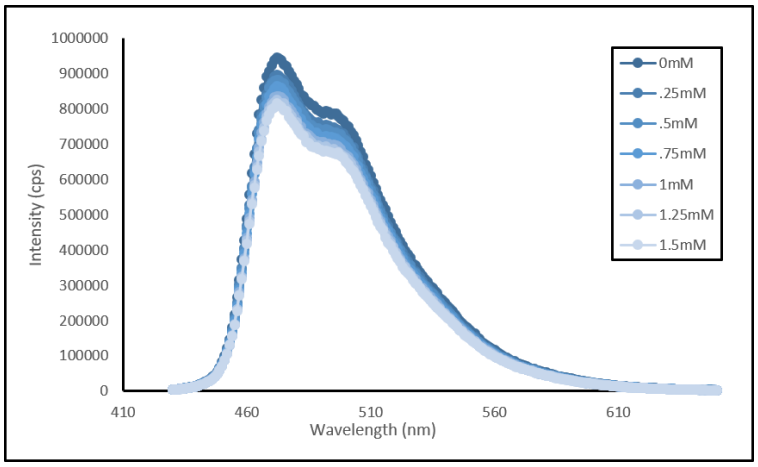

Figure 3.5.76 Stern Vollmer Quenching with 4-methylbenezenethiol

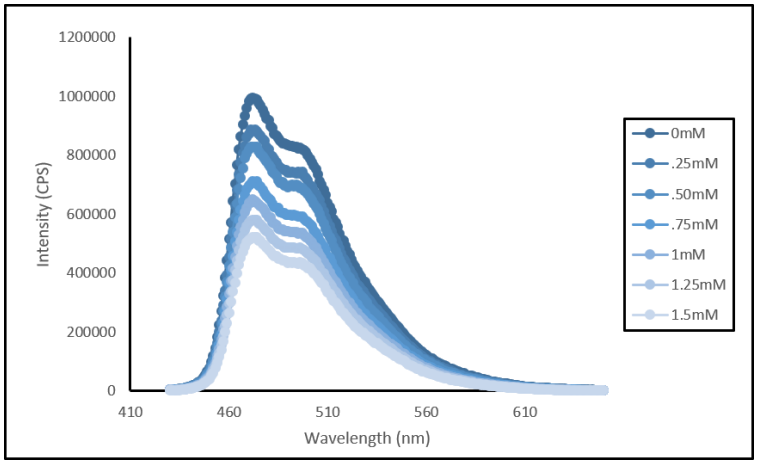

Figure 3.5.77 Stern Vollmer Quenching with 4-methyl diphenyldisulfide

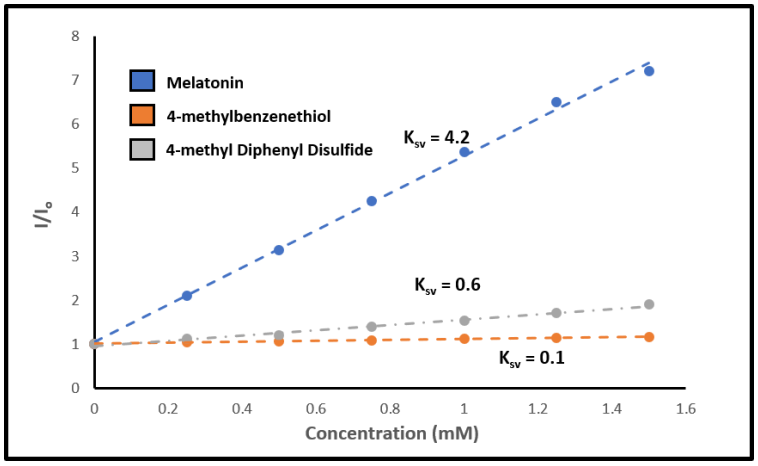

Figure 3.5.78 K_{sv} constant measurement of Stern Vollmer plots

3.5.11 Mechanistic Experiments

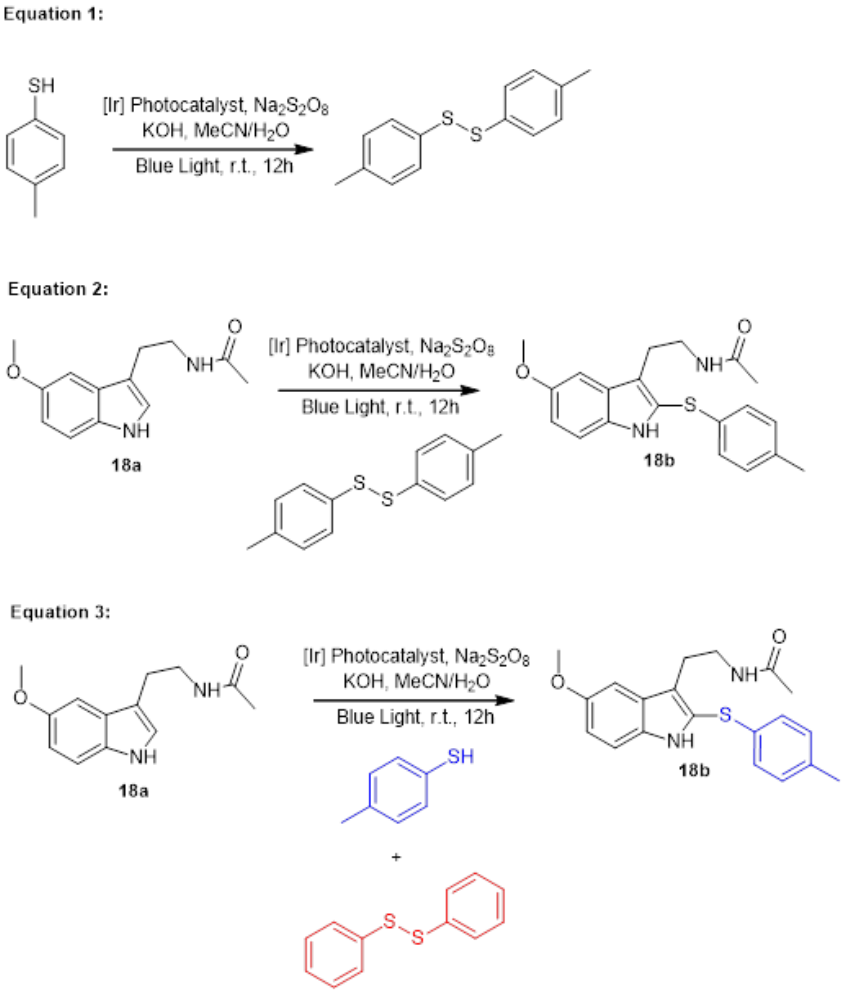

Figure 3.5.79 Control Experiments to Probe Mechanism of Sulfenylation

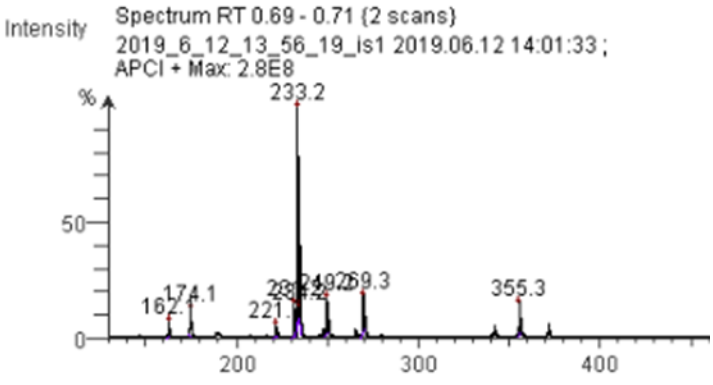

Figure 3.5.80 Mass Spectrum of Cross Experiment Showing Disulfide Byproduct

3.6 Acknowledgements

The contents in Chapter 3 are in part a reformatted reprint of the following manuscript, with permission from the Thieme Connect: Dinh, A; Nguyen, A; Millan Aceves E.; Albright, S.; Cedano, M.; Smith D.; Gustafson, J. “Photocatalytic Oxidative C-H Thiolation: Synthesis of Benzothiazoles and Sulfenylated Indoles.” *Synlett* **2019** *30* 1648-1655. I was a primary author for the manuscript, providing work for optimization, substrate scope evaluation and mechanistic studies for all reactions. Ashley Nguyen is a co-author on the manuscript and provided data for optimization and substrate scope evaluation. Ernesto Millan Aceves and Samuel Albright contributed equally to substrate scope evaluation. Mario Cedano is a graduate student experienced in electrochemistry, and he assisted in teaching me about utilizing cyclic voltammetry. Dr. Diane Smith gave insightful conversations and feedback on electrochemical mechanisms and provided the facilities to run cyclic voltammetry. The dissertation author was the primary researcher for the data presented. Support of this work by the National Science Foundation is acknowledged (CHE-1664565).

CHAPTER 4: Toward a Catalytic Atroposelective Synthesis of Diaryl Ethers Through C(sp^2)-H Alkylation with Nitroalkanes

4.0 Thieme Copyright

4.1 Atropisomerism

Chirality is a foundational chemistry concept that is introduced when one is initially taught organic chemistry, usually through point chirality. In point chirality, a molecule must have four unique substitutions about an atom which allows it to exist in two unique non-superimposable mirror images (Figure 4.1.1). However, there are multiple types of chirality which include axial chirality, also known as atropisomerism. Atropisomerism is a type of chirality that arises from differential substitutions about a bond as opposed to one singular atom, typically between two sp^2 hybridized atoms. While point chirality involves racemization by bonding formation and breakage, racemization of atropisomers can occur simply via rotation of the sp^2-sp^2 which is a dynamic process. If the substitutions about the axis are small, free bond rotation can occur without little energy as an interconverting mixture. If the steric bulk of the adjacent groups increase, the barrier

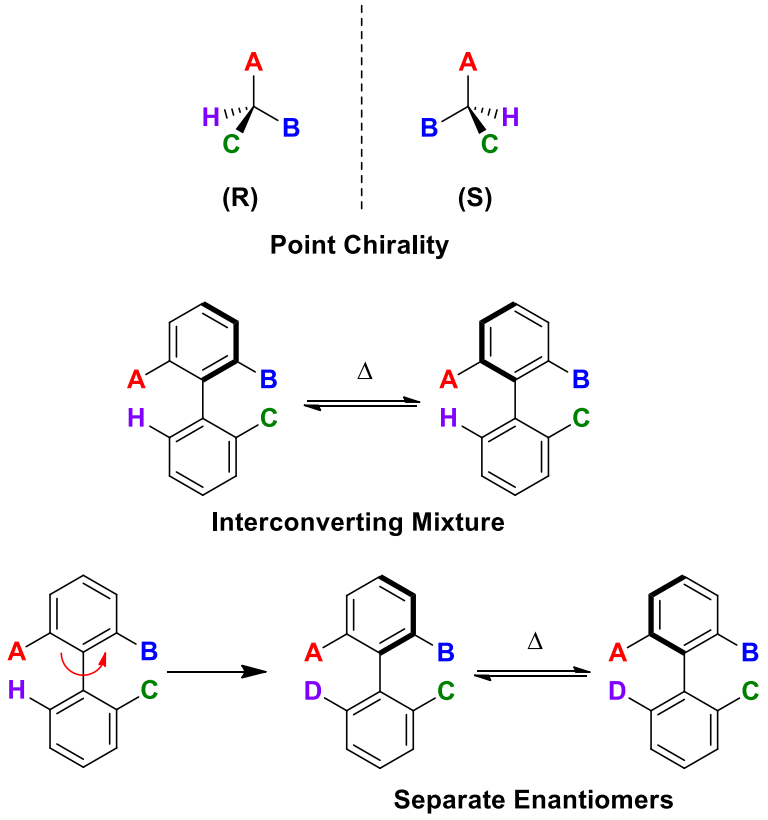

Figure 4.1.1 Point Chirality versus Axial Chirality/Atropisomerism

to rotation will increase to prevent interconversion, resulting in two distinct atropisomeric enantiomers on certain time scales.

The stereochemical stability of atropisomers has been generally classified by LaPlante into three categories based on the amount of energy needed for the chiral axis to racemize and overcome the barrier to rotation.[124,125] Class 1 atropisomers possess barriers to rotation of less than 20 kcal/mol and racemize on the second to minute time scale at room temperature; the chirality of these molecules are often disregarded and considered "achiral". Class 2 atropisomers have a barrier to rotation between 20-28 kcal/mol and racemize on the hour to month time scale at room temperature. Class 3 atropisomers possess a barrier to rotation of >28 kcal/mol and racemize on the year or longer time scale at room temperature.[126]

4.2 Atropisomerism in Medicinal Chemistry

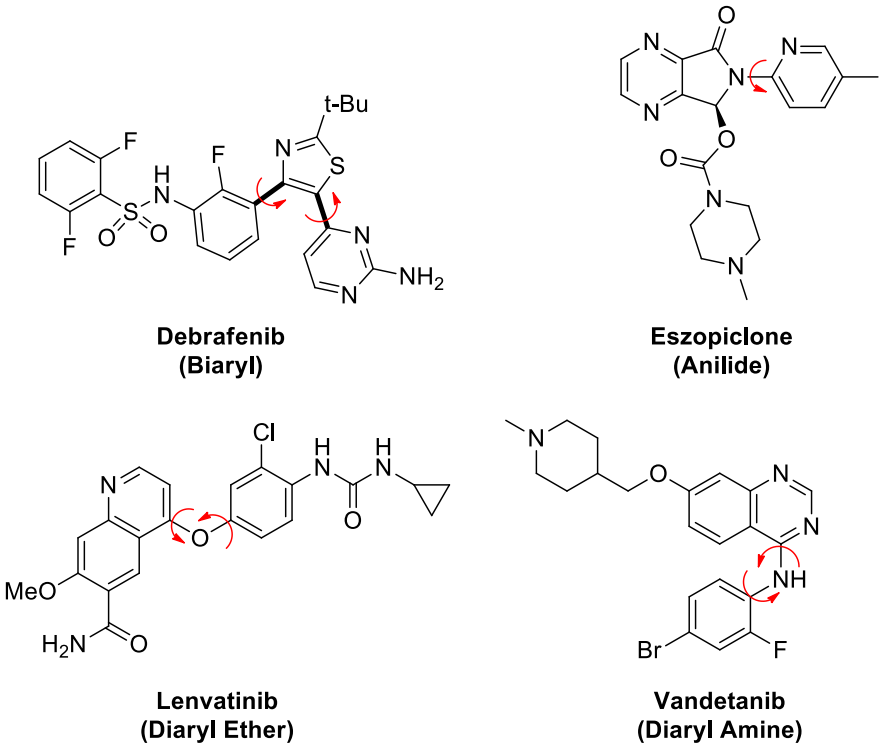

Debrafenib (Biaryl) | **Eszopiclone (Anilide)**

Lenvatinib (Diaryl Ether) | **Vandetanib (Diaryl Amine)**

Figure 4.2.1 Drugs that Possess Atropisomeric Scaffolds

There are many examples of Class 1 atropisomers as pharmaceuticals and chemical probes. A recent review contained an analysis of atropisomeric prevalence; out of approximately 1900 small molecule drugs in the US FDA Drug Bank, approximately 15% of FDA-approved small molecules contain at least one atropisomeric axis, with the vast majority as rapidly interconverting Class 1 atropisomers.[127] Additionally, a review published from our lab found that since 2011, 30% of all drugs have one or more interconverting axes of chirality, and 85% of drugs that act as kinase inhibitors, a class of proteins that is heavily target in drug discovery, are almost entirely comprised of Class 1 atropisomers (Figure 4.2.1). One reason for this finding is that the most common reactions in medicinal chemistry (i.e. Suzuki cross couplings, nucleophilic aromatic substitution, amide couplings) can give rise to sp^2-sp^2 scaffolds.[6] While these drugs are treated like achiral

molecules, these ligands will bind to their target protein in a specific conformation, meaning the target will have a selective preference for one atropisomer over the other.[128]

4.3 Atropisomerism and Dihedral Angle Control as a Selectivity Filter for Kinase Inhibitor Design

Aberrant kinase activity is implicated in many diseases such as cancer and autoimmune disorders. Because of this, kinases have become utilized as a common therapeutic target in medicinal chemistry. Most small molecule kinase inhibitors are defined as Type-I inhibitors, which means they are competitors for the active site of kinases that bind ATP. One significant drawback to this strategy is that the kinase active site is highly conserved among the over 500 different kinases in the human body. Therefore, selectivity for one target is a difficult uunmet challenge in the design of Type-I small molecule inhibitors. Drugs that are non-selective will give rise to negative side effects that can be just as harmful to the patient as the actual disease. For non-selective kinase inhibitors that are used to treat cancer, the drug will be applied to extend the patient's life while the negative side effects can only be tolerated.

Stable atropisomerism is typically avoided in the current drug discovery "industry standard" when possible.[124,129] However, our lab realized that atropisomerism is ubiquitous in kinase inhibitors and that selectivity is still an unmet need in kinase inhibition; hence our lab hypotheiszed that we could use a kinase's conformational preference as a general selectivity filter in kinase inhibition. Control of these atropisomeric scaffolds would have the potential to represent a general and useful tool for medicinal chemistry.

To test this hypothesis as a proof-of-concept, my lab colleagues synthesized atropisomerically stable compounds of a Class 1 non-selective tyrosine kinase inhibitor

Table 4.3.1 Atropisomerism as a Selectivity Filter for Kinase Inhibitors

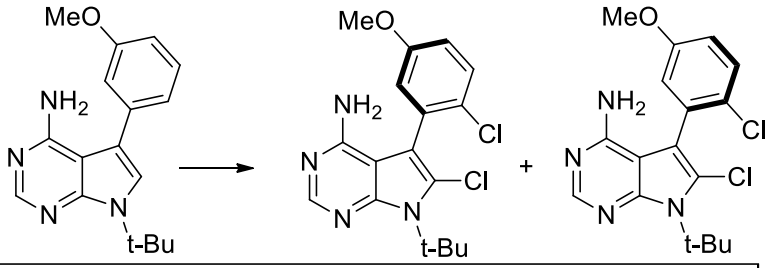

Kinase	Parent IC_{50}	(S) IC_{50}	(R) IC_{50}
Src	151+/-9	1193+/-170	5570+/-970
EGFR	641+/-54	>10,000	>10,000
Yes	92+/-11	727+/-177	895+/-90
Ret	128+/-3	7659+/-754	1857+/-482
Abl	245+/-19	1432+/-210	>10,000

pyrrolopyrimidine parent compound (Table 4.3.1).[130] The axis was locked into place via chlorination methodology introduced in Chapter 1 to form stable atropisomers **(S)** and **(R)**. The parent compound and both of the corresponding atropisomers were tested across a small panel of kinases to measure their activity via IC_{50} values. Interestingly, both the **(S)** and **(R)** were more selective than the parent compound and rigidifcation of the atropisomeric axis decoupled the acitivty of each rotational isomer. Despite the order of magnitude loss in potency, this was the first example of exploiting atropisomerism as a selectivity filter. In a subsequent paper, our lab was able to optimize these small molecule inhibitors for Ret and EGFR kinase to increase potency while maintaining this high ratio of selectivity against other kinase inhibitors.[131] Based on work by Davis Smith, Sean Toenjes and many other colleagues in the Gustafson lab, they were able to show the utility of atropisomeric scaffolds in medicinal chemistry, a concept that is only beginning to build momentum over the last decade.

4.4 Development of Atroposelective Methodologies

As mentioned in the previous section, research from our group and others have demonstrated that atropisomeric conformations can be leveraged to modulate the potency and target selectivity of lead compounds via the synthesis of stereochemically stable atropisomeric analogues.[130–132] Hence, there is a need to obtain atropisomeric enantiopure pharmaceutical scaffolds. There has a been a long-standing challenge in industry, as chemists are more likely to rely on brute force, utilizing non-chiral methodologies and separating the enantiomers by HPLC separation on a chiral stationary phase.[133,134] Over the past decade, there have been notable examples of atroposelective methodologies, with many of them focusing on enantioselective functionalziation of biaryls; the Gustafson has also developed synthetic methodologies for biologically relevant heterocycles such as quinolines, quinones and lesser known atropisomeric manifolds such as *N*-aryl quinoids and diaryl ethers.[135–139] Other seminal work has included Smith, who has shown that nucleophilic substitution of of BINOL-type ligands can be synthesized atroposelectively via simple alkylation and sulfenylation.[140,141] Miller has shown that

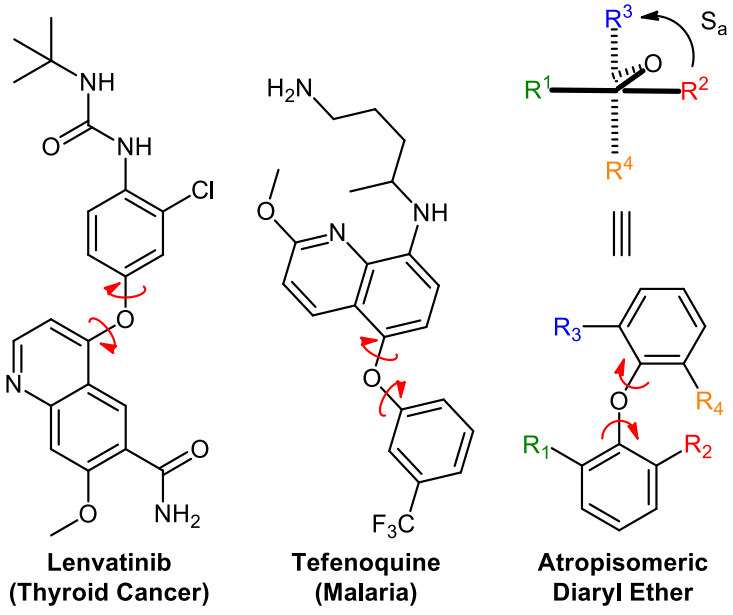

Figure 4.4.1 Illustrative Examples of Diaryl Ethers

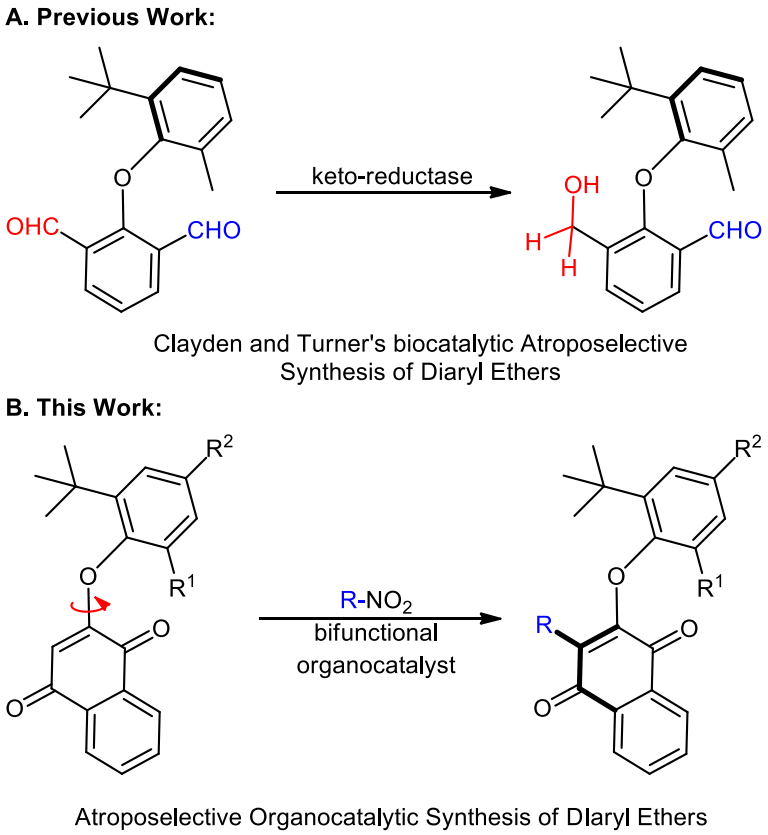

Scheme 4.4.1 Previous route towards diaryl ethers and proposed atroposelective alkylation

enantioselective methodologies with peptide catalysts can be applied to complex natural products such as Vancomycin[56,142,143]

While numerous methodologies of atroposelective biaryls have been developeed, diaryl ethers are another type of atropisomer that have been largely overlooked by the enantioselective catalysis community despite their prevalence in natural products, exemplified by the macrocyclic diaryl ethers in Vancomycin. Furthermore, atropisomerically unstable diaryl ethers are common motifs in drug discovery (Figure 4.4.1). Thus far, the literature involving diaryl ethers is highlighted by some nice diastereoselective examples en route to Vancomycin[144] and several excellent studies by Clayden and coworkers[145–149] wherein they characterized the stereochemical stabilities of differently substituted diaryl ethers, and developed diastereoselective routes to atropisomeric diaryl ethers. Notably, in collaboration with Turner, they disclosed the only catalytic

atroposelective route towards diaryl ethers currently in the literature, employing oxidase or reductase enzymes to desymmetrize prochiral diaryl ethers (Scheme 4.4.1A).

4.5 Discussion

Other than these groundbreaking examples, work on the catalytic atroposelective synthesis of diaryl ethers has been scarce. Perhaps the major reason for this is that diaryl ethers possess two axes (Figure 4.4.1) that can complicate reaction development, analysis and in some cases, result in racemization at a lower-than-expected energy via a concerted gearing mechanism.[146,150] When defining the chirality of diaryl ethers, Clayden and others have made an analogy to atropisomeric biaryl systems, defining chirality based on the orientation of the substituents across both aryl planes when looking down one aryl-ether axis (see Figure 4.4.1, priority assigned in example according to R group's number).

Recent work from our group has focused on the atroposelective synthesis of naphthoquinone-based biaryls via the rigidification of a rapidly interconverting axis via a 1,4-nucleophilic addition into the quinone.[138,139] As there is a lack of enantioselective routes towards atropisomeric diaryl ethers, I decided to test whether this approach could be extended to this scaffold (Scheme 4.4.1B). I chose to evaluate naphthoquinones such as **4.1** (see Table 4.5.1) where the aryl groups possessed a large *tert*-butyl group and a 2nd smaller substituent *ortho*-to the ether axis, as Clayden has shown that having one large quaternary substituent is often a prerequisite to obtain stereochemically stable diaryl ethers.

While evaluating nucleophiles for the addition into **4.1**, we observed that the use of nitromethane in the presence of excess Cs_2CO_3 and tetrabutylammonium bromide (TBAB) resulted in the isolation of a C(sp^2)-H methylated product **4.1a** (Table 4.5.1, entry 1), in line with seminal work reported by Mukherjee.[151,152] Quinine derived quaternary amines with hydroxyl

Table 4.5.1 Optimization of C(sp)^2-H Methylation of 4.1

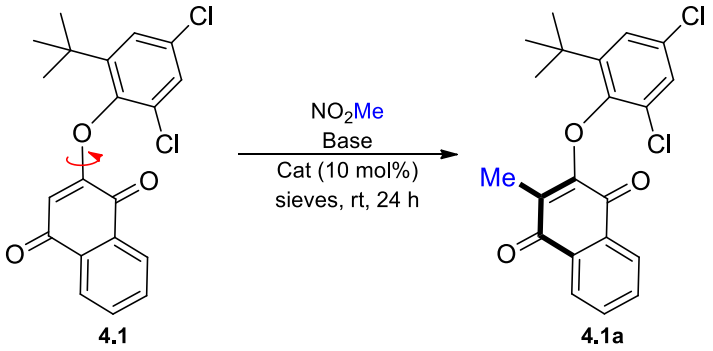

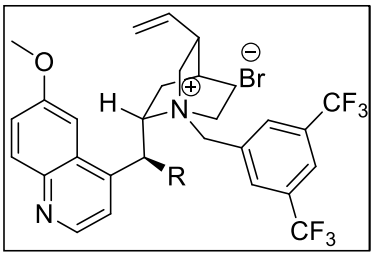

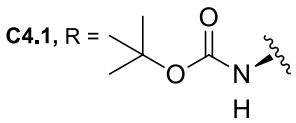

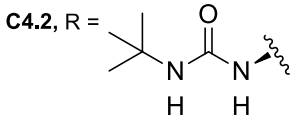

Entry	Solvent	Catalyst	Base	Sieves	Yield (%)	er[b]
1	PhMe	**TBAB**	Cs_2CO_3	-	18	---
2	PhMe	**C4.1**	Cs_2CO_3	-	18	62:38
3	PhMe	**C4.2**	Cs_2CO_3	-	17	85:15
4	PhMe/H_2O	**C4.2**	Cs_2CO_3	-	40	50:50
5	PhMe	**C4.2**	Na_2CO_3	-	20	60:40
6	PhMe	**C4.2**	K_2CO_3	-	15	65:35
7	PhMe	**C4.2**	K_3PO_4	-	60	80:20
8	PhMe	**C4.2**	K_3PO_4	4Å	51	75:25
9	PhMe	**C4.1**	K_3PO_4	4Å	36	64:36
10	PhMe	**C4.2**	K_3PO_4	3Å	68	81:19
11	CH_2Cl_2	**C4.2**	K_3PO_4	3Å	38	68:32
12	MTBE	**C4.2**	K_3PO_4	3Å	71	73:27

substitution at the cinchona alkaloid *C*-9 position gave nearly no observable selectivities (see experimental section 4.6.3 for details). On the other hand, catalyst **C4.1,** which has a *C*-9 stereochemically inverted Boc-protected amine (entry 2), yielded preliminary levels of

enantioselectivity, albeit with low conversions to **4.1a**. The selectivity could be further improved to an enantiomeric ratio (er) of 85:15 when *tert*-butyl urea-containing catalyst **C4.2** was used.

The addition of water, or the use of other carbonate bases, resulted in a loss in selectivity with minimal increase in yield (entries 4-6), however the use of tribasic potassium phosphate (entry 7) resulted in an increase in yield to 60% with only a slight drop in selectivity (er of 80:20) when compared to Cs_2CO_3. Finally, in line with Mukherjee's work, we found that the addition of 3Å molecular sieves resulted in yields of **4.1a** approaching 70% with a small increase in selectivity to 81:19 er (entry 10). While these selectivities may be considered moderate, **4.1** can be further enantioenriched via trituration out of isopropanol to allow access of **4.1a** in greater than 97:3 er. **4.1a** proved to be moderately stable, with an experimentally determined barrier to rotation at 65 ˚C of 26.6 kcal/mol, likely resulting in what LaPlante calls a 'Class 2 atropisomer" that would be expected to display significant racemization at room temperature over the course of a few weeks.

Extensive experimentation failed to yield further increases in er. Nonetheless, we decided to evaluate the conditions in Table 4.5.1, entry 10 across several differentially substituted substrate analogs (Scheme 4.5.1). Substrate **4.2**, where the aryl group possesses a 6-methyl substitution, resulted in a decrease in yield and enantioselectivity in the isolated product **4.2a** to 54% yield with an er of 71:29. Substrate **4.3**, which possesses a 4-phenyl and 6-methyl substitution yielded **4.3a** with similar selectivities. These results could be explained by an increase in electron density on the ether, reducing the electrophilicity of the quinone. Diaryl ether **4.4**, which possesses an electron deficient *para*-aryl ring, reinforces this hypothesis as the reaction proceeded with a large increase in yield of **4.4a** while retaining the moderate enantioselectivity (er of 71:29). Substrate **4.5,** which possesses 4-phenyl and 2-chloro substitution on the aryl ring also yielded moderate selectivities

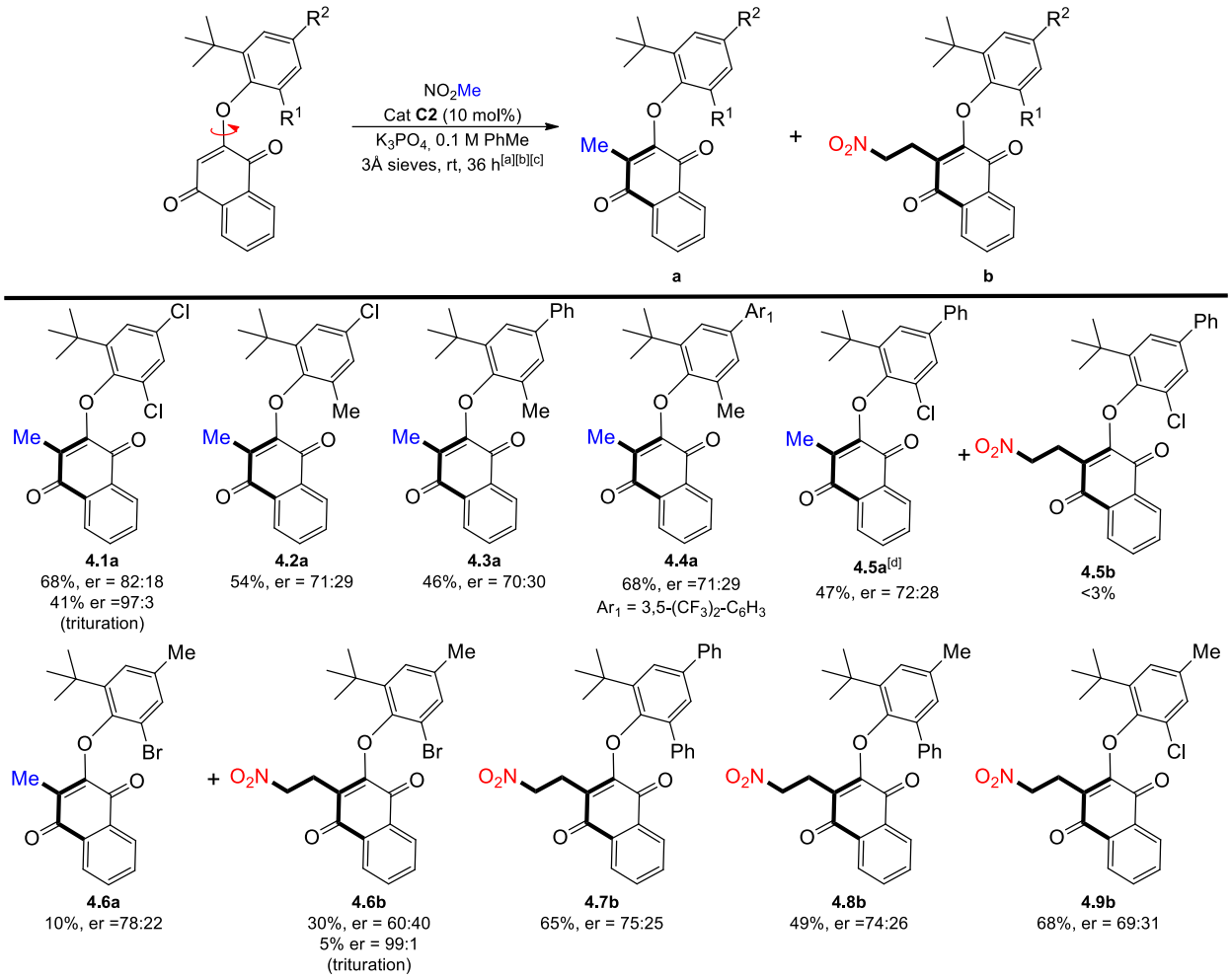

Scheme 4.5.1 Substrate Scope of Diaryl Ether Methylation and Nitroethylation

and yields of **4.5a** (47% yield, 72:28 er); however, we also observed small amounts of 'nitroethylated' **4.5b** (*vide infra)*. Substrate **4.6,** which possesses 6-Br substitution, yielded a 1:3 mixture of methylated **4.6a** (10%) and **'**nitroethylated' **4.6b** (30%) yield. Interestingly, while **4.6a** was obtained in 78:22 er, **4.6b** was obtained in only 60:40 er. One round of trituration with hexanes allowed for isolation of **4.6b** in 99:1 er, albeit in low overall yield. Substrate **4.7**, which possesses 4,6-diphenyl substitution yielded exclusively 'nitroethylated' **4.7b** with a 75:25 er. We observed similar results with **4.8** and **4.9** which gave 'nitroethylated' **4.8b** and **4.9b** with similar yields and selectivities.

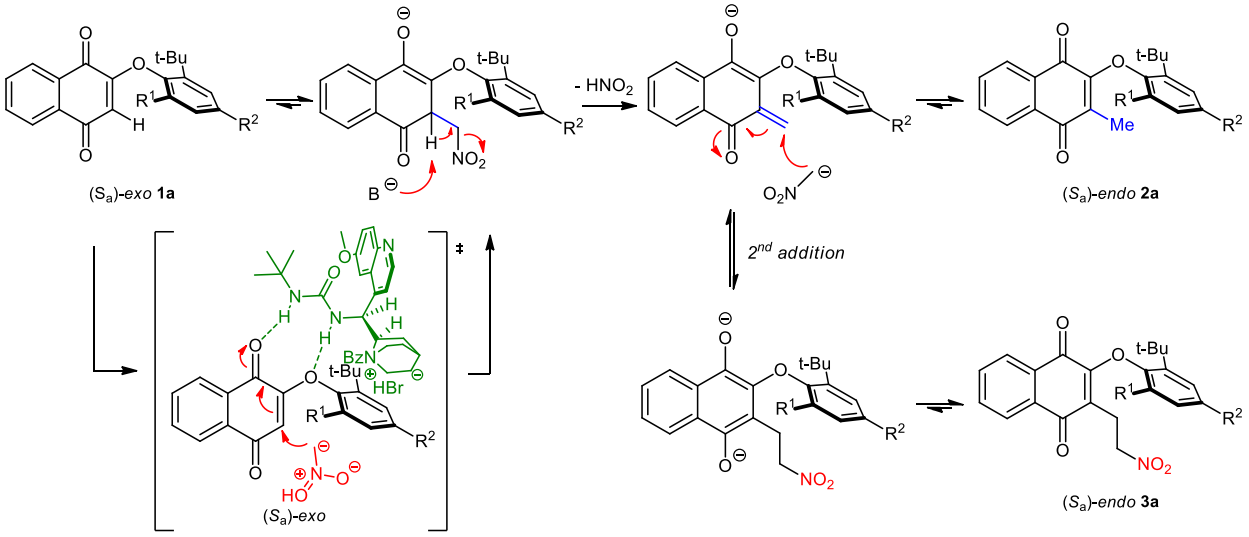

Scheme 4.5.2 Mechanistic Proposal to Explain Nitroethylated Byproduct

Referring back to Mukherjee's hypothesized mechanism of C(sp^2)-H alkylation using nitroalkanes, I postulate that our diaryl ether substrates proceed via a quinone methide intermediate.[151] If this intermediate is long lived enough, then another equivalent of nitronate anion can add 1,4 into the quinone-methide to yield the 'nitroethylated' product (Scheme 4.5.2). While the exact mechanism of quinone-methide stabilization is unknown, I suspect it is due to a subtle electronic effect as 'nitroethylation' is only observed with substrates that possess electron neutral or donating substitution *para*- to the ether.

I next sought to define the stereochemical induction of this reaction. Though I was unable to obtain suitable crystals, I compared experimental and computational circular dichroism (CD) spectra, a method that is gaining acceptance in the stereochemical community.[153–155] I obtained CD spectra of highly enantioenriched (er >97:3) **4.1a** and compared it to computational CD spectra of **4.1a** of all possible stable conformations about both ether axes (Scheme 4.5.3). This analysis suggests that the major product is in the S_a configuration with the proximal quinone carbonyl *endo*- to the aryl ring (S_a-*endo*).

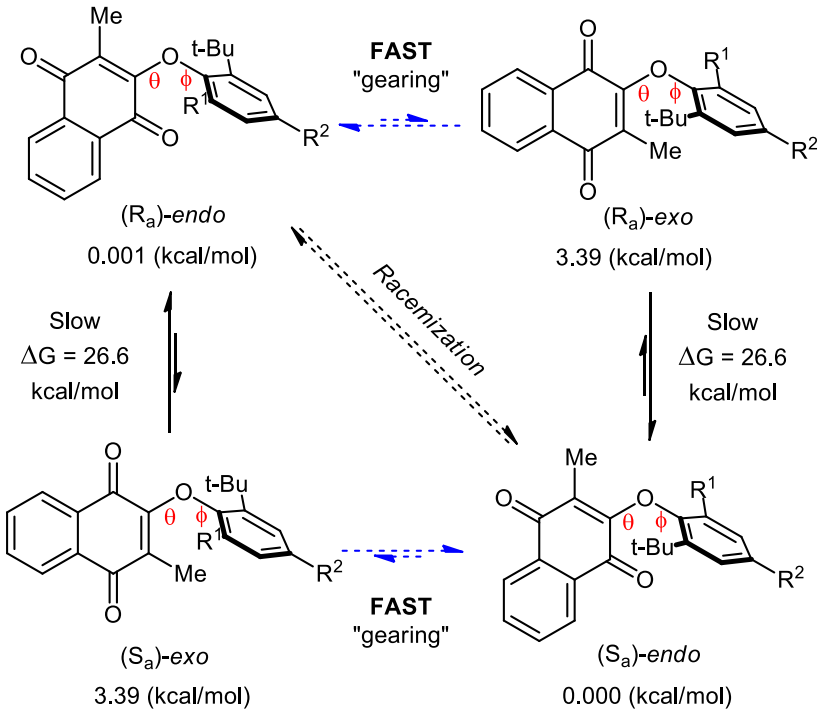

Scheme 4.5.3 Conformational Energy Simulations of 4.1a

As I generated these conformations for the computational CD studies I observed striking differences in their predicted energies (Scheme 4.5.3). For example, the *Sa-endo* conformation of **4.1a** is predicted to be significantly more stable than the *Sa-exo* conformation. Interestingly, I observed the opposite trend for the starting material **4.1**, with the *exo*- conformation being more stable (see experimental section 4.6.8 for more details).

To further investigate this, I generated contour energy maps of the rotational landscape about both axes (Scheme 4.5.4) of the diaryl ether. Consistent with results from Clayden,[146] these maps demonstrate that there is a low energy pathway for interconversion between the *exo*- and *endo*- conformations of a given enantiomer that proceeds via a concerted gearing mechanism. Thus, it is likely that the *exo*- conformation of the starting material is more stable and will likely be the conformation that interacts with the catalyst, however, the addition of the methyl group will lead to an immediate conformational gear shift to the *endo*- enantiomers.

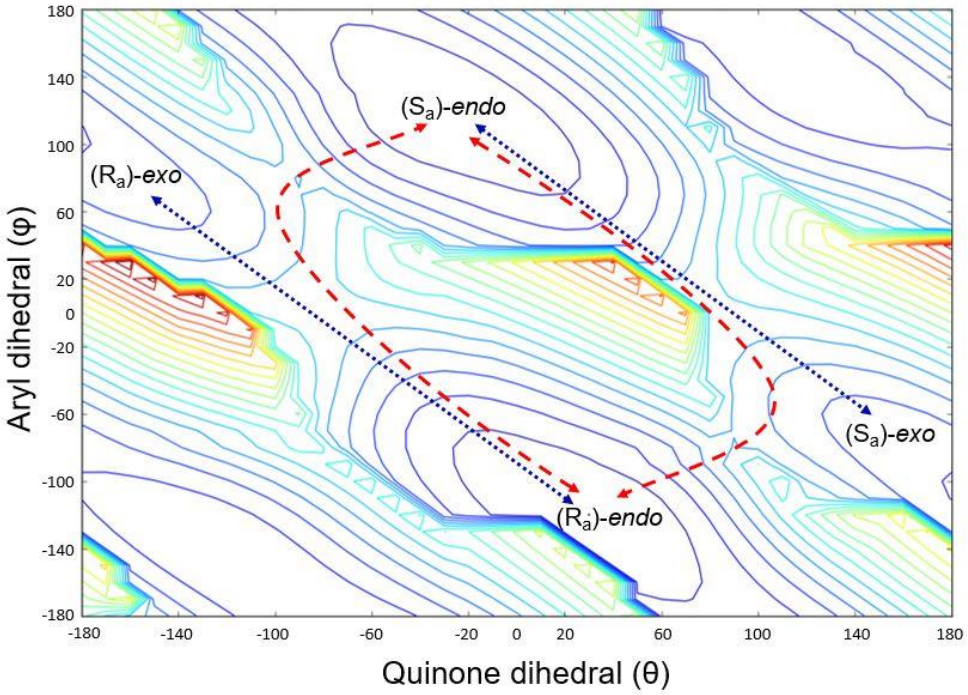

Scheme 4.5.4 Contour Energy Maps of 4.1a, Gearing Mechanism

My working model for stereoinduction is shown in the proposed transition state in Scheme 4.5.2, in which I propose that the urea moiety of the catalyst will hydrogen bond with both the ether oxygen and one of the quinone carbonyls of the lower energy *exo*- diaryl ether conformation. From here, the diaryl ether is preorganized into the S_a-atropisomer to avoid steric interactions between the *tert*-butyl group and the quinuclidinium that would be present in the R_a atropisomer/catalyst complex. I postulate that the hydrogen bonding will activate the diaryl ether for nucleophilic attack by the nitronate anion, which will go through the elimination of HNO_2 followed by tautomerization, or subsequent attack of another equivalent of nitronate and oxidation towards the 'nitroethylated' byproduct. At this point, it is likely that both products will rapidly relax to the *endo*- conformation, perhaps providing a release mechanism from the catalyst.

In conclusion I have disclosed to the best of our knowledge the first example of a small molecule catalytic synthesis of diaryl ethers. While our selectivities were moderate-to-good, highly enantioenriched ethers can be accessed via trituration. I also discussed several mechanistic aspects

of this work. I hope that these studies will serve as a starting place for future efforts towards the enantioselective syntheses of diaryl ethers and related atropisomers with biological relevance.

4.6 Experimental Section

4.6.1 General Information

All ^{1}H and ^{13}C NMR spectra were recorded on a Varian VNMRS 400 MHz or Varian Inova 500 MHz at room temperature. All chemical shifts were reported in parts per million (δ) and were internally referenced to residual protio solvents, unless otherwise noted. All spectral data were reported as follows: chemical shift (multiplicity [singlet (*s*), doublet (*d*), triplet (*t*), quartet (*q*), and multiplet (*m*)], coupling constants [Hz], integration). Carbon spectra were recorded with complete proton decoupling. Most fluorine spectra were recorded with internal fluorine standards (i.e. trifluoroacetic acid, trifluorotoluene). Conventional mass spectra were obtained using Advion expression^{s} CMS APCI/ASAP. For cross-coupling reactions, 1,4-dioxane and deionized H_2O were degassed under nitrogen flushing for 30 minutes. For the chlorination of substrates, purchased (*N*)-halosuccinimide was recrystallized from water before use. For nucleophilic aromatic substitution reactions, an Anton Paar Monowave 400 microwave reactor was utilized. All other chemicals used were purchased from Sigma Aldrich, TCI, Frontier Scientific, Acros Organics, Strem, Oakwood, Cambridge Isotope Laboratories, or Fisher and were used as received without further purification or recrystallization. All flash column chromatography (FCC) was performed using Grade 60 Silica gel (230-400 mesh) purchased from Fisher Scientific. All TLC preparatory plates were performed using Grade 60 Silica gel with fluorescent indicator F_{254} and were purchased from Fischer Scientific. Enantiomeric ratios (*er*) were determined by 1) HPLC analysis employing chiral stationary phase column specified for each individual experiment and 2) comparison of each sample with respective racemic mixtures. All data acquired were recorded on HP Agilent 1100 HPLC using Chiral Technologies Inc. Daicel Group Chiralpak IA Normal Phase chiral columns.

4.6.2 Abbreviations

NXS	*N*-(halogen)-succinimide
DCM	Dichloromethane
PhMe	Toluene
EtOAc	Ethyl Acetate
DMF	Dimethylformamide
r.t.	Room temperature
HCl	Hydrochloric Acid
NO_2Me	Nitromethane
M.S.	Molecular Sieves
Conc.	Concentration (M)
Equiv	Equivalents
LiCl	Lithium Chloride

4.6.3 Reaction Optimization

Table 4.6.1 Full Optimization Table for Enantioselective Methylation of 4.1

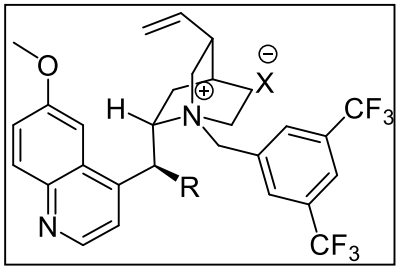

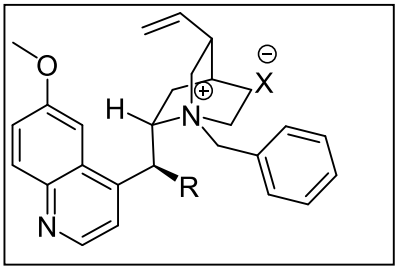

C1 R = 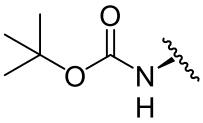 X = Br

C2 R = 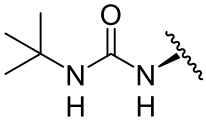 X = Br

C3 R = OH, X = Cl
C4 R = OH, X = Br
C5 R = OH, X = I
C6 R = OAc, X = Br

C7 R = OH, X = Cl
C8 R = OH, X = Br
C9 R = OH, X = I

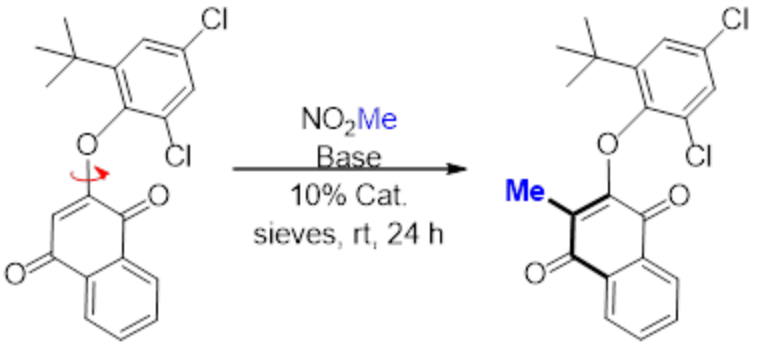

Entry	Solvent	Catalyst	Base	Sieves	Yield (%)	er
1	PhMe	TBAB	Cs_2CO_3	-	18	---
2	PhMe	**C1**	Cs_2CO_3	-	18	62:38
3	PhMe	**C2**	Cs_2CO_3	-	17	85:15
4	PhMe	**C3**	Cs_2CO_3	-	25	52:48
5	PhMe	**C4**	Cs_2CO_3	-	21	54:46
6	PhMe	**C5**	Cs_2CO_3	-	30	55:45
7	PhMe	**C6**	Cs_2CO_3	-	25	57:43
8	PhMe	**C7**	Cs_2CO_3	-	23	51:49
9	PhMe	**C8**	Cs_2CO_3	-	20	54:46
10	PhMe	**C9**	Cs_2CO_3	-	10	51:49
11	PhMe/H_2O	**C2**	Cs_2CO_3	-	40	50:50
12	NO_2Me	**C2**	Cs_2CO_3	-	71	50:50
13	PhMe	**C2**	Na_2CO_3	-	20	60:40
14	PhMe	**C2**	K_2CO_3	-	15	65:35
15	PhMe	**C2**	K_3PO_4	-	60	80:20
16	PhMe	**C2**	K_3PO_4	4Å	51	75:25
17	PhMe	**C1**	K_3PO_4	4Å	36	64:36
18	PhMe	**C2**	K_3PO_4	3Å	68	81:19
19	CH_2Cl_2	**C2**	K_3PO_4	3Å	38	68:32
20	MTBE	**C2**	K_3PO_4	3Å	71	73:27
21	$CHCl_3$	**C2**	K_3PO_4	3Å	45	60:40

To a scintillation vial was added 10 mg 3Å powdered M.S. with an oven dried stir bar. The sieves were activated with a Bunsen burner and toluene was syringed into the vial (0.1M). 2-(2-(*tert*-butyl)-4,6-dichlorophenoxy)naphthalene-1,4-dione (1 equiv), base (10 equiv), catalyst (0.1 equiv) and nitromethane (10 equiv) were added sequentially. The reaction was stirred at room temperature for 36 hours. The mixture was then diluted with toluene and filtered over Celite to remove excess base and molecular sieves. Purification with flash column chromatography (Hexanes:DCM 100:0 to 80:20) afforded the desired methylated product. All optimization trials were done in triplicate, with overall yield and enantioselectivity shown as an average.

4.6.4 General Procedures to Synthesize Diaryl Ether Substrates

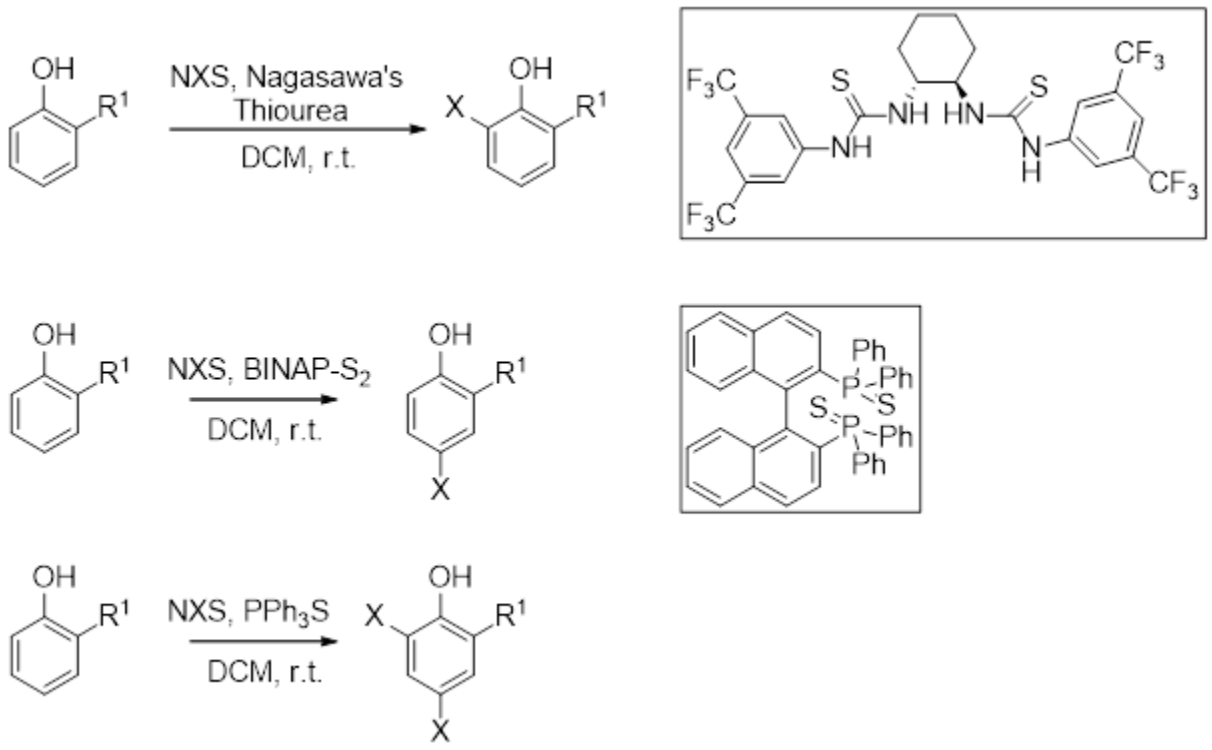

Figure 4.6.1 General Halogenation Procedure of Phenols

To phenol (1.0 equiv) was added NXS (1.0 or 2.0 equiv, X = Cl, Br), Lewis Base catalyst (2% to 5%) in 0.1M DCM. The reaction was stirred at room temperature for 12 hours. The mixture was then washed three times with $NaHCO_3$. The organic layer was collected and the aqueous layer

was extracted three times with DCM. The organic layers were combined, dried with Na_2SO_4 and concentrated *in vacuo* to yield crude products. Purification through normal phase flash column chromatography (hexanes:EtOAc::100:0 to 95:5) afforded the desired product. Selectivity of *ortho*-monohalogenated phenols was given by 1,1'-((*1R,2R*)-cyclohexane-1,2-diyl)bis(3-(3,5-bis(trifluoromethyl)phenyl) thiourea) (Nagasawa's Thiourea) while selectivity of *para*-monohalogenated phenols was given by 2,2'-Bis(diphenyl-phosphino)-1,1'-binaphthyl (BINAP)-disulfide catalyst. Triphenylphosphine sulfide catalyst was used for disubstituted halogenations. The catalyst selection is in agreeance with the literature.[156]

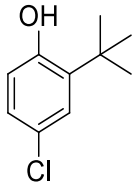

Figure 4.6.2 Precursor 2-(*tert*-butyl)-4-chlorophenol

Prepared and purified according to the general procedure: To 2-(*tert*-butyl)phenol (2 g, 13.3 mmol) was added *N*-chlorosuccinimide (1.8 g, 13.3 mmol) and 2,2'-Bis(diphenyl-phosphino)-1,1'-binaphtyl (BINAP)-disulfide (182 mg, 0.3 mmol) in DCM. The synthesis and spectral data of 2-(*tert*-butyl)-4-chlorophenol was in agreeance with the literature.[156]

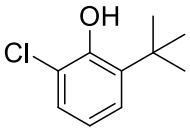

Figure 4.6.3 Precursor 2-(*tert*-butyl)-6-chlorophenol

Prepared and purified according to the general procedure: To 2-(*tert*-butyl)phenol (2 g, 13.3 mmol) was added *N*-chlorosuccinimide (1.8 g, 13.3mmol) and 1,1'-((*1R,2R*)-cyclohexane-1,2-diyl)bis(3-(3,5-bis(trifluoromethyl)phenyl) thiourea) (196 mg, 0.3 mmol) in DCM. The synthesis and spectral data of 2-(*tert*-butyl)-6-chlorophenol was in agreeance with the literature.[156]

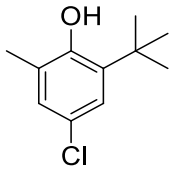

Figure 4.6.4 Precursor 2-(*tert*-butyl)-4-chloro-6-methylphenol

Prepared and purified according to the general procedure: To 2-(*tert*-butyl)-6-methylphenol (4 g, 23.4 mmol) was added *N*-chlorosuccinimide (3.1 g, 23.4 mmol) and triphenylphosphine sulfide (344 mg, 1.2 mmol) in DCM. 4.6 g (quantitative yield) of 2-(*tert*-butyl)-4-chloro-6-methylphenol was isolated as a clear oil. **^{1}H NMR (500 MHz, $CDCl_3$)** δ 7.12 (d, J = 2.0 Hz, 1H), 7.00 (d, J = 2.3 Hz, 1H), 4.73 (s, 1H), 2.24 (s, 3H), 1.41 (s, 9H). **^{13}C NMR (126 MHz, $CDCl_3$)** δ 151.21, 137.46, 127.90, 125.10, 124.65, 34.71, 29.53, 15.91. **MS (APCI): Calculated for** $C_{11}H_{16}ClO$ $[M+H]^+$ = 199.1. Found 199.1 m/z.

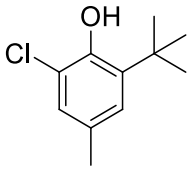

Figure 4.6.5 Precursor 2-(*tert*-butyl)-6-chloro-4-methylphenol

Prepared and purified according to the general procedure: To 2-(*tert*-butyl)-4-methylphenol (4 g, 23.4 mmol) was added *N*-chlorosuccinimide (3.1 g, 23.4 mmol) and triphenylphosphine sulfide (344 mg, 1.2 mmol) in DCM. 4.6 g (quantitative yield) of 2-(*tert*-butyl)-6-chloro-4-methylphenol was isolated as a pale yellow oil. **^{1}H NMR (500 MHz, $CDCl_3$)** δ 7.04 (d, J = 1.3 Hz, 1H), 6.99 (d, J = 1.4 Hz, 1H), 5.69 (s, 1H), 2.27 (s, 3H), 1.41 (s, 9H). **^{13}C NMR (126 MHz, $CDCl_3$)** δ 147.36, 137.12, 129.56, 126.51, 120.47, 35.10, 29.36, 20.68. **MS (APCI): Calculated for** $C_{11}H_{16}ClO$ $[M+H]^+$ = 199.1. Found 199.1 m/z.

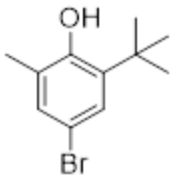

Figure 4.6.6 Precursor 4-bromo-2-(*tert*-butyl)-6-methylphenol

Prepared and purified according to the general procedure: To 2-(*tert*-butyl)-6-methylphenol (4 g, 24.4 mmol) was added *N*-bromosuccinimide (4.34 g, 24.4 mmol) and triphenylphosphine sulfide (359 mg, 1.2 mmol) in DCM. The synthesis and spectra data of 4-bromo-2-(*tert*-butyl)-6-methylphenol was in agreeance with the literature.[157]

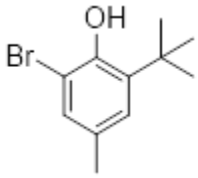

Figure 4.6.7 Precursor 2-bromo-6-(*tert*-butyl)-4-methylphenol

Prepared and purified according to the general procedure: To 2-(*tert*-butyl)-4-methylphenol (2 g, 12.2 mmol) was added *N*-bromosuccinimide (2.17 g, 12.2 mmol) and triphenylphosphine sulfide (180 mg, 0.6 mmol) in DCM. 2.8 g (96% yield) of 2-bromo-6-(tert-butyl)-4-methylphenol was isolated as a clear oil. **^{1}H NMR (500 MHz, $CDCl_3$)** δ 7.18 (d, J = 0.7 Hz, 1H), 7.03 (d, J = 0.7 Hz, 1H), 5.64 (s, 1H), 2.28 (s, 3H), 1.41 (s, 9H). **^{13}C NMR (126 MHz, $CDCl_3$)** δ 148.11, 137.17, 130.20, 129.58, 127.35, 111.87, 35.26, 29.37, 20.56. **MS (APCI): Calculated for** $C_{11}H_{16}BrO$ $[M+H]^+$ = 244.1. Found 244.1 m/z.

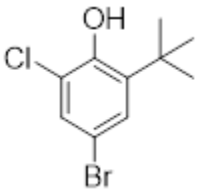

Figure 4.6.8 Precursor 4-bromo-2-(*tert*-butyl)-6-chlorophenol

Prepared according to the general procedure: To 2-(*tert*-butyl)-6-chlorophenol (1.60 g, 8.7 mmol) was added *N*-bromosuccinimide (1.54 g, 8.7 mmol) and triphenylphosphine sulfide (51.0 mg, 0.2 mmol) in DCM. 2.12 g (93% yield) of 4-bromo-2-(*tert*-butyl)-6-chlorophenol was isolated as a pale yellow oil. **^{1}H NMR (500 MHz, $CDCl_3$)** δ 7.37 (d, J = 2.3 Hz, 1H), 7.29 (d, J = 2.4 Hz, 1H), 5.85 (s, 1H), 1.40 (s, 9H). **^{13}C NMR (126 MHz, $CDCl_3$)** δ 148.99, 139.38, 129.05, 128.64, 121.51, 111.72, 35.47, 29.11. **MS (APCI): Calculated for** $C_{10}H_{13}BrClO$ $[M+H]^+$ = 263.0. Found 263.0 m/z

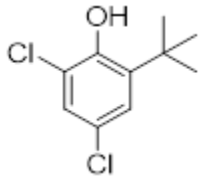

Figure 4.6.9 Precursor 2-(*tert*-butyl)-4,6-dichlorophenol

Prepared according to the general procedure: To 2-(*tert*-butyl)phenol (4 g, 26.8 mmol) was added *N*-chlorosuccinimide (7.88 g, 59.0 mmol) and triphenylphosphine sulfide (392 mg, 1.33 mmol) in DCM. 5.76 g (98% yield) of 2-(*tert*-butyl)-4,6-dichlorophenol was isolated as a clear oil. **^{1}H NMR (500 MHz, $CDCl_3$)** δ 7.24 (d, J = 2.6 Hz, 1H), 7.17 (d, J = 2.5 Hz, 1H), 5.82 (s, 1H), 1.41 (s, 9H). **^{13}C NMR (126MHz, $CDCl_3$)** δ 148.51, 138.93, 126.22, 125.83, 124.69, 121.12, 35.46, 29.10. **MS (APCI): Calculated for** $C_{10}H_{13}Cl_2O$ $[M+H]^+$ = 219.0. Found 219.0 m/z

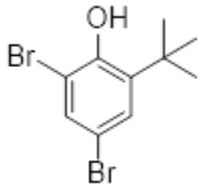

Figure 4.6.10 Precursor 2,4-dibromo-6-(*tert*-butyl)phenol

Prepared according to the general procedure: To 2-(*tert*-butyl)phenol (4 g, 26.6 mmol) was added *N*-bromosuccinimide (10.4 g, 58.6 mmol), triphenylphosphine sulfide (392 mg, 1.33 mmol) in DCM. 6.2 g (76% yield) of 2,4-dibromo-6-(*tert*-butyl)phenol was obtained as a clear oil. **^{1}H NMR (500 MHz, $CDCl_3$)** δ 7.50 (d, J = 2.4 Hz, 1H), 7.33 (d, J = 1.8 Hz, 1H), 5.80 (s, 1H), 1.40

(s, 9H). **^{13}C NMR (126MHz, $CDCl_3$)** δ 149.75, 139.39, 131.46, 129.78, 112.45, 112.22, 35.62, 29.12. **MS (APCI): Calculated for** $C_{10}H_{13}Br_2O$ $[M+H]^+$ = 309.0. Found 309.0 m/z.

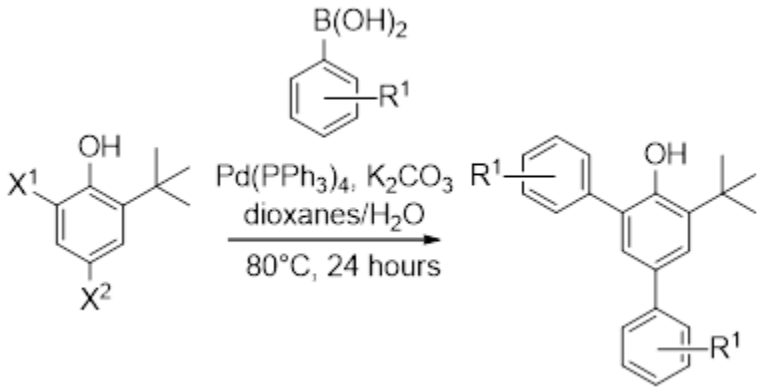

Figure 4.6.11 General Procedure for Suzuki Cross Coupling of Phenols

To phenol (1.0 equiv) was added substituted phenylboronic acid (1.2 or 2.5 equiv), $Pd(PPh_3)_4$, (0.05 equiv) and K_2CO_3 (4.0 equiv). The mixture was placed under vacuum then backfilled with argon for three cycles. To this mixture was added degassed 1,4-dioxane (100mg/mL) and water (300 mg/mL). The reaction was refluxed for 24 hours at 80 ˚C. The crude mixture was quenched with 5% LiCl, diluted with EtOAc and washed with H_2O and brine (3x each). The organic layer was collected, and the aqueous was extracted three times with EtOAc. The organic layers were combined, dried with Na_2SO_4 and concentrated *in vacuo* to yield crude products. Purification through flash column chromatography (hexanes:EtOAc::100:0 to 95:5) afforded the desired product (~45% to 80%). Completion of the reaction can be accelerated using a microwave reactor for 4 hours at 110 ˚C.

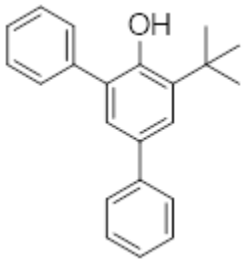

Figure 4.6.12 Precursor 5'-(*tert*-butyl)-[1,1'3',1''-terphenyl]-4'-ol

Prepared according to the general procedure: To 2,4-dibromo-6-(*tert*-butyl)phenol (2 g, 6.5 mmol) was added phenylboronic acid (1.99 g, 16.4 mmol), $Pd(PPh_3)_4$ (377 mg, 0.3 mmol) and K_2CO_3 (3.6 g, 26.2 mmol). The reaction was purged under vacuum, backfilled with argon and degassed 1,4-dioxane and water was added. The reaction was refluxed for 24 hours at 80 ˚C. 1.3 g (65% yield) was isolated as a thick brownish oil. **^{1}H NMR (500 MHz, $CDCl_3$)** δ 7.62-7.60 (m, 2H), 7.57 (d, *J* = 2.3 Hz, 1H), 7.55-7.54 (m, 4H), 7.46-7.43 (m, 3H), 7.36 (d, *J* = 2.3 Hz, 1H), 7.34-7.33 (m, 1H), 5.52 (s, 1H), 1.53 (s, 9H). **^{13}C NMR (126MHz, $CDCl_3$)** δ 150.67, 141.39, 137.18, 136.56, 132.91, 129.59, 129.54, 129.16, 128.69, 128.16, 126.88, 126.62, 126.58, 125.64, 35.15, 29.69. **MS (APCI): Calculated for** $C_{22}H_{23}O$ $[M+H]^+$ = 303.4. Found 303.4 m/z

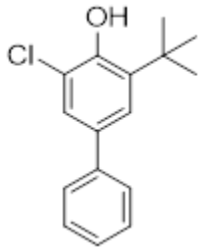

Figure 4.6.13 Precursor 3-(*tert*-butyl)-5-chloro-[1,1'-biphenyl]-4-ol

Prepared according to the general procedure: To 4-bromo-2-(*tert*-butyl)-6-chlorophenol (806 mg, 3.06 mmol) was added phenylboronic acid (447 mg, 3.67 mmol), $Pd(PPh_3)_4$ (173 mg, 0.15 mmol) and K_2CO_3 (1.69 g, 12.24 mmol). The reaction was purged under vacuum, backfilled with argon and degassed 1,4-dioxane and water was added. The reaction was refluxed for 24 hours at 80 ˚C. 535 mg (67% yield) of 3-(*tert*-butyl)-5-chloro-[1,1'-biphenyl]-4-ol was isolated as a clear oil. **^{1}H NMR (400 MHz, $CDCl_3$)** δ 7.54-7.51 (m, 2H), 7.45-7.41 (m, 4H), 7.34 (dt, 1H), 5.89 (s, 1H), 1.47 (s, 9H). **^{13}C NMR (126MHz, $CDCl_3$)** δ 149.12, 140.34, 137.70, 133.67, 128.80, 127.04, 126.81, 124.93, 124.82, 121.32, 35.40, 29.38. **MS (APCI): Calculated for** $C_{16}H_{18}ClO$ $[M+H]^+$ = 261.1. Found 261.1 m/z

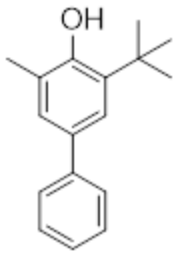

Figure 4.6.14 Precursor 3-(*tert*-butyl)-5-methyl-[1,1'-biphenyl]-4-ol

Prepared according to the general procedure: To 4-bromo-2-(*tert*-butyl)-6-methylphenol (1 g, 4.1 mmol) was added phenylboronic acid (600 mg, 4.91 mmol) $Pd(PPh_3)_4$ (71 mg, 0.06 mmol) and K_2CO_3 (2.2 g, 16.4 mmol). The reaction was purged under vacuum, backfilled with argon and degassed 1,4-dioxane and water. The reaction was refluxed for 24 hours at 80 ˚C. 490 mg (50% yield) of 3-(*tert*-butyl)-5-methyl-[1,1'-biphenyl]-4-ol was isolated as a white solid. **^{1}H NMR (500 MHz, $CDCl_3$)** δ 7.58-7.56 (m, 2H), 7.45-7.42 (m, 2H), 7.41 (d, J = 2.3 Hz, 1H), 7.32 (ddt, J = 8.6, 7.1, 1.3 Hz, 1H), 7.27 (d, J = 2.3 Hz, 1H), 4.83 (s, 1H), 2.35 (s, 3H), 1.50 (s, 9H). **^{13}C NMR (126MHz, $CDCl_3$)** δ 152.33, 141.63, 135.89, 133.04, 128.62, 127.31, 126.88, 126.44, 124.13, 123.34, 34.69, 29.81, 16.17. **MS (APCI): Calculated for** $C_{17}H_{21}O$ $[M+H]^+$ = 241.3. Found 241.3 m/z.

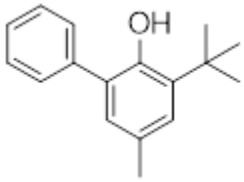

Figure 4.6.15 Precursor 3-(*tert*-butyl)-5-methyl-[1,1'-biphenyl]-2-ol

Prepared according to the general procedure: To 2-bromo-6-(*tert*-butyl)-4-methylphenol (678 mg, 2.79 mmol) was added phenylboronic acid (374 mg, 3.07 mmol), $Pd(PPh_3)_4$ (161 mg, 0.14 mmol), and K_2CO_3 (964 mg, 6.97 mmol). The reaction was purged under vacuum, backfilled with argon and degassed 1,4-dioxane and water. The reaction was refluxed for 24 hours at 80 ˚C. 3-(*tert*-butyl)-5-methyl-[1,1'-biphenyl]-2-ol (605 mg, 90% yield) was isolated as a dark orange oil.

^{1}H NMR (400 MHz, $CDCl_3$) δ 7.53 – 7.45 (m, 4H), 7.43 – 7.40 (m, 1H), 7.13 (d, *J* = 2.1 Hz, 1H), 6.92 (d, *J* = 2.2 Hz, 1H), 5.31 (s, 1H), 2.33 (s, 3H), 1.46 (s, 9H). **^{13}C NMR (126 MHz, $CDCl_3$)** δ 148.71, 137.43, 135.96, 129.50, 129.36, 128.69, 128.58, 128.28, 127.86, 127.28, 34.83, 29.64, 20.79. **MS (APCI): Calculated for** $C_{17}H_{21}O$ $[M+H]^+$ = 241.3. Found 241.3 m/z.

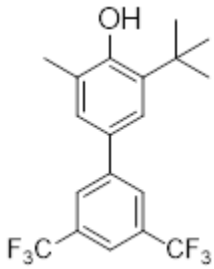

Figure 4.6.16 Precursor 3-(*tert*-butyl)-5-methyl-3',5'-bis(trifluoromethyl)-[1,1'-biphenyl]-4-ol

Prepared according to the general procedure: To 4-bromo-2-(*tert*-butyl)-6-methylphenol (1 g, 4.1 mmol) was added 3,5-Bis(trifluoromethyl)phenylboronic acid (1.3 g, 4.9 mmol), $Pd(PPh_3)_4$ (237 mg, 0.21 mmol), and K_2CO_3 (2.2 g, 16.4 mmol). The reaction was purged under vacuum, backfilled with argon and degassed 1,4-dioxane and water. The reaction was refluxed for 24 hours at 80 ˚C. 3-(*tert*-butyl)-5-methyl-3',5'-bis(trifluoromethyl)-[1,1'-biphenyl]-4-ol (450 mg, 30% yield) was isolated as a light yellow solid. **^{1}H NMR (400 MHz, $CDCl_3$)** δ 7.93 (s, 2H), 7.78 (s, 1H), 7.35 (d, *J* = 1.9 Hz, 1H), 7.25 (d, *J* = 1.7 Hz, 1H), 2.35 (s, 3H), 1.48 (s, 9H). **^{13}C NMR (126 MHz, $CDCl_3$)** δ 153.57, 143.73, 136.60, 132.00, 131.74, 130.04, 127.44, 126.75, 124.57, 124.14, 123.96, 122.40, 119.99, 119.93, 34.73, 29.69, 16.08. **^{19}F NMR (470 MHz, CDCl3)** δ -62.81. **MS (APCI): Calculated for** $C_{19}H_{19}F_6O$ $[M+H]^+$ = 377.3. Found 377.3 m/z

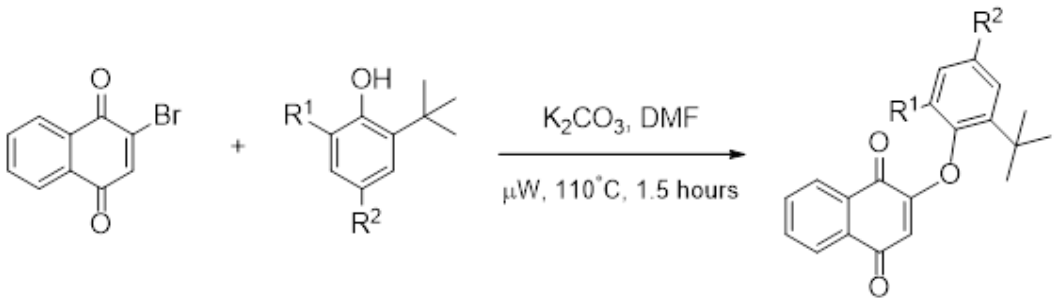

Figure 4.6.17 General Procedure for Nucleophilic Aromatic Substitution of Diaryl Ether Naphthoquinones

To a microwave reaction vessel was added 2-bromonaphthalene-1,4-dione (1.0 equiv), trisubstituted *tert*-butyl phenol (1.0 equiv), K_2CO_3 (3.0 equiv) and anhydrous DMF (1 M). The reaction was stirred in a microwave reactor at 110 ˚C for 1.5 hours. The mixture was then diluted with EtOAc, transferred into a separatory funnel and neutralized and washed with 4 M HCl (3x). The aqueous layer was then extracted with EtOAc (3x) and the combined organic layers were dried over Na_2SO_4 and concentrated *in vacuo*. Purification with flash column chromatography (hexanes:EtOAc::100:0 to 95:5). Recrystallization with hexanes combined with sonication afforded the desired products (~10% to 50% yield).

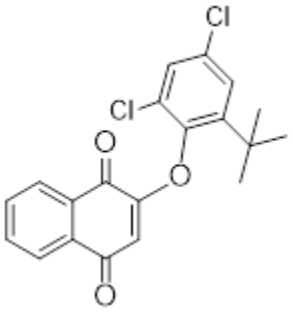

Figure 4.6.18 2-(2-(*tert*-butyl)-4,6-dichlorophenoxy)naphthalene-1,4-dione (4.1)

Prepared according to the general procedure: To a microwave reaction vessel was added 2-bromonaphthalene-1,4-dione (1 g, 4.2 mmol), 2-(*tert*-butyl)-4,6-dichlorophenol (924 mg, 4.2 mmol), K_2CO_3 (1.7 g, 12.7 mmol) and anhydrous DMF. The reaction was stirred in a microwave reactor at 110 ˚C for 1.5 hours. 2-(2-(*tert*-butyl)-4,6-dichlorophenoxy)naphthalene-1,4-dione (456 mg, 29% yield) was isolated as a bright yellow solid. **^{1}H NMR (400 MHz, $CDCl_3$)** δ 8.22 – 8.20

(m, 1H), 8.10 – 8.07 (m, 1H), 7.79 – 7.77 (m, 2H), 7.38 (q, 2H), 5.80 (s, 1H), 1.36 (s, 9H). **^{13}C NMR (101 MHz, $CDCl_3$)** δ 184.62, 178.93, 157.84, 146.05, 145.85, 134.49, 133.64, 132.01, 131.96, 131.03, 128.65, 128.20, 127.17, 126.83, 126.30, 114.01, 35.78, 30.37. **MS (APCI): Calculated for** $C_{20}H_{16}Cl_2O_3$ $[M+H]^+$ = 375.3. Found 375.3 m/z.

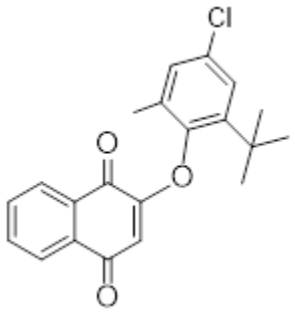

Figure 4.6.19 2-(2-(*tert*-butyl)-4-chloro-6-methylphenoxy)naphthalene-1,4-dione (4.2)

Prepared according to the general procedure: To a microwave reaction vessel was added 2-bromonaphthalene-1,4-dione (322 mg, 1.36 mmol), 2-(*tert*-butyl)-4-chloro-6-methylphenol (270 mg, 1.36 mmol), K_2CO_3 (563 mg, 4.1 mmol) and anhydrous DMF. The reaction was stirred in a microwave reactor at 110 °C for 1.5 hours. 2-(2-(*tert*-butyl)-4-chloro-6-methylphenoxy)naphthalene-1,4-dione (149 mg, 31% yield) as a bright yellow solid. **^{1}H NMR (500 MHz, $CDCl_3$)** δ 8.21 – 8.20 (m, 1H), 8.09 – 8.07 (m, 1H), 7.80 – 7.76 (m, 2H), 7.29 – 7.28 (m, 1H), 7.14 – 7.13 (m, 1H), 5.75 (s, 1H), 2.11 (s, 3H), 1.33 (s, 9H). **^{13}C NMR (126 MHz, $CDCl_3$)** δ 184.75, 179.34, 158.68, 147.98, 144.09, 134.51, 133.56, 132.25, 132.03, 131.53, 131.07, 129.56, 126.79, 126.33, 126.27, 113.27, 35.24, 30.59, 16.65. **MS (APCI): Calculated for** $C_{21}H_{20}ClO_3$ $[M+H]^+$ = 354.8. Found 354.8 m/z.

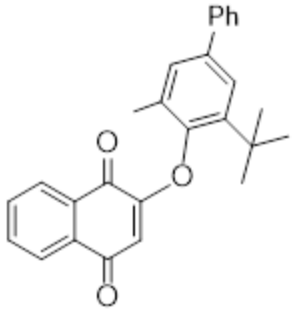

Figure 4.6.20 2-((3-(*tert*-butyl)-5-methyl-[1,1'-biphenyl]-4-yl)oxy)naphthalene-1,4-dione (4.3)

Prepared according to the general procedure: To a microwave reaction vessel was added 2-bromonaphthalene-1,4-dione (345 mg, 1.5 mmol), 3-(*tert*-butyl)-5-methyl-[1,1'-biphenyl]-4-ol (350 mg, 1.5 mmol), K_2CO_3 (605 mg, 4.5 mmol) and anhydrous DMF. The reaction was stirred in a microwave reactor at 110 ˚C for 1.5 hours. 2-((3-(*tert*-butyl)-5-methyl-[1,1'-biphenyl]-4-yl)oxy)naphthalene-1,4-dione (144 mg, 25% yield) was isolated as a bright yellow solid. **^{1}H NMR (500 MHz, $CDCl_3$)** δ 8.24-8.22 (m, 1H), 8.10-8.08 (m, 1H), 7.79-7.77 (m, 2H), 7.58-7.56 (m, 2H), 7.51 (d, *J* = 2.3 Hz, 1H), 7.48-7.44 (m, 2H), 7.39-7.35 (m, 1H), 7.34 (d, *J* = 1.5 Hz, 1H), 5.85 (s, 1H), 2.19 (s, 3H), 1.40 (s, 9H). **^{13}C NMR (126 MHz, $CDCl_3$)** δ 185.03, 179.57, 159.06, 148.96, 142.34, 140.72, 139.25, 134.45, 133.50, 132.13, 131.19, 130.66, 128.80, 128.67, 127.40, 127.20, 126.81, 126.25, 125.11, 113.34, 35.18, 30.88, 16.91. **MS (APCI): Calculated for** $C_{27}H_{25}O_3$ $[M+H]^+$ = 397.2 Found 397.2 m/z.

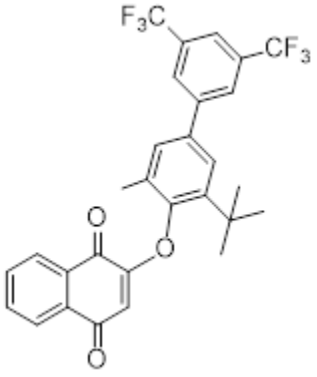

Figure 4.6.21 2-((3-(*tert*-butyl)-5-methyl-3',5'-bis(trifluoromethyl)-[1,1'-biphenyl]-4-yl)oxy)naphthalene-1,4-dione (4.4)

Prepared according to the general procedure: To a microwave reaction vessel was added 2-bromonaphthalene-1,4-dione (315 mg, 1.3 mmol), 3-(*ter*t-butyl)-5-methyl-3',5'-bis(trifluoromethyl)-[1,1'-biphenyl]-4-ol (500 mg, 1.33 mmol), K_2CO_3 (553 mg, 4.0 mmol) and anhydrous DMF. The reaction was stirred in a microwave reactor at 110 ˚C for 1.5 hours. 2-((3-(*tert*-butyl)-5-methyl-3',5'-bis(trifluoromethyl)-[1,1'-biphenyl]-4-yl)oxy)naphthalene-1,4-dione (95 mg, 13% yield) was isolated as a bright yellow solid. **^{1}H NMR (500 MHz, $CDCl_3$)** δ 8.24-8.22 (m, 1H), 8.10-8.08 (m, 1H), 7.99 (d, *J* = 1.5 Hz, 2H), 7.88 (s, 1H), 7.80-7.77 (m, 2H), 7.50 (d, *J* = 1.5 Hz, 1H), 7.37 (d, *J* = 1.5 Hz, 1H), 5.81 (s, 1H), 2.23 (s, 3H), 1.42 (s, 9H). **^{13}C NMR (126 MHz, $CDCl_3$)** δ 184.81, 179.38, 158.74, 150.18, 143.37, 142.89, 136.40, 134.54, 133.60, 132.30, 132.07, 132.03, 131.64, 131.13, 128.92, 127.32, 127.30, 126.85, 126.30, 125.20, 124.42, 122.25, 121.07, 113.38, 35.29, 30.79, 16.92. **^{19}F NMR (470 MHz, CDCl3)** δ -62.79. **MS (APCI): Calculated for** $C_{29}H_{22}F_6O_3$ $[M+H]^+$ = 533.5. Found 533.5 m/z.

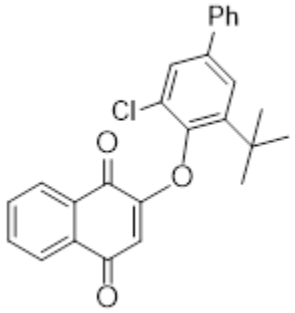

Figure 4.6.22 2-((3-(*tert*-butyl)-5-chloro-[1,1'-biphenyl]-4-yl)oxy)naphthalene-1,4-dione (4.5)

Prepared according to the general procedure: To a microwave reaction vessel was added 2-bromonaphthalene-1,4-dione (334 mg, 1.3 mmol), 3-(*tert*-butyl)-5-chloro-[1,1'-biphenyl]-4-ol (303 mg, 1.3 mmol), K_2CO_3 (530 mg, 3.8 mmol) and anhydrous DMF. The reaction was stirred in a microwave reactor at 110 ˚C for 1.5 hours. 2-((3-(*tert*-butyl)-5-chloro-[1,1'-biphenyl]-4-yl)oxy)naphthalene-1,4-dione (121 mg, 22% yield) was isolated as a yellow solid. **^{1}H NMR (500**

MHz, $CDCl_3$) δ 8.27-8.21 (m, 1H), 8.10-8.08 (m, 1H), 7.80-7.77 (m, 2H), 7.58-7.55 (m, 4H), 7.50-7.46 (m, 2H), 7.42-7.40 (m, 1H), 5.89 (s,1H), 1.42 (s, 9H). **^{13}C NMR (101 MHz, $CDCl_3$)** δ 184.89, 179.15, 158.24, 146.26, 144.68, 140.25, 139.37, 134.42, 133.58, 132.04, 131.13, 128.98, 128.02, 127.65, 127.53, 127.16, 126.82, 126.27, 125.62, 114.06, 35.66, 30.63. **MS (APCI): Calculated for** $C_{26}H_{21}ClO_3$ $[M+H]^+$ = 417.9 Found 417.9 m/z.

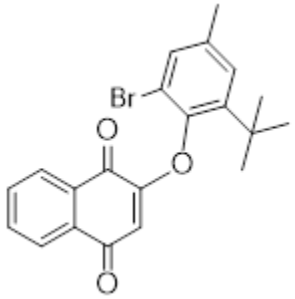

Figure 4.6.23 2-(2-bromo-6-(*tert*-butyl)-4-methylphenoxy)naphthalene-1,4-dione (4.6)

Prepared according to the general procedure: To a microwave reaction vessel was added 2-bromonaphthalene-1,4-dione (600 mg, 2.5 mmol), 2-bromo-6-(*tert*-butyl)-4-methylphenol (615 mg, 4.2 mmol) K_2CO_3 (875 mg, 6.3 mmol) and DMF. The reaction was stirred in a microwave reactor at 110 ˚C for 1.5 hours. 2-(2-bromo-6-(*tert*-butyl)-4-methylphenoxy)naphthalene-1,4-dione (87 mg, 9% yield) was obtained as a bright yellow solid. **^{1}H NMR (500 MHz, $CDCl_3$)** δ 8.23-8.21 (m, 1H), 8.09-8.07 (m, 1H), 7.78-7.76 (m, 2H), 7.33 (dd, J = 2.1, 0.8 Hz, 1H), 7.20 (dd, J = 2.0, 0.8 Hz, 1H), 5.79 (s, 1H), 2.35 (s, 3H), 1.34 (s, 9H). **^{13}C NMR (126 MHz, $CDCl_3$)** δ 184.89, 179.28, 158.50, 145.76, 144.15, 137.34, 134.36, 133.50, 132.53, 132.08, 131.16, 128.27, 126.80, 126.23, 116.69, 114.30, 35.43, 30.71, 20.95. **MS (APCI): Calculated for** $C_{21}H_{19}BrO_3$ $[M+H]^+$ = 400.3. Found 400.3 m/z.

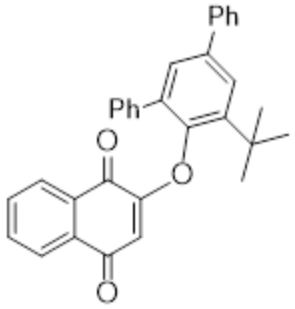

Figure 4.6.24 2-((5'-(*tert*-butyl)-[1,1':3',1''-terphenyl]-4'-yl)oxy)naphthalene-1,4-dione (4.7)

Prepared according to the general procedure: To a microwave reaction vessel was added 2-bromonaphthalene-1,4,-dione (157 mg, 0.6 mmol, 5'-(*tert*-butyl)-[1,1':3',1''-terphenyl]-4'-ol (200 mg, 0.6mmol), K_2CO_3 (273 mg, 1.98 mmol) and anhydrous DMF. The reaction was stirred in a microwave reactor at 110 ˚C for 1.5 hours. **2-((5'-(*tert*-butyl)-[1,1':3',1''-terphenyl]-4'-yl)oxy)naphthalene-1,4-dione** (98 mg, 32% yield) was isolated as a yellowish-orange solid. **^{1}H NMR (400 MHz, $CDCl_3$)** δ 8.06-8.03 (m, 1H), 7.90-7.89 (m, 1H), 7.67-7.61 (m, 5H), 7.51-7.46 (m, 5H), 7.41-7.39 (m, 1H), 7.24-7.22 (m, 2H), 7.13-7.09 (m, 1H), 5.73 (s, 1H), 1.46 (s, 1H). **^{13}C NMR (101 MHz, $CDCl_3$)** δ 184.59, 179.06, 158.43, 147.83, 143.14, 140.53, 139.55, 137.57, 135.33, 134.05, 133.19, 131.66, 130.74, 128.87, 128.57, 128.37, 127.64, 127.55, 127.23, 126.41, 126.27, 125.91, 114.15, 35.37, 30.75. **MS (APCI): Calculated for** $C_{32}H_{26}O_3$ $[M+H]^+$ = 458.6. Found 458.6 m/z.

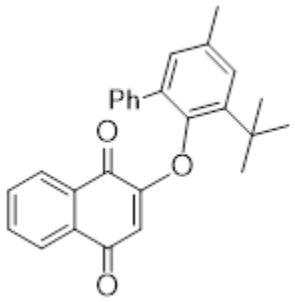

Figure 4.6.25 2-((3-(*tert*-butyl)-5-methyl-[1,1'-biphenyl]-2-yl)oxy)naphthalene-1,4-dione (4.8)

Prepared according to the general procedure: To a microwave reaction vessel was added 2-bromonaphthalene-1,4-dione (197 mg, 0.8 mmol), 3-(*tert*-butyl)-5-methyl-[1,1'-biphenyl]-2-ol (200 mg, 0.8 mmol), K_2CO_3 (345 mg, 2.5 mmol) and anhydrous DMF. The reaction was stirred in a microwave reactor at 110 ˚C for 1.5 hours. 2-((3-(*tert*-butyl)-5-methyl-[1,1'-biphenyl]-2-yl)oxy)naphthalene-1,4-dione (36 mg, 11% yield) was isolated as an orange-yellow solid. **^{1}H NMR (500 MHz, $CDCl_3$)** δ 8.04 – 8.01 (m, 1H), 7.90 – 7.87 (m, 1H), 7.65 – 7.63 (m, 2H), 7.42 – 7.38 (m, 2H), 7.26 (d, *J* = 1.6 Hz, 1H), 7.23 – 7.19 (m, 2H), 7.11 – 7.08 (m, 2H), 5.65 (s, 1H), 2.41 (s, 3H), 1.39 (s, 9H). **^{13}C NMR (101 MHz, $CDCl_3$)** δ 184.64, 179.16, 158.63, 146.09, 142.37, 137.70, 135.98, 134.71, 133.97, 133.11, 131.67, 130.75, 130.08, 128.81, 128.43, 127.98, 127.39, 126.37, 125.85, 113.96, 35.04, 30.73, 21.21. **MS (APCI): Calculated for** $C_{27}H_{25}O_3$ $[M+H]^+$ = 397.2 Found 397.2 m/z.

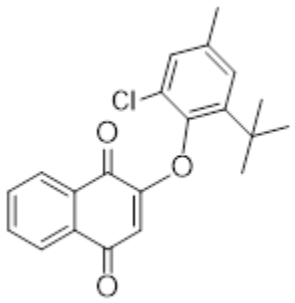

Figure 4.6.26 2-(2-(*tert*-butyl)-6-chloro-4-methylphenoxy)naphthalene-1,4-dione

Prepared according to the general procedure: To a microwave reaction vessel was added 2-bromonaphthalene-1,4-dione (1 g, 4.2 mmol), 2-(*tert*-butyl)-6-chloro-4-methylphenol (834 mg, 4.2 mmol) K_2CO_3 (1.7 g, 12.7 mmol) and anhydrous DMF. The reaction was stirred in a microwave reactor at 110 ˚C for 1.5 hours. **2-(2-(*tert*-butyl)-6-chloro-4-methylphenoxy)naphthalene-1,4-dione** (355 mg, 24% yield) was isolated as a bright yellow solid. **^{1}H NMR (400 MHz, $CDCl_3$)** δ 8.22-8.20 (m, 1H), 8.09-8.06 (m, 1H), 7.78-7.75 (m, 2H), 7.16 (d, 2H), 5.80 (s, 1H), 2.35 (s, 3H), 1.34 (s, 9H). **^{13}C NMR (101 MHz, $CDCl_3$)** δ 184.91,

179.24, 158.39, 144.66, 143.94, 136.89, 134.34, 133.49, 132.05, 131.14, 129.26, 127.42, 126.84, 126.76, 126.20, 113.91, 35.32, 30.61, 21.07. **MS (APCI): Calculated for** $C_{21}H_{20}ClO_3$ $[M+H]^+$ = 354.8. Found 354.8 m/z

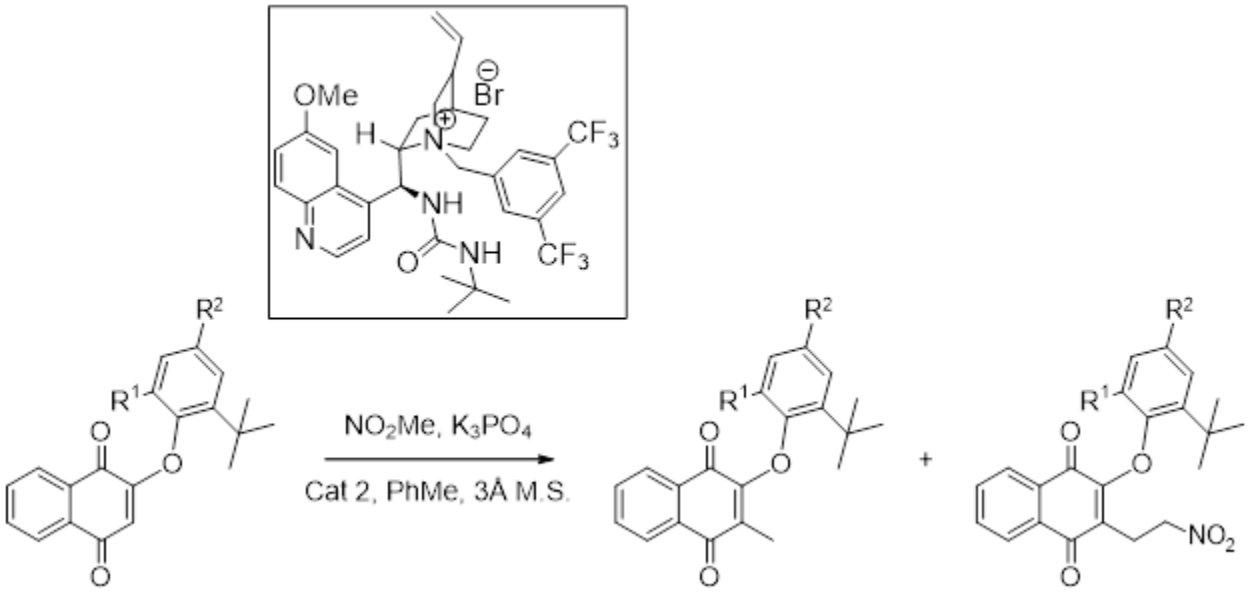

Figure 4.6.27 General Procedure for Methylation of Diaryl Ether Naphthoquinones

To a scintillation vial, 10 mg 3Å powdered M.S. was added with an oven dried stir bar. The sieves were activated with a Bunsen burner and toluene was syringed into the vial (0.1M). Diaryl ether naphthoquinone (1 equiv), potassium phosphate tribasic (10 equiv), quaternary ammonium salt (*1S,4S,5R*)-1-(3,5-bis(trifluoromethyl)benzyl)-2-((S)-(3-(*tert*-butyl)ureido)(6-methoxyquinolin-4-yl)methyl)-5-vinylquinuclidin-1-ium bromide (**C2**, 0.1 equiv) and nitromethane (10 equiv) were added sequentially. The reaction was stirred at room temperature for 36 hours. The mixture was then diluted with toluene and filtered over Celite to remove excess base and molecular sieves. Purification with flash column chromatography (hexanes:DCM::100:0 to 80:20) afforded the desired methylated and "nitroethylated" products. (~3% to 68% yield). **Note:** All substrates afforded a mixture of both products: shown below is the characterization of the major product.

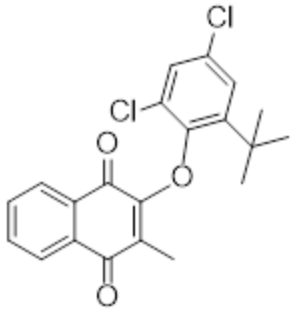

Figure 4.6.28 2-(2-(*tert*-butyl)-4,6-dichlorophenoxy)-3-methylnaphthalene-1,4-dione (4.1a)

Prepared according to the general procedure: To a scintillation vial was added 10 mg 3Å powdered molecular sieves with an oven dried stir bar, 2-(2-(*tert*-butyl)-4,6-dichlorophenoxy)naphthalene-1,4-dione (10 mg, 0.026 mmol) Catalyst 2, (2 mg, 0.0026 mmol), K_3PO_4, (55 mg, 0.26 mmol), nitromethane (16 mg, 0.26 mmol) and toluene (0.1M, 260 uL). The reaction was stirred at room temperature for 36 hours. 2-(2-(*tert*-butyl)-4,6-dichlorophenoxy)-3-methylnaphthalene-1,4-dione (68 % yield) was isolated as a bright yellow solid. Conversion of both products afforded a 10:1 ratio of **4.1a:4.1b. ^{1}H NMR (400 MHz, $CDCl_3$)** δ 8.13 (dd, J = 7.7, 1.3 Hz, 1H), 7.91 (dd, J = 7.5, 1.5 Hz, 1H), 7.72 (td, J = 7.5, 1.5 Hz, 1H), 7.66 (td, J = 7.5, 1.5 Hz, 1H), 7.32 (d, J = 2.5 Hz, 1H), 7.18 (d, J = 2.5 Hz, 1H), 2.26 (s, 3H), 1.38 (s, 9H). **^{13}C NMR (101 MHz, $CDCl_3$)** δ 185.01, 178.23, 154.23, 150.33, 142.76, 134.01, 133.37, 131.95, 130.49, 129.17, 128.39, 127.62, 126.47, 126.40, 126.29, 125.23, 35.85, 29.99, 9.73. **MS (APCI): Calculated for** $C_{21}H_{18}Cl_2O_3$ $[M+H]^+$ = 390.3. Found 390.3 m/z.

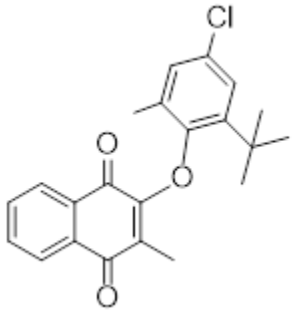

Figure 4.6.29 2-(2-(*tert*-butyl)-4-chloro-6-methylphenoxy)-3-methylnaphthalene-1,4-dione (4.2a)

Prepared according to the general procedure: To a scintillation vial was added 10 mg 3Å powdered molecular sieves with an oven dried stir bar, 2-(2-(*tert*-butyl)-4-chloro-6-methylphenoxy)naphthalene-1,4-dione (10 mg, 0.026 mmol) Catalyst 2, (2 mg, 0.0026mmol), K_3PO_4, (55 mg, 0.26 mmol), nitromethane (17 mg, 0.26 mmol) and toluene (0.1M, 260 uL). The reaction was stirred at room temperature for 36 hours**.** 2-(2-(*tert*-butyl)-4-chloro-6-methylphenoxy)-3-methylnaphthalene-1,4-dione (54% yield) was isolated as an orange solid. Conversion of both products afforded a 13:1 ratio of **4.2a:4.2b**. **^{1}H NMR (500 MHz, $CDCl_3$)** δ 8.12 (dd, *J* = 7.7, 1.3 Hz, 1H), 7.93 (dd, *J* = 7.6, 1.3 Hz, 1H), 7.73 (td, *J* = 7.6, 1.4 Hz, 1H), 7.66 (td, *J* = 7.5, 1.4 Hz, 1H), 7.25 (d, *J* = 2.9 Hz, 1H), 6.97 (d, *J* = 3.4 Hz, 1H), 2.21 (s, 3H), 2.00 (s, 3H), 1.36 (s, 9H). **^{13}C NMR (126 MHz, $CDCl_3$)** δ 185.06, 178.51, 154.50, 152.87, 141.40, 134.02, 133.36, 131.92, 130.60, 129.36, 129.10, 128.85, 127.91, 126.43, 126.25, 125.55, 35.36, 30.27, 16.97, 9.70. **MS (APCI): Calculated for** $C_{22}H_{21}ClO_3$ $[M+H]^+$ = 369.9. Found 369.9 m/z.

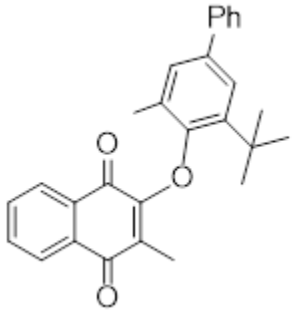

Figure 4.6.30 2-((3-(*tert*-butyl)-5-methyl-[1,1'-biphenyl]-4-yl)oxy)-3-methylnaphthalene-1,4-dione (4.3a)

Prepared according to the general procedure: To a scintillation vial was added 10 mg 3Å powdered molecular sieves with an oven dried stir bar, 2-((3-(*tert*-butyl)-5-methyl-[1,1'-biphenyl]-4-yl)oxy)naphthalene-1,4-dione (10 mg, 0.026 mmol) Catalyst 2, (2 mg, 0.0026 mmol), K_3PO_4, (55 mg, 0.26mmol), nitromethane (16 mg, 0.26 mmol) and toluene (0.1M, 260 uL). The reaction was stirred at room temperature for 36 hours. 2-((3-(*tert*-butyl)-5-methyl-[1,1'-biphenyl]-4-yl)oxy)-3-methylnaphthalene-1,4-dione (46% yield) was isolated as an orange oil. Conversion of

both products afforded a 12:1 ratio of **4.3a:4.3b**. **^{1}H NMR (500 MHz, $CDCl_3$)** δ 8.14-8.13 (m, 1H), 7.99-7.97 (m, 1H), 7.74(td, *J* = 7.5, 1.4 Hz, 1H), 7.68 (td, *J* = 7.5, 1.4 Hz, 1H), 7.63 – 7.61 (m, 2H), 7.54 (d, *J* = 2.3 Hz, 1H), 7.45 (dd, *J* = 8.4, 7.0 Hz, 2H), 7.36 – 7.33 (m, 1H), 7.23 (dd, *J* = 2.3, 0.8 Hz, 1H), 2.24 (s, 3H), 2.12 (s, 3H), 1.45 (s, 9H). **^{13}C NMR (126 MHz, $CDCl_3$)** δ 178.61, 176.55, 154.84, 153.87, 141.10, 139.77, 136.95, 133.94, 133.28, 132.01, 128.62, 128.09, 127.92, 127.61, 127.11, 126.91, 126.44, 126.22, 124.35, 109.99, 98.23, 35.32, 30.53, 29.71, 17.31, 9.73. **MS (APCI): Calculated for** $C_{28}H_{27}O_3$ $[M+H]^+$ = 411.5. Found 411.5 m/z.

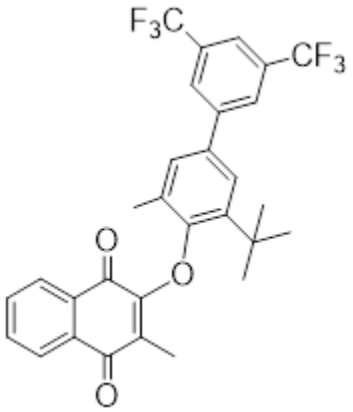

Figure 4.6.31 2-((3-(*tert*-butyl)-5-methyl-3',5'-bis(trifluoromethyl)-[1,1'-biphenyl]-4-yl)oxy)-3-methylnaphthalene-1,4-dione (4.4a)

Prepared according to the general procedure: To a scintillation vial was added 10 mg 3Å powdered molecular sieves with an oven dried stir bar, 2-((3-(*tert*-butyl)-5-methyl-3',5'-bis(trifluoromethyl)-[1,1'-biphenyl]-4-yl)oxy)naphthalene-1,4-dione (14 mg, 0.027 mmol) Catalyst 2, (2 mg, 0.0027 mmol), K_3PO_4, (57 mg, 0.27 mmol), nitromethane (17 mg, 0.26 mmol) and toluene (0.1M, 270 uL). The reaction was stirred at room temperature for 36 hours. 2-((3-(*tert*-butyl)-5-methyl-3',5'-bis(trifluoromethyl)-[1,1'-biphenyl]-4-yl)oxy)-3-methylnaphthalene-1,4-dione (68% yield) was isolated as a yellow oil. Conversion of both products afforded a 13:1 ratio of **4.4a:4.4b**. **^{1}H NMR (500 MHz, $CDCl_3$)** δ 8.15 (dd, *J* = 7.8, 1.3 Hz, 1H), 8.02 (d, *J* = 1.5 Hz, 2H), 7.96 (dd, *J* = 7.7, 1.3 Hz, 1H), 7.85 (d, *J* = 2.4 Hz, 1H), 7.75 (td, *J* = 7.5, 1.4 Hz, 1H), 7.69

(td, *J* = 7.5, 1.4 Hz, 1H), 7.51 (d, *J* = 2.4 Hz, 1H), 7.24 (d, *J* = 2.4, 1H), 2.29 (s, 3H), 2.14 (s, 3H), 1.46 (s, 9H). **^{13}C NMR (126 MHz, $CDCl_3$)** δ 185.07, 178.53, 155.15, 154.64, 143.28, 140.61, 134.10, 133.93, 133.39, 132.06, 131.96, 130.56, 128.72, 128.51, 128.30, 128.14, 127.17, 126.46, 126.30, 124.37, 35.40, 31.59, 30.44, 29.71, 22.66, 17.29, 14.13, 9.79. **^{19}F NMR (470 MHz, CDCl3)** δ -62.78 **MS (APCI): Calculated for** $C_{30}H_{24}F_6O_3$ $[M+H]^+$ = 547.5. Found 547.5 m/z.

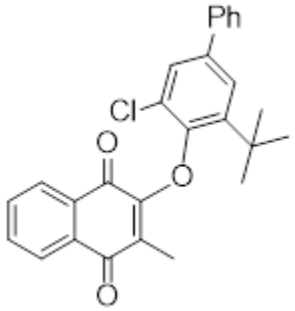

Figure 4.6.32 2-((3-(*tert*-butyl)-5-chloro-[1,1'-biphenyl]-4-yl)oxy)-3-methylnaphthalene-1,4-dione (4.5a)

Prepared according to the general procedure: To a scintillation vial was added 10 mg 3Å powdered molecular sieves with an oven dried stir bar, 2-((3-(*tert*-butyl)-5-chloro-[1,1'-biphenyl]-4-yl)oxy)naphthalene-1,4-dione (11 mg, 0.027 mmol) Catalyst 2, (2 mg, 0.0027 mmol), K_3PO_4, (57 mg, 0.27 mmol), nitromethane (17 mg, 0.26 mmol) and toluene (0.1M, 270 uL). The reaction was stirred at room temperature for 36 hours**.** 2-((3-(*tert*-butyl)-5-chloro-[1,1'-biphenyl]-4-yl)oxy)-3-methylnaphthalene-1,4-dione (47% yield) was isolated as an orange solid. Conversion of both products afforded a 6:1 ratio of **2e:3e**. **^{1}H NMR (400 MHz, $CDCl_3$)** δ 8.13 (dd, *J* = 7.8, 1.1 Hz, 1H), 7.94 (dd, *J* = 7.6, 1.9 Hz, 1H), 7.72 (td, *J* = 7.5, 1.4 Hz, 1H), 7.66 (td, *J* = 7.5, 1.4 Hz, 1H), 7.58 – 7.56 (m, 3H), 7.46 – 7.43 (m, 2H), 7.40 (d, *J* = 2.3 Hz, 1H), 7.37 – 7.34 (m, 1H), 2.29 (s, 3H), 1.45 (s, 9H). **^{13}C NMR (126 MHz, $CDCl_3$)** δ 185.18, 178.32, 154.64, 150.86, 141.52, 139.88, 137.61, 133.91, 133.29, 132.06, 130.66, 128.80, 128.12, 127.49, 127.07, 126.64, 126.42, 126.26, 124.97, 35.79, 30.27, 29.71, 22.70, 14.13, 9.74. **MS (APCI): Calculated for** $C_{27}H_{23}ClO_3$ $[M+H]^+$ = 431.9. Found 431.9 m/z.

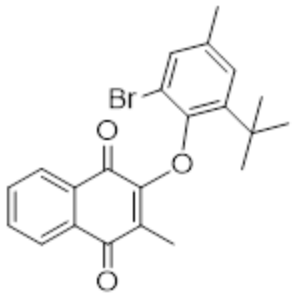

Figure 4.6.33 2-(2-bromo-6-(*tert*-butyl)-4-methylphenoxy)-3-methylnaphthalene-1,4-dione (4.6a)

Prepared according to the general procedure: To a scintillation vial was added 10 mg 3Å powdered molecular sieves with an oven dried stir bar, 2-(2-bromo-6-(*tert*-butyl)-4-methylphenoxy)naphthalene-1,4-dione (14 mg, 0.027 mmol) Catalyst 2, (2 mg, 0.0027 mmol), K_3PO_4, (57 mg, 0.27 mmol), nitromethane (17 mg, 0.26 mmol) and toluene (0.1M, 270 uL). The reaction was stirred at room temperature for 36 hours. 2-(2-bromo-6-(*tert*-butyl)-4-methylphenoxy)-3-methylnaphthalene-1,4-dione (10% yield) was isolated as a dark orange oil. **^{1}H NMR (500 MHz, $CDCl_3$)** δ 8.12 – 8.10 (m, 1H), 7.94 – 7.92 (m, 1H), 7.70 (td, J = 7.6, 1.4 Hz, 1H), 7.64 (td, J = 7.5, 1.4 Hz, 1H), 7.17 (ddd, J = 9.0, 2.1, 0.8 Hz, 2H), 2.34 (s, 3H), 2.24 (s, 3H), 1.37 (s, 9H). **^{13}C NMR (126 MHz, $CDCl_3$)** δ 185.18, 181.89, 134.81, 133.78, 133.21, 131.53, 127.56, 126.40, 126.16, 113.86, 109.99, 35.54, 31.93, 30.30, 29.70, 29.37, 22.70, 20.93, 14.12, 9.79. **MS (APCI): Calculated for** $C_{22}H_{21}BrO_3$ $[M+H]^+$ = 414.0. Found 414.0 m/z.

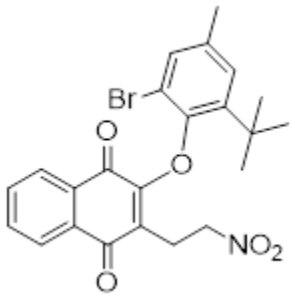

Figure 4.6.34 2-(2-bromo-6-(*tert*-butyl)-4-methylphenoxy)-3-(2-nitroethyl)naphthalene-1,4-dione (4.6b)

Prepared according to the general procedure: To a scintillation vial was added 10 mg 3Å powdered molecular sieves with an oven dried stir bar, 2-(2-bromo-6-(*tert*-butyl)-4-methylphenoxy) naphthalene-1,4-dione (14 mg, 0.027mmol) Catalyst 2, (2 mg, 0.0027 mmol), K_3PO_4, (57 mg, 0.27 mmol), nitromethane (17 mg, 0.26 mmol) and toluene (0.1M, 270 uL). The reaction was stirred at room temperature for 36 hours. 2-(2-bromo-6-(*tert*-butyl)-4-methylphenoxy)-3-(2-nitroethyl)naphthalene-1,4-dione (30% yield) was isolated as an orange solid. **^{1}H NMR (500 MHz, $CDCl_3$)** δ 8.13 (dd, J = 7.6, 1.3 Hz, 1H), 7.93 (dd, J = 7.7, 1.3 Hz, 1H), 7.75 (td, J = 7.6, 1.4 Hz, 1H), 7.68 (td, J = 7.5, 1.4 Hz, 1H), 7.21 (d, J = 2.0 Hz, 1H), 7.17 (d, J = 2.2 Hz, 1H), 4.80 – 4.68 (m, 2H), 3.59 (ddd, J = 13.2, 9.0, 6.9 Hz, 1H), 3.43 (ddd, J = 13.2, 8.8, 6.0 Hz, 1H), 2.35 (s, 3H), 1.37 (s, 9H). **^{13}C NMR (126 MHz, $CDCl_3$)** δ 184.16, 177.98, 155.80, 149.75, 135.52, 134.29, 133.68, 131.66, 130.66, 128.41, 127.85, 127.48, 126.70, 126.41, 124.44, 71.98, 35.54, 30.32, 29.70, 22.44, 20.94. **Calculated for** $C_{23}H_{22}BrNO_5$ $[M+H]^+$ = 473.3. Found 473.3 m/z.

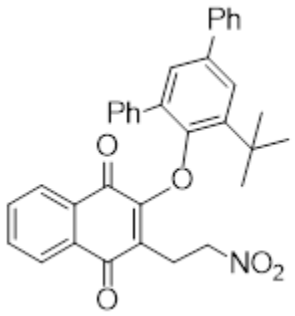

Figure 4.6.35 2-((5'-(*tert*-butyl)-[1,1':3',1''-terphenyl]-4'-yl)oxy)-3-(2-nitroethyl)naphthalene-1,4-dione (4.7b)

Prepared according to the general procedure: To a scintillation vial was added 10 mg 3Å powdered molecular sieves with an oven dried stir bar, 2-((5'-(*tert*-butyl)-[1,1':3',1''-terphenyl]-4'-yl)oxy)naphthalene-1,4-dione (14 mg, 0.027 mmol) Catalyst 2, (2 mg, 0.0027 mmol), K_3PO_4, (57 mg, 0.27 mmol), nitromethane (17 mg, 0.26 mmol) and toluene (0.1M, 270 uL). The reaction was

stirred at room temperature for 36 hours. 2-((5'-(*tert*-butyl)-[1,1':3',1"-terphenyl]-4'-yl)oxy)-3-(2-nitroethyl)naphthalene-1,4-dione (65% yield) was isolated as a dark orange solid. Conversion of both products afforded a 1:7 ratio of **2g:3g ^{1}H NMR (500 MHz, $CDCl_3$)** δ 7.91 – 7.89 (m, 1H), 7.86 – 7.82 (m, 1H), 7.73 (d, *J* = 2.3 Hz, 1H), 7.67 – 7.63 (m, 4H), 7.47 – 7.44 (m, 2H), 7.39 – 7.34 (m, 1H), 7.29 (d, *J* = 2.4 Hz, 1H), 7.14 – 7.10 (m, 2H), 7.03 – 6.97 (m, 3H), 4.63 – 4.60 (m, 2H), 3.33 (dt, *J* = 13.3, 7.9 Hz, 1H), 3.17 (dt, *J* = 13.3, 7.5 Hz 1H), 1.53 (s, 9H). **^{13}C NMR (126 MHz, $CDCl_3$)** δ 183.89, 177.83, 156.54, 152.79, 140.65, 139.96, 137.71, 137.05, 133.81, 133.35, 132.39, 131.11, 130.44, 128.72, 128.12, 127.86, 127.69, 127.18, 127.16, 126.23, 125.94, 125.90, 124.61, 72.87, 35.50, 30.34, 22.88. **MS (APCI): Calculated for** $C_{34}H_{25}NO_5$ $[M+H]^+$ = 532.7. Found 532.7 m/z.

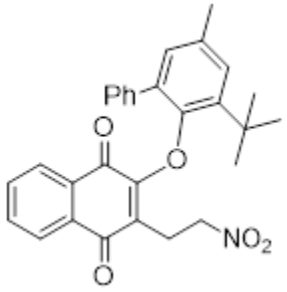

Figure 4.6.36 2-((3-(*tert*-butyl)-5-methyl-[1,1'-biphenyl]-2-yl)oxy)-3-(2-nitroethyl)naphthalene-1,4-dione (4.8b)

Prepared according to the general procedure: To a scintillation vial was added 10 mg 3Å powdered molecular sieves with an oven dried stir bar, 2-((3-(*tert*-butyl)-5-methyl-[1,1'-biphenyl]-2-yl)oxy)naphthalene-1,4-dione (50 mg, 0.13 mmol), Catalyst 2 (7 mg, 0.013mmol), K_3PO_4 (267 mg, 1.3 mmol), nitromethane (77 mg, 1.3 mmol) and toluene (0.1M, 1.3 mL). The reaction was stirred at room temperature for 36 hours. 2-((3-(*tert*-butyl)-5-methyl-[1,1'-biphenyl]-2-yl)oxy)-3-(2-nitroethyl)naphthalene-1,4-dione (49% yield) was isolated as a dark orange solid. Conversion of both products afforded a 1:5 ratio of **2h:3h**. **^{1}H NMR (500 MHz, $CDCl_3$)** δ 7.90 – 7.88 (m, 1H), 7.83 – 7.81 (m, 1H), 7.66 – 7.61 (m, 2H), 7.31 (dd, *J* = 2.3, 0.7 Hz, 1H), 7.06 – 7.05 (m, 2H),

6.98 – 6.96 (m, 3H), 6.87 (dd, *J* = 2.2, 0.8 Hz, 1H), 4.62 – 4.56 (m, 2H), 3.30 (dt, *J* = 13.2, 7.8 Hz, 1H), 3.15 (ddd, *J* = 13.2, 7.6, 6.6 Hz, 1H), 2.41 (s, 3H), 1.46 (s, 9H). **^{13}C NMR (126 MHz, $CDCl_3$)** *δ* 183.92, 177.93, 156.66, 151.08, 139.31, 137.85, 133.72, 133.60, 133.28, 131.85, 131.19, 131.09, 130.35, 129.50, 128.04, 127.81, 127.65, 126.21, 125.83, 124.36, 72.87, 35.20, 30.33, 29.71, 22.78, 21.19, 14.13. **MS (APCI): Calculated for** $C_{29}H_{27}NO_5$ $[M+H]^+$ = 470.5. Found 470.5 m/z.

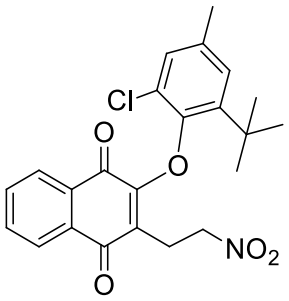

Figure 4.6.37 2-(2-(*tert*-butyl)-6-chloro-4-methylphenoxy)-3-(2-nitroethyl)naphthalene-1,4-dione (4.9b)

Prepared according to the general procedure: To a scintillation vial was added 10 mg 3Å powdered molecular sieves with an oven dried stir bar, 2-(2-(*tert*-butyl)-6-chloro-4-methylphenoxy)naphthalene-1,4-dione (10 mg, 0.026 mmol), Catalyst 2, (2 mg, 0.0026 mmol), K_3PO_4, (55 mg, 0.26 mmol), nitromethane (17 mg, 0.26 mmol) and toluene (0.1M, 260 uL). The reaction was stirred at room temperature for 36 hours. 2-(2-(*tert*-butyl)-6-chloro-4-methylphenoxy)-3-(2-nitroethyl)naphthalene-1,4-dione (68% yield) was isolated as an orange-yellow solid. Conversion of both products afforded a 1:5 ratio of **2i:3i**. **^{1}H NMR (500 MHz, $CDCl_3$)** *δ* 8.15 (ddd, *J* = 7.7, 1.4, 0.6 Hz, 1H), 7.95 (ddd, *J* = 7.6, 1.4, 0.5 Hz, 1H), 7.77 (td, *J* = 7.5, 1.4 Hz, 1H), 7.70 (td, *J* = 7.5, 1.4 Hz, 1H), 7.18 (dd, *J* = 2.1, 0.7 Hz, 1H), 7.02 (dd, *J* = 2.2, 0.7 Hz, 1H), 4.74 (qdd, *J* = 13.0, 8.7, 6.5 Hz, 2H), 3.61 (ddd, *J* = 13.3, 8.8, 6.9 Hz, 1H), 3.45 (ddd, *J* = 13.3, 8.7, 6.2 Hz, 1H), 2.36 (d, *J* = 0.7 Hz, 3H), 1.39 (s, 9H). **^{13}C NMR (126 MHz, $CDCl_3$)** *δ* 184.20, 178.06, 155.95, 148.79, 140.97, 134.91, 134.33, 133.70, 131.64, 130.63, 128.49, 127.12,

126.69, 126.43, 124.40, 123.96, 72.19, 35.47, 30.26, 22.36, 21.06. **MS (APCI): Calculated for** $C_{23}H_{22}ClNO_5$ $[M+H]^+$ = 428.8. Found 428.8 m/z.

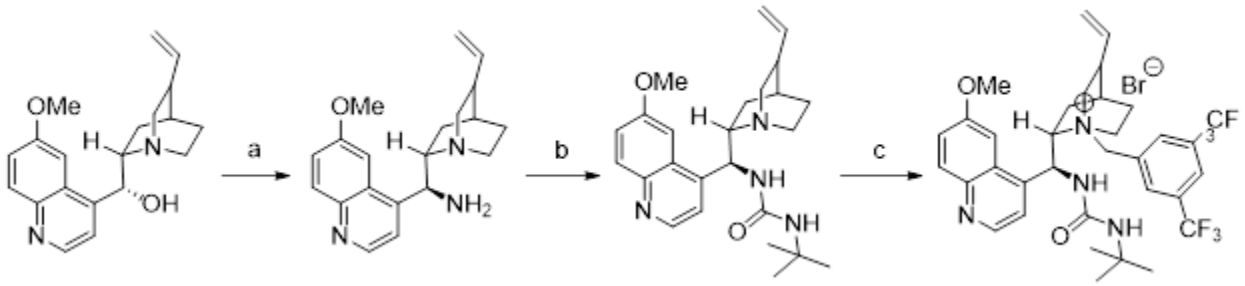

Figure 4.6.38 Synthesis of Cinchona Alkaloid Quaternary Ammonium Salt Catalysts

Step a: 9-amino (9-deoxy) *epi*-quinine was converted to the respective primary amine with inverted stereochemistry, as shown in previous literature.[158]

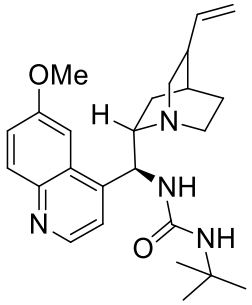

Figure 4.6.39 1-(*tert*-butyl)-3-((*S*)-(6-methoxyquinolin-4-yl)((*1R,2S,4R*)-quinuclidin-2-yl)methyl)urea, C4.2 catalyst precursor

Step b: To an oven-dried round bottom flask was added (S)-(6-methoxyquinolin-4-yl)((1R,2S,4R)-quinuclidin-2-yl)methanamine (1.0 equiv, 3.08 mmol). Anhydrous THF (1M) was added to the flask and *tert*-butyl isocyanate (1.5 equiv, 4.62 mmol). The reaction was stirred at room temperature for 4 hours. The mixture was then purified by flash column chromatography (DCM:MeOH::100:0 to 94:6) to afford the desired product, 1-(*tert*-butyl)-3-((*S*)-(6-methoxyquinolin-4-yl)((*1R,2S,4R*)-quinuclidin-2-yl)methyl)urea (90% yield). **^{1}H NMR (500 MHz, $CDCl_3$)** δ 8.74 (d, J = 4.5 Hz, 1H), 8.02 (d, J = 9.2 Hz, 1H), 7.84 (s, 1H), 7.41 – 7.39 (m, 2H), 6.59 (s, 1H), 5.81 (ddd, J = 17.2, 10.4, 6.7 Hz, 1H), 5.52 (s, 1H), 5.26 – 5.22 (m, 2H), 4.26 (td, J = 10.8, 4.9 Hz, 1H), 4.03 (s, 3H), 3.68 (dd, J = 13.8, 10.5 Hz, 1H), 3.47 (s, 3H), 3.45 – 3.38

(m, 1H), 3.23 – 3.09 (m, 1H), 2.73 (q, *J* = 8.1 Hz, 1H), 2.12 – 1.94 (m, 4H), 1.30 (s, 9H). **^{13}C NMR (126 MHz, $CDCl_3$)** δ 158.60, 156.52, 147.47, 141.93, 136.70, 131.78, 128.15, 122.54, 117.73, 101.81, 59.29, 56.11, 54.18, 50.65, 41.34, 36.73, 29.25, 26.93, 25.03, 24.47. **Calculated for** $C_{25}H_{34}N_4O_2$ $[M+H]^+$ = 423.5. Found 423.5 m/z.

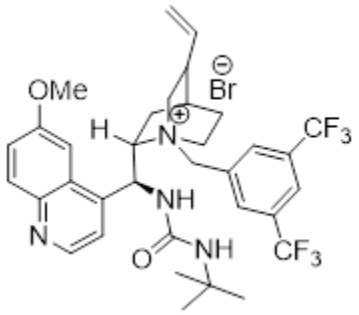

Figure 4.6.40 (*1R,2S,4R*)-1-(3,5-bis(trifluoromethyl)benzyl)-2-((*S*)-(3-(*tert*-butyl)ureido)(6-methoxyquinolin-4-yl)methyl)quinuclidin-1-ium bromide, C4.2

Step c: To an oven-dried round bottom flask was added 1-(*tert*-butyl)-3-((*S*)-(6-methoxyquinolin-4-yl)((*1R,2S,4R*)-quinuclidin-2-yl)methyl)urea (1.0 equiv, 1.63 mmol). Anhydrous MeOH (0.5M) was added to the flask and 1-(bromomethyl)-3,5-bis(trifluoromethyl)benzene (1.5 equiv, 2.44 mmol). The reaction mixture was then refluxed at 70 ˚C for 24 hours. The crude mixture was purified by two rounds of flash column chromatography (EtOAc:MeOH 9:1 and DCM:MeOH 20:1) to afford the desired product, (*1R,2S,4R*)-1-(3,5-bis(trifluoromethyl)benzyl)-2-((*S*)-(3-(*tert*-butyl)ureido)(6-methoxyquinolin-4-yl)methyl)quinuclidin-1-ium bromide (54% yield). **^{1}H NMR (500 MHz, $CDCl_3$)** δ 8.84 (d, *J* = 4.7 Hz, 1H), 8.17 (dd, *J* = 10.5, 7.0 Hz, 2H), 8.09 (s, 2H), 8.04 (s, 1H), 7.57 (d, *J* = 11.4 Hz, 1H), 7.46 (dd, *J* = 9.2, 2.5 Hz, 1H), 7.19 – 7.12 (m, 1H), 6.93 (d, *J* = 10.7 Hz, 1H), 6.49 (s, 1H), 6.15 (t, *J* = 10.2 Hz, 1H), 5.88 (ddd, *J* = 17.3, 10.4, 7.0 Hz, 1H), 5.39 – 5.24 (m, 3H), 4.67 – 4.41 (m, 3H), 4.03 (s, 3H), 3.46 (dd, *J* = 12.8, 10.2 Hz, 1H), 3.23 – 3.10 (m, 1H), 2.67 – 2.55 (m, 1H), 2.35 (s, 1H), 2.16 (ddd, *J* = 44.2, 25.4, 12.2 Hz, 2H), 1.94 (s, 1H), 1.35 (s, 9H). **^{13}C NMR (126 MHz, $CDCl_3$)** δ 159.40, 155.69, 134.40, 133.67, 133.32, 132.98, 130.34,

129.01, 128.20, 127.23, 126.62, 125.27, 124.79, 124.71, 123.89, 121.18, 120.24, 119.57, 104.99, 100.57, 81.93, 67.32, 63.76, 59.47, 56.00, 51.25, 49.24, 37.60, 28.12, 27.63, 26.84, 24.85. **^{19}F NMR (470 MHz, CDCl3)** δ -62.73. **Calculated for** $C_{34}H_{39}BrF_6N_4O_2[M+H]^+$ = 730.5. Found 730.5 m/z and 423.5 m/z fragmentation.

4.6.5 NMR Spectra

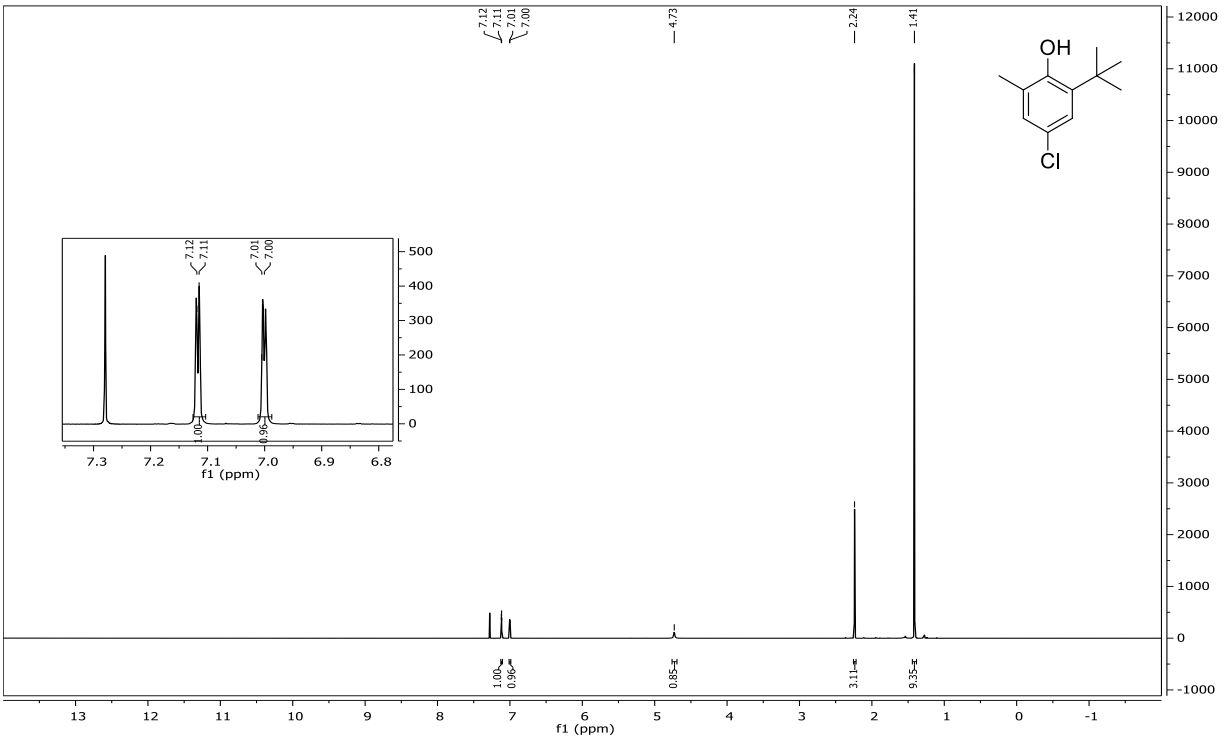

Figure 4.6.41 500 MHz ^{1}H Spectrum of 2-(*tert*-butyl)-4-chloro-6-methylphenol

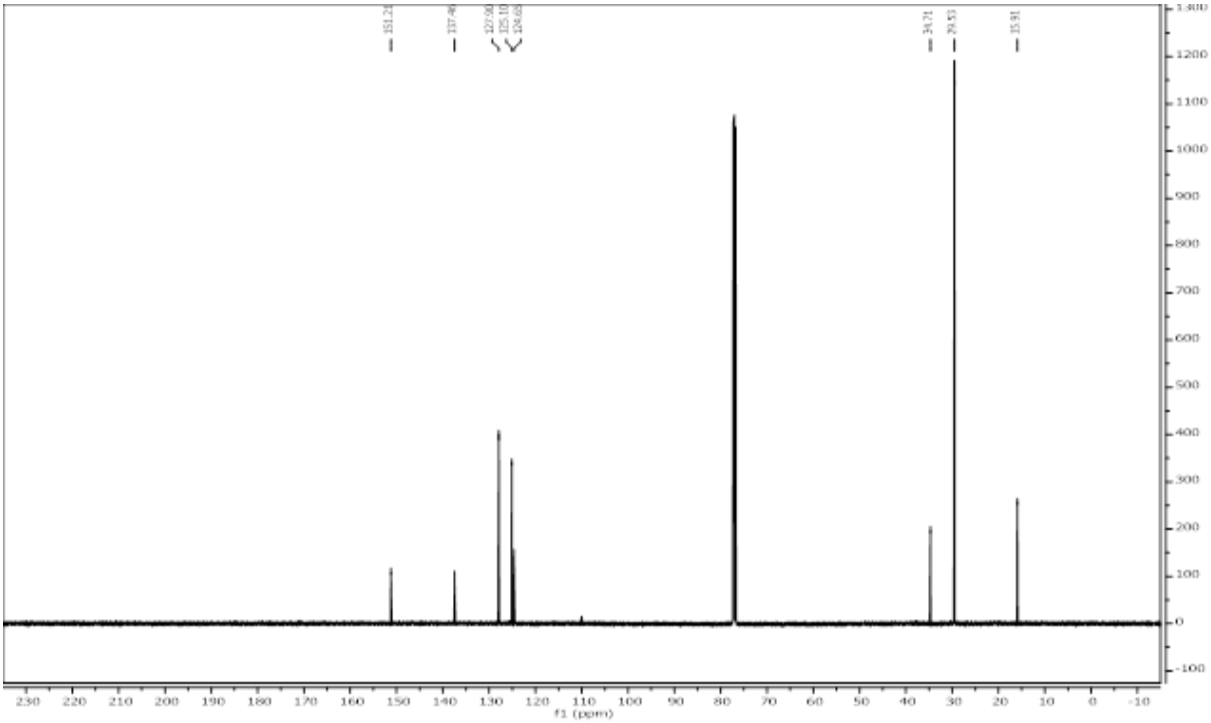

Figure 4.6.42 126 MHz ^{13}C Spectrum of 2-(*tert*-butyl)-4-chloro-6-methylphenol

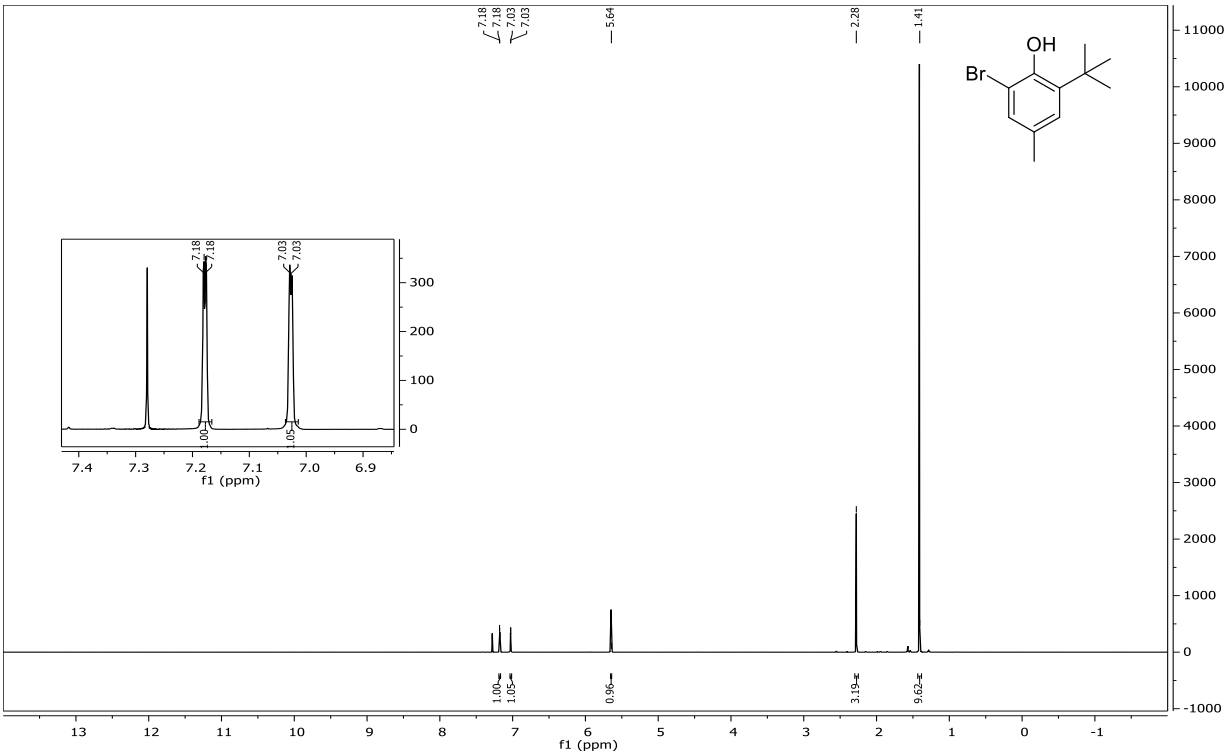

Figure 4.6.43 500 MHz ^{1}H Spectrum of 2-bromo-6-(*tert*-butyl)-4-methylphenol

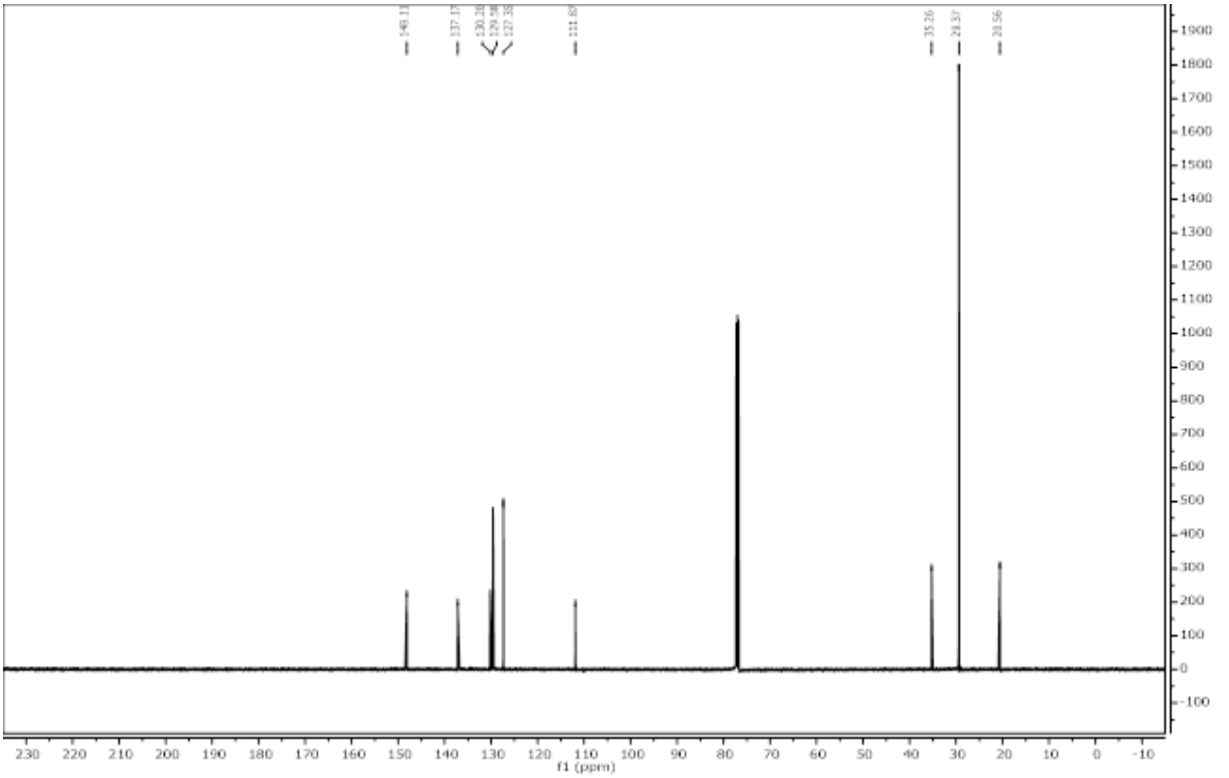

Figure 4.6.44 126 MHz ^{13}C Spectrum of 2-bromo-6-(*tert*-butyl)-4-methylphenol

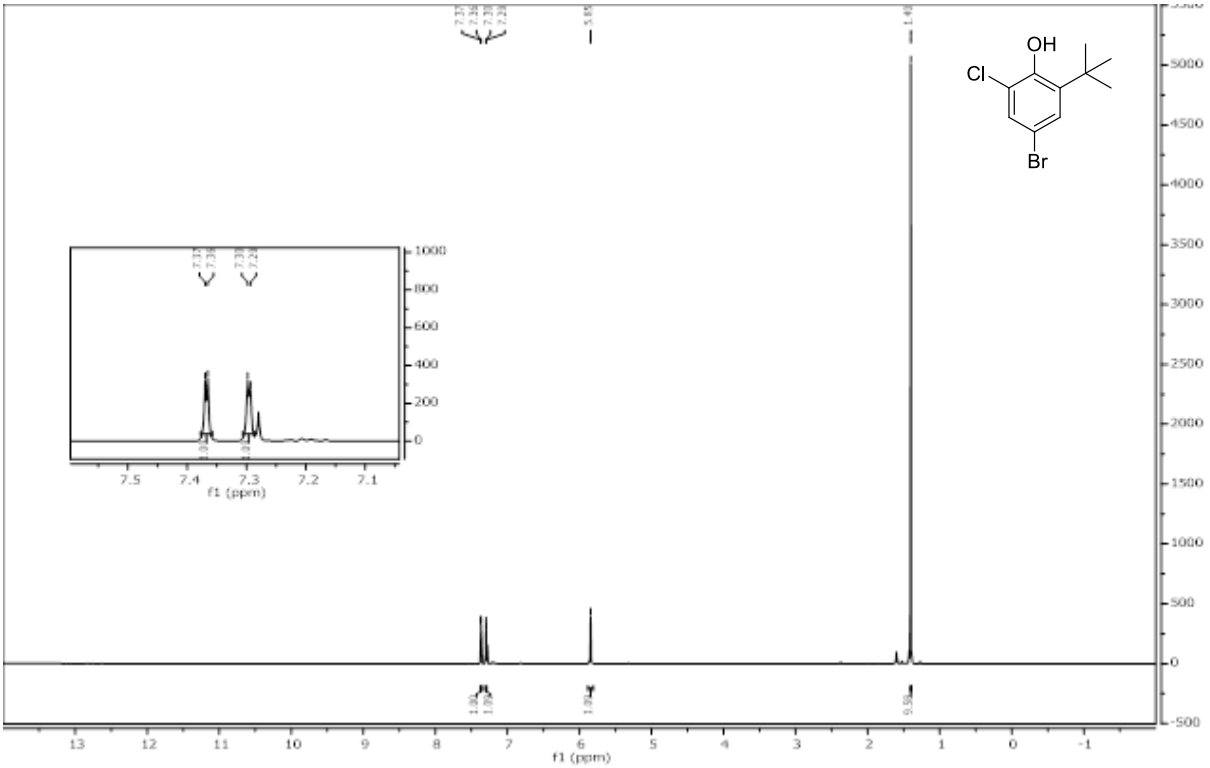

Figure 4.6.45 500 MHz ^{1}H Spectrum of 4-bromo-2-(*tert*-butyl)-6-chlorophenol

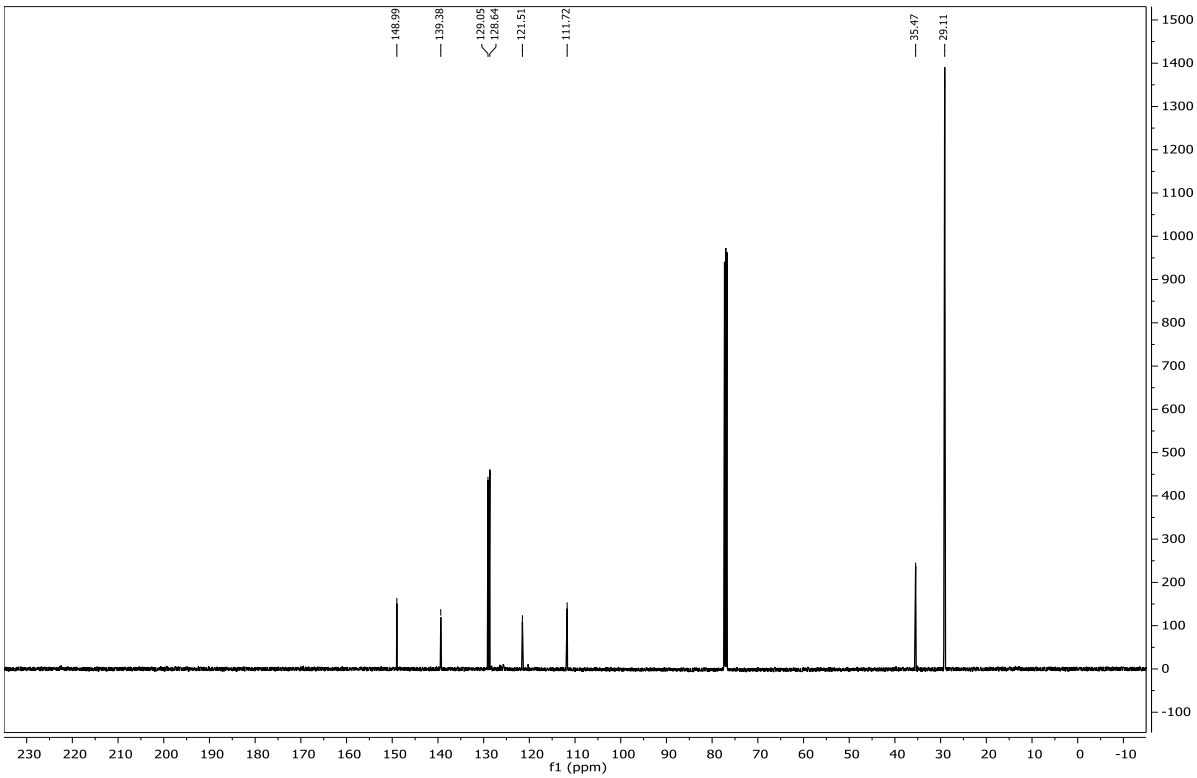

Figure 4.6.46 126 MHz ^{13}C Spectrum of 4-bromo-2-(*tert*-butyl)-6-chlorophenol

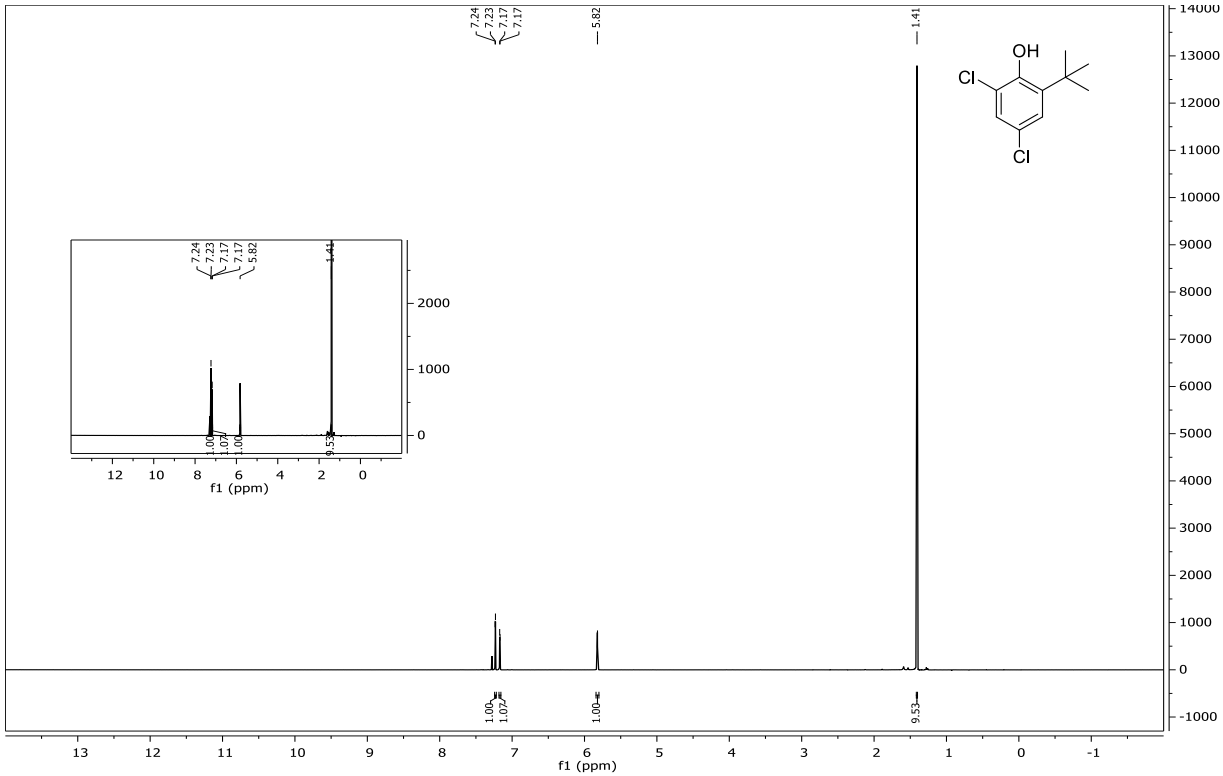

Figure 4.6.47 500 MHz ^{1}H Spectrum of 2-(*tert*-butyl)-4,6-dichlorophenol

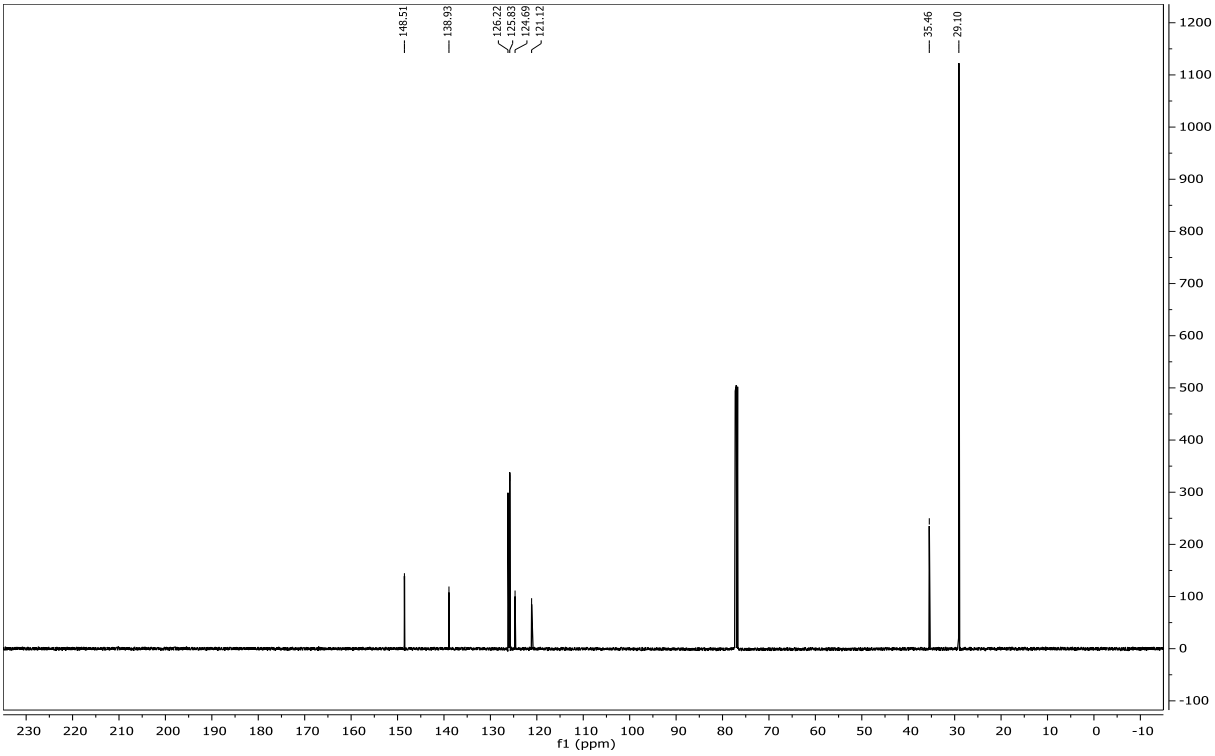

Figure 4.6.48 126 MHz ^{13}C Spectrum of 2-(*tert*-butyl)-4,6-dichlorophenol

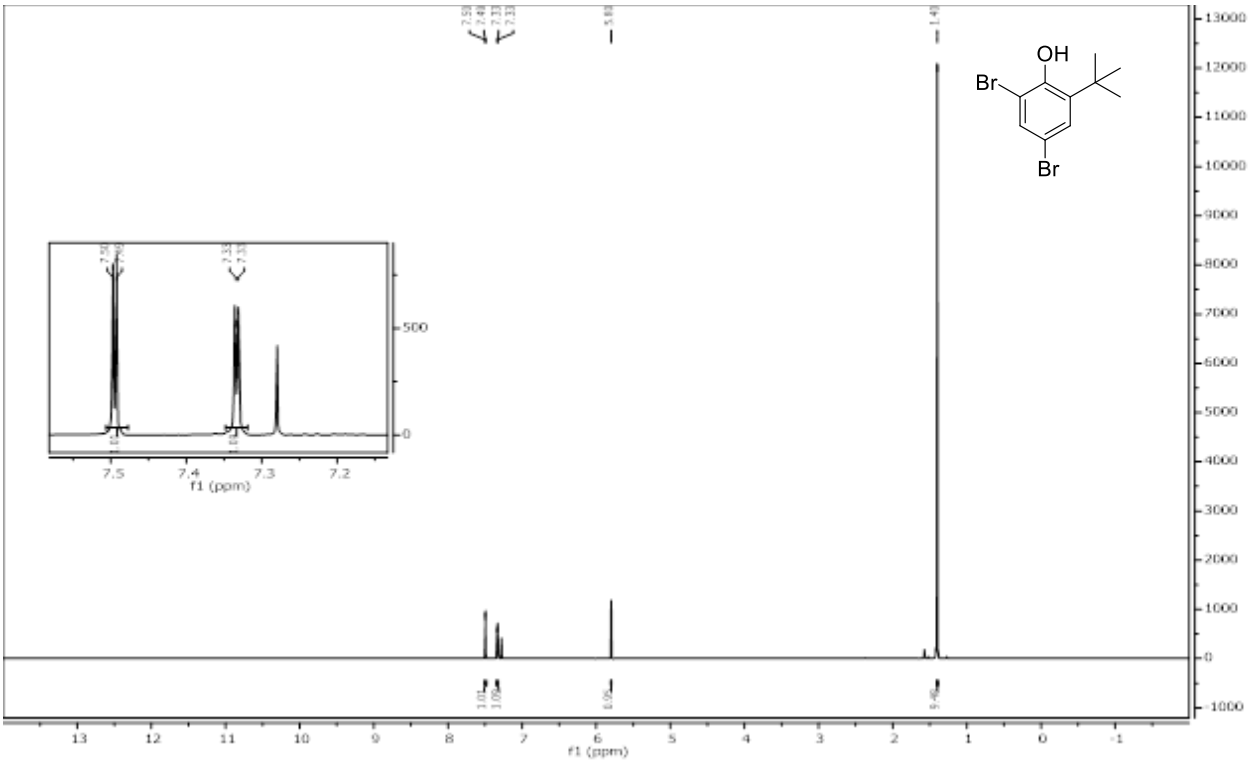

Figure 4.6.49 500 MHz ^{1}H Spectrum of 2,4-dibromo-6-(*tert*-butyl)phenol

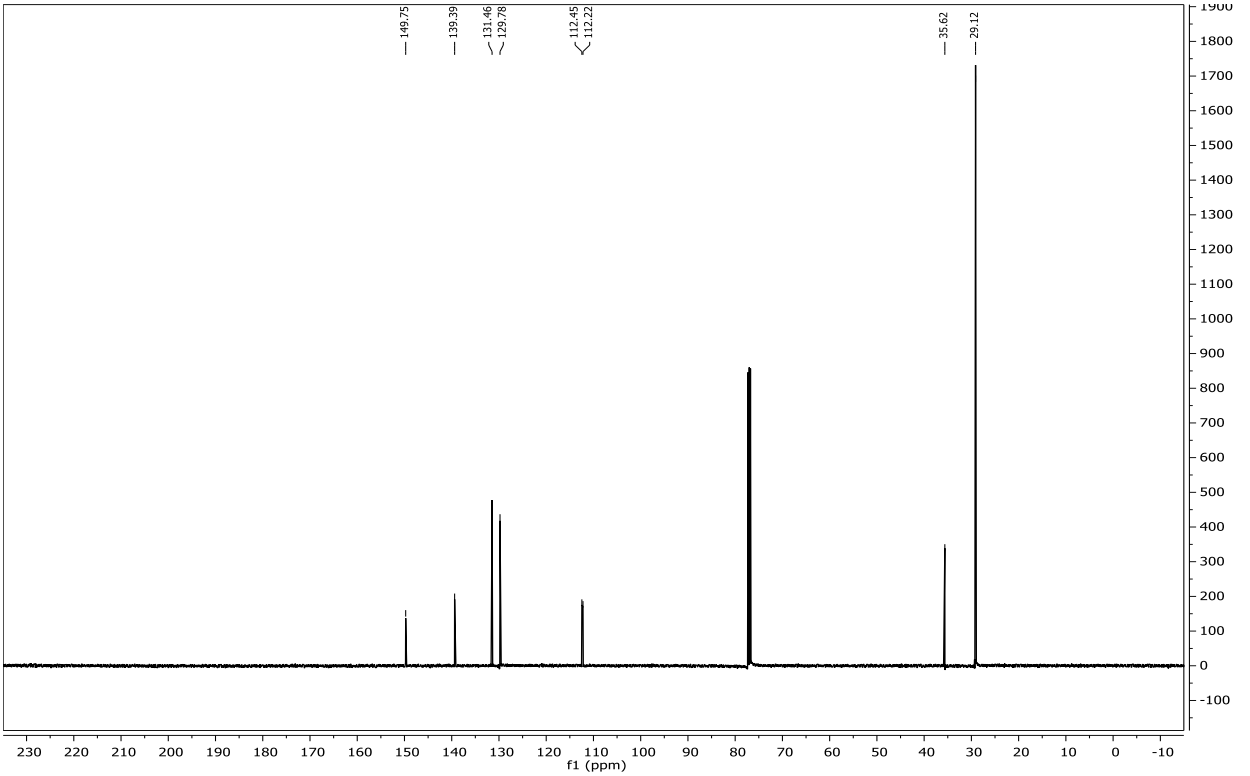

Figure 4.6.50 126 MHz ^{13}C Spectrum of 2,4-dibromo-6-(*tert*-butyl)phenol

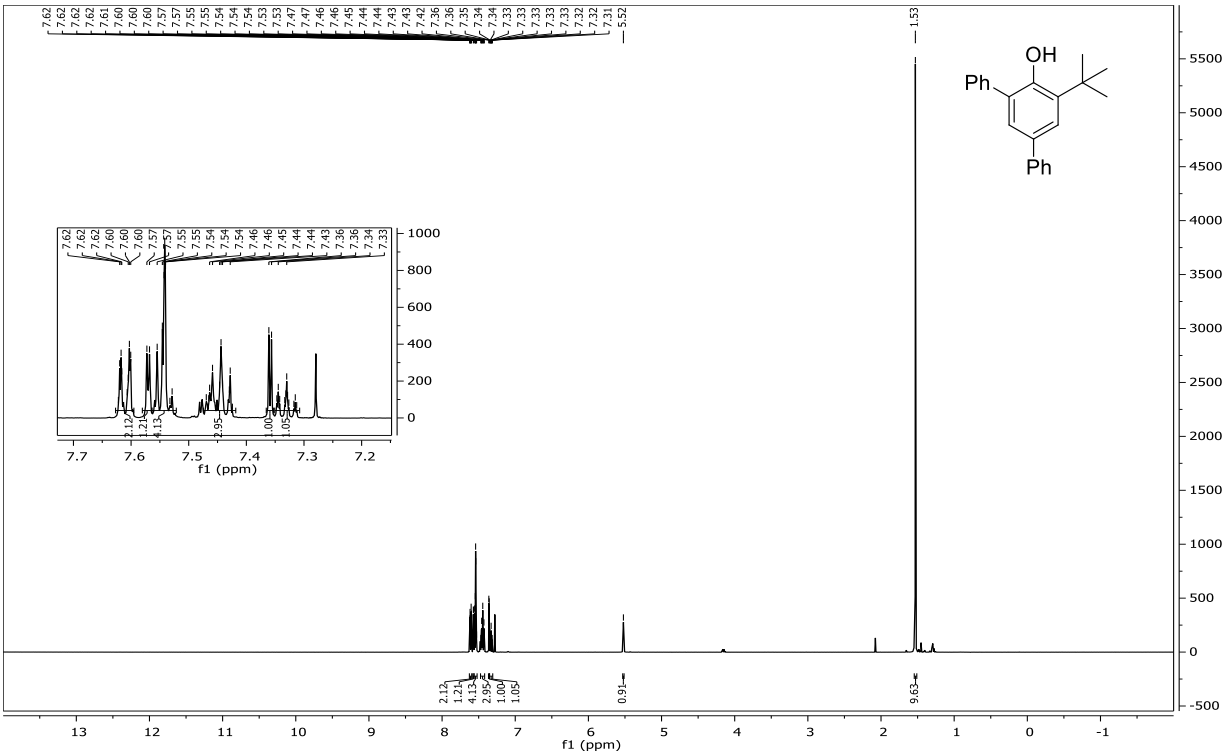

Figure 4.6.51 500 MHz ^{1}H Spectrum of 5'-(*tert*-butyl)-[1,1':3',1''-terphenyl]-4'-ol

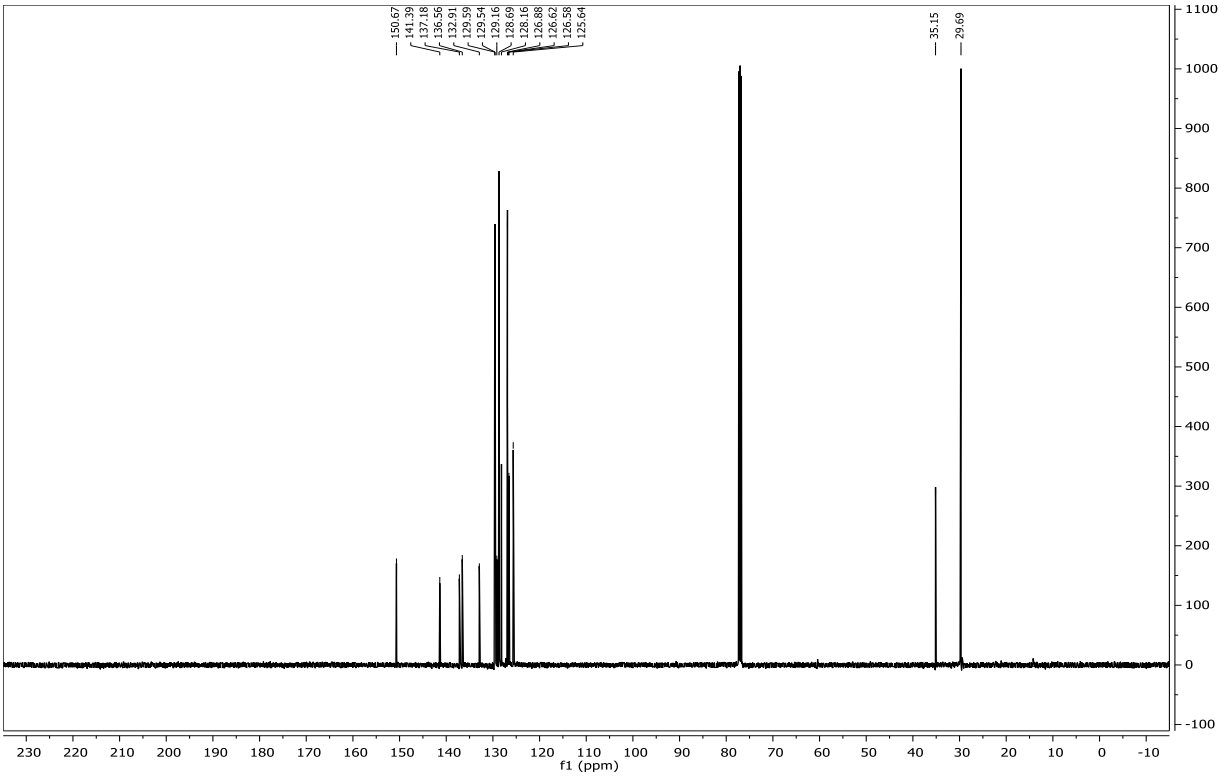

Figure 4.6.52 126 MHz ^{13}C Spectrum of 5'-(*tert*-butyl)-[1,1':3',1''-terphenyl]-4'-ol

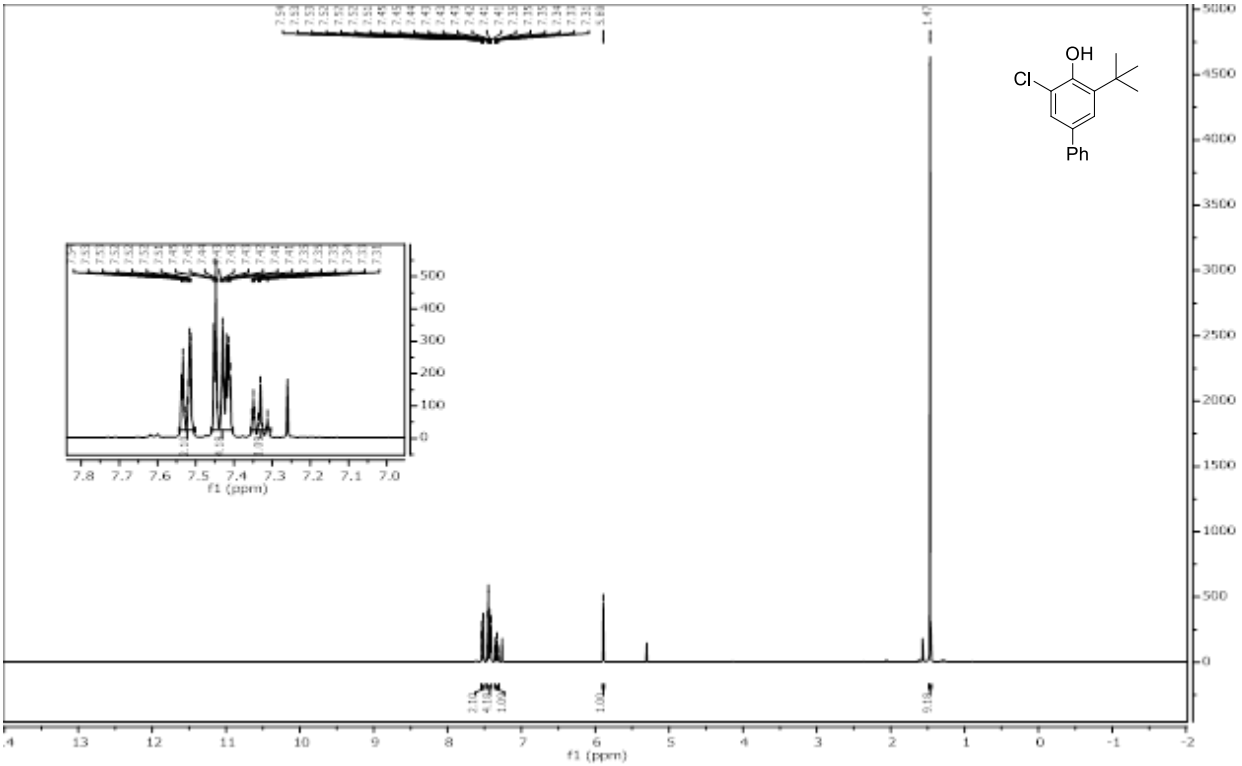

Figure 4.6.53 400 MHz ^{1}H Spectrum of 3-(*tert*-butyl)-5-chloro-[1,1'-biphenyl]-4-ol

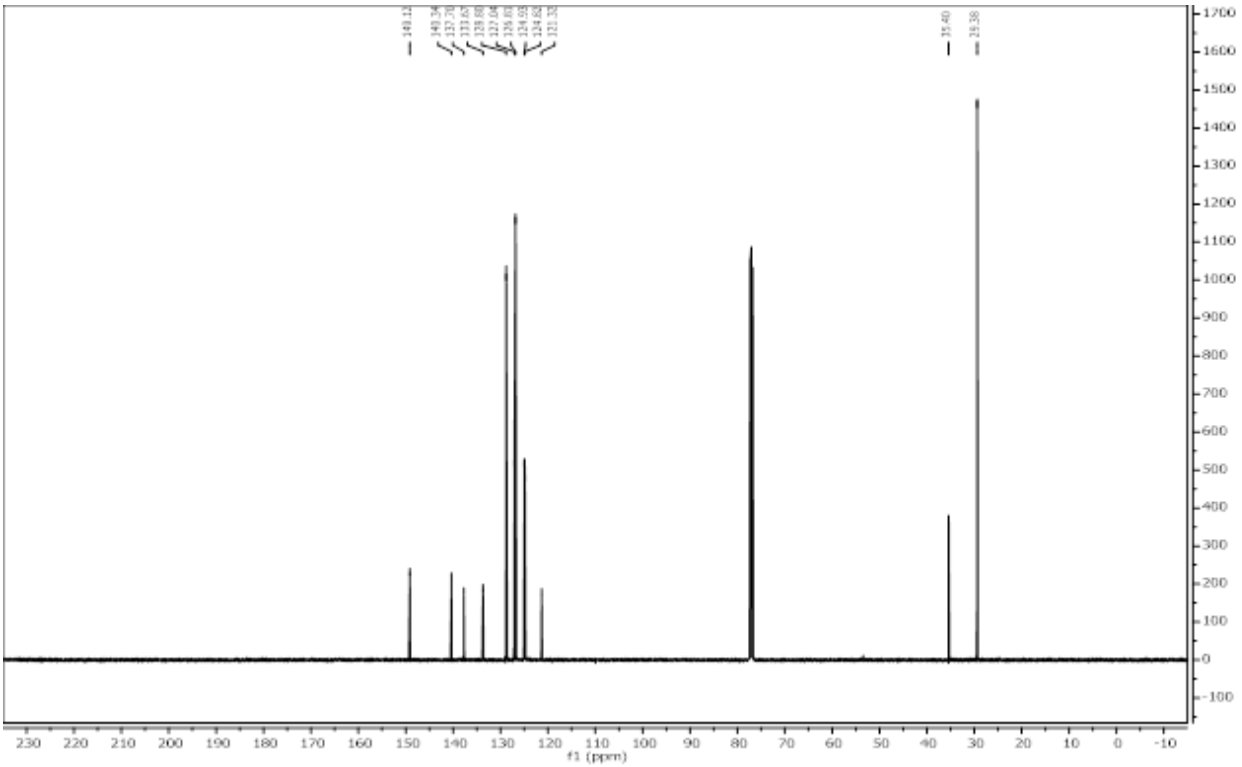

Figure 4.6.54 125 MHz ^{13}C Spectrum of 3-(*tert*-butyl)-5-chloro-[1,1'-biphenyl]-4-ol

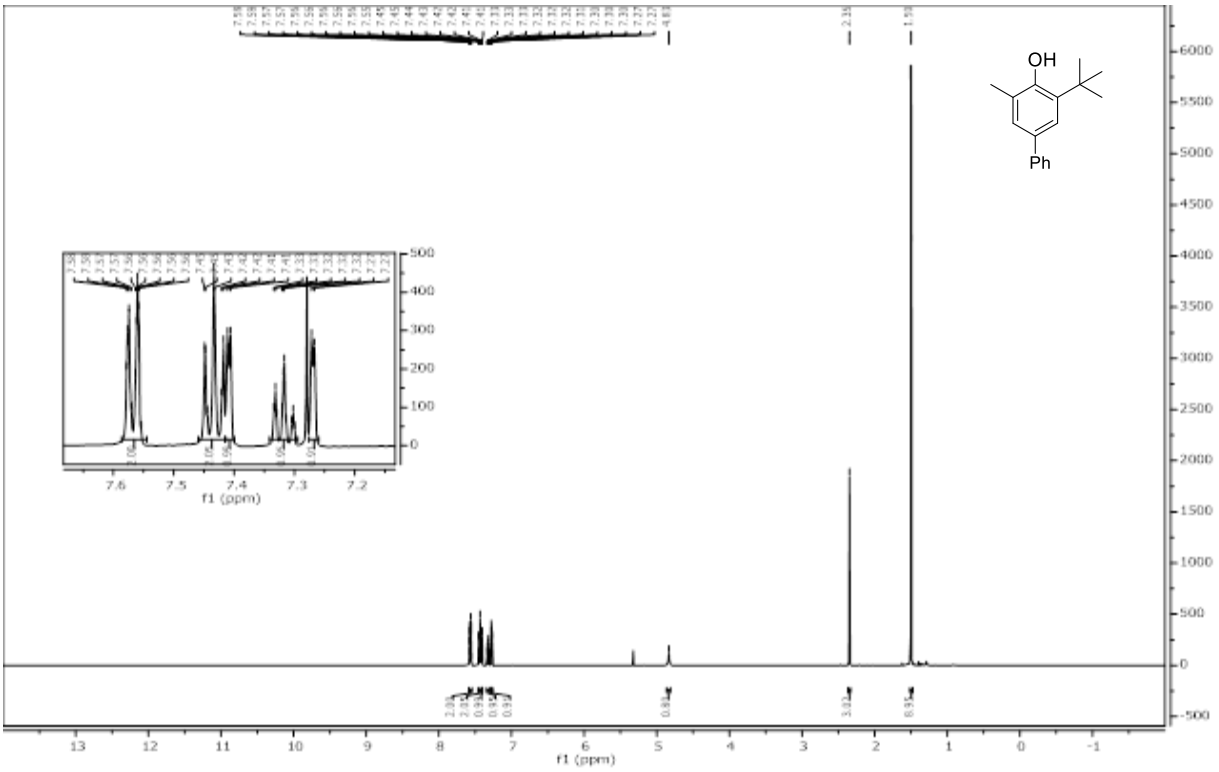

Figure 4.6.55 500 MHz ^{1}H Spectrum of 3-(*tert*-butyl)-5-methyl-[1,1'-biphenyl]-4-ol

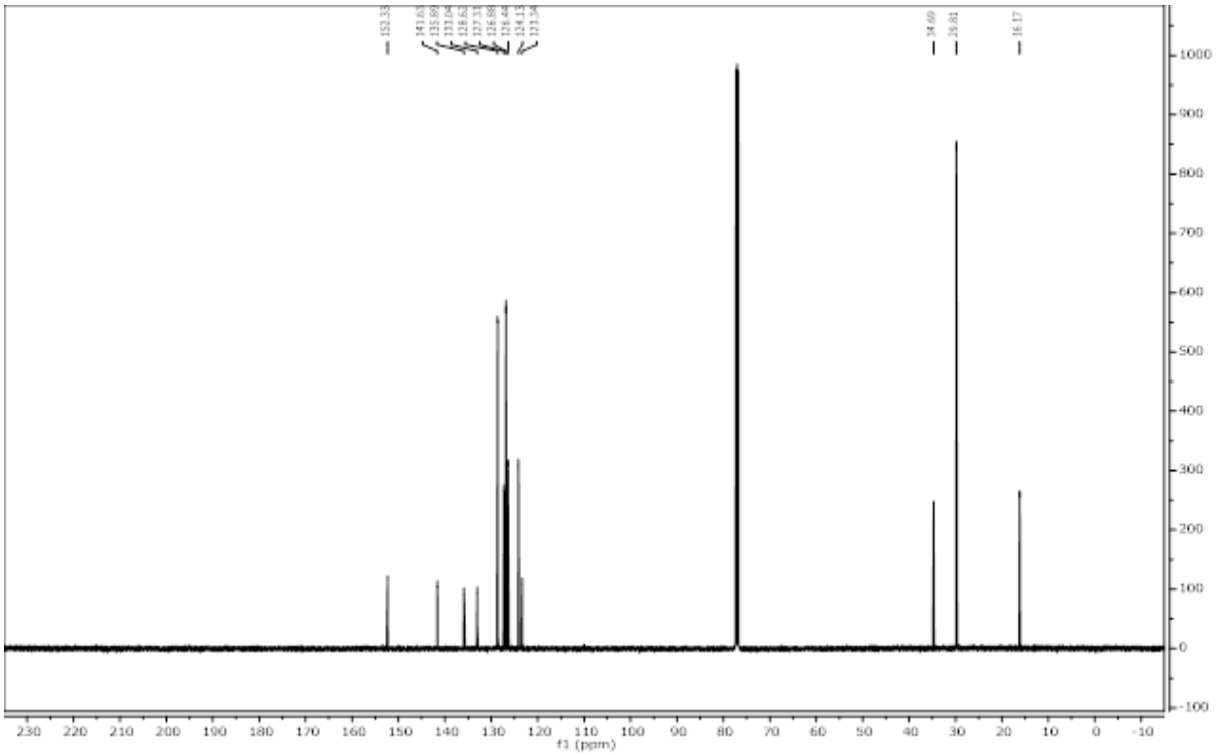

Figure 4.6.56 126 MHz ^{13}C Spectrum of 3-(*tert*-butyl)-5-methyl-[1,1'-biphenyl]-4-ol

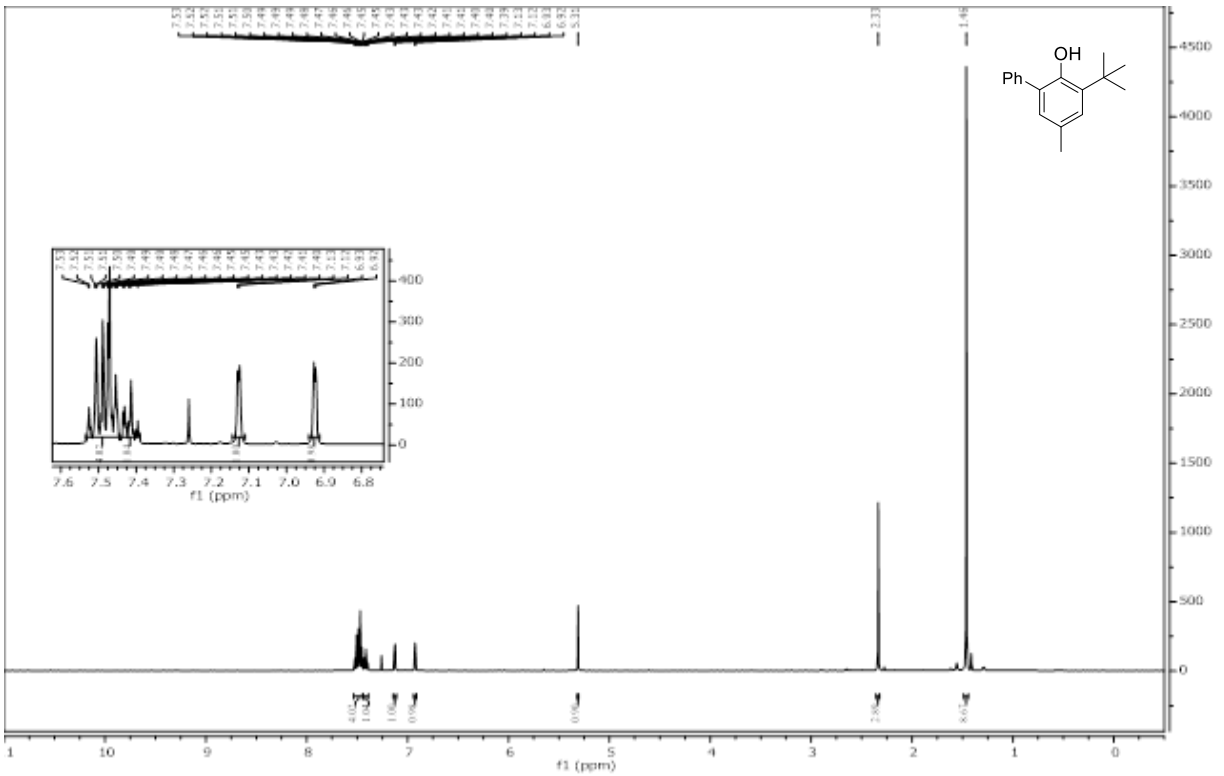

Figure 4.6.57 400 MHz ^{1}H Spectrum of 3-(*tert*-butyl)-5-methyl-[1,1'-biphenyl]-2-ol

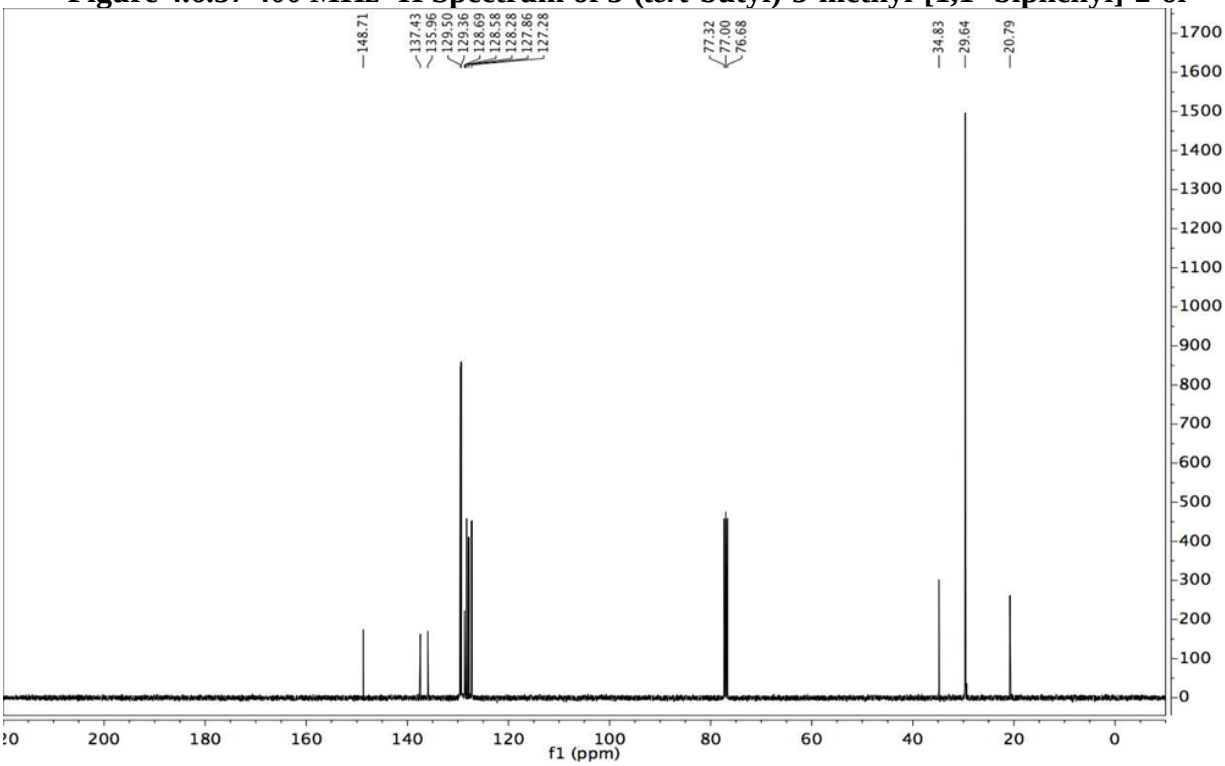

Figure 4.6.58 126 MHz ^{13}C Spectrum of 3-(*tert*-butyl)-5-methyl-[1,1'-biphenyl]-2-ol

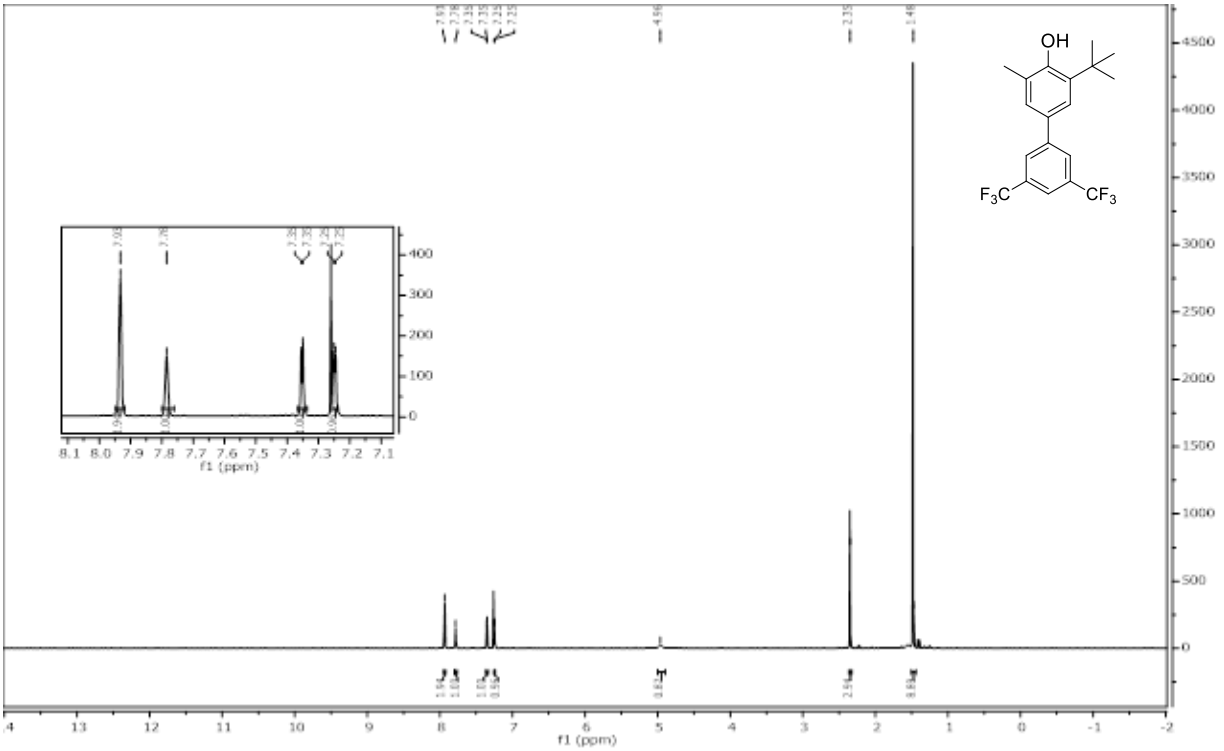

Figure 4.6.59 400 MHz ^{1}H Spectrum of 3-(*tert*-butyl)-5-methyl-3',5'-bis(trifluoromethyl)-[1,1'-biphenyl]-4-ol

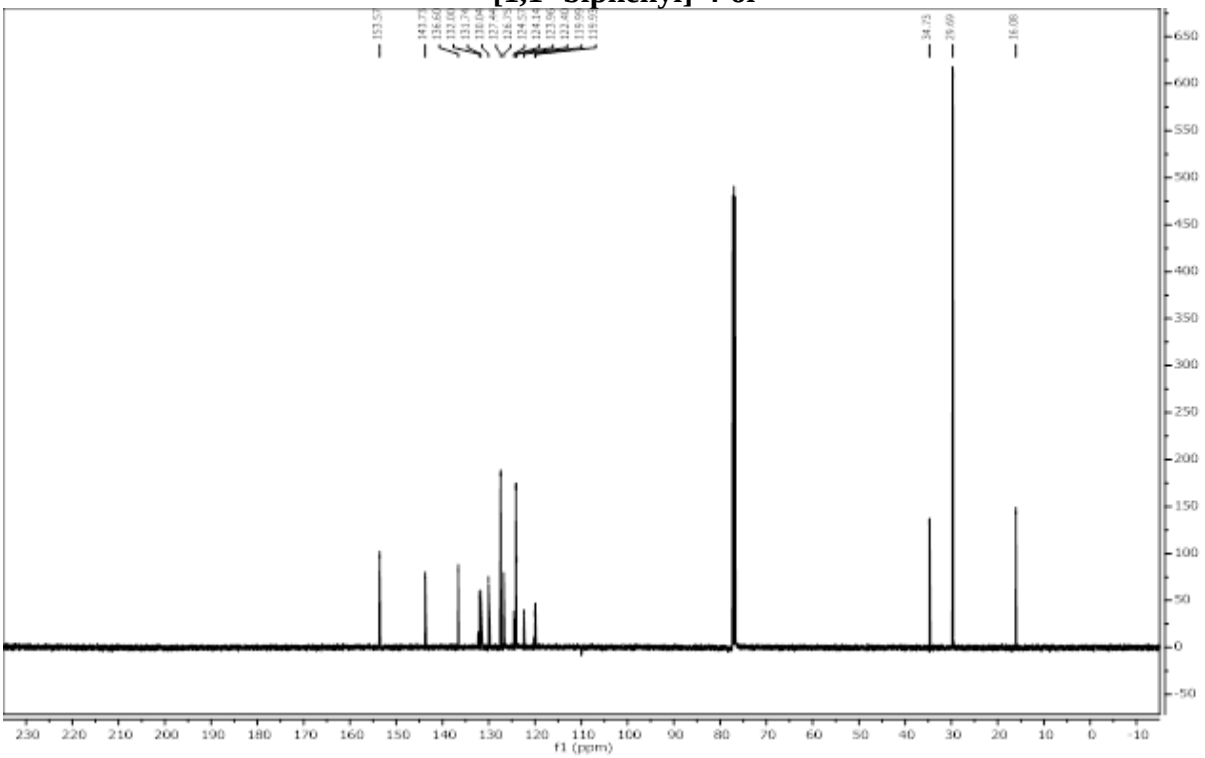

Figure 4.6.60 126 MHz ^{13}C Spectrum of 3-(*tert*-butyl)-5-methyl-3',5'-bis(trifluoromethyl)-[1,1'-biphenyl]-4-ol

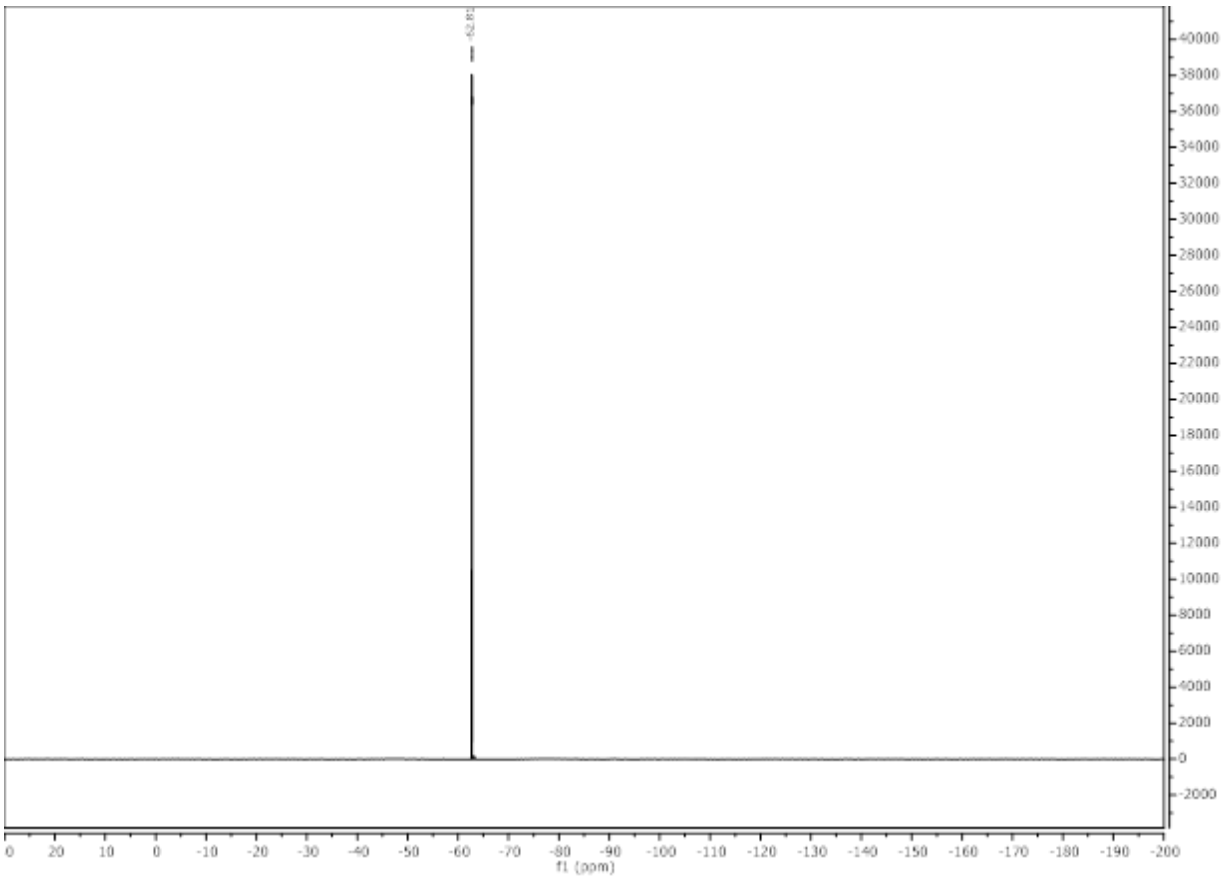

Figure 4.6.61 470 MHz ^{19}F Spectrum of 3-(*tert*-butyl)-5-methyl-3',5'-bis(trifluoromethyl)-[1,1'-biphenyl]-4-ol

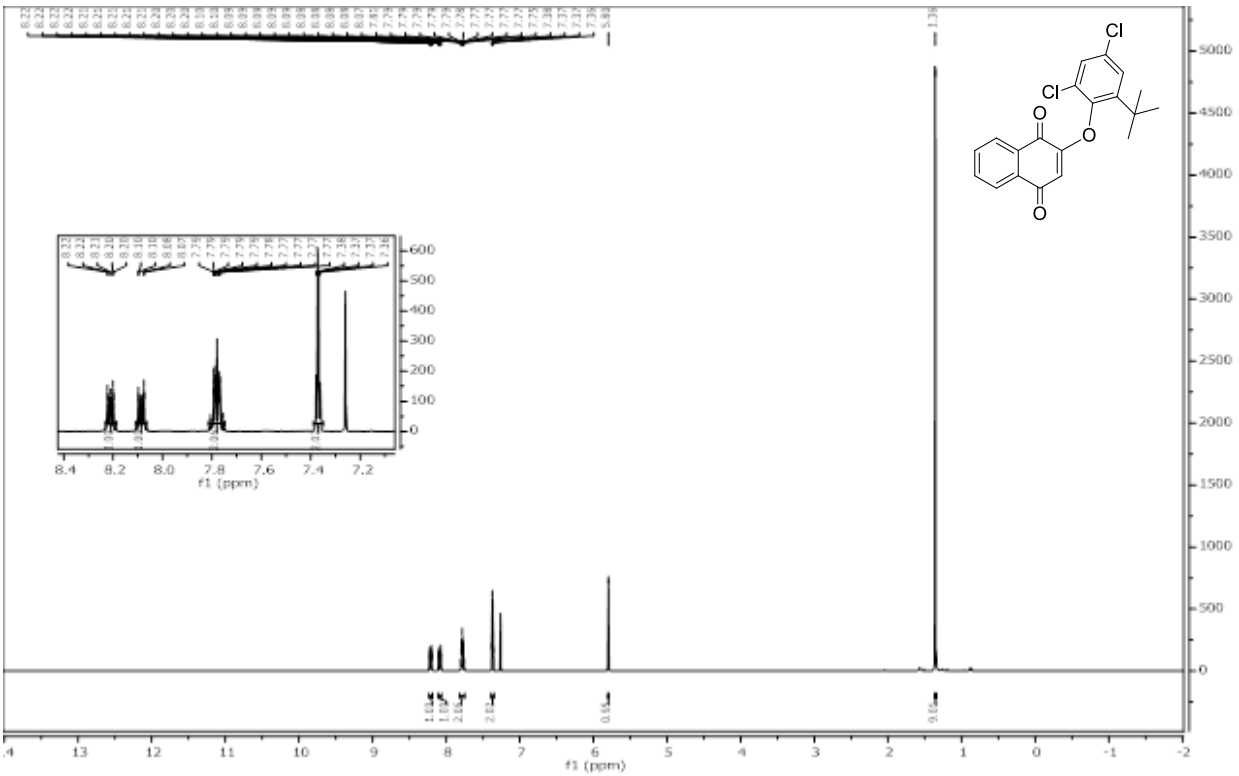

Figure 4.6.62 400 MHz ^{1}H Spectrum of 2-(2-(*tert*-butyl)-4,6-dichlorophenoxy)naphthalene-1,4-dione (4.1)

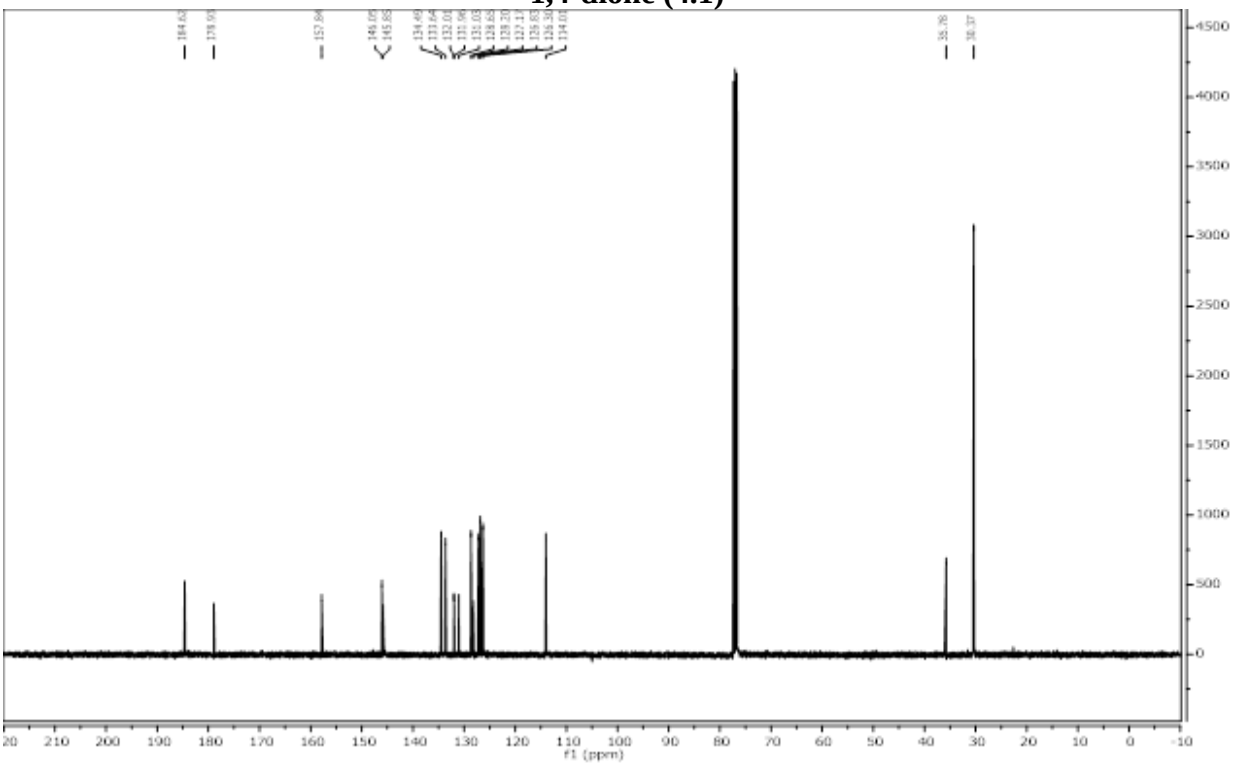

Figure 4.6.63 101 MHz ^{13}C Spectrum of 2-(2-(*tert*-butyl)-4,6-dichlorophenoxy)naphthalene-1,4-dione (4.1)

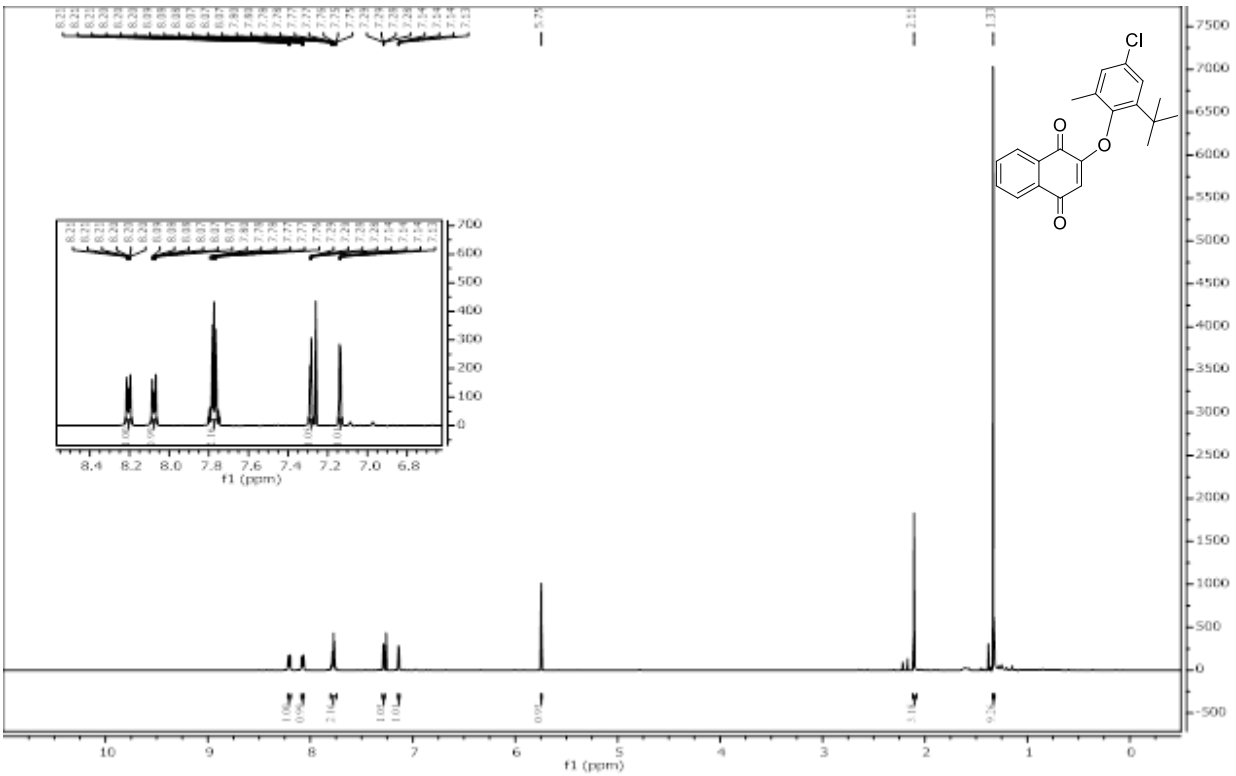

Figure 4.6.64 500 MHz ^{1}H Spectrum of 2-(2-*tert*-butyl)-4-chloro-6-methylphenoxy)naphthalene-1,4-dione (4.2)

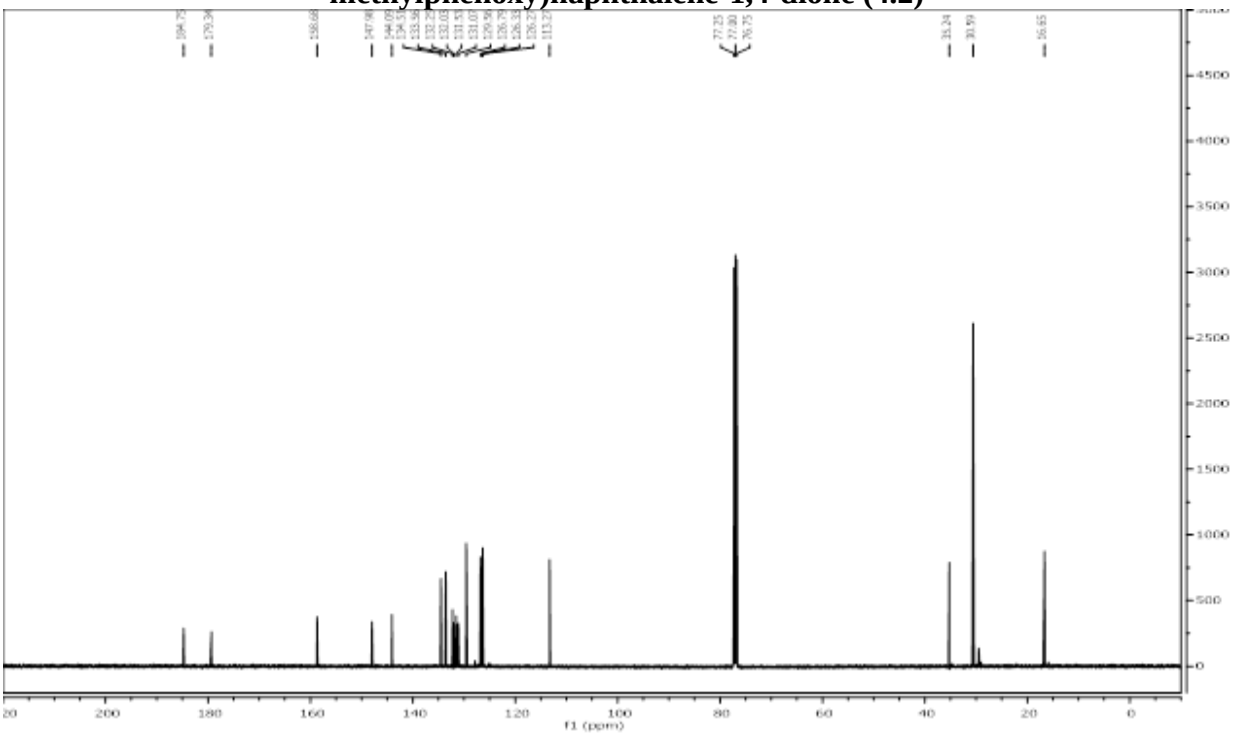

Figure 4.6.65 126 MHz ^{13}C Spectrum of 2-(2-*tert*-butyl)-4-chloro-6-methylphenoxy)naphthalene-1,4-dione (4.2)

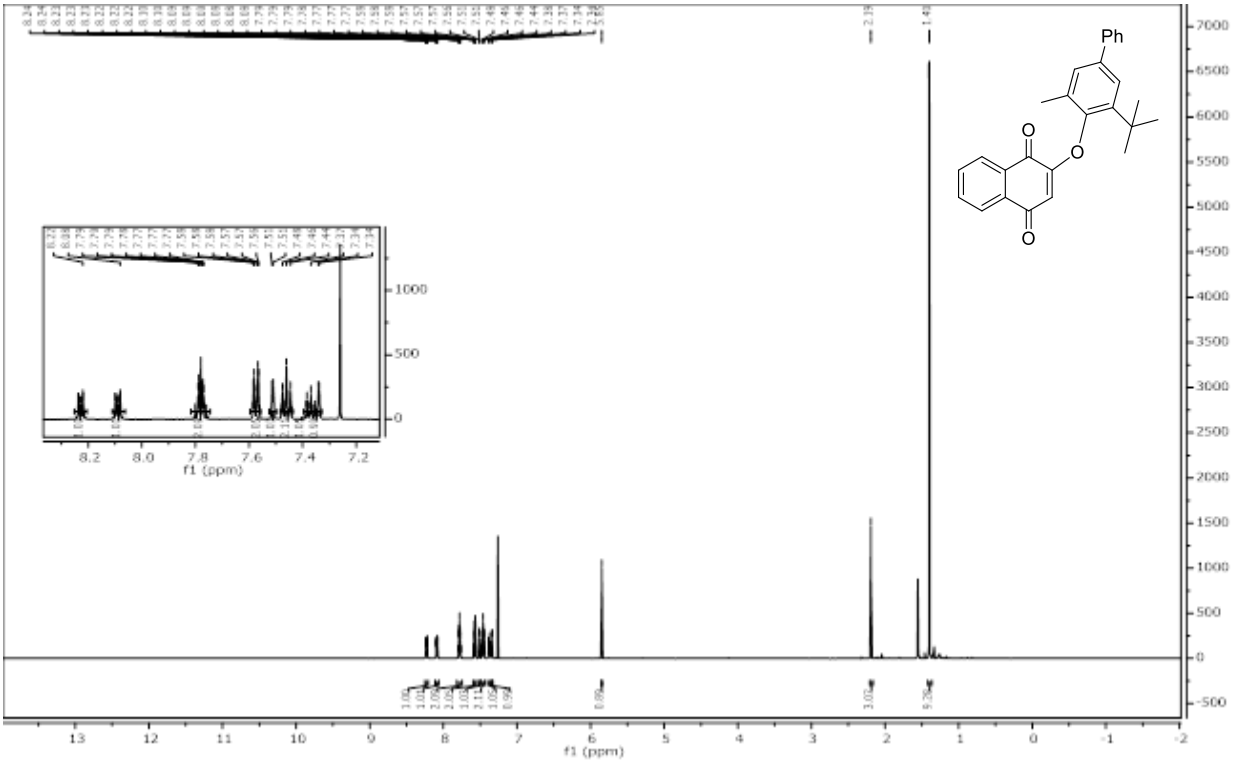

Figure 4.6.66 500 MHz ^{1}H Spectrum of 2-((3-(*tert*-butyl)-5-methyl-[1,1'-biphenyl]-4-yl)oxy)naphthalene-1,4-dione) (4.3)

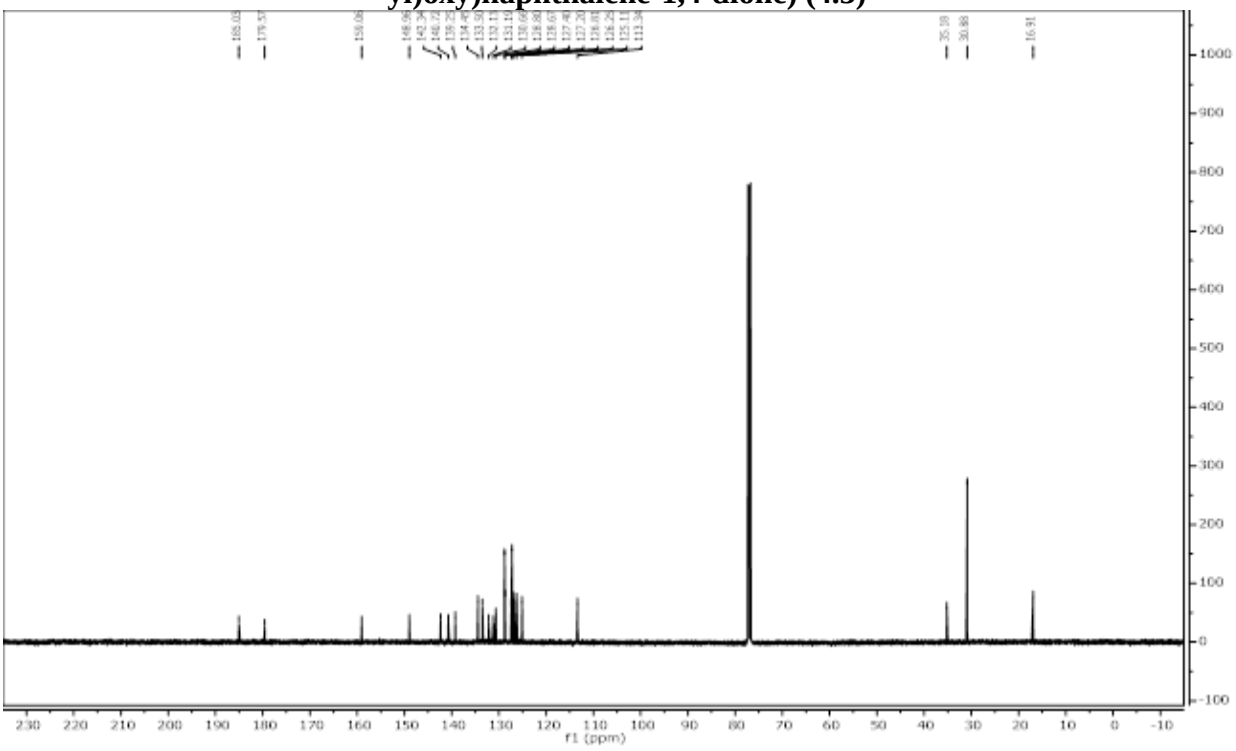

Figure 4.6.67 126 MHz ^{13}C Spectrum of 2-((3-(*tert*-butyl)-5-methyl-[1,1'-biphenyl]-4-yl)oxy)naphthalene-1,4-dione) (4.3)

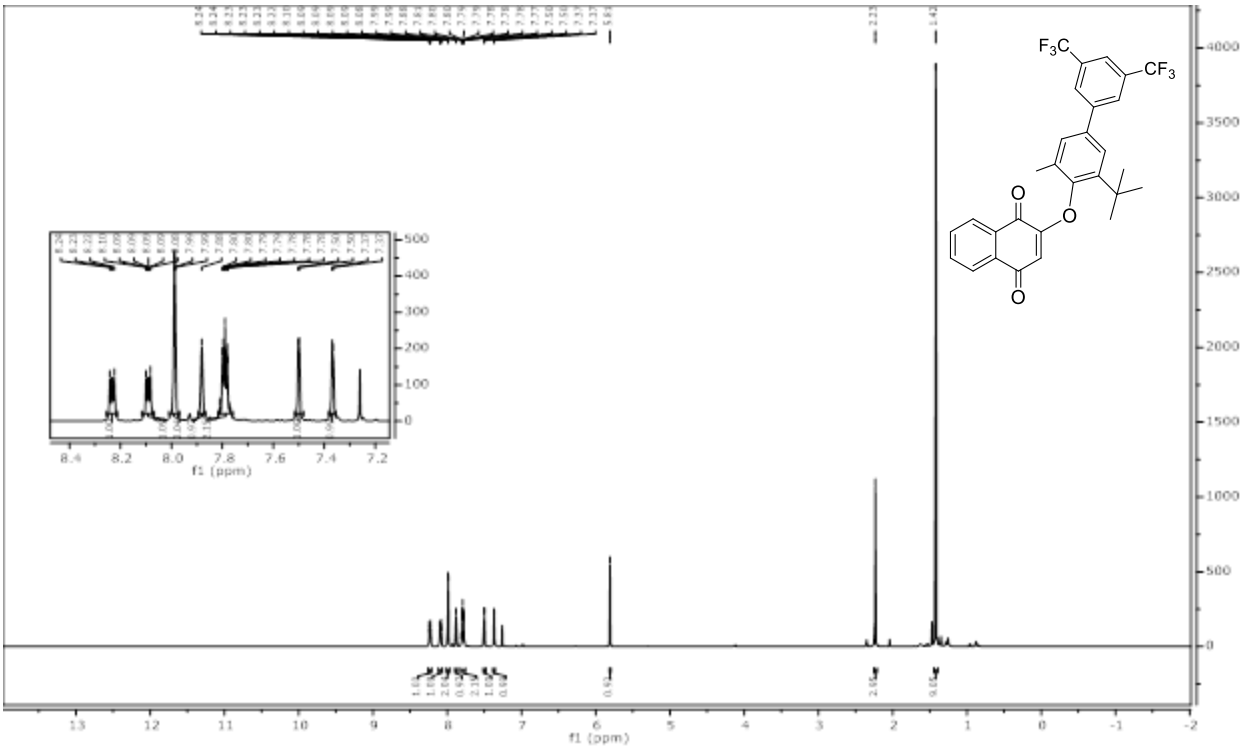

Figure 4.6.68 500 MHz ^{1}H Spectrum of 2-((3-(*tert*-butyl)-5-methyl-3',5'-bis(trifluoromethyl)-[1,1'-biphenyl]-4-yl)oxy)naphthalene-1,4-dione (4.4)

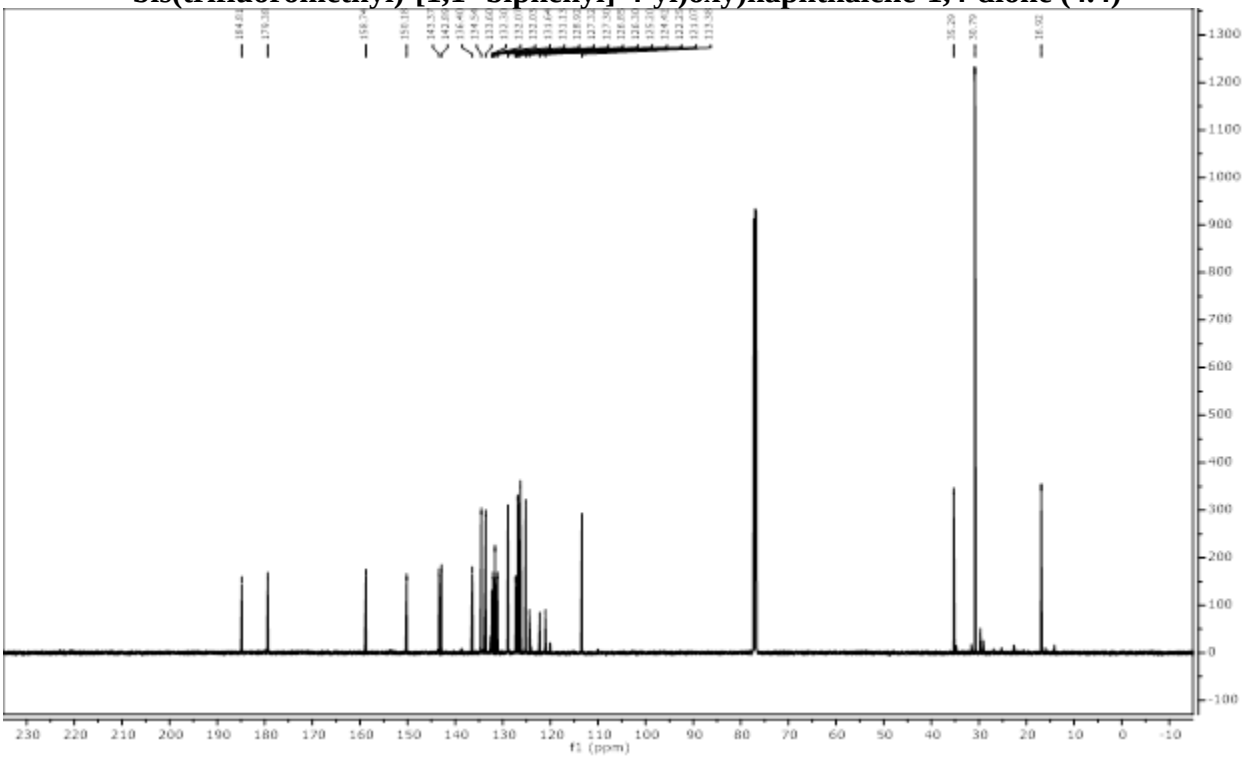

Figure 4.6.69 126 MHz ^{13}C Spectrum of 2-((3-(*tert*-butyl)-5-methyl-3',5'-bis(trifluoromethyl)-[1,1'-biphenyl]-4-yl)oxy)naphthalene-1,4-dione (4.4)

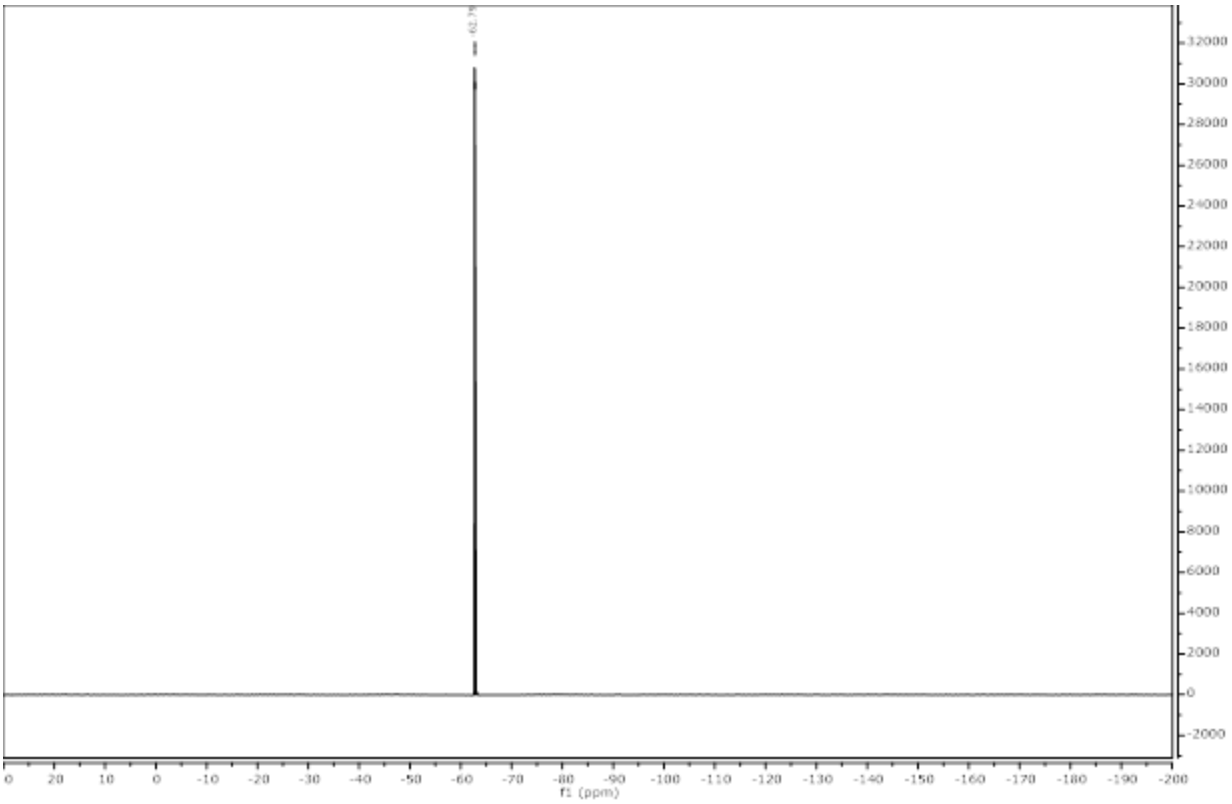

Figure 4.6.70 470 MHz ^{19}F Spectrum of 2-((3-(*tert*-butyl)-5-methyl-3',5'-bis(trifluoromethyl)-[1,1'-biphenyl]-4-yl)oxy)naphthalene-1,4-dione (4.4)

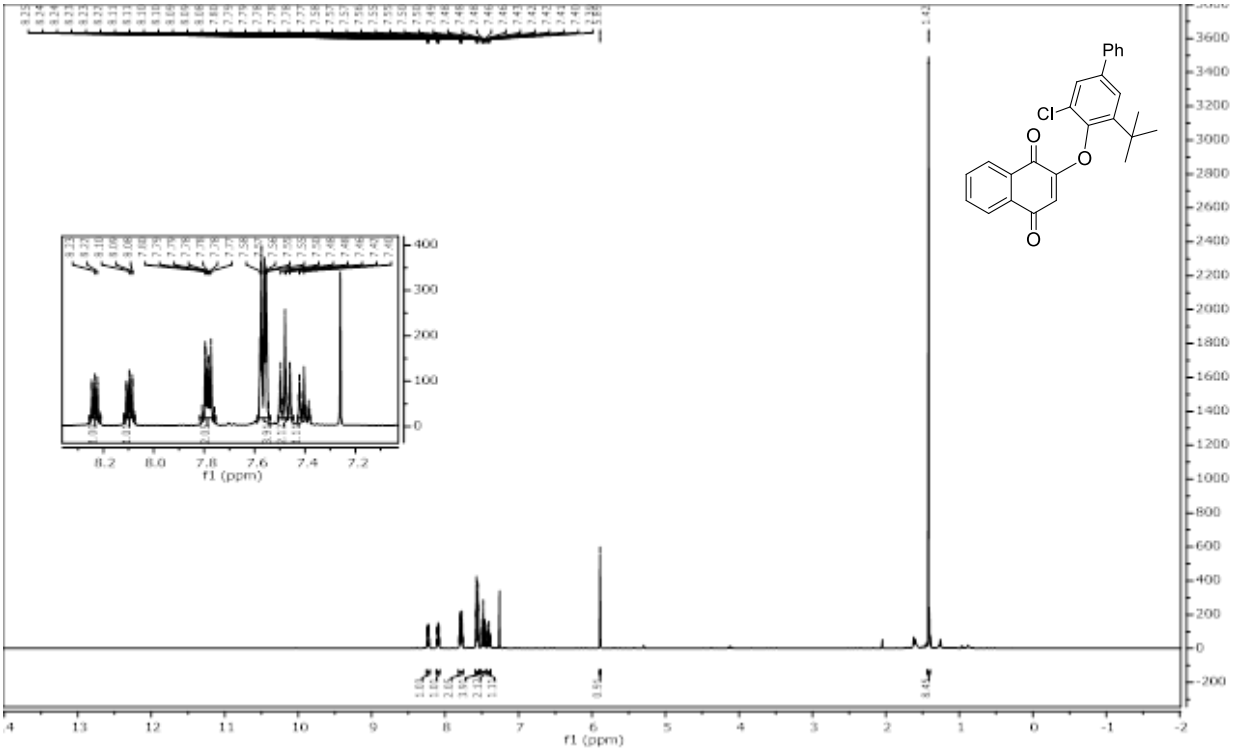

Figure 4.6.71 500 MHz ^{1}H Spectrum of 2-((3-(*tert*-butyl)-5-chloro-[1,1'-biphenyl]-4-yl)oxy)naphthalene-1,4-dione (4.5)

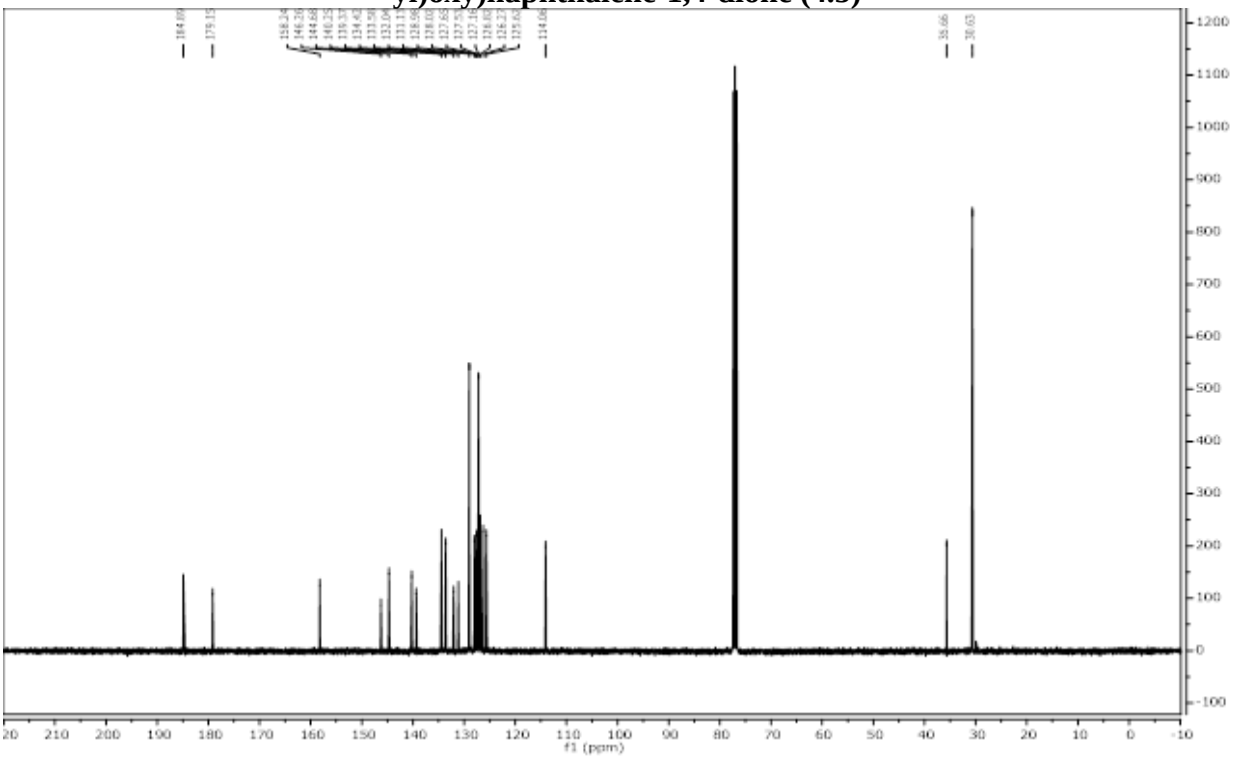

Figure 4.6.72 101 MHz ^{13}C Spectrum of 2-((3-(*tert*-butyl)-5-chloro-[1,1'-biphenyl]-4-yl)oxy)naphthalene-1,4-dione (4.5)

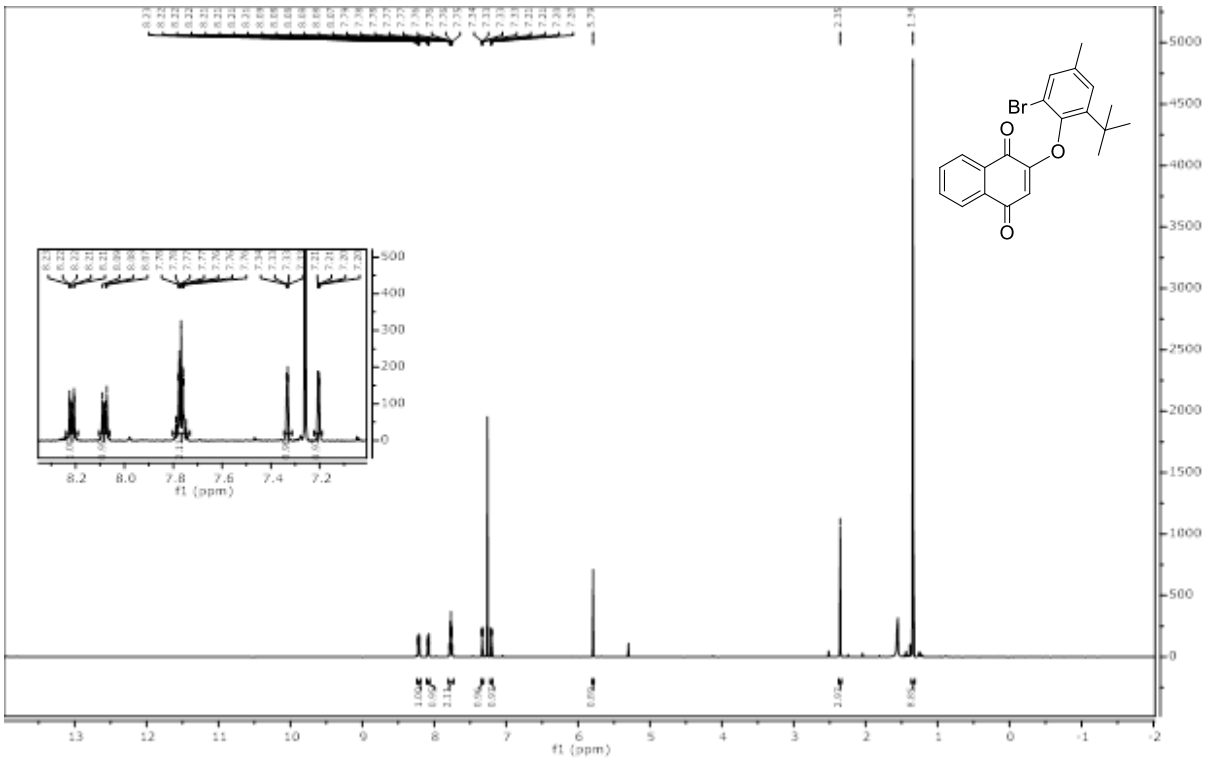

Figure 4.6.73 500 MHz ^{1}H Spectrum of 2-(2-bromo-6-(*tert*-butyl)-4-methylphenoxy)naphthalene-1,4-dione (4.6)

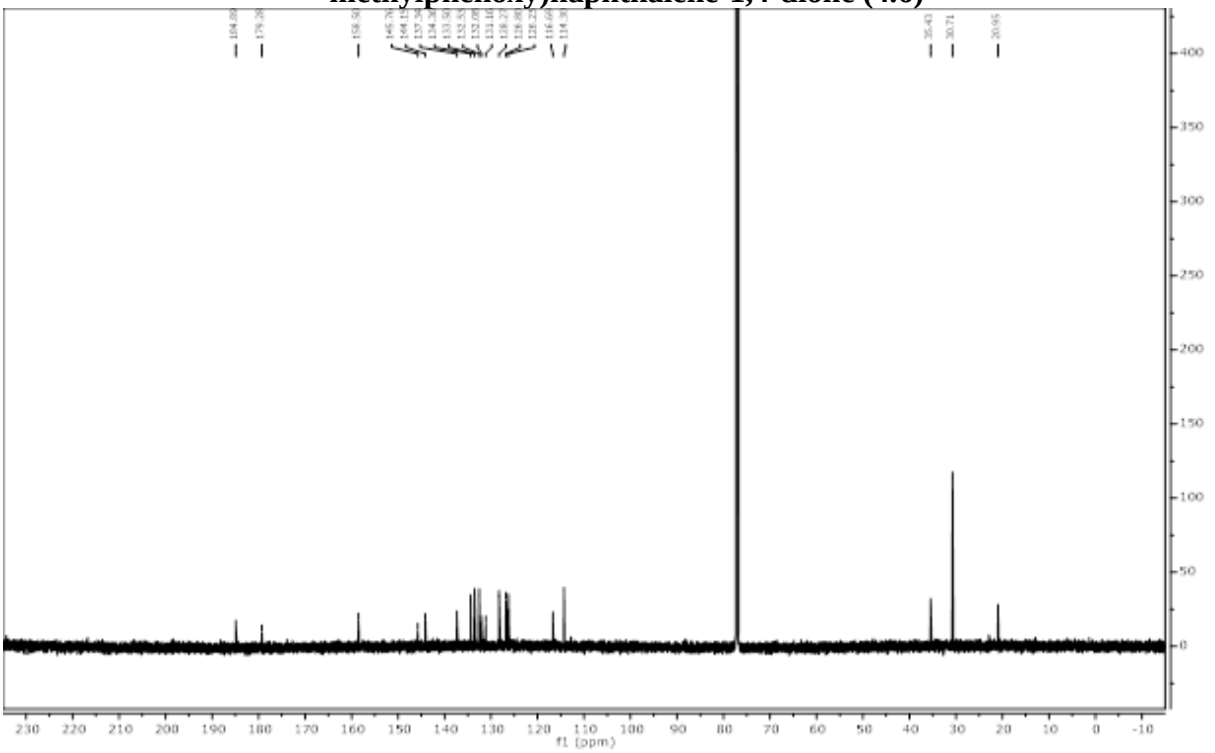

Figure 4.6.74 126 MHz ^{13}C Spectrum of 2-(2-bromo-6-(*tert*-butyl)-4-methylphenoxy)naphthalene-1,4-dione (4.6)

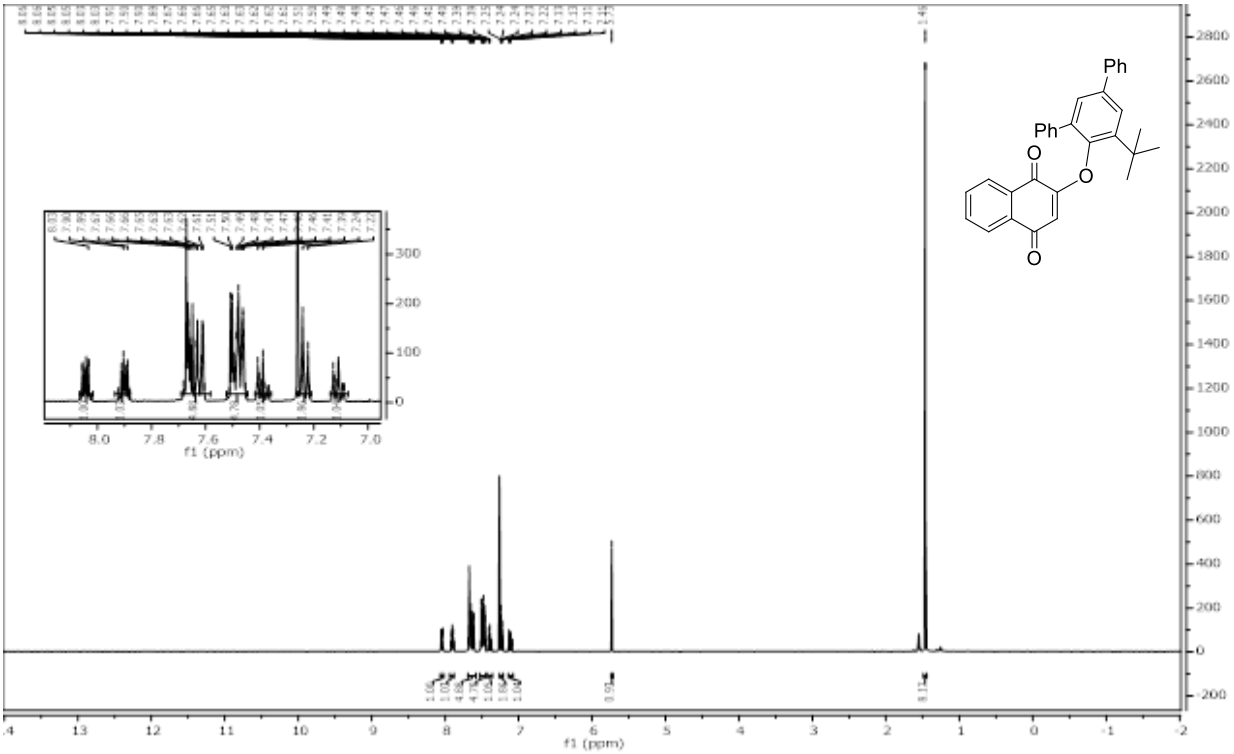

Figure 4.6.75 400 MHz ^{1}H Spectrum of 2-((5'-(*tert*-butyl)-[1,1':3',1''-terphenyl]-4'-yl)oxy)naphthalene-1,4-dione) (4.7)

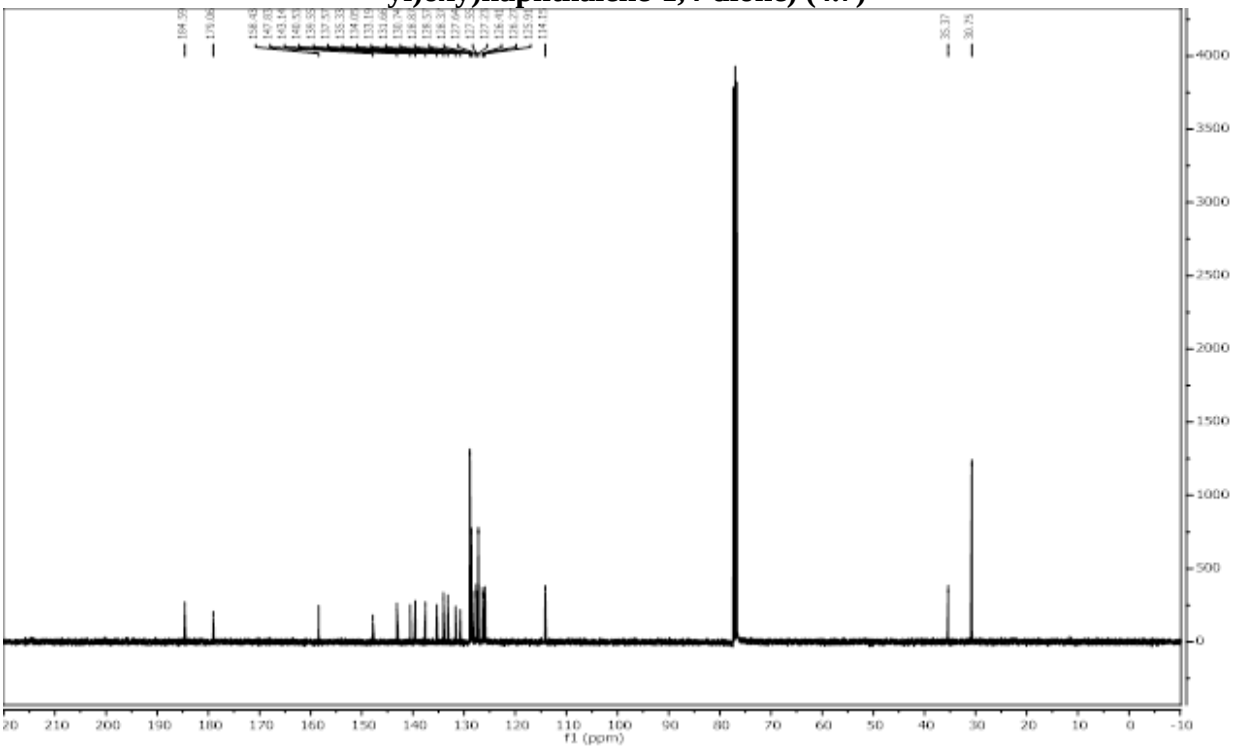

Figure 4.6.76 101 MHz ^{13}C Spectrum of 2-((5'-(*tert*-butyl)-[1,1':3',1''-terphenyl]-4'-yl)oxy)naphthalene-1,4-dione) (4.7)

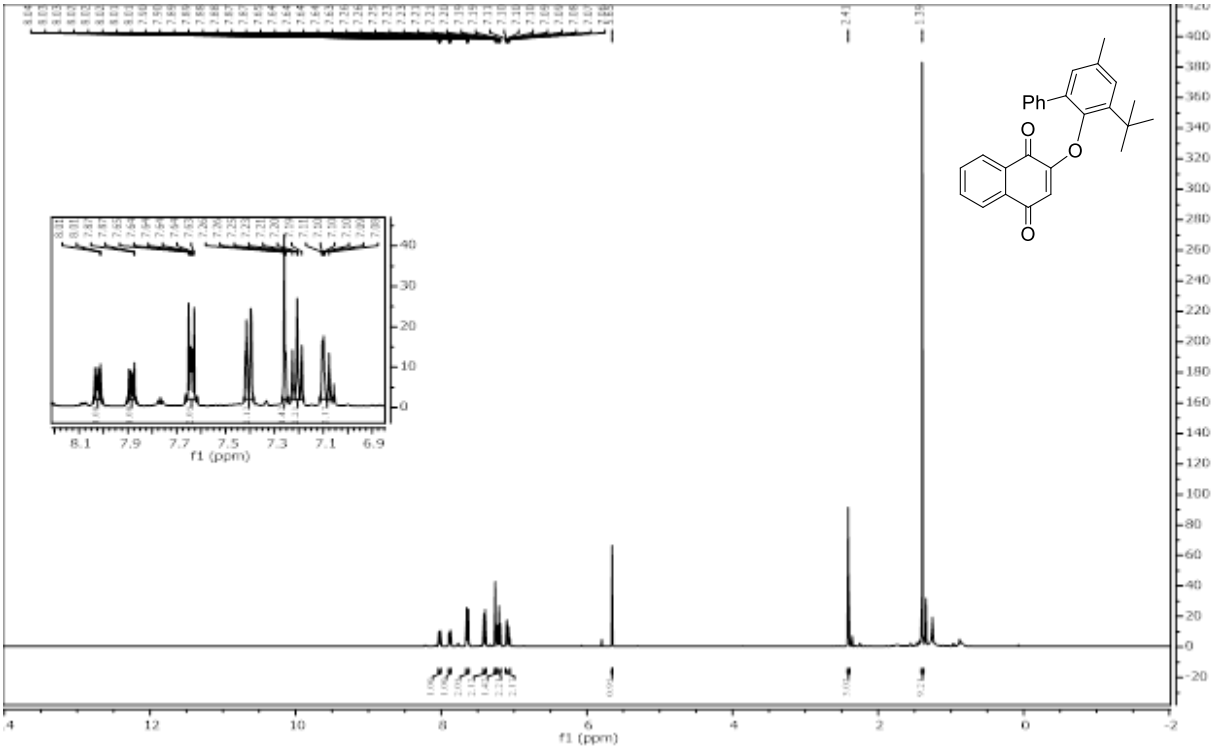

Figure 4.6.77 500 MHz ^{1}H Spectrum of 2-((3-*tert*-butyl)-5-methyl-[1,1'-biphenyl]-2-yl]-2-yl)oxy)naphthalene-1,4-dione (4.8)

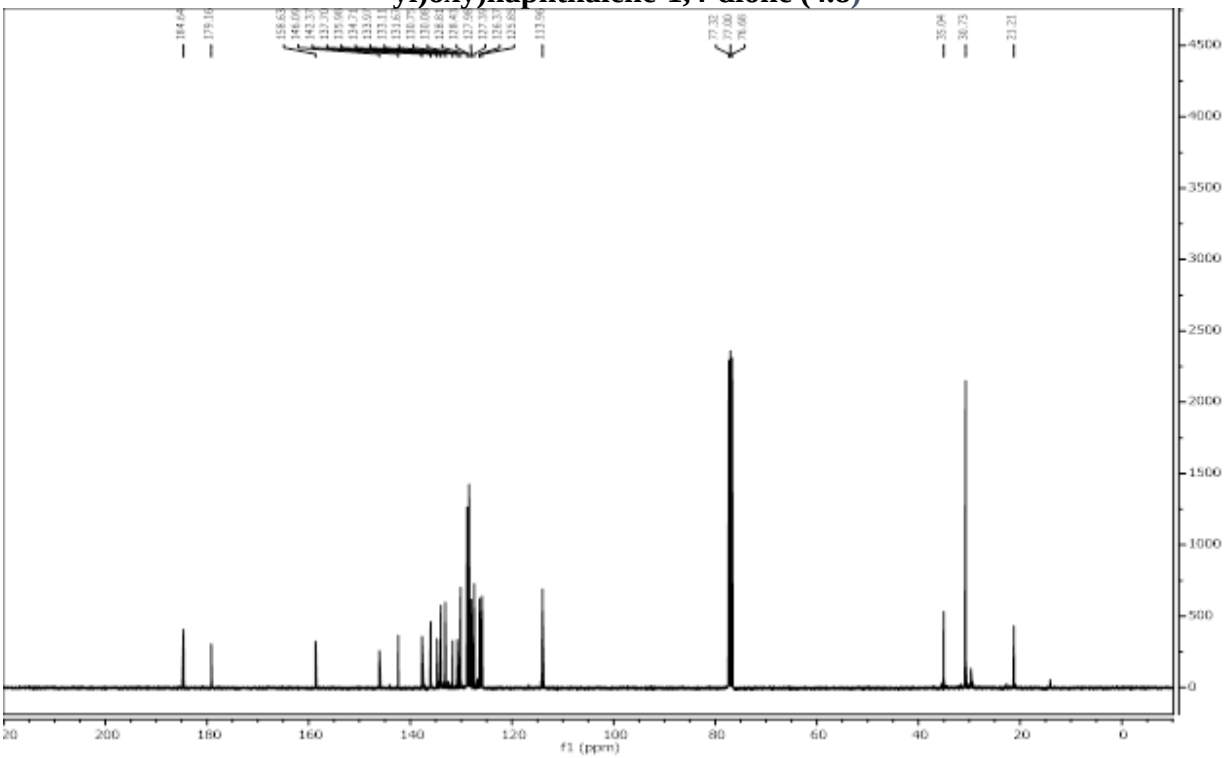

Figure 4.6.78 101 MHz ^{13}C Spectrum of 2-((3-*tert*-butyl)-5-methyl-[1,1'-biphenyl]-2-yl]-2-yl)oxy)naphthalene-1,4-dione (4.8)

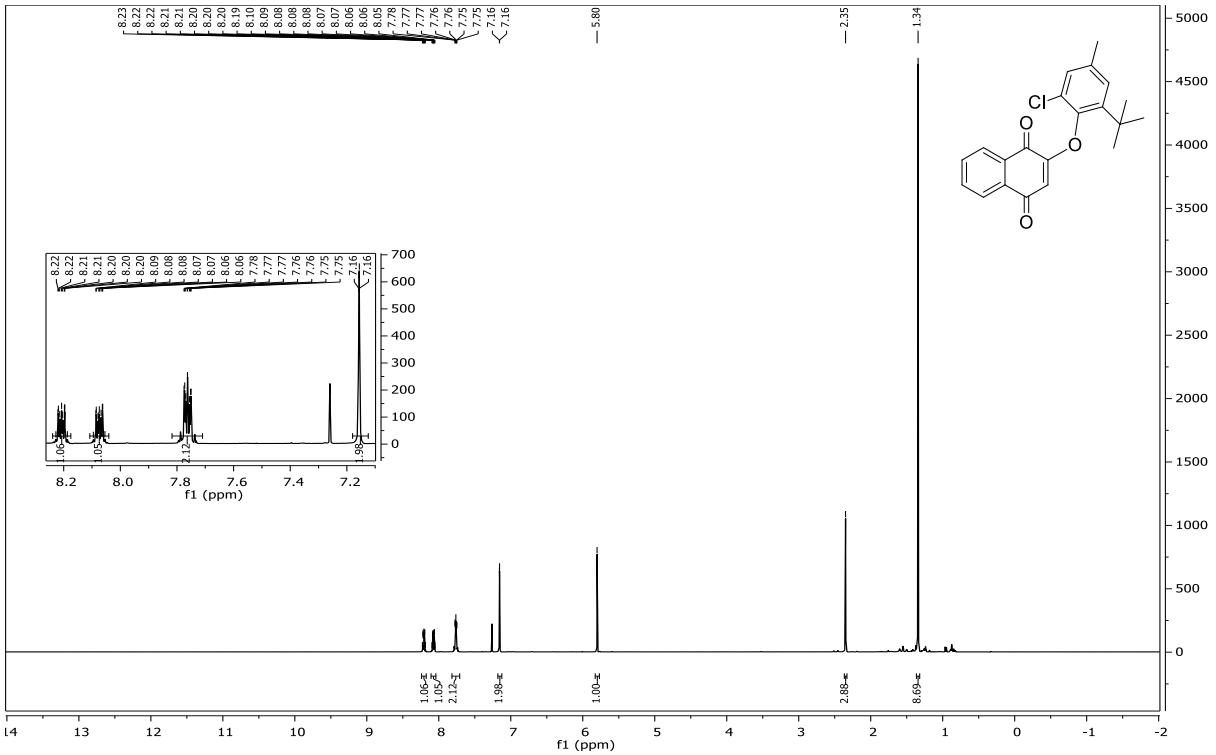

Figure 4.6.79 400 MHz ^{1}H Spectrum of 2-(2-(*tert*-butyl)-6-chloro-4-methylphenoxy)naphthalene-1,4-dione (4.9)

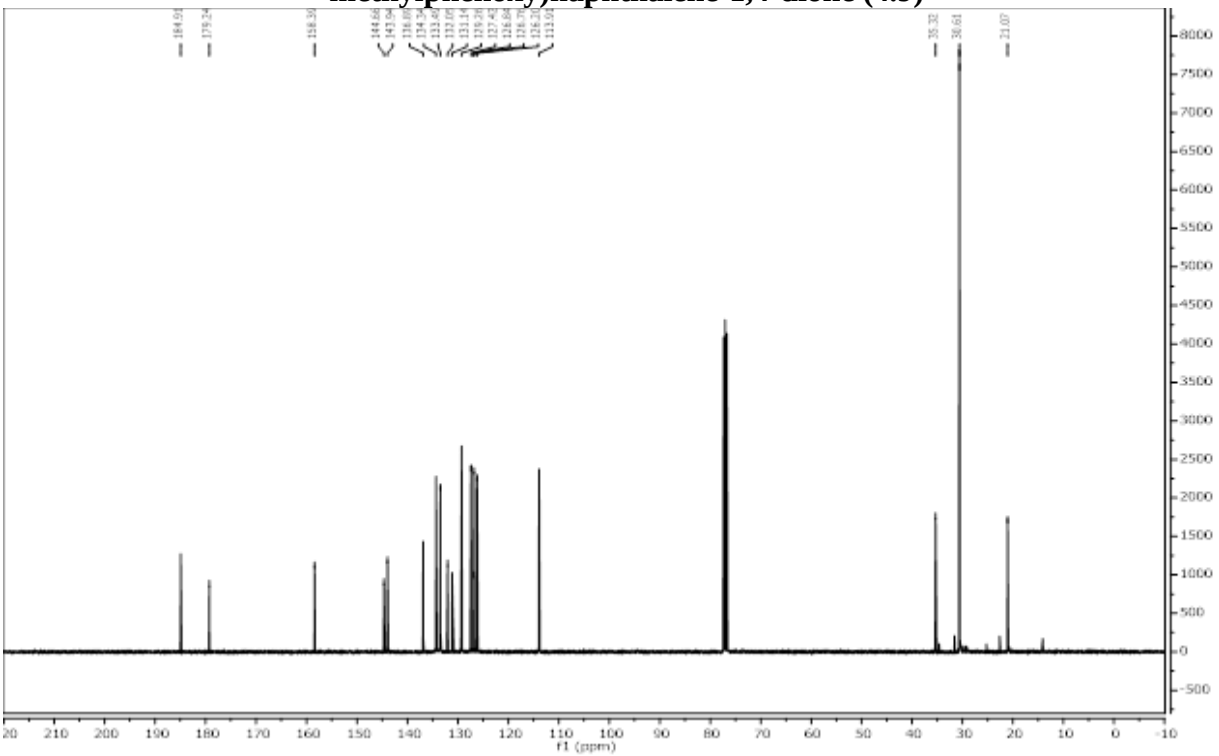

Figure 4.6.80 101 MHz ^{13}C Spectrum of 2-(2-(*tert*-butyl)-6-chloro-4-methylphenoxy)naphthalene-1,4-dione (4.9)

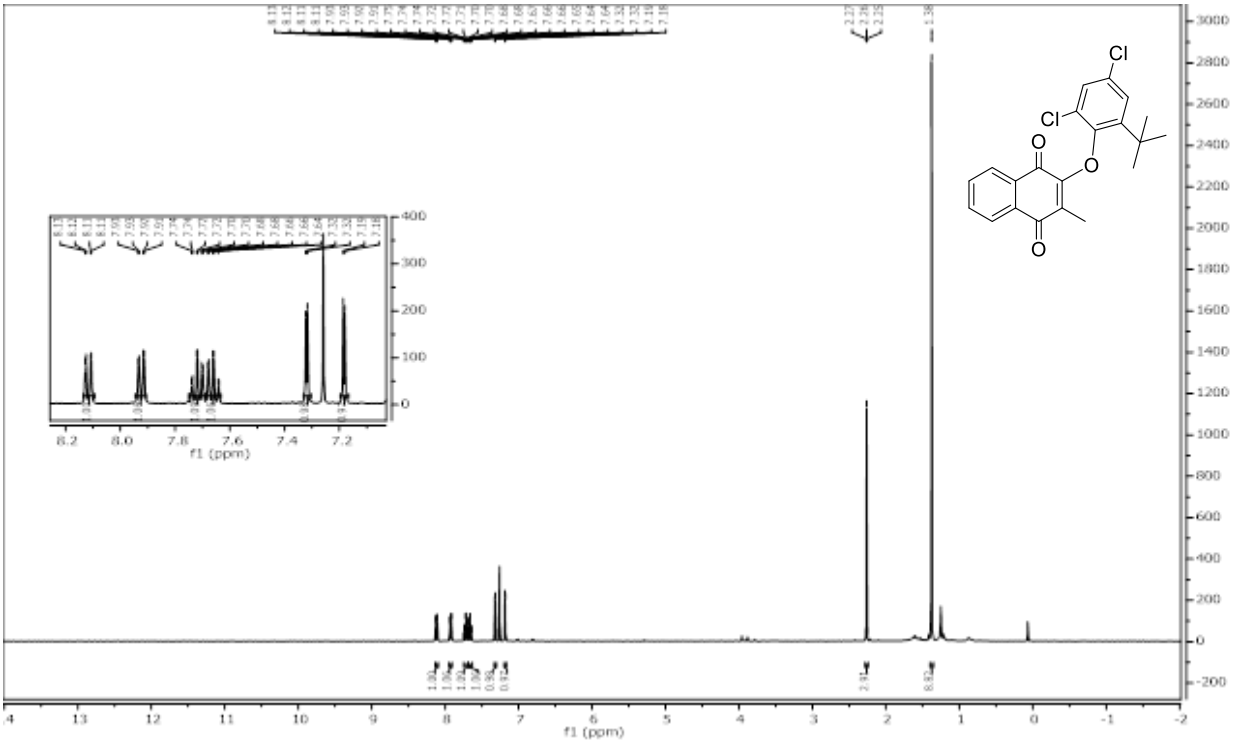

Figure 4.6.81 400 MHz ^{1}H Spectrum of 2-(2-(*tert*-butyl)-4,6-dichlorophenoxy)-3-methylnaphthalene-1,4-dione (4.1a)

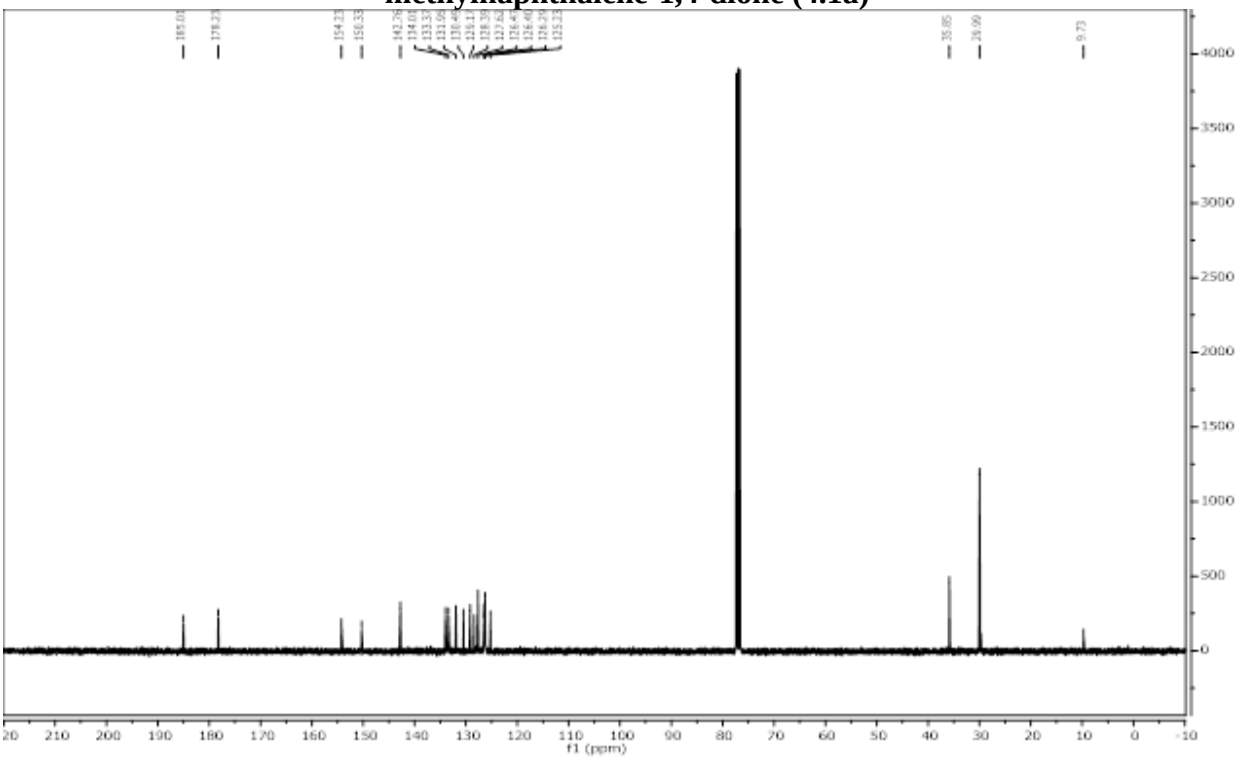

Figure 4.6.82 101 MHz ^{13}C Spectrum of 2-(2-(*tert*-butyl)-4,6-dichlorophenoxy)-3-methylnaphthalene-1,4-dione (4.1a)

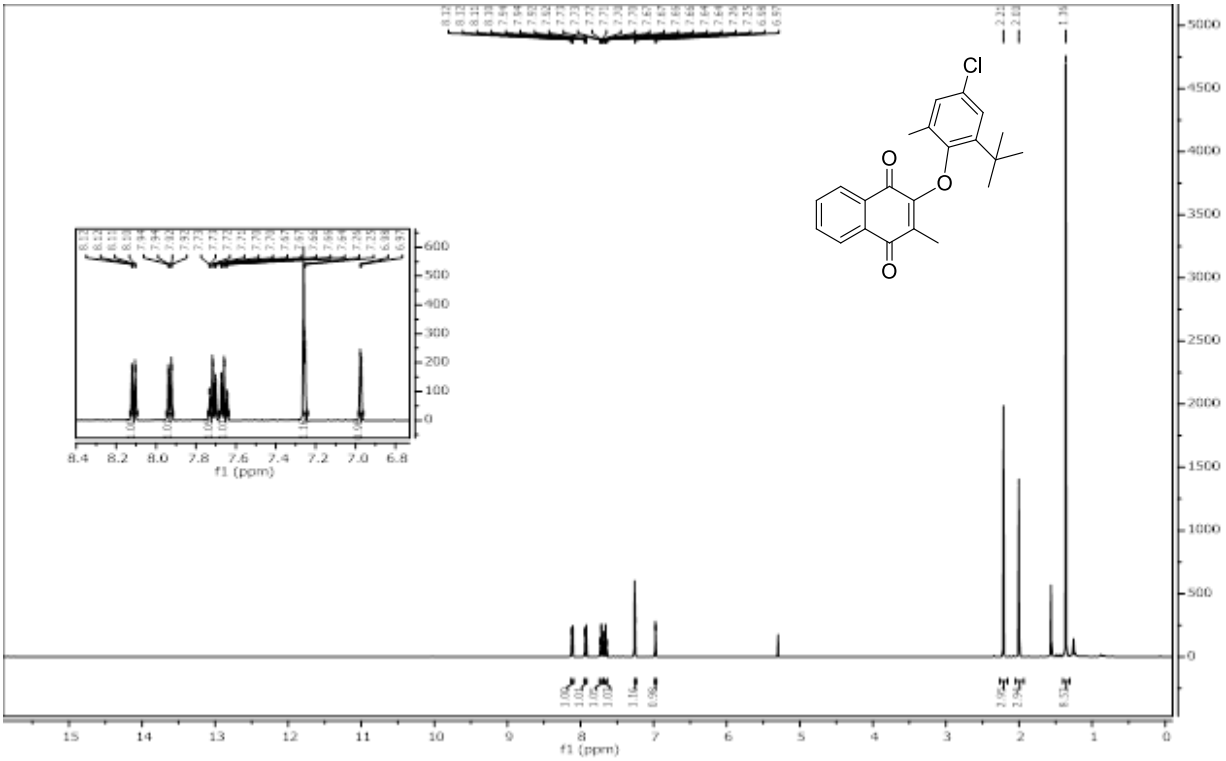

Figure 4.6.83 500 MHz ^{1}H Spectrum of 2-(2-(*tert*-butyl)-4-chloro-6-methylphenoxy)-3-methylnaphthalene-1,4-dione (4.2a)

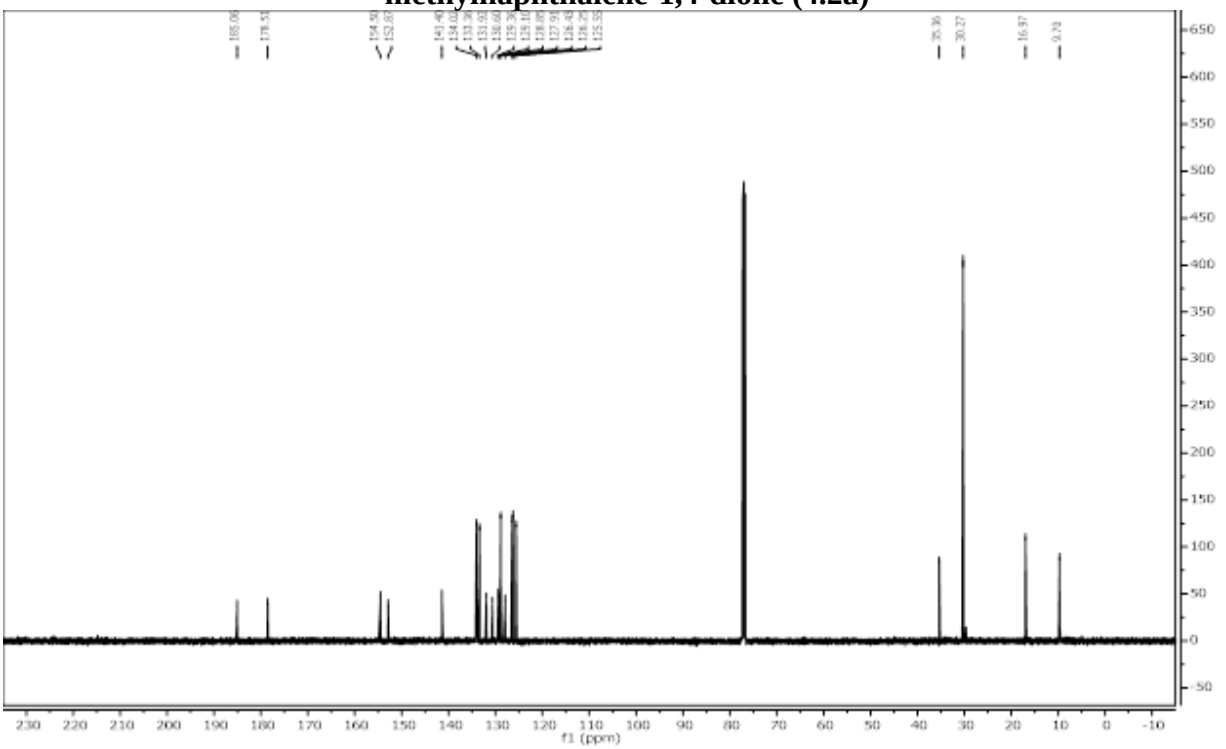

Figure 4.6.84 126 MHz ^{13}C Spectrum of 2-(2-(*tert*-butyl)-4-chloro-6-methylphenoxy)-3-methylnaphthalene-1,4-dione (4.2a)

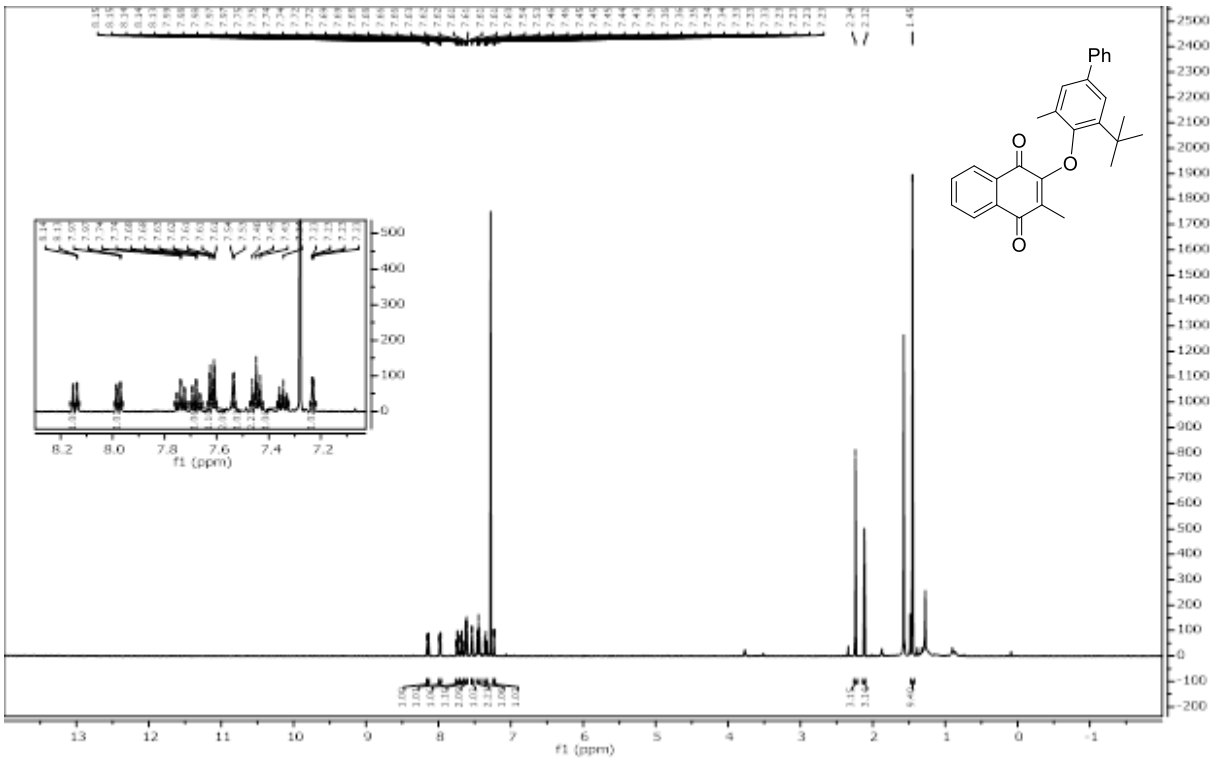

Figure 4.6.85 500 MHz ^{1}H Spectrum of 2-((3-(*tert*-butyl)-5-methyl-[1,1'-biphenyl]-4-yl)oxy)-3-methylnaphthalene-1,4-dione (4.3a)

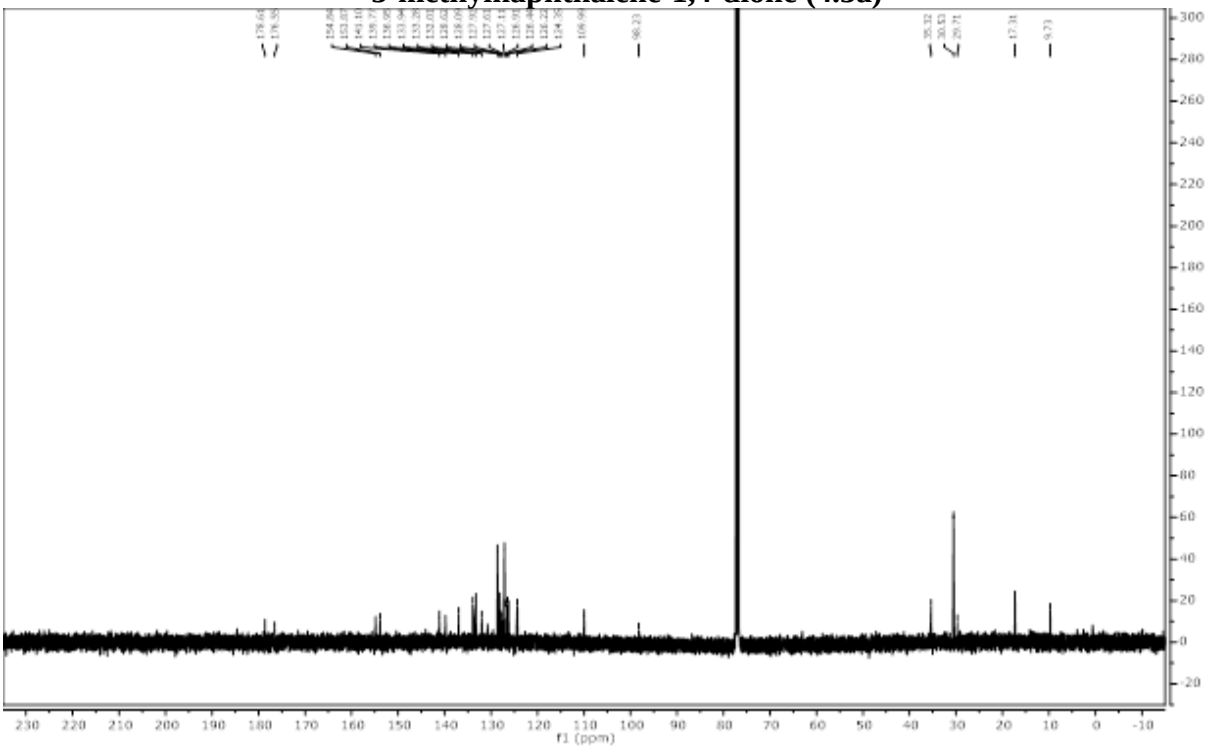

Figure 4.6.86 126 MHz ^{13}C Spectrum of 2-((3-(*tert*-butyl)-5-methyl-[1,1'-biphenyl]-4-yl)oxy)-3-methylnaphthalene-1,4-dione (4.3a)

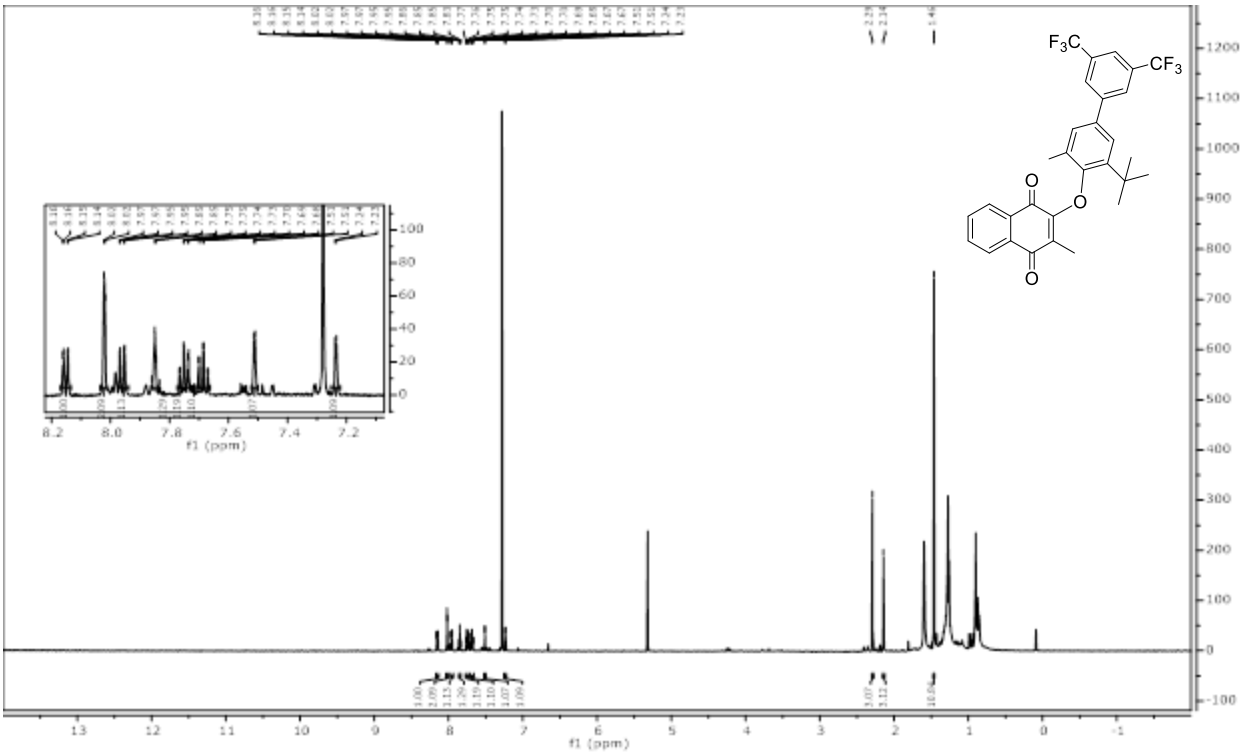

Figure 4.6.87 500 MHz ^{1}H Spectrum of 2-((3-(*tert*-butyl)-5-methyl-3',5'-bis(trifluoromethyl)-[1,1'-biphenyl]-4-yl)oxy)-3-methylnaphthalene-1,4-dione (4.4a)

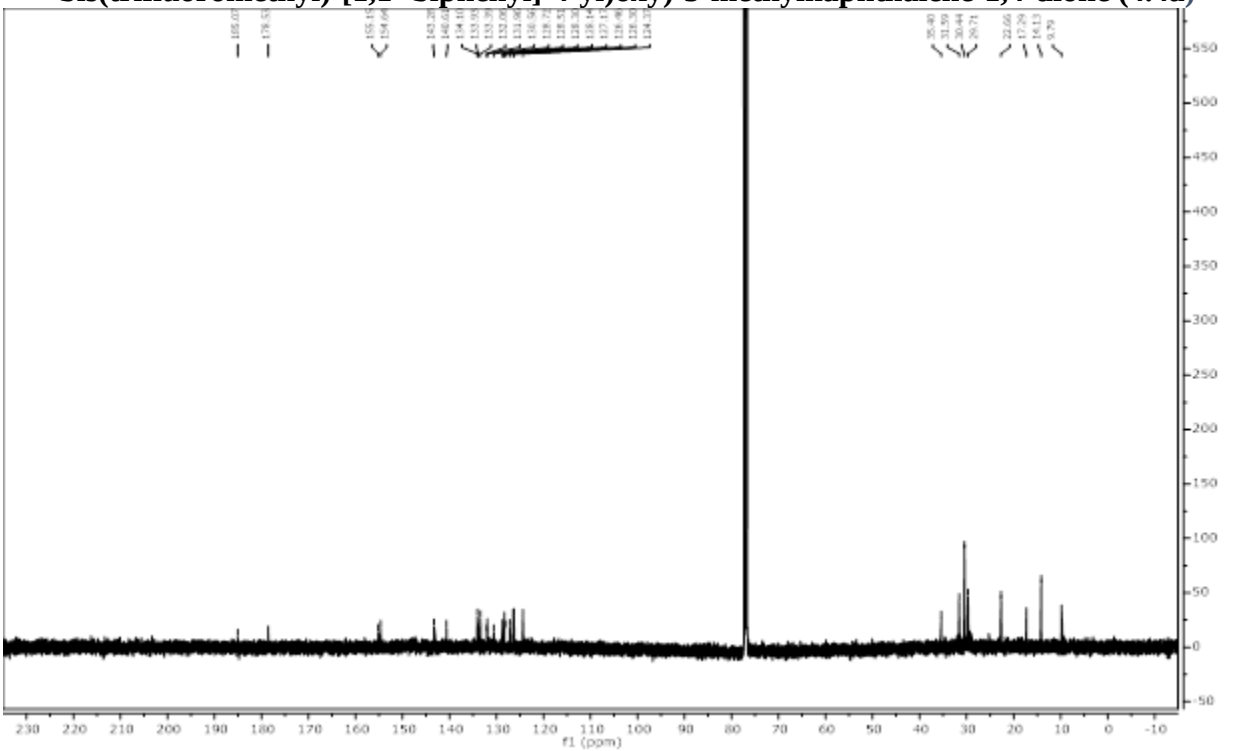

Figure 4.6.88 126 MHz ^{13}C Spectrum of 2-((3-(*tert*-butyl)-5-methyl-3',5'-bis(trifluoromethyl)-[1,1'-biphenyl]-4-yl)oxy)-3-methylnaphthalene-1,4-dione (4.4a)

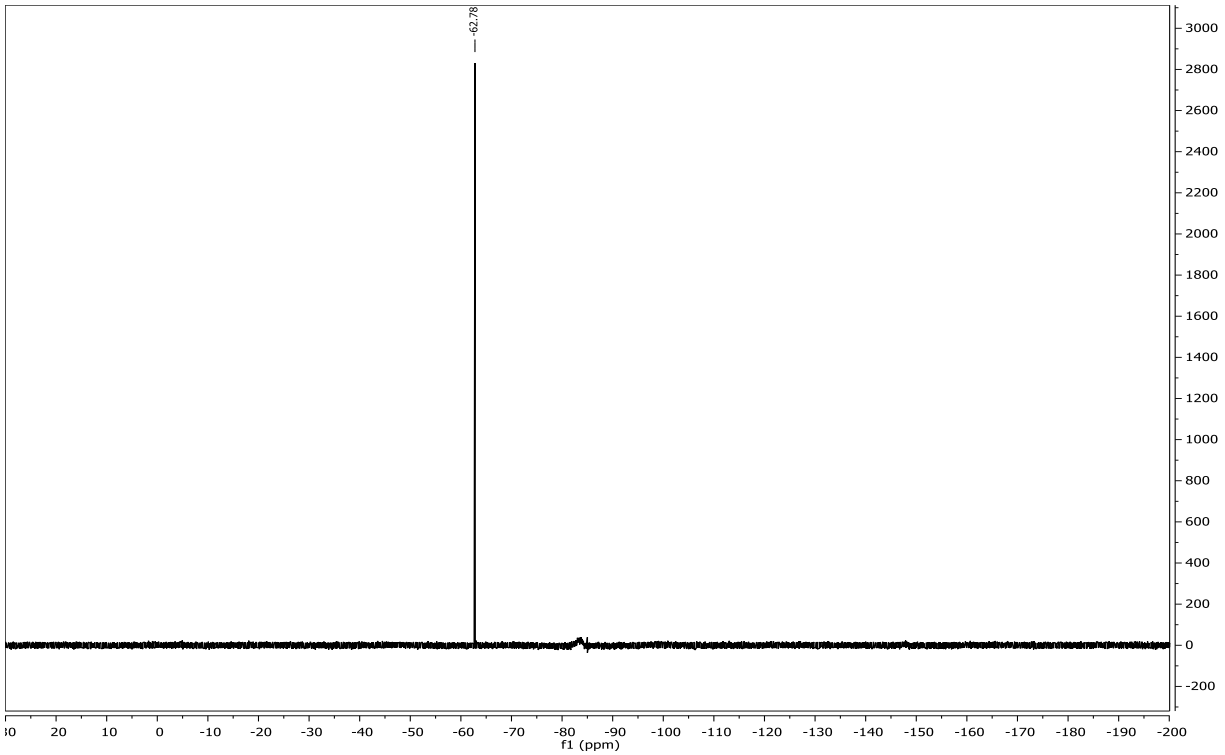

Figure 4.6.89 470 MHz ^{19}F Spectrum of 2-((3-(*tert*-butyl)-5-methyl-3',5'-bis(trifluoromethyl)-[1,1'-biphenyl]-4-yl)oxy)-3-methylnaphthalene-1,4-dione (4.4a)

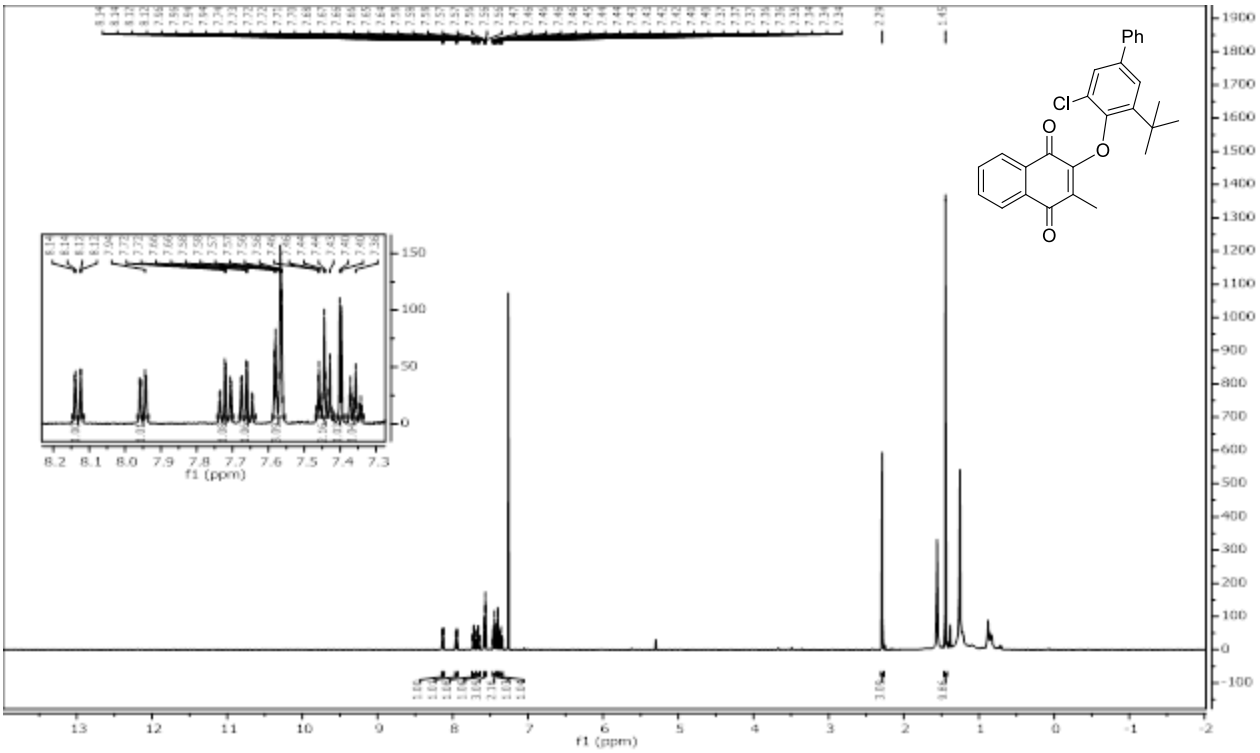

Figure 4.6.90 400 MHz ^{1}H Spectrum of 2-((3-(*tert*-butyl)-5-chloro-[1,1'-biphenyl]-4-yl)oxy)-3-methylnaphthalene-1,4-dione (4.5a)

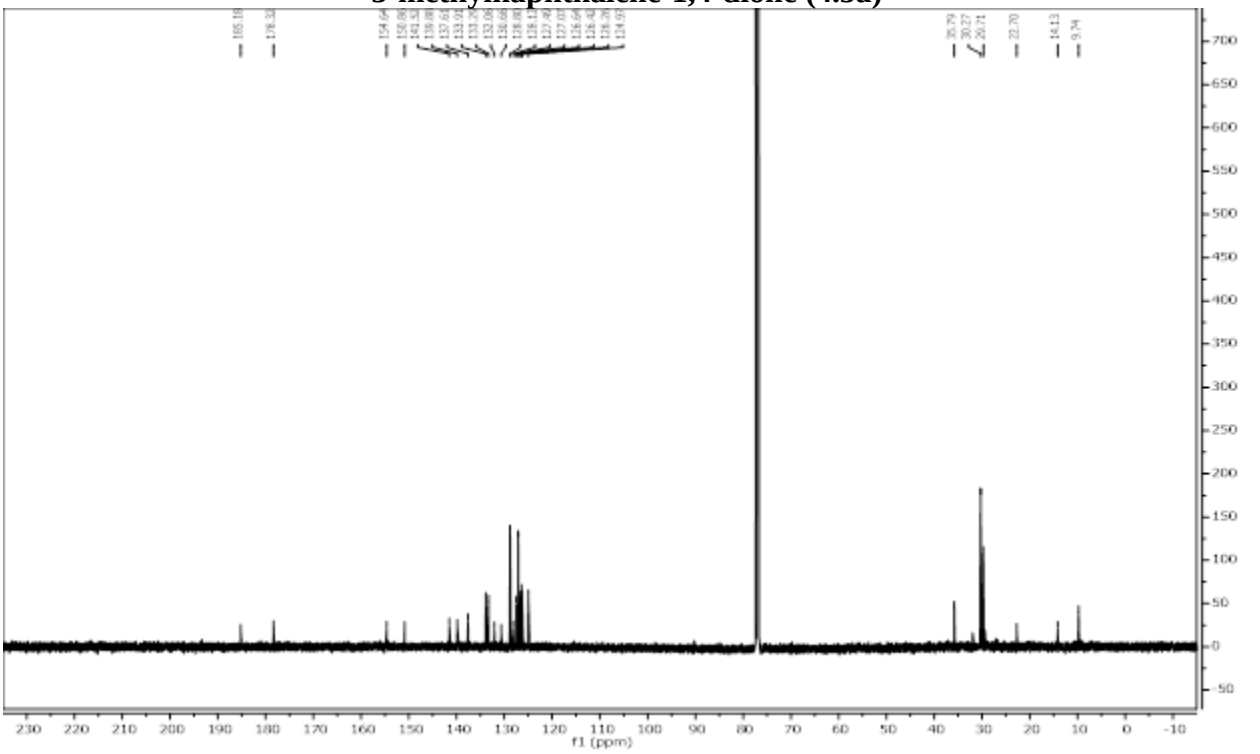

Figure 4.6.91 126 MHz ^{13}C Spectrum of 2-((3-(*tert*-butyl)-5-chloro-[1,1'-biphenyl]-4-yl)oxy)-3-methylnaphthalene-1,4-dione (4.5a)

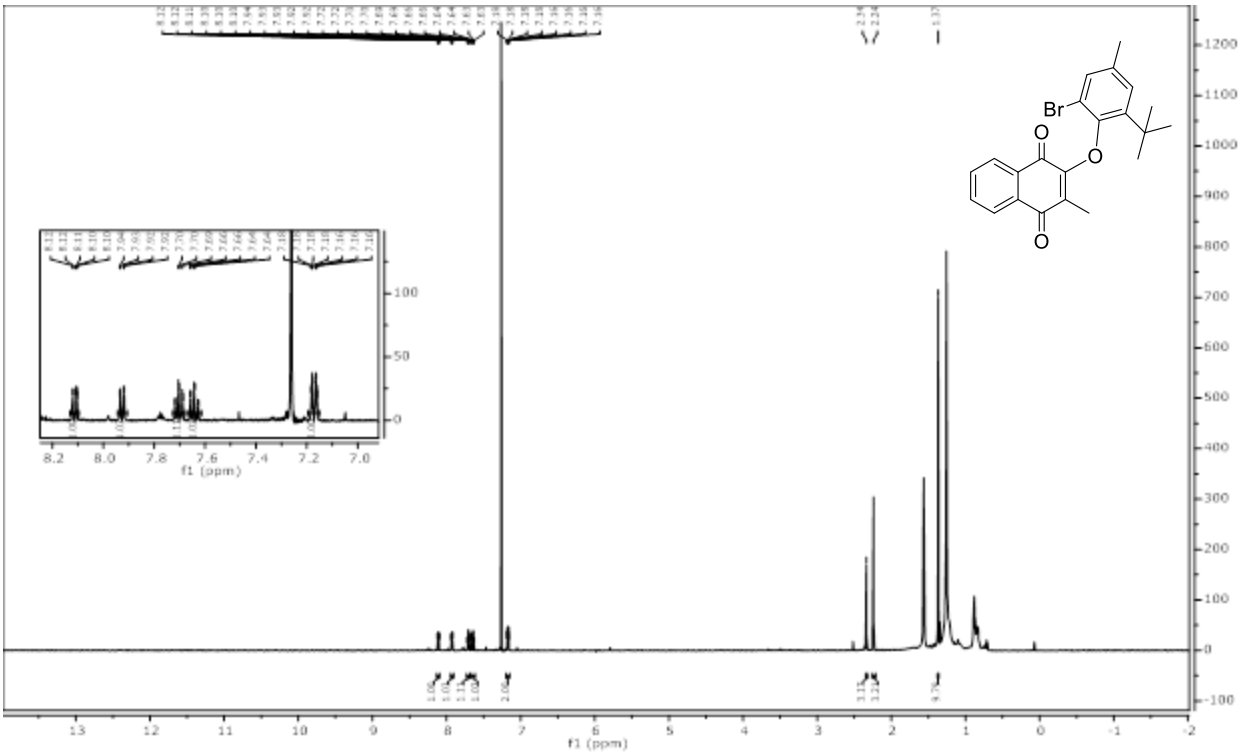

Figure 4.6.92 500 MHz ^{1}H Spectrum of 2-(2-bromo-6-(*tert*-butyl)-4-methylphenoxy)-3-methylnaphthalene-1,4-dione (4.6a)

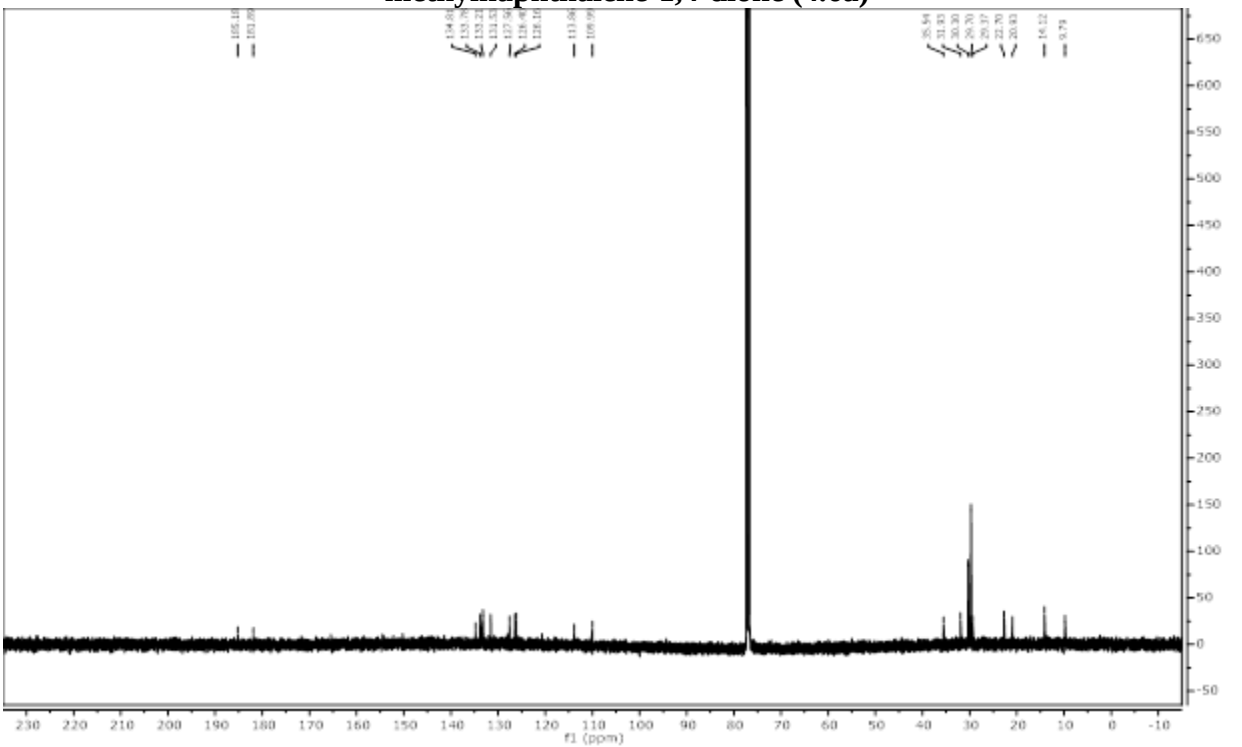

Figure 4.6.93 126 MHz ^{13}C Spectrum of 2-(2-bromo-6-(*tert*-butyl)-4-methylphenoxy)-3-methylnaphthalene-1,4-dione (4.6a)

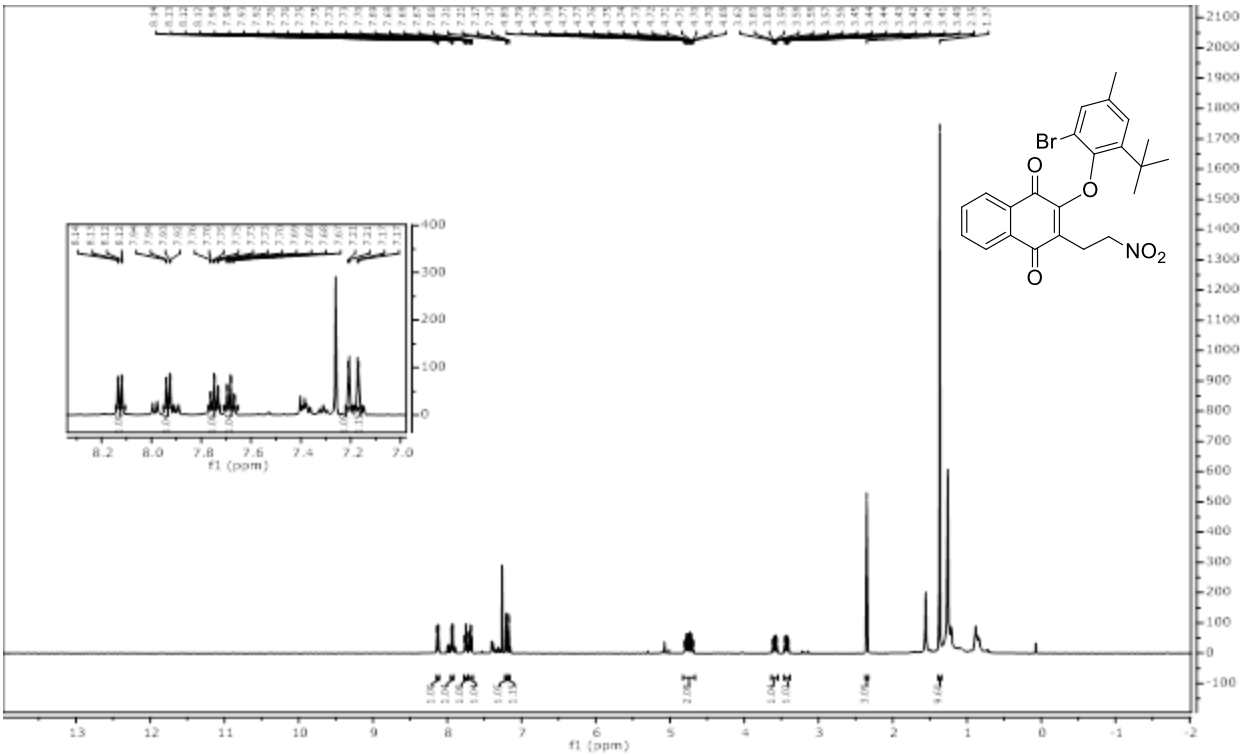

Figure 4.6.94 500 MHz ^{1}H Spectrum of 2-(2-bromo-6-(*tert*-butyl)-4-methylphenoxy)-3-(2-nitroethyl)naphthalene-1,4-dione (4.6b)

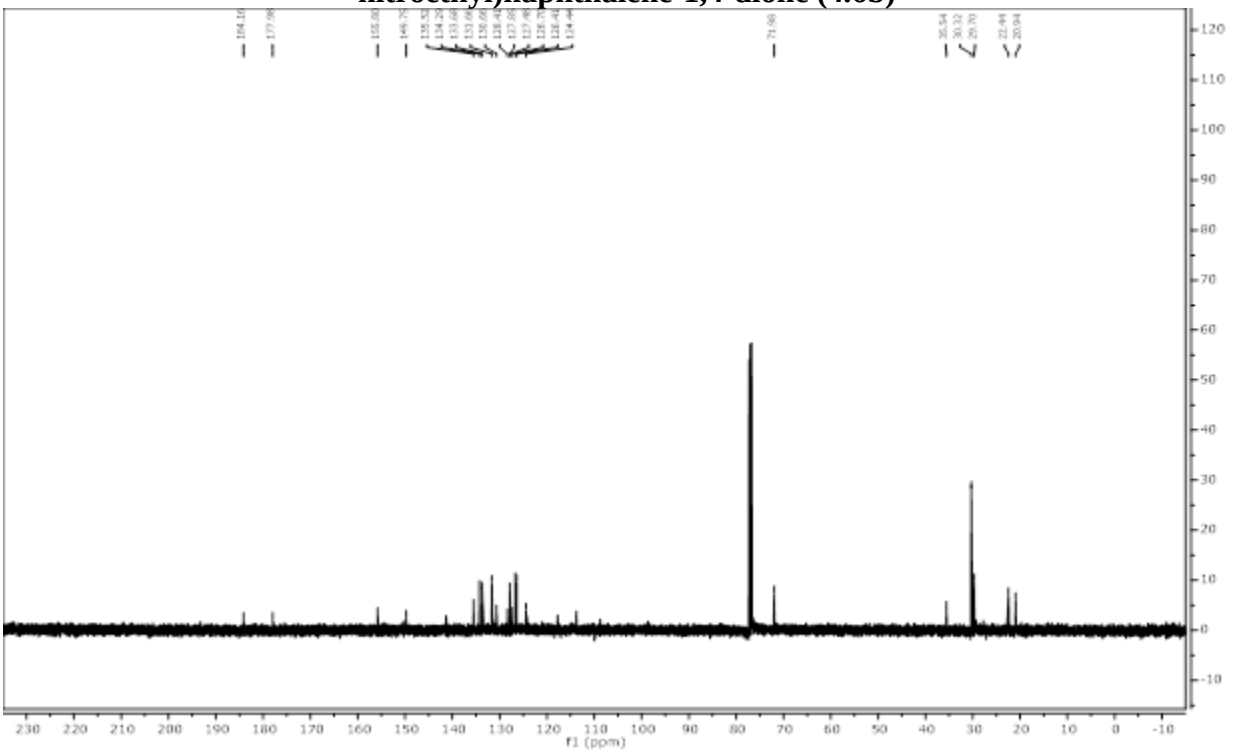

Figure 4.6.95 126 MHz ^{13}C Spectrum of 2-(2-bromo-6-(*tert*-butyl)-4-methylphenoxy)-3-(2-nitroethyl)naphthalene-1,4-dione (4.6b)

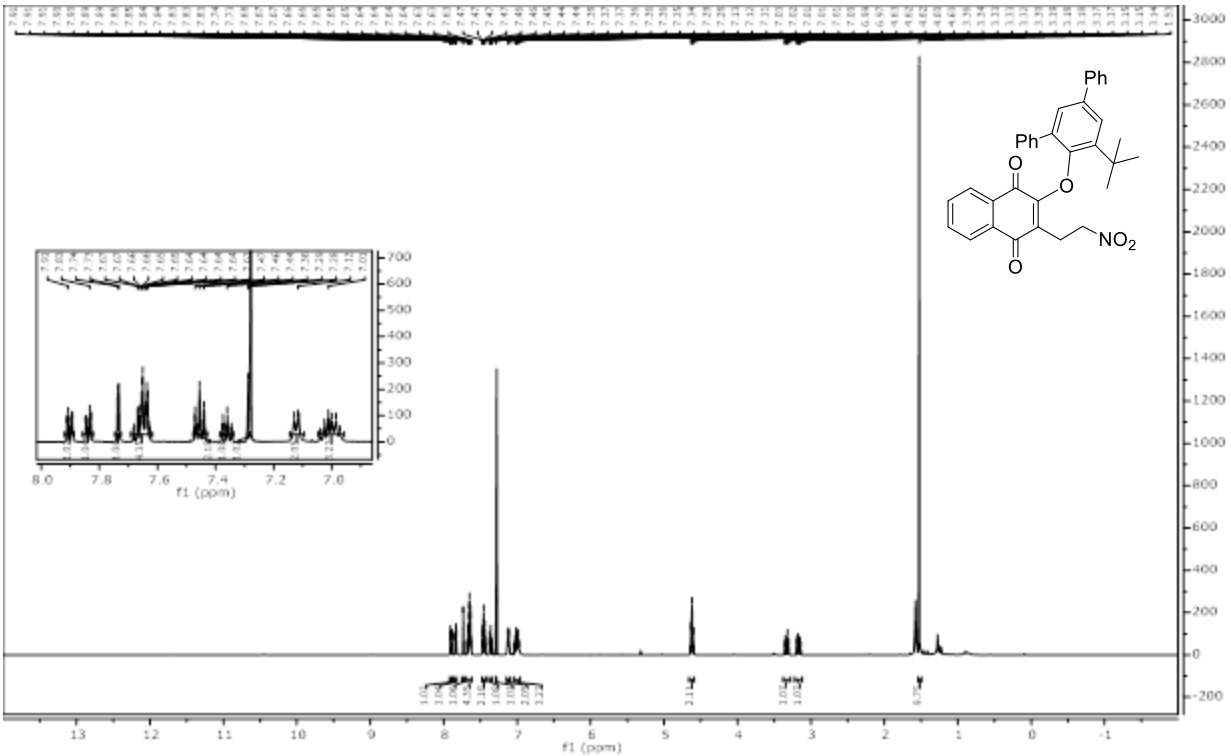

Figure 4.6.96 500 MHz ^{1}H Spectrum of 2-((5'-(*tert*-butyl)-[1,1':3',1''-terphenyl]-4'-yl)oxy)-3-(2-nitroethyl)naphthalene-1,4-dione (4.7b)

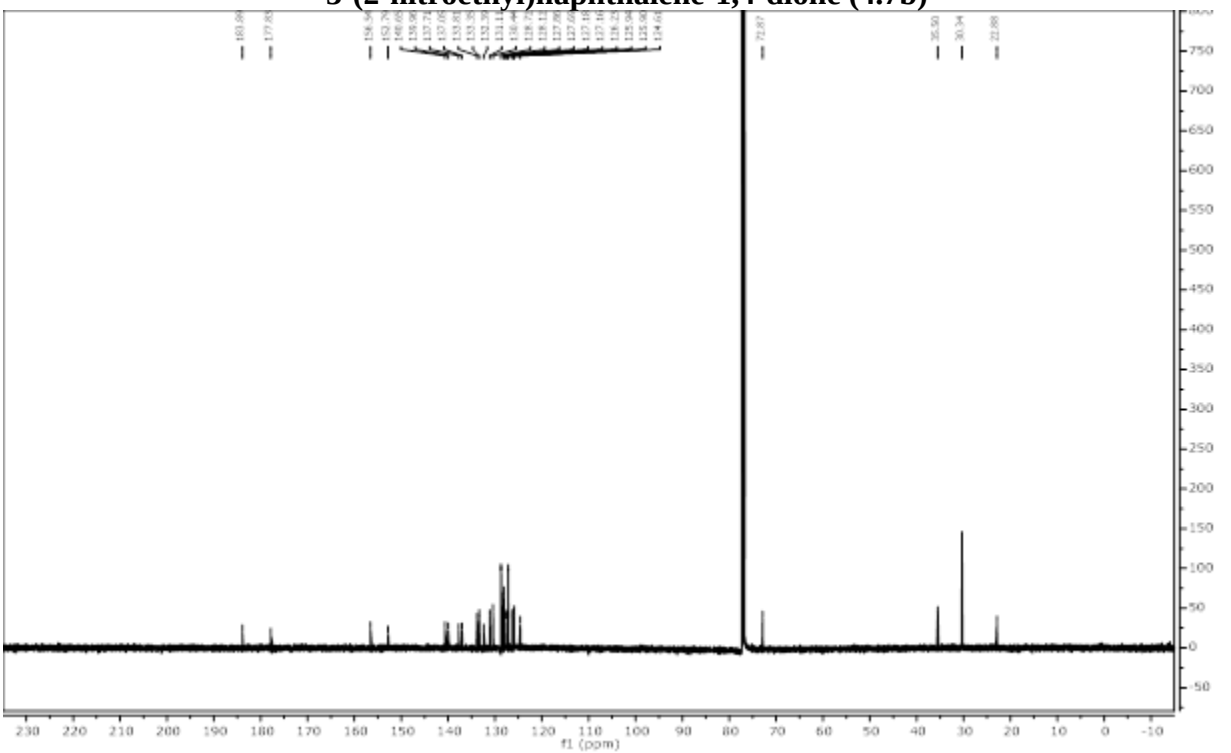

Figure 4.6.97 126 MHz ^{13}C Spectrum of 2-((5'-(*tert*-butyl)-[1,1':3',1''-terphenyl]-4'-yl)oxy)-3-(2-nitroethyl)naphthalene-1,4-dione (4.7b)

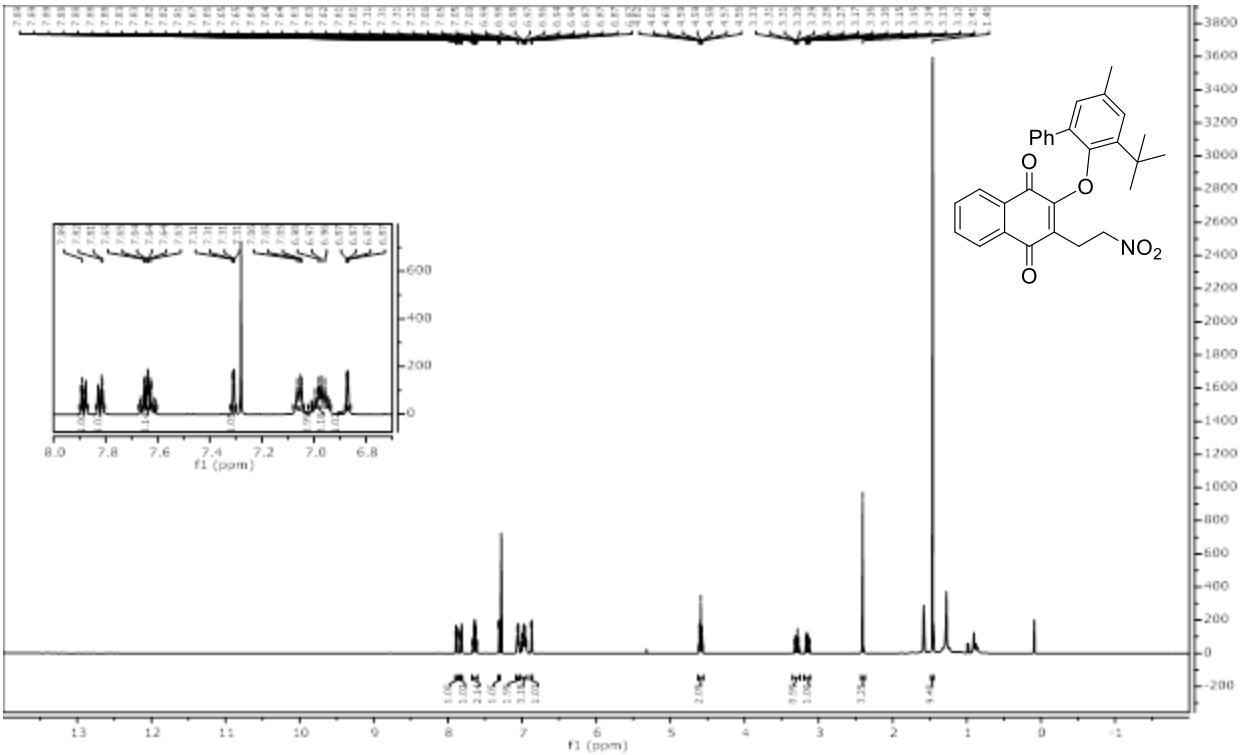

Figure 4.6.98 500 MHz ^{1}H Spectrum of 2-((3-(*tert*-butyl)-5-methyl-[1,1'-biphenyl]-2-yl)oxy)-3-(2-nitroethyl)naphthalene-1,4-dione (4.8b)

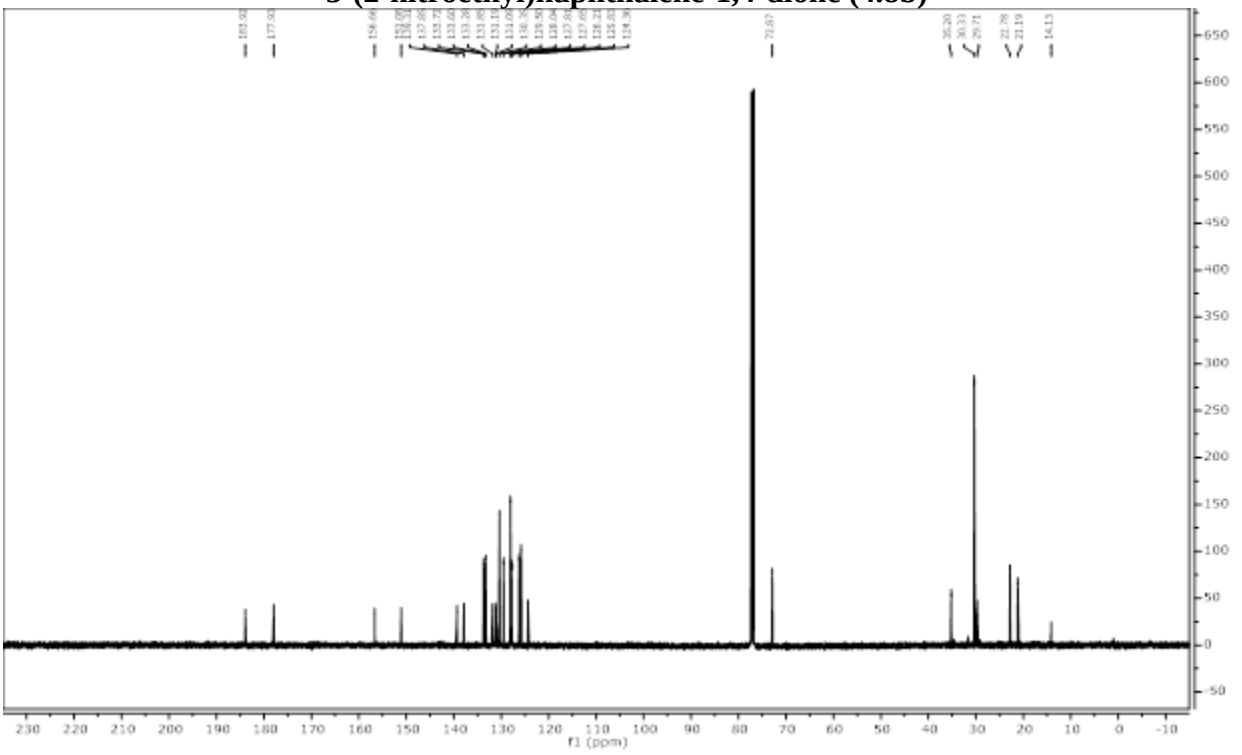

Figure 4.6.99 126 MHz ^{13}C Spectrum of 2-((3-(*tert*-butyl)-5-methyl-[1,1'-biphenyl]-2-yl)oxy)-3-(2-nitroethyl)naphthalene-1,4-dione (4.8b)

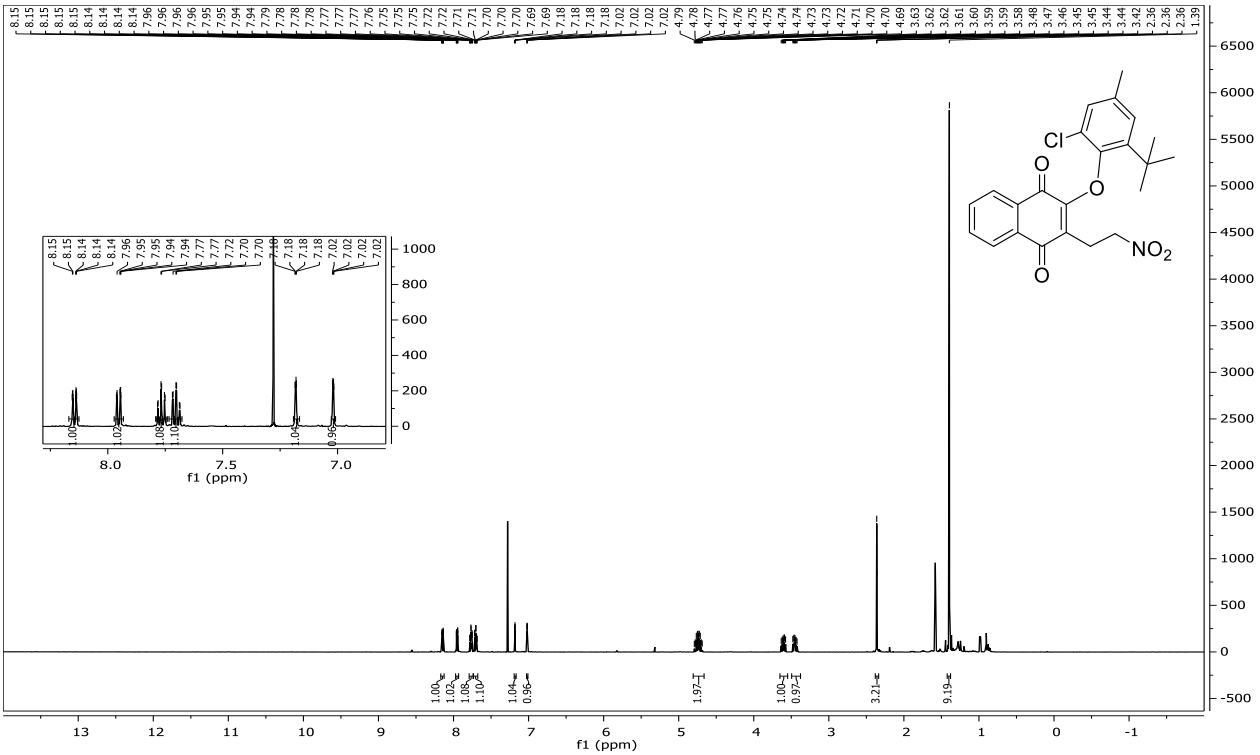

Figure 4.6.100 500 MHz ^{1}H Spectrum of 2-(2-(*tert*-butyl)-6-chloro-4-methylphenoxy)-3-(2-nitroethyl)naphthalene-1,4-dione (4.9b)

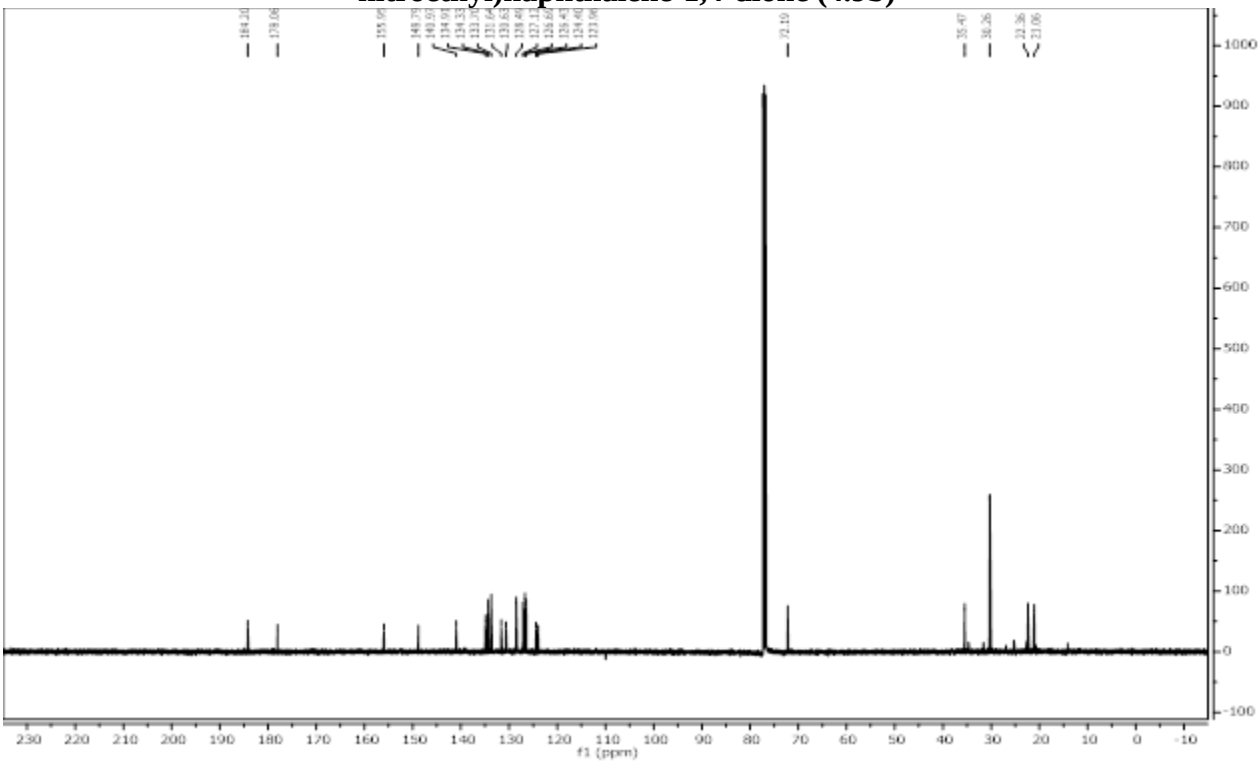

Figure 4.6.101 126 MHz ^{13}C Spectrum of 2-(2-(*tert*-butyl)-6-chloro-4-methylphenoxy)-3-(2-nitroethyl)naphthalene-1,4-dione (4.9b)

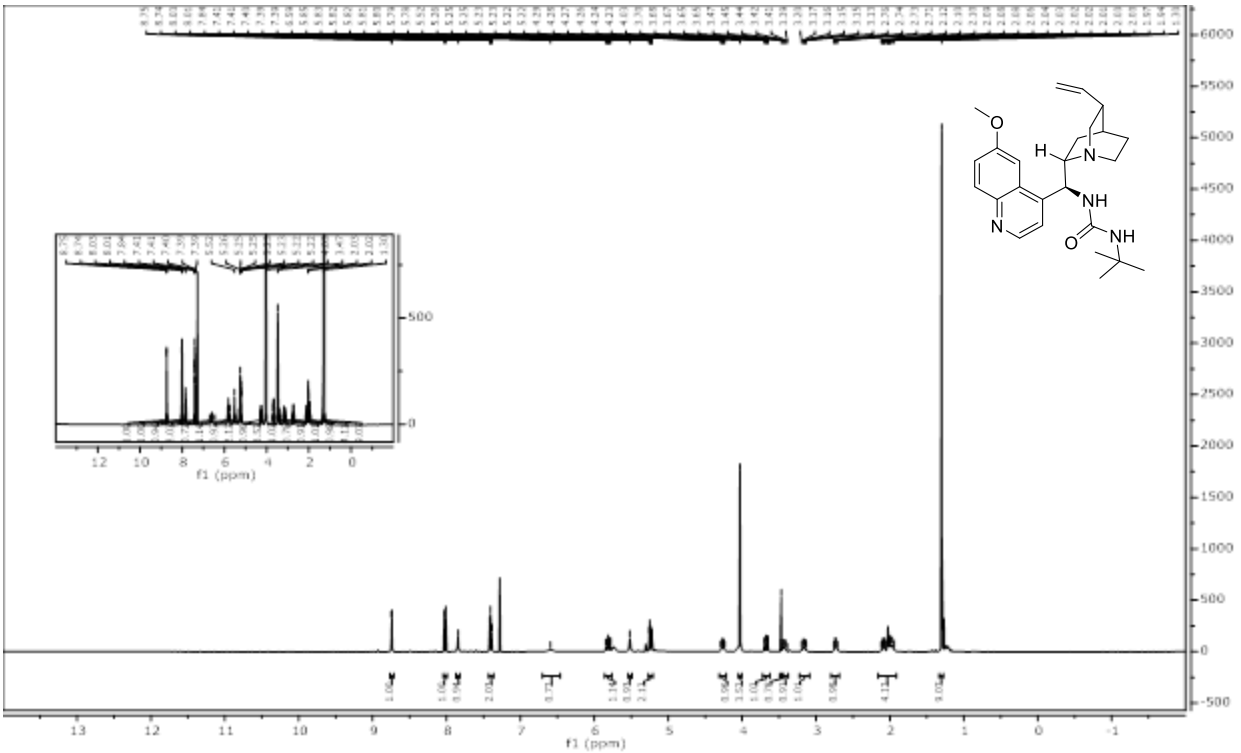

Figure 4.6.102 500 MHz ^{1}H Spectrum of -(*tert*-butyl)-3-((S)-(6-methoxyquinolin-4-yl)((1S,2S,4S,5R)-5-vinylquinuclidin-2-yl)methyl)urea

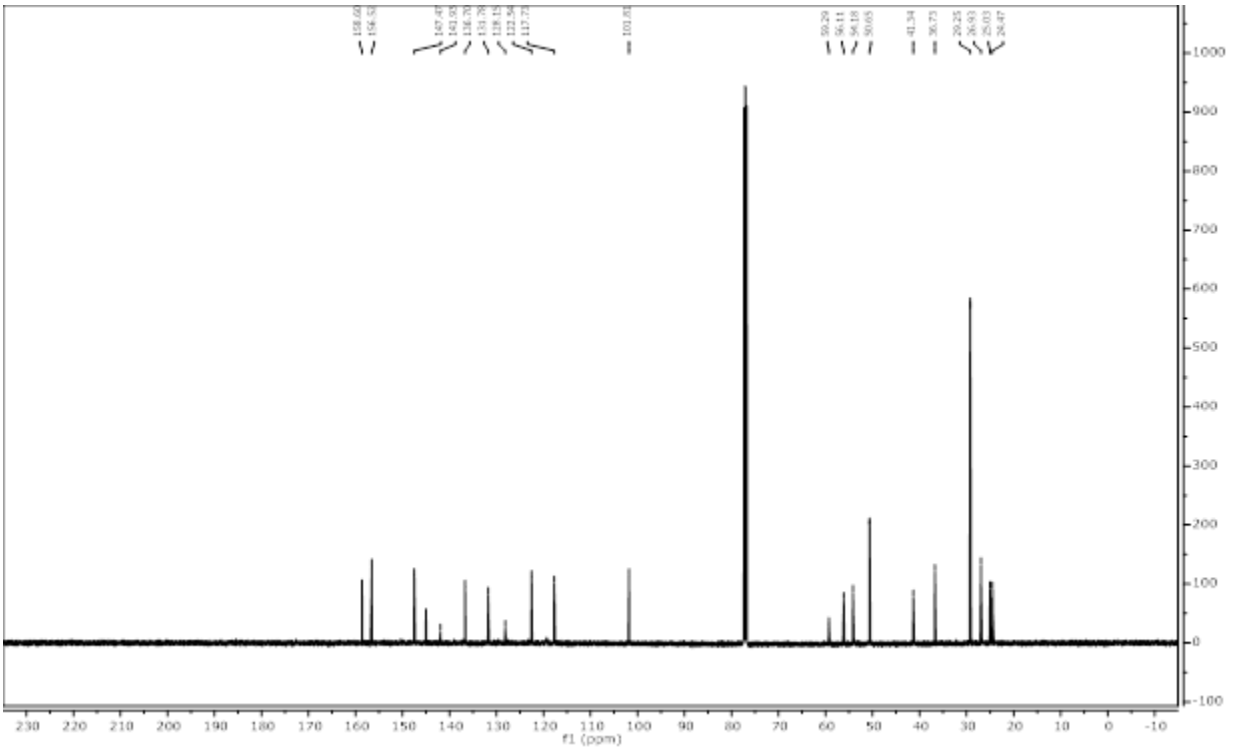

Figure 4.6.103 126 MHz ^{13}C Spectrum of -(*tert*-butyl)-3-((S)-(6-methoxyquinolin-4-yl)((1S,2S,4S,5R)-5-vinylquinuclidin-2-yl)methyl)urea

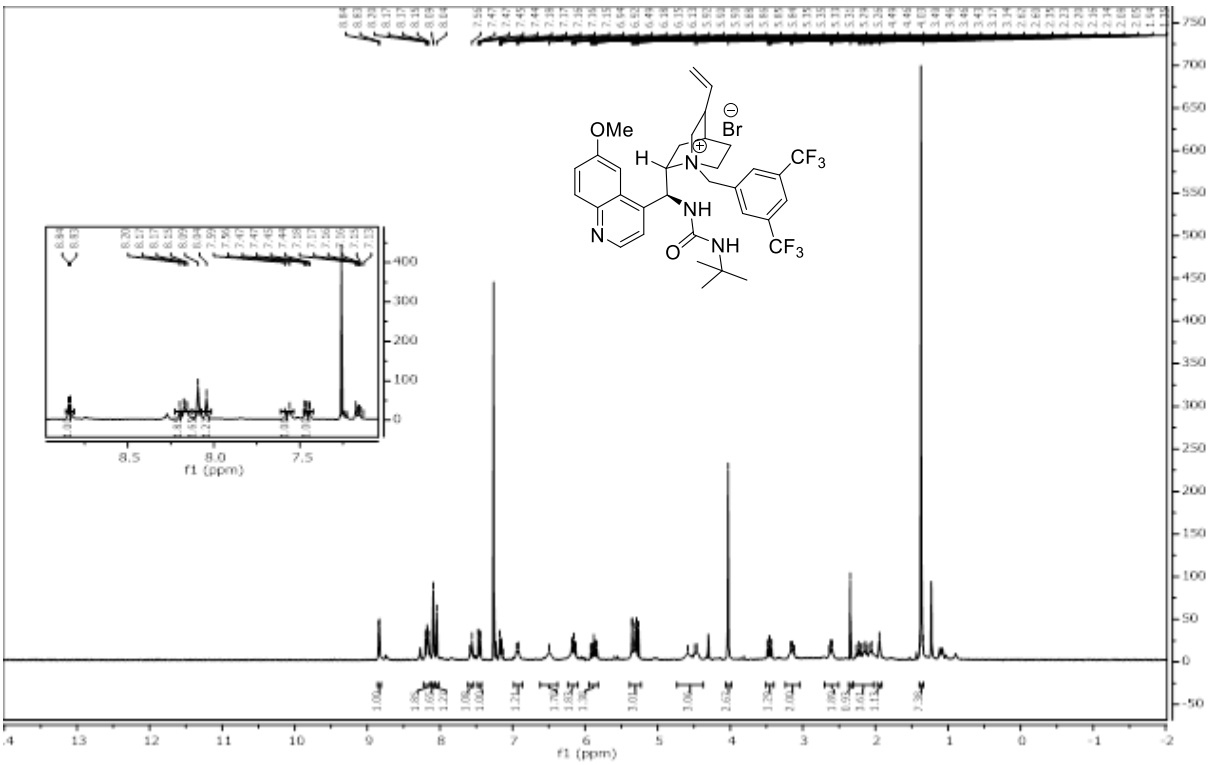

Figure 4.6.104 500 MHz ^{1}H Spectrum of (1S,2S,4S)-1-(3,5-bis(trifluoromethyl)benzyl)-2-((S)-(3-(*tert*-butyl)ureido)(6-methoxyquinolin-4-yl)methyl)-5-vinylquinuclidin-1-ium bromide, C4.2

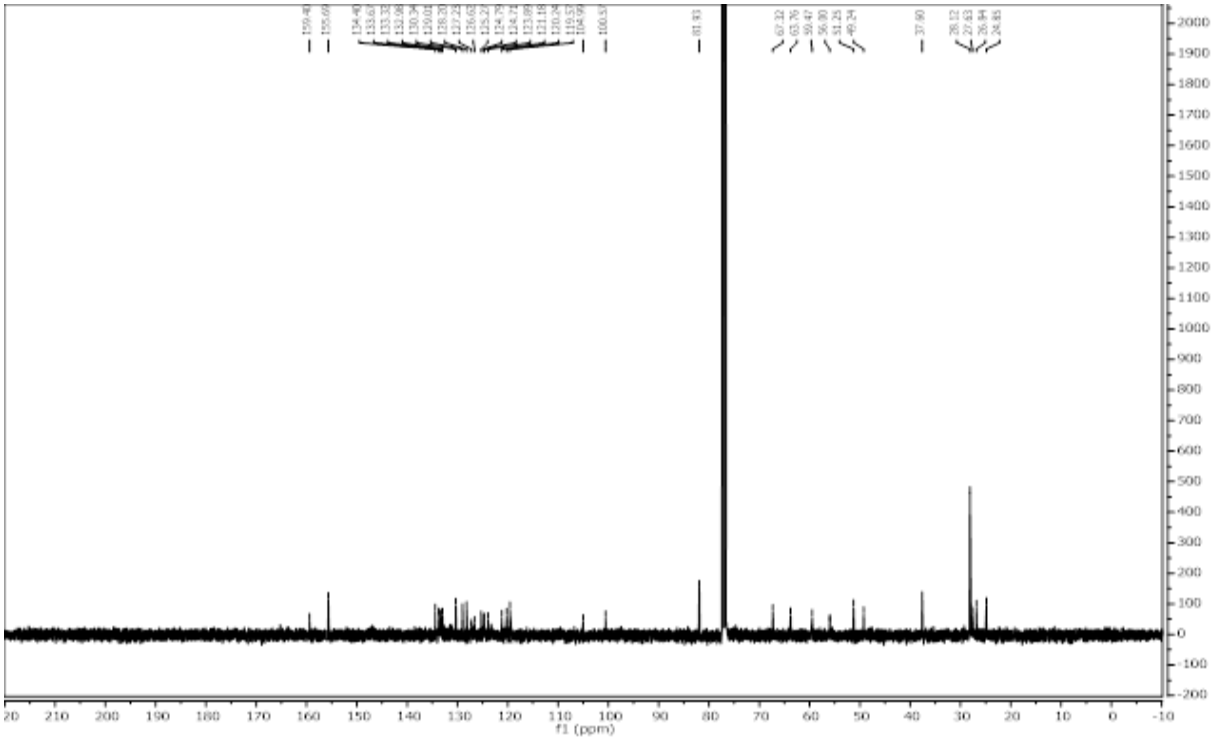

Figure 4.6.105 126 MHz ^{13}C Spectrum of (1S,2S,4S)-1-(3,5-bis(trifluoromethyl)benzyl)-2-((S)-(3-(*tert*-butyl)ureido)(6-methoxyquinolin-4-yl)methyl)-5-vinylquinuclidin-1-ium bromide, C4.2

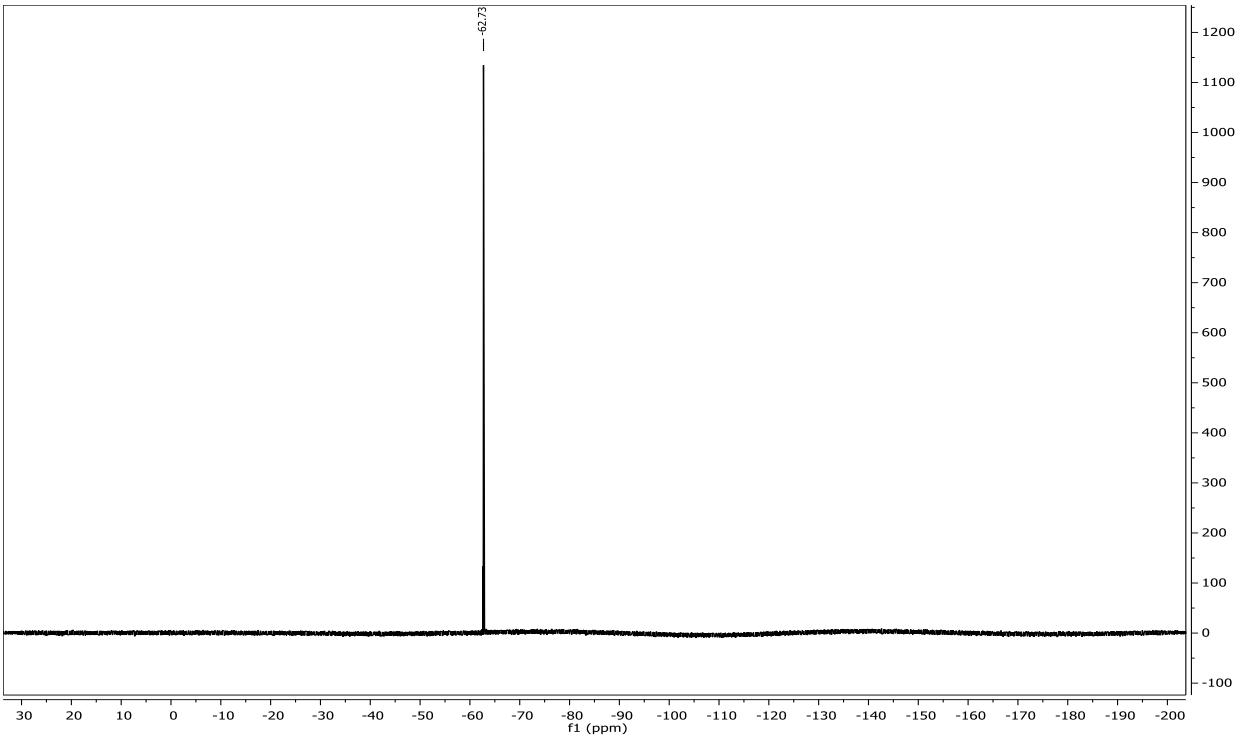

Figure 4.6.106 470 MHz ^{19}F Spectrum of (1S,2S,4S)-1-(3,5-bis(trifluoromethyl)benzyl)-2-((S)-(3-(*tert*-butyl)ureido)(6-methoxyquinolin-4-yl)methyl)-5-vinylquinuclidin-1-ium bromide, C4.2

4.6.6 Chiral HPLC Traces of Diaryl Ether Substrates

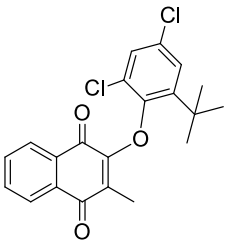

4.1a was measured with HPLC analysis using Chiralpak IA, Hexanes/EtOH (98:2), flow rate =1.0 mL/min, tR = 5.0 min (major), tR = 5.9 min (minor)

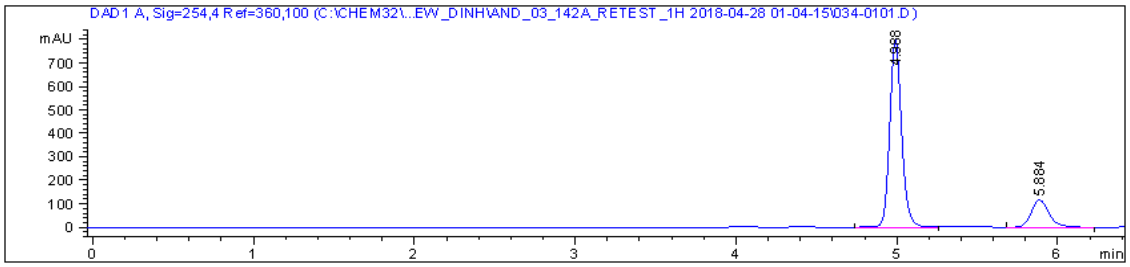

Peak #	RetTime [min]	Type	Width [min]	Area [mAU*s]	Height [mAU]	Area %
1	4.988	BV	0.0777	4105.18018	801.57135	82.0746
2	5.884	VB	0.1179	896.58795	116.39131	17.9254

Figure 4.6.107 Asymmetric HPLC Trace of 4.1a

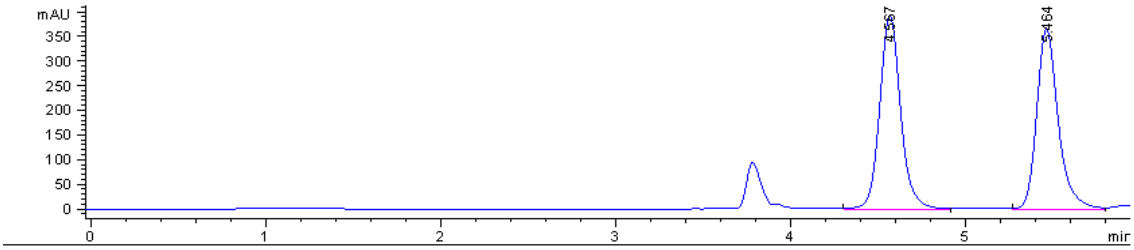

Peak #	RetTime [min]	Type	Width [min]	Area [mAU*s]	Height [mAU]	Area %
1	4.567	BB	0.1292	3275.67261	393.37134	51.2073
2	5.464	BV	0.1296	3121.21143	365.76187	48.7927

Figure 4.6.108 Racemic Standard of 4.1a

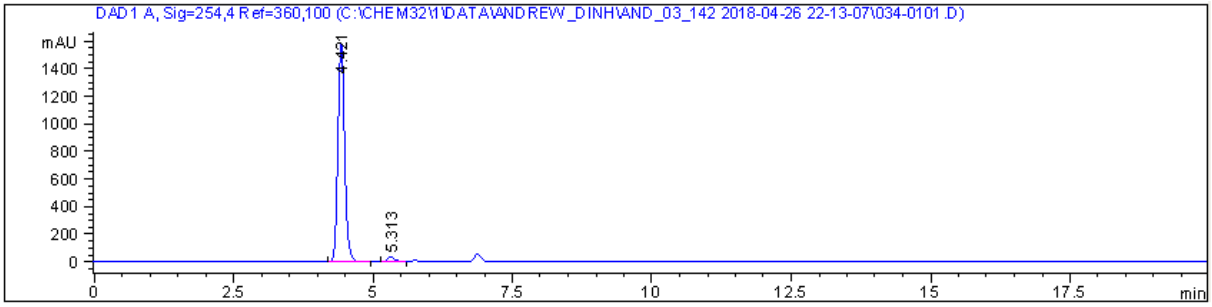

Peak #	RetTime [min]	Type	Width [min]	Area [mAU*s]	Height [mAU]	Area %
1	4.421	BB	0.1304	1.33866e4	1587.70508	97.5132
2	5.313	BV	0.1411	341.38641	35.83386	2.4868

Figure 4.6.109 Trituration 4.1a

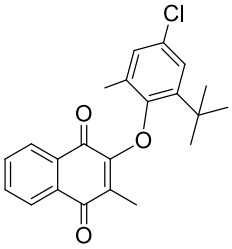

4.2a was measured with HPLC analysis using Chiralpak IA, Hexanes/EtOH (98:2), flow rate =1.0 mL/min, tR = 5.0 min (major), tR = 5.8 min (minor)

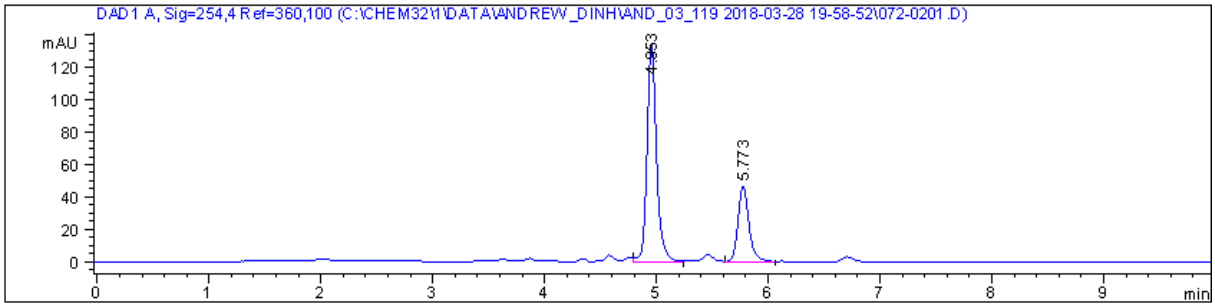

Peak #	RetTime [min]	Type	Width [min]	Area [mAU*s]	Height [mAU]	Area %
1	4.953	VB	0.0896	803.96399	134.81461	71.3692
2	5.773	VB	0.1041	322.52240	46.94880	28.6308

Figure 4.6.110 Asymmetric HPLC Trace of 4.2a

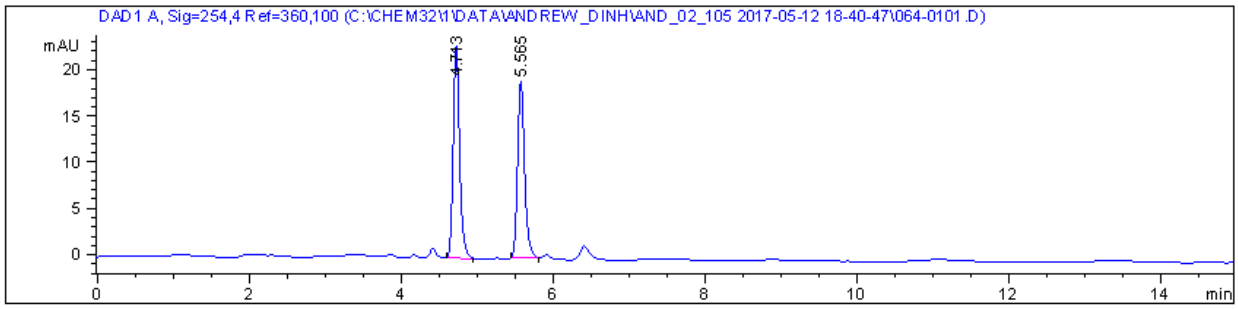

Peak #	RetTime [min]	Type	Width [min]	Area [mAU*s]	Height [mAU]	Area %
1	4.713	BB	0.0887	135.63530	23.04148	52.3367
2	5.565	BB	0.0973	123.52370	19.13589	47.6633

Figure 4.6.111 Racemic Standard of 4.2a

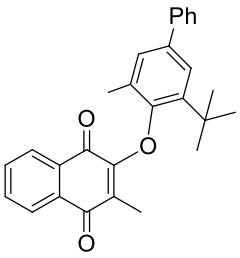

4.3a was measured with HPLC analysis using Chiralpak IA, Hexanes/EtOH (96:4), flow rate =1.0 mL/min, tR = 4.4 min (major), tR = 5.2 min (minor)

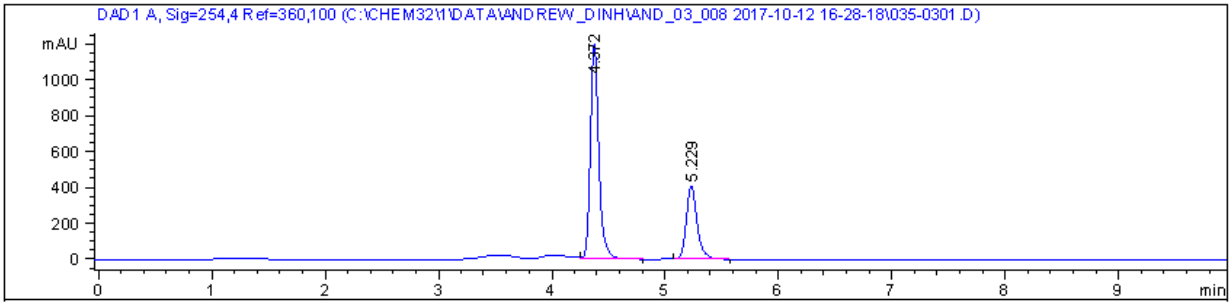

Peak #	RetTime [min]	Type	Width [min]	Area [mAU*s]	Height [mAU]	Area %
1	4.372	VB	0.0787	6258.12500	1202.74805	69.6881
2	5.229	VB	0.1016	2722.07007	409.23978	30.3119

Figure 4.6.112 Asymmetric HPLC Trace of 4.3a

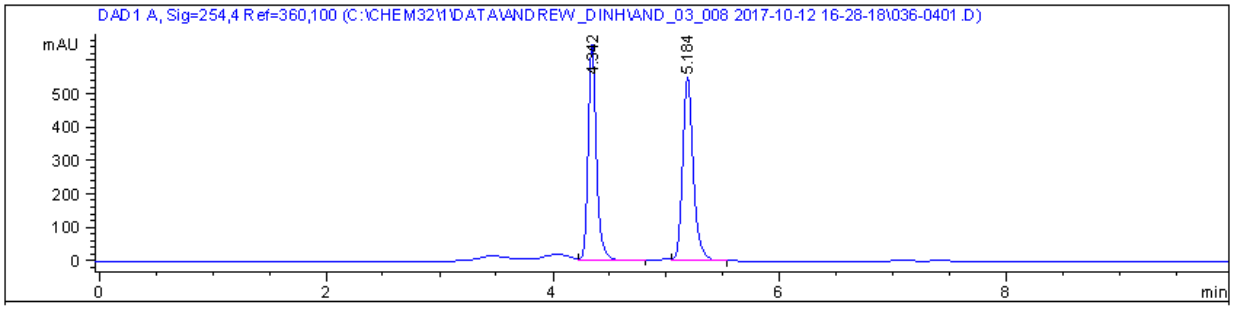

Peak #	RetTime [min]	Type	Width [min]	Area [mAU*s]	Height [mAU]	Area %
1	4.342	VV	0.0779	3325.92383	647.61902	47.9729
2	5.184	VB	0.0989	3607.00000	547.42578	52.0271

Figure 4.6.113 Racemic Standard of 4.3a

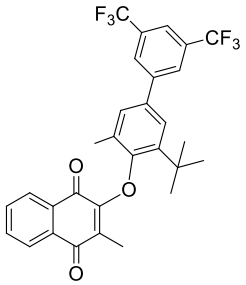

4.4a was measured with HPLC analysis using Chiralpak IA, Hexanes/EtOH (98:2), flow rate =1.0 mL/min, tR = 5.5 min (major), tR = 5.0 min (minor). Impurity in the racemic standard is residual toluene.

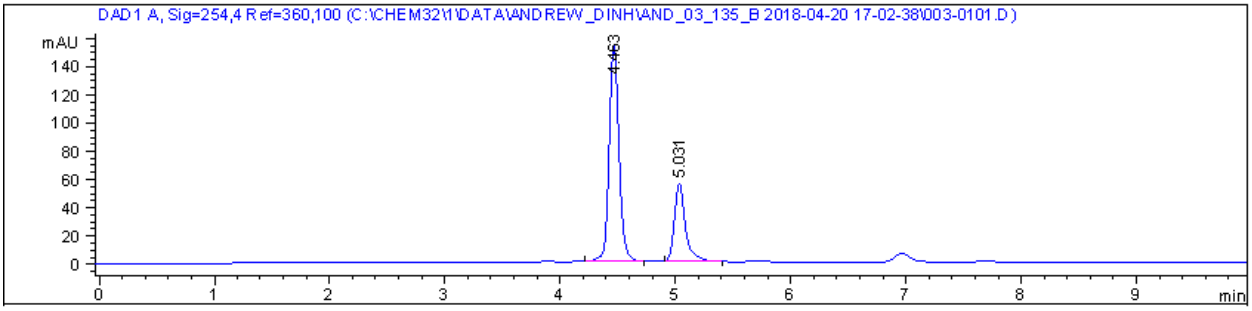

Peak #	RetTime [min]	Type	Width [min]	Area [mAU*s]	Height [mAU]	Area %
1	4.463	VB	0.0894	917.71234	154.20961	71.4409
2	5.031	BB	0.0996	366.86374	55.15306	28.5591

Figure 4.6.114 Asymmetric HPLC Trace of 4.4a

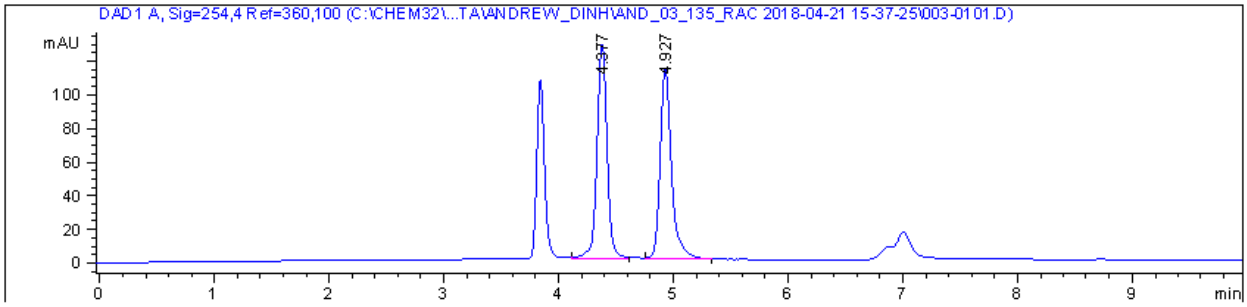

Peak #	RetTime [min]	Type	Width [min]	Area [mAU*s]	Height [mAU]	Area %
1	4.377	VB	0.0942	792.94629	128.21320	50.1479
2	4.927	BB	0.1050	788.26831	113.49321	49.8521

Figure 4.6.115 Racemic Standard of 4.4a

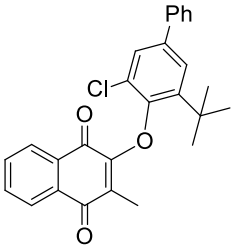

4.5a was measured with HPLC analysis using Chiralpak IA, Hexanes/EtOH (98:2), flow rate =1.0 mL/min, tR = 5.9 min (major), tR = 7.0 min (minor).

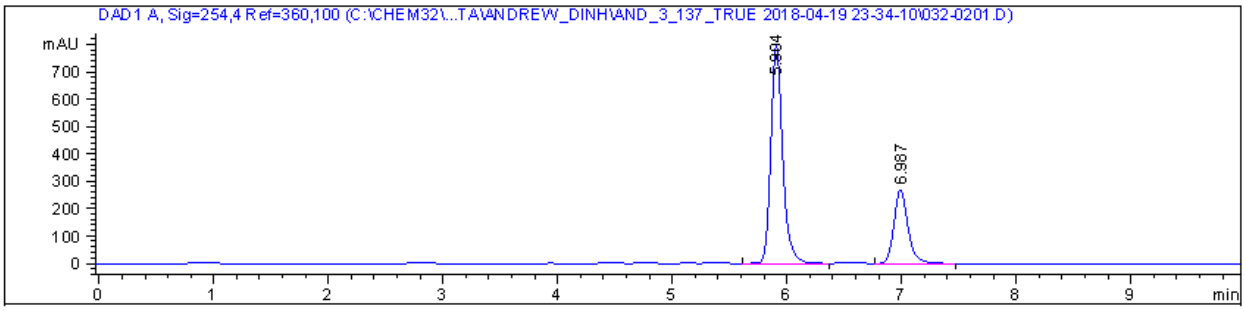

Peak #	RetTime [min]	Type	Width [min]	Area [mAU*s]	Height [mAU]	Area %
1	5.904	VB	0.1100	5756.98926	799.68353	71.4089
2	6.987	VB	0.1312	2305.02124	271.15060	28.5911

Figure 4.6.116 Asymmetric HPLC Trace of 4.5a

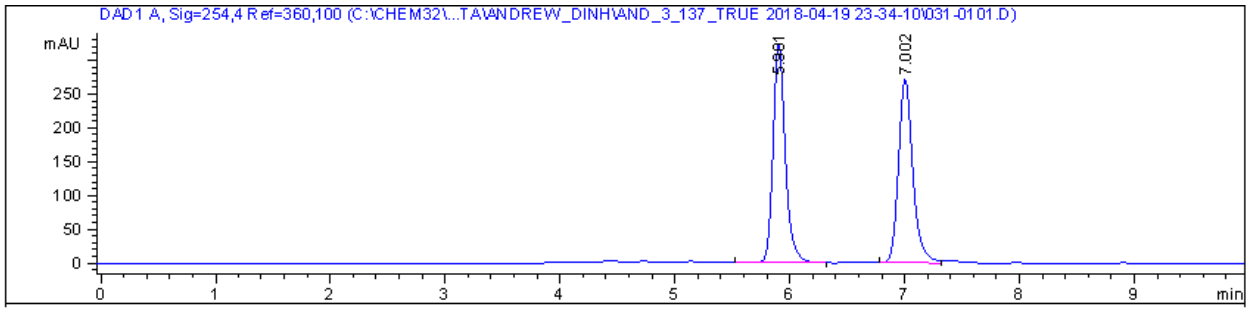

Peak #	RetTime [min]	Type	Width [min]	Area [mAU*s]	Height [mAU]	Area %
1	5.901	VB	0.1130	2410.62524	323.34933	50.4165
2	7.002	VV	0.1318	2370.79150	271.82770	49.5835

Figure 4.6.117 Racemic Standard of 4.5a

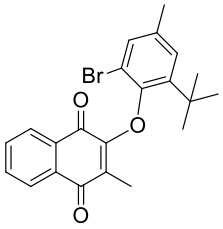

4.6a was measured with HPLC analysis using Chiralpak IA, Hexanes/EtOH (98:2), flow rate =1.0 mL/min, tR = 4.6 min (major), tR = 5.8 min (minor).

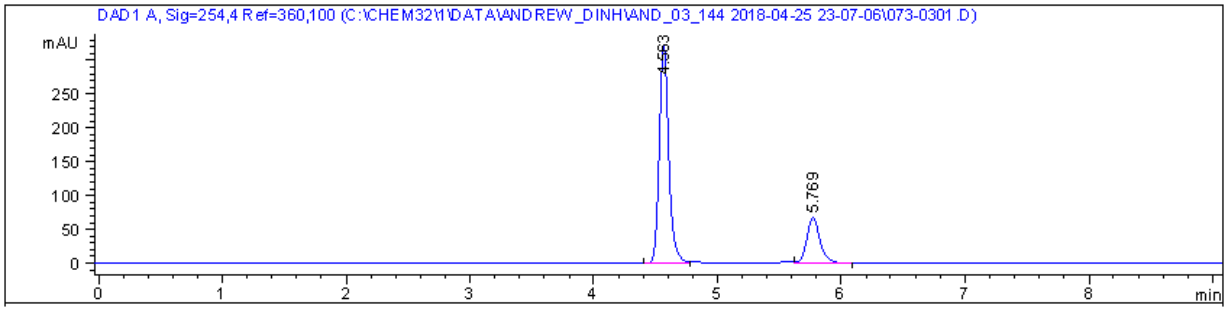

Peak #	RetTime [min]	Type	Width [min]	Area [mAU*s]	Height [mAU]	Area %
1	4.563	BV	0.0800	1719.89160	323.83951	77.3804
2	5.769	VB	0.1129	502.75204	67.49429	22.6196

Figure 4.6.118 Asymmetric HPLC Trace of 4.6a

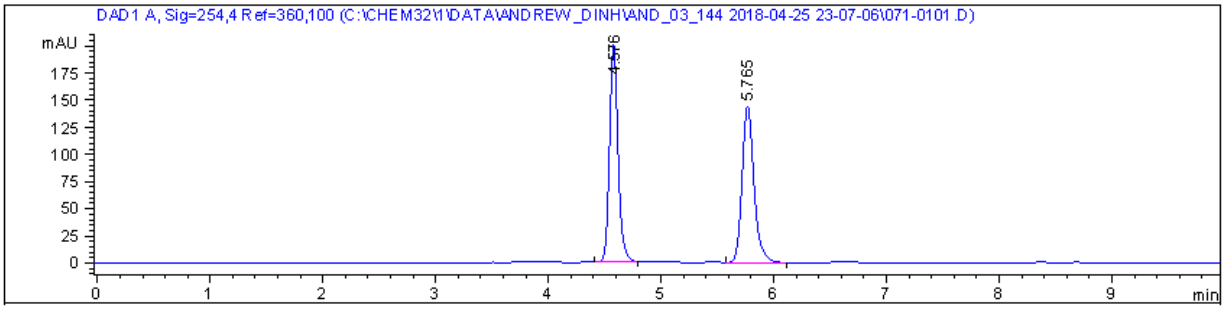

Peak #	RetTime [min]	Type	Width [min]	Area [mAU*s]	Height [mAU]	Area %
1	4.576	VV	0.0802	1074.40698	201.48393	50.0848
2	5.765	VB	0.1121	1070.76819	145.07361	49.9152

Figure 4.6.119 Racemic Standard of 4.6a

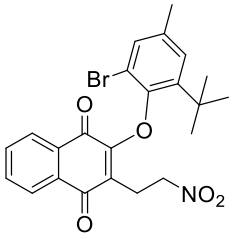

4.6b was measured with HPLC analysis using Chiralpak IA, Hexanes/EtOH (98:2), flow rate =1.0 mL/min, tR = 8.1 min (major), tR = 16.2 min (minor).

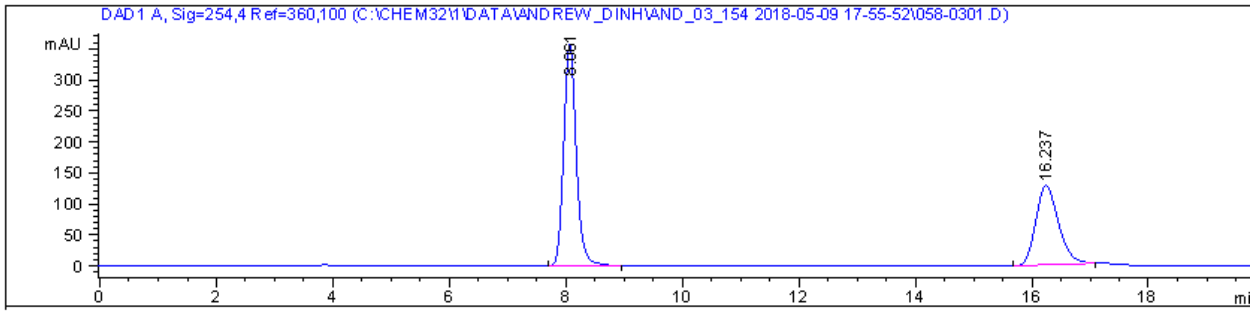

Peak #	RetTime [min]	Type	Width [min]	Area [mAU*s]	Height [mAU]	Area %
1	8.061	BB	0.2295	5367.76660	356.86658	60.7634
2	16.237	BB	0.4208	3466.11353	127.65877	39.2366

Figure 4.6.120 Asymmetric HPLC Trace of 4.6b

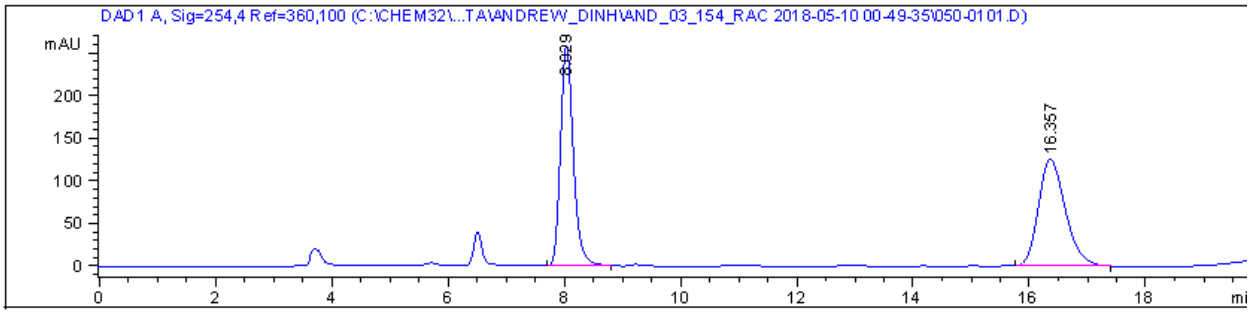

Peak #	RetTime [min]	Type	Width [min]	Area [mAU*s]	Height [mAU]	Area %
1	8.029	BB	0.2355	3981.21558	258.77649	49.5089
2	16.357	BB	0.4944	4060.19482	125.84195	50.4911

Figure 4.6.121 Racemic Standard of 4.6b

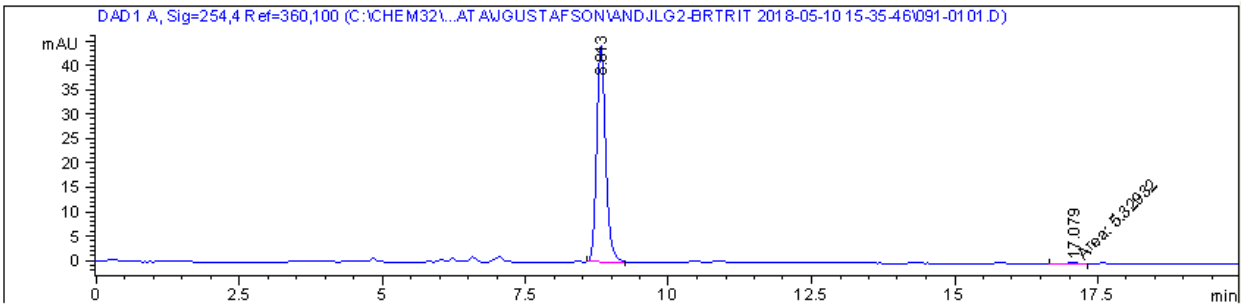

Peak #	RetTime [min]	Type	Width [min]	Area [mAU*s]	Height [mAU]	Area %
1	8.813	BB	0.1683	487.28937	44.32355	98.9182
2	17.079	MF	0.4003	5.32932	2.21900e-1	1.0818

Figure 4.6.122 Trituration of 4.6b

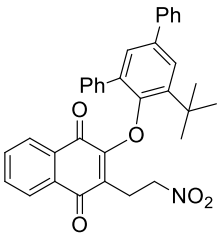

4.7b was measured with HPLC analysis using Chiralpak IA, Hexanes/EtOH (98:2), flow rate =1.0 mL/min, tR = 11.5 min (major), tR = 14.5 min (minor).

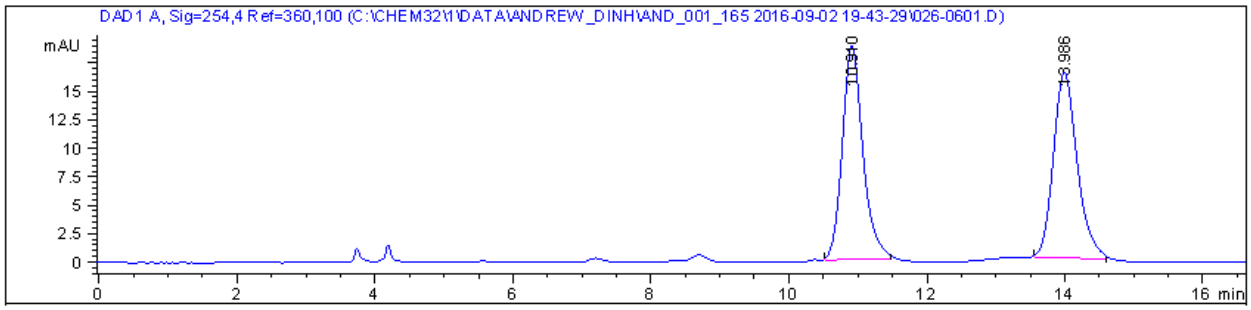

Peak #	RetTime [min]	Type	Width [min]	Area [mAU*s]	Height [mAU]	Area %
1	10.910	BB	0.3126	391.22586	18.81389	49.8337
2	13.986	BB	0.3669	393.83698	16.35851	50.1663

Figure 4.6.123 Asymmetric HPLC Trace of 4.7b

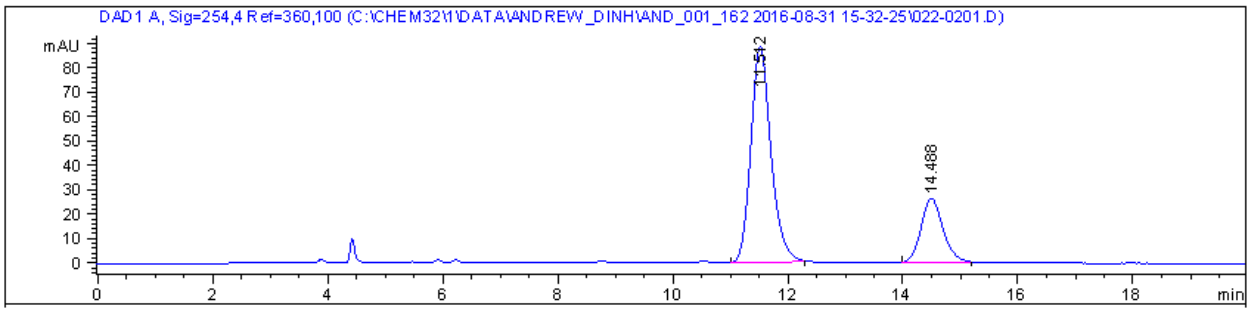

Peak #	RetTime [min]	Type	Width [min]	Area [mAU*s]	Height [mAU]	Area %
1	11.512	BB	0.3700	2155.02759	88.52171	75.3606
2	14.488	BB	0.4075	704.59515	26.39163	24.6394

Figure 4.6.124 Racemic Standard of 4.7b

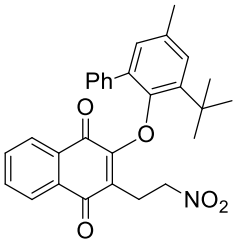

4.8b was measured with HPLC analysis using Chiralpak IA, Hexanes/EtOH (98:2), flow rate =1.0 mL/min, tR = 8.1 min (major), tR = 13.1 min (minor). Impurity in the racemic mixture is residual toluene.

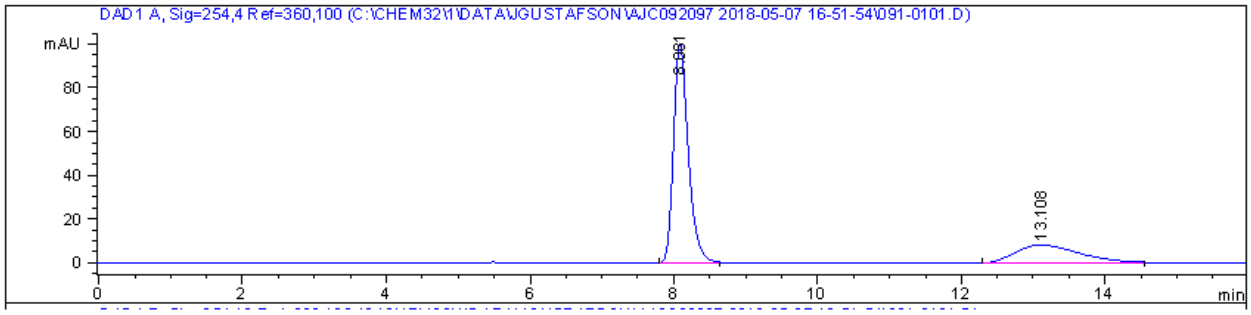

Peak #	RetTime [min]	Type	Width [min]	Area [mAU*s]	Height [mAU]	Area %
1	8.081	BB	0.2167	1431.36230	100.16615	73.8344
2	13.108	BB	0.7365	507.24976	8.21321	26.1656

Figure 4.6.125 Asymmetric HPLC Trace of 4.8b

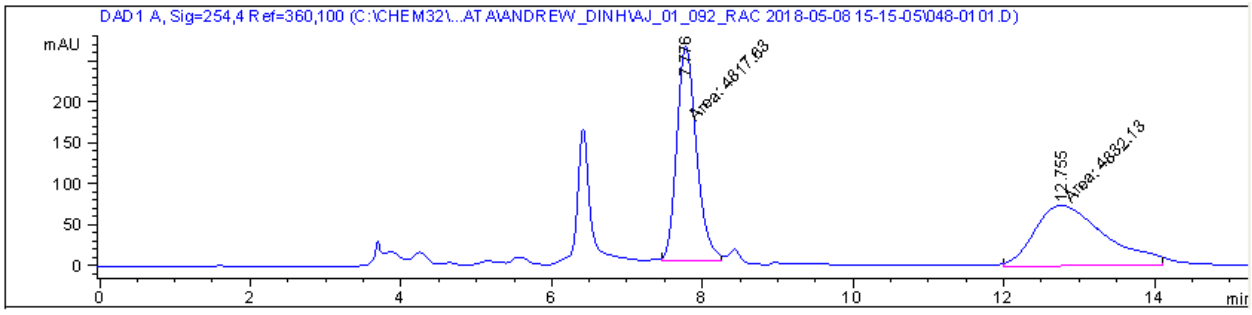

Peak #	RetTime [min]	Type	Width [min]	Area [mAU*s]	Height [mAU]	Area %
1	7.776	MM	0.3057	4817.62549	262.66818	49.9249
2	12.755	MM	1.0916	4832.12500	73.77547	50.0751

Figure 4.6.126 Racemic Standard of 4.8b

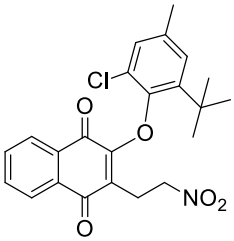

4.9b was measured with HPLC analysis using Chiralpak IA, Hexanes/EtOH (90:10), flow rate =1.0 mL/min, tR = 4.6 min (major), tR = 5.8 min (minor).

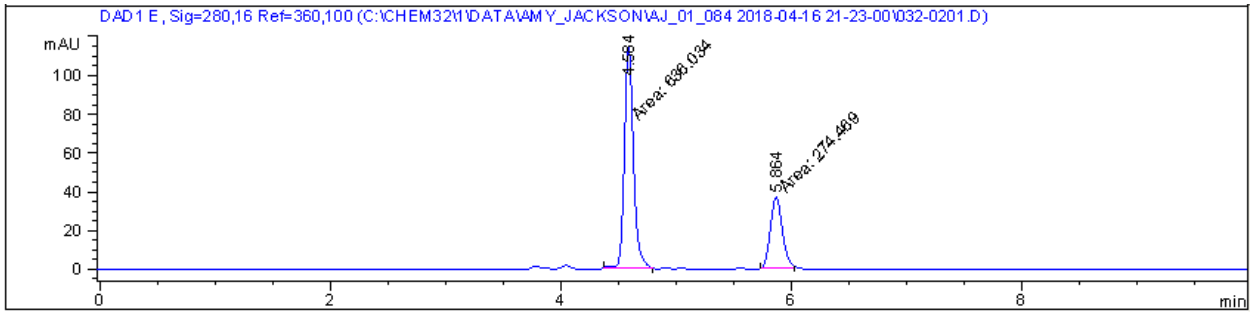

Peak #	RetTime [min]	Type	Width [min]	Area [mAU*s]	Height [mAU]	Area %
1	4.584	VB	0.0840	711.49005	129.65094	69.1417
2	5.864	VB	0.1165	317.54114	41.84821	30.8583

Figure 4.6.127 Asymmetric HPLC Trace of 4.9b

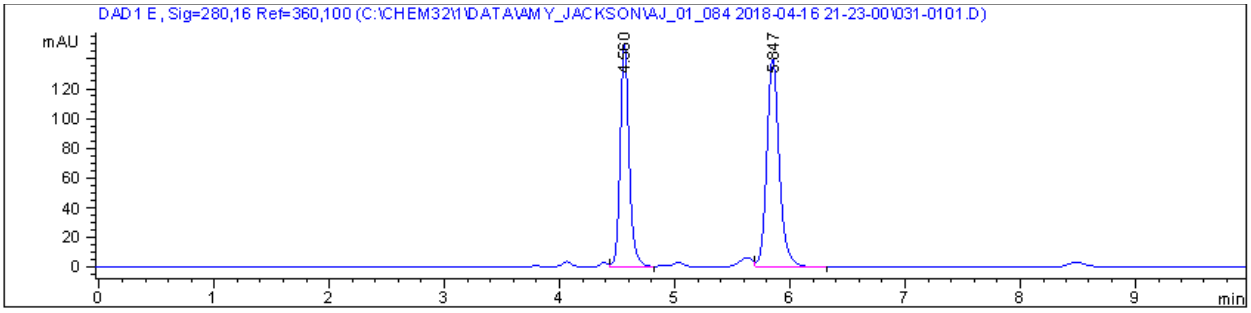

Peak #	RetTime [min]	Type	Width [min]	Area [mAU*s]	Height [mAU]	Area %
1	4.560	VV	0.0833	917.87030	169.09950	43.3285
2	5.847	VB	0.1137	1200.53003	159.73799	56.6715

Figure 4.6.128 Racemic Standard of 4.9b

4.6.7 Racemization Kinetics to Measure the Barrier to Rotation

Enantiomerically enriched atropisomeric analogues post-alkylation were tested for barrier to rotation measurements using the similar procedures from the literature.[4]

Enantiomerically enriched atropisomeric analogue of interest (<50 mg) was dissolved in ~1.5 mL of toluene. The solution was then heated at a constant temperature for a two hour period with 30 minute intervals. At each time point, a 100-200 µL aliquot was isolated and quenched in an HPLC vial with room temperature 100% HPLC hexanes or 2-propanol. Each sample was then injected into the chiral HPLC system. Barrier to rotation measurement is determined from an average of two trials.

The ee% vs. time (s) was plotted to determine the rate constant k_{obs} (i.e. the slope of the pseudo first-order kinetics) at the selected temperature using the following equation:

$$k_{obs} = \frac{\ln\left(\frac{1}{ee\%}\right)}{t}$$

From this, the racemization rate constant k_{rac} was determined using the following equation:

$$k_{rac} = \frac{k_{obs}}{2}$$

The average k_{rac} was determined by taking the average of the k_{rac} of each trial. From this, substitution into the Eyring equation was performed to determine the barrier to rotation:

$$\Delta G = RT \ln\left(\frac{T k_b}{k_{rac} h}\right)$$

in which ΔG is the barrier to rotation measurement, R is the gas constant, T is the constant temperature, k_b is the Boltzmann distribution constant, and h is Planck's constant.

To determine $t_{1/2}$ at 37 °C (physiological temperatures):

$$t_{1/2} = \frac{\left(\frac{k_b T e^{\frac{-\Delta G}{RT}}}{\ln 2}\right)}{\ln 2}$$

in which $t_{1/2}$ is the half-life to racemization in seconds. This unit can be converted into hours, days, or years.

Barrier to Rotation of **4.1a**

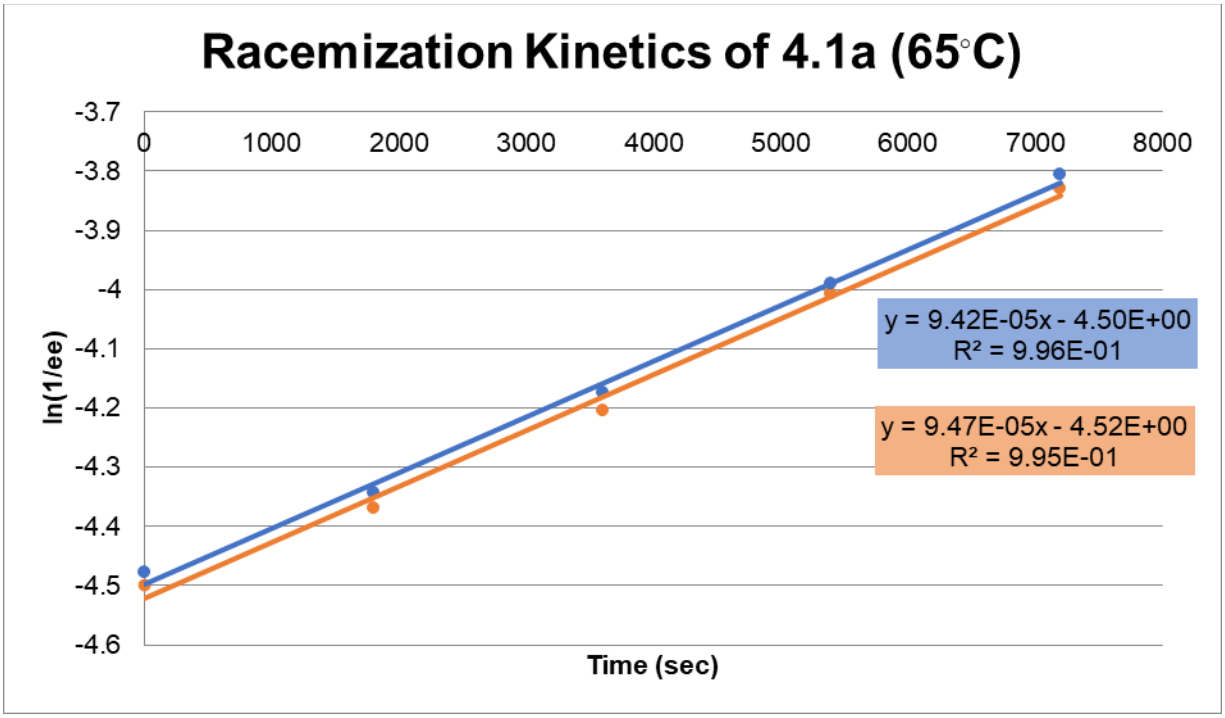

Figure 4.6.129 Barrier to Rotation Measurements of 4.1a

Time (s)	Trial Run 1 (ee%)	Trial 1 [ln(1/ee%)]	Trial Run 2 (ee%)	Trial 2 [ln(1/ee%)]
0	88	-4.477336814	90	-4.49980967
1800	77	-4.343805422	79	-4.369447852
3600	65	-4.17438727	67	-4.204692619
5400	54	-3.988984047	55	-4.007333185
7200	45	-3.80666249	46	-3.828641396

Average K_{obs} = 9.45e^{-05}, Average k_{rac}= 4.72e^{-05}
Average ΔG = 26.6 kcal/mol
Calculated $t_{1/2}$ (25°C) = ~39 days

Barrier to Rotation of **4.7b**

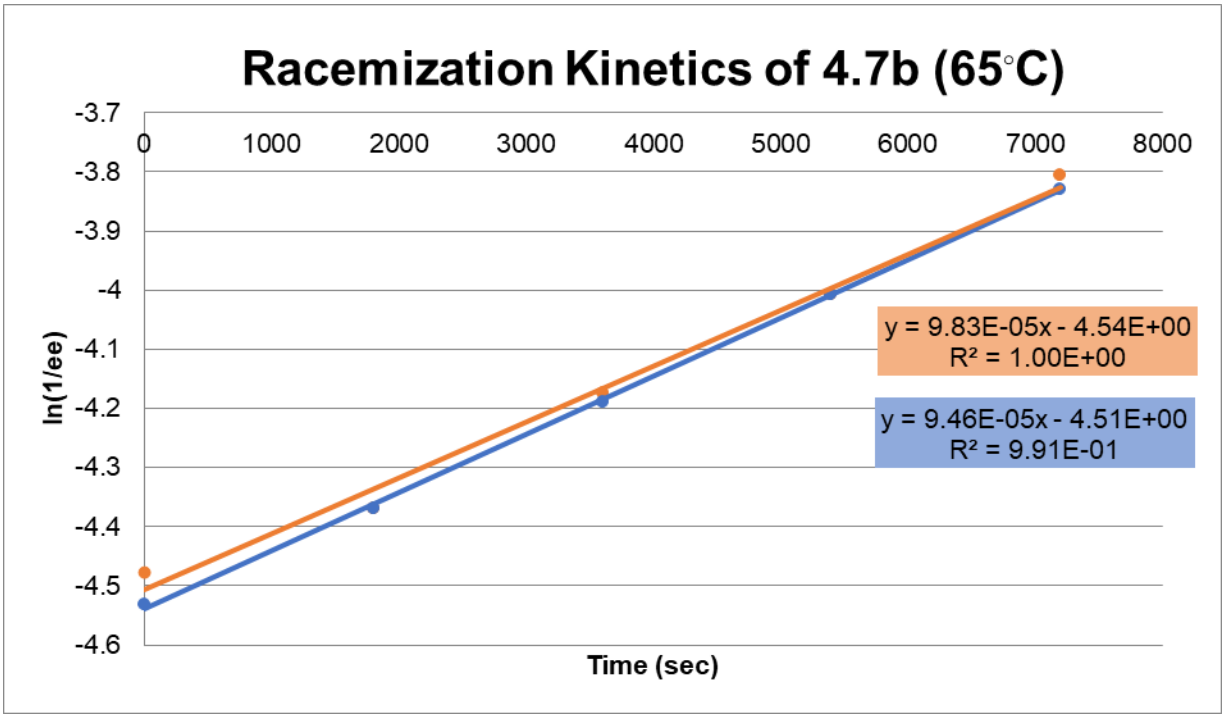

Figure 4.6.130 Barrier to Rotation Measurements of 4.7b

Time (s)	Trial Run 1 (ee%)	Trial 1 [ln(1/ee%)]	Trial Run 2 (ee%)	Trial 2 [ln(1/ee%)]
0	93	-4.532599493	8	-4.477336814
1800	79	-4.369447852	79	-4.369447852
3600	66	-4.189654742	65	-4.17438727
5400	55	-4.007333185	55	-4.007333185
7200	46	-3.828641396	45	-3.80666249

Average K_{obs} = 9.65e^{-05}, Average k_{rac}= 4.82e^{-05}
Average ΔG = 26.6 kcal/mol
Calculated $t_{1/2}$ (25°C) = ~38 days

4.6.8 Computational Geometries/energies and CD Spectra

All geometry optimizations and frequency calculations were performed in Gaussian 09 using density functional theory, B3LYP/6-31(d) in gas phase. Calculated CD spectras were calculated from the four minimized conformations using TD-DFT B3LYP/6-31(d) CPCM (EtOH) n=25. Circular dichroism spectra were collected at 25°C on an Aviv model 420 CD spectrophotometer using a 1 mm cuvette. Study compounds were dissolved in 100% ethanol (500 uM) and spectra collected from 340 to 200 nm at 1 nm intervals using a 1 nm bandwidth and 2 s averaging time. The contour plot was designed using Maestro 11.4 software from Schrödinger. The coordinate Scan function was utilized under the Structure Analysis task. The specific simulation conditions are as follows: MMFF (force field), no solvent, charges from force field and extended cutoff. The dihedral options were selected in the scan option, with angle intervals of 10 degrees and Incorporate = Do not incorporate.

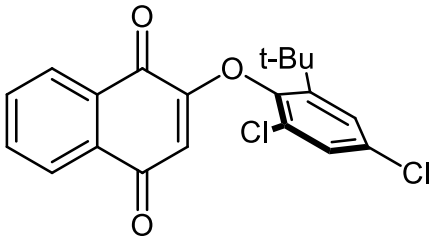

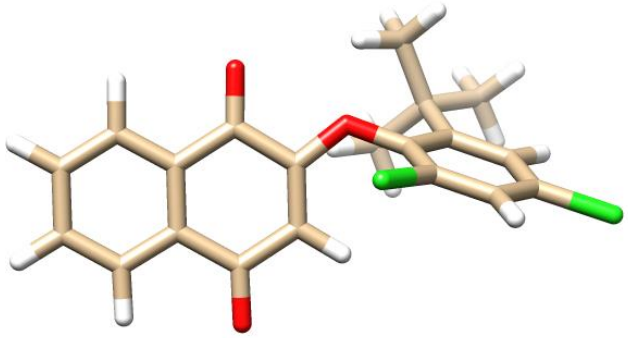

Figure 4.6.131 Computational Energies of 4.1 (S_a)-*exo*

Energy relative to other **4.1** conformations: 0 kcal/mol

Zero-point correction = 0.311977 (Hartree/Particle)
Thermal correction to Energy = 0.334354
Thermal correction to Enthalpy = 0.335299
Thermal correction to Gibbs Free Energy = 0.259564
Sum of electronic and zero-point Energies = -1917.505557
Sum of electronic and thermal Energies = -1917.483179
Sum of electronic and thermal Enthalpies = -1917.482235

Sum of electronic and thermal Free Energies = -1917.557970

Center Number	Atomic Number	Atomic Type	Coordinates (Angstroms) X	Y	Z
1	6	0	5.938052	0.405032	-0.454326
2	6	0	4.692184	0.754023	-0.971382
3	6	0	3.526360	0.266027	-0.371152
4	6	0	3.613432	-0.571516	0.756205
5	6	0	4.865687	-0.914210	1.270637
6	6	0	6.024524	-0.428607	0.665866
7	1	0	6.842931	0.781924	-0.922612
8	1	0	4.599384	1.400845	-1.837742
9	6	0	2.205670	0.651978	-0.934042
10	6	0	2.375324	-1.093295	1.413640
11	1	0	4.906510	-1.559622	2.142024
12	1	0	6.997416	-0.698459	1.067244
13	6	0	1.079216	-0.724750	0.824166
14	6	0	0.992117	0.059007	-0.271597
15	8	0	2.083740	1.418238	-1.877287
16	8	0	2.431595	-1.805654	2.411283
17	8	0	-0.144046	0.455688	-0.896690
18	6	0	-1.390902	0.001211	-0.493430
19	6	0	-2.306370	0.903141	0.093490
20	6	0	-1.768377	-1.314533	-0.801565
21	6	0	-3.571469	0.392353	0.417409
22	6	0	-3.030308	-1.800548	-0.469828
23	6	0	-3.915268	-0.931109	0.152928
24	1	0	-4.313168	1.028679	0.878911
25	1	0	-3.307271	-2.820539	-0.705824
26	6	0	-1.967445	2.392241	0.345433
27	6	0	-3.187852	3.164027	0.890996
28	1	0	-3.519506	2.787085	1.865158
29	1	0	-2.910037	4.214348	1.026858
30	1	0	-4.036871	3.136598	0.198985
31	6	0	-1.545609	3.076868	-0.979666
32	1	0	-0.636851	2.646367	-1.403227
33	1	0	-2.344423	3.000234	-1.726483
34	1	0	-1.363491	4.142054	-0.794149
35	6	0	-0.838991	2.522266	1.396123
36	1	0	-1.125740	2.048929	2.342269
37	1	0	0.098716	2.074558	1.063379
38	1	0	-0.645402	3.582740	1.595545
39	17	0	-5.513832	-1.508551	0.593651
40	17	0	-0.671700	-2.375950	-1.657287
41	1	0	0.201685	-1.133045	1.313597

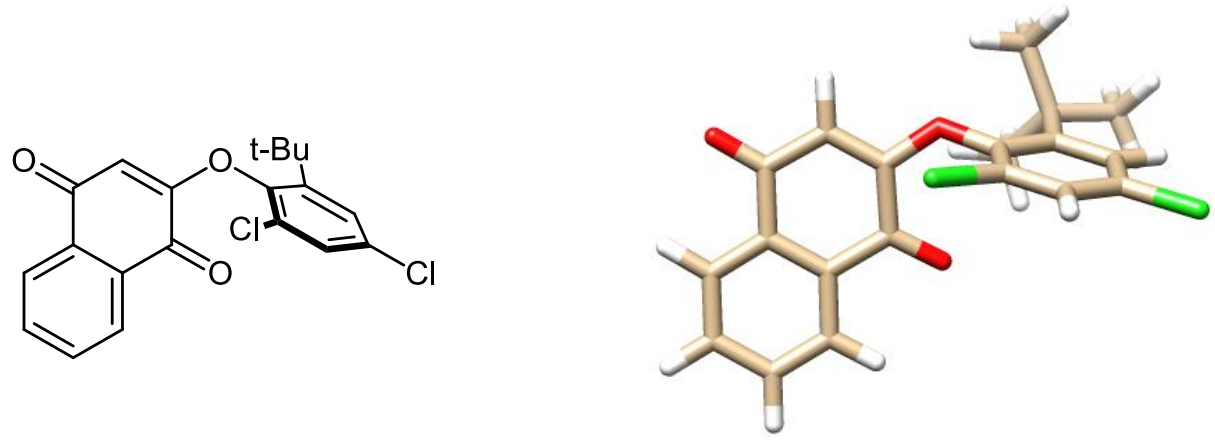

Figure 4.6.132 Computational Energies of 4.1 (S_a)-*endo*

Energy relative to other **4.1** conformations: +1.25 kcal/mol
Zero-point correction = 0.311684 (Hartree/Particle)
Thermal correction to Energy = 0.334105
Thermal correction to Enthalpy = 0.335049
Thermal correction to Gibbs Free Energy = 0.259544
Sum of electronic and zero-point Energies = -1917.503858
Sum of electronic and thermal Energies = -1917.481437
Sum of electronic and thermal Enthalpies = -1917.480493
Sum of electronic and thermal Free Energies = -1917.555998

Center Number	Atomic Number	Atomic Type	Coordinates (Angstroms) X	Y	Z
1	6	0	-4.600183	-1.208736	-2.261116
2	6	0	-3.264326	-0.952386	-2.014050
3	6	0	-2.888823	-0.327502	-0.839437
4	6	0	-3.850931	0.047131	0.086896
5	6	0	-5.185162	-0.205810	-0.162497
6	6	0	-5.560334	-0.835511	-1.335419
7	1	0	-4.890503	-1.695629	-3.170023
8	1	0	-2.507282	-1.230119	-2.717801
9	6	0	-1.453049	-0.058241	-0.609129
10	6	0	-3.465741	0.725883	1.350517
11	1	0	-5.910329	0.093861	0.565355
12	1	0	-6.595631	-1.033331	-1.527057
13	6	0	-2.025405	0.934069	1.571447
14	6	0	-1.109779	0.567529	0.697921
15	8	0	-0.598898	-0.309319	-1.433439
16	8	0	-4.292869	1.080250	2.166841
17	8	0	0.211863	0.853214	0.966360
18	6	0	1.329506	0.132839	0.563205
19	6	0	2.364379	0.809361	-0.088754
20	6	0	1.465702	-1.199275	0.877095
21	6	0	3.492389	0.072957	-0.419710

22	6	0	2.583812	-1.923228	0.542314
23	6	0	3.583666	-1.262592	-0.112388
24	1	0	4.309818	0.533934	-0.923480
25	1	0	2.661988	-2.958034	0.793007
26	6	0	2.277263	2.314243	-0.405613
27	6	0	3.532276	2.807770	-1.158812
28	1	0	3.649629	2.306914	-2.113347
29	1	0	3.419902	3.868080	-1.350959
30	1	0	4.433247	2.673527	-0.571345
31	6	0	2.181885	3.110883	0.916949
32	1	0	1.312276	2.815268	1.481931
33	1	0	3.067736	2.943450	1.519717
34	1	0	2.114210	4.171236	0.696759
35	6	0	1.055495	2.609986	-1.306453
36	1	0	1.070840	1.980383	-2.187495
37	1	0	0.131455	2.444500	-0.779581
38	1	0	1.085854	3.648289	-1.618305
39	17	0	5.081715	-2.171044	-0.578195
40	17	0	0.156322	-2.058702	1.781453
41	1	0	-1.736442	1.393973	2.491348

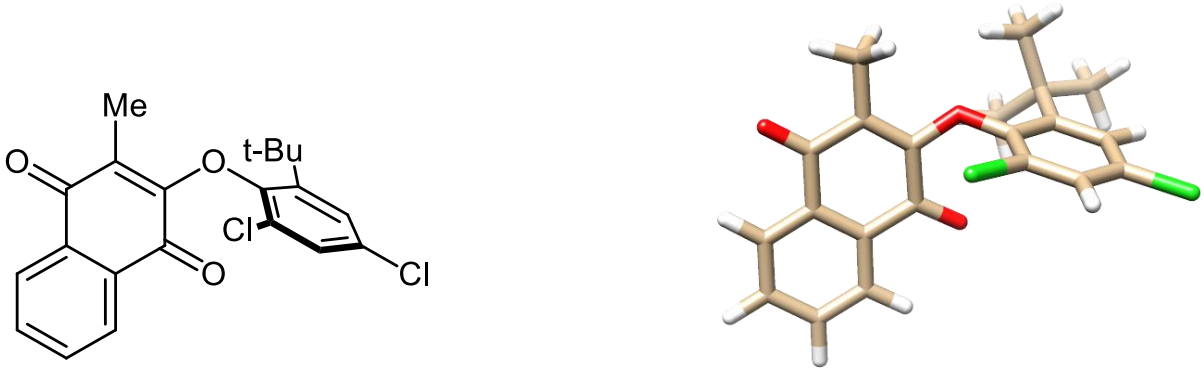

Figure 4.6.133 Computational Energies of 4.1a (R_a)-*endo*

Energy relative to other **4.1a** conformations: 0 kcal/mol

Number of imaginary frequencies: 0

Zero-point correction = 0.339493 (Hartree/Particle)
Thermal correction to Energy = 0.363694
Thermal correction to Enthalpy = 0.364638
Thermal correction to Gibbs Free Energy = 0.285118
Sum of electronic and zero-point Energies = -1956.797125
Sum of electronic and thermal Energies = -1956.772925
Sum of electronic and thermal Enthalpies = -1956.771980
Sum of electronic and thermal Free Energies = -1956.851501

Center Number	Atomic Number	Atomic Type	Coordinates (Angstroms) X	Y	Z

1	6	0	-4.410178	-1.982690	-2.106276
2	6	0	-3.078161	-1.641877	-1.878201
3	6	0	-2.759150	-0.707650	-0.887716
4	6	0	-3.778283	-0.109170	-0.128733
5	6	0	-5.111600	-0.451745	-0.365662
6	6	0	-5.425802	-1.387463	-1.350768
7	1	0	-4.658530	-2.710770	-2.873320
8	1	0	-2.272952	-2.085758	-2.454311
9	6	0	-1.336706	-0.338380	-0.666070
10	6	0	-3.449254	0.891053	0.930204
11	1	0	-5.882136	0.025097	0.230981
12	1	0	-6.463528	-1.653371	-1.531849
13	6	0	-2.021375	1.210410	1.187842
14	6	0	-1.050615	0.602038	0.459888
15	8	0	-0.435926	-0.761149	-1.380052
16	8	0	-4.339810	1.426217	1.584059
17	8	0	0.239982	0.989318	0.696124
18	6	0	1.355133	0.199729	0.454368
19	6	0	2.398230	0.721302	-0.342120
20	6	0	1.507027	-1.026106	1.115796
21	6	0	3.543088	-0.073152	-0.484932
22	6	0	2.649799	-1.803878	0.956910
23	6	0	3.657943	-1.311646	0.141076
24	1	0	4.367931	0.266270	-1.095193
25	1	0	2.743541	-2.754957	1.466210
26	6	0	2.318006	2.114915	-1.009164
27	6	0	3.568813	2.406087	-1.865942
28	1	0	3.683903	1.688630	-2.686421
29	1	0	3.469640	3.401432	-2.311698
30	1	0	4.489691	2.406726	-1.272344
31	6	0	2.243741	3.207124	0.086599
32	1	0	1.362693	3.088341	0.720623
33	1	0	3.133505	3.178562	0.726170
34	1	0	2.197079	4.198254	-0.380690
35	6	0	1.091665	2.219869	-1.947651
36	1	0	1.084616	1.406277	-2.679956
37	1	0	0.148023	2.193592	-1.401575
38	1	0	1.132224	3.170721	-2.492186
39	17	0	5.118498	-2.262562	-0.088640
40	17	0	0.253591	-1.620908	2.191581
41	6	0	-1.701051	2.196409	2.274285
42	1	0	-0.958053	1.784497	2.965560
43	1	0	-1.274292	3.117005	1.856856
44	1	0	-2.610467	2.452274	2.819706

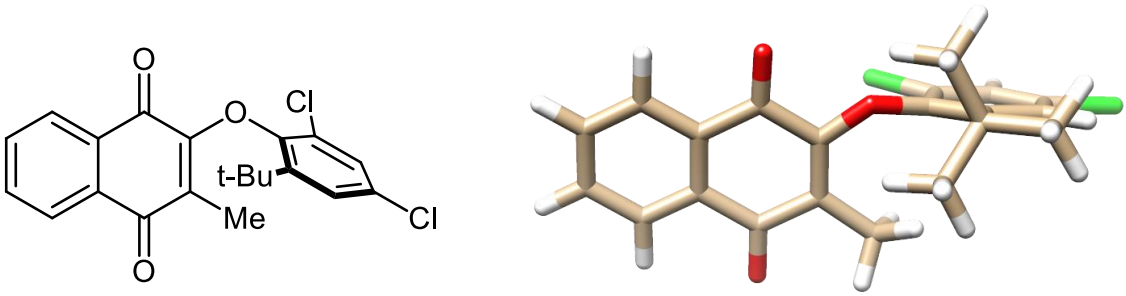

Figure 4.6.134 Computational Energies of 4.1a (R_a)-*exo*

Energy relative to **4.1a** conformations: +3.39 kcal/mol

Number of imaginary frequencies: 0

Zero-point correction = 0.339947 (Hartree/Particle)
Thermal correction to Energy = 0.363938
Thermal correction to Enthalpy = 0.364882
Thermal correction to Gibbs Free Energy = 0.286063
Sum of electronic and zero-point Energies = -1956.791273
Sum of electronic and thermal Energies = -1956.767282
Sum of electronic and thermal Enthalpies = -1956.766337
Sum of electronic and thermal Free Energies = -1956.845156

Center Number	Atomic Number	Atomic Type	Coordinates (Angstroms) X	Y	Z
1	6	0	-5.893374	0.427835	-0.997553
2	6	0	-4.592959	0.802019	-1.329524
3	6	0	-3.523980	0.379919	-0.532562
4	6	0	-3.759388	-0.412265	0.601360
5	6	0	-5.066452	-0.781228	0.931457
6	6	0	-6.129397	-0.363873	0.131908
7	1	0	-6.724638	0.751342	-1.617700
8	1	0	-4.383043	1.416056	-2.199142
9	6	0	-2.139619	0.773050	-0.893065
10	6	0	-2.627562	-0.850908	1.468636
11	1	0	-5.225448	-1.391143	1.814443
12	1	0	-7.144516	-0.654021	0.388340
13	6	0	-1.230744	-0.470301	1.103922
14	6	0	-1.024201	0.240323	-0.035055
15	8	0	-1.893149	1.500341	-1.843592
16	8	0	-2.841508	-1.514606	2.478891
17	8	0	0.166605	0.675788	-0.540276
18	6	0	1.393293	0.069710	-0.376454
19	6	0	2.477520	0.865726	0.062680
20	6	0	1.598560	-1.257599	-0.781520
21	6	0	3.724516	0.237095	0.168112
22	6	0	2.847407	-1.864273	-0.663939

23	6	0	3.897204	-1.103512	-0.170572
24	1	0	4.585981	0.790421	0.514752
25	1	0	2.987340	-2.894501	-0.967302
26	6	0	2.317182	2.372941	0.374448
27	6	0	3.658304	3.008406	0.797590
28	1	0	4.419311	2.930125	0.013289
29	1	0	3.499483	4.074246	0.991958
30	1	0	4.058588	2.564609	1.716543
31	6	0	1.320339	2.597677	1.536832
32	1	0	0.312834	2.253792	1.297317
33	1	0	1.655092	2.086572	2.447318
34	1	0	1.258304	3.668891	1.761830
35	6	0	1.831590	3.118866	-0.895005
36	1	0	2.552415	2.998755	-1.712092
37	1	0	0.859009	2.764163	-1.240951
38	1	0	1.747792	4.190586	-0.678092
39	17	0	5.483595	-1.838740	0.000090
40	17	0	0.300216	-2.190915	-1.498917
41	6	0	-0.166276	-0.961116	2.048167
42	1	0	0.218515	-1.940343	1.736053
43	1	0	0.679007	-0.275657	2.116411
44	1	0	-0.608167	-1.092904	3.037716

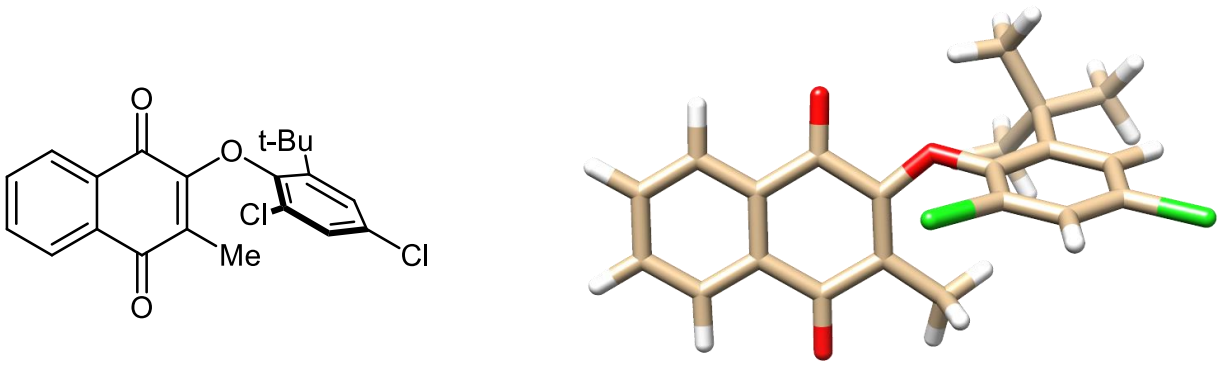

Figure 4.6.135 Computational Energies of 4.1a (S_a)-*exo*

Energy relative to **4.1a** conformations: +3.39 kcal/mol

Number of imaginary frequencies: 0

Zero-point correction = 0.339947 (Hartree/Particle)
Thermal correction to Energy = 0.363938
Thermal correction to Enthalpy = 0.364882
Thermal correction to Gibbs Free Energy = 0.286063
Sum of electronic and zero-point Energies = -1956.791273
Sum of electronic and thermal Energies = -1956.767282
Sum of electronic and thermal Enthalpies = -1956.766337
Sum of electronic and thermal Free Energies = -1956.845156

Center Number	Atomic Number	Atomic Type	Coordinates (Angstroms) X	Y	Z
1	6	0	5.893374	0.427835	-0.997553
2	6	0	4.592959	0.802019	-1.329524
3	6	0	3.523980	0.379919	-0.532562
4	6	0	3.759388	-0.412265	0.601360
5	6	0	5.066452	-0.781228	0.931457
6	6	0	6.129397	-0.363873	0.131908
7	1	0	6.724638	0.751342	-1.617700
8	1	0	4.383043	1.416056	-2.199142
9	6	0	2.139619	0.773050	-0.893065
10	6	0	2.627562	-0.850908	1.468636
11	1	0	5.225448	-1.391144	1.814443
12	1	0	7.144516	-0.654021	0.388340
13	6	0	1.230744	-0.470301	1.103922
14	6	0	1.024201	0.240323	-0.035055
15	8	0	1.893149	1.500341	-1.843592
16	8	0	2.841507	-1.514606	2.478891
17	8	0	-0.166605	0.675788	-0.540276
18	6	0	-1.393293	0.069710	-0.376454
19	6	0	-2.477520	0.865726	0.062680
20	6	0	-1.598560	-1.257599	-0.781520
21	6	0	-3.724516	0.237095	0.168112
22	6	0	-2.847407	-1.864273	-0.663940
23	6	0	-3.897204	-1.103512	-0.170572
24	1	0	-4.585981	0.790420	0.514752
25	1	0	-2.987340	-2.894501	-0.967302
26	6	0	-2.317182	2.372941	0.374448
27	6	0	-3.658304	3.008406	0.797590
28	1	0	-4.058588	2.564609	1.716543
29	1	0	-3.499483	4.074245	0.991959
30	1	0	-4.419311	2.930125	0.013289
31	6	0	-1.831590	3.118866	-0.895005
32	1	0	-0.859010	2.764163	-1.240951
33	1	0	-2.552415	2.998756	-1.712092
34	1	0	-1.747792	4.190586	-0.678092
35	6	0	-1.320340	2.597677	1.536832
36	1	0	-1.655092	2.086572	2.447318
37	1	0	-0.312834	2.253792	1.297317
38	1	0	-1.258304	3.668891	1.761830
39	17	0	-5.483595	-1.838740	0.000090
40	17	0	-0.300216	-2.190915	-1.498917
41	6	0	0.166276	-0.961115	2.048167
42	1	0	-0.679008	-0.275657	2.116411
43	1	0	-0.218515	-1.940343	1.736054
44	1	0	0.608167	-1.092903	3.037716

2a (S_a)-*endo*:

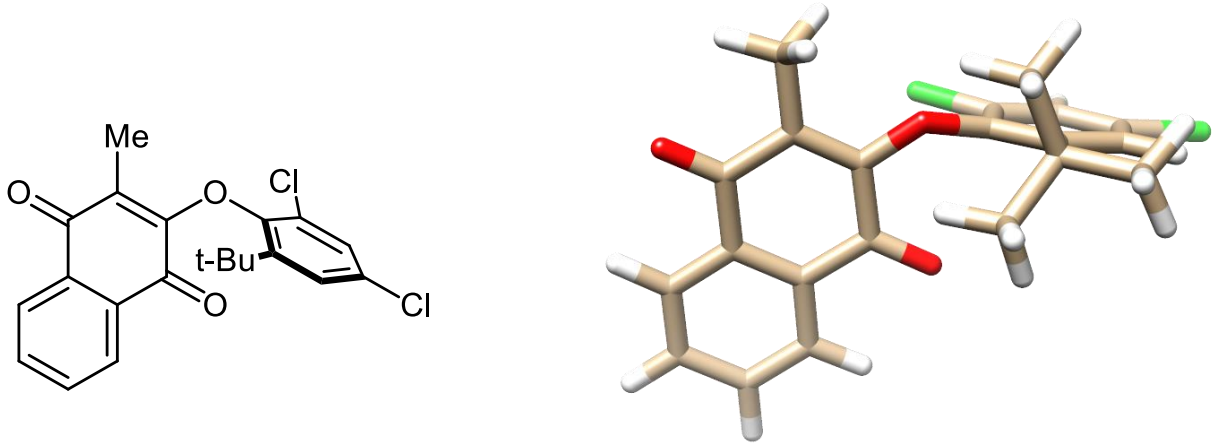

Figure 4.6.136 Computational Energies of 4.1a (S_a)-*endo*

Energy relative to **4.1a** conformations: 0 kcal/mol

Number of imaginary frequencies: 0

Zero-point correction = 0.339493 (Hartree/Particle)
Thermal correction to Energy = 0.363694
Thermal correction to Enthalpy = 0.364638
Thermal correction to Gibbs Free Energy = 0.285118
Sum of electronic and zero-point Energies = -1956.797126
Sum of electronic and thermal Energies = -1956.772925
Sum of electronic and thermal Enthalpies = -1956.771981
Sum of electronic and thermal Free Energies = -1956.851501

Center Number	Atomic Number	Atomic Type	Coordinates (Angstroms) X	Y	Z
1	6	0	4.410309	-1.982201	-2.106715
2	6	0	3.078270	-1.641536	-1.878512
3	6	0	2.759224	-0.707555	-0.887798
4	6	0	3.778343	-0.109183	-0.128703
5	6	0	5.111683	-0.451608	-0.365760
6	6	0	5.425920	-1.387074	-1.351101
7	1	0	4.658693	-2.710080	-2.873938
8	1	0	2.273071	-2.085346	-2.454690
9	6	0	1.336752	-0.338439	-0.666018
10	6	0	3.449266	0.890767	0.930473
11	1	0	5.882205	0.025144	0.230972
12	1	0	6.463658	-1.652864	-1.532285
13	6	0	2.021374	1.209991	1.188203
14	6	0	1.050636	0.601856	0.460025
15	8	0	0.435973	-0.761291	-1.379968
16	8	0	4.339799	1.425842	1.584447
17	8	0	-0.239958	0.989120	0.696322

18	6	0	-1.355199	0.199669	0.454387
19	6	0	-2.398180	0.721380	-0.342145
20	6	0	-1.507218	-1.026187	1.115768
21	6	0	-3.543095	-0.072966	-0.485063
22	6	0	-2.650058	-1.803815	0.956765
23	6	0	-3.658123	-1.311491	0.140885
24	1	0	-4.367872	0.266576	-1.095353
25	1	0	-2.743920	-2.754916	1.466024
26	6	0	-2.317799	2.115034	-1.009123
27	6	0	-3.568532	2.406375	-1.865968
28	1	0	-4.489440	2.407075	-1.272421
29	1	0	-3.469229	3.401733	-2.311660
30	1	0	-3.683647	1.688977	-2.686492
31	6	0	-1.091404	2.219938	-1.947542
32	1	0	-0.147797	2.193541	-1.401422
33	1	0	-1.084402	1.406398	-2.679904
34	1	0	-1.131852	3.170833	-2.492009
35	6	0	-2.243495	3.207178	0.086708
36	1	0	-3.133304	3.178664	0.726213
37	1	0	-1.362503	3.088263	0.720784
38	1	0	-2.196700	4.198325	-0.380523
39	17	0	-5.118736	-2.262271	-0.088957
40	17	0	-0.253865	-1.621153	2.191553
41	6	0	1.701010	2.195707	2.274897
42	1	0	1.274222	3.116396	1.857709
43	1	0	0.958011	1.783600	2.966056
44	1	0	2.610393	2.451468	2.820416

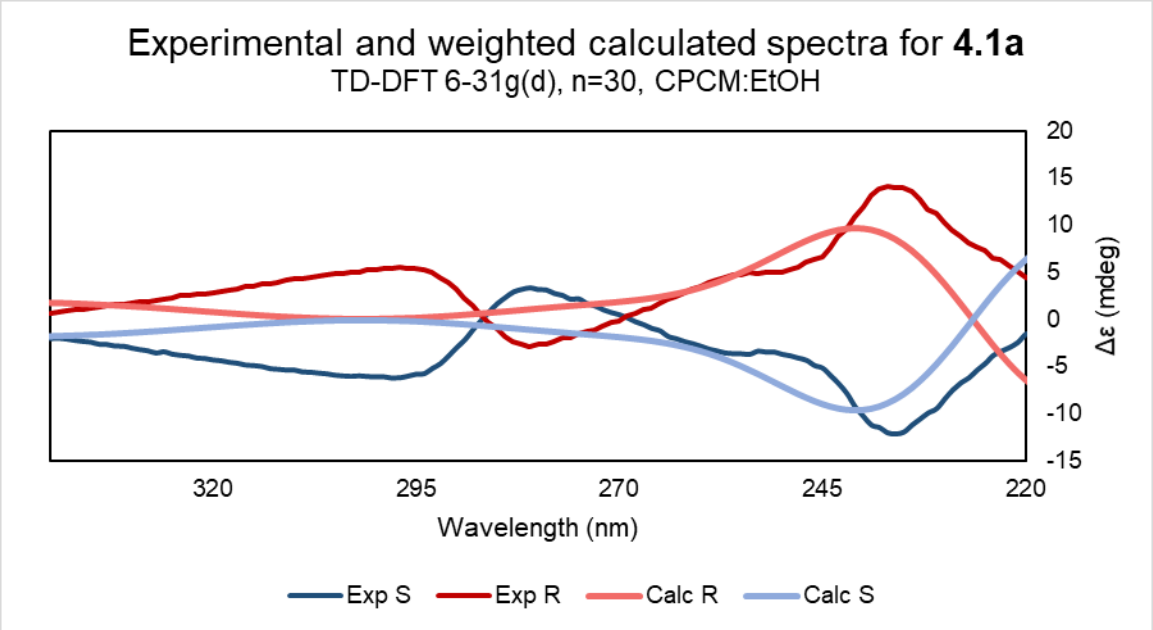

Figure 4.6.137 Experimental and Calculated Spectra for 4.1a

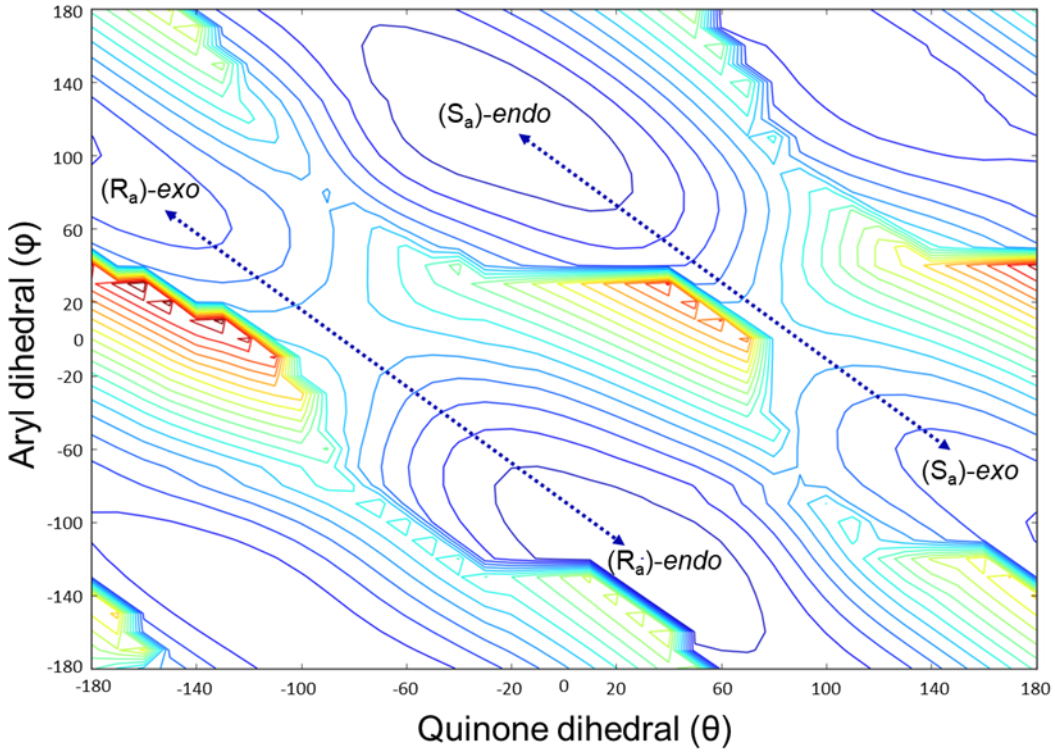

Figure 4.6.138 MMFF Contour Plot of Various (*Sa*)-4.1a conformations Labeled with Circled Shaded According to their Relative DFT-calculated Energies

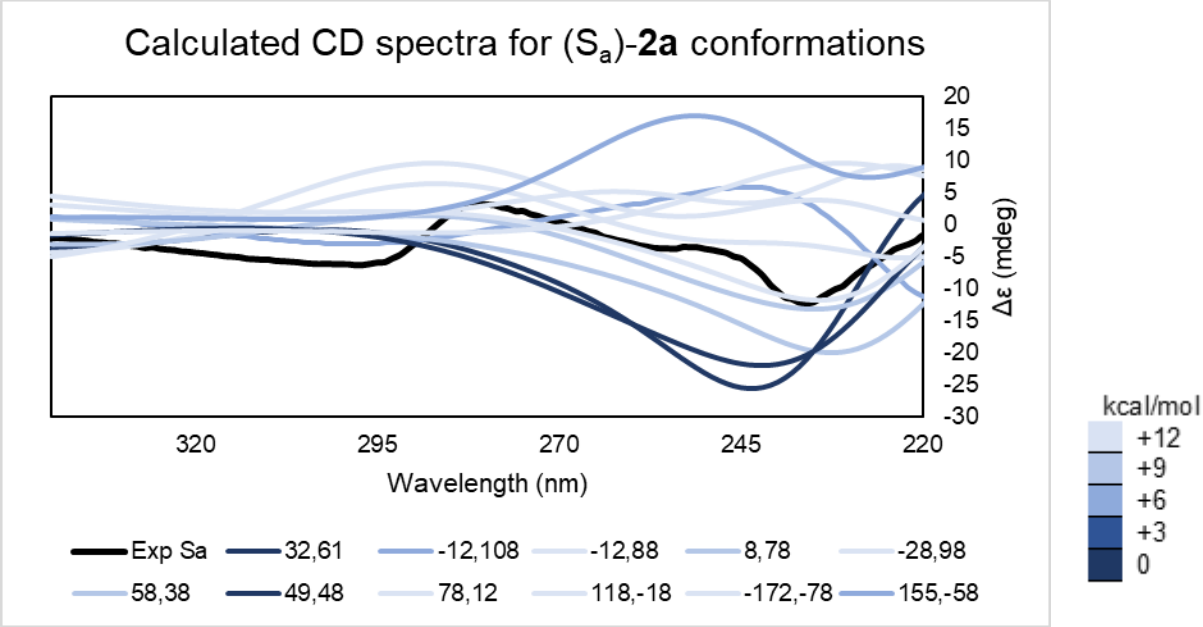

Figure 4.6.139 Energies for Multiple Conformations of (*Sa*)-4.1a and Weighted to Obtain the Predicted (Sa)-4.1a CD Spectra in Figure 4.6.137

Gaussian 09, Revision D.01. M. J. Frisch, G. W. Trucks, H. B. Schlegel, G. E. Scuseria, M. A. Robb, J. R. Cheeseman, G. Scalmani, V. Barone, B. Mennucci, G. A. Petersson, H. Nakatsuji, M. Caricato, X. Li, H. P. Hratchian, A. F. Izmaylov, J. Bloino, G. Zheng, J. L. Sonnenberg, M. Hada, M. Ehara, K. Toyota, R. Fukuda, J. Hasegawa, M. Ishida, T. Nakajima, Y. Honda, O. Kitao, H. Nakai, T. Vreven, J. A. Montgomery, Jr., J. E. Peralta, F. Ogliaro, M. Bearpark, J. J. Heyd, E. Brothers, K. N. Kudin, V. N. Staroverov, T. Keith, R. Kobayashi, J. Normand, K. Raghavachari, A. Rendell, J. C. Burant, S. S. Iyengar, J. Tomasi, M. Cossi, N. Rega, J. M. Millam, M. Klene, J. E. Knox, J. B. Cross, V. Bakken, C. Adamo, J. Jaramillo, R. Gomperts, R. E. Stratmann, O. Yazyev, A. J. Austin, R. Cammi, C. Pomelli, J. W. Ochterski, R. L. Martin, K. Morokuma, V. G. Zakrzewski, G. A. Voth, P. Salvador, J. J. Dannenberg, S. Dapprich, A. D. Daniels, O. Farkas, J. B. Foresman, J. V. Ortiz, J. Cioslowski, and D. J. Fox, Gaussian, Inc., Wallingford CT, 2013.

4.7 Acknowledgements

The contents in Chapter 4 are in part a reformatted reprint of the following manuscript, with permission from the Thieme Connect: Dinh, A.; Noorbehesht, R.; Toenjes, S.; Jackson, A.; Saputra, M.; Maddox, S.; Gustafson, J. "Toward a Catalytic Atroposelective Synthesis of Diaryl Ethers Through C(sp^2)-H Alkylation with Nitroalkanes" *Synlett* **2018**, *29*, 2155-2160. I provided work for optimization, substrate scope evaluation, stereoinductive characterization of molecules and mechanistic studies of the reaction. Ryan Noorbehesht assisted in optimization of the reaction. Sean Toenjes provided *in silico* data to predict relative energy values of conformational states of the synthesized product and elucidated possible stereoinductive mechanisms. Amy Jackson and Mirza Saputra assisted in substrate scope evaluation. Sean Maddox's previous manuscripts were inspiration for the project described in this chapter and deserves authorship. The dissertation author was the primary researcher for the data presented. Support of this work by the National Institute of Health is acknowledged (1R35GM124637).

References

(1) Cernak, T.; Dykstra, K. D.; Tyagarajan, S.; Vachal, P.; Krska, S. W. The Medicinal Chemist's Toolbox for Late Stage Functionalization of Drug-like Molecules. *Chem. Soc. Rev.* **2016**, *45* (3), 546–576.

(2) He, J.; Wasa, M.; Chan, K. S. L.; Shao, Q.; Yu, J. Q. Palladium-Catalyzed Transformations of Alkyl C-H Bonds. *Chem. Rev.* **2017**, *117* (13), 8754–8786.

(3) Qin, Y.; Zhu, L.; Luo, S. Organocatalysis in Inert C-H Bond Functionalization. *Chem. Rev.* **2017**, *117* (13), 9433–9520.

(4) Gutekunst, W. R.; Baran, P. S. C-H Functionalisation in Organic Synthesis. *Chem. Soc. Rev.* **2011**, *40* (4), 1845–2040.

(5) Engle, K. M.; Mei, T.; Wasa, M.; Yu, J. Weak Coordination as a Powerful Means for Developing Broadly Useful C-H Functionalization Reactions. *Acc. Chem. Res.* **2012**, *45* (6), 788–802.

(6) Brown, Dean G, B. Analysis of Past and Present Synthetic Methodologies on Medicinal Chemistry: Where Have All the New Reactions Gone? *J. Med. Chem* **2016**, *59* (10), 4443–4458.

(7) Wencel-Delord, J.; Glorius, F. C-H Bond Activation Enables the Rapid Construction and Late-Stage Diversification of Functional Molecules. *Nat. Chem.* **2013**, *5* (5), 369–375.

(8) Abid Masood, M.; Farrant, E.; Morao, I.; Bazin, M.; Perez, M.; Bunnage, M. E.; Fancy, S. A.; Peakman, T. Lead Diversification. Application to Existing Drug Molecules: Mifepristone 1 and Antalarmin 8. *Bioorganic Med. Chem. Lett.* **2012**, *22* (1), 723–728.

(9) Blakemore, D. C.; Castro, L.; Churcher, I.; Rees, D. C.; Thomas, A. W.; Wilson, D. M.; Wood, A. To Transform Drug Discovery. *Nat. Chem.* **2018**, *10*, 383–394.

(10) Zaldini Hernandes, M.; Melo Cavalcanti, S. T.; Rodrigo Moreira, D. M.; Filgueira de Azevedo Junior, W.; Cristina Lima Leite, A. Halogen Atoms in the Modern Medicinal Chemistry: Hints for the Drug Design. *Curr. Drug Targets* **2010**, *11* (3), 303–314.

(11) Auffinger, P.; Hays, F. A.; Westhof, E.; Ho, P. S. Halogen Bonds in Biological Molecules. *Proc. Natl. Acad. Sci. U. S. A.* **2004**, *101* (48), 16789–16794.

(12) Andrea, V.; P., H. The Role of Halogen Bonding in Inhibitor Recognition and Binding by Protein Kinases. *Curr. Top. Med. Chem.* **2007**, *7* (14), 1336–1348.

(13) Jiang, S.; Zhang, L.; Cui, D.; Yao, Z.; Gao, B.; Lin, J.; Wei, D. The Important Role of Halogen Bond in Substrate Selectivity of Enzymatic Catalysis. *Sci. Rep.* **2016**, *6* (February), 1–7.

(14) McGrath, N. A.; Brichacek, M.; Njardarson, J. T. A Graphical Journey of Innovative Organic Architectures That Have Improved Our Lives. *J. Chem. Educ.* **2010**, *87* (12), 1348–1349.

(15) Biffis, A.; Centomo, P.; Del Zotto, A.; Zecca, M. Pd Metal Catalysts for Cross-Couplings and Related Reactions in the 21st Century: A Critical Review. *Chem. Rev.* **2018**, *118* (4), 2249–2295.

(16) Zou, Y.; Melvin, J. E.; Gonzales, S. S.; Spafford, M. J.; Smith, A. B. Total Synthesis of (-)-Nodulisporic Acid D. *J. Am. Chem. Soc.* **2015**, *137* (22), 7095–7098.

(17) Jang, Y. J.; Yoon, H.; Lautens, M. Rh-Catalyzed Domino Addition-Enolate Arylation: Generation of 3-Substituted Oxindoles via a Rh(III) Intermediate. *Org. Lett.* **2015**, *17* (15), 3895–3897.

(18) Fritch, P. C.; McNaughton-Smith, G.; Amato, G. S.; Burns, J. F.; Eargle, C. W.; Roeloffs, R.; Harrison, W.; Jones, L.; Wickenden, A. D. Novel KCNQ2/Q3 Agonists as Potential Therapeutics for Epilepsy and Neuropathic Pain. *J. Med. Chem.* **2010**, *53* (2), 887–896.

(19) Tsvelikhovsky, D.; Buchwald, S. L. Synthesis of Heterocycles via Pd-Ligand Controlled Cyclization of 2-Chloro-N-(2-Vinyl)Aniline: Preparation of Carbazoles, Indoles, Dibenzazepines, and Acridines. *J. Am. Chem. Soc.* **2010**, *132* (40), 14048–14051.

(20) Martin, R.; Buchwald, S. L. Palladium-Catalyzed Suzuki - Miyaura Cross- Coupling Reactions Employing Dialkylbiaryl Phosphine Ligands. *Acc. Chem. Res.* **2008**, *41* (11), 1461–1473.

(21) Cho, E. J.; Senecal, T. D.; Kinzel, T.; Zhang, Y.; Watson, D. A.; Buchwald, S. L. The Palladium-Catalyzed Trifluoromethylation of Aryl Chlorides. *Science.* **2010**, *328* (5986), 1679–1681.

(22) Surry, D. S.; Buchwald, S. L. Dialkylbiaryl Phosphines in Pd-Catalyzed Amination: A User's Guide. *Chem. Sci.* **2011**, *2* (1), 27–50.

(23) Choi, J.; Fu, G. C. Transition Metal-Catalyzed Alkyl-Alkyl Bond Formation: Another Dimension in Cross-Coupling Chemistry. *Science.* **2017**, *356* (6334).

(24) Podgoršek, A.; Zupan, M.; Iskra, J. Oxidative Halogenation with "Green" Oxidants: Oxygen and Hydrogen Peroxide. *Angew. Chem. Int. Ed.* **2009**, *48* (45), 8424–8450.

(25) Prebil, R.; Laali, K. K.; Stavber, S. Metal and H2O2 Free Aerobic Oxidative Aromatic Halogenation with [RNH3] [NO3-]/HX and [BMIM(SO3H)][NO3)x(X)y] (X = Br, Cl) as Multifunctional Ionic Liquids. *Org. Lett.* **2013**, *15* (9), 2108–2111.

(26) Himabindu, V.; Parvathaneni, S. P.; Rao, V. J. PhI(OAc)2/NaX-Mediated Halogenation

Providing Access to Valuable Synthons 3-Haloindole Derivatives. *New J. Chem.* **2018**, *42* (23), 18889–18893.

(27) Rajesh, K.; Somasundaram, M.; Saiganesh, R.; Balasubramanian, K. K. Bromination of Deactivated Aromatics: A Simple and Efficient Method. *J. Org. Chem.* **2007**, *72* (15), 5867–5869.

(28) Close, A. J.; Kemmitt, P.; Mark Roe, S.; Spencer, J. Regioselective Routes to Orthogonally-Substituted Aromatic MIDA Boronates. *Org. Biomol. Chem.* **2016**, *14* (28), 6751–6756.

(29) Bergström, M.; Suresh, G.; Naidu, V. R.; Unelius, C. R. N-Iodosuccinimide (NIS) in Direct Aromatic Iodination. *European J. Org. Chem.* **2017**, *2017* (22), 3234–3239.

(30) Zhou, C. Y.; Li, J.; Peddibhotla, S.; Romo, D. Mild Arming and Derivatization of Natural Products via an In(OTf) 3-Catalyzed Arene Iodination. *Org. Lett.* **2010**, *12* (9), 2104–2107.

(31) Racys, D. T.; Warrilow, C. E.; Pimlott, S. L.; Sutherland, A. Highly Regioselective Iodination of Arenes via Iron(III)-Catalyzed Activation of N-Iodosuccinimide. *Org. Lett.* **2015**, *17* (19), 4782–4785.

(32) Su, J.; Zhang, Y.; Chen, M.; Li, W.; Qin, X.; Xie, Y.; Qin, L.; Huang, S.; Zhang, M. A Copper Halide Promoted Regioselective Halogenation of Coumarins Using N-Halosuccinimide as Halide Source. *Synlett* **2019**, *30* (5), 630–634.

(33) Chung, W. J.; Vanderwal, C. D. Stereoselective Halogenation in Natural Product Synthesis. *Angew. Chem. Int. Ed.* **2016**, *55* (14), 4396–4434.

(34) Terazaki, M.; Shiomoto, K. I.; Mizoguchi, H.; Sakakura, A. Thioureas as Highly Active Catalysts for Biomimetic Bromocyclization of Geranyl Derivatives. *Org. Lett.* **2019**, *21* (7), 2073–2076.

(35) Maddox, S. M.; Nalbandian, C. J.; Smith, D. E.; Gustafson, J. L. A Practical Lewis Base Catalyzed Electrophilic Chlorination of Arenes and Heterocycles. *Org. Lett.* **2015**, *17* (4), 1042–1045.

(36) Bovonsombat, P.; Sophanpanichkul, P.; Pandey, A.; Tungsirisurp, S.; Limthavornlit, P.; Chobtumskul, K.; Kuhataparuk, P.; Sathityatiwat, S.; Teecomegaet, P. Novel Regioselective Aromatic Chlorination via Catalytic Thiourea Activation of N-Chlorosuccinimide. *Tetrahedron Lett.* **2015**, *56* (17), 2193–2196.

(37) Xiong, X.; Yeung, Y. Y. Highly Ortho-Selective Chlorination of Anilines Using a Secondary Ammonium Salt Organocatalyst. *Angew. Chem. Int. Ed.* **2016**, *55* (52), 16101–16105.

(38) Xiong, X.; Yeung, Y. Y. Ammonium Salt-Catalyzed Highly Practical Ortho-Selective Monohalogenation and Phenylselenation of Phenols: Scope and Applications. *ACS Catal.*

2018, *8* (5), 4033–4043.

(39) Xiong, X.; Tan, F.; Yeung, Y. Y. Zwitterionic-Salt-Catalyzed Site-Selective Monobromination of Arenes. *Org. Lett.* **2017**, *19* (16), 4243–4246.

(40) Song, S.; Li, X.; Wei, J.; Wang, W.; Zhang, Y.; Ai, L.; Zhu, Y.; Shi, X.; Zhang, X.; Jiao, N. DMSO-Catalysed Late-Stage Chlorination of (Hetero)Arenes. *Nat. Catal.* **2019**, *3*, 107–115.

(41) Denmark, S. E.; Beutner, G. L. Lewis Base Catalysis in Organic Synthesis. *Angew. Chem. Int. Ed.* **2008**, *47*, 1560–1638.

(42) Gutmann, V. Empirical Approach to Molecular Interactions. *Coord. Chem. Rev.* **1975**, *15* (2–3), 207–237.

(43) Nishii, Y.; Ikeda, M.; Hayashi, Y.; Kawauchi, S.; Miura, M. Triptycenyl Sulfide: A Practical and Active Catalyst for Electrophilic Aromatic Halogenation Using N- Halosuccinimides. *J. Am. Chem. Soc.* **2019**, *142* (3), 1621–1629.

(44) Denmark, S. E.; Kuester, W. E.; Burk, M. T. Catalytic, Asymmetric Halofunctionalization of Alkenes-a Critical Perspective. *Angew. Chem. Int. Ed.* **2012**, *51* (44), 10938–10953.

(45) Denmark, S. E.; Burk, M. T. Lewis Base Catalysis of Bromo- and Iodolactonization, and Cycloetherification. *Proc. Natl. Acad. Sci.* **2010**, *107* (48), 20655–20660.

(46) Denmark, S. E.; Burk, M. T. Development and Mechanism of an Enantioselective Bromocycloetherification Reaction via Lewis Base / Chiral Brønsted Acid Cooperative Catalysis. *Chirality*. **2014**, *355* (July 2013), 344–355.

(47) Lindsay Smith, J. R.; McKeer, L. C. High Site-Selectivity in the Chlorination of Electron-Rich Aromatic Compounds by N-Chlorammonium Salts. *Tetrahedron Lett.* **1983**, *24* (30), 3117–3120.

(48) Watson, W. D. Regioselective Para Chlorination of Activated Aromatic Compounds. *J. Org. Chem.* **1985**, *50* (12), 2145–2148.

(49) Gnaim, J. M.; Sheldon, R. A. Selective Ortho-Chlorination of Phenol Using Sulfuryl Chloride in the Presence of t-Butylaminomethyl Polystyrene as a Heterogeneous Amine Catalyst. *Tetrahedron Lett.* **2004**, *45* (46), 8471–8473.

(50) Qian, G.; Hong, X.; Liu, B.; Mao, H.; Xu, B. Rhodium-Catalyzed Regioselective C-H Chlorination of 7-Azaindoles Using 1,2-Dichloroethane. *Org. Lett.* **2014**, *16* (20), 5294–5297.

(51) Zhang, Y.; Shibatomi, K.; Yamamoto, H. Lewis Acid Catalyzed Highly Selective Halogenation of Aromatic Compounds. *Synlett* **2005**, No. 18, 2837–2842.

(52) Neufeldt, S. R.; Sanford, M. S. Controlling Site Selectivity in Palladium-Catalyzed C-H Bond Functionalization. *Acc. Chem. Res.* **2012**, *45* (6), 936–946.

(53) Rodriguez, R. A.; Pan, C.; Yabe, Y.; Kawamata, Y.; Eastgate, M. D.; Baran, P. S. Palau ' Chlor : A Practical and Reactive Chlorinating Reagent. *J. Am. Chem. Soc.* **2014**, *136*, 23–26.

(54) Wang, M.; Zhang, Y.; Wang, T.; Wang, C.; Xue, D.; Xiao, J. Story of an Age-Old Reagent: An Electrophilic Chlorination of Arenes and Heterocycles by 1-Chloro-1,2-Benziodoxol-3-One. *Org. Lett.* **2016**, *18* (9), 1976–1979.

(55) Samanta, R. C.; Yamamoto, H. Selective Halogenation Using an Aniline Catalyst. *Chemistry* **2015**, *21* (34), 11976–11979.

(56) Pathak, T. P.; Miller, S. J. Site-Selective Bromination of Vancomycin. *J. Am. Chem. Soc.* **2012**, *134* (14), 6120–6123.

(57) Payne, J. T.; Andorfer, M. C.; Lewis, J. C. Regioselective Arene Halogenation Using the FAD-Dependent Halogenase RebH. *Angew. Chem. Int. Ed.* **2013**, *52* (20), 5271–5274.

(58) Andorfer, M. C.; Park, H. J.; Vergara-Coll, J.; Lewis, J. C. Directed Evolution of RebH for Catalyst-Controlled Halogenation of Indole C–H Bonds. *Chem. Sci.* **2016**, *7* (6), 3720–3729.

(59) Xiong, X.; Zheng, T.; Wang, X.; Tse, Y.-L. S.; Yeung, Y.-Y. Access to Chiral Bisphenol Ligands (BPOL) through Desymmetrizing Asymmetric Ortho-Selective Halogenation. *Chem* **2020**, *6*, 1–14.

(60) Quin, L. D.; Williams, A. *Practical Interpretation of P-31 NMR Spectra and Computer Assisted Structure Verification*; Advanced Chemistry Development, Inc., 2004.

(61) Ashtekar, K. D.; Marzijarani, N. S.; Jaganathan, A.; Holmes, D.; Jackson, J. E.; Borhan, B. A New Tool To Guide Halofunctionalization Reactions: The Halenium Affinity (HalA) Scale. *J. Am. Chem. Soc.* **2014**, *136* (38), 13355–13362.

(62) Gnaim, J. M.; Sheldon, R. A. Highly Regioselective Ortho-Chlorination of Phenol with Sulfuryl Chloride in the Presence of Amines. *Tetrahedron Lett.* **1995**, *36* (22), 3893–3896.

(63) Yu, M.; Snider, B. B. Syntheses of Chloroisosulochrin and Isosulochrin and Biomimetic Elaboration to Maldoxin, Maldoxone, Dihydromaldoxin, and Dechlorodihydromaldoxin. *Org. Lett.* **2011**, *13* (16), 4224–4227.

(64) Ohkubo, K.; Hirose, K.; Fukuzumi, S. Solvent-Free One-Step Photochemical Hydroxylation of Benzene Derivatives by the Singlet Excited State of 2,3-Dichloro-5,6-Dicyano-p-Benzoquinone Acting as a Super Oxidant. *Chem. - A Eur. J.* **2015**, *21* (7), 2855–

2861.

(65) Kotoučová, H.; Strnadová, I.; Kovandová, M.; Chudoba, J.; Dvořáková, H.; Cibulka, R. Biomimetic Aerobic Oxidative Hydroxylation of Arylboronic Acids to Phenols Catalysed by a Flavin Derivative. *Org. Biomol. Chem.* **2014**, *12* (13), 2137–2142.

(66) Dong, Z.; Le, X.; Liu, Y.; Dong, C.; Ma, J. Metal Organic Framework Derived Magnetic Porous Carbon Composite Supported Gold and Palladium Nanoparticles as Highly Efficient and Recyclable Catalysts for Reduction of 4-Nitrophenol and Hydrodechlorination of 4-Chlorophenol. *J. Mater. Chem. A* **2014**, *2* (44), 18775–18785.

(67) Keane, M. A.; Gomez-Quero, S.; Cardenas-Lizana, F.; Shen, W. Alumina-Supported Ni-Au: Surface Synergistic Effects in Catalytic Hydrodechlorination. *ChemCatChem* **2009**, *1* (2), 270–278.

(68) Marzi, E.; Mongin, F.; Spitaleri, A.; Schlosser, M. Fluorophenols and (Trifluoromethyl)Phenols as Substrates of Site-Selective Metalation Reactions: To Protect or Not to Protect. *European J. Org. Chem.* **2001**, *15*, 2911–2915.

(69) Townsend, C. A.; Davis, S. G.; Christensen, S. B.; Link, J. C.; Lewis, C. P. Methoxymethyl-Directed Aryl Metalation. Total Synthesis of (.+-.)-Averufin. *J. Am. Chem. Soc.* **1981**, *103* (23), 6885–6888.

(70) Yoon, T. P.; Jacobsen, E. N. Privileged Chiral Catalysts. *Science.* **2003**, *299*, 1691–1693.

(71) Zhang, Z.; Schreiner, P. R. (Thio)Urea Organocatalysis - What Can Be Learnt from Anion Recognition? *Chem. Soc. Rev.* **2009**, *38* (4), 1187–1198.

(72) Schreiner, P. R.; Wittkopp, A. H-Bonding Additives Act like Lewis Acid Catalysts. *Org. Lett.* **2002**, *4* (2), 217–220.

(73) Sohtome, Y.; Tanatani, A.; Hashimoto, Y.; Nagasawa, K. Development of Bis-Thiourea-Type Organocatalyst for Asymmetric Baylis-Hillman Reaction. *Tetrahedron Lett.* **2004**, *45* (29), 5589–5592.

(74) Mittal, N.; Lippert, K. M.; De, C. K.; Klauber, E. G.; Emge, T. J.; Schreiner, P. R.; Seidel, D. A Dual-Catalysis Anion-Binding Approach to the Kinetic Resolution of Amines: Insights into the Mechanism via a Combined Experimental and Computational Study. *J. Am. Chem. Soc.* **2015**, *137* (17), 5748–5758.

(75) Busschaert, N.; Kirby, I. L.; Young, S.; Coles, S. J.; Horton, P. N.; Light, M. E.; Gale, P. A. Squaramides as Potent Transmembrane Anion Transporters. *Angew. Chem. Int. Ed.* **2012**, *51* (18), 4426–4430.

(76) Ghosh, D.; Gupta, N.; Abdi, S. H. R.; Nandi, S.; Khan, N. U. H.; Kureshy, R. I.; Bajaj, H. C. Organocatalyzed Enantioselective Allylation of Isatins by Using a Chiral Amino Alcohol

Derived Squaramide as Catalyst. *Eur. J. Org. Chem.* **2015**, *2015* (13), 2801–2806.

(77) Xu, H. J.; Liang, Y. F.; Cai, Z. Y.; Qi, H. X.; Yang, C. Y.; Feng, Y. S. CuI-Nanoparticles-Catalyzed Selective Synthesis of Phenols, Anilines, and Thiophenols from Aryl Halides in Aqueous Solution. *J. Org. Chem.* **2011**, *76* (7), 2296–2300.

(78) Magano, J.; Chen, M. H.; Clark, J. D.; Nussbaumer, T. 2-(Diethylamino)Ethanethiol, a New Reagent for the Odorless Deprotection of Aromatic Methyl Ethers. *J. Org. Chem.* **2006**, *71* (18), 7103–7105.

(79) Pallavicini, M.; Fumagalli, L.; Gobbi, M.; Bolchi, C.; Colleoni, S.; Moroni, B.; Pedretti, a; Rusconi, C.; Vistoli, G.; Valoti, E. QSAR Study for a Novel Series of Ortho Disubstituted Phenoxy Analogues of Alpha1-Adrenoceptor Antagonist WB4101. *Eur. J. Med. Chem.* **2006**, *41* (9), 1025–1040.

(80) Nagata, R.; Maruta, K.; Iwai, K.; Kitoh, M.; Ushiroda, K.; Yoshida, K. Pyrrole Derivative. Eur. Pat. Appl. p EP1386913.

(81) Cee, V. J.; Downing, N. S. A One-Pot Method for the Synthesis of 2-Aminobenzimidazoles and Related Heterocycles. *Tetrahedron Lett.* **2006**, *47* (22), 3747–3750.

(82) Denmark, S. E.; Kalyani, D.; Collins, W. R. Preparative and Mechanistic Studies toward the Rational Development of Catalytic, Enantioselective Selenoetherification Reactions. *J. Am. Chem. Soc.* **2010**, *132* (44), 15752–15765.

(83) Luo, J.; Cao, Q.; Cao, X.; Zhao, X. Selenide-Catalyzed Enantioselective Synthesis of Trifluoromethylthiolated Tetrahydronaphthalenes by Merging Desymmetrization and Trifluoromethylthiolation. *Nat. Commun.* **2018**, *9* (1), 1–9.

(84) Liu, X.; Liang, Y.; Ji, J.; Luo, J.; Zhao, X. Chiral Selenide-Catalyzed Enantioselective Allylic Reaction and Intermolecular Difunctionalization of Alkenes: E Fficient Construction of C-SCF 3 Stereogenic Molecules. *J. Am. Chem. Soc.* **2018**, *140* (14), 4782–4786.

(85) Luo, J.; Liu, Y.; Zhao, X. Chiral Selenide-Catalyzed Enantioselective Construction of Saturated Trifluoromethylthiolated Azaheterocycles. *Org. Lett.* **2017**, *19* (13), 3434–3437.

(86) See, J. Y.; Yang, H.; Zhao, Y.; Wong, M. W.; Ke, Z.; Yeung, Y. Desymmetrizing Enantio- and Diastereoselective Selenoetherification through Supramolecular Catalysis. *ACS Catal.* **2018,** *8*, 850-858.

(87) Liu, X.; An, R.; Zhang, X.; Luo, J.; Zhao, X. Enantioselective Trifluoromethylthiolating Lactonization Catalyzed by an Indane-Based Chiral Sulfide. *Angew. Chem. Int. Ed.* **2016**, *55* (19), 5846–5850.

(88) Wolfard, J.; Xu, J.; Zhang, H.; Chung, C. K. Synthesis of Chiral Tryptamines via a

Regioselective Indole Alkylation. *Org. Lett.* **2018**, *20* (17), 5431–5434.

(89) Gardelli, C.; Wada, H.; Ray, A.; Caffrey, M.; Llinas, A.; Shamovsky, I.; Tholander, J.; Larsson, J.; Sivars, U.; Hultin, L.; et al. Identification and Pharmacological Profile of an Indane Based Series of Ghrelin Receptor Full Agonists. *J. Med. Chem.* **2018**, *61* (14), 5974–5987.

(90) Dunbar, K. L.; Scharf, D. H.; Litomska, A.; Hertweck, C. Enzymatic Carbon − Sulfur Bond Formation in Natural Product Biosynthesis. *Chem. Rev.* **2017**, *117* (8), 5521–5577.

(91) Johannesson, P.; Lindeberg, G.; Johansson, A.; Nikiforovich, G. V; Gogoll, A.; Synnergren, B.; Gre, M. Le; Nyberg, F.; Karlen, A.; Hallberg, A. Vinyl Sulfide Cyclized Analogues of Angiotensin II with High Affinity and Full Agonist Activity at the AT 1 Receptor. *J. Med. Chem* **2002**, *45* (9), 1767–1777.

(92) Kazemi, M.; Shiri, L.; Kohzadi, H.; Kazemi, M.; Shiri, L.; Kohzadi, H. Recent Advances in Aryl Alkyl and Dialkyl Sulfide Synthesis. *Phosphorus, Sulfure, Silicon Relat. Elem.* **2015**, *190* (7), 978–1003.

(93) Marcantoni, E.; Massaccesi, M.; Petrini, M.; Bartoli, G.; Bellucci, M. C.; Bosco, M.; Sambri, L. A Novel Route to the Vinyl Sulfide Nine-Membered Macrocycle Moiety of Griseoviridin. *J. Org. Chem* **2000**, *65* (10), 4553–4559.

(94) Vazquez-prieto, M. A.; Miatello, R. M. Molecular Aspects of Medicine Organosulfur Compounds and Cardiovascular Disease. *Mol. Aspects Med.* **2010**, *31* (6), 540–545.

(95) Vouillamoz, J.; Entenza, M.; Hohl, P.; Moreillon, P. LB11058 , a New Cephalosporin with High Penicillin-Binding Protein 2a Affinity and Activity in Experimental Endocarditis Due to Homogeneously Methicillin-Resistant Staphylococcus Aureus. *Antimicrob Agents Chemother* **2004**, *48* (11), 4322–4327.

(96) Takimiya, K.; Osaka, I.; Mori, T.; Nakano, M. Organic Semiconductors Based on [1] Benzothieno[3,2-*b*][1] Benzothiophene Substructure. *Acc. Chem. Res.* **2014**, *47* (5), 1493–1502.

(97) Gill, R.; Rawal, R.; Bariwal, J. Recent Advances in the Chemistry and Biology of Benzothiazoles. *Arch. Pharm. Chem. Life Sci.* **2015**, *348* (3), 155–178.

(98) Lee, C.; Liu, Y.; Badsara, S. S. Transition-Metal-Catalyzed C-S Bond Coupling Reaction. *Chem. Asian J.* **2014**, *9* (3), 706–722.

(99) Beletskaya, I. P.; Ananikov, V. P. Transition-Metal-Catalyzed C - S , C - Se , and C - Te Bond Formation via Cross-Coupling and Atom-Economic Addition Reactions. *Chem. Rev.* **2011**, *111* (3), 1596–1636.

(100) Vasquez-cespedes, S.; Ferry, A.; Candish, L.; Glorius, F. Heterogeneously Catalyzed Direct

C-H Thiolation of Heteroarenes *Angew. Chem. Int. Ed.* **2015**, *54* (19), 5772–5776.

(101) Stavber, S. Recent Advances in the Application of Selectfluor TMF-TEDA-BF4 as a Versatile Mediator or Catalyst in Organic Synthesis. *Molecules* **2011**, *16* (8), 6432–6464.

(102) Schlosser, K. M.; Krasutsky, A. P.; Hamilton, H. W.; Reed, J. E.; Sexton, K. A Highly Efficient Procedure for 3-Sulfenylation of Indole-2-Carboxylates. *Org. Lett.* **2004**, *6* (5), 819–821.

(103) Tudge, M.; Tamiya, M.; Savarin, C.; Humphrey, G. R. Development of a Novel , Highly Efficient Halide-Catalyzed Sulfenylation of Indoles. *Org. Lett.* **2006**, *8* (54), 565–568.

(104) Gillis, M.; Greene, L.; Thompson, A. Preparation of Sulfenyl Pyrroles. *Synlett* **2009**, *2009* (1), 112–116.

(105) Matsugi, M.; Murata, K.; Nambu, H.; Kita, Y. An Efficient Sulfenylation of Aromatics Using Highly Active Quinone Mono O , S -Acetal Bearing a Pentafluorophenylthio Group. *Tetrahedron Lett.* **2001**, *42* (6), 1077–1080.

(106) Nalbandian, C. J.; Brown, Z. E.; Alvarez, E.; Gustafson, J. L. Lewis Base/Bronsted Acid Dual-Catalytic C–H Sulfenylation of Aromatics. *Org. Lett.* **2018**, *20* (11), 3211–3214.

(107) Nalbandian, C. J.; Miller, E. M.; Toenjes, S. T.; Gustafson, J. L. A Conjugate Lewis Base-Brønsted Acid Catalyst for the Sulfenylation of Nitrogen Containing Heterocycles under Mild Conditions. **2017**, *53* (9), 1494–1497.

(108) Shaw, M. H.; Twilton, J.; Macmillan, D. W. C. Photoredox Catalysis in Organic Chemistry. *J. Org. Chem.* **2016**, *81* (16), 6898–6926.

(109) Prier, C. K.; Rankic, D. A.; Macmillan, D. W. C. Visible Light Photoredox Catalysis with Transition Metal Complexes : Applications in Organic Synthesis. *Chem. Rev.* **2013**, *113* (7), 5322–5363.

(110) Romero, N. A.; Nicewicz, D. A. Organic Photoredox Catalysis. *Chem. Rev*. **2016**, *116* (17) 10075–10166.

(111) Takeda, H.; Ishitani, O. Development of Efficient Photocatalytic Systems for CO2 Reduction Using Mononuclear and Multinuclear Metal Complexes Based on Mechanistic Studies. *Coord. Chem. Rev.* **2010**, *254* (3–4), 346–354.

(112) Buzzetti, L.; Crisenza, G. E. M.; Melchiorre, P. Mechanistic Studies in Photocatalysis. *Angew. Chem. Int. Ed.* **2019**, *58*, 2–20.

(113) Smith, J. M.; Harwood, S. J.; Baran, P. S. Radical Retrosynthesis. *Acc. Chem Res.* **2018**. *51* (8), 1807-1817.

(114) Wang, C.; Dixneuf, P.; Soule, J.-F. Photoredox Catalysis for Building C−C Bonds from C(Sp^2)−H Bonds. *Chem. Rev.* **2018**, *118* (16), 7532–7585.

(115) Zhang, G.; Liu, C.; Yi, H.; Meng, Q.; Bian, C.; Chen, H.; Jian, J.; Wu, L.; Lei, A. External Oxidant-Free Oxidative Cross-Coupling: A Photoredox Cobalt-Catalyzed Aromatic C − H Thiolation for Constructing C−S Bonds. *J. Am. Chem. Soc.* **2015**, *137* (29), 9273–9280.

(116) Qian, X.; Li, S.; Song, J.; Xu, H. TEMPO-Catalyzed Electrochemical C−H Thiolation: Synthesis of Benzothiazoles and Thiazolopyridines from Thioamides. *ACS Catal.* **2017**, *7* (4), 2730–2734.

(117) Rahaman, R.; Das, S.; Barman, P. Visible-Light-Induced Regioselective Sulfenylation of Imidazopyridines with Thiols under Transition Metal-Free Conditions. *Green Chem.* **2018**, *20* (1), 141–147.

(118) Guo, W.; Tan, W.; Zhao, M.; Tao, K.; Zheng, L.; Wu, Y.; Chen, D.; Fan, X. Photocatalytic Direct C-S Bond Formation: Facile Acces to 3-Sulfenylindoles via Metal-Free C-3 Sulfenylation of Indoles with Thiophenols. *RSC Adv.* **2017**, *7* (60), 37739–37742.

(119) Das, A.; Maity, M.; Malcherek, S.; König, B.; Rehbein, J. Synthesis of Aryl Sulfides via Radical – Radical Cross Coupling of Electron-Rich Arenes Using Visible Light Photoredox Catalysis. *Beilstein J. Org. Chem.* **2018**, *14* (1), 2520–2528.

(120) Ayonon, A.; Nalbandian, C.; Guillemard, L.; Gustafson, J. Benzylic Bromination Catalyzed by Triphenylphosphine Selenide via Lewis Basic Activation. *Tetrahedron Lett.* **2017**, *58* (30), 2940–2943.

(121) Cruz, C. L.; Nicewicz, D. A. Mechanistic Investigations into the Cation Radical Newman − Kwart Rearrangement. *ACS Catal.* **2019**, *9*, 3926–3935.

(122) Morse, P. D.; Nicewicz, D. A. Chemical Science Divergent Regioselectivity in Photoredox-Catalyzed Hydrofunctionalization Reactions of Unsaturated Amides and Thioamides. *Chem. Sci.* **2015**, *6* (1), 270–274.

(123) Denes, F.; Pichowicz, M.; Povie, G.; Renaud, P. Thiyl Radicals in Organic Synthesis. *Chem. Rev.* **2014**, *114* (5), 2587–2693.

(124) Laplante, S. R.; Fader, L. D.; Fandrick, K. R.; Fandrick, D. R.; Hucke, O.; Kemper, R.; Miller, S. P. F.; Edwards, P. J. Assessing Atropisomer Axial Chirality in Drug Discovery and Development. *J. Med. Chem.* **2011**, *54* (20), 7005–7022.

(125) Laplante, S. R.; Edwards, P. J.; Fader, L. D.; Jakalian, A.; Hucke, O. Revealing Atropisomer Axial Chirality in Drug Discovery. *ChemMedChem* **2011**, *6* (3), 505–513.

(126) Toenjes, S. T.; Gustafson, J. L. Atropisomerism in Medicinal Chemistry : Challenges and Opportunities. *Future Med. Chem.* **2018**, *10* (4), 409–422.

(127) Law, V.; Knox, C.; Djoumbou, Y.; Jewison, T.; Guo, A. C.; Liu, Y.; MacIejewski, A.; Arndt, D.; Wilson, M.; Neveu, V.; et al. DrugBank 4.0: Shedding New Light on Drug Metabolism. *Nucleic Acids Res.* **2014**, *42* (D1), 1091–1097.

(128) Zask, A.; Murphy, J.; Ellestad, G. Biological Stereoselectivity of Atropisomeric Natural Products and Drugs. *Chirality* **2013**, *25*, 265–274.

(129) Clayden, J.; Moran, W. J.; Edwards, P. J.; Laplante, S. R. The Challenge of Atropisomerism in Drug Discovery. *Angew. Chem. Int. Ed.* **2009**, *48* (35), 6398–6401.

(130) Smith, D. E.; Marquez, I.; Lokensgard, M. E.; Rheingold, A. L.; Hecht, D. A.; Gustafson, J. L. Exploiting Atropisomerism to Increase the Target Selectivity of Kinase Inhibitors. *Angew. Chem. Int. Ed.* **2015**, *54* (40), 11754–11759.

(131) Toenjes, S. T.; Garcia, V.; Maddox, S. M.; Dawson, G. A.; Ortiz, M. A.; Piedrafita, F. J.; Gustafson, J. L. Leveraging Atropisomerism to Obtain a Selective Inhibitor of RET Kinase with Secondary Activities towards EGFR Mutants. *ACS Chem. Biol.* **2019**, *14* (9), 1930–1939.

(132) Watterson, S. H.; De Lucca, G. V.; Shi, Q.; Langevine, C. M.; Liu, Q.; Batt, D. G.; Beaudoin Bertrand, M.; Gong, H.; Dai, J.; Yip, S.; et al. Discovery of 6-Fluoro-5-(R)-(3-(S)-(8-Fluoro-1-Methyl-2,4-Dioxo-1,2-Dihydroquinazolin-3(4H)-Yl)-2-Methylphenyl)-2-(S)-(2-Hydroxypropan-2-Yl)-2,3,4,9-Tetrahydro-1H-Carbazole-8-Carboxamide (BMS-986142): A Reversible Inhibitor of Bruton's Tyrosine Kinase (BT. *J. Med. Chem.* **2016**, *59* (19), 9173–9200.

(133) Dai, J.; Wang, C.; Traeger, S. C.; Discenza, L.; Obermeier, M. T.; Tymiak, A. A.; Zhang, Y. The Role of Chromatographic and Chiroptical Spectroscopic Techniques and Methodologies in Support of Drug Discovery for Atropisomeric Drug Inhibitors of Bruton's Tyrosine Kinase. *J. Chromatogr. A* **2017**, *1487*, 116–128.

(134) Mamane, V.; Aubert, E.; Peluso, P.; Cossu, S. Synthesis, Resolution, and Absolute Configuration of Chiral 4,4′-Bipyridines. *J. Org. Chem.* **2012**, *77* (6), 2579–2583.

(135) Bringmann, G.; Mortimer, A. J. P.; Keller, P. A.; Gresser, M. J.; Garner, J.; Breuning, M. Atroposelective Synthesis of Axially Chiral Biaryl Compounds. *Angew. Chem. Int. Ed.* **2005**, *44* (34), 5384–5427.

(136) Bringmann, G.; Tasler, S.; Pfeifer, R. M.; Breuning, M. The Directed Synthesis of Axially Chiral Ligands, Reagents, Catalysts, and Natural Products through the "Lactone Methodology." *J. Organomet. Chem.* **2002**, *661* (1–2), 49–65.

(137) Cardenas, M. M.; Toenjes, S. T.; Nalbandian, C. J.; Gustafson, J. L. Enantioselective Synthesis of Pyrrolopyrimidine Scaffolds through Cation-Directed Nucleophilic Aromatic Substitution. *Org. Lett.* **2018**, *20* (7), 2037–2041.

(138) Vaidya, S. D.; Toenjes, S. T.; Yamamoto, N.; Maddox, S. M.; Gustafson, J. L.; Vaidya, S. D.; Toenjes, S. T.; Yamamoto, N.; Maddox, S. M.; Gustafson, J. L. Catalytic Atroposelective Synthesis of N-Aryl Quinoid Compounds Catalytic Atroposelective Synthesis of N -Aryl Quinoid Compounds. *J. Am. Chem. Soc.* **2020**, *142*, 2198–2203.

(139) Maddox, S. M.; Dawson, G. A.; Rochester, N. C.; Ayonon, A. B.; Moore, C. E.; Rheingold, A. L.; Gustafson, J. L. Enantioselective Synthesis of Biaryl Atropisomers via the Addition of Thiophenols into Aryl-Naphthoquinones. *ACS Catal.* **2018**, *8*, 5443-5447

(140) Jolliffe, J. D.; Armstrong, R. J.; Smith, M. D. Catalytic Enantioselective Synthesis of Atropisomeric Biaryls by a Cation-Directed O-Alkylation. *Nat. Chem.* **2017**, *9* (6), 558–562.

(141) Armstrong, R. J.; Smith, M. D. Catalytic Enantioselective Synthesis of Atropisomeric Biaryls: A Cation-Directed Nucleophilic Aromatic Substitution Reaction. *Angew. Chem. Int. Ed.* **2014**, *53* (47), 12822–12826.

(142) Gustafson, J. L.; Lim, D.; Miller, S. J. Dynamic Kinetic Resolution of Biaryl Asymmetric Bromination. *Science.* **2010**, *328* (4), 1251–1255.

(143) Barrett, K. T.; Miller, S. J. Enantioselective Synthesis of Atropisomeric Benzamides through Peptide-Catalyzed Bromination. *J. Am. Chem. Soc.* **2013**, *135* (8), 2963–2966.

(144) Nicolaou, K. C.; Boddy, C. N. C. Atropselective Macrocyclization of Diaryl Ether Ring Systems: Application to the Synthesis of Vancomycin Model Systems. *J. Am. Chem. Soc.* **2002**, *124* (35), 10451–10455.

(145) Clayden, J.; Kubinski, P. M.; Sammiceli, F.; Helliwell, M.; Diorazio, L. Sulfoxides as "traceless" Resolving Agents for the Synthesis of Atropisomers by Dynamic or Classical Resolution. *Tetrahedron Lett.* **2004**, *60* (20), 4387–4397.

(146) Betson, M. S.; Clayden, J.; Worrall, C. P.; Peace, S. Three Groups Good, Four Groups Bad? Atropisomerism in Ortho-Substituted Diaryl Ethers. *Angew. Chem. Int. Ed.* **2006**, *45* (35), 5803–5807.

(147) Clayden, J.; Worrall, C. P.; Moran, W. J.; Helliwell, M. Enantioselective Synthesis of an Atropisomeric Diaryl Ether. *Angew. Chem. Int. Ed.* **2008**, *47* (17), 3234–3237.

(148) Yuan, B.; Page, A.; Worrall, C. P.; Escalettes, F.; Willies, S. C.; McDouall, J. J. W.; Turner, N. J.; Clayden, J. Biocatalytic Desymmetrization of an Atropisomer with Both an Enantioselective Oxidase and Ketoreductases. *Angew. Chem. Int. Ed.* **2010**, *49* (39), 7010–7013.

(149) Staniland, S.; Adams, R. W.; McDouall, J. J. W.; Maffucci, I.; Contini, A.; Grainger, D. M.; Turner, N. J.; Clayden, J. Biocatalytic Dynamic Kinetic Resolution for the Synthesis of

Atropisomeric Biaryl N-Oxide Lewis Base Catalysts. *Angew. Chem. Int. Ed.* **2016**, *55* (36), 10755–10759.

(150) Iwamura, H.; Mislow, K. Stereochemical Consequences of Dynamic Gearing. *Acc. Chem. Res.* **1988**, *21* (4), 175–182.

(151) Manna, M. S.; Mukherjee, S. Organocatalytic Enantioselective Formal C(Sp2)-H Alkylation. *J. Am. Chem. Soc.* **2015**, *137* (1), 130–133.

(152) Sarkar, R.; Mukherjee, S. Catalytic Enantioselective Desymmetrization of Norbornenoquinones via C(Sp 2)–H Alkylation. *Org. Lett.* **2016**, *18* (23), 6160–6163.

(153) Diedrich, C.; Grimme, S. Systematic Investigation of Modern Quantum Chemical Methods to Predict Electronic Circular Dichroism Spectra. *J. Phys. Chem. A* **2003**, *107* (14), 2524–2539.

(154) Berova, N.; Bari, L. Di; Pescitelli, G. Application of Electronic Circular Dichroism in Configurational and Conformational Analysis of Organic Compounds. *Chem. Soc. Rev.* **2007**, *36* (6), 914–931.

(155) Li, X.-C.; Ferreira, D.; Ding, Y. Determination of Absolute Configuration of Natural Products: Theoretical Calculation of Electronic Circular Dichroism as a Tool. *Curr. Org. Chem.* **2010**, *14* (16), 1678–1697.

(156) S. Maddox, A. Dinh, F. Armenta, J. Um, J. G. The Catalyst-Controlled Regiodivergent Chlorination of Phenols. *Org. Lett.* **2016**, *18* (21), 5476–5479.

(157) Jähnert, T.; Hager, M. D.; Schubert, U. S. Assorted Phenoxyl-Radical Polymers and Their Application in Lithium-Organic Batteries. *Macromol. Rapid Commun.* **2016**, *37*, 725–730.

(158) Cassani, C.; Martín-Rapún, R.; Arceo, E.; Bravo, F.; Melchiorre, P. Synthesis of 9-Amino(9-Deoxy)Epi Cinchona Alkaloids, General Chiral Organocatalysts for the Stereoselective Functionalization of Carbonyl Compounds. *Nat. Protoc.* **2013**, *8* (2), 325–344.